LEABHARLANN CHOLÁISTE NA TRÍONÓIDE, BAILE ÁTHA CLIATH | TRINITY COLLEGE LIBRARY DUBLIN
Ollscoil Átha Cliath | The University of Dublin

Terms and Conditions of Use of Digitised Theses from Trinity College Library Dublin

Copyright statement

All material supplied by Trinity College Library is protected by copyright (under the Copyright and Related Rights Act, 2000 as amended) and other relevant Intellectual Property Rights. By accessing and using a Digitised Thesis from Trinity College Library you acknowledge that all Intellectual Property Rights in any Works supplied are the sole and exclusive property of the copyright and/or other IPR holder. Specific copyright holders may not be explicitly identified. Use of materials from other sources within a thesis should not be construed as a claim over them.

A non-exclusive, non-transferable licence is hereby granted to those using or reproducing, in whole or in part, the material for valid purposes, providing the copyright owners are acknowledged using the normal conventions. Where specific permission to use material is required, this is identified and such permission must be sought from the copyright holder or agency cited.

Liability statement

By using a Digitised Thesis, I accept that Trinity College Dublin bears no legal responsibility for the accuracy, legality or comprehensiveness of materials contained within the thesis, and that Trinity College Dublin accepts no liability for indirect, consequential, or incidental, damages or losses arising from use of the thesis for whatever reason. Information located in a thesis may be subject to specific use constraints, details of which may not be explicitly described. It is the responsibility of potential and actual users to be aware of such constraints and to abide by them. By making use of material from a digitised thesis, you accept these copyright and disclaimer provisions. Where it is brought to the attention of Trinity College Library that there may be a breach of copyright or other restraint, it is the policy to withdraw or take down access to a thesis while the issue is being resolved.

Access Agreement

By using a Digitised Thesis from Trinity College Library you are bound by the following Terms & Conditions. Please read them carefully.

I have read and I understand the following statement: All material supplied via a Digitised Thesis from Trinity College Library is protected by copyright and other intellectual property rights, and duplication or sale of all or part of any of a thesis is not permitted, except that material may be duplicated by you for your research use or for educational purposes in electronic or print form providing the copyright owners are acknowledged using the normal conventions. You must obtain permission for any other use. Electronic or print copies may not be offered, whether for sale or otherwise to anyone. This copy has been supplied on the understanding that it is copyright material and that no quotation from the thesis may be published without proper acknowledgement.

A multi-proxy palaeoceanographic investigation of slope deposits on the Porcupine Bank, NE Atlantic Ocean

Submitted to the University of Dublin for the degree of Doctor of Philosophy

2010

Nicholas Liam Owen

Declaration

This thesis has not been submitted as an exercise for a degree at this or any other University and is entirely the candidate's own work, with the inclusion of unpublished work by a joint project acknowledged in the text wherever included. The candidate agrees that the Library may lend or copy the thesis upon request.

Signed.....

TRINITY COLLEGE
3 0 MAR 2012
LIBRARY DUBLIN
Thesis 9368

Summary

High resolution imaging of the continental slope west of the Porcupine Bank by the Irish National Seabed Survey reveals an area that is smooth and relatively undisturbed. The area lacks evidence of debris flows and canyon complexes that are prevalent on most other slope sections of the Rockall Trough, presenting a unique opportunity to examine cores along a depth transect without the issue of major down slope redistribution of sediments. Previous examinations of cores from the study area have revealed an absence of sedimentological evidence for significant gravity related remobilization and suggested that a record of bottom current activity interacting with the sea-floor is preserved.

For this study, a multi-proxy palaeoceanographic investigation of these deposits is made from a depth transect consisting of seven gravity cores. However, in order to assess the potential value of these units for palaeoceanographic purposes, it is first necessary to assess the quality, resolution and integrity of the records preserved at different depths. This is undertaken by correlation of individual *%Neogloboquadrina pachyderma* (sin.) curves with reference curves to identify hiatuses and episodes with low sedimentation rates and to develop age models for each core. Key results of this exercise include the identification of a significant hiatus in two cores which appears to span large parts of Marine Isotope Stage 3. Fragmentation of foraminiferal tests are used to identify units which are likely to have suffered from post-mortem modification, with results showing that, in some instances, interglacial units are poorly preserved compared to glacials. Transfer functions were performed on fossil assemblages of planktonic foraminifera to attempt to reconstruct sea surface temperatures, although the lack of good modern analogues for most samples suggests that mixing of samples could be a significant problem. However, an absence of sub-polar taxa suggests that sea-ice may have formed and been retained over the Porcupine Bank. A key finding in this regard is

that this proposed episode of sea-ice cover corresponds to the proposed maximum extent of the British Irish Ice Sheet during the last glacial (16-27 kyr B.P.), as suggested by some authors in previous works, but also highlights variations within this interval. The effect of glacial-interglacial variations on water mass flux and the resulting effect on sea surface temperatures can also be inferred from geochemical analysis and suggest that when Glacial North Atlantic Intermediate Water / Antarctic Intermediate Water flux crosses a threshold value in glacials / interglacials (respectively), this appears to result in stable SSTs in the North Atlantic region. Heinrich events also impact on the palaeoceanography of this site, and could produce a response to the migration of the polar front over this area as part of Dansgaard-Oeschger events. The spatial and temporal distribution of assemblages of benthic foraminifera was also examined to provide information on benthic productivity, which in some cases can be related to surface production. It is difficult to determine the precise mechanisms causing variation in the spatial distribution of benthic foraminifera on this part of the continental slope. No obvious species response to proposed episodes of enhanced bottom current activity can be identified, and no taxa display a clear correlation to any of the geochemical proxy / tracer data. However, a response to productivity variations is apparent when the known ecological preferences of certain taxa are considered. This (in more than one way) appears to exert overwhelmingly the biggest influence on species distributions on the slope for the larger size fraction. Comparing down slope productivity, sedimentological and species diversity data appears to suggest that the diversity of assemblages of benthic foraminifera is responding to a dynamic equilibrium between food supply and environmental stability. For the smaller size fraction, mixing both within and between cores appears to be more prevalent and suggests that proxy data based on small particle size data should be treated with due caution.

Acknowledgements

I would like to thank my supervisor, Dr. Robin Edwards, for his guidance and discussions throughout the study. Lee Toms is thanked for supplying data and figures to be applied in this thesis, as well as some interesting discussions. Dr. Peter Haughton and Prof. Pat Shannon are acknowledged for also providing some insightful comments and discussion throughout the project. The technical support staff at Trinity College Dublin (Neil Kearney, Mags Duncan, Francis Hendron, Noel McGinley and Dr. Robbie Goodhue) are thanked for their support. At Cardiff University, Jenny Riker is thanked especially for her assistance and guidance with respect to the HR-ICP-MS analysis, as are Drs. Carrie Lear and Stephen Barker for helpful discussions prior to and following the analyses. Drs. Jeremy Young, Andy Henderson and Robert Wynn Jones (BNHM) are also acknowledged.

I would also like to especially thank my mother, step-father, grandmother, brother and sister for their support during the study. My fiancée and best friend, Kiara, is thanked for her unequivocal support and comfort during some of the more challenging parts of this project.

A multi-proxy palaeoceanographic investigation of slope deposits on the Porcupine Bank, NE Atlantic Ocean

Title Page

Declaration

Summary

Acknowledgements

Page

Chapter 1

1.1 Introduction 1

1.2 Databases and sources 3

1.3 Aims and objectives 3

Chapter 2: Regional setting and previous work

2.1 Introduction 12

2.2 Modern oceanography of Porcupine Bank and related areas 13

2.3 Stratigraphy 21

2.4 Palaeoceanography of Porcupine Bank and related areas 28

2.5 Ecology of modern benthic foraminifera 42

2.6 Sedimentology 49

Chapter 3: Methods

3.1 Sample extraction and preparation 55

3.2 Sample examination under light microscopy 59

3.3 Estimating the degree of post-mortem modification of assemblages 61

3.4 Taxonomy and Scanning Electron Microscopy 66

3.5 Age model development and correlation 68

3.6 Transfer function based sea surface temperature reconstructions 74

3.7 Geochemical analyses 82

3.8 Statistical analysis of data 112

3.9 Ecology of benthic foraminifera 115

Chapter 4: Taxonomy

4.1 Introduction 119

4.2 Taxonomic descriptions of benthic foraminifera 120

4.3 List of plates (benthic foraminifera) 173

4.4 Taxonomy of planktonic foraminifera 178

Chapter 5: Age model development and fragmentation

5.1 Introduction 195

5.2 Results 196

5.3 Discussion 220

5.4 Comparison with nannofossils biostratigraphy and lithostratigraphy 225

5.5 Summary and conclusions 228

Chapter 6: Planktonic foraminifera

6.1 Introduction 229

6.2 Reliability of sea surface temperature reconstructions 230

6.3 Results 235

6.4 Discussion 253

6.5 Summary and conclusions 262

Chapter 7: Geochemistry

7.1 Introduction 264

7.2 Planktonic stable isotope data from core 9/97-10 267

7.3 Preliminary whole core assessment of geochemical data 268

7.4 Results of benthic geochemical analysis 271

7.5 Down slope patterns in geochemical data 278

7.6 Discussion 286

7.7 Summary 301

Chapter 8: Benthic foraminifera

8.1 Introduction 307

8.2 Results 308

8.3 Temporal variations in assemblage 330

8.4 Statistical analysis of assemblage data 336

8.5 Discussion 355

8.6 Summary 372

Chapter 9: Synthesis

9.1 Integrity of the record 376

9.2 Inferences from assemblage / geochemical data 382

9.3 Wider implications 394

Chapter 10

10.1 Outline 417

10.2 Addressing the research questions 417

10.3 Recommendations for further research 426

References 430

Appendices

List of Tables

Chapter 1

Table 1.1. Appendices of raw and processed data used in this study.

Chapter 2

Table 2.1. Outline of the modern properties of the major water masses that currently interact with the Porcupine Bank, or possibly did in the past. Data from Sarnthein et al. (1994); Bertram et al. (1995); Barringer and Price (1999); New and Smythe-Wright (2001); Read (2001) and Hall and Chan (2004).

Chapter 3

Table 3.1. Details of cores used in this study.

Table 3.2. Properties studied from each size fraction.

Table 3.3. Ecological and other significance of the key taxa picked onto reference slides.

Table 3.4. Precision and reproducibility of the trace element ratios of interest and comparable publications.

Chapter 5

Table 5.1. Dating and correlation methods applied to each core, with reference curves used and resulting correlation coefficients.

Chapter 6

Table 6.1. Root Mean Squared Error of Prediction (RMSEP) values for each transfer function method from each core. MAT = Modern Analogue Technique, WAPLS = Weighted averaging, partial least squares and ML = Maximum Likelihood). Note the relatively high value for the winter SST reconstruction of core 9/97-20 using the Maximum Likelihood method. DC (%) refers to the percentage of fossil samples for which a good modern analogue is present in the training set, based on the percentage of samples with a dissimilarity coefficient less than 5%.

Chapter 7

Table 7.1 Summary of the geochemical proxies examined in this study, their primary utility, what they are combined / compared with to perform reconstructions.

Chapter 8

Table 8.1. Eigenvalues and the percentage variance for each principal component.

List of figures

Chapter 1

Figure 1.1. Map of the Rockall Trough region with modern ocean circulation. Abbreviations: PAB=Porcupine Abyssal Plain; PSB=Porcupine Seabight; RT=Rockall Trough; PB=Porcupine Bank; HS=Hebrides Shelf; RB=Rockall Bank; HT=Hatton Trough; HB=Hatton Bank; IB=Iceland Basin; NAC=North Atlantic Current; SEC=Slope Edge Current; NSDW=Norwegian Sea Deep Water; and LSW=Labrador Sea Water. From Øvrebø *et al.* (2006).

Figure 1.2. Bathymetric profile of the study area, with the positions of Transect 1 and Transect 2 highlighted. The positions of cores examined in the previous study by Øvrebø *et al.* (2006) are highlighted. Modified from Øvrebø *et al.* (2006).

Figure 1.3. Lithostratigraphic correlation of Transect 1, as proposed by Toms (in prep.). For lithostratigraphic key, see Appendix G. Alternations of pink and blue colours are related to

interglacial-glacial climate variations respectively. Arrows indicate the positions of radiocarbon dating points.

Figure 1.4. Calcareous nannofossil biostratigraphy of Transect 1, as proposed by Toms (in prep.). For lithostratigraphic key, see Appendix G. Blue and pink backgrounds represent glacials and interglacials respectively, with colours in the bars representing the relative abundance of species of calcareous nannofossil.

Figure 1.5. Lithostratigraphic correlation of Transect 2, as proposed by Toms (in prep.). S1-11 = surface number. Numbers above and between the cores refer to distance (in km) between core sites. Blue core labels refer to cores incorporated into the correlation from Øvrebø (2005). For lithostratigraphic key, see Appendix G.

Figure 1.6. Division of labour diagram for the two Ph.D. projects, this study (Nick Owen, TCD) and the concurrent project at UCD (Lee Toms, UCD).

Chapter 2

Figure 2.1. Geostrophic velocity recorded for the North East North Atlantic Ocean. Note the strength and direction of the currents at 1000m, 2000m and 3000m on the Porcupine Bank (red square). Modified from Ocean Data View, based on data from Bersch (1995).

Figure 2.2. Potential temperature (°C) sections of the top 1000m of the Porcupine Bank (red square), modified from Read (2001).

Figure 2.3. The main water masses impinging on the Porcupine Bank, modified from Read (2001). Transect highlighted (red line) in smaller, left-hand panel. SAIW = Sub Arctic Intermediate Water, ISOW = Iceland-Scotland Overflow Water, WNAW = Western North

Atlantic Water, ENAW = Eastern North Atlantic Water, AAIW = Antarctic Intermediate Water, LSW = Labrador Sea Water, NEADW = North East Atlantic Deep Water, AABW = Antarctic Bottom Water.

Figure 2.4. Cenozoic stratigraphic column modified from Gibbard *et al.* (2009). The portion of the Quaternary period examined in this thesis is highlighted by the red square.

Figure 2.5. Oxygen isotope stratigraphy of the last 1.8 million years (Lisiecki and Raymo 2005). This curve is based on a stack of 57 globally distributed benthic $\delta^{18}O$ curves. The numbers adjacent to the curve represent marine isotope stages. Modified from Bassinot (2007).

Figure 2.6. Models of the cumulative ice cover of the British Irish Ice Sheet during the last glacial based on three experiments (a-c), modified from Hubbard *et al.* (2009).

Figure 2.7. The GISP-II ice core record of Stuiver *et al.* (1997). The stadial-interstadial variations of MIS 3 are highlighted. HE = Heinrich Event.

Figure 2.8. Reconstructed summer and winter sea surface temperature records of the previous 500ka from Kandiano and Bauch (2003) based on three distinct transfer functions (Modern Analogue Technique - MAT, Revised Analogue Method - RAM and Transfer Function Technique - TFT). Interglacials are highlighted (1-11).

Figure 2.9. Modelled circulation of the North Atlantic based on the presence / absence of Mediterranean Outflow Water modified from Rahmstorf (1997). Numbers = °C.

Figure 2.10. (a) Modern distributions of NADW and AABW based on Phosphorus concentrations (arrows indicate relative flow speed) and (b) reconstructed distributions of GNAIW and AABW based on $\delta^{13}C_{benthic}$ (Lynch-Stieglitz *et al.* 2007), with the distribution of sample points highlighted by black dots.

Figure 2.11. Multi-proxy record of Peck *et al.* (2007) from the Porcupine Seabight. Negative $\delta^{13}C_{benthic}$ excursions are highlighted (black squares). Blue vertical bars highlight episodes of surface ocean stratification, orange and pink vertical bars indicate Heinrich events. Green line data = core SO75-26KL, Black line data = MD01-2461, Purple line data = NEAP4K. For sedimentation rates, black line = radiocarbon-based sedimentation rate, red line = tuned. Arrows adjacent to benthic $\delta^{18}O$ data denote tie-points.

Figure 2.12. From Scourse *et al.* (2009), a conceptual model displaying the proposed relationship between the dynamics of the BIIS with the migration of the polar front (A) through a D–O cycle from the GISP-II record (B), with the position of this study area highlighted.

Figure 2.13. The TROX model, which explains the effect of controls (productivity and oxygenation) on the distribution of benthic foraminifera in the sediment (Jorissen *et al.* 1995).

Figure 2.14. Migration of peaks in BFAR from the North Atlantic to Arctic Ocean with proposed velocities (v) estimated from the distance between stations and dates at which peaks occurred. Modified from Nees *et al.* (1997).

Figure 2.15. 3D bathymetry map showing the position of cores studied by Øvrebø *et al.* (2006). Note the large canyon complex to the south and the area examined in this study highlighted by the red square. Modified from Øvrebø *et al.* (2006).

Figure 2.16. Depositional model proposed by Øvrebø *et al.* (2006). Note the changing position and strength of currents along the slope at different time intervals, and the resulting sedimentary units.

Chapter 3

Figure 3.1. Sampling positions highlighted either side of a large cobble present in core 9/97-10. Photograph courtesy of Toms (pers. comm.).

Figure 3.2. Flow-chart indicating the sample preparation procedure employed in this study.

Figure 3.3. Dissolution series of modern planktonic foraminifera (based on Hemleben *et al.* 1989). Note the relative position of *N.pachyderma* compared to taxa such as *G.bulloides* and *G.ruber* highlighted by the red squares (Modified from Kucera 2007). Grayscale shading of symbols denotes habitat preferences in terms of sea surface temperature, from cold (light grey) to tropical (black).

Figure 3.4. Relationship between coiling direction of *N.pachyderma* and mean sea surface temperature. Modified from Kucera (2007), where *N.pachyderma* (dext.) is labeled *N.incompta*.

Figure 3.5. Wiggle-matching method employed to correlate the *%N.pachyderma* (sin.) curve (green line) from core 9/97-10 with the benthic $\delta^{18}O$ curve (red line) of McManus *et al.* (1999). Note that the core depth axis of the *%N.pachyderma* (sin.) curve has altered. Yellow shading indicates interglacials (odd numbers 5-11) as proposed by calcareous nannofossil biostratigraphy (Toms in prep.), with stars indicating radiocarbon dating points.

Figure 3.6. Calcareous nannofossil biostratigraphy of Transect 1, as proposed by Toms *et al.* (in prep.). Blue and pink background represents glacial-interglacial units respectively. Colours in bars represent the relative abundance of the calcareous nannofossil highlighted.

Figure 3.7. Calculation of reservoir ages using the correlation of *%N.pachyderma* (sin.) from core 9/97-27/2 (green line in lower panel) to GISP-II ($\delta^{18}O$, red line in lower panel). The

letters a and b refer to uncorrected ^{14}C AMS radiocarbon dates provided by Toms (pers. comm.). Blue shaded areas represent absent stadials in the core 9/97-27/2 record.

Figure 3.8. Diagram illustrating the expansion of sea-ice cover during the Last Glacial Maximum based on the distribution of the sub-polar species group (Kucera *et al.* 2005). Green shading = seasonal sea-ice, orange shading = open sea.

Figure 3.9. Flow chart indicates the procedure followed for performing stable isotope analyses using the CF-IRMS.

Figure 3.10. Flow-chart illustrating the procedure followed for cleaning and preparing samples prior to trace metal analysis using the HR-ICP-MS.

Figure 3.11. LM photographs highlighting contaminants (clay minerals and manganese nodules) that need to be removed during the contaminant picking stage.

Figure 3.12. LM photograph showing the picked foraminiferal shell material and the separated contaminants.

Figure 3.13. The relationship between the concentration of Barium and Alkalinity in the Pacific Ocean, from Jaquet *et al.* (2005).

Figure 3.14. The relationship between the concentration of cadmium and phosphorus in the Pacific Ocean, modified from Lacan *et al.* (2005).

Figure 3.15. Plot of end-member compositions of different water masses, modified from Rickaby and Elderfield (2005). Open square = Glacial North Atlantic Intermediate Water, Open circle = Mediterranean Outflow Water, Open cross = North Atlantic Deep Water and Closed square = Antarctic Bottom Water. Mixing with Antarctic Intermediate Water would result in a distinctive air-sea exchange signature.

Figure 3.16. Proposed relationship between Mg/Ca recorded in *C.wuellerstorfi* and temperature, as proposed by Martin *et al.* (2002).

Figure 3.17. The effect of variations in ice volume, salinity (evaporation and precipitation) on $\delta^{18}O_{sw}$ and of temperature on $\delta^{18}O_{shell}$ from Ravelo and Hillaire-Marcel (2007). T = temperature and f = function.

Figure 3.18. The distribution of $\delta^{13}C$ with water depth in the North East Atlantic Ocean, from Bertram *et al.* (1995).

Figure 3.19. Illustration of the various factors that can influence $\delta^{13}C_{DIC}$ and $\delta^{13}C_{shell}$ from Ravelo and Hillaire-Marcel (2007).

Figure 3.20. An example of the paired cluster and DCA method used to determine lithofacies assemblage zone groups (LFAZs) for core 9/97-10. The lithofacies classification scheme is courtesy of Toms (pers. comm.).

Figure 3.21. The proposed relationship between the percentage of *C.wuellerstorfi* from the >250μm size fraction and sea-floor flux rates, from Altenbach *et al.* (1999). Note the scatter around the linear trend line.

Chapter 4

Figure 4.1. Light microscope image of *Fissurina porcupinensis* sp. nov. Note the distinctive surface ornamentation.

Chapter 5

Figure 5.1. Correlation window with *%N.pachyderma* (sin.) data from core 9/97-10 (green curve) correlated to the benthic oxygen isotope profile of ODP site 980 (red curve). Blue lines indicate tie-points. Yellow shading indicates Marine Isotope Stages (numbers above graphs) based on calcareous nannofossil biostratigraphy. Stars indicated ^{14}C AMS radiocarbon dated samples, with adjacent numbers indicating age kyr B.P.

Figure 5.2. Result of overlaying the *%N.pachyderma* (sin.) curve (green line) on to the benthic oxygen isotope profile of ODP site 980 (red line). Note the relatively poor record between 200 and ~330 kyr B.P.

Figure 5.3.(a) Variations in sedimentation rate with depth and (b) age-depth plot for core 9/97-10.

Figure 5.4. Fragmentation indices for the upper 83cm of core 9/97-10. FLS refers to the Le and Shackleton (1992) index.

Figure 5.5. Result of overlaying the $\delta^{18}O_{planktonic}$ record from core 9/97-10 from this study (red line) with that from Øvrebø *et al.* (2006) – (green line).

Figure 5.6. Stable isotope data from Øvrebø *et al.* (2006) plotted against data obtained in this study (Owen 2009). Data from this study that plots separately from that of Øvrebø *et al.* (2006) is highlighted by the grey oval.

Figure 5.7. Spectral analysis of the $\delta^{18}O_{planktonic}$ curve from core 9/97-10. Note the high power peaks at eccentricity (100kyr) and precession (19kyr) frequencies.

Figure 5.8.(a) Variations in sedimentation rate with depth and (b) age-depth plot for core 9/97-03.

Figure 5.9. Fragmentation indices for the whole of core 9/97-03. FLS refers to the Le and Shackleton (1992) index.

Figure 5.10.(a) Variations in sedimentation rate with depth and (b) age-depth plot for core 9/97-04.

Figure 5.11. Fragmentation indices for the upper 88cm of core 9/97-04. FLS refers to the Le and Shackleton (1992) index.

Figure 5.12.(a) Variations in sedimentation rate with depth and (b) age-depth plot for core 9/97-14.

Figure 5.13. Fragmentation indices for the upper 95cm of core 9/97-14. FLS refers to the Le and Shackleton (1992) index.

Figure 5.14. Fragmentation indices for the whole of core 9/97-08 and an approximate stratigraphy for the upper 82cm. FLS refers to the Le and Shackleton (1992) index.

Figure 5.15.(a) Variations in sedimentation rate with depth and (b) age-depth plot for core 9/97-27/2.

Figure 5.16. Fragmentation indices for the whole of core 9/97-27/2. FLS refers to the Le and Shackleton (1992) index.

Figure 5.17. Correlation of the MAT reconstructed SSTs for core 9/97-27/2 (green line) with the $\delta^{18}O$ record of GISP-II (red line). Blue lines indicate tie-points, stars denote the positions of ^{14}C AMS radiocarbon dated points.

Figure 5.18.(a) Variations in sedimentation rate with depth and (b) age-depth plot for core 9/97-20.

Figure 5.19. Fragmentation indices for the whole of core 9/97-20. FLS refers to the Le and Shackleton (1992) index.

Figure 5.20. Correlation of the $\delta^{18}O$ curve of ODP Site 980 with *%N.pachyderma* (sin.) data from cores (a) 9/97-10, (b) 9/97-03, (c) 9/97-04 and (d) 9/97-14. Yellow shading indicates interglacials (numbered) as suggested by calcareous nannofossil biostratigraphy, with tie-points highlighted.

Figure 5.21. Correlation of the GISP-II $\delta^{18}O$ curve with *%N.pachyderma* (sin.) data from cores (a) 9/97-27/2 and (b) 9/97-20. Stars indicate ^{14}C AMS radiocarbon dating points (from Toms pers. comm.), with tie-points indicated.

Figure 5.21. Calcareous nannofossil biostratigraphy of cores along Transect 1, modified from Toms (in. prep.). Blue and pink backgrounds indicate glacial and interglacial stages respectively. Coloured bars represent the relative abundance of species of calcareous nannofossil.

Chapter 6

Figure 6.1. Scatter plots showing the relationship between observed SSTs and reconstructed (estimated) values from each transfer function (as calculated from the sample data in core 9/97/10). Note the linear relationship in (a) compared to the relationships in (b) and (c).

Figure 6.2. Linear relationship between reconstructed summer and winter sea surface temperatures of core 9/97-10 from MAT.

Figure 6.3.(a) Subpolar species group, (b) *%N.pachyderma* (sin.) and (c) abundance of warm water oligotrophic taxa for core 9/97-10. Grey shading highlights intervals where *N.pachyderma* (sin.) is ≥60%.

Figure 6.4. Reconstructed summer and winter SSTs and seasonal differences for MAT (red lines), WAPLS (blue lines) and ML (black lines) for core 9/97-10. Dissimilarity coefficients for each sample are presented, with the 20th percentile indicated by the dashed line. The vast majority of samples are above this, suggesting a relative lack of good modern analogues.

Figure 6.5.(a) Subpolar species group, (b) *%N.pachyderma* (sin.) and (c) abundance of warm water oligotrophic taxa for core 9/97-03. Grey shading highlights intervals where *N.pachyderma* (sin.) is ≥60%.

Figure 6.6. Reconstructed summer and winter SSTs and seasonal differences for MAT (red lines), WAPLS (blue lines) and ML (black lines) for core 9/97-03. Dissimilarity coefficients for each sample are presented, with the 20th percentile indicated by the dashed line. The vast majority of samples are above this, suggesting a relative lack of good modern analogues.

Figure 6.7.(a) Subpolar species group, (b) *%N.pachyderma* (sin.) and (c) abundance of warm water oligotrophic taxa for core 9/97-04. Grey shading highlights intervals where *N.pachyderma* (sin.) is ≥60%.

Figure 6.8. Reconstructed summer and winter SSTs and seasonal differences for MAT (red lines), WAPLS (blue lines) and ML (black lines) for core 9/97-04. Dissimilarity coefficients for each sample are presented, with the 20th percentile indicated by the dashed line. The vast majority of samples are above this, suggesting a relative lack of good modern analogues.

Figure 6.9.(a) Subpolar species group, (b) *%N.pachyderma* (sin.) and (c) abundance of warm water oligotrophic taxa for core 9/97-14. Grey shading highlights intervals where *N.pachyderma* (sin.) is ≥60%.

Figure 6.10. Reconstructed summer and winter SSTs and seasonal differences for MAT (red lines), WAPLS (blue lines) and ML (black lines) for core 9/97-14. Dissimilarity coefficients for each sample are presented, with the 20th percentile indicated by the dashed line. The vast majority of samples are above this, suggesting a relative lack of good modern analogues.

Figure 6.11. Composite MAT derived sea surface temperature record for intermediate depth (1230-2118m water depth) cores. Splicing sections are highlighted (4 = 9/97-04, 10 = 9/97-10 and 3 = 9/97-03). Red line indicates summer values, blue line indicates winter value. Grey shading highlights interglacials.

Figure 6.12.(a) Subpolar species group, (b) *%N.pachyderma* (sin.) and (c) abundance of warm water oligotrophic taxa for core 9/97-27/2. Grey shading highlights intervals where *N.pachyderma* (sin.) is ≥60%. Blue shading indicates intervals where sub-polar species group are absent.

Figure 6.13. Reconstructed summer and winter SSTs and seasonal differences for MAT (red lines), WAPLS (blue lines) and ML (black lines) for core 9/97-27/2. Dissimilarity coefficients for each sample are presented, with the 20th percentile indicated by the dashed line. The majority of samples are above this, suggesting a relative lack of good modern analogues.

Figure 6.14.(a) Subpolar species group, (b) *%N.pachyderma* (sin.) and (c) abundance of warm water oligotrophic taxa for core 9/97-20. Grey shading highlights intervals where *N.pachyderma* (sin.) is ≥60%. Blue shading indicates intervals where sub-polar species group are absent.

Figure 6.15. Reconstructed summer and winter SSTs and seasonal differences for MAT (red lines), WAPLS (blue lines) and ML (black lines) for core 9/97-20. Dissimilarity coefficients for each sample are presented, with the 20th percentile indicated by the dashed line. The majority of 'cold' samples are below this, suggesting they may have good modern analogues.

Figure 6.16. Composite MAT derived sea surface temperature record for deep (>2118m water depth) cores. Splicing sections are highlighted (20 = 9/97-20, 27 = 9/97-27/2). Red line indicates summer values, blue line indicates winter value. Grey shading highlights Holocene (left area) and Marine Isotope Stage 3 (right area).

Chapter 7

Figure 7.1. Down core (a) delta$^{18}O_{planktonic}$, (b) delta$^{13}C_{planktonic}$, (c) SST derived from delta$^{18}O_{planktonic}$, (d) Summer SST derived from MAT (red line) and WA-PLS (blue line) and (e) Winter SST derived from MAT (red line) and WA-PLS for core 9/97-10.

Figure 7.2. Fragmentation index versus Mg/Ca values for cores (a) 9/97-10, (b) 9/97-04, (c) 9/97-14 and (d) 9/97-27/2. The whole core dataset is plotted in (e).

Figure 7.3. Scatter plot of whole core Mn/Ca vs. Cd/Ca values, with all of the samples from core 9/97/27/II recording concentrations above 150 μmol/mol.

Figure 7.4. Down core multi-element / calcium and stable isotope ratios for core 9/97-10 (1260m water depth).

Figure 7.5. Down core multi-element / calcium and stable isotope ratios for core 9/97-04 (1502m water depth).

Figure 7.6. Down core multi-element / calcium and stable isotope ratios for core 9/97-14 (2118m water depth).

Figure 7.7. Down core multi-element / calcium and stable isotope ratios for core 9/97-27/2 (2756m water depth).

Figure 7.8. Down slope bottom water temperature variations from four cores for the last interglacial to Holocene; 9/97-10 (1260m water depth), 9/97-04 (1502m water depth), 9/97-14 (2118m water depth), 9/97-27/2 (2756m water depth).

Figure 7.9. Reconstructed $\delta^{18}O_{sw}$ values for cores (a) 9/97-10 (1260m water depth), (b) 9/97-04 (1502m water depth), (c) 9/97-14 (2118m water depth) and (d) 9/97-27/II (2756m water depth) for the time interval 0-125 kyr B.P.

Figure 7.10. Down slope carbon isotope ratios from four cores for the last interglacial to Holocene; 9/97-10 (1260m water depth), 9/97-04 (1502m water depth), 9/97-14 (2118m water depth), 9/97-27/2 (2756m water depth).

Figure 7.11. Down slope reconstructed phosphorus concentrations from three cores for the last interglacial to Holocene; 9/97-10 (1260m water depth), 9/97-04 (1502m water depth), 9/97-14 (2118m water depth).

Figure 7.12. Plots of reconstructed phosphorus concentrations versus $\delta^{13}C_{benthic}$ for cores (a) 9/97-10, (b) 9/97-04 and (c) 9/97-14. End-member compositions are derived following the methodology of Rickaby and Elderfield (2005). Open square = GNAIW, open circle = MOW (Mediterranean Outflow Water), open cross = NADW, full square = AABW. Green dots refer to Holocene samples, blue dots to last glacial samples and red dots to last interglacial

samples. Samples which are removed vertically along the air-sea exchange parameter are considered to be mixed with AAIW.

Figure 7.13. Water mass stratification reconstructions along the slope for two time periods; the last interglacial (95-125 kyr B.P.) and Marine Isotope Stage 3 (30-60 kyr B.P.). Blue arrows indicate the relative increase or decrease in refractory nutrient supply and blue stars indicate bottom water dysoxia. Curved arrows indicate mixing of water masses.

Figure 7.14. Water mass stratification reconstructions along the slope for two time periods; the Marine Isotope Stage 2 (11.5-30 kyr B.P.) and the Holocene (0-11.5 kyr B.P.). Blue arrows indicate the relative increase or decrease in refractory nutrient supply and blue stars indicate bottom water dysoxia. Curved arrows indicate mixing of water masses.

Chapter 8

Figure 8.1. Down core distribution of taxa and assemblages zones from the 250-500μm size fraction (9/97-08). Also BFAR and fragmentation data.

Figure 8.2. Down core distribution of taxa from the 63-250μm size fraction (9/97-08). Also BFAR and fragmentation data.

Figure 8.3. Down core distribution of taxa and assemblages zones from the 250-500μm size fraction (9/97-10). Also BFAR and fragmentation data.

Figure 8.4. Down core distribution of taxa from the 63-250μm size fraction (9/97-10). Also BFAR and fragmentation data.

Figure 8.5. Down core distribution of taxa and assemblages zones from the 250-500μm size fraction (9/97-03). Also BFAR and fragmentation data.

Figure 8.6. Down core distribution of taxa and assemblages zones from the 250-500μm size fraction (9/97-04). Also BFAR and fragmentation data.

Figure 8.7. Down core distribution of taxa from the 63-250μm size fraction (9/97-04). Also BFAR and fragmentation data.

Figure 8.8. Down core distribution of taxa and assemblages zones from the 250-500μm size fraction (9/97-14). Also BFAR and fragmentation data.

Figure 8.9. Down core distribution of taxa from the 63-250μm size fraction (9/97-14). Also BFAR and fragmentation data.

Figure 8.10. Down core distribution of taxa and assemblages zones from the 250-500μm size fraction (9/97-27/2). Also BFAR and fragmentation data.

Figure 8.11. Down core distribution of taxa from the 63-250μm size fraction (9/97-27/2). Also BFAR and fragmentation data.

Figure 8.12. Down core distribution of taxa and assemblages zones from the 250-500μm size fraction (9/97-20). Also BFAR and fragmentation data.

Figure 8.13. Scatter plot of all core BFAR data versus fragmentation index.

Figure 8.14. Variation of BFAR through time down slope for cores 9/97-10 (1260m water depth), 9/97-04 (1502m water depth), 9/97-14 (2118m water depth), 9/97-27/2 (2756m water depth) and 9/97-20 (3073m water depth).

Figure 8.15. Fisher's Alpha diversity index for each interval; (a) Last interglacial, (b) Last glacial, (c) Holocene.

Figure 8.16. Whole dataset cluster analysis for the larger size fraction (250-500μm). Samples ending in _8 are from core 9/97-08, ending in _10 from core 9/97-10 etc. Inter-core clustering is highlighted by the red square.

Figure 8.17. Cluster analysis (bootstrapped) of the larger size fraction for cores 9/97-10 and 9/97-03 (ending in _3).

Figure 8.18. Position in cores 9/97-10 and 9/97-03 of cluster pairs X and Y.

Figure 8.19. Cluster analysis of the larger size fraction for cores 9/97-27/2 (ending in _27) and 9/97-20.

Figure 8.20. Position in cores 9/97-27/2 and 9/97-20 of cluster pair Z.

Figure 8.21a Principle components analysis (component 1 versus component 2) of the whole large fraction dataset, with important taxa highlighted. Samples ending in _8 are from core 9/97-08, ending in _10 from core 9/97-10 etc.

Figure 8.21a and b. Principle components analysis (component 2 versus component 3, top graph; component 3 versus component 4, bottom graph) of the whole dataset. Samples ending in _8 are from core 9/97-08, ending in _10 from core 9/97-10 etc.

Figure 8.22. Principle components analysis of samples from cores 9/97-08 (a), 9/97-10 (b), 9/97-04 (c), 9/97-14 (d), 9/97-27/2 (e).

Figure 8.23. Detrended correspondence analysis of samples from different time slices; (a) Holocene, (b) Last glacial and (c) Last interglacial. Samples ending in _8 are from core 9/97-08, ending in _10 from core 9/97-10 etc.

Figure 8.24. Cluster analysis of the small size fraction data (63-250μm) for cores (a) 9/97-08, (b) 9/97-10, (c) 9/97-04, (d) 9/97-14 and (e) 9/97-27/2.

Figure 8.25. Principle components analysis of the whole small size fraction dataset. Samples ending in _8 are from core 9/97-08, ending in _10 from core 9/97-10 etc.

Figure 8.26. Detrended correspondence analysis of the small and large size fraction data for cores (a) 9/97-08, (b) 9/97-10, (c) 9/97-04, (d) 9/97-14 and 9/97-27/2. Samples ending with the core label (e.g. _8 for core 9/97-08) are from the small size fraction.

Figure 8.27. Mid slope diversity maximum produced by dynamic equilibrium of benthic foraminifera populations with nutrient supply and environmental stability.

Chapter 9

Figure 9.1. Multi-proxy record of MIS 3 in core 9/97-27/2. Note the strong negative delta13C value (arrow) approximately 4kyrs before H4 (as dated by Peck et al. 2007 - grey band). For MAT SST, red line = summer values, blue line = winter values. IRD (%) is the percentage of IRD grains in the greater than 150 micron size fraction, courtesy of Toms (in prep.).

Figure 9.2. Particle size analysis results for core 9/97-27/2, courtesy of Toms (in prep.).

Figure 9.3. Comparison of MAT derived SST summer values from the composite SST record of Chapter 6 with the benthic $\delta^{18}O$ record of Poli *et al.* (2000) for MIS 11-13 (10.2, 10.3 etc. refer to sub-stages of each marine isotope stage). Note the step-wise increase in the SST values at the termination of the MIS 12 glacial in the composite SST record.

Figure 9.4. Stability of SSTs (MAT derived from core 9/97-10, red line = summer values, blue line = winter values) and the maximum fluxes of AAIW / GNAIW during MIS 5 and MIS 2 respectively according to benthic geochemistry.

Figure 9.5. Correlation of lithofacies assemblage zone groups from cores 9/97-10, 9/97-03 and 9/97-04 during MIS 5. Note the position of a potential boundary between cores 9/97-04 and 9/97-14 which corresponds to the AAIW / NADW boundary proposed by benthic geochemistry.

Figure 9.6. Comparison of benthic foraminifera relative abundance with particle size data (courtesy of Toms in prep.), SSTs (red line = summer values, blue line = winter values), BFAR and overall water mass influence in core 9/97-10.

Figure 9.7. Migration of the polar front (red line) over this study area at (a) 40.8 kyr B.P. (BFAR peak 1), (b) 39 kyr B.P. (Heinrich event 4 as dated by Peck *et al.* 2007) and (c) 37.7kyr B.P. (BFAR peak 2). Map courtesy of Toms (in prep.).

Figure 9.8. Comparison of geochemical proxy data from three cores (9/97-10, 9/97-14 and 9/97-27/2) with Heinrich events (as dated by Peck *et al.* 2007, pink and orange shading) and the three phases (I-IIIa and b) of perennial sea-ice development (grey shading), as suggested by the planktonic foraminifera assemblages data of core 9/97-20.

Figure 9.9. Particle size analysis results for core 9/97-10, courtesy of Toms (in prep.).

Figure 9.10. Record of benthic $\delta^{13}C$ and $\delta^{18}O$ from the Gulf of Cadiz (Voelker *et al.* 2006) and the benthic record of phosphorus concentrations and $\delta^{13}C$ in core 9/97-10. The sample which records the influence of MOW is highlighted.

List of Plates

Scale bar represents 250μm for all specimens

Plate 1

Fig. 1a and b = *Siphotextularia rolhauseni* Phleger and Parker 1951 – TCD.59237

Fig. 2 = *Eggerella bradyi* (Cushman 1911) – TCD.59237

Fig.3a-c = *Karreriella bradyi* (Cushman 1911) – TCD.59230

Fig. 4 = *Amphicoryna scalaris* (Batsch 1791) – TCD.59236

Fig.5 = *Astacolus hyalacrulus* Loeblich and Tappan 1953 – TCD.59238

Fig.6 = *Dentalina communis* (d'Orbigny 1826) – TCD.59236

Fig. 7 = *Dentalina baggi* (Galloway and Wissler 1927) – TCD.59236

Plate 2

Fig. 1a-b = *Spiroloculina rotunda* d'Orbigny 1826 – TCD.59233

Fig. 2a-b = *Quinqueloculina seminulum* (Linné 1758) – TCD.59238

Fig. 3a-b = *Quinqueloculina arctica* Cushman 1933 – TCD.59238

Fig. 4 = *Quinqueloculina stalkeri* Loeblich and Tappan 1953 – TCD.59238

Fig. 5 = *Quinqueloculina striata* d'Orbigny 1826 – TCD.59238

Fig. 6 = *Quinqueloculina elongata* Natland 1938 – TCD.59238

Plate 3

Fig. 1 = *Pyrgo oblonga* (d'Orbigny 1826) – TCD.59238

Fig. 2 = *Pyrgo lacernula* (Schwager 1866) – TCD.59238

Fig. 3 = *Pyrgo sarsi* (Schlumberger 1891) – TCD.59238

Fig. 4a-b = *Pyrgo murrhina* (Schwager 1866) – TCD.59238

Fig. 5 = *Pyrgo* sp. 1 – TCD.59238

Fig. 6 = *Triloculina tricarinata* Reuss 1867 – TCD.59237

Fig. 7a-b = *Sigmoilopsis schlumbergeri* (Silvestri 1904) – TCD.59230

Plate 4

Fig. 1 = *Oolina apiopleura* (Loeblich and Tappan 1953) – TCD.59236

Fig. 2 = *Oolina heronalleni?* Jones 1984 – TCD.59236

Fig. 3 = *Oolina hexagona* (Williamson 1858) – TCD.59236

Fig. 4a-e = *Oolina melo* (d'Orbigny 1826) – TCD.59236

Fig. 5a-b = *Oolina intercalata* Jones 1984 – TCD.59236

Fig. 6a-b = *Oolina squamosa* (Montagu 1803) – TCD.59236

Plate 5

Fig. 1a-b = *Fissurina marginata* (Montagu 1803) – TCD.59237

Fig. 2 = Fissurina sp. 2 – TCD.59237

Fig. 3a-b = *Fissurina porcupinensis* sp. nov. – TCD.59223

Fig. 4 = *Fissurina* sp. 1 – TCD.59237

Fig. 5a-b = *Fissurina varioperforata* (Buchner 1940) – TCD.59237

Plate 6

Fig. 1a-b = *Pseudofissurina mccullochae* Jones 1984 – TCD.59237

Fig. 2 = *Lagena sulcata* (Walker and Jacob 1789) – TCD.59237

Fig. 3a-b = *Pseudosolenina borealis* Jones 1984 – TCD.59237

Fig. 4 = *Lagena* sp. 1 – TCD.59237

Fig. 5a-b = *Solenina radiata* (Seguenza 1862) – TCD.59237

Fig. 6 = *Lagena* sp. 2 – TCD.59237

Plate 7

Fig. 1a-c = *Bulimina inflata* (Seguenza 1862) – TCD.59224

Fig. 2a-b = *Bulimina aculeata* (d'Orbigny 1826) – TCD.59224

Fig. 3 = *Bulimina marginata* (d'Orbigny 1826) – TCD.59223

Fig. 4a-c = *Ruprtina stabilis* Wallich 1877 – TCD.59225

Fig. 5 = *Nummoloculina irregularis* (d'Orbigny 1826) - – TCD.59238

Plate 8

Fig. 1a-b = *Bolivina albatrossi* Cushman 1922 – TCD.59236

Fig. 2a-b = *Bolivina pseudopunctata* Höglund 1947 – TCD.59236

Fig. 3a-b = *Bolivina spinescens* Cushman 1911 – TCD.59236

Fig. 4a-b = *Bolivina subspinescens* Cushman 1922 – TCD.59236

Fig. 5a-b = *Brizalina robusta* Brady 1884 – TCD.59236

Plate 9

Fig. 1a-c = *Fursenkoina complanata* (Egger 1895) – TCD.59238

Fig. 2a-b = *Stainforthia* (*Fursenkoina*) *fusiformis* (Egger 1895) – TCD.59238

Fig. 3a-c = *Virgulina advena* Cushman 1922 – TCD.59238

Plate 10

Fig. 1a-c = *Hoeglundia elegans* (d'Orbigny 1826) – TCD.59229

Fig. 2a-c = *Triffarina angulosa* (Williamson 1858) – TCD.59229

Fig. 3a-b = *Ehrenbergina serrata* Reuss 1850 – TCD.59233

Plate 11

Fig. 1a-c = *Alabaminella weddellensis* (Earland 1936) – TCD.59237

Fig. 2a-c = *Cassidulina laevigata* d'Orbigny 1826 – TCD.59238

Fig. 3 = *Epistominella exigua* (Brady 1884) – TCD.59238

Fig. 4 = *Eponides pusillus* (Parr 1950) – TCD.59238

Fig. 5 = *Nonionella turgida* (Williamson 1858) – TCD.59238

Plate 12

Fig. 1a-c = *Gyroidina soldanii* d'Orbigny 1826 – TCD.59236

Fig. 2a-c = *Melonis barleeanum* (Williamson 1858) – TCD.59227

Fig. 3a-c = *Pullenia bulloides* (d'Orbigny 1826) – TCD.59225

Plate 13

1a-b = *Turborotalita quinqueloba* (Natland 1938) – TCD.59232

2 = *Orbulina universa* d'Orbigny 1839 – TCD.59233

3a-c = *Globigerina bulloides* d'Orbigny 1826 – TCD.59232

4a-c = *Globigerinoides ruber* (d'Orbigny 1839) – TCD.59233

Plate 14

1a-c = *Globorotalia inflata* (d'Orbigny 1839) – TCD.59234

2a-c = *Globorotalia scitula* (Brady 1882) – TCD.59234

3a-c = *Globorotalia hirsuta* (d'Orbigny 1839) – TCD.59234

4a-c = *Globorotalia truncatulinoides* (d'Orbigny 1839) – TCD.59234

Plate 15

1a-b = *Neogloboquadrina pachyderma* (dextral) (Ehrenberg 1861) – TCD.59233

2a-c = *Neogloboquadrina pachyderma* (sinistral) (Ehrenberg 1861) – TCD.59233

3a-c = *Globigerinella siphonifera* (d'Orbigny 1839) – TCD.59233

List of Appendices

Appendix A - Planktonic foraminifera assemblage data

Appendix B – Benthic foraminifera assemblage data, large and small size fractions

Appendix C – Geochemistry data (including equations used)

Appendix D – BFAR, Fragmentation indices

Appendix E – Age model data and reservoir ages

Appendix F – Principle components scores

Appendix G – Lithofacies classification scheme

Chapter 1

1.1 Introduction

This study is part of a project that seeks to better understand the record of oceanographic currents on submarine slopes west of Ireland, in order to assess possible links and feedbacks between changes in deeper level oceanographic circulation and climate oscillations that occurred onshore during the Quaternary. The project is entitled 'Deposits of thermohaline currents on slopes west of Ireland – implications for climate change' and is financially supported by Science Foundation Ireland under Grant Number 06/RFP/GEO030.

Whereas variations in atmospheric radiocarbon can provide a proxy for global thermohaline circulation (Clark *et al.* 2002), regional indications of palaeocirculation rely on extracting information from the deposits of bottom currents on the ocean floor. When bottom currents exceed the threshold velocity for sediment transport, sediment on the sea floor is transported and redeposited to create a variety of erosional and depositional structures (e.g. erosion surfaces, moats, mounds and channels) that can reveal the former activity of currents (White *et al.* 2005; Øvrebø *et al.* 2006). Transport by along slope currents can also impart a distinctive texture to the sediment, and influence oxygenation, productivity and biotic activity on the sea floor (Rasmussen *et al.* 2002).

Although a link between thermohaline circulation and global climate is widely suspected (e.g. Broecker 1998; Barker *et al.* 2009), the precise nature of the relationship remains unclear. The western seaboard of Ireland and the 'gateway' Rockall Trough (Fig. 1.1) is critically placed on a possible fairway for northward moving, slope-parallel currents that would have advected warmer water to higher latitudes during interglacial and interstadial periods as part of

the sub-polar gyre system (Hatun *et al.* 2005). Whilst significant advances have been made in dating the Irish glacial record, information from the offshore record will complement and advance these. The onshore last glacial record in Ireland is rather fragmentary and still poorly dated (Coxon 2001) so a better appreciation of events offshore will help understand the structure of the onshore record; the offshore record can also be compared with more complete proxy records from onshore NW Europe. Study of the deposits over the whole slope will address the presence of different water masses at different levels in the water column during glacial, interstadial and interglacial times. The modern ocean structure is complex and it is likely that it has been so in the past. To date, deep sea proxy records have mainly focused on vertical profiles in a single core, often in deep water. A multi-core approach is critical to mapping how different parts of the slope responded to glacial climate change, but this is often not possible in the Rockall Trough region due to instabilities in the slopes either side.

With greater knowledge of the Irish far-offshore arising from the Irish National Seabed Survey and recent exploratory drilling in the Rockall region (e.g. RRS Challenger cruise 1999), a critical area of smooth and relatively undisturbed slope has been identified to the west of the Porcupine Bank (Fig. 1.2). Although the gradients here are locally steep (up to 10° on the lower slope), this area is unusual in that there is little evidence for the surficial slide scars and debris flow lobes that generally characterize the slopes flanking the Rockall Trough (Shannon *et al.* 2001). This suggests that this site would be suitable for examining cores along a depth transect through this area.

1.2 Databases and sources

The raw data used in this study are presented in the Appendices as outlined in Table 1.1. This study uses the graphic logs, lithostratigraphic correlation and nannofossil biostratigraphic scheme (Figs. 1.3-1.5), grain size and ice-rafted debris data of a concurrent PhD project undertaken at UCD by Toms (in prep.). The uncorrected ^{14}C AMS radiocarbon dates used in this study (Appendix E) were also obtained by Toms. All data or interpretations presented in this thesis that are originally from Toms (in prep.) are highlighted accordingly. A diagram illustrating the different areas of research covered between this project and the concurrent project at UCD and how they relate to each other is given in Figure 1.8.

Appendix	Data
A	Planktonic foraminifera assemblage data
B	Benthic foraminifera assemblage data, Large and Small size Fractions
C	Geochemistry data (incl. equations used)
D	BFAR, Fragmentation Indices
E	Age model data and reservoir ages
F	Principle components scores
G	Lithofacies classification scheme

Table 1.1. Appendices of raw and processed data used in this study.

1.3 Aims and objectives

The main objective of this project is to assess the quality of the palaeoceanographic record preserved in contourite deposits on the slope of the Porcupine Bank. In order to determine this, the following characteristics will be described for the slope deposits:

- Taxonomy of benthic foraminifera (Chapter 4)

- Distribution in space / time of assemblages of benthic foraminifera (large versus small size fractions)
- Relationships between bio- and lithostratigraphy
- Stratigraphic integrity and establishment of chronologies (Chapter 5)
- Fragmentation indices

This objective will then be achieved by addressing the following research questions:

1. Is there evidence of physical (e.g. bottom-current sorting/winnowing, inclusion of allochthonous material) and / or chemical (e.g. dissolution) taphonomic processes distorting any original climate records?
2. Do indicators of preservation potential vary systematically either within cores or down slope?

Achieving the first objective will enable the identification of portions of the record which are suitable for further study, using a multi-proxy approach to extract information about changes in the palaeoceanography of the Porcupine Bank region during the Late Quaternary. This will form the basis of the following objectives where, quality of the record permitting, the following research questions will be addressed:

3. What were the surface oceanographic conditions under which these deposits formed?
4. How did the influence of Southern Component Water in this region vary between the Last Interglacial and the Holocene?
5. How does productivity vary through both time and space at this site?
6. Did the core of a bottom current vary in strength and positioning along the slope following glacial-interglacial climate variations, as proposed by Øvrebø *et al.* (2006)?

The third question will be addressed by examining assemblages of planktonic foraminifera and using these to perform transfer functions using comparative analyses with modern assemblages (Chapter 6). This should enable the extraction of valuable information on both seasonal differences in sea surface temperatures and the presence or otherwise of sea-ice. Question four will be addressed by applying a combination of trace element and stable isotope analyses to identify the relative strength of the Southern versus Northern Component Water influences and how this has varied (Chapter 7). Answering the next question will rely on applying the known ecological preferences of modern assemblages of benthic foraminifera (which today display a strong relationship with productivity) to principal components of the fossil assemblages to decipher the parameters causing significant variation in assemblages (Chapter 8). The final question will be addressed by examining evidence from the distribution of assemblages of benthic foraminifera as well as the distribution of key species of benthic foraminifera that are known to rely on lateral currents for feeding (Chapters 8 and 9).

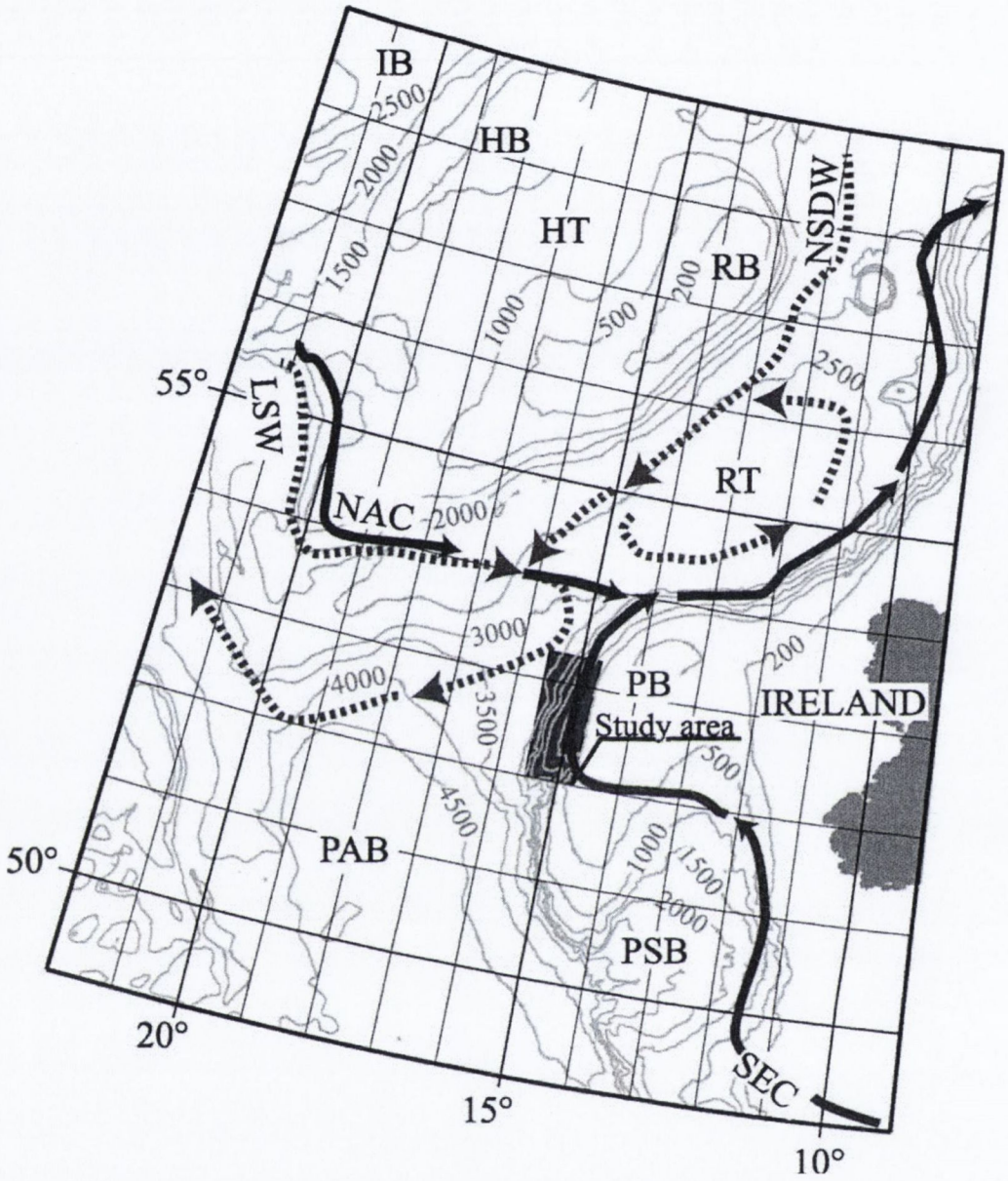

Figure 1.1. Map of the Rockall Trough region with modern ocean circulation. Abbreviations: PAB=Porcupine Abyssal Plain; PSB=Porcupine Seabight; RT=Rockall Trough; PB=Porcupine Bank; HS=Hebrides Shelf; RB=Rockall Bank; HT=Hatton Trough; HB=Hatton Bank; IB=Iceland Basin; NAC=North Atlantic Current; SEC=Slope Edge Current; NSDW=Norwegian Sea Deep Water; and LSW=Labrador Sea Water. From Øvrebo *et al.* (2006).

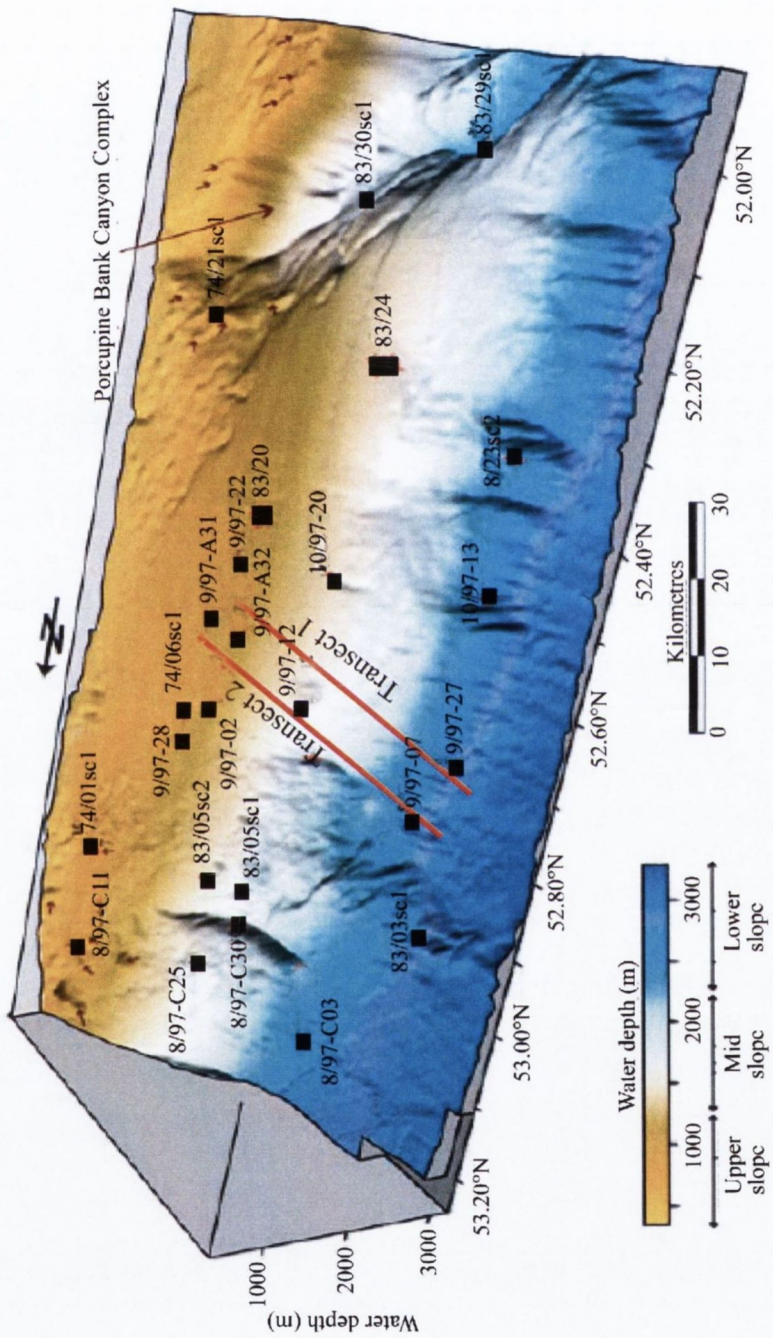

Figure 1.2. Bathymetric profile of the study area, with the positions of Transect 1 and Transect 2 highlighted. The positions of cores examined in the previous study by Øvrebø *et al.* (2006) are highlighted. Modified from Øvrebø *et al.* (2006).

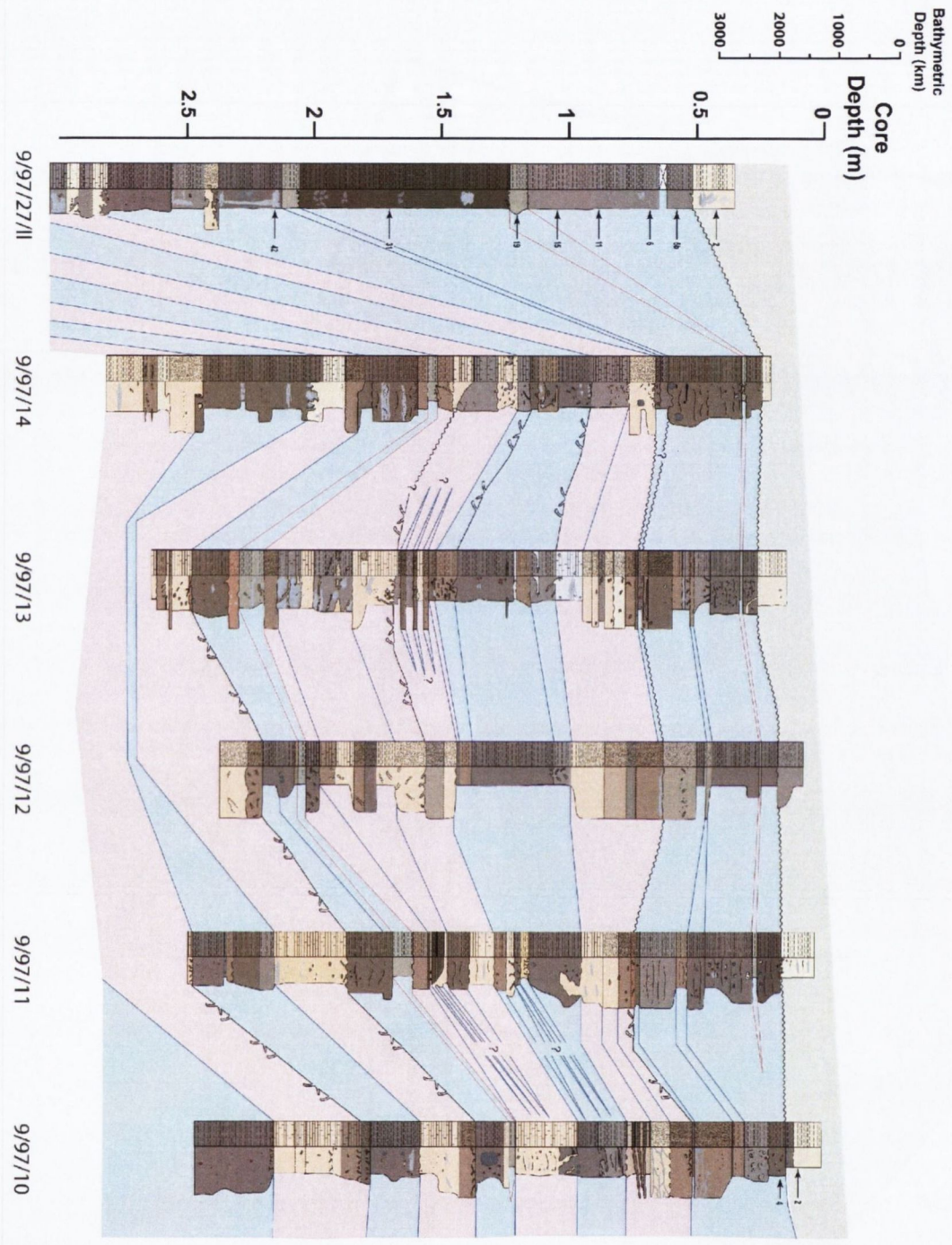

Figure 1.3. Lithostratigraphic correlation of Transect 1, as proposed by Toms (in prep.). For lithostratigraphic key, see Appendix G. Alternations of pink and blue colours are related to interglacial-glacial climate variations respectively. Arrows indicate the positions of radiocarbon dating points.

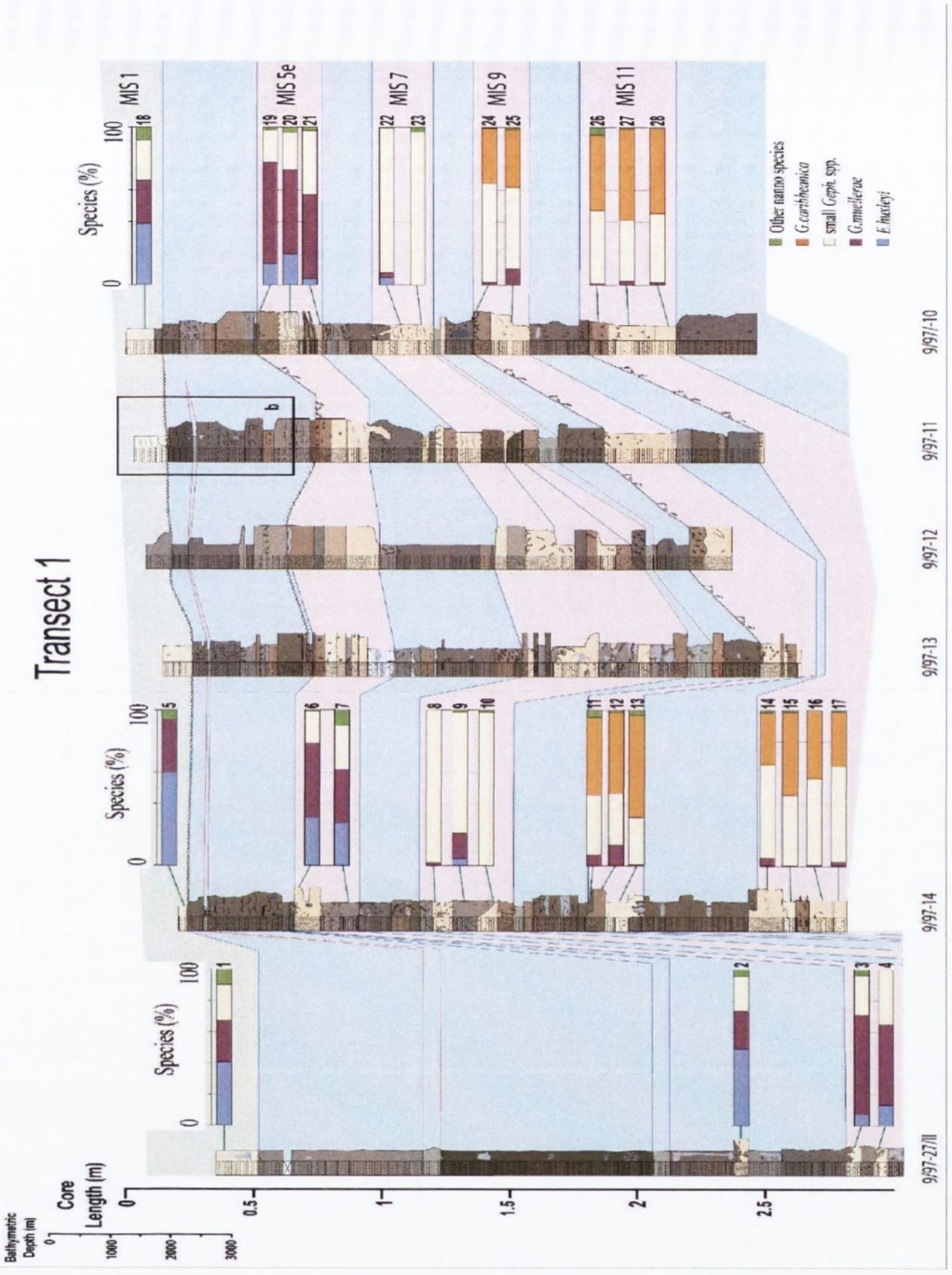

Figure 1.4. Calcareous nannofossil biostratigraphy of Transect 1, as proposed by Toms (in prep.). For lithostratigraphic key, see Appendix G. Blue and pink backgrounds represent glacials and interglacials respectively, with colours in the bars representing the relative abundance of species of calcareous nannofossil.

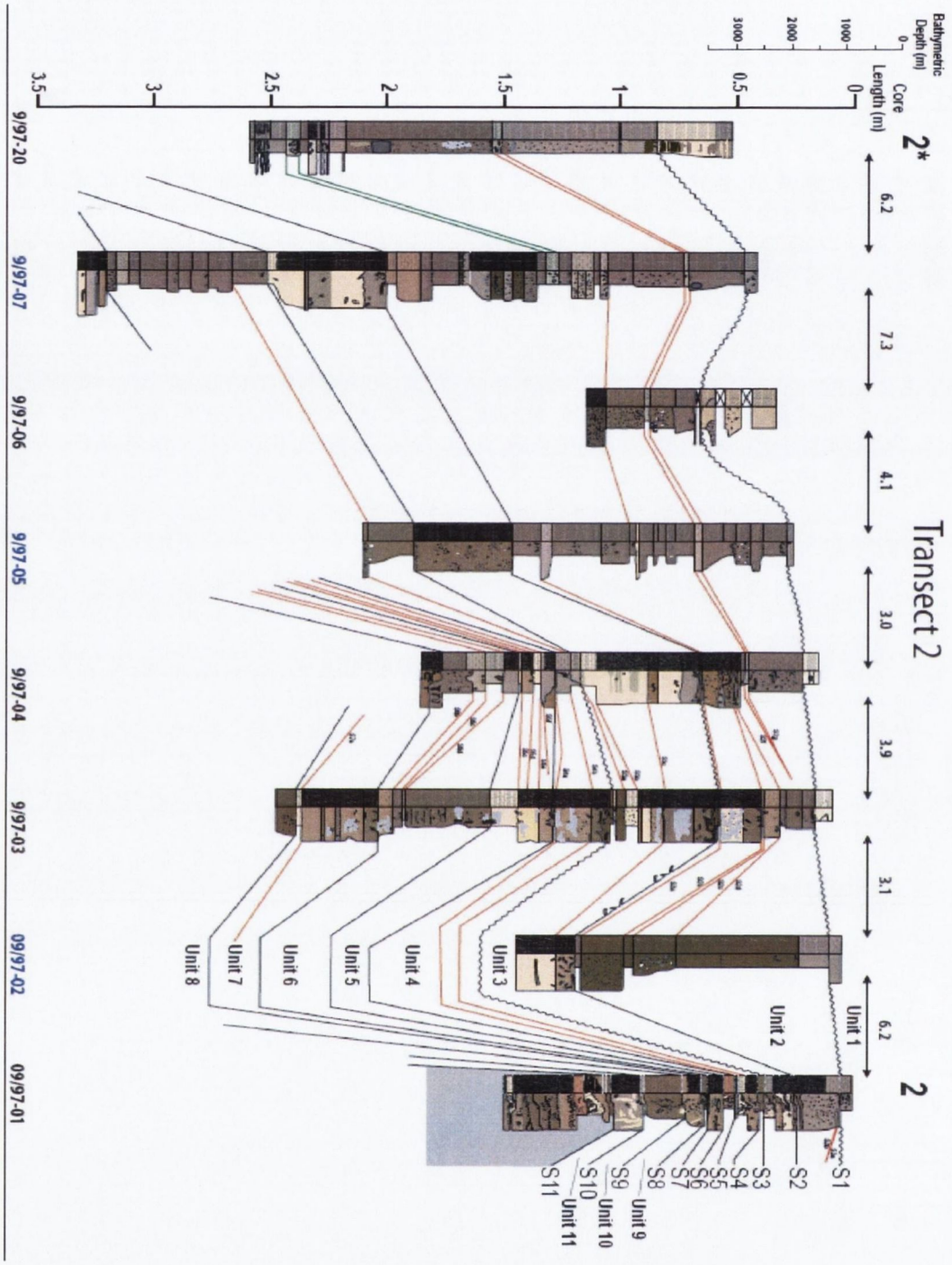

Figure 1.5. Lithostratigraphic correlation of Transect 2, as proposed by Toms (in prep.). S1-11 = surface number. Numbers above and between the cores refer to distance (in km) between core sites. Blue core labels refer to cores incorporated into the correlation from Øvrebø (2005). For lithostratigraphic key, see Appendix G.

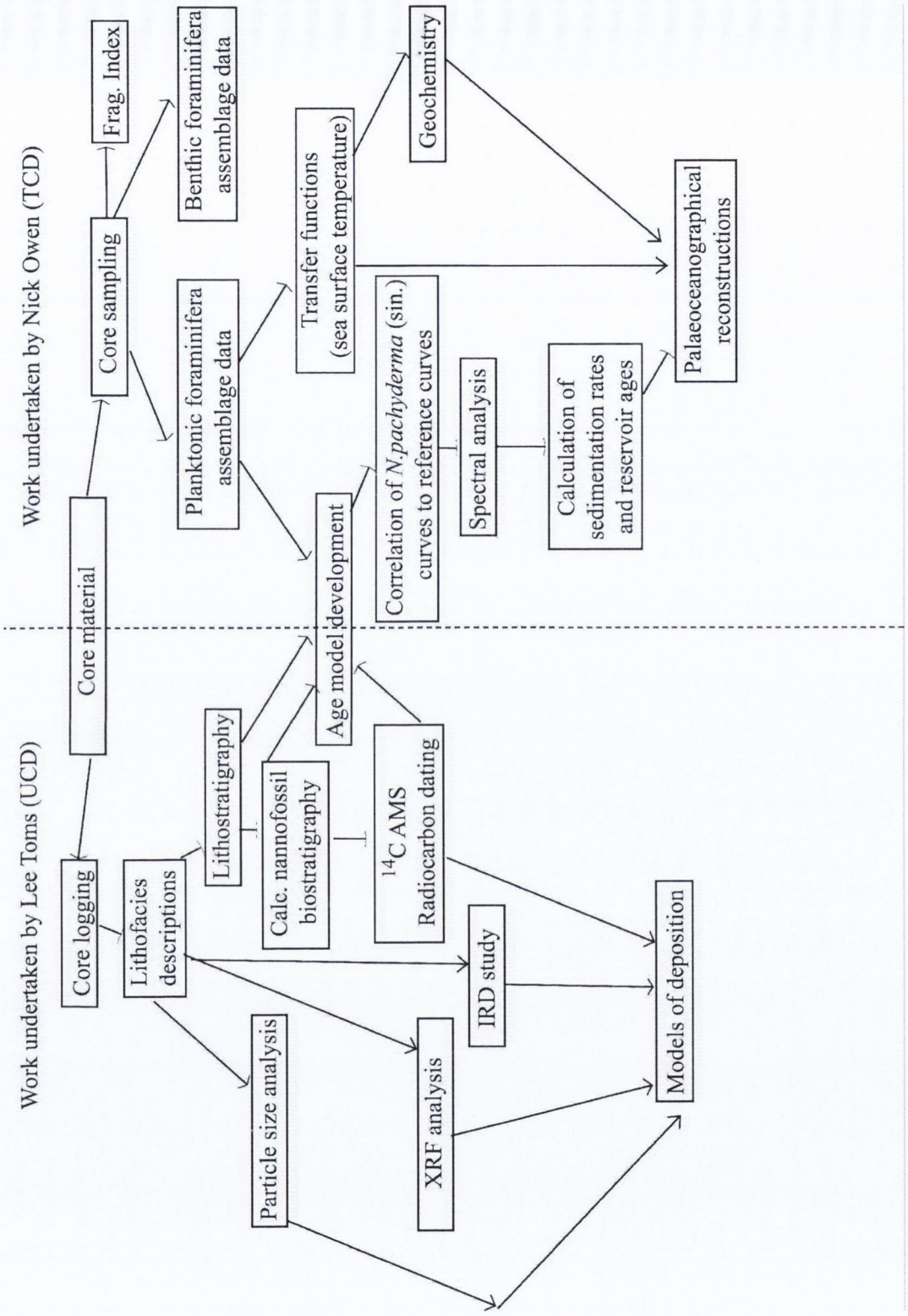

Figure 1.6. Division of labour diagram for the two Ph.D. projects, this study (Nick Owen, TCD) and the concurrent project at UCD (Lee Toms, UCD).

Chapter 2 – Regional setting and previous work

2.1. Introduction

The northeast North Atlantic Ocean has been the focus of extensive, multi-disciplinary research for over twenty years (McIntyre *et al.* 1972; Gooday and Lambshead 1989; Thomas *et al.* 1995; Øvrebo *et al.* 2006). Research groups have been developed with the specific aim of increasing our understanding of palaeo and modern oceanographic processes in the region (i.e. NEAPACC, BOFS, CLIMAP, Ellett Line, CONVEX-91). This is because the NE Atlantic plays a crucial role in driving meridional overturning circulation (MOC), with exchanges between warm, surface waters flowing north from the tropics and cold, dense, deeper water flowing south from the Nordic and Labrador Seas (Broecker 1991). Changes in the site(s)/amount/pace of downwelling in these polar regions can have a significant impact on oceanic circulation and, therefore, global climate (Clark *et al.* 2002). It is therefore crucial to study the relationship of sub-surface ocean circulation to alterations in past climate.

The first studies of foraminifera from the NE Atlantic region were published by Parker and Jones (1865), Carpenter *et al.* (1870) and Brady (1884). More recent studies have been conducted by Weston and Murray (1984), Murray *et al.* (1986) and Lukashina (1983, 1988a, b). Several studies have looked at the assemblages of foraminifera in regions closely adjoining the Porcupine Bank. Gooday (1988, 1999), Gooday *et al.* (1995, 1998) and Smart & Gooday (1997) examined samples of live assemblages of foraminifera from the Porcupine Abyssal Plain, with a particular focus on responses to seasonal phytodetritus deposits. Gooday (1986a, b) and Gooday and Lambshead (1989) studied assemblages from the Porcupine Seabight.

Weston (1985) compared live and dead assemblages on the Porcupine Seabight with those from the Western Approaches.

The deposits on the western slopes of the Porcupine Bank were studied in great detail by British Petroleum during the 1970s to assess their potential as a hydrocarbon reservoir (i.e. Coles *et al.* 1996). An extensive survey of micropalaeontological material (mainly foraminifera and ostracoda) resulted from M.Sc. research projects conducted at the University of Wales at Aberystwyth (material and theses currently stored at the British Museum of Natural History, London). Significant results included a benthic foraminiferal stratigraphy for the Cenozoic (Wilson 1982; unpublished) and also faunal associations with hydrocarbon seeps (Coles *et al.* 1996). The contourite deposits that form the basis of this study were examined by Øvrebø *et al.* (2006).

2.2. Modern oceanography of the Porcupine Bank and related areas

The gross physical oceanography of the modern Atlantic Ocean is strongly influenced by gyre systems (Hatun *et al.* 2005) and Atlantic Meridional Overturning Circulation (AMOC; e.g. McManus *et al.* 2004). The gyre systems of the North Atlantic Ocean redistribute warm, saline surface waters from the tropics towards the polar regions. This saline water cools, increases in density and is convected downwards to form deep water (e.g. NADW in the North Atlantic) which is then redistributed throughout the North Atlantic region, again under the influence of the gyre systems (Read 2001). Gyre systems are particularly important at continental margins as they are responsible for the formation of stable, geostrophic currents

that can impinge on the sea floor (Fig. 2.1) and some studies have suggested that they may expand and contract due to glacial-interglacial oscillations (Hatun *et al.* 2005).

Convection centres in the North Atlantic region are sensitive to increases in freshwater inputs. Dickson *et al.* (1996) suggest that the North Atlantic gyre and, specifically, changes of salinity within it (such as occurred during the 'Great Salinity Anomaly', of the 1960s) act as a feedback mechanism to co-ordinate convective activity in the North Atlantic between the Labrador Sea and Greenland/Iceland Seas. Changes in North Atlantic Oscillation (NAO) are an important source of season to decade scale climatic variability in this region (Hurrell 1995). The NAO is the result of an atmospheric pressure gradient between Iceland and the Azores. Variations in the strength of this gradient are considered to result in climatic variations in the North Atlantic region over annual or decadal timescales (Cook *et al.* 1998). In the Dickson *et al.* (1996) study, variations in convective history of the Labrador Sea are compared to alterations in NAO. During the 'Great Salinity Anomaly', reduced wind stress resulted in reduced Ekman divergence, allowing fresher water to spread over the convective centre of the Labrador Sea. This slowed and eventually interrupted the formation of Labrador Sea Water (LSW). An opposite trend was observed in the Nordic convective centres, and this was considered to show that changes in convection at these two sites are linked via the sub-polar gyre.

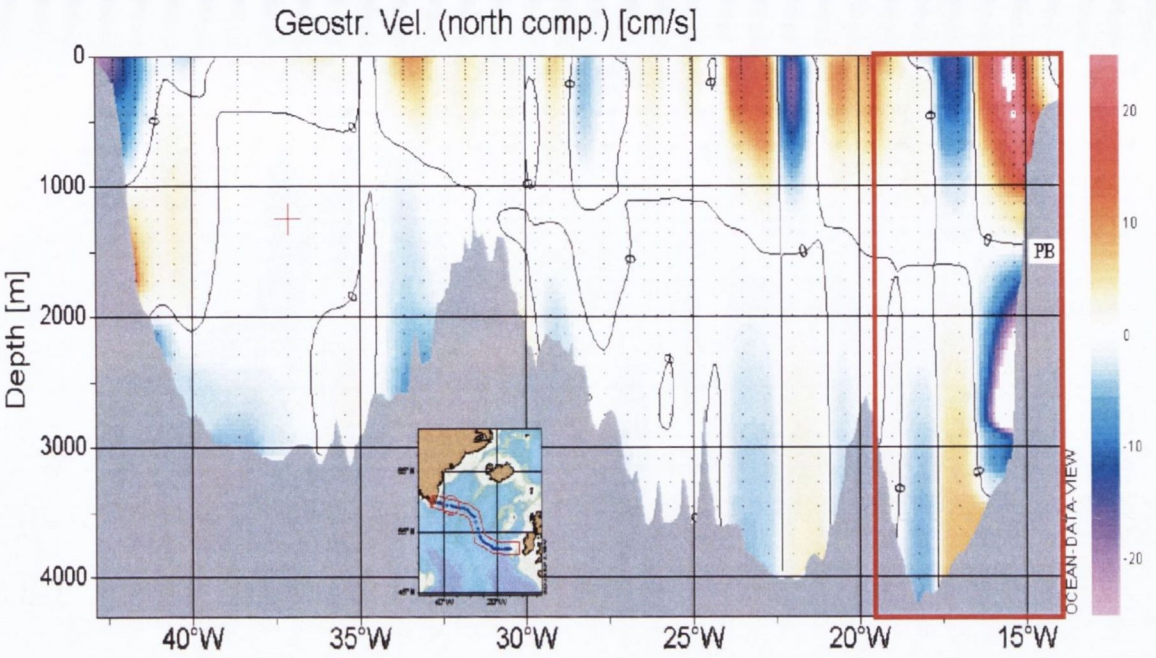

Figure 2.1. Geostrophic velocity recorded for the North East North Atlantic Ocean. Note the strength and direction of the currents at 1000m, 2000m and 3000m on the Porcupine Bank (red square). Modified from Ocean Data View, based on data from Bersch (1995).

The western flank of the Porcupine Bank is currently ventilated by water masses from a variety of source regions (Read 2001). An outline of the different water masses and their properties is given in Table 2.1.

The main currents and water masses of interest in this project are the surface components (North Atlantic Current, Shelf Edge Current and possibly Mediterranean Outflow Water) and intermediate to deep water masses (Antarctic Intermediate Water, Labrador Sea Water, Eastern North Atlantic Deep Water and Antarctic Bottom Water).

Read (2001) provides a detailed model of the current oceanography of this region (see Figures 2.2 and 2.3), which is strongly influenced by the sub-polar gyre. This model is constructed

using geostrophic calculations based on recent CTD measurements from a series of transects from a survey named CONVEX-91. The model assumes a horizon of no motion between different water masses. The results of the survey (CONVEX-91) and modelling (Read 2001) has revealed bottom waters for the Porcupine Abyssal Plain are relatively enriched in nutrients, particularly silicate. They are also relatively low in dissolved oxygen and have a constant temperature-salinity relationship. This is indicative of Antarctic Bottom Water (AABW), although modified by mixing with North Atlantic Deep Water (NADW). In the Rockall Trough itself, bottom water silicate concentrations are high (>25μmol/l), due possibly to the lack of a northern source water in this basin (see Read 2001, Figure 12).

At intermediate depths, Labrador Sea Water (LSW) is easily identified by salinity and potential vorticity minima and a temperature minimum at depths between 1000-1800 dbar (Read 2001). The vertical extent of the salinity minimum is 500m in the Rockall Trough and is also the deepest salinity minimum in the basin. At near surface depths, there is a high salinity maximum at 600m. This possibly represents Mediterranean Outflow Water (MOW), which reaches near surface depths in this part of the North Atlantic, due to

Water mass	Abbreviation	Current depth range (m)	Core locality (m)	Salinity (max or min, ppt)	Temp. °C	Nutrient content	Source	Ba / Ca	$\delta^{13}C$	Oxygen content	Cd / Ca	Presence in study area
Antarctic Intermediate Water	AAIW	1000-2200m	1200m and 2000m	Low	2-3°C	Rich	Southern Ocean	High	Low	Low	High	Definite but mixed
Mediterranean Outflow Water	MOW	500-~1200m?	~600m	36.5	12	Depleted	Mediterranean	No data	Conspicuous	High	No data	Debatable
Labrador Sea Water	LSW	1000-1800m	1600-1900m	34.92	3.3	Poor	Labrador Sea	No data	No data	No data	No data	Definite, mixed
Eastern North Atlantic Deep Water	ENADW	~2000-3000m	2300-2500m	34.94	2.8-3.0	Poor	Nordic Sea	Poor	High (1.23-1.3)	High	Low	Definite, mixed
Antarctic Bottom Water	AABW	Below 3000m	Below 3000m	Low	2.25	Rich silicate	Southern Ocean	Rich	Low	Low	High	Definite

Table 2.1. Outline of the modern properties of the major water masses that currently interact with the Porcupine Bank, or possibly did in the past. Data from Sarnthein et al. (1994); Bertram et al. (1995); Barringer and Price (1999); New and Smythe-Wright (2001); Read (2001) and Hall and Chan (2004).

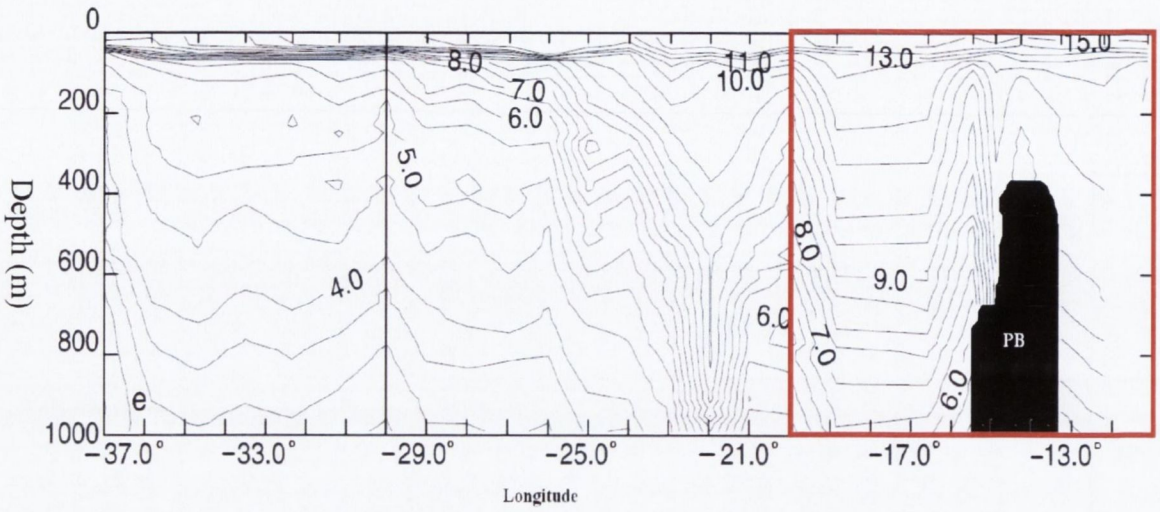

Figure 2.2. Potential temperature (°C) sections of the top 1000m of the Porcupine Bank (red square), modified from Read (2001).

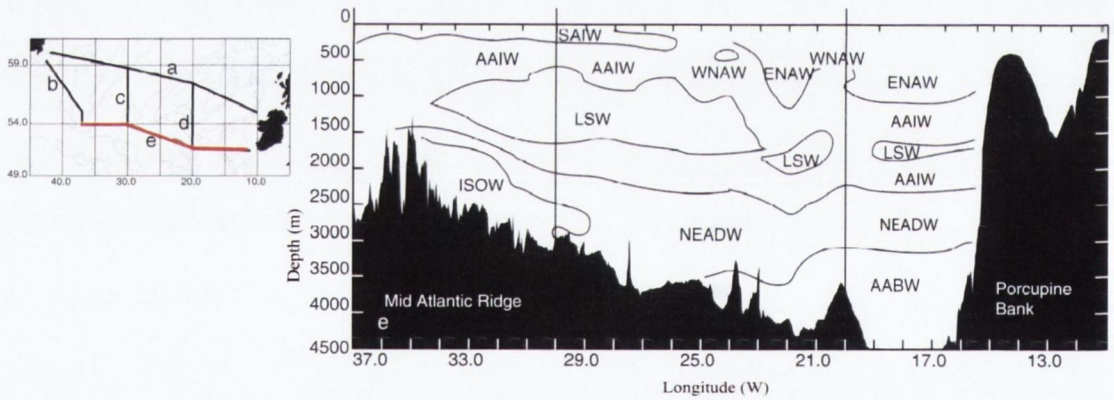

Figure 2.3. The main water masses impinging on the Porcupine Bank, modified from Read (2001). Transect highlighted (red line) in smaller, left-hand panel. SAIW = Sub Arctic Intermediate Water, ISOW = Iceland-Scotland Overflow Water, WNAW = Western North Atlantic Water, ENAW = Eastern North Atlantic Water, AAIW = Antarctic Intermediate Water, LSW = Labrador Sea Water, NEADW = North East Atlantic Deep Water, AABW = Antarctic Bottom Water.

mixing and freshening with other water masses (New and Smythe-Wright 2001). During winter, deep convective mixing potentially entrains MOW into ENAW, a surface North Atlantic water mass (New *et al.* 2001; Read 2001).

New and Smythe-Wright (2001) also provide a detailed study of the different water masses in the Rockall Trough. They reported a Shelf Edge Current (SEC) associated with a high salinity core in the upper 400m. At intermediate depths, LSW (1600-1900m) was observed (identified by a salinity minimum). NADW was also present (identified by a salinity maximum around 2500m) in the Rockall Trough, with AABW found below 3000m (identified by a characteristic high silicate content).

There is currently debate concerning the fate of MOW in this region (Reid 1979; McCartney and Mauritzen 2001; New *et al.* 2001). The Nordic Sea contains high salinity surface waters of unknown origin. Reid (1979) suggested that MOW is able to flow into the Nordic Sea, with MOW shoaling from depths of 1200m in the Rockall Trough to less than 600m depth at the Wyville-Thomson Ridge. Measuring flow rates over the Wyville-Thomson Ridge shows that flow directly over the ridge is southward and descending, rather than northward and ascending, which subsequently disproved this hypothesis (McCartney and Mauritzen 2001). Subsequent computer modelling by New *et al.* (2001) suggests that MOW reaches as far north as the Porcupine Bank from the Straits of Gibraltar, then becomes partially incorporated into Shelf Edge Current. New *et al.* (2001) used three models to show where MOW is most likely to flow. Their results agree with McCartney and Mauritzen (2001), not Reid (1979). But New *et al.* (2001) go further to suggest that the source of saline water in the Nordic Sea is a mixture of NAC and ENAW and probable convergences with SEC (White and Bowyer 1997).

The oceanography of the NE Atlantic is further complicated by regional topographic features. This is suggested by White *et al.* (1998), in their study of nutrient distributions in surface waters surrounding the Porcupine Bank. They recorded higher nutrient levels within a dense dome of relatively (to values on either side) cold, less saline water located directly above the Porcupine Bank. This suggests that an oceanographic phenomenon known as a Taylor column might exert a strong, seasonal influence on the distribution of nutrients in this region. Taylor columns form when a fluid flows over an obstruction (e.g. the Porcupine Bank), with the main flow deflected either side of the obstruction. This traps cold, nutrient rich waters on top of the bank. This is important because Taylor columns have been suggested as a mechanism that causes the retention of sea-ice in other regions (Martin and Drucker 1997). Sea-ice formation would have implications for productivity, as it would prevent phytoplankton from acquiring sunlight for photosynthesis, as well as increasing the albedo effect in this region.

Intermediate nepheloid layers are horizons in the water column above the sea floor that contain a large amount of suspended material. They potentially form as a result of the actions of internal waves (Hawley 2004; Puig *et al.* 2004), which form at the interface between fluids of differing densities (e.g. NADW and AABW). These features have also been observed in the modern Porcupine Bank environment (Dickson and McCave 1986; White *et al.* 2005) and could provide a physical barrier between core sites during intervals where water mass stratification is occurring.

The Rockall Trough region also experiences deep convective mixing to 600m water depth, with mixing to 1000m during severe storms (Meincke 1986). This has implications for

mixing of shallow – intermediate depth water masses in this region, producing a homogenized water mass above the limit of deep convection (Read 2001).

2.3. Stratigraphy

Gibbard *et al.* (2009) divide the Pleistocene epoch into three sub-epochs; Early, Middle and Late (see Fig. 2.4). For this project, only the Middle Pleistocene to present will be studied. The base of the Middle Pleistocene (or Ionian) is dated at 781 kyr B.P. and is defined by the start of the Brunhes Polarity Chron (Shackleton *et al.* 1990). The base of the Late Pleistocene (or Tarantian) is dated at 126 kyr B.P. on the basis of the expansion of forest tree pollen above 50% in the Amsterdam Terminal Borehole (Cleveringa *et al.* 2000; Gibbard 2003). The Pleistocene – Holocene transition is dated at 11 700 years calendar yr b2k +/- 99 yrs (before 2000 A.D.), with the stratotype located within the NGRIP (North Greenland Ice Core Project) ice core (Walker *et al.* 2009). It is defined on the basis of the identification of the first signs of warming following Greenland Stadial 1.

Marine Isotope Stages (MIS) are commonly used to correlate discrete sections based on their oxygen isotope profile (e.g. Emiliani 1955; Emiliani 1972; Shackleton and Opdyke 1973; Hays *et al.* 1976; Chappell and Shackleton 1986; Shackleton 1987; McManus *et al.* 1999; Øvrebo *et al.* 2006; Peck *et al.* 2007). These stages can be subdivided into two main types (see Fig. 2.5 for summary) which alternate throughout the Late Quaternary; interglacial (or 'warm' periods) and glacial (or 'cold' periods). The pacing and relative durations of glacial-interglacial stages is mainly considered to be orbitally paced although there is still

considerable debate regarding the exact mechanisms driving glacial-interglacial climate variations (Ridgwell *et al.* 1999; Raymo *et al.* 2004; Ruddiman 2006; Tziperman *et al.* 2006).

Marine isotope stages 12 and 11 are considered to have been the 'coldest' glacial and 'warmest' interglacial respectively (Kandiano and Bauch 2003). Particularly in Europe, the marine isotope stage 12 glaciation was the largest of the Late Quaternary glaciations (Donner 1995). The second largest (in terms of ice sheet expansion) is thought to be the previous glacial (MIS 2). Conversely, marine isotope stage 11 has produced some of the warmest reconstructed SSTs (Kandiano and Bauch 2003) and the lightest benthic $\delta^{18}O$ values (McManus *et al.* 1999) of the previous five hundred thousand years. Marine isotope stage 11 has also been proposed as an analogue for the current interglacial (Petit *et al.* 1999; Loutre and Berger 2003; EPICA 2004), although the extent of this proposed analogy has been queried recently (Kandiano and Bauch 2007). An examination of the transition from MIS 12 to MIS 11 by Hall and Becker (2006), which focused on changes in the velocity of the Deep Western Boundary Current (DWBC) revealed no obvious step-wise warming trend, which suggests that Termination V was not analogous to the MIS 2 to MIS 1 transition (Termination I).

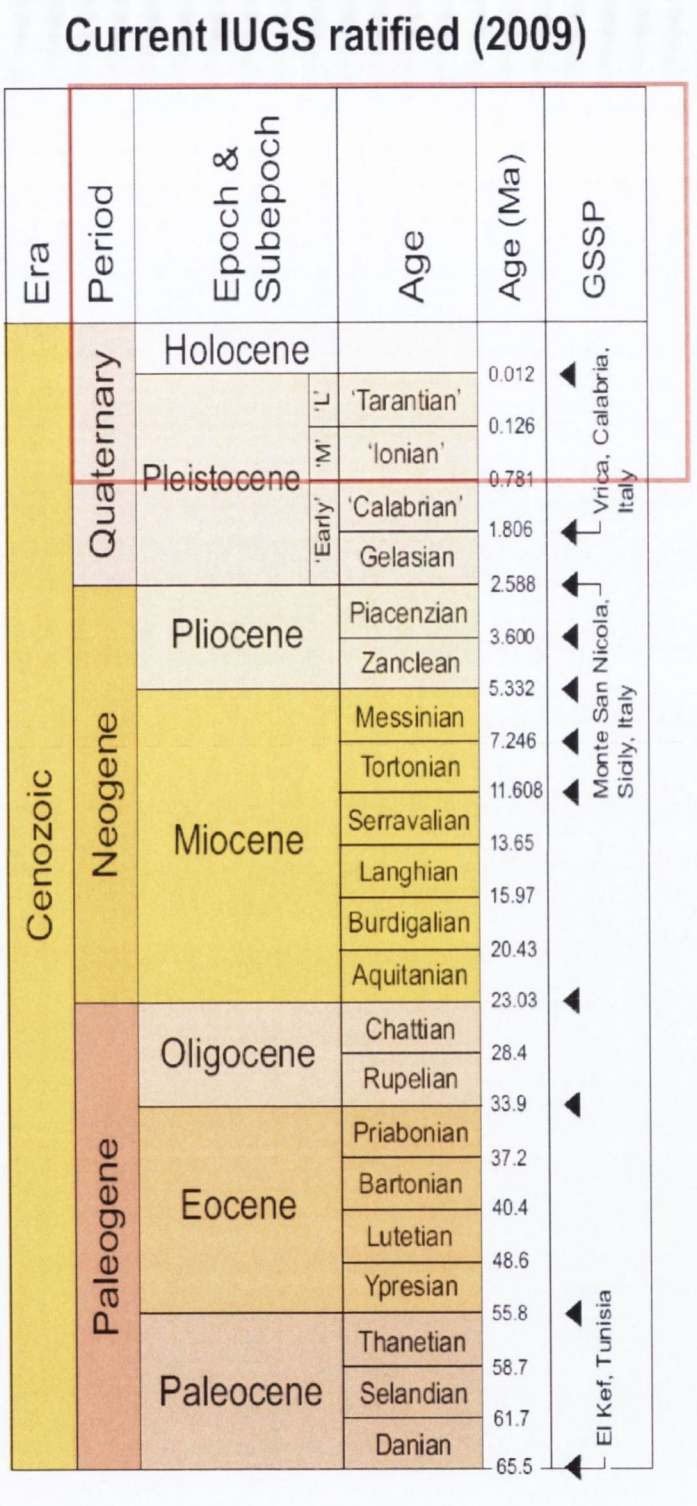

Figure 2.4. Cenozoic stratigraphic column modified from Gibbard *et al.* (2009). The portion of the Quaternary period examined in this thesis is highlighted by the red square.

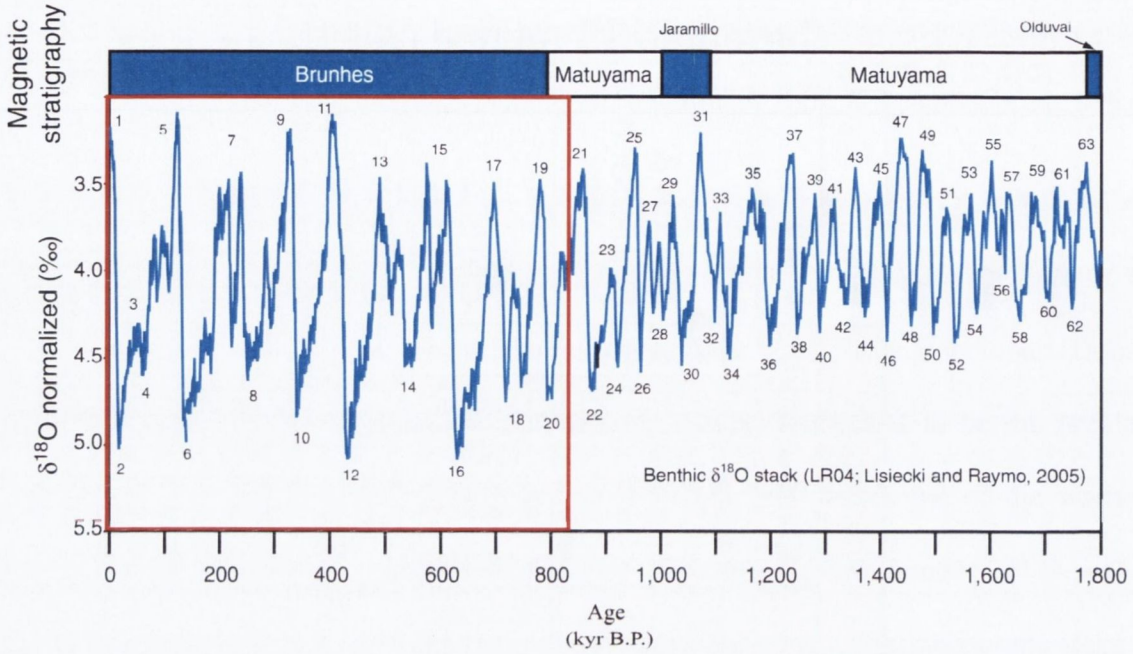

Figure 2.5. Oxygen isotope stratigraphy of the last 1.8 million years (Lisiecki and Raymo 2005). This curve is based on a stack of 57 globally distributed benthic $\delta^{18}O$ curves. The numbers adjacent to the curve represent marine isotope stages. Modified from Bassinot (2007). The red box indicates the period covered by the records presented in this thesis.

It should be noted that this interval (MIS 12 and 11) is within the Mid Brunhes Dissolution Interval (approx. 600-200 ka), a period of enhanced carbonate dissolution that even affected sites that were relatively shallow (e.g. Droxler *et al.* 1990; Barker *et al.* 2006; Huybers 2009). During this interval, a shift in global pelagic carbonate production occurred, potentially caused by the initiation and / or expansion of coral reef formation on continental shelves (e.g. Droxler *et al.* 1997). Expanding coral reef systems will have required an increase in the $CaCO_3$ budget of the oceans to maintain the pelagic ecosystem in the state it was prior to this interval. This did not occur and dissolution resulted (Crowley 1985; Hoddell *et al.*

2000; Heinrich *et al.* 2002), despite an apparent lack of increase in atmospheric CO_2 or ocean surface pCO_2 (Petit *et al.* 1999; Barker and Elderfield 2002). However, it has been proposed that pelagic production or flux rates (the rate at which food particles are transported to the seafloor) increased significantly during this interval, particularly during MIS 11 (Barker *et al.* 2006) and resulted in the removal of excess carbon from the sea-surface and the maintenance of pCO_2 levels.

The growth, maximum extent and deglaciation of the British Irish Ice Sheet (Fig. 2.6) and the potential impact of this ice sheet on global or regional climate via AMOC has received much attention (e.g. Boulton *et al.* 1985; 1991; McCabe 1987; Scourse *et al.* 2000; Knutz *et al.* 2001; Wilson *et al.* 2001; Bowen *et al.* 2002; Knutz *et al.* 2007; Peck *et al.* 2007; Fretwell *et al.* 2008). Most studies appear to concur that the maximum extent of the BIIS occurred during MIS 2, approximately 14-30 kyr B.P. (Knutz *et al.* 2001; Wilson *et al.* 2001) and that this coincided with the onshore Glenavy stadial (McCabe *et al.* 1998; Richter *et al.* 2001), although there are considered to be variations on the timing of the maximum extent in different sectors (Knight 2006; O'Cofaigh and Evans 2007; Hubbard *et al.* 2009) and dating uncertainties remain problematic for some regions (Knight 2006; Clark *et al.* 2009). The apparently complex and dynamic nature of the BIIS adds to the dating uncertainty, with the results of recent modelling experiments proposing that the three main ice accumulation centres varied between being interdependent and being independent (Hubbard *et al.* 2009).

Stadial – interstadial variations during the last glacial period (MIS 2-4) should be observed in cores with a well-developed stratigraphy for the last glacial (Fig. 2.7). These are smaller scale and shorter climate variations compared to glacial-interglacial changes (Grootes *et al.* 1993; Grootes and Stuiver 1997). Other 'cycles' or events of interest to this time interval

include Dansgaard-Oeschger events (Dansgaard *et al.* 1993; Chapman and Maslin 1999) and Heinrich events (Bond *et al.* 1999). Dansgaard-Oeschger (D-O) events or 'cycles' have been observed globally (Dansgaard *et al.* 1993; Voelker 2003; EPICA 2006) but there is still considerable debate concerning their causal mechanisms, how they might relate to other phenomena (such as Heinrich events, discussed below) and if they are a cyclical phenomenon or episodic (Bond *et al.* 1999; Voelker 2003; Rahmstorff 2003; Braun *et al.* 2005; Rahmstorff 2006).

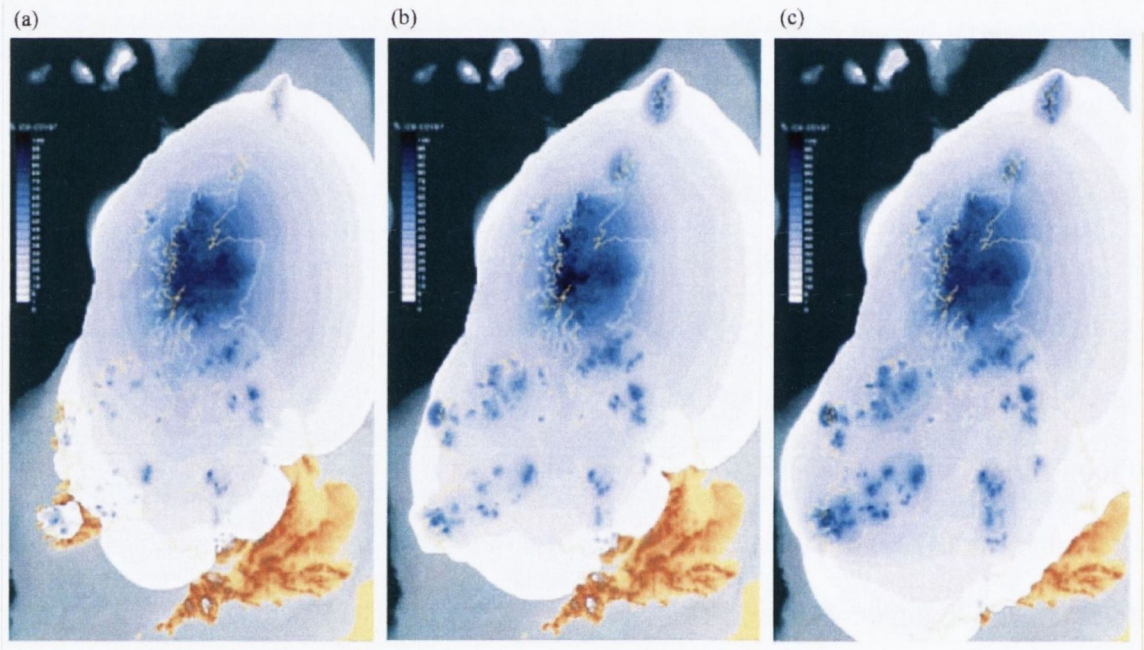

Figure 2.6. Models of the cumulative ice cover of the British Irish Ice Sheet during the last glacial based on three experiments (a-c), modified from Hubbard *et al.* (2009).

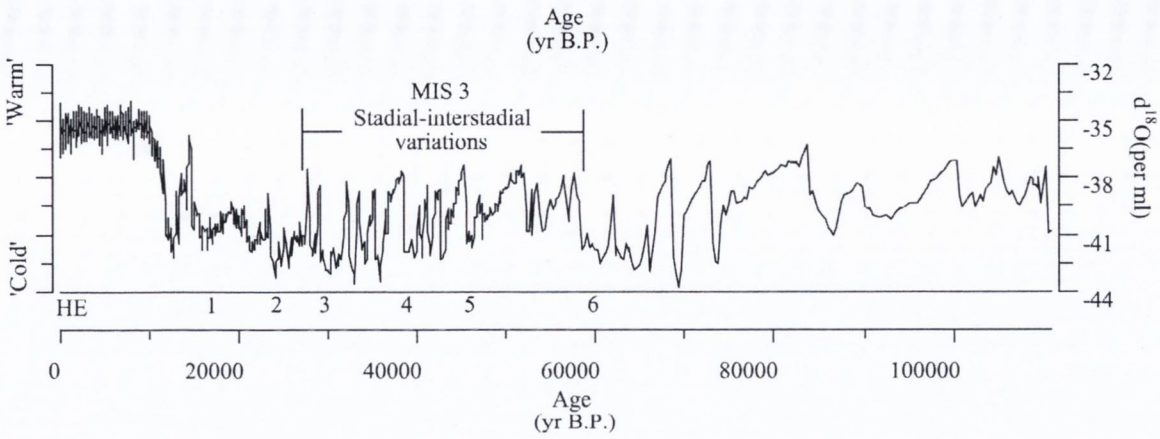

Figure 2.7. The GISP-II ice core record of Stuiver *et al.* (1997). The stadial-interstadial variations of MIS 3 are highlighted. HE = Heinrich Event.

Heinrich-events are considered to be the result of rapid (Maslin *et al.* 2001; Roche *et al.* 2004), large-scale (Ruddiman 1977) deteriorations of northern hemisphere ice sheets (Heinrich 1988), in particular the Laurentide Ice Sheet, which caused perturbations in global climate (Cacho *et al.* 1999; Vidal *et al.* 1999; Claussen *et al.* 2003; Genty *et al.* 2003) with potential implications for human migration into Europe (Sepulchre *et al.* 2008). There were six Heinrich events during the last glacial (HE 1-6), although some authors include the Younger Dryas (e.g. Bond and Lotti 1995) as a seventh Heinrich event labelled H0. In this study, the term Younger Dryas will be applied. Some models of Heinrich event causal mechanisms have been proposed (Stocker 1998; Vidal *et al.* 1999; Sarnthein *et al.* 2001; Moros *et al.* 2002; Flükiger *et al.* 2006; Peck *et al.* 2007) but each is problematic. Some authors have linked D-O events to Heinrich events (Seidov and Maslin 1999; Seidov and Maslin 2001; Dickson *et al.* 2008) via deepwater processes, but the precise nature of this proposed link is debatable (MacAyeal 1993). One of the problems in trying to develop a

model for Heinrich event initiation is that each event, when studied in detail, displays a distinctive set of conditions. The palaeoceanographic characteristics of Heinrich events are discussed in more detail in Section 2.4. Heinrich events 1 and 2 each display distinctive peaks in detrital, dolomitic carbonate (e.g. Peck *et al.* 2007), a clear indication of a Hudson strait source. The provenance and distribution of IRD are consistent in suggesting a mainly Laurentide Ice Sheet origin (Bond *et al.* 1992). Heinrich event 3 has a distinctive ice rafted detritus (IRD) signature (both in terms of provenance and distribution) when compared to other Heinrich events (Gwiazda *et al.* 1996) and it has been suggested that this event initiated in Europe (Scourse *et al.* 2000), rather than in North America. Also, foraminiferal tests appear to be more corroded during this event rather than the two later events (Gwiazda *et al.* 1996). Heinrich event 4 has a high detrital carbonate component (e.g. Peck *et al.* 2007) but occurred during Marine Isotope Stage 3, which was influenced by a very different oceanography and ice volume compared to Heinrich events 1 and 2 (Grousett *et al.* 2000).

2.4. Palaeoceanography of the Porcupine Bank and related areas

The study of palaeoceanography has primarily focused on the reconstruction of deep water mass distributions (e.g. Sarnthein *et al.* 1994; Lynch-Stieglitz *et al.* 2007) and reconstructing various parameters (such as sea surface temperature). The oceanography of the NE Atlantic region has changed significantly in response to glacial-interglacial cycles (e.g. McIntrye *et al.* 1972; Sarnthein *et al.* 1994). McIntyre *et al.* (1972) studied evidence for large-scale surface water mass movements in the North Atlantic over the last 225 kyr. Using the modern biogeography of planktonic foraminifera and calcareous nannoplankton, they

determined that the distribution of polar and sub-tropical surface water masses in the region have altered significantly during this time, largely as a response to glacial-interglacial changes. They recorded carbonate minima dominated by *N.pachyderma* (sin.) and carbonate maxima with influxes of tropical taxa (i.e. *Globigerinoides ruber*). Key results from this study included the identification of four strong southward penetrations of cold water and IRD during the last 225kyr, with only one major northward penetration of sub-tropical taxa.

The CLIMAP (Climate: Long rage Investigation, Mapping and Prediction) project was the first to use transfer functions to estimate sea surface temperature (SST) using the relative abundance of species of planktonic foraminifera (CLIMAP 1976, 1981). One of the aims of the project was to reconstruct surface temperatures (both terrestrial and marine) for Earth during the Last Glacial Maximum (LGM, defined at 18 ka for CLIMAP) and for the last interglacial. However, the reconstructed values were largely incompatible with climate models (Yin and Battisti 2001) and some questions remained over the reliability of reconstructed values for some regions. For example, Prell (1985) applied the method used to modern Pacific Ocean assemblages and found that this produced unrealistic SST values.

The GLAMAP (Glacial Atlantic Mapping and Prediction) project followed CLIMAP, and developed and applied a new technique, SIMMAX (acronym for a modern analogue technique using a similarity technique), for reconstructing sea surface temperatures (Pflaumann *et al.* 1996; 2003) for the LGM. Strict limits on age control and selection / rejection of samples were applied (Pflaumann *et al.* 2003). The MARGO (Multi-proxy Approach for the Reconstruction of the Glacial Ocean surface) project is the most recent large-scale application of the transfer function technique (three separate methods, SIMMAX, RAM (Revised Analogue Method) and Automated Neural Networks were applied in this study) to

determine palaeo SSTs for the last glacial maximum (Kucera *et al.* 2005). A compilation of planktonic Mg/Ca derived SSTs and dinoflagellate data were also available to compare with the results produced using this method (Barker *et al.* 2005; de Vernal *et al.* 2005). Key MARGO findings included a consistent 10°C cooling in the sub-polar North Atlantic Ocean and a 4-6°C cooling at the tropics during the LGM. However, problems with the reconstructions remained, particularly where the different reconstructions applied differed significantly in their reconstructed values.

Kandiano and Bauch (2003) provide a record of reconstructed SSTs for the North Atlantic Ocean over the last 500 000 years (Fig. 2.8). The authors used three separate transfer function methods in their study. Their record is similar to that of McManus *et al.* (1999), with glacial-interglacial temperature changes indicating the presence of MISs 1-13. It is suggested that MIS 1, 5 and 11 experienced the warmest SSTs over this time period and that glacial-interglacial temperature changes were on average 8-10°C in amplitude.

Peck *et al.* (2008) provides a high resolution (millennial scale) record of SST adjacent to the BIS between 8-55 kyr B.P based on Mg/Ca. Their reconstructed values suggested a warm (6-10°C) SST prevailed during the LGM at the Porcupine Seabight, despite the relative proximity to the BIIS. An excellent recent critique and estimation of the extent of sea-ice cover during the LGM using Mg/Ca and $\delta^{18}O_{planktonic}$ is provided by Meland *et al.* (2005). In this reconstruction, the authors propose that sea-ice extent was limited to latitudes higher than 60°N during the LGM. There are no samples in close proximity to the western flank of the Porcupine Bank used in this study.

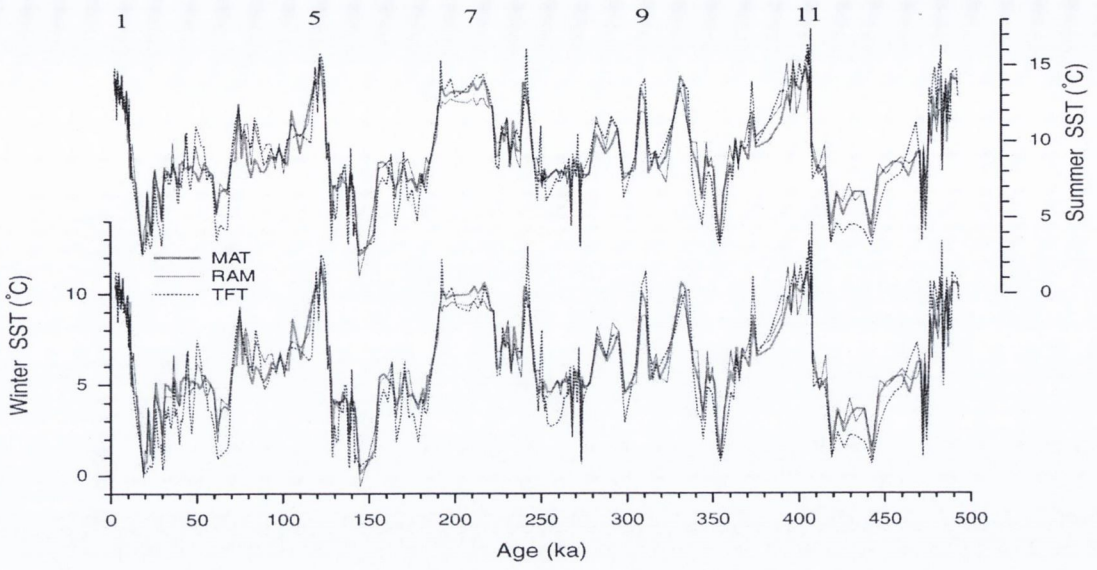

Figure 2.8. Reconstructed summer and winter sea surface temperature records of the previous 500ka from Kandiano and Bauch (2003) based on three distinct transfer functions (Modern Analogue Technique - MAT, Revised Analogue Method - RAM and Transfer Function Technique - TFT). Interglacials are highlighted (1-11).

Sarnthein *et al.* (1994) proposes three modes of deep water circulation associated with the formation of NADW. This is based on the $\delta^{13}C_{benthic}$ record from *C.wuellerstorfi* (4000-5000 specimens from 95 core locations) over the last 30 000 years. These modes are:

1. **Modern** – source region the same as modern
2. **Glacial** - source region of end-member NADW shifted from the Norwegian-Greenland Sea to an area south of Iceland.

3. **Enhanced melt water episode** (i.e. Younger Dryas or Heinrich Event) - the spread of glacial meltwater over the North Atlantic led to a short-term ventilation minimum below 1800m.

The authors also reported that the flux of MOW varied largely independently of the variations in deepwater circulation over the last 30 000 years. It is unclear if this would have any impact on the palaeoceanography surrounding the Porcupine Bank, given the probable lack of MOW in this region of the modern NE Atlantic Ocean (See Section 2.2). Rahmstorf (1997) modelled the impact of a dam on the River Nile, which, as proposed by Johnson (1997), would increase the salinity of MOW (by reducing freshwater flux) and impact on thermohaline circulation by causing an increase in SSTs in the Labrador Sea region. However, the results of the modelling exercise (Fig. 2.9) suggested that increasing the salinity of MOW would have a negligible impact on thermohaline circulation in the North Atlantic region.

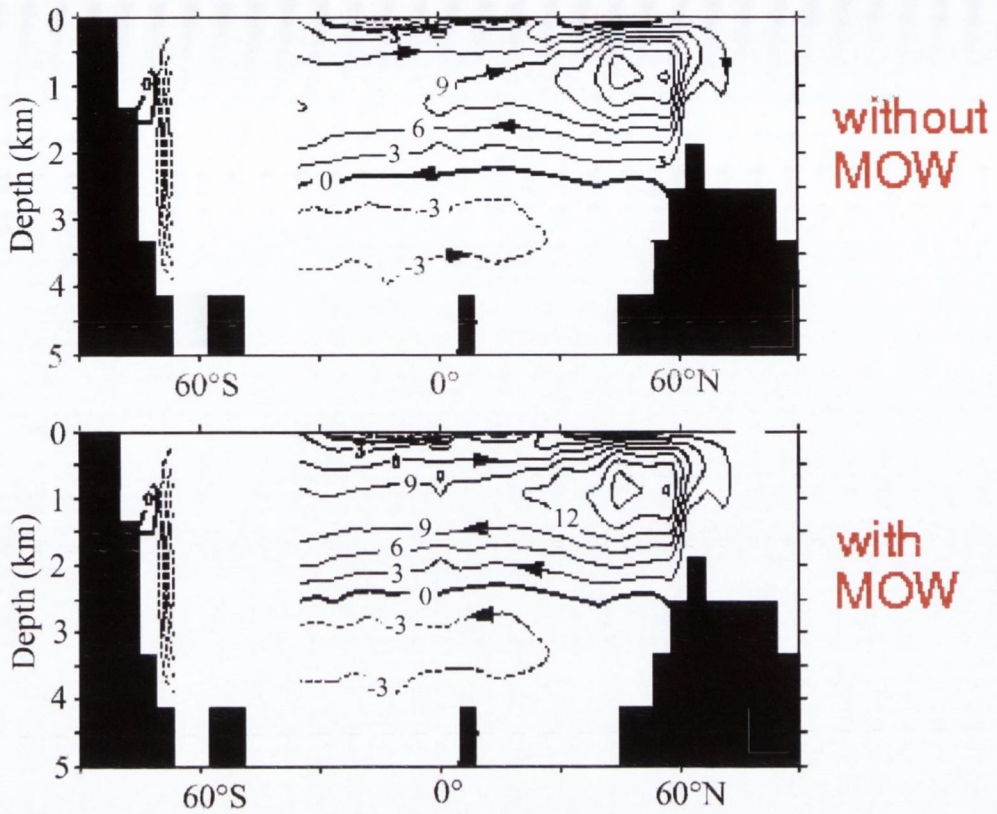

Figure 2.9. Modelled circulation of the North Atlantic based on the presence / absence of Mediterranean Outflow Water modified from Rahmstorf (1997). Numbers = °C.

A recent paper by Thornalley *et al.* (2009) indicates that AMOC is heavily influenced by sub-polar gyre dynamics, which modulate large-amplitude millennial variability. The study examined reconstructed salinity records for the surface and near thermocline layers during the Holocene to the south of Iceland. Their results suggested a pre-8.2ka interval of large differences in surface-thermocline salinity followed by a post-8.2ka interval of smaller differences. Interestingly, all intervals of Labrador Sea freshening correspond with an increase in salinity south of Iceland. This suggests that a negative feedback of salinity exists

between the Labrador Sea and the water entering the Nordic-Greenland Seas, facilitated by the expansion / contraction of the sub-polar gyre.

Lynch-Stieglitz *et al.* (2007) provides a recent synthesis of deep-water mass distributions during the LGM based on benthic carbon isotope values (Fig. 2.10). Their reconstruction shows a strong GNAIW influence during the LGM in the Atlantic Ocean, with the GNAIW /AABW 'boundary' located at approximately 2000m water depth in the North Atlantic.

Hillaire-Marcel *et al.* (2001) used micropalaeontology (dinocyst assemblages and foraminiferal stable isotope data) to examine the density structure of the water column for Labrador Sea Water. The results imply that LSW has only formed in this region over the last 7000 years and did not form during the last glacial or previous interglacial. This has

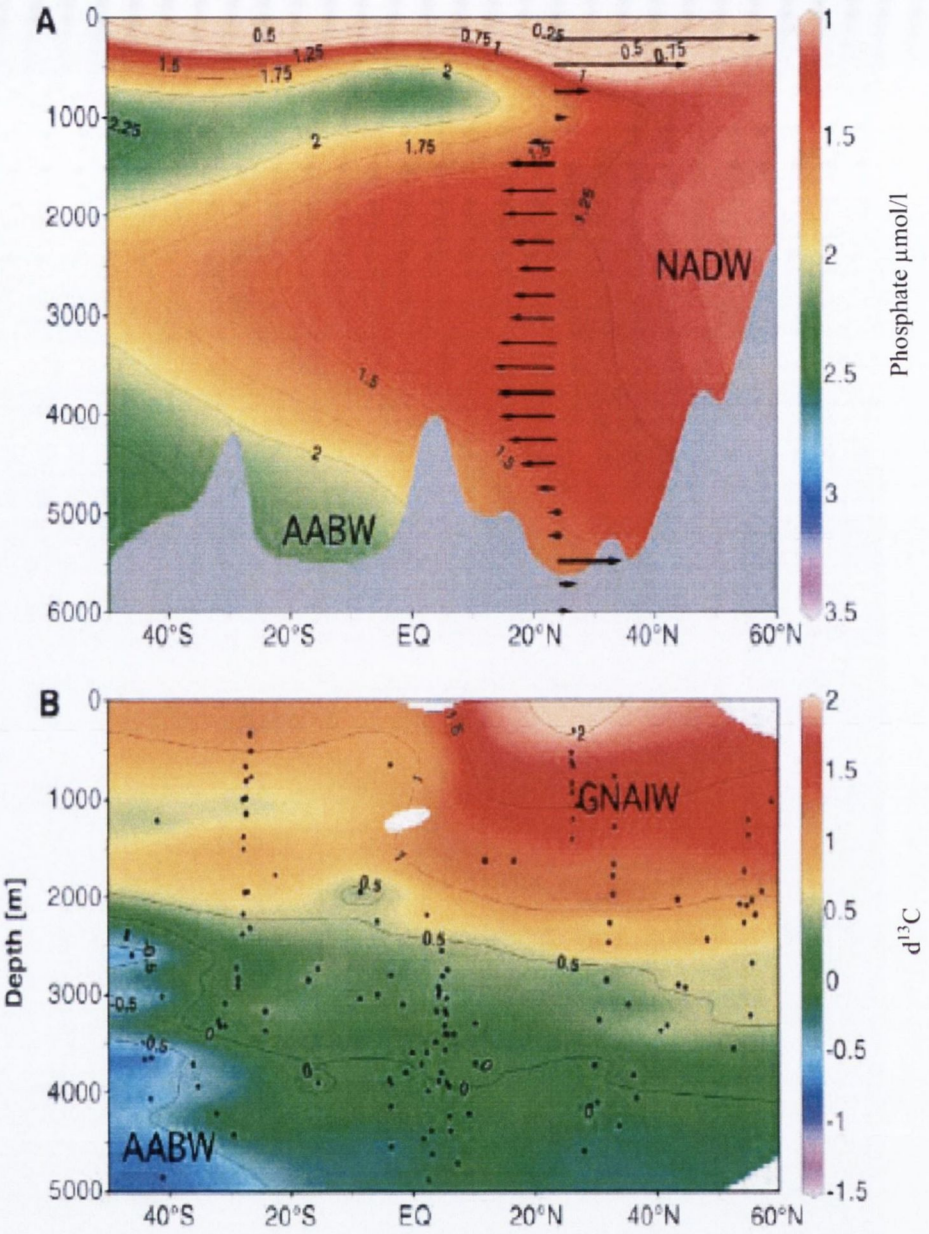

Figure 2.10. (a) Modern distributions of NADW and AABW based on Phosphorus concentrations (arrows indicate relative flow speed) and (b) reconstructed distributions of GNAIW and AABW based on $\delta^{13}C_{benthic}$ (Lynch-Stieglitz *et al.* 2007), with the distribution of sample points highlighted by black dots.

significant implications for palaeoceanographic reconstructions, as it suggests that NADW may have formed elsewhere. It also has implications for interpreting the palaeoceanography of the previous interglacial, particularly in light of the proposed compensatory nature of deep water formation between the Labrador Sea regions and the Nordic Seas (see above, Dickson *et al.* 1996).

The recovery of cores with high sedimentation rates has enabled the study of episodes of abrupt climate change from the last glacial (e.g. Peterson *et al.* 2000; Peck *et al.* 2007). Heinrich events have received considerable attention due to their apparent effects on AMOC (e.g. Roche *et al.* 2004). There is considerable interest in the palaeoceanographic conditions that precede, occur during and follow Heinrich events (e.g. Vidal *et al.* 1999; Peck *et al.* 2007). Several models exist which attempt to explain the mechanisms that lead to the occurrence of a Heinrich event. The binge-purge model (MacAyeal 1993) of ice-rafting associated with the Laurentide Ice Sheet proposes that heat build-up at the base of the ice sheet (after it has reached a sufficient mass, or the "binge" phase) acts to gradually lubricate the base. The mass of the ice sheet, combined with a lubricated base is then considered to be sufficient to facilitate the rapid collapse of part of the ice sheet (the "purge" phase). This model perhaps goes some way to explain the relatively rapid (750-250 yrs) duration of Heinrich events (MacAyeal 1993; Roche *et al.* 2004) but excludes atmospheric climate as a factor in controlling the periodicity of the events.

Heinrich events occur during stadial episodes (Bond and Lotti 1995) in the North Atlantic region and similar events are observed in the Southern Ocean (Vidal *et al.* 1999; Kanfoush *et al.* 2000). Some authors link the two via Dansgaard-Oeschger cycles (or events) which are rapid (one cycle = 1.47 kyrs) climate variations linked to stadial-interstadial changes recorded

in the Greenland Ice Sheet cores (e.g. GISP-II, NGRIP) and in some marine sediment cores (Bond and Lotti 1995). It is not clear if the link between D-O events and Heinrich events is causal (Bond *et al.* 1999; Maslin *et al.* 2001) or coincidental (MacAyeal 1993).

The potential role of other ice sheets besides the Laurentide Ice Sheet (such as the British Irish Ice Sheet and Fenno-Scandinavian Ice Sheet) also needs to be considered (Knutz *et al.* 2007). During the last glacial period, the Porcupine Bank was situated close the edge of the British Irish Ice Sheet (BIIS; Knutz *et al.* 2007). This is reflected in periodic influxes of IRD observed in some cores (Øvrebo *et al.* 2006). The extent and influence of the BIIS in this region is not well constrained, however. The temporal relation of IRD fluxes from the BIIS compared with IRD fluxes from the Laurentide Ice Sheet requires further understanding (Grousset *et al.* 2000). Because the Porcupine Bank is located outside the IRD belt linked to Heinrich Events (HE) identified by Ruddiman (1977), it has been proposed that some IRD recovered in cores from this locality originated from the BIIS, as opposed to the Laurentide Ice Sheet (Grousset *et al.* 2000).

Peck *et al.* (2007) presented a high resolution multi-proxy study of the last glacial and early Holocene (8-43 kyr B.P.) from an adjacent region, the Porcupine Seabight (Fig. 2.11). Their study was based on a core from an intermediate water depth (1153m) and is based primarily on benthic $\delta^{13}C$ values (which can vary due to a range of factors (see Chapter 3). This study demonstrated a reduction in GNAIW ventilation preceding three Heinrich events (H1, H2 and H4), with the authors invoking a NWEIS (North West European Ice Sheet) initiation. However, Scourse *et al.* (2009) examined IRD data (flux and provenance) combined with *%N.pachyderma* (sin.) to determine the growth and dynamics of the British Irish Ice Sheet during the last glacial (MIS 2-3). Their data showed a gradual southward

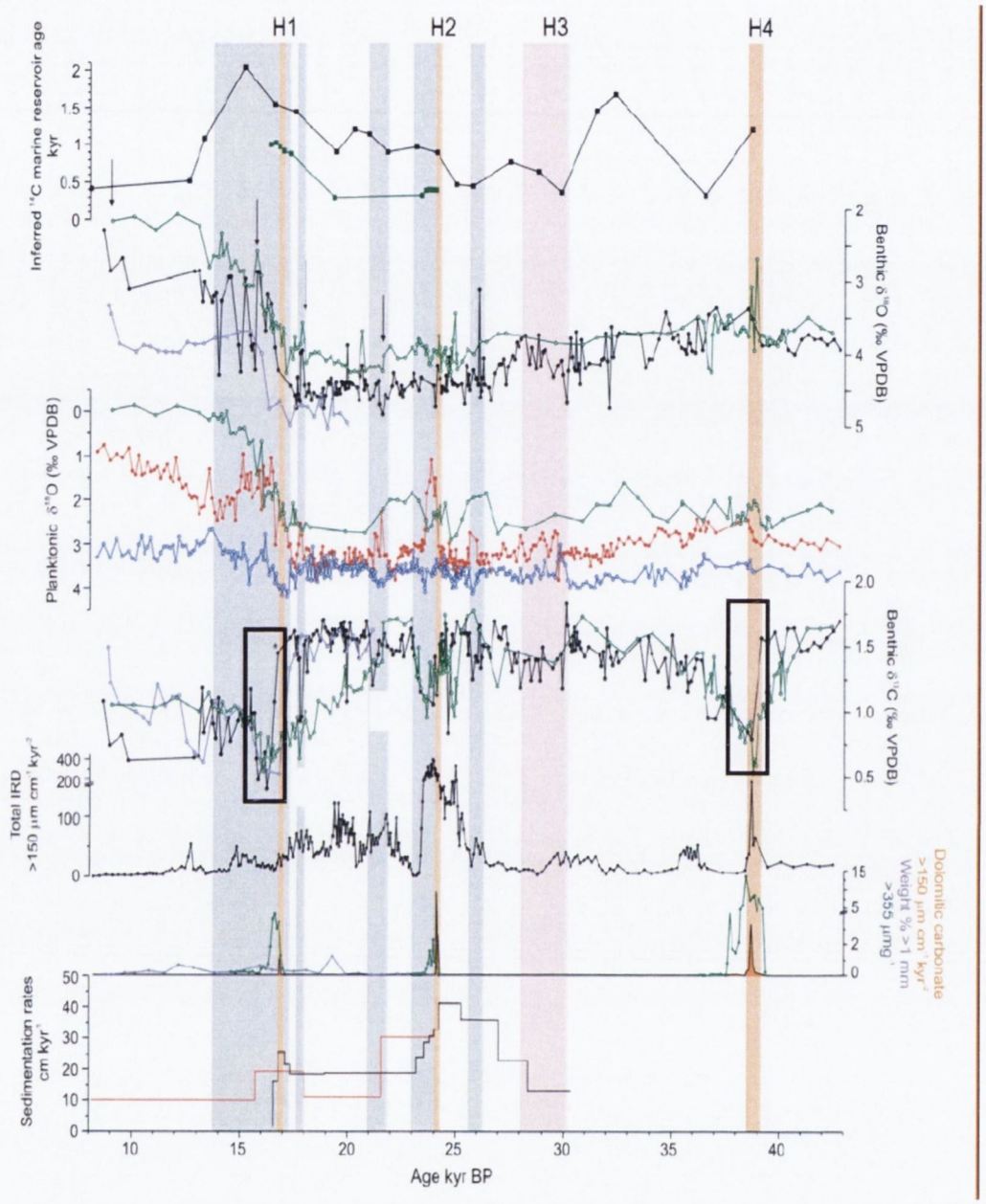

Figure 2.11. Multi-proxy record of Peck *et al.* (2007) from the Porcupine Seabight. Negative $\delta^{13}C_{benthic}$ excursions are highlighted (black squares). Blue vertical bars highlight episodes of surface ocean stratification, orange and pink vertical bars indicate Heinrich events. Green line data = core SO75-26KL, Black line data = MD01-2461, Purple line data = NEAP4K. For sedimentation rates, black line = radiocarbon-based sedimentation rate, red line = tuned. Arrows adjacent to Benthic $\delta^{18}O$ data denote tie-points.

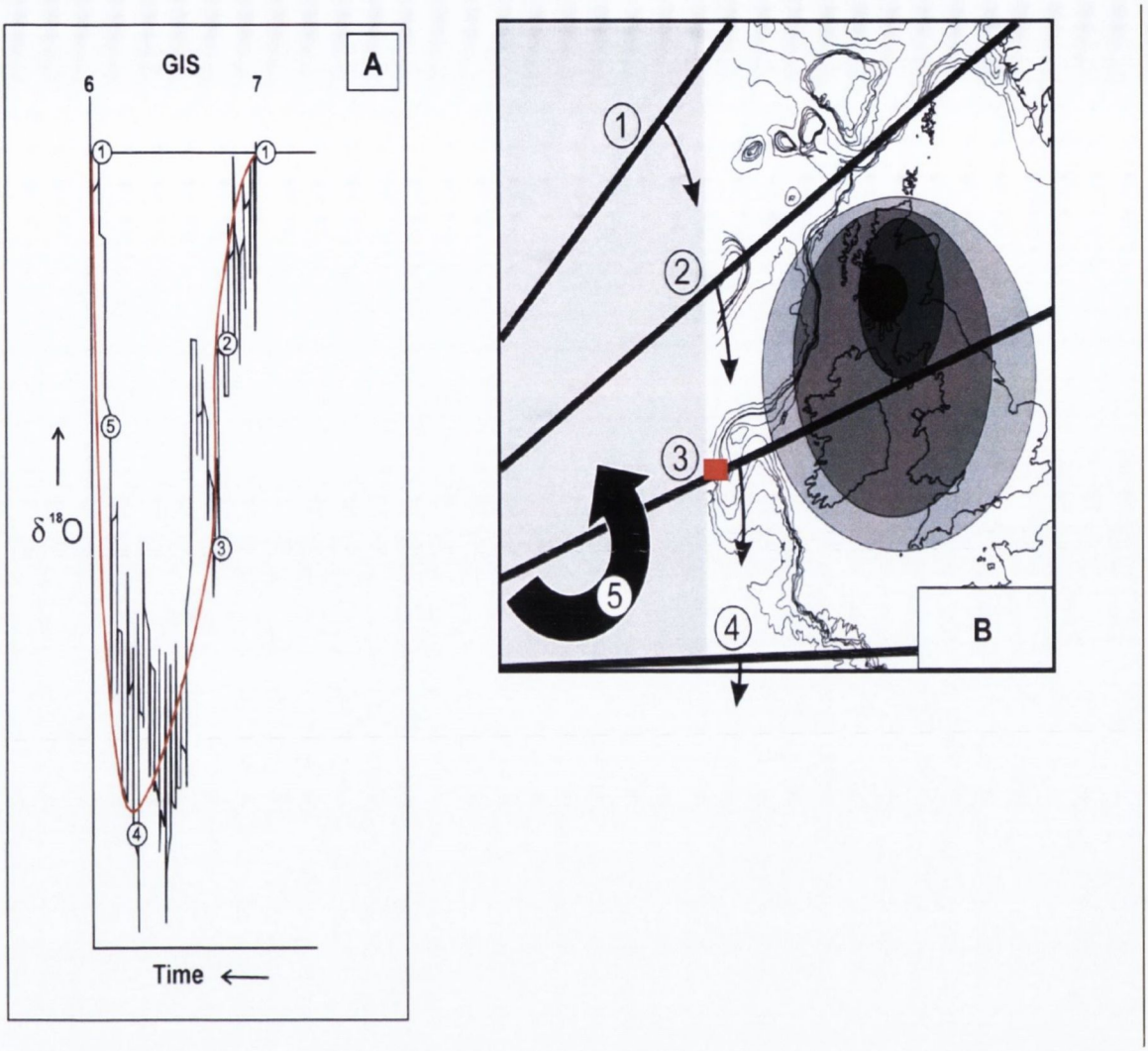

Figure 2.12. From Scourse *et al.* (2009), a conceptual model displaying the proposed relationship between the dynamics of the BIIS with the migration of the polar front (A) through a D–O cycle from the GISP-II record (B), with the position of this study area highlighted.

migration of the polar front followed by a northward migration (Fig. 2.12), which appeared to follow Dansgaard-Oeschger climate oscillations in the GISP-II record. This challenges the proposal that such oceanographic events as interpreted by Peck *et al.* (2007) were precursors

to Heinrich events and are perhaps actually part of the longer term millennial-scale climate variability.

Bertram *et al.* (1995) studied Cd/Ca and $\delta^{13}C_{benthic}$ at intermediate (1000-2000m) and deep (>2000m) water depths from the LGM to present values. The results can be summarised as follows:

- Intermediate – $\delta^{13}C_{benthic}$ increase, Cd / Ca decrease during LGM
- Deep – $\delta^{13}C_{benthic}$ decrease, Cd/Ca increase during LGM.

This suggests that the glacial NE Atlantic was strongly stratified and that rapid ventilation of the glacial ocean to depths down to 2000m by cold, nutrient-depleted surface waters occurred. They also suggested that AABW and NADW shoaled significantly during the last glacial, compared to their Holocene distributions. The mechanisms causing the apparent anti-phasing between northern and southern sourced waters during the last glacial were not identified.

The bipolar seesaw hypothesis (Broecker 1998; Dokken and Nisancioglu 2004) provides an explanation for the anti-phase relationships observed between northern and southern hemisphere climate variations during the last glacial. This has since been modified and incorporated into the 'thermal bipolar seesaw' hypothesis (Stocker and Johnsen 2003), and predicts that changes in ocean circulation that cause warming in the North Atlantic region result in cooling in the Southern Ocean and vice versa. This link has been demonstrated recently (EPICA 2006). There is still uncertainty regarding the exact mechanisms driving this bipolar seesaw, particularly how the northern and southern regions are linked (Schmittner *et*

al. 2003; Wunsch 2003; Rickaby and Elderfield 2005; Peck *et al.* 2007) and regarding the relative timing of the climate variations in the two polar regions (Barker *et al.* 2009).

Rickaby and Elderfield (2005), following on from Broecker (1998) and Lassen *et al.* (2002) who proposed that the relative densities of AAIW and NADW may be significant in stabilising northern hemisphere climate during interglacials via a salinity feedback, examined AAIW influence during Termination I. Their results suggested that during the last deglaciation, AAIW and NADW are closer to each other in terms of relative density and that when the density difference is reversed or reinforced due to the input of freshwater at convection centres, this can cause the collapse of GNAIW formation during the last glacial. This does not occur during the Holocene or (presumably) the last interglacial where the influx of 'warm, salty' AAIW acts to stabilise the North Atlantic region, resulting in stable climates in the northern hemisphere. This hypothesis relies on Southern Ocean variations in climate leading variations in northern hemisphere climate. More data are needed on the relative densities of AAIW and NADW (or the glacial equivalent) during the last glacial to test this hypothesis.

The importance (or otherwise) of Mediterranean Outflow Water (MOW) during the last glacial is debatable. Some authors suggest that variations in MOW would have little net effect on circulation in the North Atlantic (e.g. Rahmstorff 1997) where as others have suggested that it could be an important salt source for this region during glacial (e.g. Voelker *et al.* 2006). Voelker *et al.* (2006) proposed that MOW played an important role in acting to stabilize northern hemisphere climate during the last glacial through the supply of salt, particularly following Heinrich events, acting to counteract the freshwater influx of these events.

2.5. Ecology of modern benthic foraminifera

The impact of changes in surface productivity on changing surface conditions, combined with variations in physical oceanography are likely to impact on the distribution of preserved assemblages of benthic foraminifera. Although the abundance of some species of benthic foraminifera display correlations with environmental parameters, most have not been related to specific conditions (i.e. Linke and Lutze 1993; Schnitker 1994) and even relationships that could be present in one locality may not exist at others. For example, *Uvigerina* spp. and *E.exigua* both responded to seasonal phytodetritus deposition in the Bay of Biscay (Fontanier *et al.* 2003), but this was not observed in the NW Pacific (Okushi *et al.* 2003), where only *E.exigua* displayed a reaction. Buliminids and Bolivinids have been linked to oxygen-depletion or even anoxia in previous studies (e.g. Corliss and Chen, 1988; Kaiho, 1994; Jorissen *et al.*, 1995; de Stigter *et al.* 1998; Fontanier *et al.* 2002). *Rupertina stabilis* is an obligate epifaunal suspension feeder that requires a steady input of nutrients throughout the year (Linke 1992). Uvigerinids are considered to be most abundant in conditions with high and pulsed nutrient input to the sea-floor and are potentially better adapted to exploit unstable environments where nutrient supply is occasionally quite high (Fontanier *et al.* 2002). *Melonis barleeanum* and *Melonis pompilioides* have been correlated to high productivity (Fariduddin and Loubere 1997) and oxygen depletion (Fontanier *et al.* 2002). *Cibicides wuellerstorfi* is an epifaunal taxon (Lutze and Thiel 1989) and has been shown to be more abundant in environments with lower productivity than *U.peregrina* (Altenbach *et al.* 1999). *Pullenia bulloides* is potentially also even more inversely correlated to increasing productivity (Altenbach *et al.* 1999). *Karreriella bradyi* and *Sigmoilopsis schlumbergeri* are both taxa that

are generally more abundant under oligotrophic productivity regimes (Kuhnt *et al.* 1999; Rasmussen *et al.* 2002). *Cibicides kullenbergi* has displayed an affinity for bottom currents and the influence of Mediterranean waters (Murray 1991). *Triffarina angulosa* has been suggested as a potential indicator taxon for the deposition of coarser sediments under the influence of bottom currents (Harloff and Mackensen 1997; Rasmussen *et al.* 2003). *Fursenkoina fusiformis* has been linked to spring bloom productivity in the Nordic Seas (Gustafsson and Nordberg 2001) and is tolerant of anoxia (Bernhard and Alve 1996; Rasmussen *et al.* 2003).

Hermelin and Scott (1985) provide a good description of the different foraminifera assemblages in the North East Atlantic region. They described 117 species from the North Atlantic Ridge, southwest of the Azores (36°N, 34°W; Water depths 538-2759m) and were able to define two assemblages. One, at 500-1500m (which they linked to NADW) dominated by *Epistominella exigua*, *Uvigerina auberiana*, *Planulina ariminensis*, and *Trifarina bradyi*. A deeper assemblage was defined at 2400-2800m (which they linked to AABW) and dominated by *Eponides bradyi*, *Epistominella exigua* and *Bolivina pseudoplicata*.

Austin and Evans (2000) also describe the modern distribution patterns of benthic foraminifera from the NE Atlantic and discuss the palaeoecological significance of their findings. They define three assemblage groups dominated by three taxa; *Cassidulina laevigata*, *Rhizammina* sp. and *Epistominella exigua*. The *Cassidulina laevigata* assemblage group occupies continental slope depths above 2000m to the north of 60.5°N. It is also located in a region of high primary productivity (>90gC/m^2/yr). The *Rhizammina* sp. assemblage group is located between 2000-2500m water depth in a region of declining surface productivity relative to the *Cassidulina laevigata* assemblage group (~70gC/m^2/yr). The

Epistominella exigua assemblage group occupies water depths >2000m. It is also associated with lower primary productivity (<45gC/m^2/yr). Infaunal taxa dominate assemblages down to 2700m water depth, with epifaunal taxa dominating assemblages below this.

Jorissen and Wittling (1999) compared live: dead ratios for different benthic species in an attempt to identify opportunistic and non-opportunistic taxa. They studied a five station surface sample transect off Cape Blanc, using samples collected in March 1994. The unique upwelling system of this area enabled a direct comparison of seasonal versus continuous upwelling-linked productivity. Samples extracted nearer the shoreline were from a region associated with continuous upwelling throughout the year. Samples located further offshore were within an area that experienced seasonal upwelling (July-August) linked to Ekman transport. The authors proposed that an increased living:dead ratio for a taxon from samples that pre-date the upwelling season would suggest that taxon is non-opportunistic. A low living: dead ratio (such as observed for *E.exigua* and *U.peregrina*) would suggest an opportunistic species, with the reproduction and growth of that species mainly occurring during the upwelling season (during March).

Gooday and Hughes (2002) performed a similar study on foraminifera assemblages from at a bathyal site in the northern Rockall Trough (NE Atlantic). The authors studied a site at 1920m water depth, comparing assemblages before (May) and after (July) a phytodetritus bloom. Rotaliid taxa (especially *Eponides pusillus* and *Nonionella iridea*) show the clearest response to phytodetritus deposits. The results of this study leads the authors to conclude that the abundance and distribution of epifaunal and some infaunal species is linked to phytodetritus deposits. It is also proposed that this phytodetritus signal should be preserved in the fossil record (due to the response from calcareous rather than arenaceous taxa). The two

main 'phytodetrital' species (*E.pusillus* and *N.iridea*) are relatively small, usually occurring in the 63-125μm size fraction, but should be well preserved in most deep sea sediments in this region.

Fontannier *et al.* (2002) studied benthic foraminifera in the Bay of Biscay in relation to organic matter input and oxygenation variations. The results suggest that oxygenation of bottom waters and sediments has only a minor role in controlling assemblage compositions of benthic foraminifera. This also suggests that variations in export productivity have a much larger impact. Another observation is that *Uvigerina peregrina* is commonly observed living beneath the most elevated taxa (Average Living Depth 0.4-1.1cm), suggesting that the stable isotope and trace element composition of its shell is not characteristic of bottom waters. The species-specific TROX model proposed by the authors (Fig. 2.13) shows the relationship of different taxa to different parameters (i.e. microhabitat, eutrophic-oligotrophic conditions).

Thomas *et al.* (1995) studied benthic foraminifera from the last 45 kyrs. The results indicate that a low abundance of "phytodetritus species" (i.e. *Epistominella exigua* and

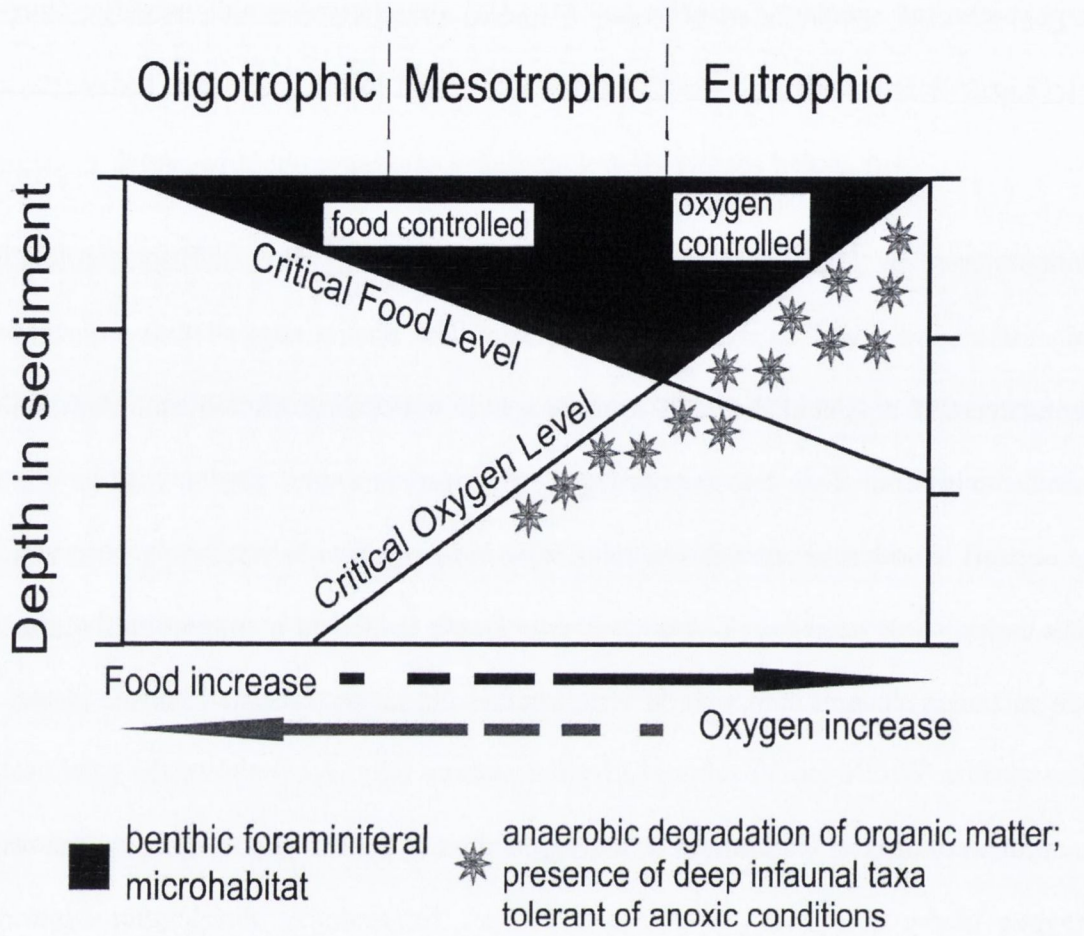

Figure 2.13. The TROX model, which explains the effect of controls (productivity and oxygenation) on the depth distribution of benthic foraminifera in the sediment (Jorissen *et al.* 1995).

Alabaminella weddellensis) occurred during the LGM. This suggests a reduction in seasonal export production, compared to modern values. The authors note that the major changes in assemblages were due to variations in productivity related taxa. This suggests that changes in assemblages of benthic foraminifera in the NE Atlantic are due to variations in surface productivity, as opposed to deep water mass circulation.

Sierro *et al.* (1999) studied the Gulf of Cadiz contourite deposits, enabling a detailed reconstruction of Mediterranean Outflow Water through time. However, the authors did not include any primary data in their report, only percentages of different groups (i.e. coccolithophores, planktonic and benthic foraminifera) complicating interpretation of their results. For example, the authors report that the percentage of benthic foraminifera per sample decreases from bottom to top. This does not differentiate between an actual decrease in the numbers of benthic foraminifera and an increase in other components (i.e. planktonic foraminifera). Schönfeld (2002) identified an 'elevated epifaunal' group of species (e.g. *C.wuellerstorfi*) that appeared to increase in relative abundance in response to enhanced bottom current activity on the Gulf of Cadiz contourite deposit. The author proposed that this group could even be used as a proxy for bottom current strength.

Attempts have been made by previous authors to quantify changes in palaeoproductivity using the accumulation of benthic foraminifera (Herguera and Berger 1992). The method used assumes that one benthic foraminiferal specimen from the >150μm is equivalent to the deposition of 1mg of carbon on the sea-floor, which is then related to surface productivity. The authors used this to investigate changes in BFAR in glacial and post-glacial sediments in the Western Equatorial Pacific. They concluded that primary productivity during the glacial period was almost twice as high as today. However, this conclusion relies on the assumption that sedimentation rates during the Holocene and LGM were approximately the same. Another application of BFAR is to investigate the migration of the polar front in the North Atlantic (Nees *et al.* 1997). Nees *et al.* (1997) assumed that peaks in BFAR observed in a series of cores along an approximately north-south transect represented the position of the polar front (a region of current high productivity; Yoder *et al.* 1994) at different times during

Termination 1 (9-12 kyr B.P.). The authors only used cores located in regions of open water, avoiding potential sites of upwelling and the results suggest that sea ice retreated at a mean velocity of 0.77km.yr^{-1} (Fig. 2.14). A linear sedimentation rate was also used in this study.

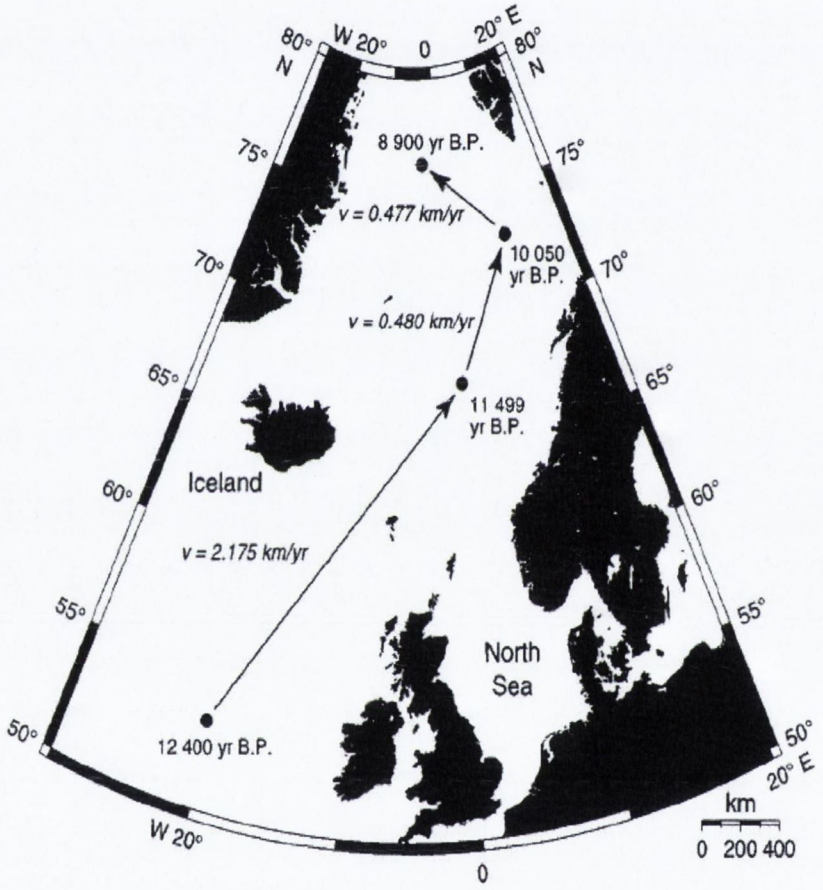

Figure 2.14. Migration of peaks in BFAR from the North Atlantic to Arctic Ocean with proposed velocities (v) estimated from the distance between stations and dates at which peaks occurred. Modified from Nees *et al.* (1997).

2.6. Sedimentology

The study of contourite deposits has expanded considerably in the last decade (Faugeres and Stow 1993; Stow *et al.* 1998; Viana *et al.* 1998; Sierro *et al.* 1999). This is because of their importance in understanding the circulation of important water masses and how this has changed in response to climatic fluctuations (Sierro *et al.* 1999). Contourites are also considered to be economically important as sources of hydrocarbons (Viana *et al.* 2007) because they are usually sand-dominated (a good reservoir rock) and are deposited mostly on continental shelves (and will, therefore, receive more organic carbon per sedimentary particle than deep marine sediments).

Contourite is defined by Faugeres and Stow (1993) as a sediment found in relatively deep water (greater than 300m) that has been deposited or significantly reworked by stable, geostrophic currents. This can include sediments affected by bottom currents acting at intermediate depths as well as those affected by major surface currents impinging on the deep sea floor. Reworked turbidite deposits are not considered contourites (Faugeres and Stow 1993).

Stow *et al.* (1998) provide a critical review of the sedimentology of biogenic contourites. The following characteristics are usually observed:

- In most cases bedding is indistinct, but may be enhanced by cyclic variations in composition.

- Primary sedimentary structures are poorly developed or absent due to thorough bioturbation.
- Many biogenic particles are fragmented and stained with iron or manganese oxides.
- Biogenic contourites typically occur in sequences on a decimetre scale that show variation in the biogenic / terrigenous ratio, which is generally linked to a grain size variation.
- This cyclic facies pattern is closely analogous to the Milankovitch cyclicity recognised in many pelagic and hemipelagic successions and is believed to be driven by the same mechanism of orbital forcing super imposed on changes in bottom current velocity (Robinson and McCave 1994).

Viana *et al.* (1998) outline the formation of modern contourites. For mid-water depth contourites (300-2000m water depth) the following factors are considered to control their formation,

1. Mid-depth sandy contourites require the presence of relatively strong, semi-permanent geostrophic currents flowing at intermediate depths within the water column, or very strong surficial geostrophic currents that are able to influence the sea floor at these depths. Short term perturbations in flow strength, during benthic storms for example, as well as longer term variations caused by climate or sea level change, can significantly affect the nature of the contourite deposit.

2. Morphology exerts a primary control on sandy contourite deposition in that it directly affects bottom-current intensity. Intensification of weaker flows is caused by flow constriction through gateways or channels and over sills between basins, by the Coriolis Effect along higher latitude continental margins, and by the local steepening or curvature of a continental slope along which flow is directed.
3. The supply of sand to mid-depth drifts is from a variety of sources both internal and external, including bottom-current erosion upstream of the drift, the pirating of direct turbidity current input, pelagic biogenic fallout, and in-situ winnowing. Long-term persistence of any of these modes of sand supply appears limited, so that individual beds are generally thin and rarely exceed 1m in thickness.
4. Climate, sea-level and tectonic factors can each influence drift accumulation and, as for the shallower-water bottom-current sands, act as the turn-on / turn-off mechanism for sand deposition.

An initial study of the contourite deposits on the Porcupine Bank was undertaken by Dr. Lena Øvrebo as part of her Ph.D. thesis at UCD (University College, Dublin). This resulted in the production of three lateral transects at 700-1000m (Transect 1), 1600-1800m (Transect 2) and 2400-2700m (Transect 3) on the basis of a shared, coherent, lithostratigraphy (Øvrebo *et al.* 2006). Of the 66 cores logged by Øvrebo (2005), most have recovered Holocene and last glacial sediments, with some cores extending deeper in time to approximately 500 kyr B.P, as determined by visual counting of glacial-interglacial sediment alternations.

Between 52°15'N and 52°45'N the slope on the Porcupine Bank is smooth (Øvrebo *et al.* 2006). This smoothness can be explained by a reduction in current strength due to the presence of a large canyon complex to the south (Figure 2.15; Øvrebo *et al.* 2006). The morphology and depositional regimes of the western slope appear to be strongly controlled by the position of geostrophic currents. Øvrebo *et al.* (2006) proposes that the core of a strong geostrophic current located at 500-1200m water depth shifted position in the past and during the late glacial, the core was located at 1200-2300m (Figure 2.16).

There are two principal modes of sedimentation on the Porcupine Bank (Øvrebo *et al.* 2006). Hemipelagic sediments (calcareous foraminifera and nannofossils) dominate interglacial episodes, with little or no terrigenous input or IRD (Øvrebo 2005). Glacial sediments consist mainly of fine-grained mud and clays, with some IRD input also observed (Øvrebo 2005). These also contain foraminifera, but the planktonic fauna is much less diverse (the benthic foraminifera were not studied). The sedimentological characteristics of the sediments deposited on the stable section of the slope (e.g. strong grain size sorting) has led to the conclusion that these are contourite deposits (Øvrebo *et al.* 2006).

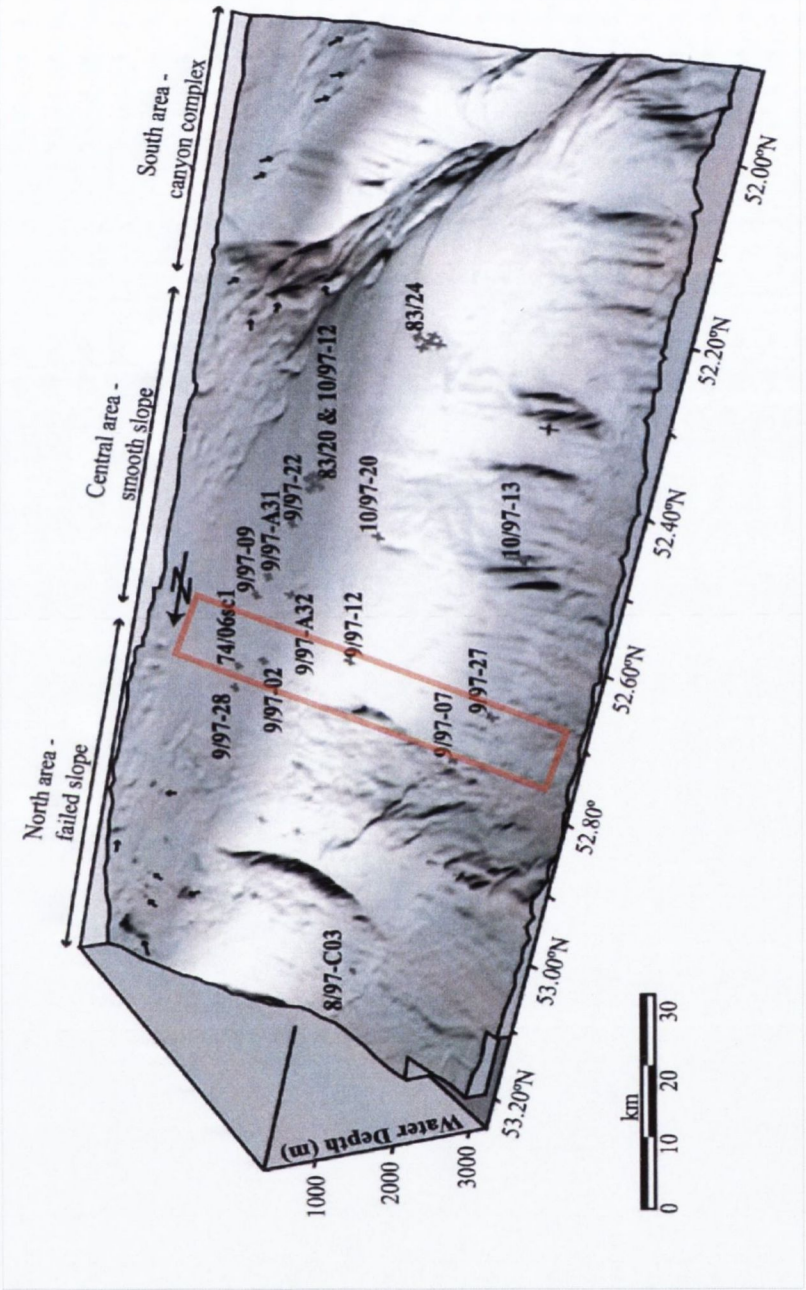

Figure 2.15. 3D bathymetry map showing the position of cores studied by Øvrebo *et al.* (2006). Note the large canyon complex to the south and the area examined in this study highlighted by the red square. Modified from Øvrebo *et al.* (2006).

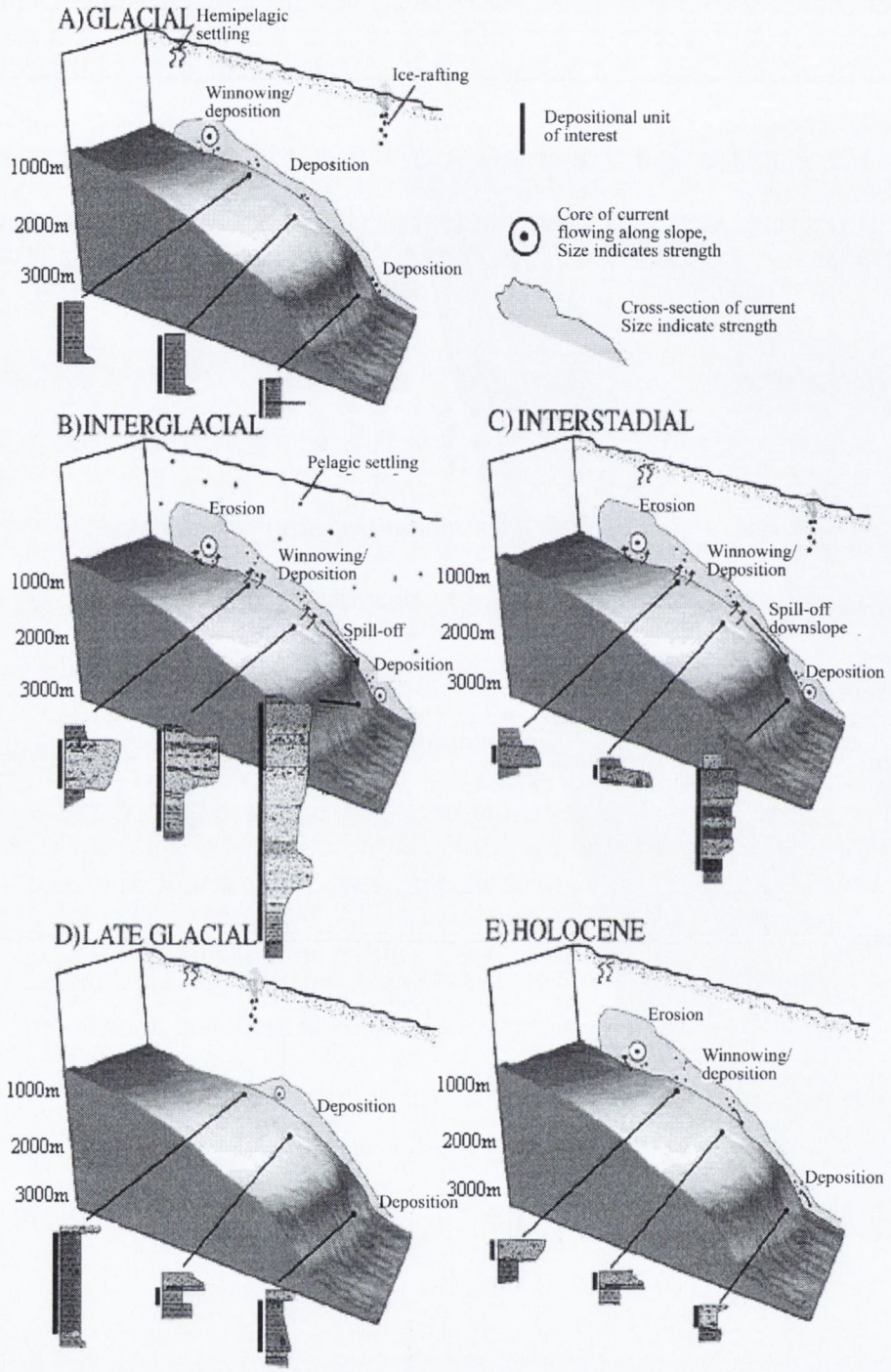

Figure 2.16. Depositional model proposed by Øvrebo *et al.* (2006). Note the changing position and strength of currents along the slope at different time intervals, and the resulting sedimentary units.

Chapter 3 – Methods

3.1 Sample extraction and preparation

Seven gravity cores were selected for this study (Table 3.1) from a total of 87 SGS cores. The cores were collected as part of the SGS (1999) coring programme. These were selected to provide two adjacent depth transects along the western flank of the Porcupine Bank to examine down slope and along slope distribution of foraminifera. This method provides an opportunity to study along-slope as well as down-slope processes affecting the distribution of foraminifera. Cores were initially sampled every 4cm with a 2cm diameter sampling device (see Fig.3.1), with higher resolution sampling undertaken over key intervals (e.g. the late Glacial – Holocene boundary in core 9/97-10) and sedimentary layers of interest (e.g. the 'grey bands' in core 9/97-27/2). In total, 441 samples were examined following the procedure outlined in Figure 3.2, providing foraminiferal data from a range of sedimentary facies. Samples of known volume (which are essential for calculating accumulation rates) were extracted and placed into labelled plastic bags. Two to five cubic centimetres (5-15g dry weight) of material was extracted for each sample.

The samples were then transported to the Geomorphology Laboratory at TCD and batches of 20-25 samples were placed in an oven to dry overnight at 50°C. Each sample was then weighed on a balance, then placed in a labelled glass beaker with ~150ml distilled water and replaced into the oven for ~3 hours. The samples were then removed from the oven and each had ~1-2g of Calgon stirred in before being washed through a 63μm sieve. Calgon was added to each sample as it removes clay particles from the surface of foraminiferal tests, without affecting the results of subsequent geochemical analyses (Green 2001). If the samples

were not sufficiently clean, this stage was repeated. The samples were then rinsed into a labelled beaker using distilled water and left overnight to dry out in the oven.

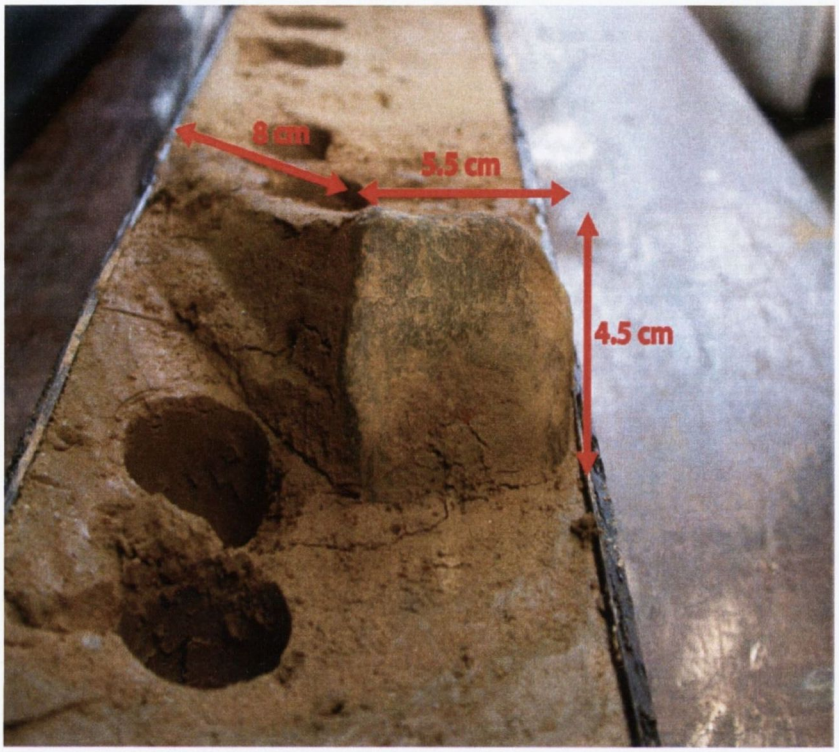

Figure 3.1. Sampling positions highlighted either side of a large cobble present in core 9/97-10. Photograph courtesy of Toms (pers. comm.).

The dry residues were then split into different size fractions (63-250μm, 250-500μm and >250μm and >150μm for benthic foraminifera accumulation rates (BFAR), planktonic census counts etc.) and poured into empty, labelled glass vials.

Core number	Core type	Longitude °E	Latitude °N	Water depth (m)	Core length (m)
9/97-03	Gravity	-15.09	52.71	1230	2.38
9/97-04	Gravity	-15.14	52.73	1502	1.70
9/97-08	Gravity	-14.97	52.60	819	1.84
9/97-10	Gravity	-15.14	52.64	1260	2.46
9/97-14	Gravity	-15.32	52.69	2118	2.61
9/97-20	Gravity	-15.41	52.80	3073	2.06
9/97-27	Gravity	-15.39	52.70	2756	2.68

Table 3.1. Details of gravity cores examined in this study.

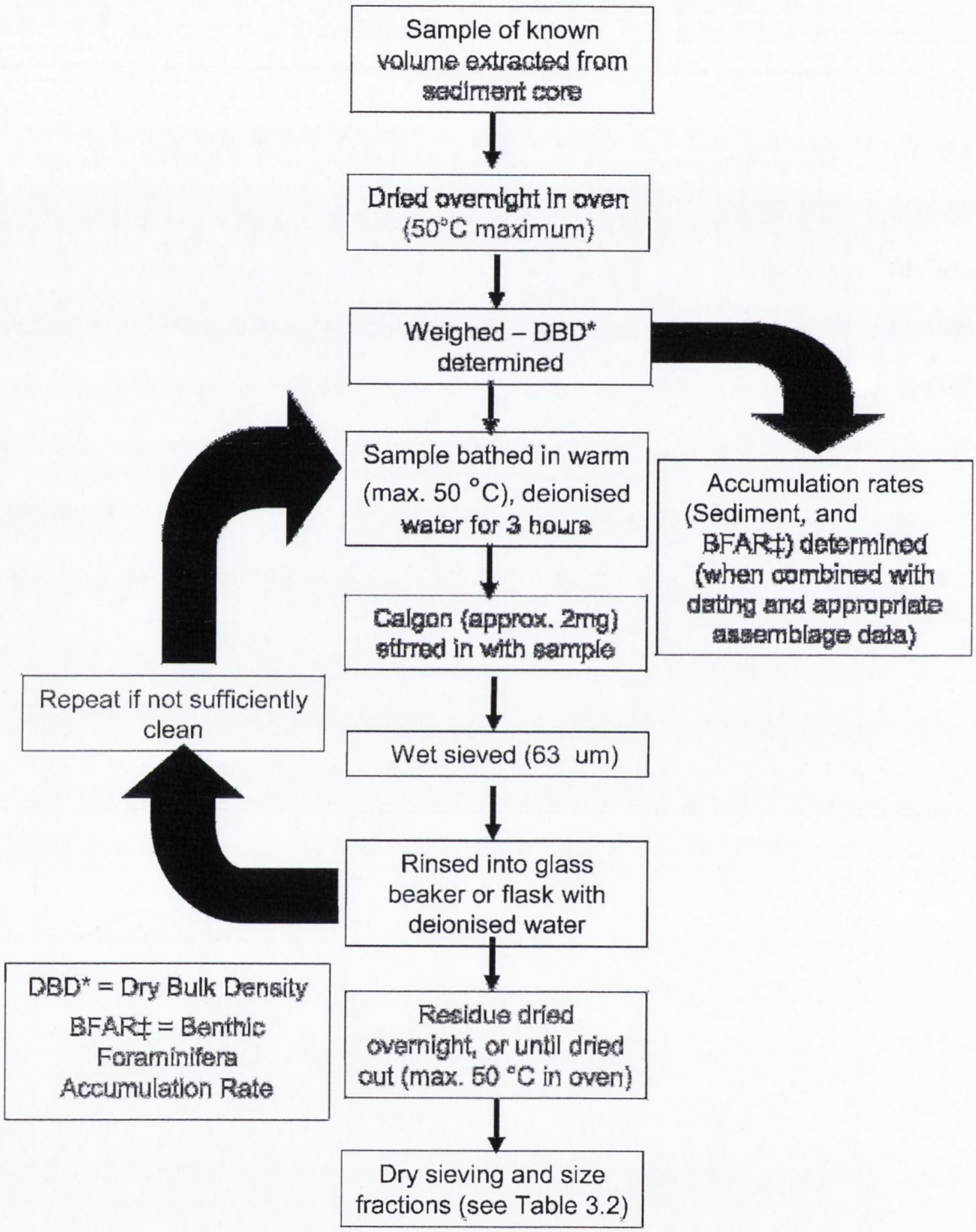

Figure 3.2. Flow-chart indicating the sample preparation procedure employed in this study.

3.2 Sample examination under light microscopy

Residues were scooped onto a black picking tray and examined using a Leica MZ6 Stereo Microscope at typical magnifications of x32. Each size fraction provides different proxy information (Table 3.2). Fifteen reference slides from each core (ten planktonic and five benthic foraminifera) were picked and logged. Specimens were picked, orientated and fixed to cardboard slides using a sable picking brush moistened with distilled water. Species of interest for ecological and taxonomic purposes (Table 3.3) were picked onto cardboard slides but not fixed (fifteen specimens per species). Reference slides were selected that would best reflect the diversity of assemblages from each core, or for key intervals. Assemblage counts of planktonic foraminifera were made from the >150μm fraction whereas for benthic foraminifera, two size fractions (63-250μm and 250-500μm) were counted.

Size fraction	**Proxy information**
63-250μm	Benthic and planktonic foraminifera species abundance
>150μm	Planktonic foraminifera species abundance, BFAR, Fragmentation Index
>250μm	Benthic foraminifera species abundance, Stable isotope and trace element picking of *Cibicides wuellerstorfi*
250-355μm	Stable isotope picking of *Globigerina bulloides*

Table 3.2. Properties studied from each size fraction.

Species	Ecological (or other) significance	Reference
Globigerina bulloides	Sea surface temperature and productivity	Kucera (2007)
Neogloboquadrina pachyderma (sin.)	Sea surface temperature	Bandy (1960)
Cibicides wuellerstorfi	Geochemical data	Rickaby and Elderfield (2005)
Cibicides kullenbergi	Bottom water conditions	Murray (1991)
Melonis barleeanum	High productivity	Loubere (1991)
Melonis pompilioides	High productivity	Loubere (1991)
Sigmoilopsis schlumbergeri	Oligotrophic conditions	Kuhnt *et al.* (1999)
Karerriella bradyi	Oligotrophic conditions	Kuhnt *et al.* (1999)
Pullenia buloides	Low productivity	Altenbach *et al.* (1999)
Bullimina aculeata	Low oxygen	Jorissen *et al.* (1995)
Bullimina marginata	Low oxygen	Jorissen *et al.* (1995)

Bullimina inflata	Low oxygen	Jorissen *et al.* (1995)
Uvigerina celtica	Seasonality	Fontanier *et al.* (2002)
Uvigerina peregrina	Seaonality	Fontanier *et al.* (2002)
Triffarina angulosa	Bottom current activity	Rasmussen *et al.* (2002)
Fissurina porcupinensis (sp. nov.)	New species	N/A

Table 3.3. Ecological and other significance of the key taxa picked onto reference slides.

3.3. Estimating the degree of post-mortem modification of assemblages

There are four main complicating factors in interpreting the faunal record from this part of the Porcupine Bank. These are listed below.

1. Bioturbation
2. Reworking by geostrophic currents and internal waves
3. Low rate of sedimentation
4. Dissolution

Each of these factors complicates any interpretation of foraminiferal assemblages. The effects of bioturbation can be determined by the observation of burrowing on the core surface. Cryptic bioturbation (i.e. bioturbation beneath the observed surface) is another potential problem and cannot be observed directly (Øvrebø *et al.* 2006). It is unlikely that any core material from this environment will contain preserved laminations. This is because the slope is well oxygenated (Read 2001) and experiences periodic influxes of food (Gooday and Hughes 2002), which is capable of supporting populations of bioturbating organisms (Thomson *et al.* 2000). The most reasonable approach is to attempt to quantify the effects of bioturbation or to account for them when interpreting the results of analyses, rather than attempting to avoid them. In this study, a 4cm sampling interval is employed in an attempt to minimise the effects of bioturbation.

Bioturbation can cause mixing of sediments of different ages (Manighetti *et al.* 1995). Manighetti *et al.* (1995) suggest using different taxa to obtain accurate ^{14}C radiometric dates for the Holocene and Last Glacial. *Globigerina bulloides* (a sub-polar taxon) should be used in Holocene sediments, with *N.pachyderma* (sin.) used in glacial sediments. This follows the simple logic that *G.bulloides* from glacial sediments are more likely to have been reworked than specimens of *N.pachyderma* (sin.). Preferential mixing of finer particles compared to larger particles (Bard 2001) will also need to be considered when interpreting size fraction data of foraminifera.

Reworking by geostrophic currents and internal waves is another factor that requires consideration. A comparison of size fractions of sediments and foraminifera should identify episodes of enhanced bottom current reworking. This is because different current velocities result in the deposition of a specific size of sedimentary particle (McCave *et al.* 1995).

Foraminifera behave slightly differently to sedimentary particles of the same size as they are usually slightly lighter and therefore require slightly lower velocities in order to settle out of suspension (Berger and Piper 1972).

The low sedimentation rate on the Porcupine Bank (Øvrebo *et al.* 2006) suggests that high resolution (sub-millennial scale) studies are impractical. Low sedimentation, combined with bioturbation suggests that most assemblages will be thoroughly mixed. However, some of the deeper and shallower cores appear to be less condensed than the core dated by Øvrebo *et al.* (2006) and could facilitate the study of high resolution variations in foraminiferal assemblages.

Another important consideration when obtaining samples for microfossil studies from cores is the phenomenon referred to as 'caving'. Because a core is obtained by drilling down-strata, this can lead to specimens appearing earlier in caved sections than they do in uncaved sections (Morris *et al.* 1999). Although this does not have a significant impact on geochemical or assemblage studies, it can and does affect the biostratigraphy. Biostratigraphy is largely based on the first occurrences of taxa in a section. Because this would not be possible in a core (due to caving) most cores are correlated using last occurrences of taxa. This assumes that the last occurrence of a taxon occurs at a uniform time across the studied area (which can be contentious). To overcome this problem, it is necessary to extract samples away from the edges of the core tube, as the process of gravity coring causes material to cave at the contact with the core barrel.

Dissolution can impact on the preservation of whole foraminiferal shells (Hemleben *et al.* 1989; Fig. 3.3) and original geochemical signatures (McCorkle *et al.* 1995; Sexton *et al.*

2006). Several methods have been developed to attempt to qualify / quantify the effects of dissolution (see Kucera 2007 for review). Le and Shackleton (1992) proposed a method for estimating the degree of dissolution a foraminiferal sample has undergone based on the number of shell fragments observed. By acknowledging the fact that multiple fragments would result from the disintegration of only one test, this method improves the linearity between the carbonate ion concentration at the sediment-water interface and fragmentation of shells (compared to the simple 'percentage of shell fragments' method of Berger (1970)). This method, however, is relatively subjective as defining what constitutes a test fragment or a 'whole test' is not straightforward. An alternative method (Broecker and Clark 2001) uses test weight to determine the degree of dissolution. This method assumes that all of the variations in test weight are due to dissolution, and could be difficult to employ if tests display evidence of shallow-burial diagenesis resulting in the addition of calcite to tests (Williams *et al.* 2007). Some geochemical proxies of dissolution exist (Stoll *et al.* 1999), but these are relatively new and potential biases / drawbacks are not yet well defined.

Some species of planktonic foraminifera are more susceptible to dissolution than others (Fig. 3.3). This will also need to be considered in relation to transfer function estimates of sea surface temperature, where census data could potentially be biased by preferential dissolution of certain 'warm water' taxa over 'cold water' species. In spite of all of these potential hindrances, initial studies suggest that the core material from the Porcupine Bank is stratigraphically coherent, even when studying to a moderately high resolution (Øvrebo *et al.* 2006).

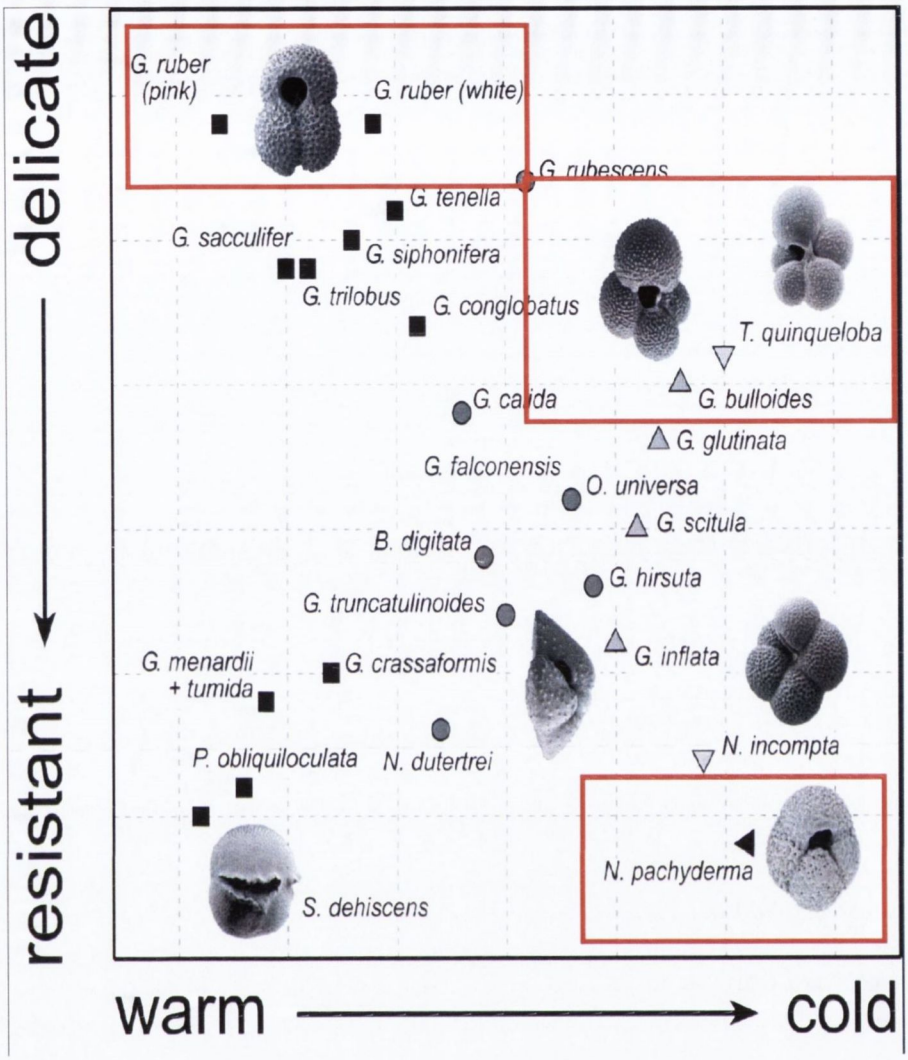

Figure 3.3. Dissolution series of modern planktonic foraminifera (based on Hemleben *et al.* 1989). Note the relative position of *N.pachyderma* compared to taxa such as *G.bulloides* and *G.ruber* highlighted by the red squares (Modified from Kucera 2007). Grayscale shading of symbols denotes habitat preferences in terms of sea surface temperature, from cold (light grey) to tropical (black).

Variation in fragmentation was estimated by counting the percentage of damaged / fragmented planktonic foraminiferal shells versus undamaged shells (referred to as the

Fragmentation Index – Berger 1970). It was crucial that all samples were prepared using a uniform protocol, and deviations from this (such as additional wet sieving stages) were recorded. Also, the fragmentation index proposed by Le and Shackleton (1992) was calculated.

Fragmentation Index (From Le and Shackleton 1992):

$$F_{LS}\ (\%) = 100 \times (F/8)/ ((F/8) + C) \qquad \text{Equation 1}$$

where F_{LS} is Fragmentation index (Le and Shackleton 1992), F is the number of fragments and C is the number of complete shells. The number of fragments are arbitrarily divided by eight to improve the linearity with dissolution, assuming that eight fragments result from the break down of a foraminiferal test (although this is logically a more realistic proposition than the 1:1 relationship implied by the Berger (1970) method). This is a modification of the most commonly used dissolution index (from Berger 1970).

3.4 Taxonomy and Scanning Electron Microscopy

3.4.1 Planktonic foraminifera

Taxonomy of planktonic foraminifera followed Kennett and Srinivasan (1983) and Hemleben *et al.* (1989) the standard references for the application of transfer functions (Pflaumann *et al.* 2003; Kucera *et al.* 2005). This was supplemented by more recent

publications, particularly regarding genetic studies of planktonic foraminifera in the North Atlantic region (i.e. Kucera and Darling 2002). This study disregarded the discrimination of different sized specimens of the planktonic foraminifer *Neogloboquadrina pachyderma* (sin.) into a 'plexus of different genotypes' as suggested by Eynaud *et al.* (pers. comm.). This was because extensive genetic studies of *N.pachyderma* (sin.) in this region have shown that there is probably only one genotype present (Darling *et al.* 2004), which implies that the 'plexus of genotypes' is in reality a 'plexus of phenotypes' and possibly the result of ontogenetic variation related to varying oceanographic conditions. At present, it is not possible to determine what environmental variable(s) this apparent phenotypic variation is a response to.

3.4.2 Benthic foraminifera

Schönfeld (2006) and Schweiger (2006) provide detailed taxonomic information on the genera *Uvigerina* and *Cibicides* respectively. Schönfeld (2006) outlined a scheme for discriminating members of the *Uvigerina peregrina* plexus based on gross test morphology and test ornamentation. This proposed scheme was followed in this study. Schweiger (2006) provided a morphological framework for discriminating between different Cibicidid species, which was also supported by molecular genetic data. This framework was applied to this study. For other taxa, a new taxonomy was developed based on comparing the specimens observed to previous taxonomies for this group (see Chapter 4).

3.4.3 Scanning Electron Microscopy

Scanning Electron Microscopy (SEM) was performed using an Hitachi S-4300 Field Emission scanning electron microscope at the Centre for Microscopy and Analysis, Trinity College Dublin (CMA). Two hundred and sixty-five specimens were prepared for SEM imaging. The specimens chosen were identified as well preserved specimens or displaying taphonomic features of interest (i.e. dissolution). If necessary, they were cleaned in a droplet of distilled water using a picking brush, before being orientated and fixed to an SEM stub, with a diagram produced to illustrate their position on the stub surface.

LM images were also produced for key taxa and to highlight important taxonomic features that are not easily observed via SEM imaging.

3.5 Age model development and correlation

The percentage of *N.pachyderma* (sin.) in the >150μm size fraction can be a useful tool in identifying glacial-interglacial or stadial-interstadial periods (Bond *et al.* 1993; Knutz *et al.* 2007). A dominance of the polar taxon *N.pachyderma* (sin.) suggests an influx of polar surface waters (Bandy 1960). This would be expected during glacial periods and the expansion of ice sheets. This should enable correlation of the *%N.pachyderma* (sin.) curve with benthic $\delta^{18}O$ curves (which vary due to the expansion / contraction of global ice volume once other factors are taken into account; e.g. Shackleton (1987)) from other sites, which can then aid age model development for individual cores and also be used to calculate reservoir ages when combined with ^{14}C AMS radiometric dating, as it has been applied in previous studies from this region (Voelker *et al.* 1998; Peck *et al.* 2006). This method provides a useful

relative dating technique, but the limited variation in the relative abundance of this species at the very coldest and warmest SSTs (Fig. 3.4) could result in an unrealistic representation of SSTs.

Cryptic speciation in *N.pachyderma*. could undermine the assumption that this morphospecies has maintained the same linear response to SST as observed at present (Ericson 1959; Bandy 1960). Cryptic speciation describes a morphospecies that has two or more genotypes, despite a lack of obvious morphological differences. This could have significant implications for palaeoceanographic reconstructions as it has been observed in modern *N.pachyderma* (Bauch *et al.* 2003). Darling *et al.* (2004) report five genotypes within the morphospecies *N.pachyderma* (sin.). Four are South Atlantic species,

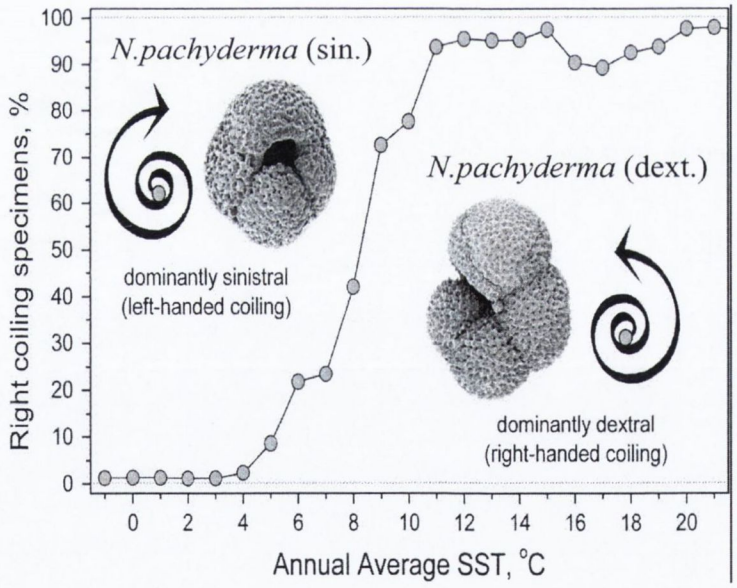

Figure 3.4. Relationship between coiling direction of *N.pachyderma* and mean sea surface temperature. Modified from Kucera (2007), where *N.pachyderma* (dext.) is labelled *N.incompta*.

with only one genotype in the Arctic region (Type I). It is also reported that approximately 3% of *N.pachyderma* (sin.) change coiling direction and produce a dextrally coiled test (Bauch *et al.* 2003). This will need to be considered if interpreting assemblages of planktonic foraminifera, particularly when applied as a proxy of sea-ice extent (see below). As only one genotype is reported in the North Atlantic, this makes the retention of the modern linear response to temperature more plausible for this region.

Øvrebo *et al.* (2006) reported cores extending as far back as MIS 13 from this section of the Porcupine Bank. Unlike for Øvrebo *et al.* (2006), who correlated their oxygen isotope profile to the record of Venz *et al.* (1999) from ODP site 982, the oxygen isotope profiles generated from the cores examined in this project were correlated to the profile produced by McManus *et al.* (1999) at ODP site 980, which was graphically correlated to existing chronologies (Shackleton *et al.* 1990). This record was selected as a reference as it is likely to provide a much higher resolution record against which the data produced in this study can be correlated with a high degree of confidence. It also provided a higher resolution record compared to ODP 982, which was unable to present a clear millennial scale resolution (Raymo *et al.* 2004). Although millennial scale variability is unlikely to be preserved in such short cores (see Table 3.1), it could be preserved during intervals of enhanced pelagic production (and flux rates).

The Greenland Ice Sheet Project II ice core (GISP-II) provides a high resolution record (centennial scale) of northern hemisphere climate variability over the previous 125 ka (Grootes and Stuiver 1997). This record of sub-millennial scale resolution is ideal for comparison / correlation with records which are likely to preserve a sub-millennial scale record, as has been shown in other studies from this region (Peck *et al.* 2007) and elsewhere

(e.g. Peterson *et al.* 2000). The record from ODP 980 is not suitable for sub-millennial scale chronological studies (McManus *et al.* 1999).

Down core data were correlated with data from other studies with an established chronology (GISP-II, Grootes *et al.* 1993; ODP 980, McManus *et al.* 1999), referred to as reference curves (see Chapter 5). This was achieved by using the splinage function in Analyseries 2.0 (Paillard *et al.* 1996). Down core *%N.pachyderma* (sin.) data (Appendix A) were pasted into the program (and referred to as the correlation curve) and the splinage function selected. The reference curves consisted of one column of age estimates and one column of corresponding $\delta^{18}O$ values. The curves were then visually displayed on the screen and likely tie-points between the two curves selected. Once the tie-points were selected, the probability of the now altered correlation curve matching the reference curve was estimated and presented as a linear correlation coefficient (r^2 value). If these proposed tie-points enhanced the correlation coefficient (i.e. increased the linear correlation coefficient) and were realistic with respect to the nannofossil biostratigraphic data and the radiocarbon dates, then the tie-points were retained. If the proposed tie-points did not improve the correlation coefficient or were unrealistic in relation to other data, then the tie-point was rejected and removed from the correlation. This process of attempting tie-point correlations was undertaken until the highest possible correlation coefficient was achieved.

Although this method was subjective (relying upon visual 'wiggle-matching' – see Fig. 3.5) it was applied within an established nannofossil biostratigraphic scheme and using radiocarbon dates (Fig. 3.6) to guide the correlation of the curves. The linear correlation estimate provided by Analyseries was also used as a guide to improve correlations. This provides an estimate (r^2) of how well the two curves have been matched, a number between 0

and 1, with 1 being a perfect match and 0 not matching. The software enabled the highest linear correlation coefficient between the two curves to be achieved. No correlated curve produced in this study had a linear correlation coefficient lower than 0.5.

Although the method outlined above represents the best method for obtaining age-depth profiles for each of the cores examined in this project, there are significant issues which need to be considered. For example, this method does not include any independent age control (except for the calcareous nannofossil data), which is potentially problematic for the deeper cores. This problem feeds into subsequent analyses (particularly BFAR calculations) and will need to be considered when assessing the results of these. Tephrochronology (e.g. Davies *et al.* 2002) can potentially solve this problem by providing an age control on the deeper cores.

Radiocarbon dating is the most commonly used method of absolute dating of organic material in the late Quaternary (e.g. Broecker *et al.* 1988; Currie *et al.* 1999; Hughen *et al.* 2000; Peterson *et al.* 2000; Fairbanks *et al.* 2005). Calculating reservoir ages for ^{14}C AMS radiocarbon dates is necessary to correct for variations in the age of surface water through time (Waelbrock *et al.* 2004). It had been assumed that the age of surface water had not varied significantly in the past (Bard *et al.* 1987; Voelker *et al.* 1998) but recent evidence shows that it is necessary to account for variations in the age of surface water (reservoir age) to improve the accuracy of absolute dates (Waelbroeck *et al.* 2004), particularly at latitudes greater than 40°N. This is particularly important when attempting to determine relative ages (i.e. 'leads' or 'lags') between events or processes at different water depths.

Reservoir ages were calculated following the correlation with the reference curves. The ^{14}C AMS dates provided by Toms (in prep.) were used as a guide in the correlation process, but it was clear that substantial (up to 1549 yrs) off-sets existed between some parts of the curves and the uncorrected ages (see Fig. 3.7). Reservoir ages were calculated by subtracting the age of the dated points suggested by the correlation from the dates suggested by ^{14}C AMS radiocarbon dating (Fig. 3.7).

For the splicing of reconstructed sea surface temperature curves in Chapter 6, the software NClip was used (Higgins *et al.* 2006). The software presented the reference curve(s) in a left-hand panel with the correlation curve(s) on the right-hand side. Each portion of each correlation curve was then visually compared with the corresponding portion of the reference curve. The 'best matching' (i.e. no or least amount of obvious hiatuses) portion from the correlation curves was selected and spliced with other 'best matching' portions to create a spliced record. It should be noted that this method is entirely subjective, with no correlation coefficient presented during the comparison of correlation and reference curves. However, this is the standard method applied when splicing IODP records (Higgins *et al.* 2006; Pälike pers. comm.).

In order to perform reliable spectral analysis from sediment core data, certain factors must be in place / considered. Sedimentation rates must be accurately determined. In this case, the combined method using calcareous nannofossil biostratigraphy and *%N.pachyderma* (sin.) with ^{14}C AMS dating outlined above should provide accurate dates for the cores. It is important to consider that turbidites can also produce cyclical sediments, which may be mistaken for orbital cycles.

Spectral analysis of the $\delta^{18}O_{planktonic}$ curve of 9/97-10 and *N.pachyderma* (sin.) percentage data was performed using the software package AnalySeries 2.0. This core was selected for this analysis as it is at the centre of a grid of gravity core transects examined by Toms (in prep.). The data were de-trended and normalized prior to the application of a Blackman-Tukey algorithm. The resulting graph (see Chapter 5) enabled identification of orbital cycles, by comparison of the ratio of peak values to the Milankovitch ratio (100kyrs : 41kyrs : 23kyrs : 19.5kyrs). Identification of the strongest peaks (highest power) in the resulting graph identified the dominant cycles pacing variations in $\delta^{18}O_{planktonic}$.

3.6 Transfer function-based sea surface temperature reconstructions

Transfer functions and analogue methods have been applied extensively in palaeoecological studies (Imbrie and Kipp 1971; Sachs *et al.* 1977; Koç *et al.* 1993; Sabin and Pisias 1996; Pflaumann *et al.* 2003; Kucera *et al.* 2005). The use of transfer functions and analogue methods to estimate sea surface temperatures has been one of the most successful applications of this method (e.g. Imbrie and Kipp 1971; CLIMAP 1976; Kucera *et al.* 2005).

Some of the advantages of the transfer function method are that it is relatively inexpensive compared to obtaining equivalent geochemical data and does not necessarily require a full understanding of the ecology of every species used, as this is normally detectable following analysis of the dataset against the desired environmental gradient.

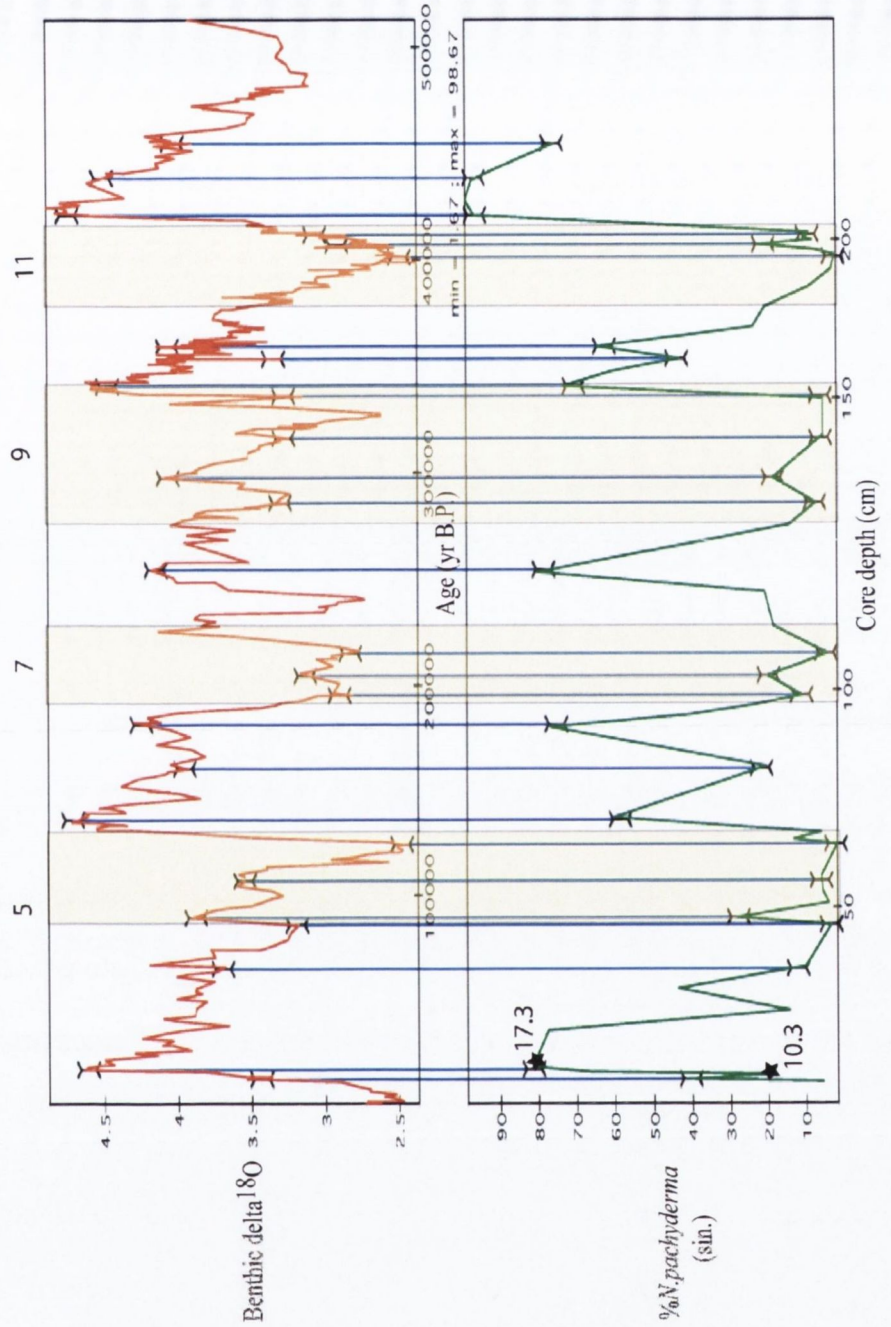

Figure 3.5. Wiggle-matching method employed to correlate the *%N.pachyderma* (sin.) curve (green line) from core 9/97-10 with the benthic $\delta^{18}O$ curve (red line) of McManus *et al.* (1999). Note that the core depth axis of the *%N.pachyderma* (sin.) curve has altered. Yellow shading indicates interglacials (odd numbers 5-11) as proposed by calcareous nannofossil biostratigraphy (Toms in prep.), with stars indicating radiocarbon dating points.

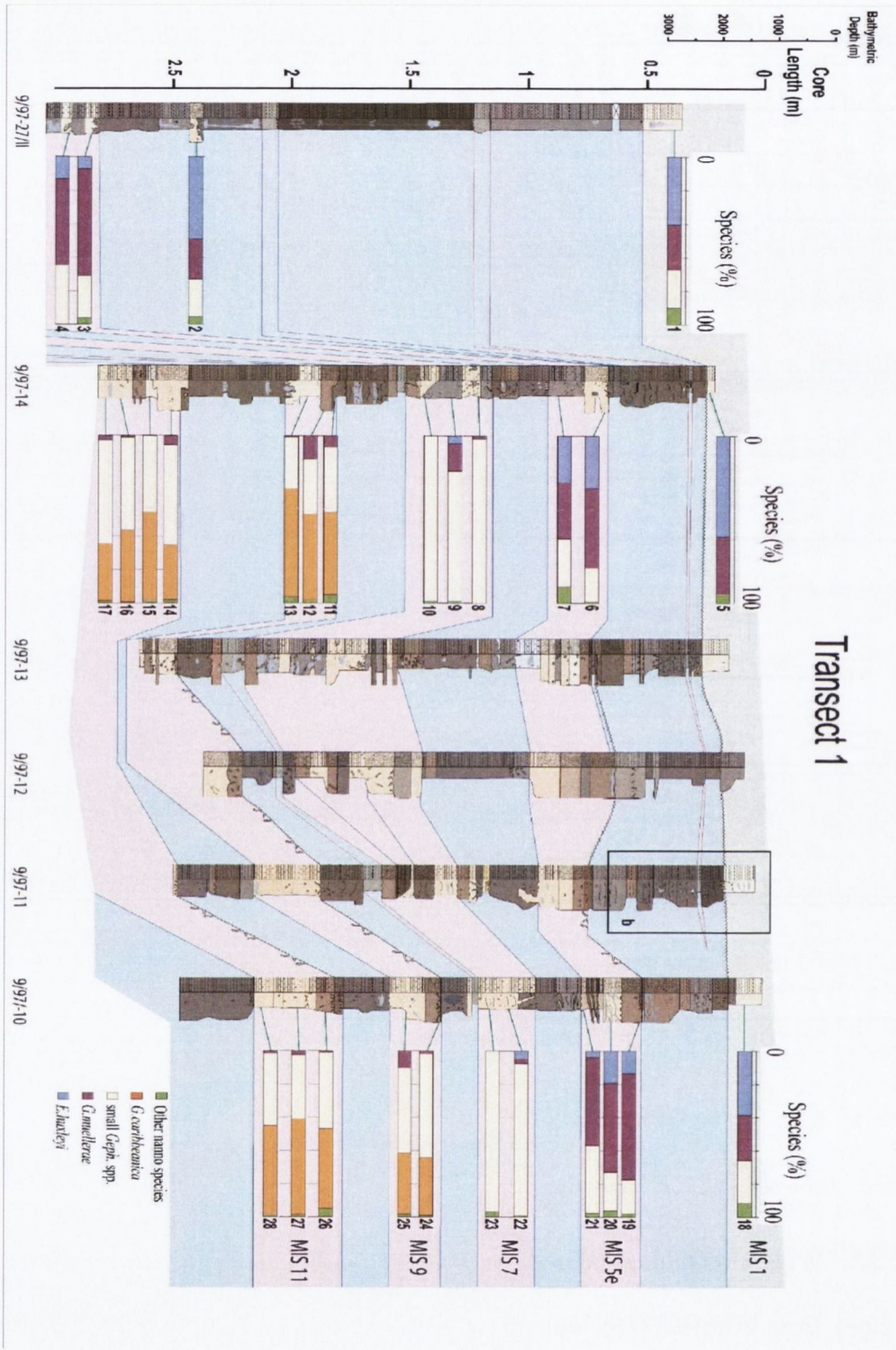

Figure 3.6. Calcareous nannofossil biostratigraphy of Transect 1, as proposed by Toms *et al.* (in prep.). Blue and pink background represents glacial-interglacial units respectively. Colours in bars represent the relative abundance of the calcareous nannofossil highlighted.

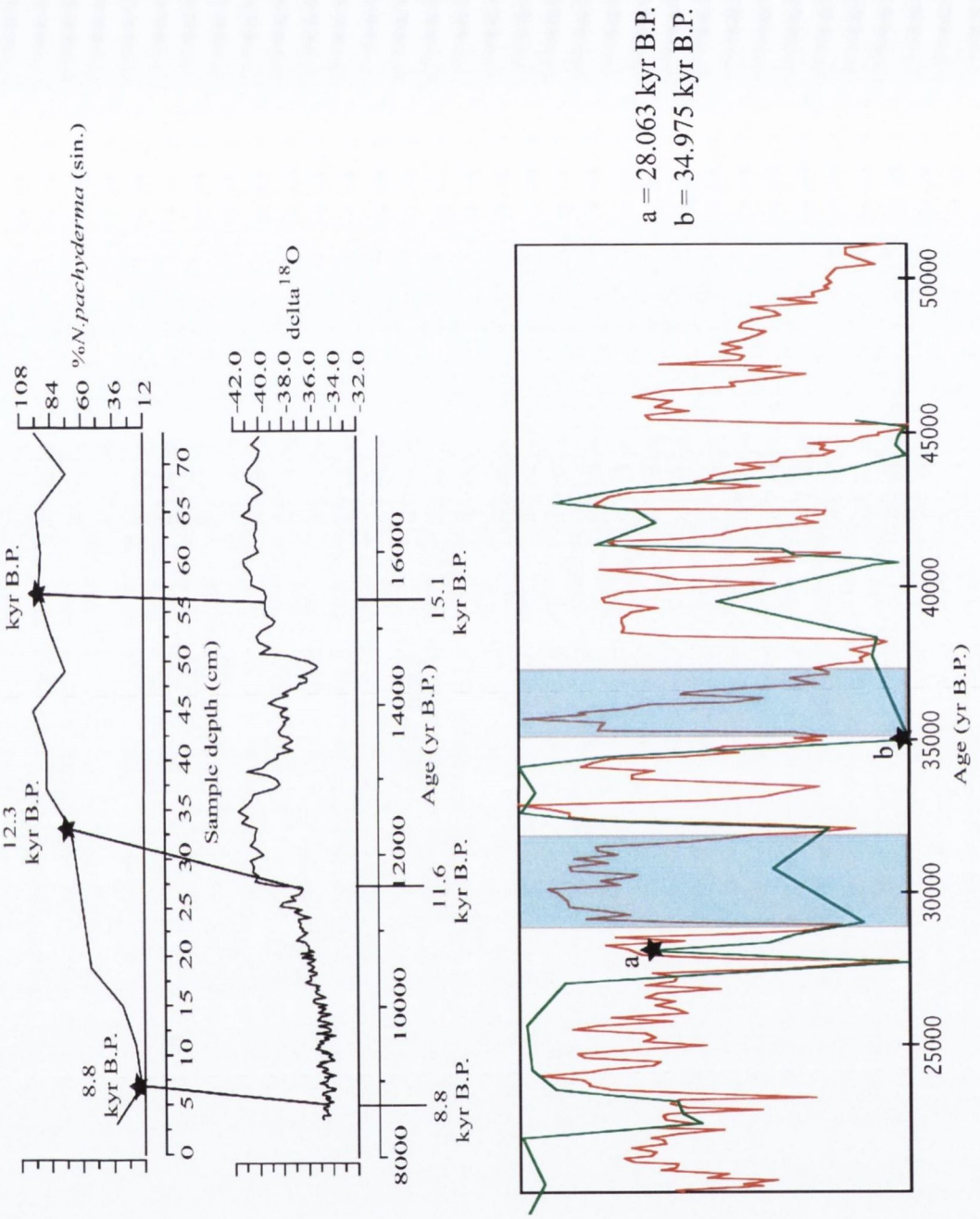

Figure 3.7. Calculation of reservoir ages using the correlation of *%N.pachyderma* (sin.) from core 9/97-27/2 (green line in lower panel) to GISP-II ($\delta^{18}O$, red line in lower panel). The letters a and b refer to uncorrected ^{14}C AMS radiocarbon dates provided by Toms (pers. comm.). Blue shaded areas represent absent stadials in the core 9/97-27/2 record.

It relies on the assumption that the group chosen are primarily affected by the stated environmental variable, although this assumption appears to be (mostly) valid with respect to planktonic foraminifera and sea surface temperature (Morey *et al.* 2005). If a species displays a strong correlation with a secondary variable, this species can be removed from the analysis.

It also relies on the acquisition and compilation of a large number of modern analogues (in this case, assemblages of planktonic foraminifera) and concurrent environmental data (sea surface temperature values) which adequately reflect the variation of fossil assemblages and the environmental conditions under which they formed. The fossil assemblages are then compared against the modern dataset using either a calibration or similarity approach (Guiot and de Vernal 2007). A few points need to be considered when discussing the results of a transfer function. Modern datasets are based on core-top assemblages of planktonic foraminifera (e.g. Pflaumann *et al.* 2003), but there is sometimes uncertainty regarding how 'recent' core top samples are (Andrews *et al.* 1999). Obtaining reliable sea surface temperatures is also potentially problematic, with some authors favouring mean annual temperatures (Morey *et al.* 2005) and others favouring seasonal (summer and winter) values (Pflaumann *et al.* 2003; Kucera *et al.* 2005). Which temperature value(s) are used is dependent on the desired information. If the purpose of applying the method is to determine the probability of sea-ice cover during different time intervals (for example), then applying seasonal values is more appropriate. However, as Morey *et al.* (2005) have shown, planktonic foraminifera are not strongly correlated with seasonal temperatures but are with mean annual temperatures. If obtaining a temperature value for a time interval is the aim, then applying mean annual temperatures is more appropriate.

Fossil assemblages can undergo a range of processes of post-mortem modification (e.g. dissolution, re-working) which have the potential to influence preserved assemblages. If evidence of post-mortem modification of assemblages is observed (e.g. fragmentation of tests, bioturbation) this will need to be considered when discussing the results of transfer functions. A dissolution interval (such as the MBDI, see Chapter 2) also has the potential to influence SST reconstructions, although it might be expected that this would result in cooler SSTs, following the dissolution series of Hemleben *et al.* (1989), which shows that colder taxa (in particular, *N.pachyerma* sin.) are more resistant to dissolution. If dissolution were occurring, it would be expected that this species would be preferentially preserved, biasing faunal census data and resulting in cooler reconstructed SSTs. In order to determine the adequacy of the modern training dataset to provide good modern analogues for the fossil assemblages, dissimilarity coefficients will be calculated. These provide a measure of the amount of dissimilarity between fossil and modern assemblages using the squared-chord method (Kandiano and Bauch 2003). In this study, the percentage of samples with a good modern analogue (within the 20% range) will be determined for each core.

Planktonic foraminiferal assemblages can also be used as an indirect proxy for the extent of perennial sea-ice cover in the past (Fig. 3.8). Kucera *et al.* (2005) demonstrated that areas of the North Atlantic which are perennially covered with sea-ice do not contain any (even small percentages, 0.3-1%) sub-polar species (specifically, *T.quinqueloba*, *G.bulloides* and *G.glutinata*). Therefore, any site (or sample) which contained only polar taxa (*N.pachyderma* sin.) was possibly under perennial sea-ice cover. This method assumes that preferential dissolution of the sub-polar species has not occurred.

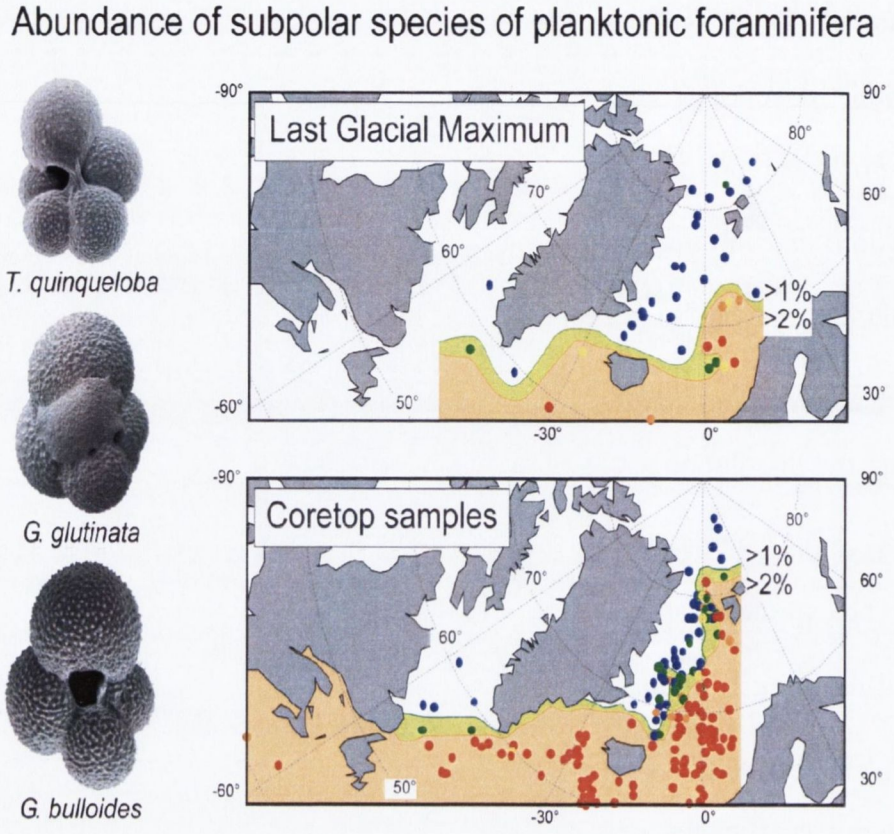

Figure 3.8. Diagram illustrating the expansion of sea-ice cover during the Last Glacial Maximum based on the distribution of the sub-polar species group (Kucera *et al.* 2005). Green shading = seasonal sea-ice, orange shading = open sea.

Transfer functions were performed on the relative abundance of planktonic foraminifera from the >150μm size fraction from six cores. These data were then compared to a modern, regional (i.e. North Atlantic only) training set consisting of 551 data points (Pflaumann *et al.* 2003) for Modern Analogue Technique (MAT), Weighted Averaging Partial Least Squares (WA-PLS) and Maximum Likelihood (ML). The training set data points consisted of modern SST values (summer and winter) coupled with modern assemblages of planktonic foraminifera. The data sets (modern data and fossil assemblages) were then loaded

onto a statistical software package (C2; Juggins 2003) and the analysis performed ('leave one out' provided cross-validation).

The Modern Analogue Technique (MAT) is a non-linear, constrained similarity transfer function (Guiot and de Vernal 2007) and has been used and modified extensively in previous studies (Hutson 1980; Prell 1985; Gersonde *et al.* 2005). The modern analogue technique employs the k-nearest neighbour algorithm. This algorithm attempts to reduce the number of distance estimations between samples. It uses the preserved assemblage data to evaluate which sample(s) from the training set it is closest too then assigns SST values (summer and winter) which reflects this. The limitations of the MAT in no-analogue conditions was demonstrated by Prell (1985), who used the CLIMAP database to reconstruct modern sea surface temperatures for some regions (e.g. the Pacific Ocean) and found that the technique did not perform adequately. The problems identified by Prell (1985) in producing reliable reconstructions of past SSTs have since been partially resolved. For example, regional databases covering each ocean now exist (Pflaumann *et al.* 1996; Kucera *et al.* 2005). Stricter criteria are now applied with respect to the selection / rejection of appropriate core-top samples (Kucera *et al.* 2005). Core-top samples are rejected on the basis of evidence of dissolution, incorporation of reworked material or not providing a recent assemblage. However, the problem of no-analogue conditions (Pflaumann *et al.* 1996) and the dominance of individual species (*N.pachyderma* sin.) at the colder end of the temperature range (Kucera *et al.* 2005) remain problematic.

Weighted averaging partial least squares (WA-PLS) is a calibration based regression technique that relies on species displaying a unimodal response to environmental parameters (Guiot and de Vernal 2007). This transfer function (or a modification of it) has also been used

in a previous planktonic foraminiferal transfer function study in Pacific and Atlantic Oceans (Morey *et al.* 2005). This method is particularly useful in evaluating the significance of secondary environmental parameters (such as salinity or productivity), which have been shown to have a relatively minor (compared to sea surface temperature) influence on the whole ocean dataset, but perhaps have a significant influence on polar assemblages of planktonic foraminifera (Morey *et al.* 2005)

Maximum Likelihood (Birks *et al.* 1995) has not been applied to planktonic foraminifera, but has been used as a complementary method to WAPLS and MAT in sea-level reconstructions (Horton and Edwards 2005). It is more regularly applied to computational phylogenetic studies (e.g. Longet and Pawlowski 2007). It is a useful method to apply when species display a unimodal response to an environmental variable (Birks *et al.* 1995) and, essentially, works by constructing a sample mean and variance, constructing a unimodal probability model from this and then selecting the most likely value that the fossil assemblage represents within this model. This is different from MAT, which only performs well within the limits of the modern analogue data and is very poor at extrapolating beyond this (Kucera *et al.* 2005).

3.7 Geochemical analysis

3.7.1 Planktonic foraminifera: *Globigerina bulloides* d'Orbigny 1826

The forty-nine planktonic samples selected for stable isotope analysis ($\delta^{13}C$ and $\delta^{18}O$) were taken from core 9/97-10 and prepared following the procedure outlined in Figures 3.2 and 3.9. This core was selected as it was considered to provide a good reference curve for

correlation with other cores in the study by Toms (in prep.). Each sample consisted of >20 specimens of *Globigerina bulloides*, from the 250-355μm size range with each sample weighing between 0.279 and 0.493mg. Specimens were carefully selected to ensure only pristine, 'glassy' specimens were chosen for analysis (Sexton *et al.* 2006). This involved picking specimens onto a droplet of water under LM and rejecting those that were opaque or 'frosty' in appearance. *G.bulloides* was selected for this analysis because it is common in almost all samples studied (see Appendix A), it has been used extensively in similar studies in this region (e.g. Peck *et al.* 2008), the ecology of this species is well documented (e.g. surface-dweller, size fractions (Spero and Lea 1996; Schiebel *et al.* 1997); genotypes (Darling *et al.* 2000); vital effects (Spero *et al.* 1997; Bemis *et al.* 1998)), it does not produce gametogenetic calcite (Bemis *et al.* 1998) and it does not interact with photosynthetic symbionts (Hemleben *et al.* 1989).

3.7.2 Benthic foraminifera: *Cibicides wuellerstorfi* (Schwager), 1866

The epifaunal species *Cibicides wuellerstorfi* was used for stable isotope analyses and prepared following the procedures outlined in Figures 3.2 and 3.6. Because the ecology of this species is well documented (e.g. Lutze and Thiel 1989), it has well established relationships to stable isotopes and trace metals of interest (i.e. Shackleton 1973; Boyle 1988; Martin *et al.* 2002; Hall and Chan 2003, 2004) and it is common at most depths along the transect studied (see Appendix B). For the stable isotope studies, >20 specimens from the >250μm size fraction were picked from each sample. Four cores were studied along a depth transect; 9/97-10, 9/97-04, 9/97-14 and 9/97-27/2. Only specimens that displayed no obvious signs of

abrasion and that appeared translucent under LM were selected for analysis and picked into tubes.

3.7.3 Analysis using the Continuous Flow – Isotope Ratio Mass Spectrometer (CF-IRMS)

The cleaned shell material (*G.bulloides* and *C.wuellerstorfi*) was weighed, and then poured into glass exetainers. These were then randomised (not in stratigraphic order) and placed onto the auto sampler (every five samples bracketed by two standards; Cranford dolomite and CO-1 or Carrara marble) of the Thermo Finnigan Delta Plus CF-IRMS in the

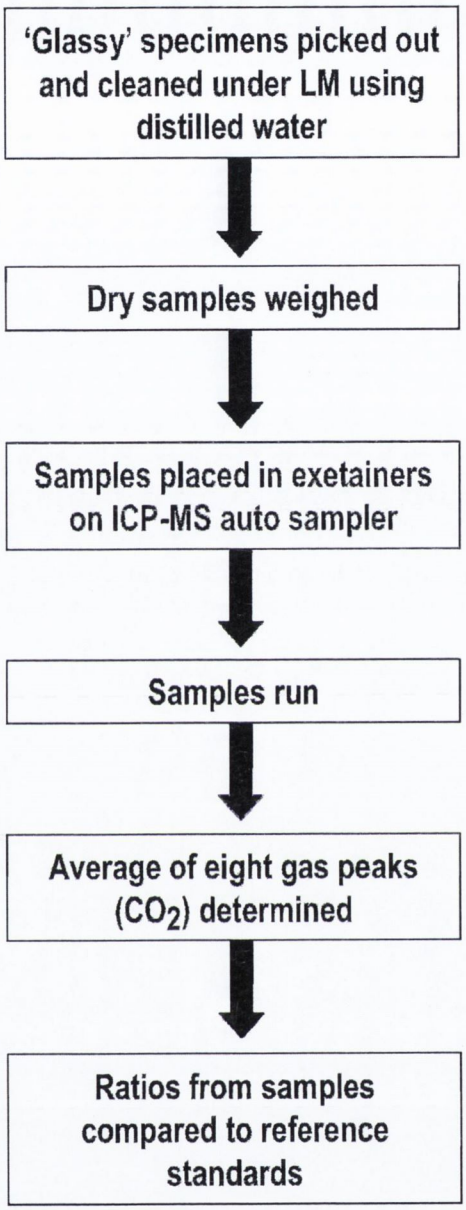

Figure 3.9. Flow chart indicates the procedure followed for performing stable isotope analyses using the CF-IRMS.

Geochemistry Laboratory at Trinity College Dublin. Each sample was dissolved dropwise in phosphoric acid (via injection into exetainers via the acid needle), releasing CO^2 gas which passed through a sampling tube in a stream of helium. This then entered the IRMS and was ionized in order to quantify the isotopic ratios of the samples and the reference material. Resulting values were reported as the mean value of the resulting eight gas peaks produced. Values of $\delta^{13}C$ and $\delta^{18}O$ were reported relative to VPDB (the "Vienna" Pee Dee Belemnite). Analytical precision was <0.1‰ and 0.03‰ for $\delta^{18}O$ and $\delta^{13}C$ respectively, comparable to other studies (e.g. Bauch *et al.* 2004).

3.7.4 Trace metal cleaning

It is important at all stages of the analysis that the samples are randomised (i.e. not in stratigraphic order); both during cleaning and the final analysis, to prevent cross contamination with samples which are adjacent in the stratigraphy (Boyle and Keigwin 1985). An outline of the cleaning procedure employed is provided in Figure 3.10.

Two glass plates were placed under a light microscope, with a large drop of deionised water (18.2MΩ) from an Elga PureLab OptionQ deionised water purifier placed on the surface of one plate. The foraminifera from the tubes were then picked onto the drop of water using a picking brush and the glass plates brought together carefully to crush the foraminifera until each of the chambers from every specimen was opened (it is not advisable to pulverise the tests at this stage as it makes the contaminant picking process more difficult). Once the tests were sufficiently crushed, contaminants were separated out. This involved picking out clay particles and manganese nodules (Fig. 3.11), which can bias the final trace metal signal. This

was completed using the light microscope set at a magnification of x32 and against both a white and a black background as manganese nodules are typically dark in colour, whereas clay particles tend to be lighter. Resulting material to be used for analysis was translucent (Fig. 3.12).

Material for the analysis was then 'painted' onto the inside of clean (acid-leached), labelled tubes (taking care not to touch the metal of the picking brush against the inside of the tube and contaminate the sample) and the sample was then left to dry overnight in an acrylic rack. The glass slides were then rinsed with deionised water and wiped clean with a paper towel, before the process was repeated with the following sample.

Samples that had completed the crushing and contaminant removal stage then underwent the clay removal step. The rack containing twenty-three or twenty-four tubes was placed in a Bassaire flow bench and each sample gently filled with deionised water (18.2MΩ). The entire rack was then gently tapped against the bench to encourage settling of the foraminifera sample to the bottom of the tube. Water was then siphoned off from each sample tube, after the siphon tip had been tip rinsed (three one second rinses with 10% HCl acid followed by three one second rinses with deionised H_2O). Great care was taken at this stage to avoid siphoning off the sample with the excess water. Once each sample had been siphoned, the tubes were one-thirds filled with deionised water, quickly tapped against the bench, and placed in an ultrasonic bath (Bransonic®) for sixty seconds. Afterwards, the rack was removed, shaken and tapped to encourage settling of foraminifera particles (but not clay particles) and the excess water siphoned off (again, after tip rinsing of the siphon tip). The samples were then refilled to one-third with deionised water before undergoing a further sixty seconds ultrasonic treatment. When the rack was removed from the ultrasonic bath, the order

of sample siphoning was altered from last time to remove cleaning bias from the final results. After sample siphoning, the samples were again filled to one-third with deionised water, ultrasonicated for sixty seconds and excess water siphoned off.

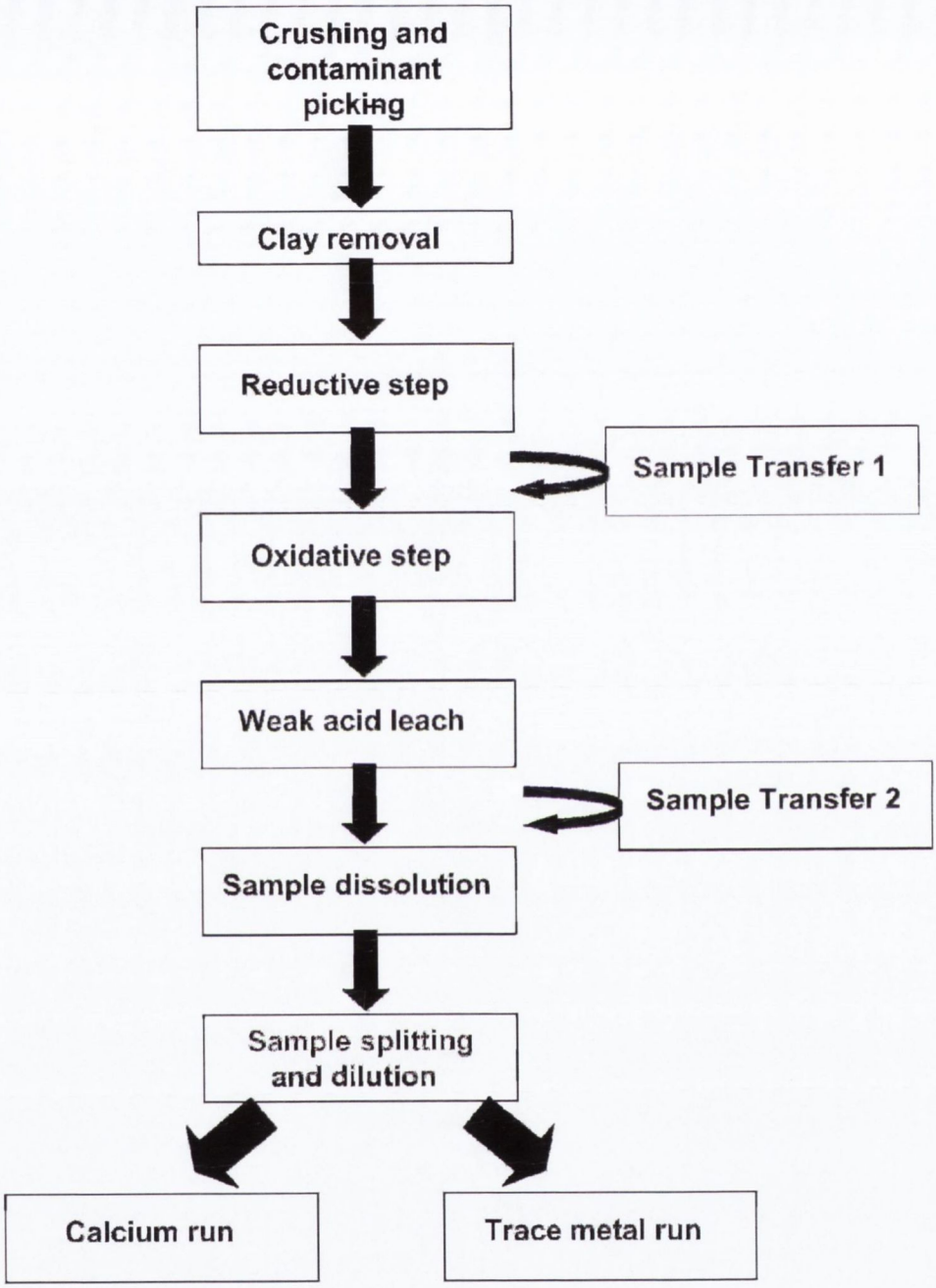

Figure 3.10. Flow-chart illustrating the procedure followed for cleaning and preparing samples prior to trace metal analysis using the HR-ICP-MS.

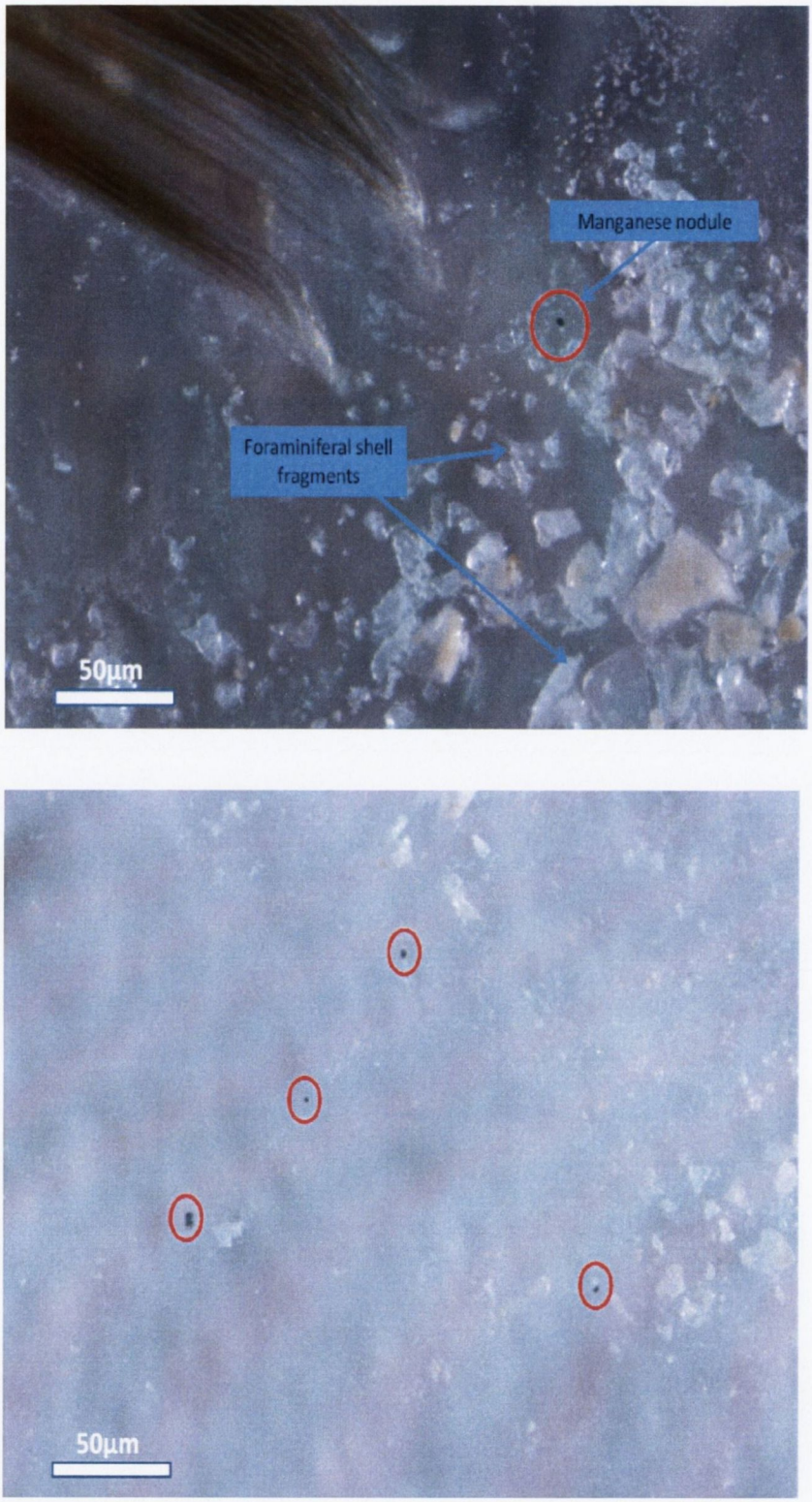

Figure 3.11. LM photographs highlighting contaminants (clay minerals and manganese nodules – inside red circles) that need to be removed during the contaminant picking stage.

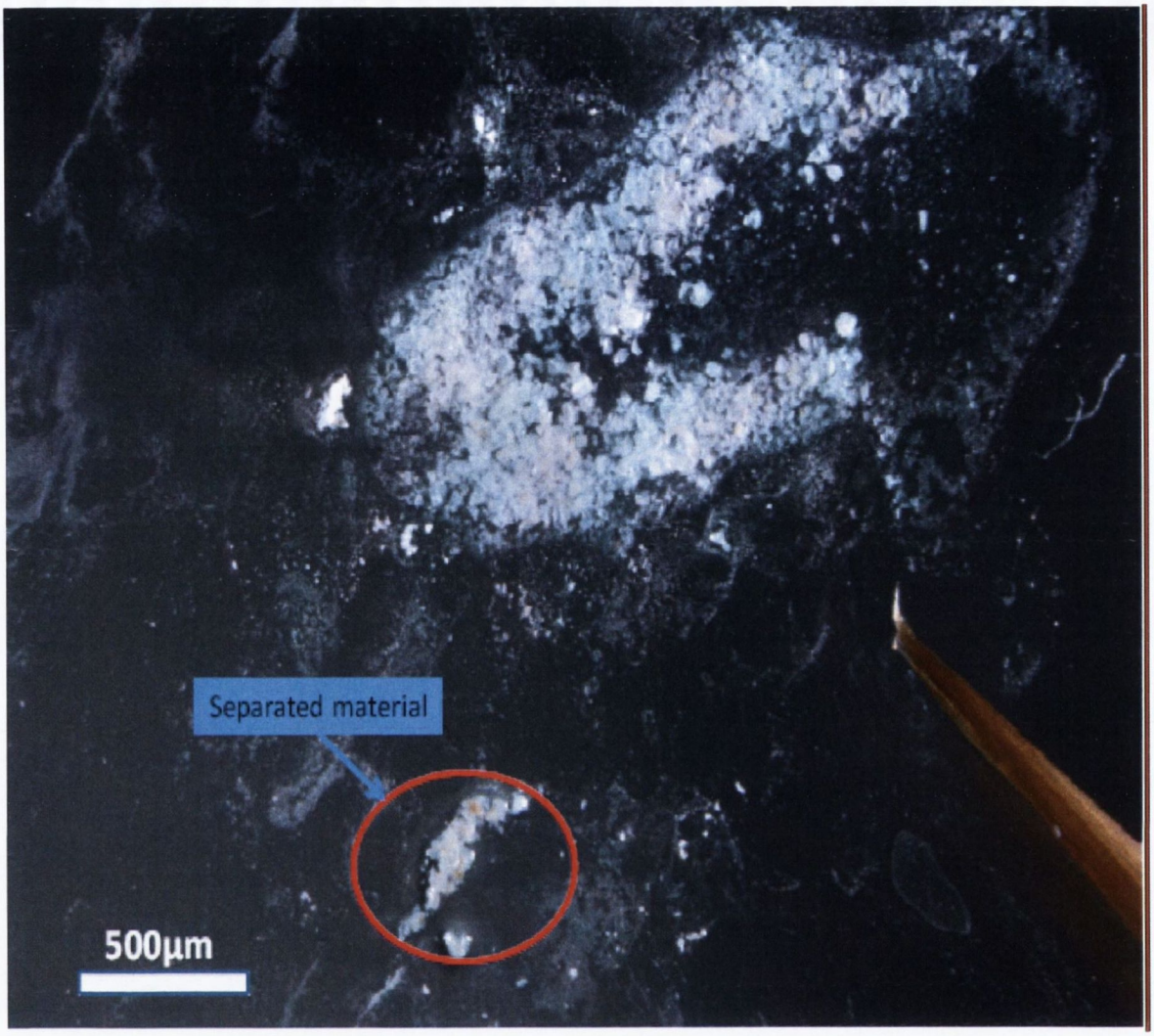

Figure 3.12. LM photograph showing the picked foraminiferal shell material and the separated contaminants.

Samples were then half filled with methanol, before undergoing one minute of ultrasonic treatment. The methanol was then siphoned off from each sample (taking care to observe that methanol is less viscous than water) and the methanol treatment was then repeated once, with the final siphoning taking care to remove as much methanol as possible.

Each tube was then filled to one-third with deionised water, quickly tapped to remove air bubbles, and ultrasonicated for one minute, before the excess water was siphoned off. This deionised water treatment phase was then repeated twice, after which the clay removal stage was completed. Ten samples were chosen at random and visually inspected under the light microscope for the presence of clay particles.

The rack was transferred from a flow bench to a fume cupboard for this stage. The purpose of this stage in the cleaning process is to remove any surface coatings from the foraminiferal tests, particularly those which would be preferentially enriched in the trace metals of interest (i.e. manganese oxide coatings preferentially enriched in cadmium; Boyle 1983). A 'casserole' dish was filled with deionised water and placed on a hotplate set at 90°C, after being rinsed with deionised water to remove any dust particles. A reducing reagent was then prepared, consisting of a mixture of 10ml Ammonia, 10ml Citric acid and ammonia mix (0.25M citric acid and ammonia solution) and 1200µl hydrous hydrazine. The ammonia and citric acid / ammonia solution were poured into the guest reagent bottle. Extreme caution was taken in the handling of the hydrous hydrazine and anything that came into direct contact with it, due to the highly toxic and extremely unstable nature of this particular chemical. Hydrous hydrazine was pipetted into the guest reagent bottle, using a tip rinsed pipette set at 600µl and the pipette tip was then expelled into a plastic bag specifically for hydrazine related waste. The guest reagent bottle was then inverted several times to mix the components. A paper towel was then placed under the rack to catch any of the solution that missed the sample tubes. A tip rinsed pipette, set at 100µl, was then used to introduce 100µl of the solution to each sample, taking care to close the lids of each of the caps firmly after filling. The pipette tip was then expelled into the hydrazine waste bag.

An acrylic plate was then bolted down on top of the sample tubes to ensure that the caps remained closed during the warm bath treatment to follow (ammonia has a high pressure when heated, making it necessary to use a bolted-down plate to ensure the caps remain closed). The rack was then placed into the 'casserole' dish for thirty minutes. Every two minutes during this thirty minute bathe, the rack was removed, tapped gently, placed in the ultrasonic bath for five seconds. After this, the rack was removed, tapped quickly and the cap tops checked to ensure that they all remained firmly closed, with the bolts tightened further as and when required.

The rack was removed from the hot water bath and the screws slowly and evenly undone and the plate lifted off. A pipette (set at 100µl) was tip rinsed, before each tube cap was carefully (with fore finger on tube cap and thumb slowly peeling back lid to avoid rapid gas release) released and the solution pipetted off into the guest reagent bottle (it is important not to merely siphon off the hydrous hydrazine at this stage, as it is highly toxic). The pipette tip was then expelled into the hydrazine waste bag.

Once this was completed for each sample, the tubes were half-filled with deionised water (with the caps also filled with deionised water). The caps were closed; the rack was then shaken and tapped to ensure the foraminiferal material settled. A tip rinsed siphon was then used to siphon off the water (including from inside the caps). This process of filling with water and siphoning off was then repeated twice.

The sample tubes were then half-filled with deionised water and placed into the hot water bath for five minutes. Meanwhile, the hydrazine waste was poured from the guest reducing reagent bottle into the hydrazine waste bottle stored in the refrigerator in the clean

lab. The guest reducing reagent bottle was then twice half-filled with deionised water and inverted vigorously several times before being dispensed into the sink. The paper towels used to mop up spilled hydrazine solution and the latex gloves used during the hydrazine handling process were then placed into the hydrazine waste bag, which was then sealed and double bagged before being placed in the waste bin.

After the samples had completed five minutes in the hot water bath, the rack was removed, quickly tapped and placed inside the ultrasonic bath for five seconds. After another quick tap, a tip rinsed siphon was used to siphon off the water. The sample tubes were then half-filled with deionised water (with the caps also filled) before the rack was tapped and the water again siphoned off. Each sample tube was then half-filled with deionised water (with the caps also filled with deionised water) before the rack was placed in the hot water bath for five minutes. After five minutes, the rack was shaken, tapped and ultrasonicated for five seconds. After a quick tap, a tip rinsed siphon was used to extract the excess water (including from the caps).

Because the reductive step (or the weak acid leach) can be potentially damaging to the sample tubes (due to the chemical treatment, as well as the heating), it is necessary at this stage to transfer the sample material to new, clean tubes to avoid contamination from damaged tubes.

The rack was transferred from the fume cupboard to the flow bench for this process. For each sample tube, a corresponding, clean sample tube was labelled in an adjacent rack. A scalpel was used to trim a pipette tip, removing approximately a quarter of the length from the tip at an angle of approximately 30° or 40°. The pipette tip was then double tip rinsed (six

rinses with 10% HCl, six rinses with deionised water), with the pipette set at 70µl. The tip was then held directly over the foraminiferal material at the base of the tube, with the plunger depressed fully. A rapid, short release of the plunger followed by the immediate removal of the tip from the water was normally sufficient to remove most of the particles from the tube bottom. This was then expelled into the corresponding, clean tube for the appropriate sample. The tip was examined closely to determine that there were no remaining foraminiferal particles, as was the original sample tube. The extraction process was repeated until no material visibly remained in the non-clean tubes, after which one final extraction step was undertaken. This process was then repeated for each sample. For this, the tip was double tip rinsed between each sample transfer, rather than a new tip used each time. Once each sample was transferred to clean tubes, a tip rinsed siphon was used to remove the excess deionised water.

The rack was transferred to the fume cupboard for this step in the cleaning process. The purpose of this stage is to remove any organic material from the foraminiferal material. A 'casserole' dish was filled with deionised water and placed onto a hotplate set at 90°C.

The oxidizing reagent was then prepared, which consisted of 15ml 0.1M NaOH mixed with 50µl H_2O_2. The NaOH was poured into the guest oxidizing reagent bottle, whereas the hydrogen peroxide was pipetted using a clean, tip rinsed pipette. The closed guest oxidizing reagent bottle was then inverted vigorously several times. A pipette, set at 250µl and tip rinsed, was then used to introduce 250µl of the reagent to each sample. The sample tube caps were then closed; the rack was tapped and then placed into the hot water bath for five minutes. After five minutes, the rack was removed, tapped and placed in the ultrasonic bath for five seconds. The rack was then removed and quickly tapped before being replaced into the hot

water bath for five minutes. After five minutes, the rack was removed, tapped against the bench and ultrasonicated for five seconds.

Then the tubes were opened and half-filled with deionised water (with the caps also filled with deionised water). The caps were closed, the rack tapped, and a tip rinsed siphon used to extract the excess water and oxidizing reagent from the tubes and the caps. This adding water – shaking – siphoning process was then repeated a further two times.

The rack was transferred to the flow bench for this step. A clean, tip rinsed pipette, set at 250µl was used to add 250µl of weak acid (0.002M HNO_3 Optima) to each sample. Tube caps were then closed and the rack tapped before being placed into the ultrasonic bath for thirty seconds. The rack was then removed, tapped and a tip rinsed siphon used to remove the acid. This process was then repeated a further three times, with the order of siphoning alternating between each repeat.

Tubes were then half-filled with deionised water (with the caps also filled with deionised water). The rack was then tapped before undergoing ultrasonic treatment for five seconds and the rack was then removed, tapped and a tip rinsed siphon used to remove the water from the tubes and the caps. Tubes were then half-filled with deionised water again (with the caps also filled with deionised water). Caps were then closed, the rack shaken and tapped, and a tip rinsed siphon used to remove the water from the tubes and the caps.

A clean, tip rinsed pipette was then used to remove any remaining water that had not been picked up by the siphon. A new, clean tip was used for each sample. Each sample was then transferred to new tubes as described above.

The tip rinse for this and subsequent steps changed from the previous method (three rinses in 10% HCl followed by three rinses in deionised water) to the following; three rinses in 10%HNO_3 (nitric acid) followed by three rinses in deionised water). This stage varies for each sample as some samples will dissolve more rapidly and in less acid than others. For consistency, the same process was used, with different samples requiring more treatment than others. Each sample had 170-250µl of acid (0.065M optima HNO_3) added at the start. The samples were then inverted four or five times before vortexing (Heidolph Reax top Vortex) for ten seconds. The sample tubes were then placed into a centrifuge (Hettich Zentrifugen Mikro 200) and centrifuged at 5000 rpm for three minutes. The samples were then left to stand in the rack in a flow bench for two hours.

After two hours, the samples were inverted and vortexed for ten seconds. The caps were then gently opened and closed to release any built up CO_2 that could be buffering the calcite dissolution. Each sample was then checked to determine the level of dissolution, between the following stages;

- Completely dissolved – no foraminiferal fragments visible
- Very nearly dissolved – two to seven foraminiferal fragments remain
- Mostly dissolved – eight to twenty foraminiferal fragments remain
- Little or no dissolution – more than twenty foraminiferal fragments remain

The following processes were then undertaken;

- Completely dissolved – removed to separate rack – no further treatment
- Very nearly dissolved – ultrasonicated for two hours
- Mostly dissolved – ultrasonicated for two hours

- Little or no dissolution – ultrasonicated for two hours, after addition of 50-100µl of additional acid.

After two hours, the samples were inverted, vortexed, opened and checked again. This time, the following steps were undertaken;

- Completely dissolved – removed to separate rack – no further treatment
- Very nearly dissolved – removed to separate rack – left overnight to complete dissolution
- Mostly dissolved – ultrasonicated for thirty minutes after addition of 25-100µl of acid
- Little or no dissolution – ultrasonicated for thirty minutes after addition of 50-125µl acid

The samples were then inverted, vortexed, opened and checked again and the above process repeated as necessary until every sample in the original rack had displayed sufficient progress in dissolving to the point where they could be left overnight without the requirement for additional acid or ultrasonic treatment.

Two clean sets of tubes labelled for trace element and calcium splits were placed in a rack on a flow bench. The dissolved samples were inverted, vortexed for ten seconds then placed into the centrifuge for three minutes at 5000 rpm. Each sample tube was then carefully brought over to the flow bench and the cap removed carefully (to avoid disturbing the pellet at the base of the tube). Using a fresh, double tip rinsed (six rinses in 10% HNO_3 followed by six rinses in deionised water) pipette for each sample set at 100ul to introduce 100ul of the dissolved solution into the sample tubes labelled for trace metal analysis.

Once the trace metal split had been transferred for each sample, the dissolved solution was re-centrifuged for a further three minutes at 5000 rpm. The sample tubes were then individually brought carefully over to the flow bench and the caps carefully removed. Using a fresh, double tip rinsed pipette for each sample, 10µl of the dissolved solution was added to the corresponding sample tube labelled for calcium analysis.

A clean, tip rinsed pipette, set at 190µl, was then used to add 190µl of 0.5M optima HNO_3 to each of the sample tubes labelled for calcium analysis. The calcium splits were then inverted and vortexed for five seconds before being placed in the centrifuge for three minutes at 5000 rpm.

The calcium splits were then analyzed in the High Resolution Inductively Coupled Mass Spectrometer (HR-ICP-MS – Thermo Finnigan Element XR) with Autosampler (Element Scientific SC E2). The samples were run with blanks (to correct raw intensities against background noise – important if dealing with low concentrations) and standards (24mM per litre calcite and 4mM per litre calcite – to track drift in the data and correct for it if necessary). This method only analyzed ^{43}Ca as ^{48}Ca suffers from interference in estimating abundance from ^{24}Mg (Riker pers. comm.). The purpose of this run is to correct for the matrix effect (Hieftje *et al.* 2002), which can interfere with trace metal analyses.

A new set of sample tubes were labelled for matrix-matched standards. A clean, double tip rinsed pipette was then used to pipette out standards totalling 350µl of standard (24 or 4mM) and acid (0.5M HNO_3). A fresh, double tip rinsed pipette was used if switching between the two standards or for switching from pipetting standard or acid.

Then 250µl of 0.5M optima HNO_3 was added to each trace element split using a clean, double tip rinsed pipette. Twelve blanks containing only 350µl 0.5M HNO_3 were also prepared, using a fresh, double tip rinsed pipette.

Each standard, trace element split sample and blank was then inverted and vortexed for five seconds. Trace element splits were then centrifuged for three minutes at 5000 rpm (this is not necessary for the blanks or standards). The samples were then run in the HR-ICP-MS. Samples were continuously checked through each run to observe any anomalous data points to ensure only plasma flicker was occurring and nothing more systematic affecting the whole batch. The resulting values were then presented as ratios, by comparing the relative intensities of the trace metals of interest against the calcium intensity (See Table 3.4). Calcium matching accuracy was ≥91%.

Trace element ratio	**Concentration**	**Max. RSD (%) (Precision)**	**Reproducibility**	**Comparable with**
Sr/Ca	mmol/mol	0.8	1%	Stoll *et al.* (1999), Yu *et al.* (2005)
Ba/Ca	µmol/mol	1	8.50%	Hall and Chan (2004)
Mg/Ca	mmol/mol	0.5	2%	Martin *et al.* (2002), Yu *et al.* (2005)
Cd/Ca	umol/mol	5	5.10%	Bertram *et al.* (1995)

Table 3.4. Precision and reproducibility of the trace element ratios of interest and comparable publications.

This study will employ a series of geochemical proxies in order to further understand the oceanographic processes that have influenced the formation of the contourite deposits on the Porcupine Bank. It is therefore necessary to understand precisely the information that could be derived from each and their limitations. Of particular interest is defining the position of key water masses through time and any changes in their properties. This section will break the proxy elements of the project down into separate components and discuss each in turn. The equations used to convert the raw trace metal and stable isotope data into the required parameters are presented in Appendix C.

Under dysoxic conditions, foraminiferal tests can develop manganese oxide coatings (Boyle 1983) and this can also cause preferential enrichment (e.g. Martin and Lea 2002; Tachikawa and Elderfield 2002) of some of the trace metals of interest (Cd/Ca and Ba/Ca). For this reason, any specimen that contained a Mn/Ca concentration greater than 150μmol/mol was excluded from this study. Also, if a linear correlation was observed between Mn/Ca and Cd/Ca values, these samples were rejected.

Sr/Ca ratios have the potential to act as a palaeothermometer, as has been observed in corals (Schrag and Linsley 2002), although this is probably not the case in benthic foraminifera (Martin *et al.* 1999). Variations in strontium concentration are also considered to reflect parameters such as sea-level change and particularly carbonate ion concentration as they co-vary with both of these parameters in the study by Stoll *et al.* (1999). Sr/Ca ratios are highly susceptible to dissolution (Stoll *et al.* 1999), so they were used as a tool to aid identification of samples which are likely to be dissolved. This assumes that variations in Sr/Ca are primarily due to changes in carbonate ion concentration.

Ba/Ca is a useful proxy for the concentration of refractory nutrients such as silica and alkalinity (Chan *et al.* 1977; Lea and Boyle 1989; Hall 2002), displaying a linear relationship with these two nutrients (e.g. Fig. 3.13). As Southern Component Water has a higher refractory nutrient content compared to Northern Component Water (Hall 2002), it should also have a higher barium concentration. It, therefore, has the potential to provide a supplementary tracer for water mass distribution along with Cd/Ca and $\delta^{13}C_{benthic}$ (see below). One problem that does occur when using Ba/Ca as a tracer is sedimentary barite formation (e.g. Bishop 1988) which can interfere with the bottom water signature. Hall and Chan (2002) proposed a value of 4μmol/mol, above which significant inorganic barite precipitation has probably occurred. Another potential issue with this tracer is that the precise mechanisms that cause Ba concentration to display a linear relationship with refractory nutrients is poorly understood.

Cd/Ca values can be used to calculate bottom water phosphorus concentrations using the equations developed by Boyle (1988, 1992) and applying the distribution coefficients used by Bertram *et al.* (1995) for the NE Atlantic Ocean. Cadmium is an excellent tracer of bottom water nutrients, having an almost identical water column profile as phosphate (Lacan *et al.* 2006; See Fig. 3.14), although the exact cause of this linear relationship (if it is not coincidental) is poorly understood at present. Southern Component Water contains higher concentrations of phosphorus and cadmium compared to Northern Component Water. The incorporation of cadmium into the calcite tests of some epifaunal foraminifera (i.e. *C.wuellerstorfi*) has been shown to occur in chemical equilibrium with the ambient water mass (Hester and Boyle 1982). A study by Elderfield *et al.* (1996) has shown that the rate of calcification of benthic foraminifera changes during life. This suggests that benthic foraminifera are an 'open' system, with the rate of reservoir "flushing" varying through their

lifetime. This implies that Cd/Ca values obtained from benthic foraminifera are average values for the lifespan of the foraminifera used. The rate of incorporation of cadmium does not appear to be directly influenced by changing temperature or salinity of the water mass (Marchitto *et al.* 2004). Alteration due to dissolution (McCorkle *et al.* 1995) has been observed but can be avoided through careful sample selection and preparation. Water depth and microhabitat can also influence the uptake of cadmium in benthic foraminifera (Tachikawa and Elderfield 2002) but the effects can be quantified (in the case of water depth) or avoided (in the case of microhabitat).

Most recent studies using cadmium as a tracer of Antarctic Bottom Water (AABW) flux in the Atlantic Ocean have focused on variations between the Holocene and Last Glacial Maximum (i.e. Marchitto *et al.* 2002).

This study examined the volumetric flux of AABW / AAIW (Antarctic Intermediate Water) in the NE Atlantic in response to stadial – interstadial variations observed in the GISP-II core. This follows up on the 'bipolar seesaw' hypothesis proposed by Broecker (1998) and enabled the response of deep water circulation to stadial – interstadial variations to be determined. This consisted of 2-3 cores being used to constrain the volumetric flux of AABW.

Phosphorus values reconstructed from foraminiferal Cd/Ca values using the equations of Boyle (1988, 1992) and Bertram *et al.* (1995) in this study were plotted against $\delta^{13}C_{benthic}$ and compared to the end-member compositions (Fig. 3.15) of Rickaby and Elderfield (2005), which were derived from previous studies (Boyle 1992; Lynch- Stieglitz *et al.* 1994; Lynch-Stieglitz and Fairbanks 1994; Bertram *et al.* 1995; Lynch-Stieglitz *et al.* 1995; Zahn *et al.*

1997). Oppo and Fairbanks (1987) identified a distinctive air-sea exchange signature in benthic $\delta^{13}C$, which the authors attributed to AAIW. This enabled AAIW influence to be distinguished from AABW when Cd/Ca and $\delta^{13}C_{benthic}$ are used in combination. This enabled the discrimination of distinctive water mass influences for each sample.

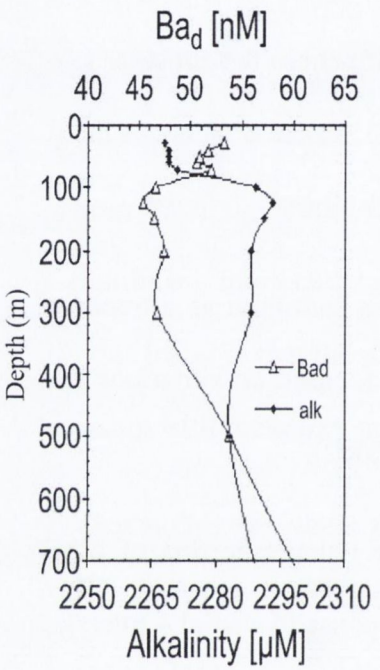

Figure 3.13. The relationship between the concentration of Barium and Alkalinity in the Pacific Ocean, from Jaquet *et al.* (2005).

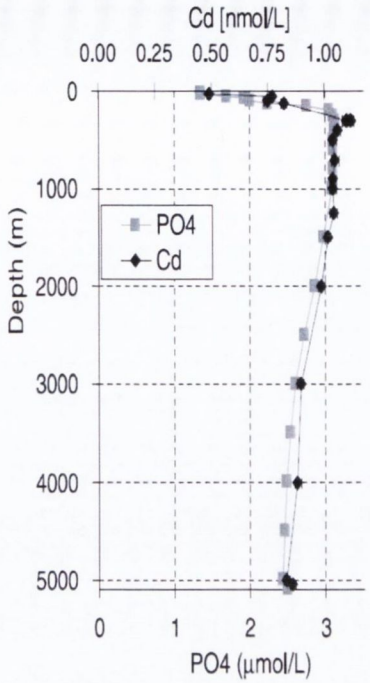

Figure 3.14. The relationship between the concentration of cadmium and phosphorus in the Pacific Ocean, from Lacan *et al.* (2005).

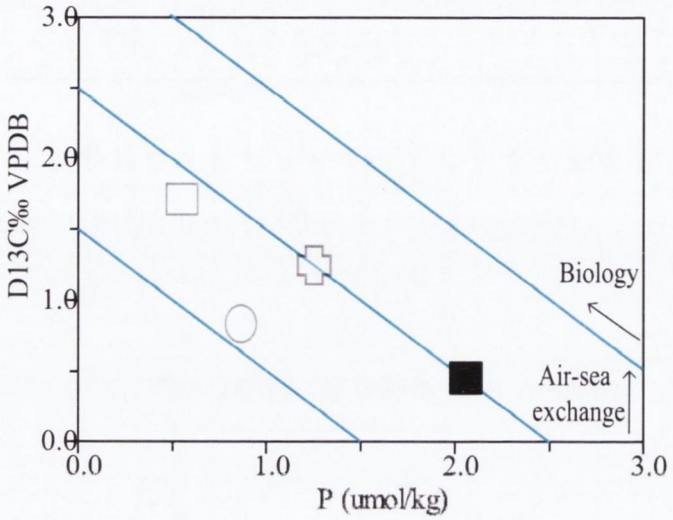

Figure 3.15. Plot of end-member compositions of different water masses, modified from Rickaby and Elderfield (2005). Open square = Glacial North Atlantic Intermediate Water, Open circle = Mediterranean Outflow Water, Open cross = North Atlantic Deep Water and Closed square = Antarctic Bottom Water. Mixing with Antarctic Intermediate Water would result in a distinctive air-sea exchange signature.

Mg/Ca ratios in foraminifera can be converted into palaeotemperatures (e.g. Rosenthal *et al.* 1997; Lear *et al.* 2000) due to the exponential relationship between Mg incorporation into foraminiferal calcite and ambient water temperature (Delaney *et al.* 1985). This method is only applicable in localities where a significant variation in temperature will occur, as there are currently large errors in absolute temperatures predicted from the calibration equation used by Martin *et al.* (2002). Mg/Ca ratios are also susceptible to dissolution (McCorkle *et al.* 1995) and appear to be affected by carbonate ion concentrations at the lower end of the temperature range (Bryan and Marchitto 2008). It is, therefore, not applicable for deeper

cores, where temperature variation is very slight. This study used the equation proposed by Martin *et al.* (2002) to calculate bottom water temperatures for this site (Fig. 3.16) but the primary aim for this was to combine the Mg/Ca derived palaeotemperatures with $\delta^{18}O_{benthic}$ to calculate $\delta^{18}O_{sw}$ (see below).

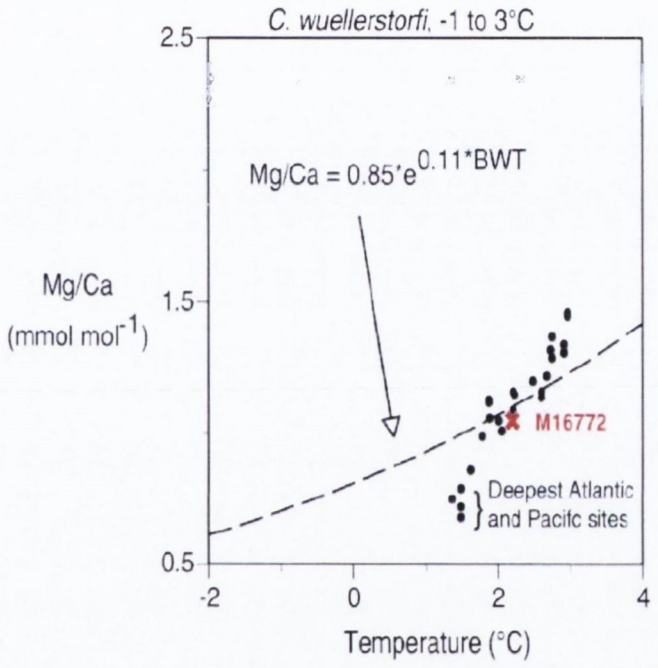

Figure 3.16. Proposed exponential relationship between Mg/Ca recorded in *C.wuellerstorfi* and temperature, as proposed by Martin *et al.* (2002).

Benthic oxygen isotope values are an extremely powerful palaeoceanographic tool (e.g. Shackleton 1974; Shackleton 1987; Lynch-Stieglitz *et al.* 1999; Siddall 2005). For this study, they were used to determine changes in bottom water density (from benthic derived $\delta^{18}O_{sw}$ values; Shackleton 1974) and surface temperature (from planktonic $\delta^{18}O$ values; Bemis *et al.* 1998). By combining the benthic data with reconstructed bottom water temperatures and

using the equation of Shackleton (1974) it was possible to calculate the $\delta^{18}O$ of seawater ($\delta^{18}O_{sw}$). As $\delta^{18}O_{sw}$ is strongly correlated with density (e.g. Lynch-Stieglitz *et al.* 1999), this provides a semi-quantitative estimate of changes in bottom water density through time for each core. Surface temperature estimates were derived from the species-specific $\delta^{18}O$-temperature equations developed by Bemis *et al.* (1998). Several factors need to be considered when applying this method, however (See Fig. 3.17).

Stable isotopes of carbon (^{13}C / ^{12}C) can be useful tools for determining the geographical origin of a deep water mass (Sarnthein *et al.* 1994; Lynch-Stieglitz *et al.* 2007) or extreme variations in productivity (Kennett *et al.* 2000; Spero and Lea 2002; Cannariato and Stott 2003) as well as identifying the position in the water column of planktonic organisms (see Fig. 3.18). Kennett *et al.* (2000) reported two strong negative carbon isotope excursions in benthic and planktonic foraminiferal data and attributed this to methane hydrate destabilisation in the Santa Barbara Basin. Methane hydrate releases have the potential to increase global temperatures and surface productivity (Dickens *et al.* 1995; Kennett *et al.* 2003). This interpretation has since been questioned by Cannariato and Stott (2003) who attributed the negative excursions to diagenetic processes. Several complicating factors hinder the use of $\delta^{13}C_{benthic}$ (Fig. 3.19). Microhabitat (Rathburn *et al.* 1996; Bickert and Wefer 1999) can significantly alter $\delta^{13}C_{benthic}$, but can be avoided by only using species with a known epifaunal microhabitat (i.e. *C.wuellerstorfi*). Enhanced productivity can also affect $\delta^{13}C_{benthic}$ isotope ratios. Schmiedl and Mackensen (1997)

studied $\delta^{13}C_{benthic}$ isotope ratio profiles from two cores from the Cape Basin, South Atlantic. The two sites have different upwelling characteristics, and this appears to have affected their $\delta^{13}C_{benthic}$ isotope profiles. It is important to quantify changes due to productivity variations

before using $\delta^{13}C_{benthic}$ isotope profiles to determine variations in deep water circulation. Dissolution is another problem (McCorkle *et al.* 1995), although this can be partially overcome by using a multi-proxy approach or by assessing the preservation state of samples examined.

One planktonic stable isotope ($\delta^{18}O$ and $\delta^{13}C$) profile for core 9/97-10 has been constructed, using the species *G.bulloides*. Stable isotopes of carbon were analysed to provide evidence that the specimens used had not formed their calcite away from the surface (see Fig. 3.18). Sea-surface temperature estimates have been derived from planktonic $\delta^{18}O$ via the species-specific relationship (see Appendix C) established by Bemis *et al.* (1998). Values for δ_{sw} were derived from Elderfield and Ganssen (2000). This should provide a suitable range of variation in δ_{sw} to cover the previous 500kyr B.P. as the Holocene and LGM (examined in Elderfield and Ganssen 2000) are considered to represent two of the warmest and coldest periods of the Late Quaternary (see Chapter 2).

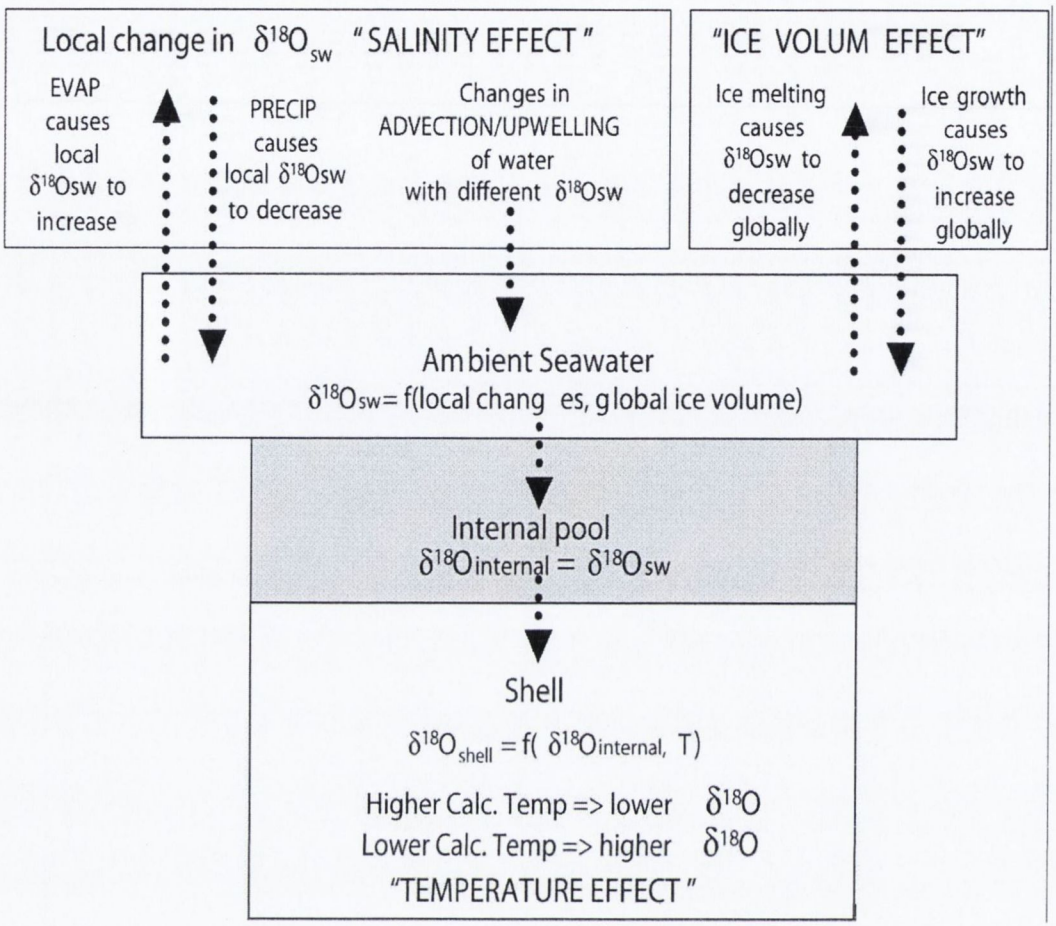

Figure 3.17. The effect of variations in ice volume, salinity (evaporation and precipitation) on $\delta^{18}O_{sw}$ and of temperature on $\delta^{18}O_{shell}$ from Ravelo and Hillaire-Marcel (2007). T = temperature and f = function.

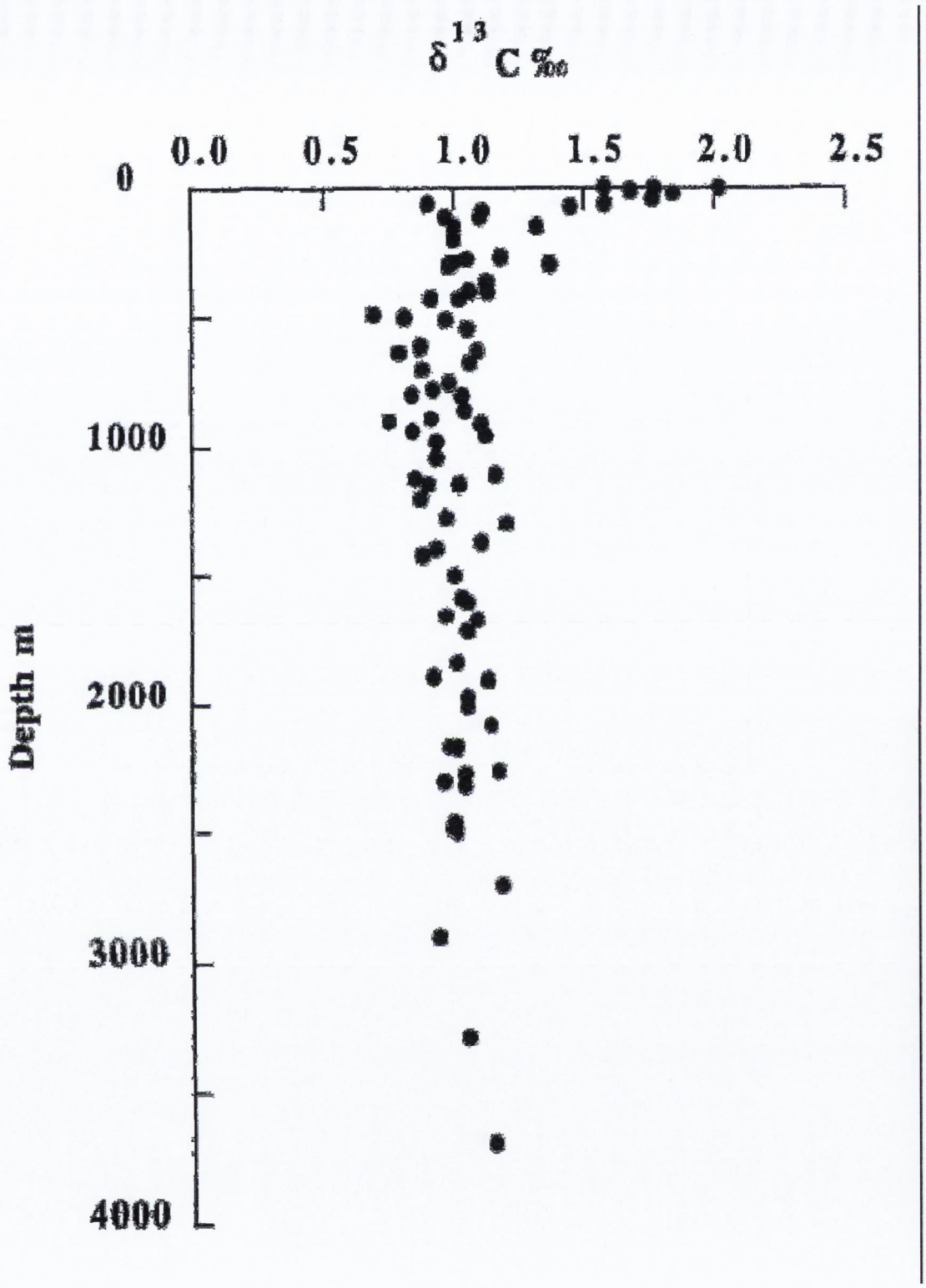

Figure 3.18. The distribution of $\delta^{13}C$ with water depth in the North East Atlantic Ocean, from Bertram *et al.* (1995).

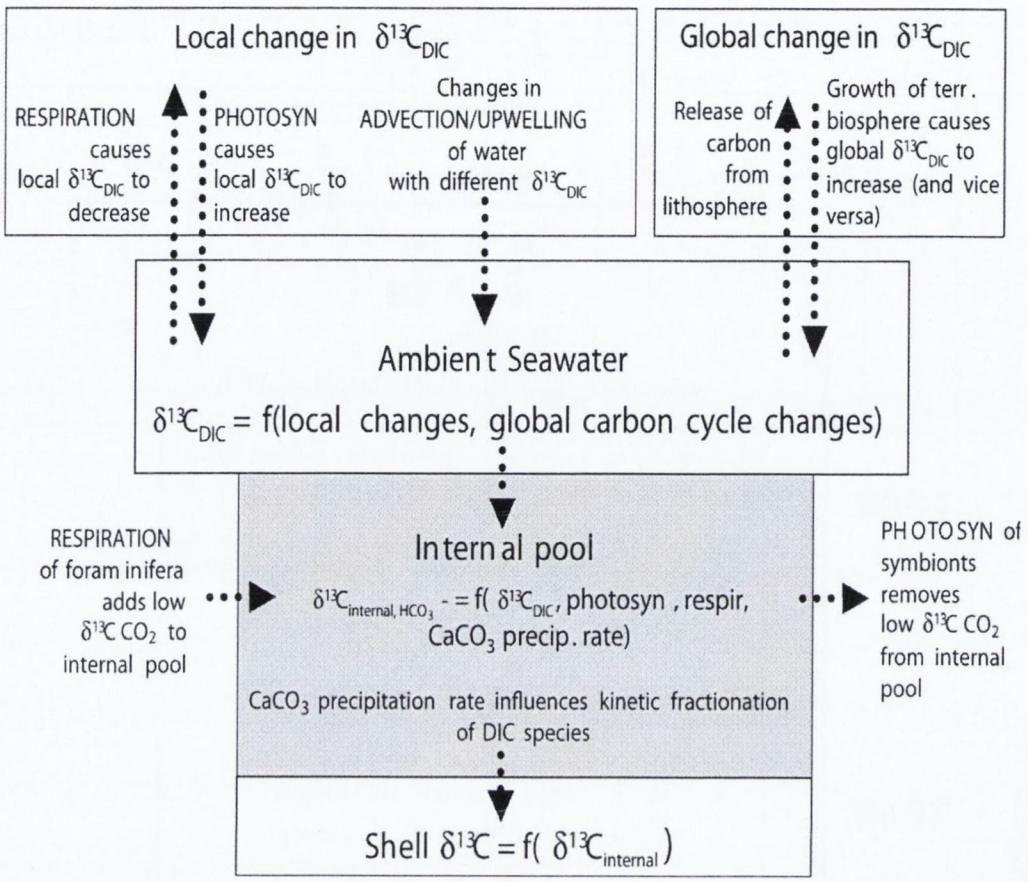

Figure 3.19. Illustration of the various factors that can influence $\delta^{13}C_{DIC}$ and $\delta^{13}C_{shell}$ from Ravelo and Hillaire-Marcel (2007).

3.8 Statistical analyses of data

3.8.1 Cluster analysis

Cluster analysis is a useful tool for grouping samples according to similarities in foraminiferal assemblages. Unconstrained Q-mode cluster analysis was used to determine (and qualify, via bootstrapping n=100) sample associations and disassociations. The method used Euclidean distance (combined with DCA) to evaluate which sample clusters were

consistent (see example Fig. 3.19). All samples with a specimen count lower than 75 and species that constituted <5% of preserved assemblages were removed prior to analysis (Fatela and Taborda 2002) when applying the Euclidean distance (Grieg-Smith 1983; Legrende and Gallagher 2001; Fatela and Taborda 2002).

3.8.2 Principle components analysis

Principle components analysis (PCA) is a useful data exploration analysis that presents the relationships between discrete samples (in this case, assemblages of foraminifera) in ordination space relative to an undetermined pair of component axes. The relative position of each sample along each axis is then considered to represent the influence of that component on the species composition of that sample. It is possible to plot the scores of individual species on top of this, to determine which species are influencing the distribution of the samples. This can aid the identification of the principle components, provided the ecological preferences of the species are well-defined.

For this study, PCA was performed on assemblages of benthic foraminifera using the PAST software application (http://folk.uio.no/ohammer/past/). Species which did not record a relative abundance greater than 4% were excluded from the analysis, as were samples which contained less than 75 specimens. Eigenvalues and the percentage of variance accounted for by each component were recorded (see Chapter 8).

It should be noted that PCA is a non-parametric analysis, so no prior knowledge of the principle components can be applied. Also, the method assumes that species or assemblages of species will have a linear or normal (Gaussian) relationship to the components (environmental variables).

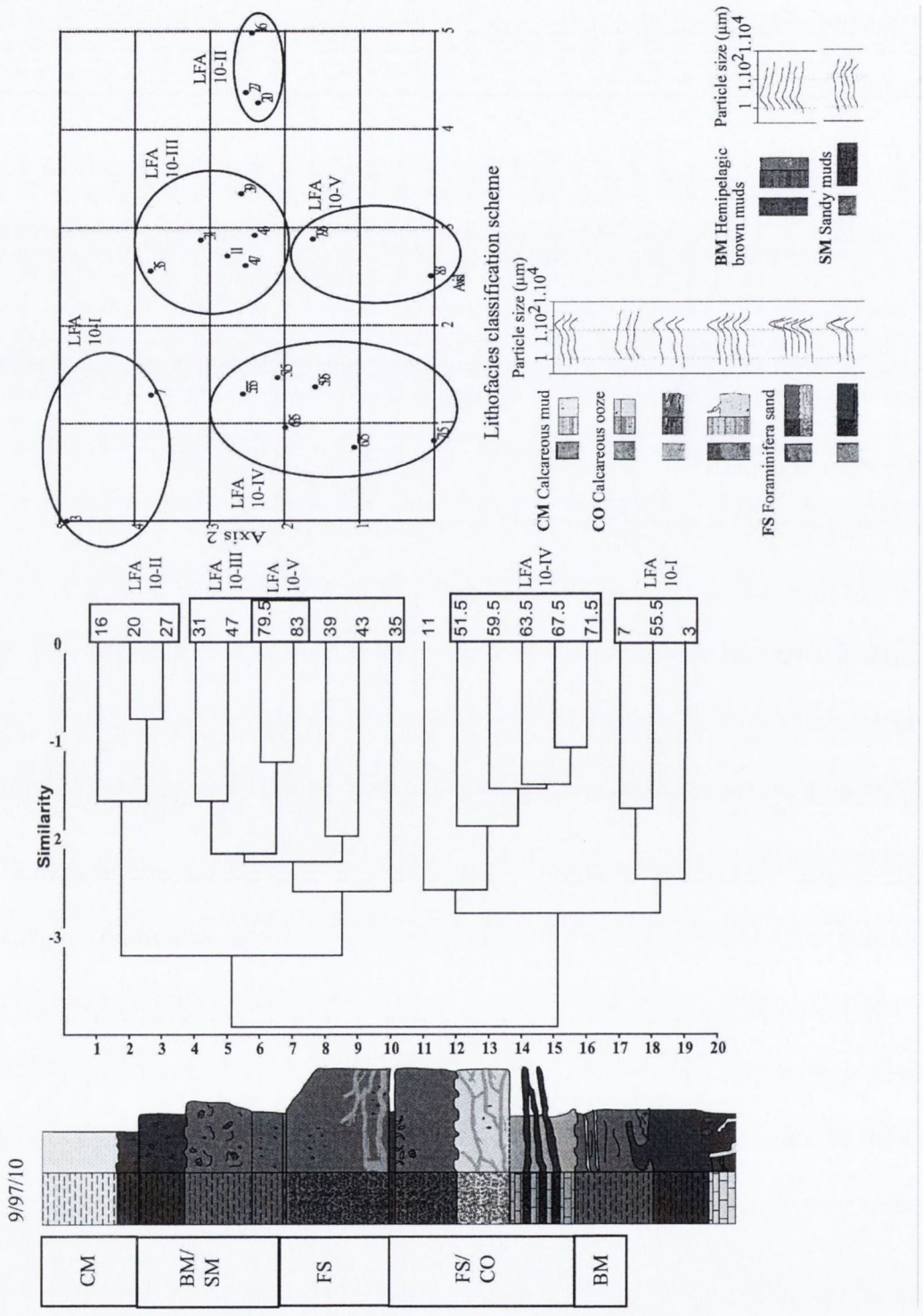

Figure 3.19. An example of the paired cluster and DCA method used to determine lithofacies assemblage zone groups (LFAZs) for core 9/97-10. The lithofacies classification scheme is courtesy of Toms (pers. comm.).

3.8.3 Detrended correspondence analysis

Detrended correspondence analysis (DCA) is a type of normalization method (Hill and Gauch 1980). It begins with a correspondence analysis, which plots the samples relative to each other in ordination space, following the calculation of eigenvalues for each sample based on the species content (Hill and Gauch 1980). This is then detrended, the arch effect common to correspondence analysis is removed. The plot results in similar samples plotting together and dissimilar samples plotting separately. This is a useful complementary analysis to cluster analysis (Birks 1992). DCA was used in combination with cluster analysis.

3.9. Ecology of benthic foraminifera

Knowledge of the ecology of modern benthic foraminifera will increase the information that can be gained from studying their fossil assemblages. Correlations between the relative abundance of benthic foraminifera species and productivity are now well established (Loubere 1991; Nees *et al.* 1997; Altenbach *et al.* 1999; Gooday and Hughes 2002). For non-symbiont bearing foraminifera, oxygenation of bottom waters and nutrient content are the controlling parameters on species distribution (Van der Zwann *et al.* 1999). However, most attention has focused on the potential of benthic foraminifera to provide quantitative estimates of palaeoproductivity (e.g. Herguera and Berger 1992; Altenbach *et al.* 1999).

This generally involved measuring changes in benthic foraminifera accumulation rate (BFAR) and assuming that every >150μm benthic foraminifera test deposited corresponded to

1mg carbon reaching the sea floor. This led to the equation, proposed by Herguera and Berger (1992) for quantifying primary productivity:

$$PP = Z*(31+1.06BFAR)/(100*[K+r\sqrt{Z}])$$

Where PP is primary production (in grams of carbon per square meter per year), Z is water depth, r and K are coefficients and BFAR is Benthic Foram Accumulation Rate (benthic foraminifera per square meter per thousand years).

The reliability of this method will depend on the taphonomic processes the benthic foraminifera assemblages have undergone. Also, the method will rely on the assumption that refractory nutrient supply is (and always has been) negligible in comparison to export production or co-varied. BFAR also does not currently account for variations in the seasonality of food supply, or the quality of organic matter that arrives at the sea floor (e.g. Guichard *et al.* 1999). For this study, the following equation (from Nees *et al.* 1997) was used to calculate BFARs:

$$\text{Specimens} \times \text{cm}^2 \times \text{kyr}^{-1}\ (\text{BFAR}) = \text{specimens} \times \text{gram}^{-1} \times \text{cm} \times \text{kyr}^{-1} \times \text{gram} \times \text{cm}^{-3}$$

Another method for quantifying flux rates has been devised by Altenbach *et al.* (1999). In this study, the authors were able to quantify organic matter flux versus primary productivity in several oceanic basins, and then compare these results to counts of benthic foraminifera.

Their results showed a positive correlation between *C.wuellerstorfi* relative abundance and organic carbon flux to the sea floor, when *C.wuellerstorfi* is restricted to a limited size range (>250μm; Figure 3.20). They also concluded that it is possible to link the relative dominance of different trophic groups (i.e. epifaunal, infaunal, opportunistic) to flux rates. Another important result is the definition of the range of flux rates occupied by each taxon. This enables threshold values of organic carbon flux to be established, providing upper and lower limits to flux rate estimates. Several other, less abundant species also display a strong correlation with flux rates (i.e. *Pyrgo murrhina, Pullenia bulloides* and *Uvigerina peregrina*).

However, the authors concluded that the presence / absence of certain species could not be used to obtain quantitative estimates of flux rates. Their study perhaps suffered from using data from regions under the influence of a range of oceanographic conditions. Also, more information is needed to determine the influence of oxygenation, seasonality and the quality of organic matter.

For this study BFAR is used as a qualitative estimate of palaeoproductivity rather than applying it as a direct proxy of primary production due to the large assumptions required to undertake this. The varied sedimentation rates that resulted from the correlation technique discussed above were used in calculating this, rather than assuming a linear sedimentation rate such as was employed by Nees *et al.* (1997).

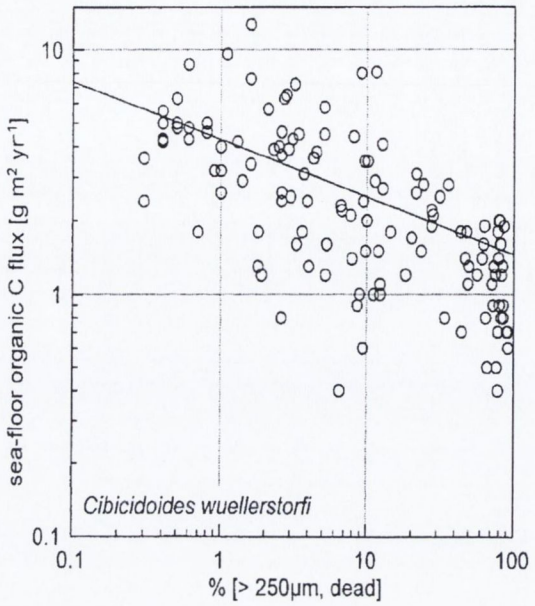

Figure 3.20. The proposed relationship between the percentage of *C.wuellerstorfi* from the >250µm size fraction and sea-floor flux rates, from Altenbach *et al.* (1999). Note the scatter around the linear trend line.

Chapter 4: Taxonomy

4.1 Introduction

Alcide d'Orbigny (1826) provided the first descriptions of the foraminifera as a separate group from the cephalopoda. Many of the taxonomic designations made in this publication are still valid today (e.g. *Globigerina bulloides* d'Orbigny 1826). Williamson (1858) provided a detailed description of several taxa (especially unilocular species). Brady (1884) described the species of foraminifera recovered from the Challenger expedition, which formed the basis of an updated version by Jones (1994).

Joseph Cushman produced a taxonomic framework for benthic foraminifera recovered from North Atlantic sediments during the early part of the 20th Century (i.e. Cushman 1911, 1923, 1940). Further new species were described by Phleger *et al.* (1953) and Barker (1960). Murray (1971) also contains plates and descriptions of some important taxa.

Jones (1984a and b) produced a taxonomic description of Late Quaternary benthic foraminifera from the Porcupine Bank region as part of a PhD thesis. The taxonomic descriptions produced for the unilocular taxa were published. Hermelin and Scott (1985) provide plates and morphological descriptions of 63 taxa from the central North Atlantic. Schönfeld (2006) is a detailed study of the biogeographic distribution of different taxa from the *Uvigerina peregrina* plexus in the NE North Atlantic. The plates and detailed morphological descriptions of the different members of the plexus enable each to be readily distinguished under LM (light microscopy). Schweiger (2006) provides a detailed taxonomic assessment of the species from the Cibicidid genus. Gooday and Hughes (2002) supply plates

and descriptions of some of the smaller taxa (i.e. *E.pusillus* and *N.iridea*). Struck (1992) contains plates of some important taxa likely to be observed in this region that are not covered by other publications. The NEAPACC CD-ROM (Austin and Evans 1999), contains photographs and brief morphological descriptions of some of the key taxa likely to be encountered in this region. For the planktonic foraminifera, the taxonomy outline by Kennett and Srinivasan (1983) and Hemleben *et al.* (1989) was followed as these are the taxonomic references used for transfer functions (see Chapter 6).

4.2. Taxonomic descriptions of benthic foraminifera

Siphotextularia rolhauseni Phleger and Parker 1951

Plate 1. Figs. 1a-b

Siphotextularia rolhauseni Phleger and Parker. Plate 1; Figs. 6-7; Description page 217 (Hermelin and Scott 1985)

Siphotextularia rolhauseni Phleger and Parker 1951, Plate 3; Figs. 13-16; Description page 59 (Jones 1984a)

Test elongate, slightly compressed in apertural view. Biserial, globose chambers. Finely agglutinated and finely perforate. Sutures depressed and distinct. Aperture sub-circular, surrounded by a raised lip.

***Eggerella bradyi* (Cushman 1911)**

Plate 1. Fig. 2

Verneuilina bradyi sp. nov. Fig. 87; Description page 54 (Cushman 1911)

Eggerella bradyi (Cushman 1933). Plate 5; Figs. 7-9; Description page 77 (Jones 1984a)

Test broad at distal end and tapering strongly towards the apical end. Chambers triserially arranged, globose with sutures depressed and clearly defined. Wall finely agglutinated, smooth and finely perforate. Aperture interiomarginal, arch-shaped and in contact with the basal suture.

***Karreriella bradyi* (Cushman 1911)**

Plate 1. Figs. 3a-c

Karreriella bradyi (Cushman 1911). Plate 5; Figs. 14-16; Description page 82 (Jones 1984a)

Karreriella bradyi (Cushman 1911). Plate 1; Fig. 8; Description page 212 (Hermelin and Scott 1985)

Test elongate, initially triserial but later chambers are biserially arranged. Sutures depressed and angle of taper low in the biserial portion and sutures elevated and angle of taper high in the triserial portion of the test. Chambers globular, fine-medium grained agglutinated composition, smooth surface, finely perforate. Aperture areal, slit shaped extending across the base of the final chamber adjacent to the basal suture, surrounded by a lip.

***Spiroloculina rotunda* d'Orbigny 1826**

Plate 2. Figs. 1a-b

Spiroloculina rotunda d'Orbigny 1826. Plate 1; Fig. 9; Description page 217 (Hermelin and Scott 1985)

Test ovate with sharply tapering ends, strongly compressed in cross-section. Wall surface is smooth. Chambers elongate and planispirally arranged. Sutures strongly depressed. Penultimate and final chamber are substantially wider than the initial chambers. Aperture is terminal, areal and located at the termination of a short, apertural neck. The aperture is sub-circular in outline.

***Quinqueloculina seminulum* (Linné 1758)**

Plate 2. Figs. 2a-b

Miliolina seminulum Linné. Plate 5; Fig. 6; Description page 157 (Brady 1884)

Quinqueloculina seminulum (Linnaeus). Plate 2; Fig. 2; Description page 24 (Part 6). (Cushman 1923)

Quinqueloculina seminulum (Linné). Plate 2; Fig. 3; Description page 216 (Hermelin and Scott 1985)

Test elongate-ovate in outline, with inflated elongate chambers. The test is sub-ovate to sub-trigonal in cross-section. Wall surface is smooth and glossy. Chamber arrangement is quinqueloculine. Sutures are very slightly depressed (if at all) and are distinct. Aperture is interiomarginal, loop-shaped and with a small tooth.

Diagnosis

This species differs from *Q.arctica* in lacking peripheral chamber compression. It lacks the striated test surface of *Q.striata* and is broader than *Q.stalkeri* and *Q.elongata*.

***Quinqueloculina arctica* Cushman 1933**

Plate 2. Figs. 3a-b

Quinqueloculina arctica Cushman 1933. Plate 5; Figs. 11-12; Description page 40 (Loeblich and Tappan 1953)

Quinqueloculina arctica Cushman 1933. Plate 2; Fig. 1; Description page 216 (Hermelin and Scott 1985)

Test elongate-ovate in outline, nearly as broad as it is long. The test is compressed sub-trigonal in cross-section. Wall surface is smooth and glossy. Chamber arrangement is quinqueloculine. Chambers are curved, elongate and compressed towards the periphery. Sutures are very slightly depressed and are distinct. Aperture is interiomarginal, loop-shaped and with a small tooth.

Diagnosis

This species is broader than *Q.stalkeri* and *Q.elongata.* It lacks the surface striations of *Q.striata* and the chambers are compressed towards the periphery, unlike *Q.seminulum.*

***Quinqueloculina striata* d'Orbigny 1826**

Plate 2. Fig. 5

Quinqueloculina striata d'Orbigny 1826. Plate 4; Fig. 2; Description page 29 (Part 6). (Cushman 1923)

Test elongate-ovate in outline, longer than it is broad. The test is compressed sub-trigonal in cross-section. Wall surface is glossy. Chamber arrangement is quinqueloculine. Chambers are curved, elongate and inflated. Chambers ornamented by very fine, sometimes discontinuous longitudinal ridges. Sutures are very slightly depressed and distinct. Aperture is interiomarginal, loop-shaped and with a small tooth.

Diagnosis

This species is more elongate than *Q.seminulum* and *Q.arctica*, and also has a clear surface ornamentation of surface striations, unlike *Q.stalkeri* and *Q.elongata.*

***Quinqueloculina stalkeri* Loeblich and Tappan 1953**

Plate 2. Fig. 4

Quinqueloculina stalkeri sp. nov. Plate 5; Fig. 12; Description page 40 (Loeblich and Tappan 1953)

Test elongate-ovate in outline, longer than it is broad. Test is sub-trigonal in cross-section. Wall surface is smooth and glossy. Chamber arrangement is quinqueloculine. Chambers are curved, elongate and inflated near the middle, but strongly compressed towards the periphery. Sutures are relatively indistinct. Aperture is interiomarginal and loop-shaped.

Diagnosis

Q.stalkeri is more elongate than *Q.seminulum*, *Q.arctica* and *Q.striata*. It has relatively indistinct sutures, unlike *Q.elongata*.

***Quinqueloculina elongata* Natland 1938**

Plate 2. Fig. 6

Quinqueloculina elongata Natland 1938. Plate 2; Fig. 2; Description page 216 (Hermelin and Scott 1985)

Test is elongate, significantly longer than it is broad. Test is ovate in cross-section. Wall surface is smooth and glossy. Chamber arrangement is quinqueloculine. Chambers are straight except at the apertural and adapertural ends of the test, where they curve strongly. Sutures are slightly depressed and distinct. Aperture is interiomarginal and elongate loop shaped with slightly raised lips.

Diagnosis

This species is more elongate than *Q.seminulum*, *Q.arctica* and *Q.striata* and has distinct sutures, unlike *Q.stalkeri*.

***Pyrgo murrhina* (Schwager 1866)**

Plate 3. Figs. 4a-b

Pyrgo murrhina (Schwager 1866). Plate 19; Figs. 6-7; Description page 71 (Cushman 1923)

Pyrgo murrhina (Schwager 1866). Plate 5; Figs. 22-24 (Phleger *et al.* 1953)

Pyrgo murrhina (Schwager 1866). Plate 8; Figs. 12-13; Description page 109 (Jones 1984a)

Test sub-circular to globose in outline, ovate in side view. Normally longer than it is broad. Wall surface is smooth, imperforate and porcelaneous. The periphery is angular, producing a

carina which surrounds the whole of the base and periphery of the final chamber. The carina edge has two very short, symmetrical projections at the base. Chamber arrangement spiroloculine, although this is obscured by the final chamber which extends over all of the previous chambers. Sutures are slightly depressed (if at all) and relatively indistinct. Aperture is terminal, areal and oval in outline. The aperture is sometimes surrounded by a slightly raised lip. A well-developed bifid tooth is present.

Diagnosis

P.murrhina is ovate in side view, unlike *P.sarsi* which is plano-convex. The aperture is surrounded by a raised lip, unlike *P.oblonga* and *Pyrgo* sp. 1. This species lacks the strong tapering at the periphery of the penultimate chamber and the short apertural neck of *P.*cf.*lacernula*.

***Pyrgo sarsi* (Schlumberger 1891)**

Plate 3. Fig. 3

Biloculina sarsi sp. nov. Plate 9; Figs. 55-59; Text-figs. 10-12; Description page 533 (Schlumberger 1891)

Pyrgo sarsi (Schlumberger 1891). Plate 8; Figs. 14-16; Description page 111 (Jones 1984a)

Test sub-circular to globose in outline, plano-convex in side view. Normally longer than it is broad. Wall surface is smooth, imperforate and porcelaneous. The periphery is angular, producing a carina which surrounds the whole of the base and periphery of the final chamber. Penultimate chamber is flattened so that the suture with the final chamber is slightly raised. Chamber arrangement is spiroloculine, but obscured by the final and penultimate chambers which envelop all of the previous chambers. The aperture is terminal, interiomarginal and is elongate-ovate in shape. The aperture contains a broad, bifid tooth which is flush with the basal suture with the previous chamber.

Diagnosis

This species is plano-convex in side view, unlike *P.murrhina*, *P.oblonga*, *Pyrgo* sp. 1 and *Pyrgo* cf. *lacernula*.

***Pyrgo oblonga* (d'Orbigny 1826)**

Plate 3. Fig. 1

Pyrgo oblonga (d'Orbigny 1826). Plate 5; Figs. 25-26 (Phleger *et al.* 1953)

Test globose in outline, ovate in side view. Normally longer than it is broad. Wall surface is smooth, imperforate and porcelaneous. The periphery is broadly rounded, lacking a carina,

although the base of the final chamber does sometimes have a broad spine projecting from the test surface. Chamber arrangement is spiroloculine, but obscured by the penultimate and final chambers. Suture slightly depressed and distinct. Aperture is terminal, areal and a broad loop-shape in outline. It contains a large, bifid tooth.

Diagnosis

This species is ovate in side view, unlike *P.sarsi*. The distinctive bifid tooth is not surrounded by a lip, unlike *P.murrhina*. The aperture is loop-shaped, unlike *Pyrgo* sp. 1 and the apertural neck of *Pyrgo* cf. *lacernula* is absent.

***Pyrgo* cf. *lacernula* (Schwager 1866)**

Plate 3. Fig. 2

Pyrgo lacernula (Schwager 1866). Plate 2; Fig. 5; Description page 216 (Hermelin and Scott 1985)

Test sub-globose in outline, ovate in side view. Longer than broad. Wall surface is smooth, imperforate and porcelaneous. The periphery is angular, producing a carina which surrounds the whole of the base and periphery of the final chamber. The carina edge has two very short, symmetrical projections at the base. Chamber arrangement spiroloculine, although this is

obscured by the final chamber which extends over all of the previous chambers. Penultimate chamber tapers strongly towards the base. Sutures are slightly depressed and distinct. Aperture is terminal, areal, raised slightly on a very short neck and surrounded by a lip. Aperture is sub-circular in outline.

Diagnosis

This species has a short apertural neck, unlike *P.murrhina*, *P.sarsi*, *P.oblonga* and *Pyrgo* sp. 1.

***Pyrgo* sp. 1**

Plate 3. Fig. 5

Test elongate-globose in outline, ovate to plano-convex in side view. Longer than broad. Wall surface is smooth, imperforate and porcelaneous. The periphery of the final chamber is angular, producing a carina which surrounds the base and periphery of the final chamber. The base of the carina is broadly crenulated. Chamber arrangement is spiroloculine, but obscured by the final and penultimate chambers which envelop all of the previous chambers. Sutures raised and distinct. Aperture is terminal, areal, and sub-quadrate in outline.

Diagnosis

This species has a sub-quadrate shaped aperture, unlike *P.murrhina*, *P.sarsi*, *P.oblonga* and *Pyrgo* cf. *lacernula*.

***Sigmoilopsis schlumbergeri* (Silvestri 1901)**

Plate 3. Figs. 7a-b

Sigmoilina schlumbergeri (Silvestri). Plate 5; Fig. 17 (Phleger *et al.* 1953)

Sigmoilopsis schlumbergeri (Silvestri). Plate 2; Fig.6; Description page 217 (Hermelin and Scott 1985)

Test elongate-ovate in outline, slightly longer than broad. Compressed in cross-section. Wall surface is agglutinated by fine to medium sized sand particles. Chamber arrangement is millioline. Sutures usually indistinct. Aperture is terminal, areal and oval.

***Triloculina tricarinata* d'Orbigny 1826**

Plate 3. Fig. 6

Triloculina tricarinata d'Orbigny 1826. Plate 2; Fig. 7; Description page 218 (Hermelin and Scott 1983)

Test elongate-ovate in outline, slightly longer than broad. Trigonal in cross-section. Wall surface is smooth and glossy. Chamber arrangement is quinqueloculine. Chambers are elongate and inflated. Sutures are slightly depressed and distinct. Aperture is areal, terminal and loop-shaped with a small tooth.

***Oolina apiopleura* (Loeblich and Tappan 1953)**

Plate 4. Fig. 1

Lagena apiopleura sp. nov. Plate 10; Figs. 14-15; Description page 59 (Loeblich and Tappan1953)

Oolina apiopleura Plate 1; Fig. 8 (Jones 1984b)

Monothalamous, test ovate, subcircular in cross-section. Chamber surface covered in strong, longitudinal ridges and grooves that extend from the base of the chamber towards the apertural

end. The ridges terminate after covering ¾ of the test. Above each of these grooves is a small pore, some of which appear to be amygdaloidal in outline. Short apertural neck.

Diagnosis

O.apiopleura differs from *O.hexagona*, *O.melo* and *O.squamosa* in only having longitudinal surface ridges as ornamentation. It possesses pores above and separate from each groove, unlike *O.heronalleni*? and *O.intercalata*.

***Oolina heronalleni?* Jones 1984**

Plate 4. Fig. 2

Oolina heronalleni? Plate 1; Fig. 16 (Jones 1984b)

Monothalamous, test ovate with rounded base and rounded apertural end. Sub-circular in cross-section. Chamber ornament consists of poorly developed longitudinal ridges. Ridges extend from the base and terminate before the apertutal end. Apertural neck is short, round and broad. Aperture is sub-circular.

Diagnosis

This species has a surface ornament consisting of longitudinal ridges, unlike *O.hexagona*, *O.squamosa* and *O.melo*. It does not possess the amygdaloidal pores of *O.apiopleura* or the long apertural neck of *O.intercalata*.

***Oolina hexagona* (Williamson 1858)**

Plate 4. Fig. 3

Lagena hexagona Williamson 1858. Plate 58; Fig. 33; Description page 472 (Brady 1884)

Lagena hexagona (Williamson 1858). Plate 4; Fig. 6; Description page 24 (Part 4). (Cushman 1923)

Oolina hexagona (Williamson 1858). Plate 14; Figs. 1-2; Description page 69 (Loeblich and Tappan 1953)

Oolina hexagona (Williamson 1858). Plate 33; Figs. 21-22; Description page 100 (McCulloch 1977)

Oolina hexagona (Williamson 1858). Plate 2; Fig. 10; Description page 214 (Hermelin and Scott 1985)

Oolina hexagona? Plate 1; Figs.17-18 (Jones 1984b)

Monothalamous, test ovate, with tapering apertural end terminating in a distinct apertural neck. Rounded base, sub-circular in cross-section. Chamber ornament consists of strongly developed longitudinal and lateral ridges resulting in a cancellate surface ornament.

Diagnosis

This species has a hexagonal surface ornamentation, unlike *O.apiopleura*, *O.heronalleni*?, *O.melo*, *O.squamosa* and *O.intercalata*.

***Oolina melo* (d'Orbigny 1826)**

Plate 4. Figs. 4a-e

Oolina melo d'Orbigny 1826. Plate 12; Fig. 8; Description page 71 (Loeblich and Tappan 1953)

Oolina cf. *melo* d'Orbigny 1826. Plate 35; Fig. 5; Description page 101 (McCulloch 1977)

Oolina melo (d'Orbigny 1826). Plate 2; Fig. 11; Description page 214 (Hermelin and Scott 1985)

Oolina sp. 1 Plate 1; Fig. 26 (Jones 1984b)

Monothalamous, test ovate with flattened base and tapering apertural end. Sub-circular in cross-section. Chamber ornament consists of poorly developed longitudinal and lateral ridges. Surface ornament reticulose, lateral ridges are straight initially from the base and curve towards the base towards the apertural end. Apertural neck is smooth and terminate in a small, sub-circular aperture.

Diagnosis

This species differs from *O.apiopleura*, *O.heronalleni*? and *O.intercalata* in having lateral surface ridges. The ridges are not raised strongly, unlike *O.squamosa* and are not hexagonally arranged as in *O.hexagona*.

***Oolina intercalata* Jones 1984**

Plate 4. Figs. 5a-b

Oolina intercalata sp. nov. Plate 1; Figs. 24-25 (Jones 1984b)

Monothalamous, chamber ovate, with finely tapering apertutal end and flattened, slightly rounded base. Sub-circular in cross-section. Series of longitudinal ridges and grooves. Three ridges are strongly developed and extend from the base to ¾ of the apertural neck. Other ridges are poorly developed and alternate between terminating before the apertural neck or

extending to the same distance as the three strongest ridges. Apertural neck is long (1/3 length of test), thin (1/7 width of test at broadest point) and ridged.

Diagnosis

This species has longitudinal surface ridges only, unlike *O.hexagona*, *O.squamosa* and *O.melo*. It possesses a long apertural neck, unlike *O.apiopleura* and *O.heronalleni*?

***Oolina squamosa* (Montagu 1803)**

Plate 4. Figs. 6a-b

Lagena squamosa Montagu. Plate 58; Figs. 28-31; Description page 471 (Brady 1884)

Lagena squamosa (Montagu). Plate 10; Figs. 3-4; Description page 51 (Part 4). (Cushman 1923)

Oolina squamosa (Montagu). Plate 13; Fig. 10; Description page 73 (Loeblich and Tappan 1953)

Oolina squamosa? Plate 1; Figs. 20-21 (Jones 1984b)

Monothalamous, test ovate with a strongly tapering apertural end. Sub-circular in cross-section. Chamber ornament consists of strongly developed longitudinal and lateral ridges which varies from reticular to cancellate between specimens, but is consistent across the whole

of the chamber wall. Apertural neck is short, smooth and terminates in a small, sub-circular aperture.

Diagnosis

This species differs from *O.apiopleura*, *O.hexagona*, *O.heronalleni*?, *O.melo* and *O.intercalata* in having a strongly developed cancellate surface ornamentation.

***Lagena sulcata* (Walker and Jacob 1789)**

Plate 6. Fig. 2

Lagena sulcata Walker and Jacob 1789. Plate 57; Fig. 33; Description page 462 (Brady 1884)

Lagena sulcata Walker and Jacob 1789. Plate 9; Fig. 5; Description page 23 (Cushman 1913)

Unilocular, ovate in outline, subcircular in cross-section, tapering towards the apertural end. Base flattened, chamber surface ornamented by longitudinal costae. The costae (approximately) halve in number via joining as the chamber tapers. Aperture terminal, present at the termination of an apertural neck, and is sub-circular in outline.

Diagnosis

L.sulcata differs from *Lagena* sp. 1 in having a less laterally compressed test and from *Lagena* sp. 2 in having more than eight longitudinal surface ridges which are not separated by strong grooves.

***Lagena* sp. 1**

Plate 6. Fig. 4

Test unilocular, subcircular in outline tapering towards the apertural end. Chamber surface (including apertural neck) covered in strongly developed, evenly spaced longitudinal grooves and ridges (normally 8 of each). Base of test is flat. Aperture, present at termination of apertural neck, is subcircular in outline.

Diagnosis

This species has eight longitudinal surface ridges and grooves as surface ornamentation, unlike *L.sulcata* and *Lagena* sp. 2.

***Lagena* sp. 2**

Plate 6. Fig. 6

Unilocular, elongate-ovate in outline, tapering towards the apertural end. Chamber surface (including apertural neck) covered with evenly spaced longitudinal ridges (approximately 6 ridges per test). Base of test is flat. Aperture, present at termination of apertural neck, is subcircular in outline.

Diagnosis

This species has less than eight longitudinal ridges and grooves as surface ornamentation, unlike *L.sulcata* and *Lagena* sp. 1.

Fissurina varioperforata **(Buchner 1940)**

Plate 5. Figs. 5a-b

Fissurina varioperforata parvicarinata subsp. nov. Plate 3; Figs. 14-15 (Jones 1984b)

Monothalamous, test sub-circular with rounded base and tapering apertural end. Compressed in apertural view, carina narrow, translucent and is present from the base to the top of the apertural neck. Pronounced apertural neck. Aperture, a narrow slit. Surface ornament consists of small pits covering the body of the chamber, but not the carina.

Diagnosis

This species has small pits covering the main body of the test, unlike *F.marginata*, *F.porcupinensis* sp. nov., *Fissurina* sp. 1 and *Fissurina* sp. 2.

***Fissurina marginata* (Montagu 1803)**

Plate 5. Figs. 1a-b

Lagena marginata Walker and Boys. Plate 59; Figs. 21-23; Description page 476 (Brady 1884)

Fissurina marginata (Montagu). Plate 14; Figs. 6-9; Description page 77 (Loeblich and Tappan 1953)

Fissurina marginata (Montagu). Plate 2; Fig. 17; Description page 208 (Hermelin and Scott 1985)

Monothalamous, test sub-circular, compressed in apertural view. Carina narrow and translucent. Slightly pronounced aperture, a narrow slit with an entosolenian tube.

Diagnosis

This species lacks the distinctive pitted and amygdaloidal surface ornamentation of *F.varioperforata* and *F.porcupinensis* sp. nov. and the ridged surface ornamentation of *Fissurina* sp. 1 and *Fissurina* sp. 2.

Fissurina porcupinensis **sp. nov.**

Plate 5. Figs. 3a-b; Figure 4.1

Holotype

Specimen extracted from core 9/97-08 (Latitude -14.97°E, Longitude 52.60°N; 819m water depth). Deposited at the Geological Museum, Trinity College Dublin, Ireland. Accession number TCD.59223 (1).

Paratypes

Eight specimens extracted from cores 9/97-08 and 9/97-10. Deposited at the Geological Museum, Trinity College Dublin, Ireland. Accession numbers TCD.59223 (2-9).

Monothalamous, test subcircular, compressed in apertural view. Keel very narrow and translucent. Pronounced apertural neck, with keel extending two-thirds of the distance of the neck. Aperture is small and sub-circular in shape. Surface ornament consists of amygdaloidal

pores covering the body of the chamber and the peripheral carina. Each pore on the main body is depressed from the main body and surrounded by a fine, radiating surface ornament, within a cancellate framework. This results in a cancellate surface ornament being observed under LM (Fig. 4.1).

Diagnosis

Fissurina porcupinensis sp. nov. is distinguished from all other species of the genus by the highly developed and distinctive surface ornamentation. The species also differs from *F.marginata* in possessing a pronounced apertural neck. It also lacks the small perforations covering the main body of the test in *F.varioperforata.*

Distribution

This taxon is observed only on the shallower to intermediate sections of the slope in this study (cores 9/97-08, 9/97-10 and 9/97-04). The highest absolute abundance of this species (13 specimens) is observed in core 9/97-08, at 23cm depth. It is present in low numbers (1-2 specimens) in core 9/97-10 and moderate numbers (1-8 specimens) in 9/97-04.

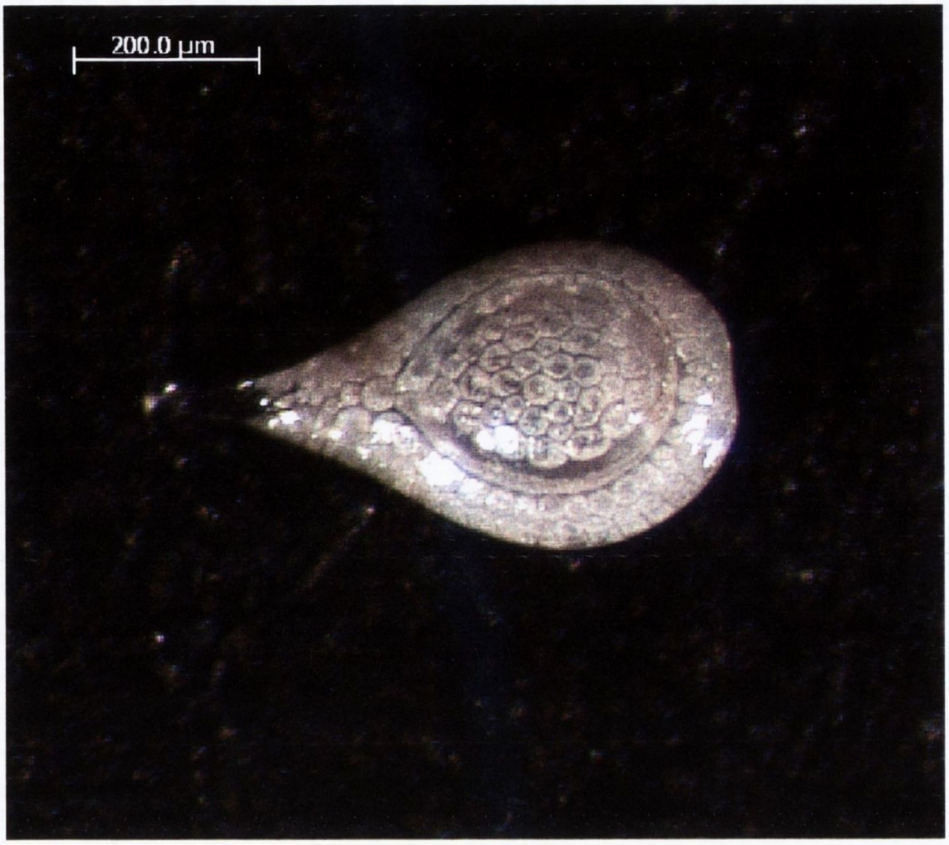

Figure 4.1. Light microscope image of *Fissurina porcupinensis* sp. nov. Note the distinctive surface ornamentation.

***Fissurina* sp. 1**

Plate 5. Fig. 4

Monothalamous. Test sub-circular with rounded base and tapering apertural end. Compressed in apertural view. Carina narrow, translucent and is present from the base to the aperture. Aperture is narrow slit. In side view, body of the chamber has three prominent ridges, one central ridge which extends from the aperture to the base of the chamber and two either side which join up at the basal end of the central ridge. Surface texture of main body is smooth.

Diagnosis

This species has three distinctive surface ridges as ornamentation, unlike *F.varioperforata*, *F.marginata*, *F.porcupinensis* sp. nov., and *Fissurina* sp. 2.

***Fissurina* sp.2**

Plate 5. Fig. 2

Monothalamous, test sub-circular with rounded base and rounded apertural end. Compressed in apertural view, carina narrow, translucent and is present from the base to the aperture. Aperture is narrow slit. Body of the test is covered in poorly developed longitudinal ridges which run discontinuously from the base to the apertural end.

Diagnosis

This species lacks the apertural neck of *F.varioperforata* and *F.porcupinensis* sp. nov. It has a surface ornament of more than three longitudinal ridges, unlike *F.marginata* and *Fissurina* sp. 1.

***Pseudofissurina mccullochae* Jones 1984**

Plate 6. Figs. 1a-b

Pseudofissurina mccullochae gen. et sp. nov. Plate 4; Figs. 25-26 (Jones 1984b)

Unilocular, subcircular in outline. Strongly compressed in apertural view. Wall smooth, finely perforated (apart from the carinae). Tricarinate, with central carina the most laterally extensive. Aperture is narrow slit in apertural view, with oral lip (usually) slightly more extensive.

***Solenina radiata* (Seguenza 1862)**

Plate 6. Figs. 5a-b

Solenina radiata amygdaloides subsp. nov. Plate 5; Figs. 11-12 (Jones 1984b)

Unilocular, test elongate-ovate in outline, hyaline and compressed in apertural view. Carinate, with the carina terminating in the lower half of the apertural neck. The carina is covered in a moderately developed radiating ornamentation. Test tapers towards the aperture, which is located at the termination of an apertural neck. The apertural neck is thin and lacks ornamentation.

***Pseudosolenina borealis* Jones 1984**

Plate 6. Figs. 3a-b

Pseudosolenina borealis gen. et sp. nov. Plate 4; Figs. 25-26 (Jones 1984b)

Monothalamous, elongate-ovate in outline, with main chamber subcircular in shape, tapering towards the aperture. Compressed in apertural view. Wall smooth, imperforate. Carinate with the carina surrounding the main chamber and extending to the termination of the apertural neck. Apertural tube is relatively short. Aperture located at the termination of the apertural neck and bounded by two (usually) equally developed lips.

***Amphicoryna scalaris* (Batsch 1791)**

Plate 1. Fig. 4

Nodosaria scalaris Batsch. Plate 63; Figs. 28-31; Description page 510 (Brady 1884)

Amphicoryna scalaris (Batsch 1791). Plate 11; Figs. 3-5; Description page 142 (Jones 1984a)

Uniserial, rectilinear. Number of chambers in specimens observed varies between 3 and 6. Chamber ornament initially well-developed longitudinal ridges, becoming poorly developed and discontinuous after chamber number two. Basal end of chambers display short, thin

processes approximately 10µm in length that extend away from the test at an approximately 45° angle. Base characterised by long (15-60µm), thin process extending away from the test at a 180° angle. Long (40-120µm) apertural neck present, with small, lateral ridges in a discontinuous coiling arrangement.

***Astacolus hyalacrulus* Loeblich and Tappan 1953**

Plate 1. Fig. 5

Astacolus hyalacrulus sp. nov. Plate 9; Fig. 4; Description page 52 (Loeblich and Tappan 1953)

Astacolus hyalacrulus Loeblich and Tappan 1953. Plate 11; Fig. 12; Description page 148 (Jones 1984a)

Test sub-circular with one flat edge aligned with the aperture. Compressed in cross-section. Planispiral, involute chamber arrangement, with chambers triagonal in shape and surrounded by a secondary outer wall. The outer wall is slightly flattened at the periphery, sometimes producing a very fine carina. Chambers grow gradually towards the apertural end. Wall surface is hyaline and imperforate. Aperture is terminal, areal and slit-shaped.

***Dentalina communis* (d'Orbigny 1826)**

Plate 1. Fig. 6

Nodosaria communis d'Orbigny 1826. Plate 62; Figs. 19-22; Description page 504 (Brady 1884)

Nodosaria communis sp. nov. Plate 12; Figs. 15-17; Description page N/a. (Part 4). (Cushman 1923)

Dentalina sp. cf. *D.communis* (d'Orbigny 1826). Plate 11; Fig. 20; Description page 154 (Jones 1984a)

Test elongate, uniserial, slightly arcuate in outline. Outer wall is imperforate. Chambers overlapping, initially sub-quadrate in outline with the final chamber ovate in shape. Apical and apertural ends taper and terminate relatively abruptly. Aperture is terminal, sub-circular and surrounded by two well-developed lips.

Diagnosis

In this species, the apical and apertural ends taper and terminate abruptly, unlike *D.baggi*.

***Dentalina baggi* (Galloway and Wissler 1927)**

Plate 1. Fig. 7

Dentalina baggi (Galloway and Wissler 1927). Plate 11; Fig. 17; Description page 152 (Jones 1984a)

Test elongate, uniserial and strongly arcuate in outline. Outer wall is imperforate. Chambers overlapping, initially sub-quatrate but becoming ovate in final chambers. Slight taper towards rounded apical end. Apertures are terminal, areal, subcircular in outline and each surrounded by two well-developed lips.

Diagnosis

There is a slight taper towards the rounded apical end in this species, unlike *D.communis*.

***Bulimina inflata* (Seguenza 1862)**

Plate 7. Figs. 1a-c

Bulimina inflata Seguenza. Plate 51; Figs. 10-13; Description page 406 (Brady 1884)

Bulimina aculeata d'Orbigny 1826. Plate 15; Figs. 9-14; Description page 214 (Jones 1984a)

Test short and broad, triserial chamber arrangement. Chambers coarsely perforate, globular and with crenulated extensions at the base of each chamber. The crenulated appearance is created by short spines extending towards the apical end joined by a thin, border (which is coarsely perforate and "wrinkled" in the later chambers). In earlier chambers, this crenulation

is strong enough to obscure the chambers almost completely. Aperture interiomarginal, slit to oval in shape, with a slightly raised border, one or two well developed lips and a tooth plate.

Diagnosis

This species has a crenulated ornamentation at the base of latter chambers, unlike *B.aculeata*, *B.marginata*, and *B.pupoides*.

***Bulimina aculeata* (d'Orbigny 1826)**

Plate 7. Figs. 2a-b

Bulimina aculeata d'Orbigny 1826. Plate 51; Figs. 7-9; Description page 406 (Brady 1884)

Bulimina aculeata (d'Orbigny 1826). Plate 6; Figs. 21-22 (Phleger *et al.* 1953)

Bulimina aculeata d'Orbigny 1826. Plate 3; Fig. 7; Description page 204 (Hermelin and Scott 1985)

Bulimina marginata d'Orbigny 1826. Plate 15; Figs. 7-8; Description page 210 (Jones 1984a)

Test elongate, tapering towards the distal end. Triserial chamber arrangement. Chambers finely perforate, globular and with short spines present at the base of each chamber. The spines extend towards the apical end, but away from the test. Spines are a mixture of both

aculeate and blunted. Sutures deep. Aperture interiomarginal, slightly depressed, slit-like and with a well-developed lip on one side.

Diagnosis

This species possesses long aculeate spines at the bases of latter chambers, unlike *B.inflata*, *B.pupoides* and *B.marginata*.

***Bullimina pupoides* d'Orbigny 1846**

Plate 7. Fig. 4

Bulimina pupoides d'Orbigny 1846. Fig. 132. Description page 84 (Cushman 1911)

Bulimina pupoides d'Orbigny 1846. Plate 20; Fig. 3; Description page 105 (Cushman 1923)

Test elongate, slightly compressed in apertural view and with a low angle of taper from the broader apertural end towards the apical end. Each end of the test is broadly rounded. Wall is smooth and finely and sparsely perforate. Initial chambers sometimes display a very finely ridged longitudinal ornamentation Chambers biserial, but development is irregular with initial chambers sub-quadrate but the final and penultimate chambers ovate (and considerably larger than the initial chambers). Sutures are slightly depressed. Aperture terminal, areal and slit-like in shape.

Diagnosis

This species does not possess any ornamentation at the base of any chambers, unlike *B.inflata*, *B.aculeata* and *B.marginata*.

***Bulimina marginata* (d'Orbigny 1826)**

Plate 7. Fig. 3

Bulimina marginata Plate 12; Figs. 10-12; Description page 269 (d'Orbigny 1826)

Bulimina marginata d'Orbigny: (Brady 1884), 405; Pl. 51; Figs. 3-5

Bulimina marginata d'Orbigny: (Cushman 1922), 91-93; Pl. 21; Figs. 4-5

Bulimina marginata d'Orbigny: (Feyling-Hansen 1964), 302, 304; Pl. 14; Figs. 2-5

Test elongate, tapering towards the distal end. Triserial chamber arrangement. Chambers finely perforate, globular and with very short spines present at the base of each chamber. The spines extend towards the apical end. Sutures deep. Aperture interiomarginal, slightly depressed, slit-like and with a well-developed lip on each side.

Diagnosis

This species possesses spines at the bases of latter chambers, unlike *B.pupoides* and *B.inflata*. The spines are less common and shorter than in *B.aculeata*.

***Globobullimina affinis* (d'Orbigny 1826)**

Plate 7. Fig. 5

Bulimina ovata d'Orbigny 1826. Plate 50; Fig. 13; Description page 400 (Brady 1884)

Globobullimina affinis (d'Orbigny 1826). Plate 6; Fig. 32 (Phleger *et al.* 1953)

Test elongate-ovate in outline, broadly rounded at apertural end and strongly tapered towards apical end. Chambers triserially arranged, sutures distinct and slightly depressed, sparsely perforate. Initial few chambers are more densely perforate, with the perforations associated with longitudinal grooves in the test outline. Chambers ovate-globose in shaped. Aperture terminal, areal and consisting of a long, curved slit.

***Nummoloculina irregularis* (d'Orbigny 1826)**

Plate 7. Fig. 6

Nummoloculina irregularis (d'Orbigny 1826). Plate 5; Figs. 19-20 (Phleger *et al.* 1953)

Biloculinella cf. irregularis (d'Orbigny 1826). Plate 20; Fig. 10; Description page 68 (McCulloch 1977)

Test lenticular, with a broadly rounded periphery. Wall calcareous and imperforate. Spiroloculine chamber arrangement, with chambers ovate and globular. Sutures not depressed and relatively indistinct. Aperture terminal, thin and arched.

***Bolivina albatrossi* (Cushman 1923)**

Plate 8. Fig. 1a-b

Bolivina albatrossi sp. nov. Plate 6; Fig. 4; Description page 31 (Part 3). (Cushman 1923)

Bolivina sp. 1. Plate 7; Figs. 27-28 (Phleger *et al.* 1953)

Bolivina (*Bolivina*) *albatrossi* Cushman 1922. Plate 20; Figs. 7-8; Description page 263 (Jones 1984a)

Test elongate, biserial. Test blade-shaped in outline and slightly compressed. Chambers recurved and tapering towards the periphery. Interiomarginal aperture, loop-shaped and with tooth plate. Latter chambers have one row of evenly spaced perforations located near the lower edge. Sutures distinct, slightly depressed.

Diagnosis

This species has a row of evenly spaced perforations at the base of each chamber, unlike *B.pseudopunctata*, *B.spinescens*, *B.subspinescens* and *B.robusta*.

***Bolivina pseudopunctata* Höglund 1947**

Plate 8. Figs. 2a-b

Bolivina punctata d'Orbigny 1826. Plate 7; Fig. 1; Description pages 42-43 (Part 3). (Cushman 1923)

Bolivina pseudopunctata Höglund 1947. Plate 20; Figs. 13-14; Description page 111 (Loeblich and Tappan 1953)

Bolivina pseudopunctata Höglund. Plate 7; Figs. 20-21 (Phleger *et al.* 1953)

Bolivina pseudopunctata Höglund. Plate 2; Fig. 18; Description page 203 (Hermelin and Scott 1985)

Test elongate, tapering towards the apical end. Biserial, slightly compressed in apertural view. Chambers compressed globular to wedge shaped. Sutures depressed. Chambers finely perforated. Interiomarginal aperture, a tapering slit with thinnest end at the suture with the penultimate chamber. Slight border developed, and a simple toothplate present.

Diagnosis

This species is much more elongate than *B.albatrossi*, *B.spinescens*, *B.subspinescens* and *B.robusta*.

***Bolivina spinescens* Cushman 1911**

Plate 8. Figs. 3a-b

Bolivina textilarioides Reuss. Plate 52; Figs. 23-25; Description page 419 (Brady 1884)

Bolivina (?*Bolivina*) *spinescens* Cushman 1911. Plate 21; Fig. 3; Description page 277 (Jones 1984a)

Bolivina subspinescens Cushman. Plate 3; Fig. 2; Description page 204 (Hermelin and Scott 1985)

Test elongate, tapering towards the apical end. Biserial, slightly compressed in apertural view. Chambers compressed, globular, gradually increasing in size away from the apical end, sutures strongly depressed. Chambers finely perforate. Peripheral bases of chambers display small spines which extend towards the apical end. Interiomarginal aperture, loop shaped and quite broad in side view.

Diagnosis

The sutures are strongly depressed in this species, unlike *B.albatrossi*, *B.pseudopunctata*, *B.subspinescens* and *B.robusta*.

***Bolivina subspinescens* Cushman 1922**

Plate 8. Figs. 4a-b

Bolivina lobata Brady. Plate 53; Figs. 22-23; Description page 425 (Brady 1884)

Bolivina (?*Bolivina*) *subspinescens* Cushman 1922. Plate 21; Fig. 9 (Not Fig. 8); Description page 280 (Jones 1984a)

Test elongate, tapering towards the apical end. Biserial chamber arrangement, slightly compressed in apertural view. Chambers globular, sutures strongly depressed. Base of chambers display a crenulated edge, with short spines extending from the base of each chamber towards the apical end. Final and penultimate chambers have a smooth surface, but earlier chambers display fine ridges which vary between discontinuous to strongly developed. Aperture interiomarginal, loop-shaped, extending from basal arch and with a well-defined border.

Diagnosis

The chamber bases in this species are crenulated, unlike *B.albatrossi*, *B.pseudopunctata*, *B.spinescens* and *B.robusta*.

***Bolivina robusta* (Brady 1884)**

Plate 8. Figs. 5a-b

Bolivina robusta Brady 1884. Plate 53; Figs. 7-9; Description page 421 (Brady 1884)

Bolivina (?*Bolivina*) *robusta* Brady 1884. Plate 21; Fig. 1; Description page 274 (Jones 1984a)

Test elongate, blade-like, strongly compressed in apertural view, tapering towards the apical end. Biserial chamber arrangement. Chambers thin, recurved slightly towards the apex. Coarsely perforate. Sutures depressed, slight carina around the apical end. Aperture interiomarginal , slit shaped extending from the basal suture and with two well-developed lips.

Diagnosis

In this species, the chambers are thin and recurved and the test is strongly compressed in apertural view, unlike *B.albatrossi*, *B.pseudopunctata*, *B.subspinescens* and *B.spinescens*.

***Fursenkoina complanata* (Egger 1895)**

Plate 9. Figs. 1a-c

Virgulina complanata Egger 1895. Plate 7; Fig. 3 (Phleger *et al.* 1953)

Fursenkoina complanata (Egger 1895). Fig. 3 (n) (Austin and Evans 2000)

Test elongate, low angle of taper towards the apical end. Slightly compressed in apertural view. Short spine extending out from the apical end. Chambers ovate, globular in shape, finely and sparsely perforate, sutures depressed. Aperture a narrow arch , interiomarginal and slightly depressed.

***Stainforthia (Fursenkoina) fusiformis* (Williamson 1858)**

Plate 9. Figs. 2a-c

Virgulina fusiformis (Williamson 1858). Plate 14; Figs. 15-18; Description page 307 (Feyling-Hansen 1964)

Fursenkoina fusiformis (Williamson 1858). Plate 77; Figs. 1-5; Description page 185 (Murray 1971)

Fursenkoina fusiformis (Williamson 1858). Plate 4; Fig. 14; Description page 210 (Hermelin and Scott 1985)

Test elongate, low angle of taper towards the apical end. Biserial chamber arrangement, with the growth axis twisting gradually through 90°. Chambers elongate-globose in shape, wall finely and sparsely perforate. Sutures depressed and distinct. Aperture is interiomarginal, slit-like in shape, extending vertically from the basal suture towards the outer margin.

***Virgulina advena* Cushman 1922**

Plate 9. Figs. 3a-c

Virgulina advena Cushman 1922. Plate 7; Figs. 1-2 (Phleger *et al.* 1953)

Virgulina (?) *advena* Cushman 1922. Plate 25; Figs. 1-3; Description page 120 (Cushman 1923)

Test elongate with a broadly rounded apical end and a straight periphery which tapers towards the apertural end. Wall calcareous and finely and sparsely perforate. Irregular biserial

chamber arrangement. Chambers tear-drop shaped, with sutures slightly depressed and indistinct. Aperture interiomarginal, terminal and elongate, surrounded by two well developed lips.

***Trifarina angulosa* (Williamson 1858)**

Plate 10. Figs. 2a-c

Uvigerina angulosa Williamson 1858. Plate 74; Figs. 15-18; Description page 576 (Brady 1884)

Triffarina angulosa (Williamson 1858). Plate 19; Figs. 10-16; Description page 256 (Jones 1984a)

Test elongate, tapering at the apical and apertural ends, tigonal in cross-section. Wall calcareous, finely and sparsely perforate. Triserial chamber arrangement with chambers slightly inflated and triagonal in outline. Chambers ornamented with longitudinal costae, with the costae at the edges of the chambers strongly developed, occasionally overlapping between overlying chambers to form carinae. Sutures distinct and depressed. Aperture at the termination of a very short neck, terminal, sub-circular. Aperture surrounded by a short lip.

***Ehrenbergina serrata* Reuss 1850**

Plate 10. Figs. 3a-b

Ehrenbergina serrata Reuss. Plate 55; Figs. 2-7; Description page 434 (Brady 1884)

Ehrenbergina trigona Goës. Plate 4; Figs. 15-16; Description page 206 (Hermelin and Scott 1985)

Test elongate, strongly tapering toward the apical end. ?Biserial chamber arrangement, sutures depressed. Chamber edges ridged with moderate sized, spines extending away from the periphery. The spines are located only at the periphery and at the base of each chamber. Chambers coarsely perforate. Aperture a curved slit, interiomarginal, with a small lip on one side.

***Hoeglundia elegans* (d'Orbigny 1826)**

Plate 10. Figs. 1a-c

Pulvinulina elegans d'Orbigny 1826. Plate 105; Figs. 3-6; Description page 699 (Brady 1884)

Hoeglundia elegans (d'Orbigny). Plate 9; Figs. 24-25 (Phleger *et al.* 1953)

Hoeglundia elegans (d'Orbigny 1826). Plate 6; Figs. 6-7; Description page 210 (Hermelin and Scott 1985)

Hoeglundia elegans (d'Orbigny 1826). Plate 24; Fig.1; Description page 316 (Jones 1984a)

Test sub-circular in outline, biconvex. Wall surface smooth, opaque, aragonitic and imperforate. Chambers arranged in a low trochospire, triagonal in shape. Periphery can sometimes have a very fine carina. Sutures distinct under LM, radial on spiral side. Aperture interiomarginal, sub-circular.

***Alabaminella weddellensis* (Earland 1936)**

Plate 11. Figs. 1a-c

Eponides weddellensis sp. nov. Plate 9; Figs. 65-67; Description page 57 (Earland 1936)

Test sub-circular in outline, biconvex and compressed in cross-section. Wall surface is smooth, hyaline and finely but sparsely perforate. Chambers are arranged in either a planispiral or very low trochospiral system. Chambers are elongate and overlapping when observed from the apical view. Sutures are distinct and slightly depressed. Aperture is interiomarginal, slit shaped and extends from the basal suture.

***Cassidulina laevigata* d'Orbigny 1826**

Plate 11. Figs. 2a-c

Cassidulina laevigata d'Orbigny 1826. Fig. 150; Description page 96 (Cushman 1911)

Cassidulina laevigata d'Orbigny 1826 subsp. *carinata* Silvestri 1896. Plate 22; Figs. 12-15; Description page 294 (Jones 1984a)

Test sub-circular in outline, biconvex and compressed in cross-section with an angular periphery. Chambers arranged into an involute planispire. Chambers elongate-ovate in outline, and curved towards the umbilical area. Wall surface is smooth and finely and sparsely perforate. Aperture interiomarginal, an elongate slit shape and with an elongate and slightly crenulated lip extending from the basal suture and covering more than half of the aperture.

***Epistominella exigua* (Brady 1884)**

Plate 11. Fig. 3

Pulvinulina exigua sp. nov. Plate 103; Figs. 13-14; Description page 696 (Brady 1884)

Eponides exigua (Brady 1884). Plate 10; Figs. 1-2; Description page 44 (Part 8). (Cushman 1923)

Epistominella exigua (Brady). Plate 9; Figs. 35-36 (Phleger *et al.* 1953)

Epistominella exigua (Brady 1884). Plate 18; Figs. 10-11; Description page 243 (Jones 1984a)

Epistominella exigua (Brady). Plate 4; Fig. 1; Description page 208 (Hermelin and Scott 1985)

Test sub-circular in outline, plano-convex with chambers arranged in a low-angle trochospire. Wall surface smooth, hyaline and imperforate. Chambers triagonal in shape. Sutures depressed and recurved slightly. Aperture interiomarginal, surrounded by a well-developed margin and elongate.

***Eponides pusillus* Parr 1950**

Plate 11. Fig. 4

Eponides pusillus Parr 1950. Plate 9; Figs. 5-6 (Phleger *et al.* 1953)

Test sub-circular in outline, biconvex with chambers arranged in an involute planispire. Compressed in cross-section. Periphery broadly rounded. Wall surface smooth and finely and densely perforate. Chambers triagonal in shape. Sutures slightly depressed and recurved towards the umbilical area. Aperture interiomarginal, a low, elongate arch with a large lip.

Nonionella turgida **(Williamson 1858)**

Plate 11. Fig. 5

Nonionella turgida (Williamson 1858). Plate 6; Figs. 1-4; Description page 15 (Part 7). (Cushman 1923)

Nonionella turgida (Williamson 1858). Plate 29; Figs. 8-10; Description page 403 (Jones 1984a)

Test elongate-ovate in outline, compressed in cross-section. Wall surface hyaline, densely and finely perforate. Chambers initially sub-quadrate, becoming lobate in the final and penultimate chambers. Final two chambers are substantially larger and more lobate than earlier chambers. Chambers arranged in an involute planispiral. Periphery rounded, sutures moderately depressed, recurved slightly. Aperture interiomarginal, a low arch along the basal suture.

Gyroidina soldanii **d'Orbigny 1826**

Plate 12. Figs. 1a-c

Gyroidina soldanii d'Orbigny. Plate 9; Figs. 1-2 (Phleger *et al.* 1953)

Gyroidina soldanii d'Orbigny 1826. Plate 5; Figs. 6-8; Description page 210 (Hermelin and Scott 1985)

Test sub-circular in outline, plano-convex. Wall surface smooth, opaque and densely but finely perforate. Chambers arranged in a low-angle trochospire. Umbilical side planar with flush sutures which are very distinct in LM. Spiral side strongly convex, with flush, radial sutures. Aperture interiomarginal, slit-shaped and with a well-developed lip.

***Melonis barleeanum* (Williamson 1858)**

Plate 12. Figs. 2a-c

Nonionina umbilieatula Montagu. Plate 109; Figs. 8-9; Description page 726 (Brady 1884)

Nonion barleeanum (Williamson 1858). Plate 6; Fig. 4 (Phleger *et al.* 1953)

Nonion barleeanum (Williamson 1858). Plate 5; Fig. 2; Description page 213 (Hermelin and Scott 1985)

Test sub-circular in outline, compressed and biconvex in cross-section. Periphery broadly and evenly rounded, with the test outline slightly tapering towards the periphery in cross-section. Chambers arranged in an involute planispiral. Chambers triagonal in shape, coarsely and

densely perforate. Sutures flush and imperforate as are the most basal portions of the chambers. Sutures are also either radial or slightly curved backwards. Aperture is interiomarginal, a low arch which extends across the whole of the basal suture with the previous chambers. Umbilicus is excavated.

Diagnosis

This species is compressed and bi-convex in cross section, unlike *M.pompilioides*. This species also has perforate sutures, unlike *M.pompilioides*.

***Melonis pompilioides* (Fichtel and Moll 1798)**

Nonionina pompilioides Fichtel and Moll. Plate 109; Figs. 10-11; Description page 727 (Brady 1884)

Nonion pompilioides (Fichtel and Moll). Plate 1; Figs. 7-11; Description page 4 (Part 7). (Cushman 1923)

Nonion pompilioides (Fichtel and Moll). Plate 6; Figs. 7-8 (Phleger *et al.* 1953)

Melonis pompilioides (Fichtel and Moll). Plate 6; Fig. 5; Description page 212 (Hermelin and Scott 1985)

Melonis pompilioides (Von Fichtel and Von Moll 1798). Plate 29; Figs. 1-2; Description page 397 (Jones 1984a)

Test sub-circular in outline, ovate in cross-section. Chambers arranged in an involute planispire with a broadly rounded periphery. Chambers sub-quadrate, coarsely and densely perforate. Sutures flush but very distinct due to imperforate surface. Umbilicus excavated and imperforate. Aperture interiomarginal, a low arch which extends across the breadth of the basal suture of the final chamber.

Diagnosis

This species is ovate in cross section and possesses imperforate sutures, unlike *M.barleeanum.*

***Pullenia bulloides* (d'Orbigny 1826)**

Plate 12. Figs. 3a-c

Pullenia sphaeroides d'Orbigny 1826. Plate 84; Figs. 12-13; Description page 615 (Brady 1884)

Pullenia bulloides (d'Orbigny 1826). Plate 10; Fig. 19 (Phleger *et al.* 1953)

Pullenia bulloides (d'Orbigny). Plate 5; Fig. 2; Description page 216 (Hermelin and Scott 1985)

Test sub-circular to globose in outline, ovate in cross-section. Wall surface smooth, opaque and finely and sparsely perforate. Chambers arranged in an involute planispire with a broadly rounded periphery. Chambers triagonal in shape. Sutures slightly depressed and indistinct. Only four chambers in the final whorl. Aperture interiomarginal, a narrow arch with a small lip.

***Rupertina stabilis* Wallich 1877**

Plate 7. Figs. 4a-c

Rupertina stabilis Wallich 1877. Plate 98; Figs. 1-12; Description page 680 (Brady 1884)

Rupertina stabilis Wallich 1877. Plate 10; Fig. 19 (Phleger *et al.* 1953)

Test outline varies between two main morphotypes; elongate with a flattened apical end and tapered apertural end and elongate with a flattened apical end and globose apertural end. The flattened base is normally imperforate with the chambers coarsely and densely perforate. In apical view, the flattened surface usually displays three or four lobes which almost meet at the centre and which appear to overlap a series of grooves in the flattened surface. Chambers are trochospirally arranged, and ovate-globose in shape. Sutures are slightly depressed and

normally either imperforate or very sparsely perforate. Aperture is terminal, areal, and loop-shaped with one, strongly developed tooth.

4.3 List of Plates (Benthic foraminifera)

Scale bar represents 250µm for all specimens

Plate 1

Fig. 1a and b = *Siphotextularia rolhauseni* Phleger and Parker 1951

Fig. 2 = *Eggerella bradyi* (Cushman 1911)

Fig.3a-c = *Karreriella bradyi* (Cushman 1911)

Fig. 4 = *Amphicoryna scalaris* (Batsch 1791)

Fig.5 = *Astacolus hyalacrulus* Loeblich and Tappan 1953

Fig.6 = *Dentalina communis* (d'Orbigny 1826)

Fig. 7 = *Dentalina baggi* (Galloway and Wissler 1927)

Plate 2

Fig. 1a-b = *Spiroloculina rotunda* d'Orbigny 1826

Fig. 2a-b = *Quinqueloculina seminulum* (Linné 1758)

Fig. 3a-b = *Quinqueloculina arctica* Cushman 1933

Fig. 4 = *Quinqueloculina stalkeri* Loeblich and Tappan 1953

Fig. 5 = *Quinqueloculina striata* d'Orbigny 1826

Fig. 6 = *Quinqueloculina elongata* Natland 1938

Plate 3

Fig. 1 = *Pyrgo oblonga* (d'Orbigny 1826)

Fig. 2 = *Pyrgo lacernula* (Schwager 1866)

Fig. 3 = *Pyrgo sarsi* (Schlumberger 1891)

Fig. 4a-b = *Pyrgo murrhina* (Schwager 1866)

Fig. 5 = *Pyrgo* sp. 1

Fig. 6 = *Triloculina tricarinata* Reuss 1867

Fig. 7a-b = *Sigmoilopsis schlumbergeri* (Silvestri 1904)

Plate 4

Fig. 1 = *Oolina apiopleura* (Loeblich and Tappan 1953)

Fig. 2 = *Oolina heronalleni?* Jones 1984

Fig. 3 = *Oolina hexagona* (Williamson 1858)

Fig. 4a-e = *Oolina melo* (d'Orbigny 1826)

Fig. 5a-b = *Oolina intercalata* Jones 1984

Fig. 6a-b = *Oolina squamosa* (Montagu 1803)

Plate 5

Fig. 1a-b = *Fissurina marginata* (Montagu 1803)

Fig. 2 = Fissurina sp. 2

Fig. 3a-b = *Fissurina porcupinensis* sp. nov.

Fig. 4 = *Fissurina* sp. 1

Fig. 5a-b = *Fissurina varioperforata* (Buchner 1940)

Plate 6

Fig. 1a-b = *Pseudofissurina mccullochae* Jones 1984

Fig. 2 = *Lagena sulcata* (Walker and Jacob 1789)

Fig. 3a-b = *Pseudosolenina borealis* Jones 1984

Fig. 4 = *Lagena* sp. 1

Fig. 5a-b = *Solenina radiata* (Seguenza 1862)

Fig. 6 = *Lagena* sp. 2

Plate 7

Fig. 1a-c = *Bulimina inflata* (Seguenza 1862)

Fig. 2a-b = *Bulimina aculeata* (d'Orbigny 1826)

Fig. 3 = *Bulimina marginata* (d'Orbigny 1826)

Fig. 4a-c = *Rupertina stabilis* Wallich 1877

Fig. 5 = *Nummoloculina irregularis* (d'Orbigny 1826)

Plate 8

Fig. 1a-b = *Bolivina albatrossi* Cushman 1922

Fig. 2a-b = *Bolivina pseudopunctata* Höglund 1947

Fig. 3a-b = *Bolivina spinescens* Cushman 1911

Fig. 4a-b = *Bolivina subspinescens* Cushman 1922

Fig. 5a-b = *Brizalina robusta* Brady 1884

Plate 9

Fig. 1a-c = *Fursenkoina complanata* (Egger 1895)

Fig. 2a-b = *Stainforthia* (*Fursenkoina*) *fusiformis* (Egger 1895)

Fig. 3a-c = *Virgulina advena* Cushman 1922

Plate 10

Fig. 1a-c = *Hoeglundia elegans* (d'Orbigny 1826)

Fig. 2a-c = *Triffarina angulosa* (Williamson 1858)

Fig. 3a-b = *Ehrenbergina serrata* Reuss 1850

Plate 11

Fig. 1a-c = *Alabaminella weddellensis* (Earland 1936)

Fig. 2a-c = *Cassidulina laevigata* d'Orbigny 1826

Fig. 3 = *Epistominella exigua* (Brady 1884)

Fig. 4 = *Eponides pusillus* (Parr 1950)

Fig. 5 = *Nonionella turgida* (Williamson 1858)

Plate 12

Fig. 1a-c = *Gyroidina soldanii* d'Orbigny 1826

Fig. 2a-c = *Melonis barleeanum* (Williamson 1858)

Fig. 3a-c = *Pullenia bulloides* (d'Orbigny 1826)

4.4. Taxonomy of planktonic foraminifera

Scale bar represents 250µm for all specimens

Plate 13

1a-b = *Turborotalita quinqueloba* (Natland 1938)

2 = *Orbulina universa* d'Orbigny 1839

3a-c = *Globigerina bulloides* d'Orbigny 1826

4a-c = *Globigerinoides ruber* (d'Orbigny 1839)

Plate 14

1a-c = *Globorotalia inflata* (d'Orbigny 1839)

2a-c = *Globorotalia scitula* (Brady 1882)

3a-c = *Globorotalia hirsuta* (d'Orbigny 1839)

4a-c = *Globorotalia truncatulinoides* (d'Orbigny 1839)

Plate 15

1a-b = *Neogloboquadrina pachyderma* (dextral) (Ehrenberg 1861)

2a-c = *Neogloboquadrina pachyderma* (sinistral) (Ehrenberg 1861)

3a-c = *Globigerinella siphonifera* (d'Orbigny 1839)

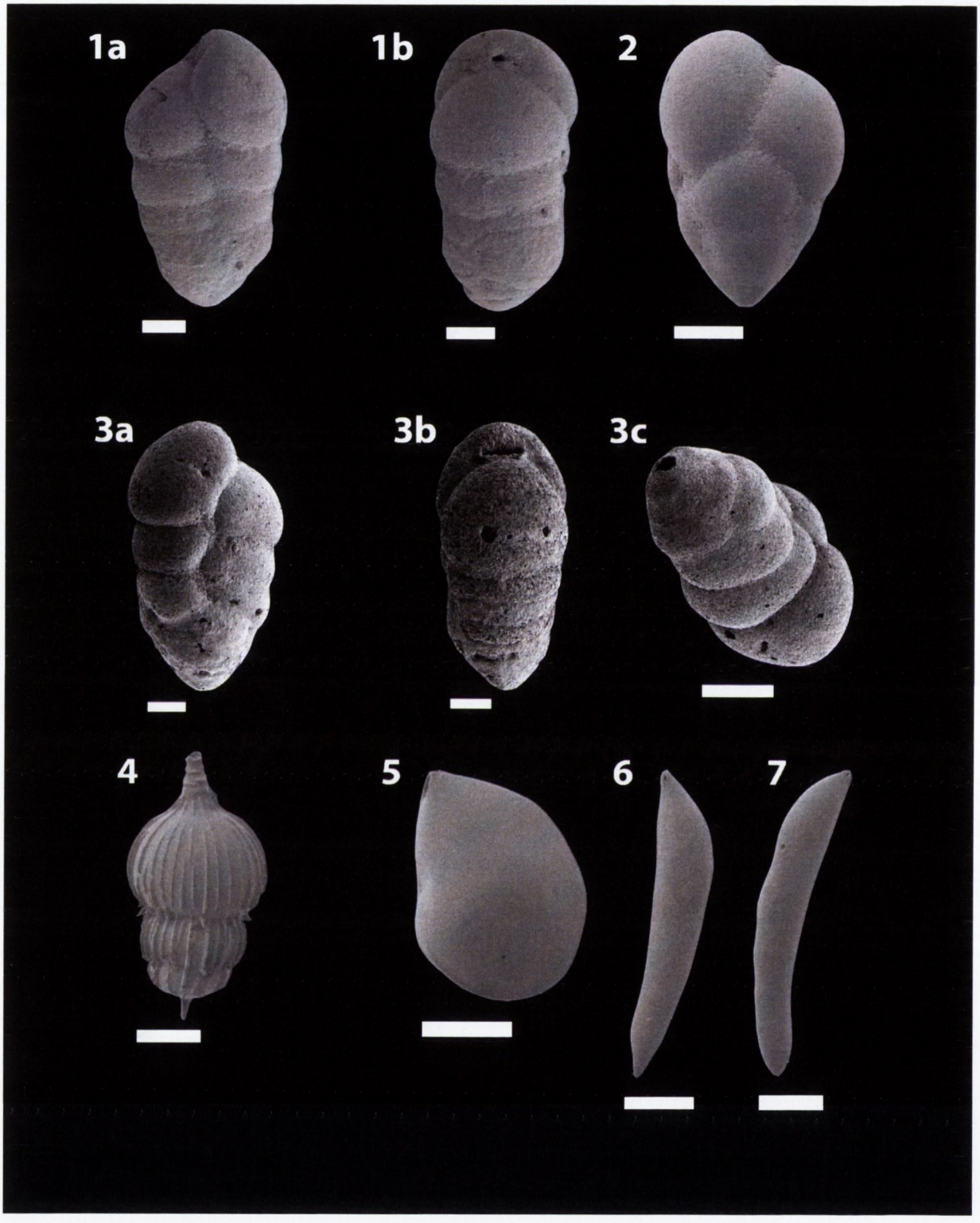

PLATE 1

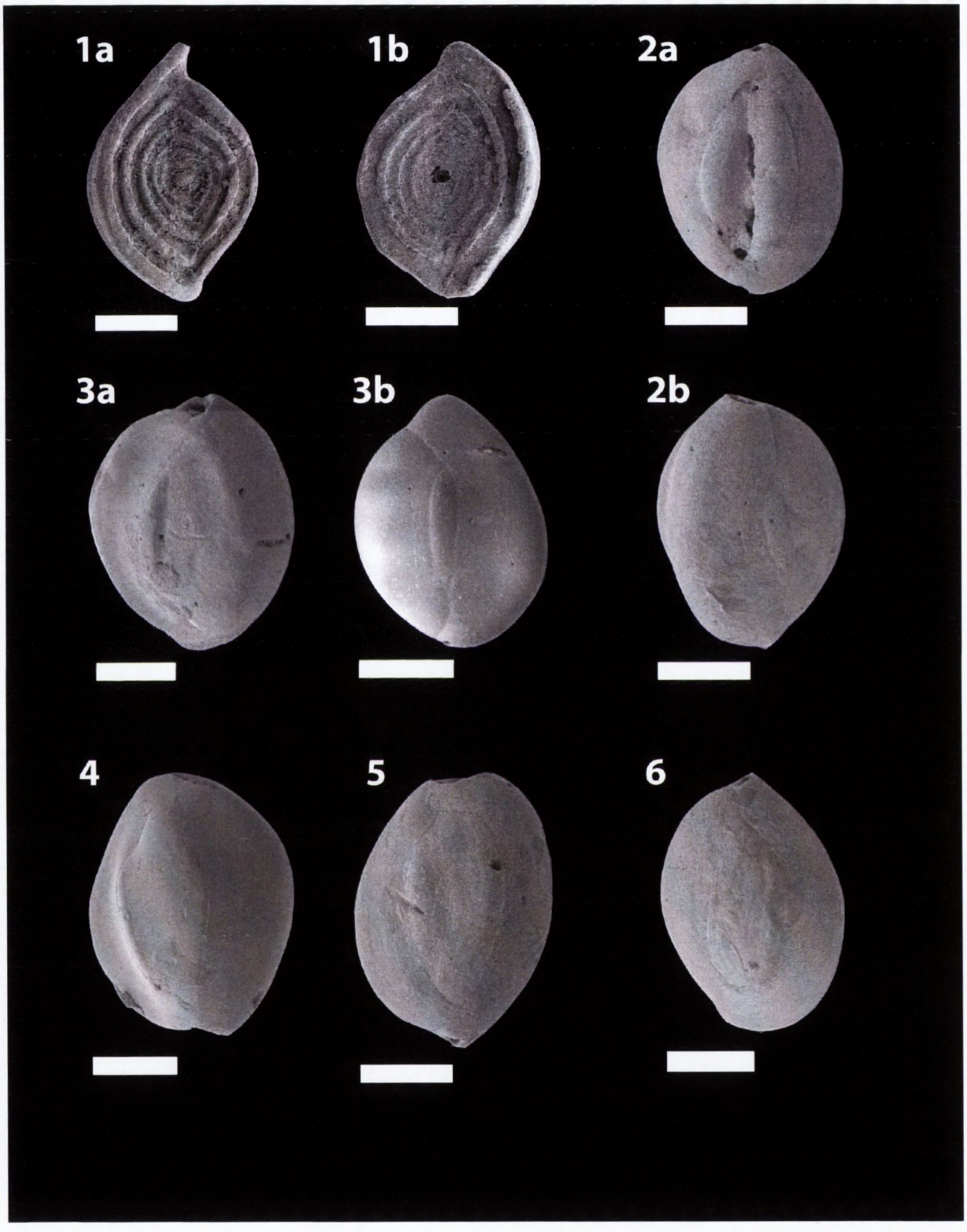

PLATE 2

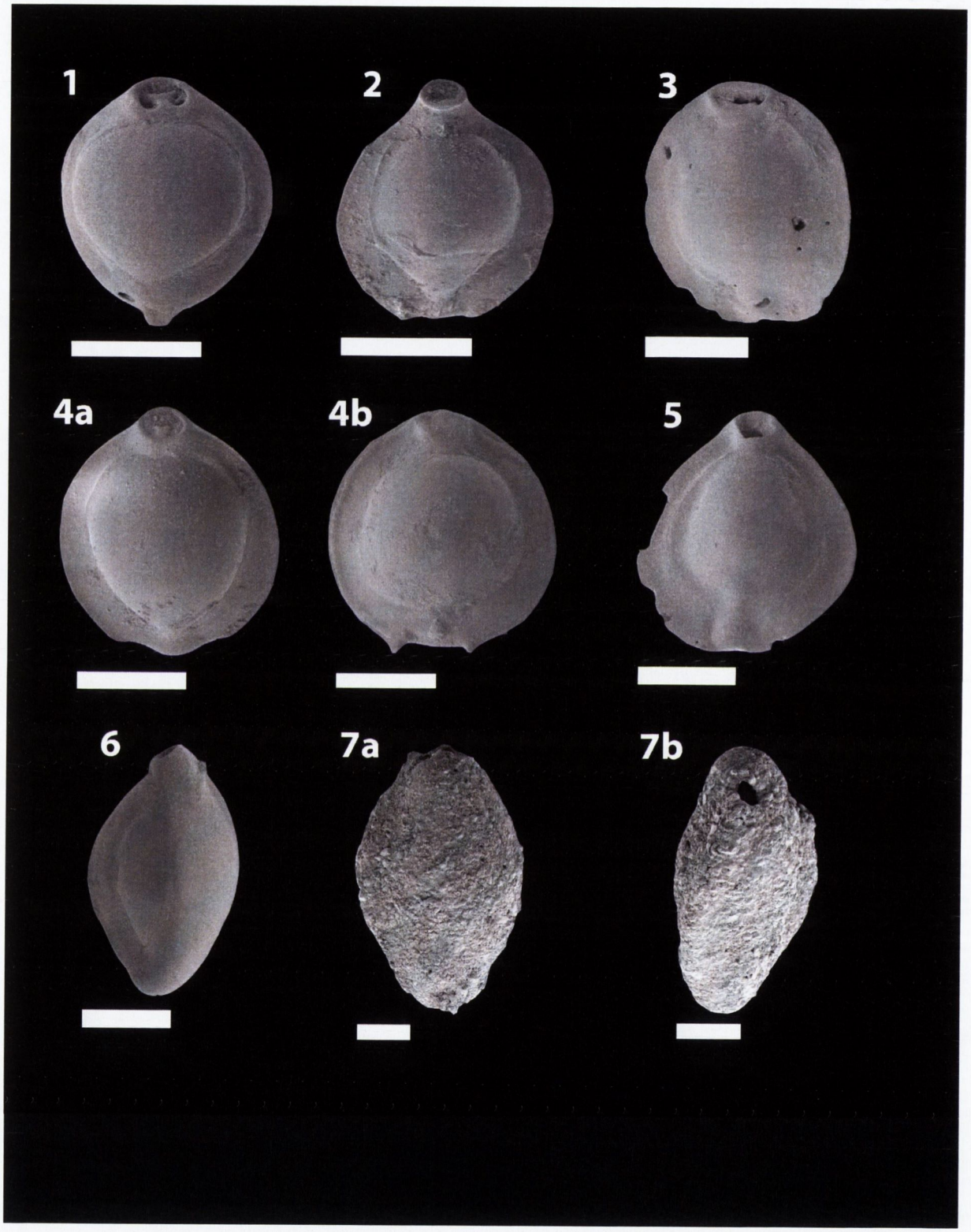

PLATE 3

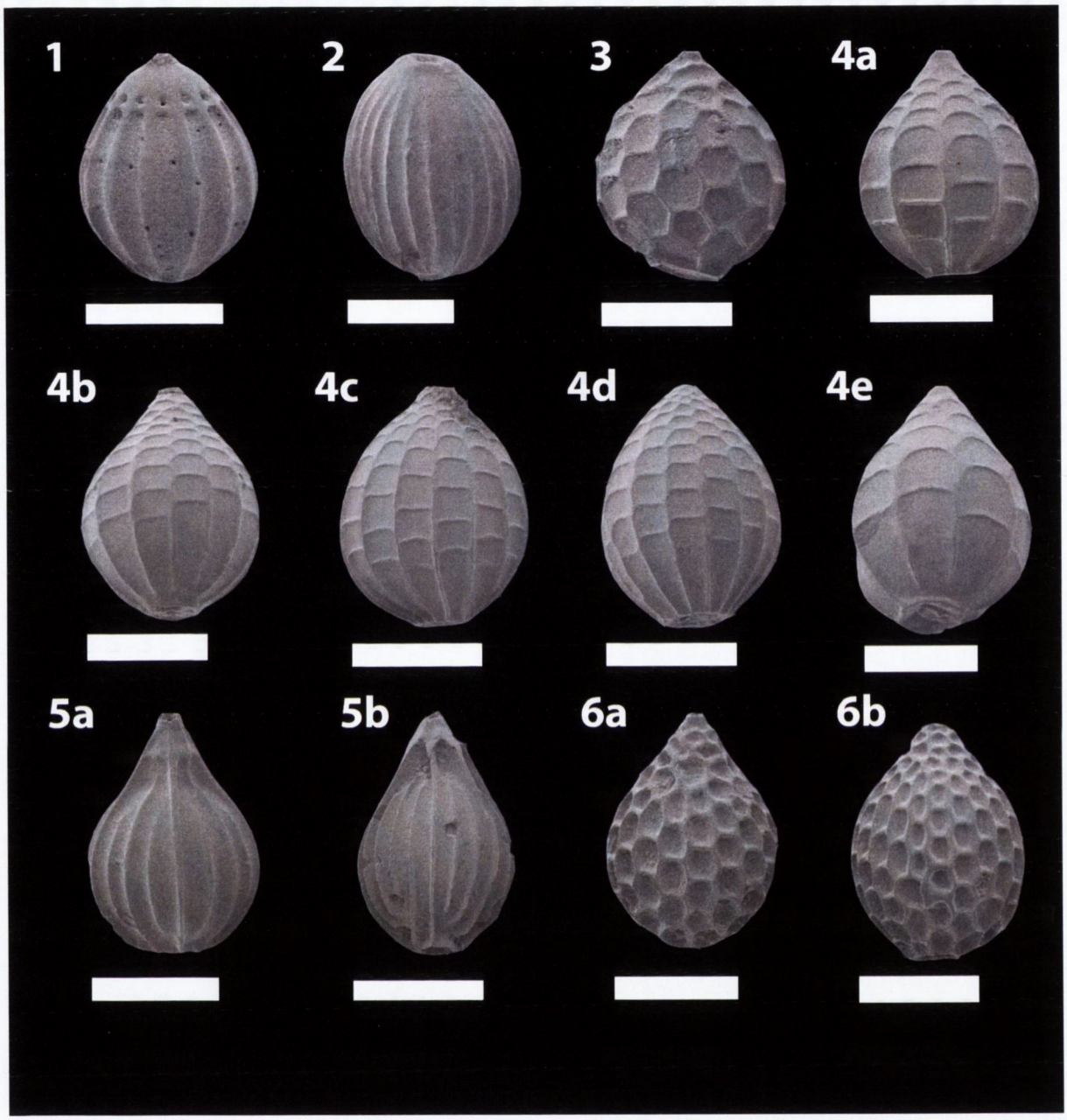

PLATE 4

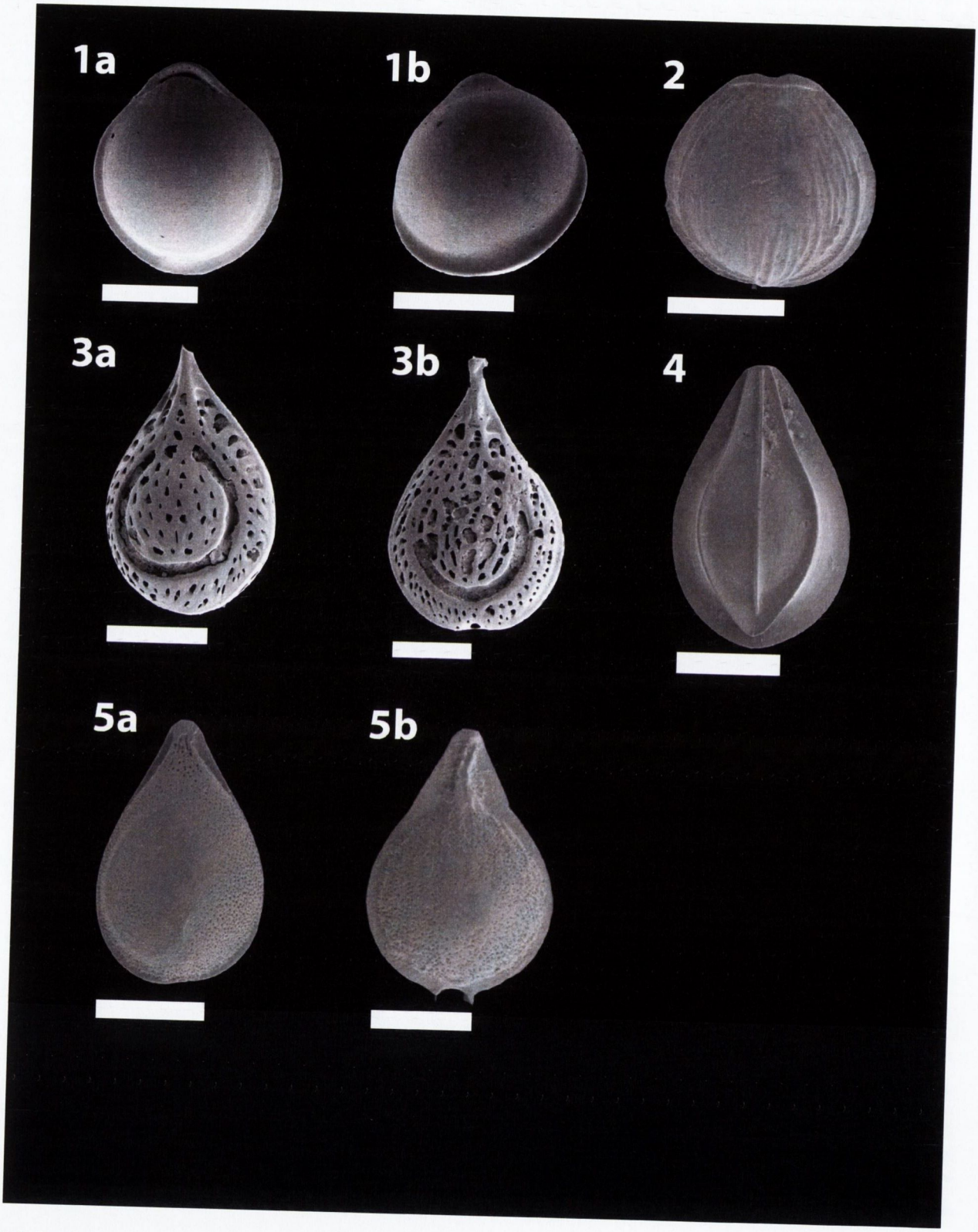

PLATE 5

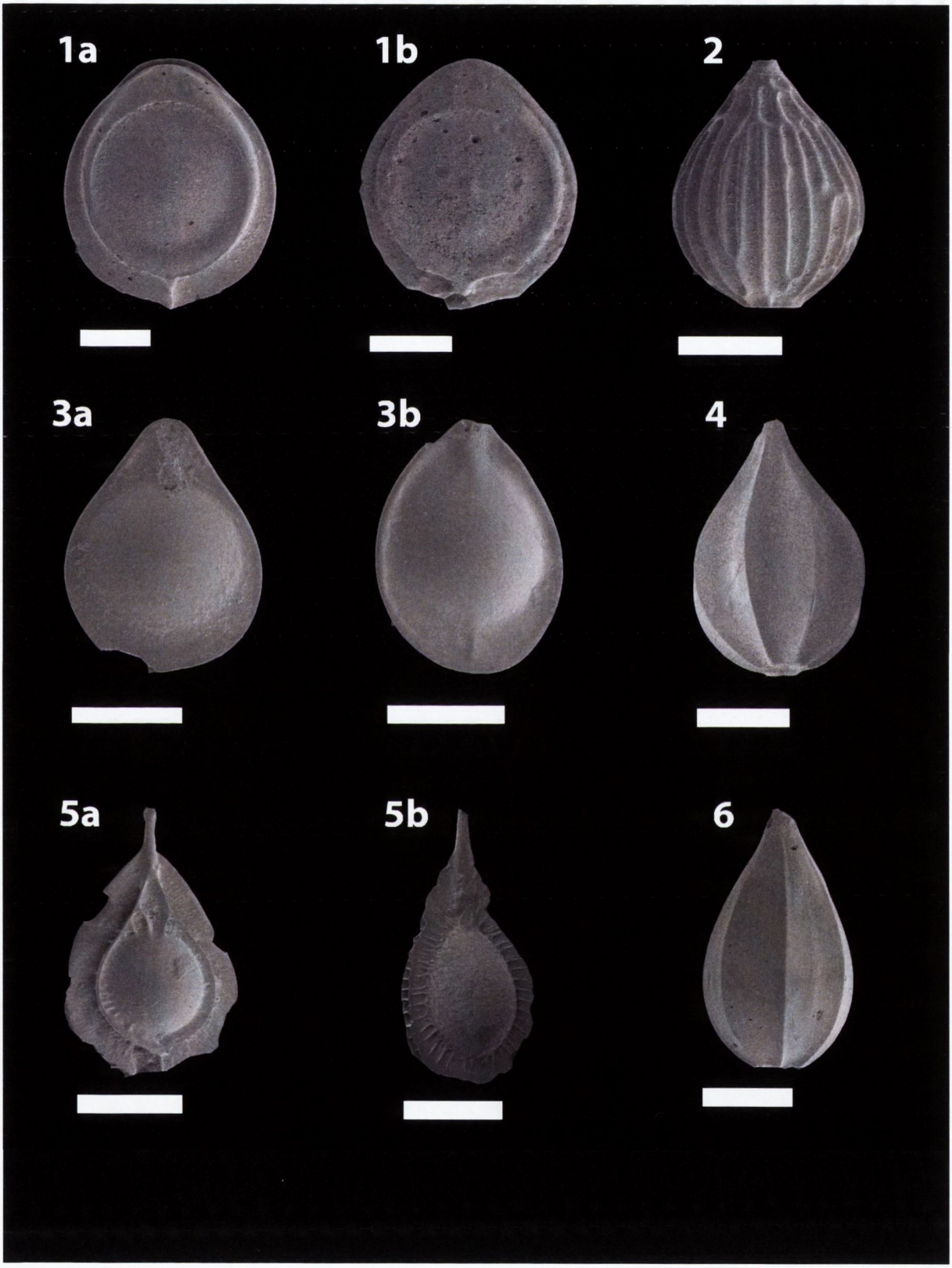

PLATE 6

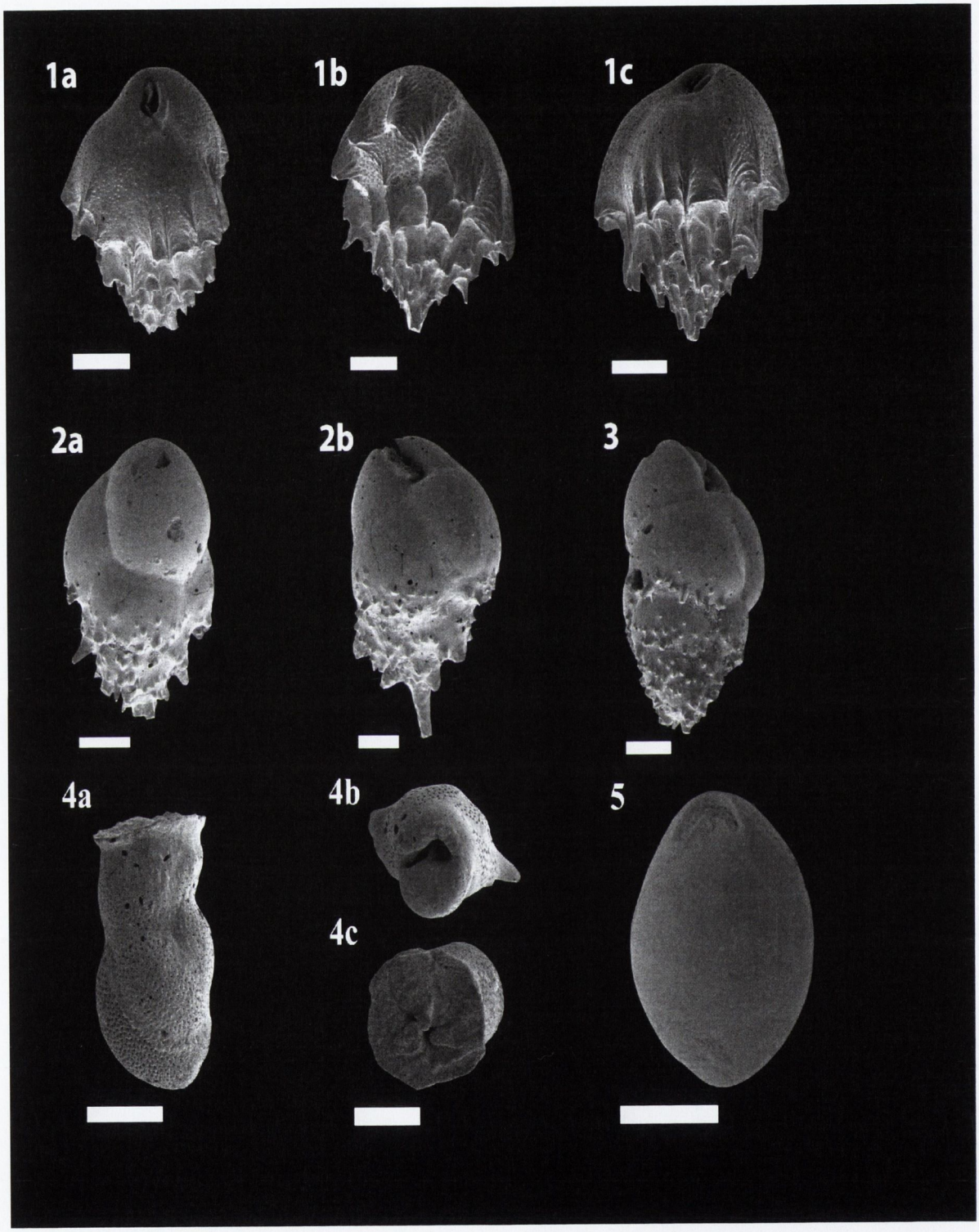

PLATE 7

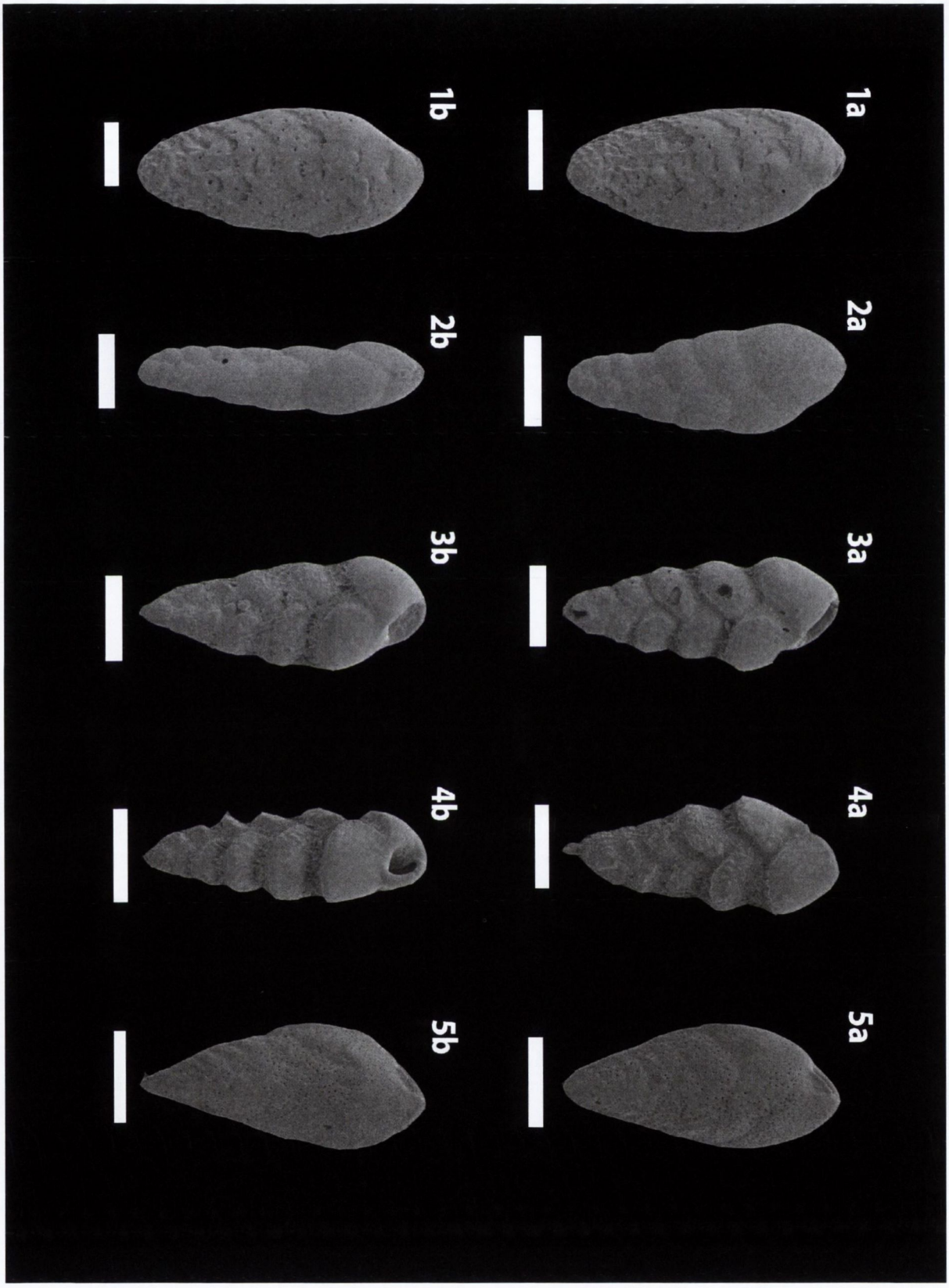

PLATE 8

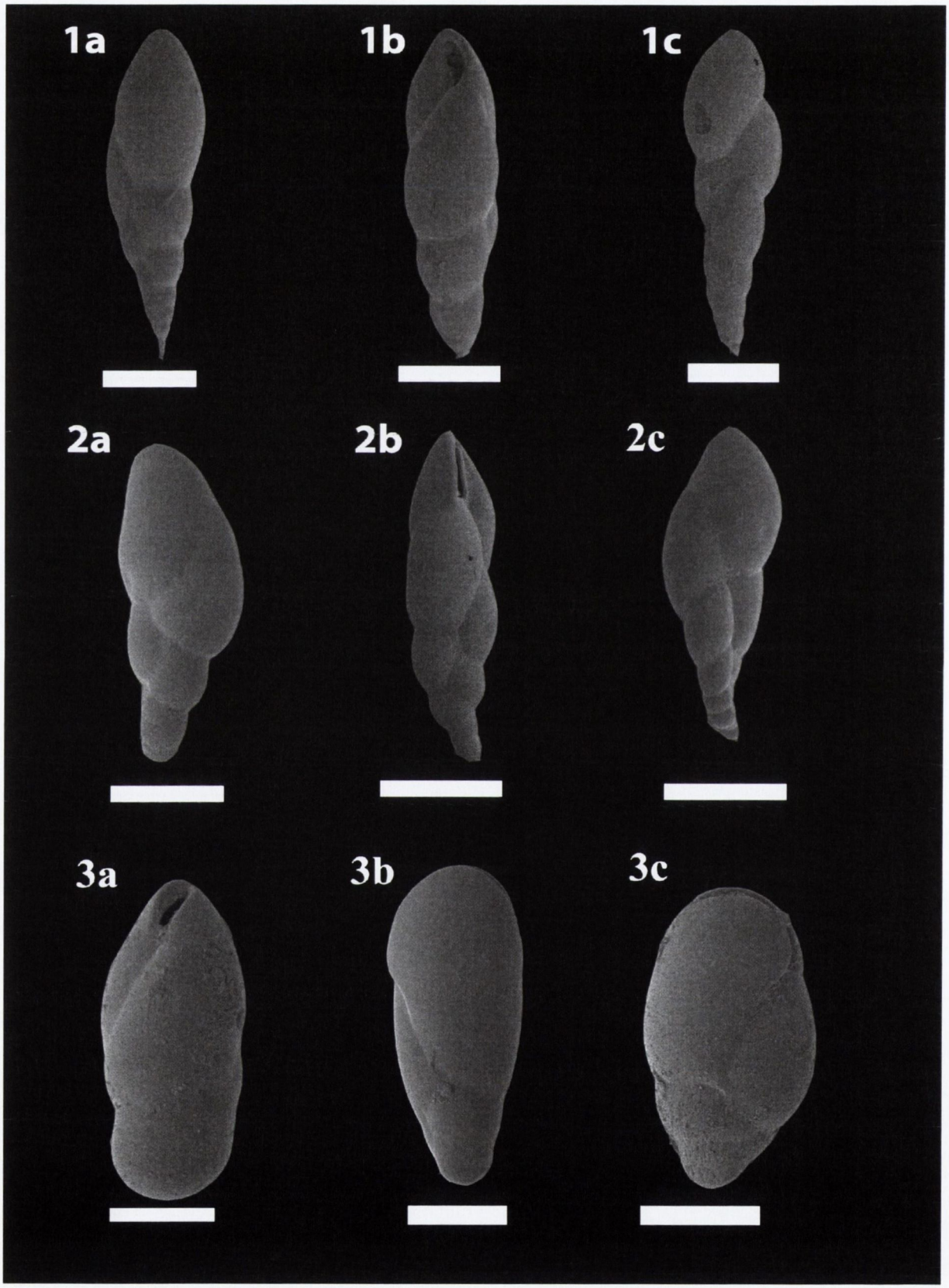

PLATE 9

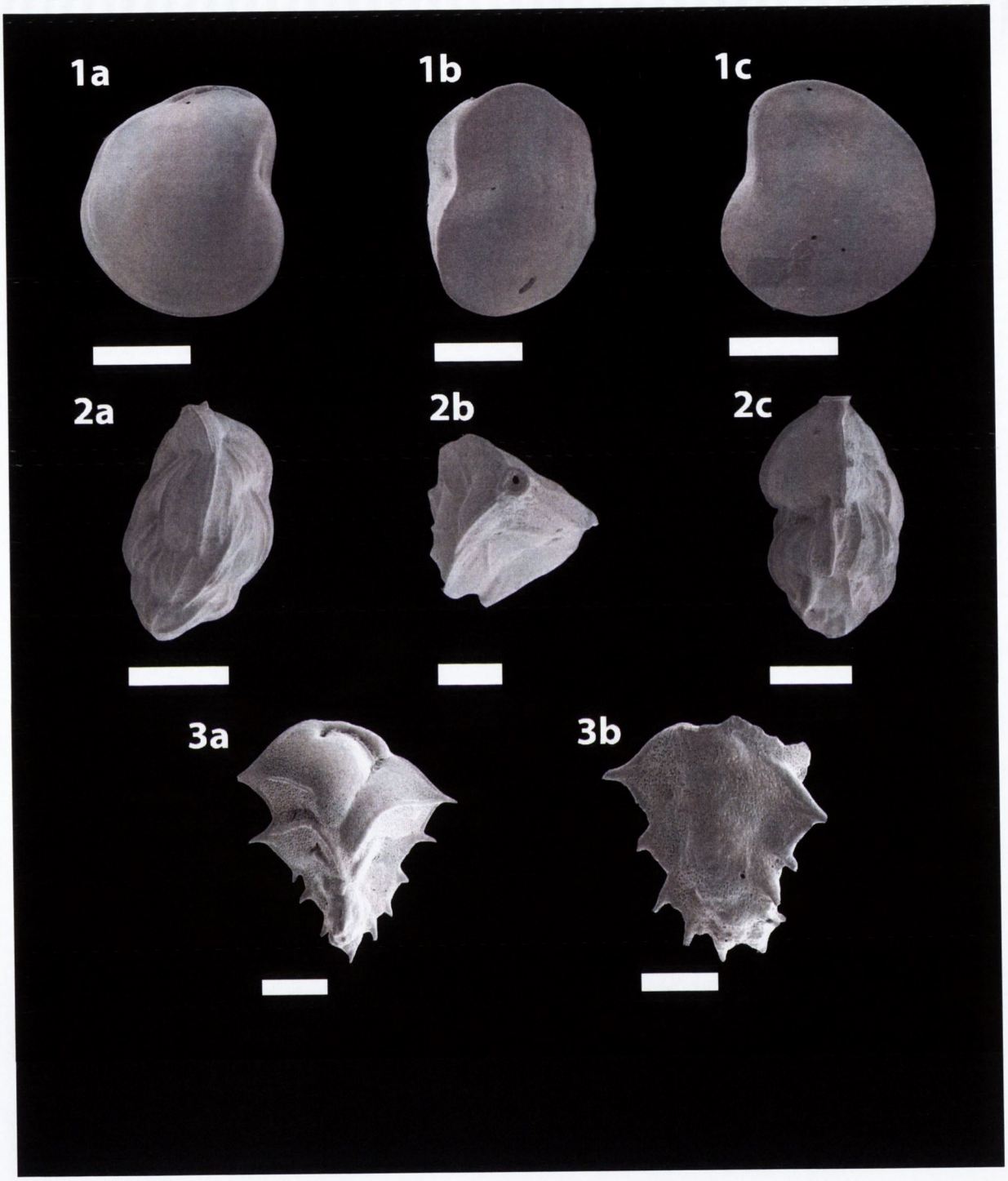

PLATE 10

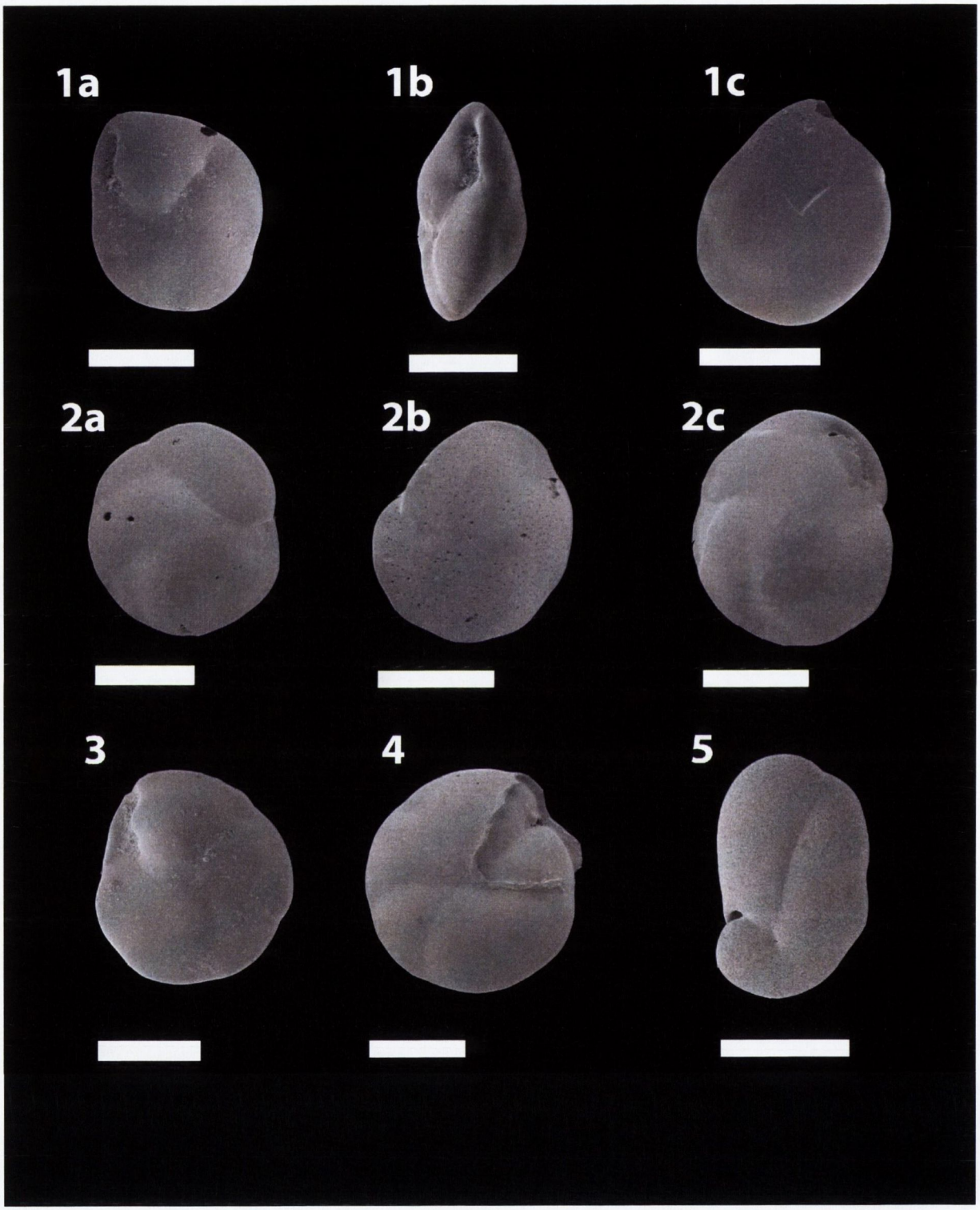

PLATE 11

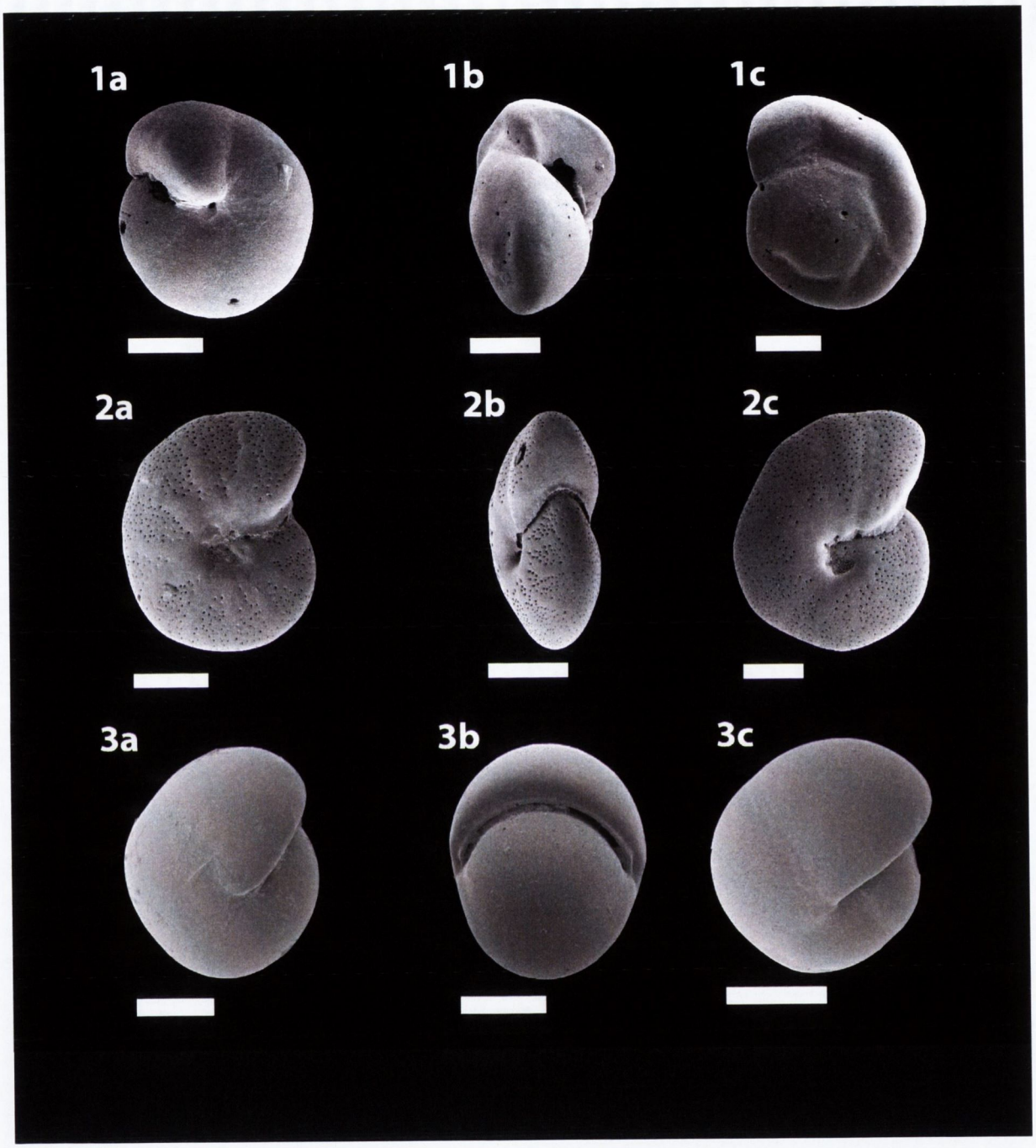

PLATE 12

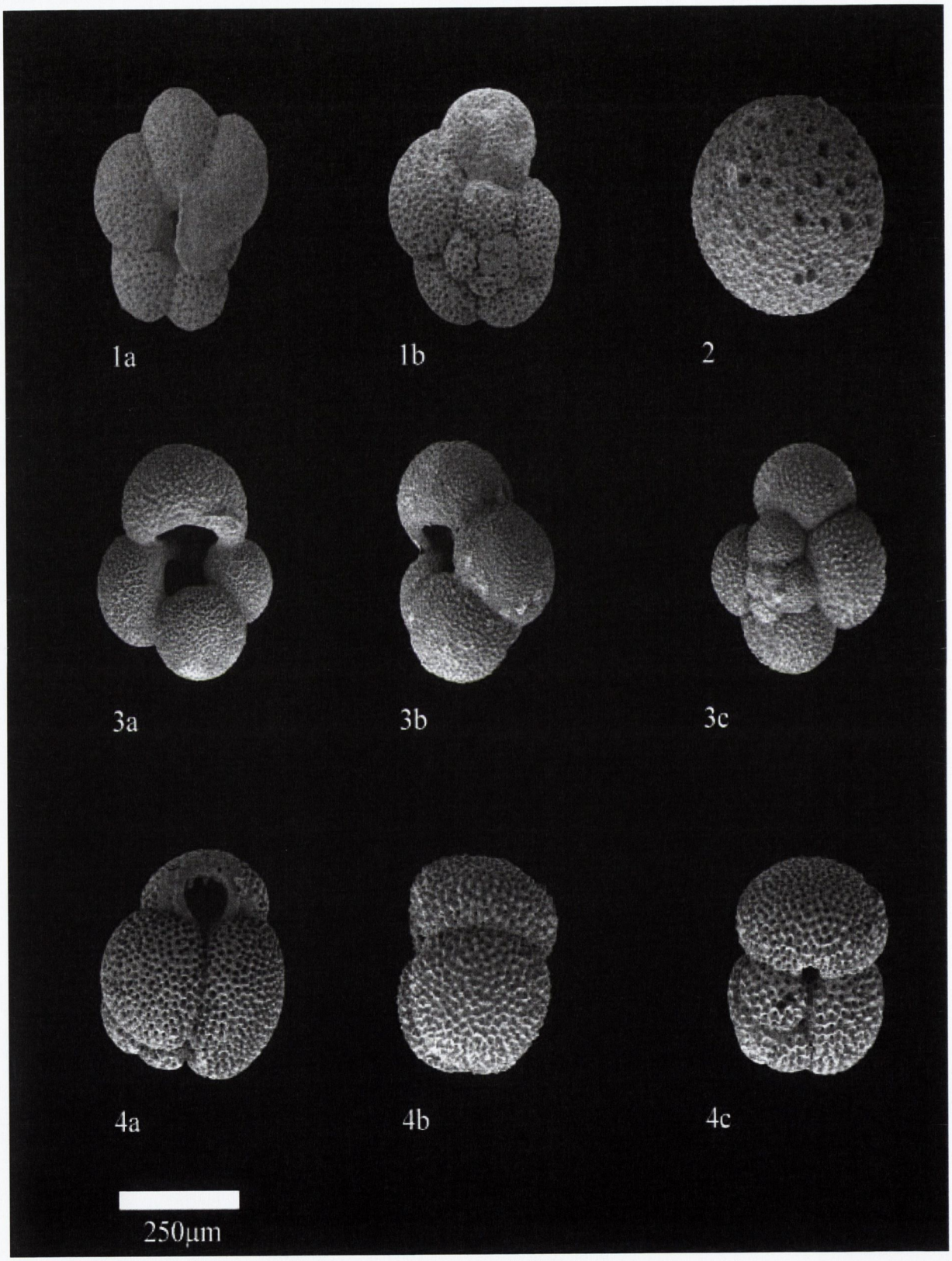

PLATE 13



PLATE 14 – Scale bar = 250µm

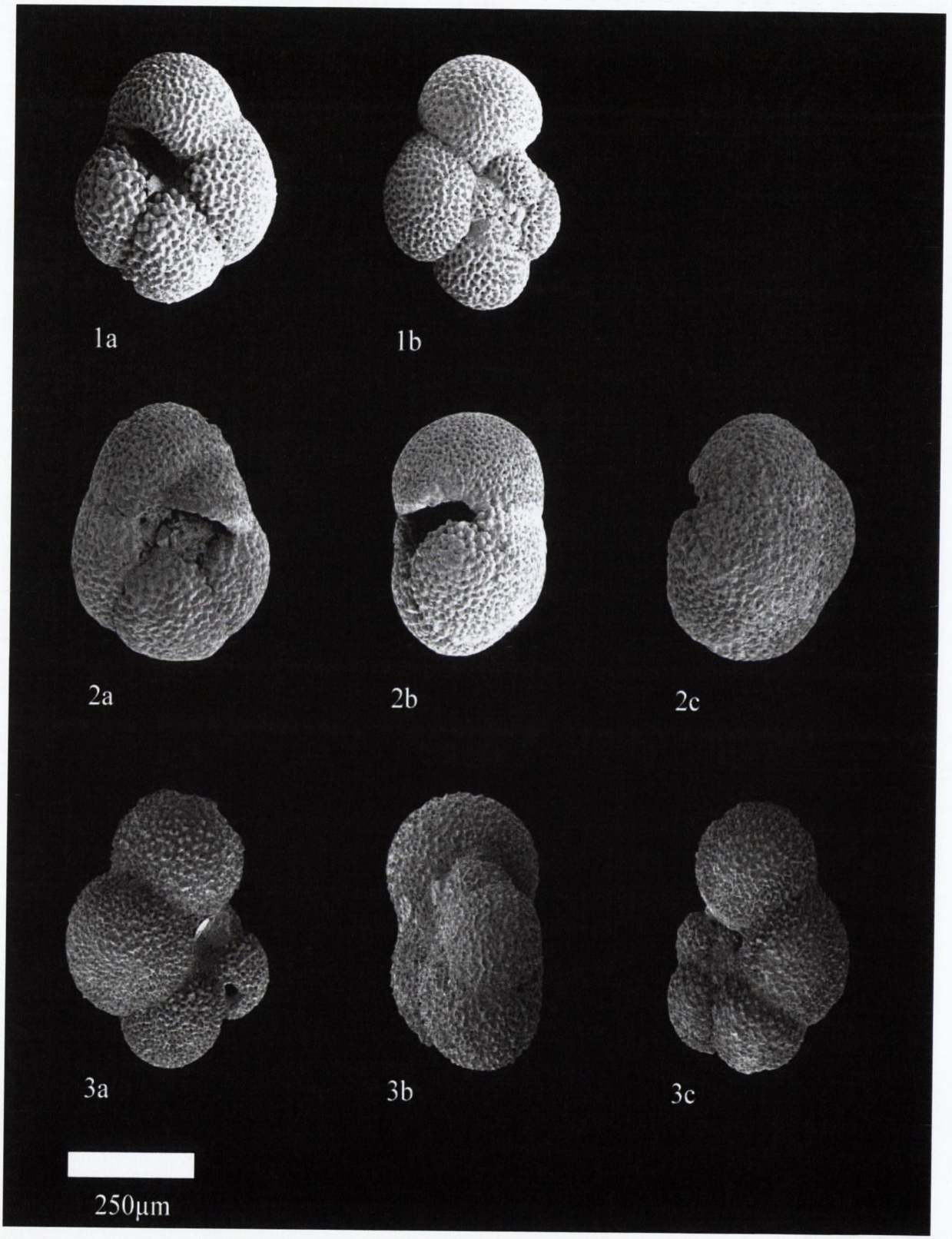

PLATE 15

Chapter 5: Age model development and fragmentation

5.1 Introduction

Developing a robust age model based on multiple lines of evidence is necessary in order to examine the relative timing of key events in the past. The chronologies presented here for the seven gravity cores examined in this study are based on correlation of *%N.pachyderma* (sin.) curves to reference curves (see Table 5.1). This follows the method outlined in Chapter 3 (see Sections 3.3 and 3.4) and has been used in previous studies from a nearby locality (e.g. Peck *et al.* 2007). A whole core chronology is established for four cores (9/97-10, 9/97-03, 9/97-27/2 and 9/97-20) which are chosen due to the lack of obvious reworking in the sedimentological record (Toms pers. comm.). For three cores (9/97-04, 9/97-14 and 9/97-08) a chronology extending back to the previous interglacial is developed. The chronologies are applied in the following chapters (Chapter 6-9). Reservoir ages for ^{14}C AMS radiocarbon dates obtained by Toms (in prep.) are calculated following the method outlined in Chapter 3. The graphic logs presented in this chapter are from Toms (in prep.).

An examination of the degree of fragmentation of a foraminiferal residue provides a qualitative estimate of the degree of dissolution that residue has undergone (see Section 3.3), highlighting samples that are likely to have undergone significant post-mortem modification. Berger (1970) proposed a threshold value of 20% above which significant dissolution / post-mortem modification has probably occurred. This will be applied to the cores used in this study, to highlight samples and intervals that have been significantly altered. An alternative method, suggested by Le and Shackleton (1992) is also applied, as it is considered that this newer method improves the linearity between fragmentation and dissolution (see Section 2.5).

A previous chronology established for this region by Øvrebø *et al.* (2006) was sufficient for the broad (glacial-interglacial) variations of interest to that study. For the purposes of this project, this chronology will need to be extended as many of the cores extend beyond the previous interglacial. It will also be necessary to produce a reliable age model for shorter-term climatic variations (e.g. stadial-interstadial variations) and events (Heinrich events). This will then aid correlations and comparisons between cores, as well as providing an independent test of the correlations and chronologies proposed by other methods (such as nannofossil biostratigraphy and lithostratigraphy).

5.2 Results

Core 9/97-10

The *%N.pachyderma* (sin.) curve for 9/97-10 is correlated with the benthic oxygen isotope profile of ODP site 980 (McManus *et al.* 1999). This record is selected as a reference for the intermediate depth cores (≤2118m water depth) as it provides a high resolution (millennial scale) record from a site that is proximal to this study area. It is also considered to provide a length of record approximately equivalent to that of core 9/97-10 (based on visual counting of 'lighter' and 'darker' coloured units revealing 6-7 glacial-interglacial cycles), as it extends back to approximately 520 kyr B.P.. Peaks and troughs in the *%N.pachyderma* (sin.) curve are correlated to those in the ODP 980 curve in the correlation window (Figs. 5.1 and 5.2). When the highest possible correlation coefficient is achieved, the process is terminated (see Section 3.4). Plotting the resultant sedimentation rates against depth (Fig.5.3a) reveals a

varied sedimentation rate. Core 9/97-10 provides a mixture of high (~2-3cm/kyrs) moderate (0.5-1cm/kyrs) and low (0.1-0.4cm/kyrs) resolution records of sedimentation from ~450 kyrs

Core ID	Correlation curve	Supplementary data	Reference curve	Correlation coefficient
9/97-10	%N.pachyderma (sin.)	Nannofossil biostrat. + 14C AMS dates (Toms in prep.)	ODP 980 (McManus et al. 1999)	$r^2 = 0.72$
9/97-03	%N.pachyderma (sin.)		ODP 980 (McManus et al. 1999)	$r^2 = 0.76$
9/97-04	%N.pachyderma (sin.)		ODP 980 (McManus et al. 1999)	$r^2 = 0.65$
9/97-14	%N.pachyderma (sin.)	Nannofossil biostrat. + 14C AMS dates (Toms in prep.)	ODP 980 (McManus et al. 1999)	$r^2 = 0.68$
9/97-08	%N.pachyderma (sin.)		ODP 980 (McManus et al. 1999)	Not applicable
9/97-27/2	%N.pachyderma (sin.)	Nannofossil biostrat. + 14C AMS dates (Toms in prep.)	GISP-II (Grootes and Stuiver 1997)	$r^2 = 0.90$ (0-94cm), $r^2 = 0.42$ (94-262cm)
9/97-20	%N.pachyderma (sin.)		GISP-II (Grootes and Stuiver 1997)	$r^2 = 0.81$

Table 5.1. Dating and correlation methods applied to each core, with reference curves used and resulting correlation coefficients.

B.P. to the Mid-Holocene, assuming an absence of significant hiatuses. The age-depth plot for this core (Fig. 5.3b) displays no evidence of any hiatuses, although there are two sharp increases in age versus depth at 30cm and 80-95cm. Reservoir ages for the two ^{14}C AMS radiocarbon dates obtained by Toms (pers. comm.) are also calculated (Appendix E) and are consistent with those recorded from adjacent areas (e.g. Waelbroeck *et al.* 2001; Peck *et al.* 2007). Fragmentation indices (Fig. 5.4) display a clear variation in line with changes in sedimentology, with higher values present in lighter coloured units and lower values in darker coloured units.

The oxygen isotope data used for correlation with the profile of Øvrebo *et al.* (2006) follow an expected pattern, with more 'negative' values in the inferred interglacial units and more 'positive' values in glacial units (Fig. 5.5). This uses the same species (*Globigerina bulloides*) as Øvrebø *et al.* (2006) and a composite plot of their data with data from this study displays significant overlap (Fig. 5.6). The only data from this study which does not overlap are those from samples which are older than those analysed by Øvrebø *et al.* (2006), who only measured samples dating back to the last interglacial (approx. 125 kyr B.P.). The palaeoceanographic implications of the $\delta^{18}O_{planktonic}$ values are discussed in Chapter 7.

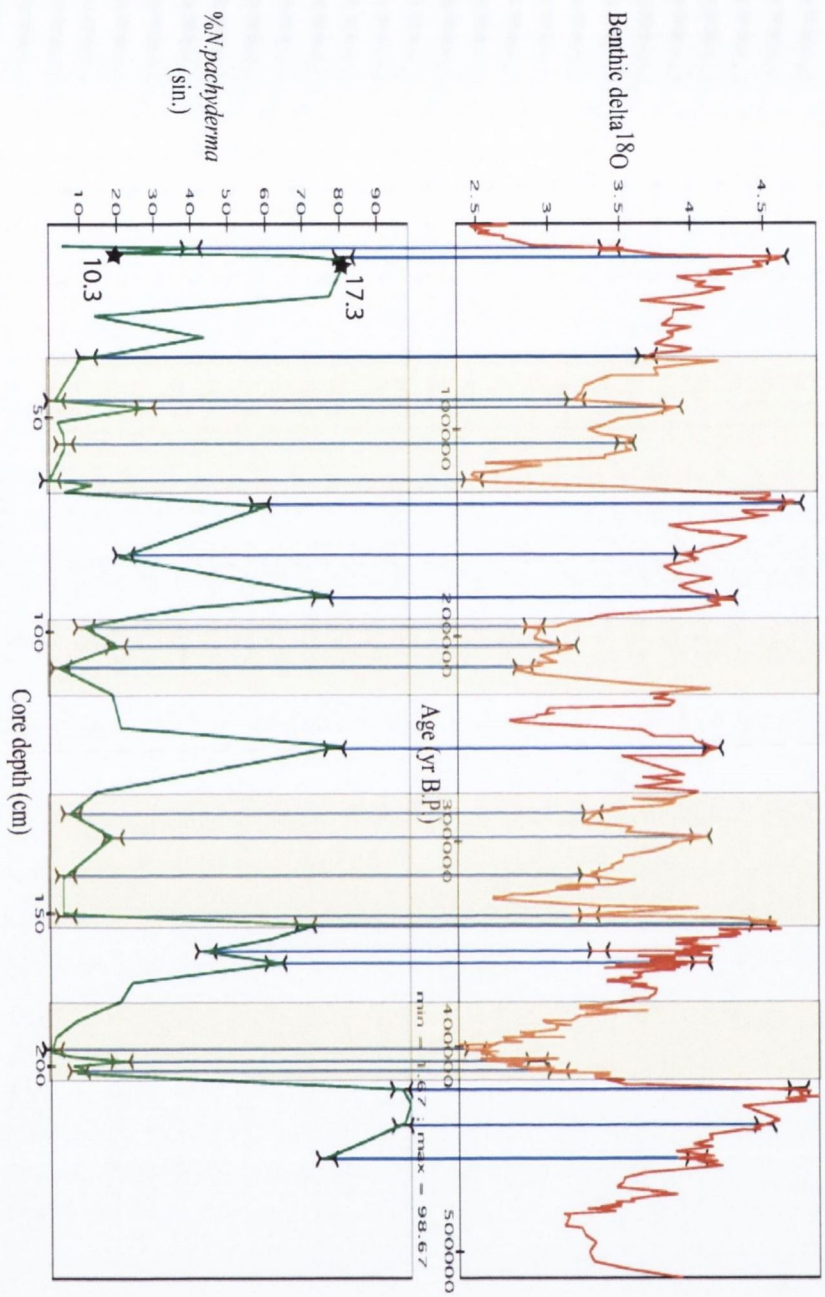

Figure 5.1. Correlation window with *%N.pachyderma* (sin.) data from core 9/97-10 (green curve) correlated to the benthic oxygen isotope profile of ODP site 980 (red curve). Blue lines indicate tie-points. Yellow shading indicates Marine Isotope Stages (numbers above graphs) based on calcareous nannofossil biostratigraphy. Stars indicated ^{14}C AMS radiocarbon dated samples, with adjacent numbers indicating age kyr B.P.

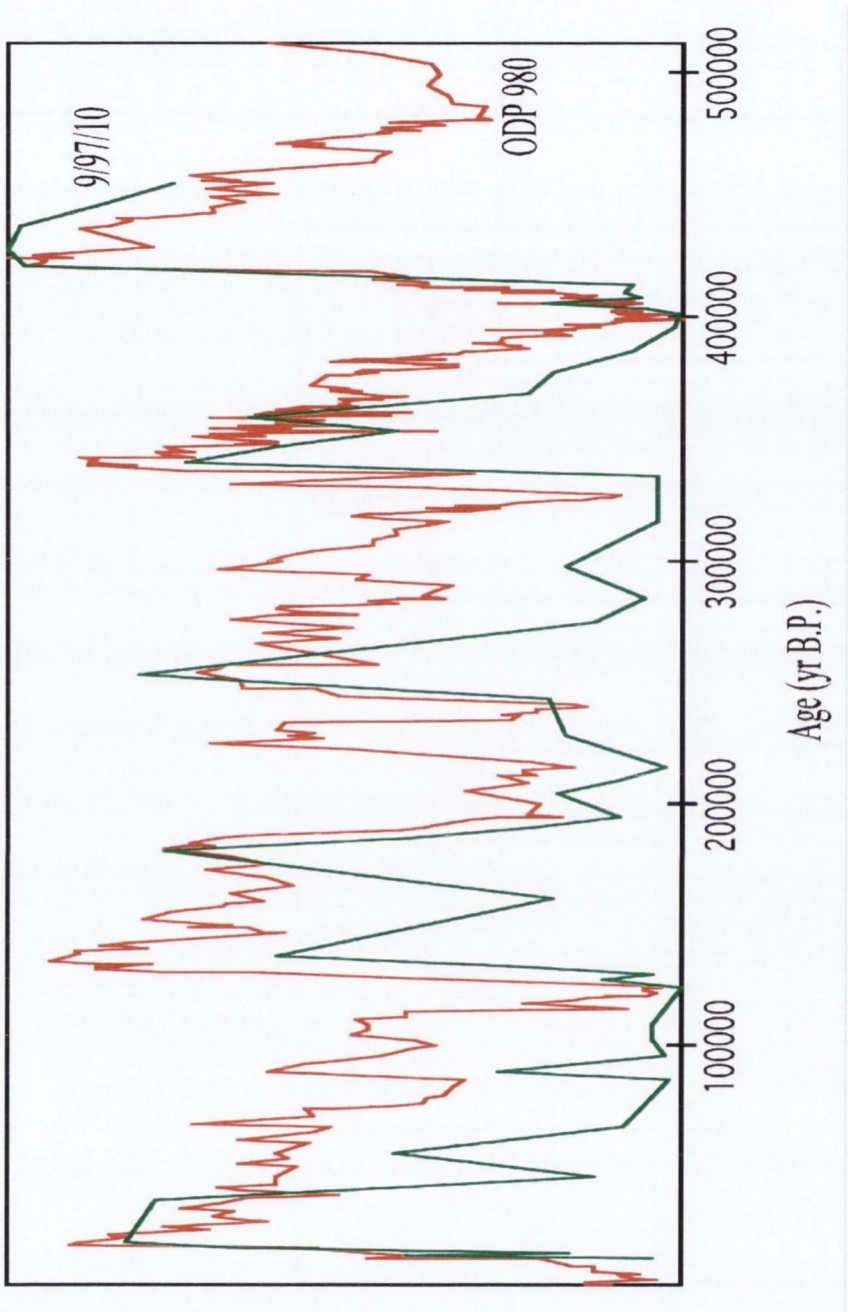

Figure 5.2. Result of overlaying the *%N.pachyderma* (sin.) curve (green line) of core 9/97-10 on to the benthic oxygen isotope profile of ODP site 980 (red line). Note the relatively poor record (or lack of correlation) between 200 and ~330 kyr B.P.

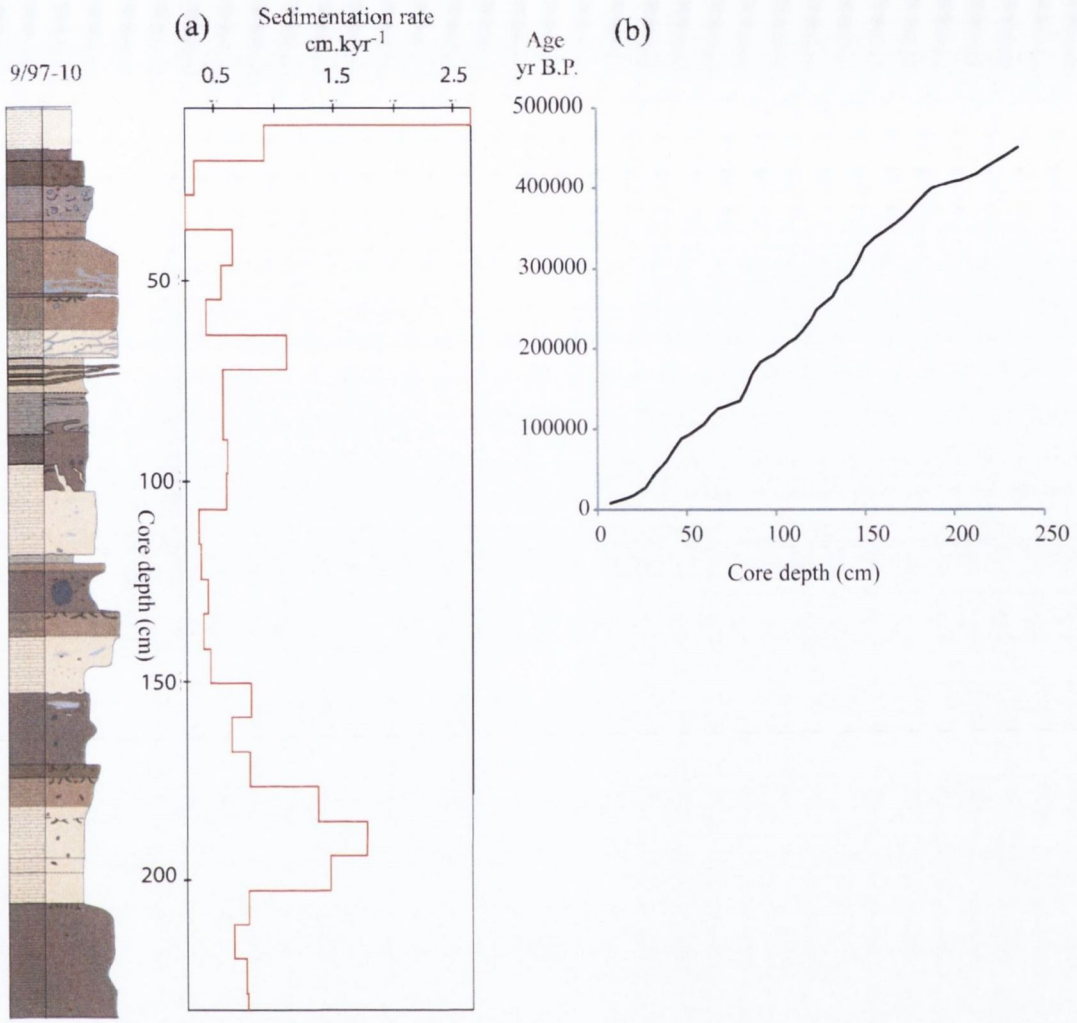

Figure 5.3. (a) Variations in sedimentation rate with depth and (b) age-depth plot for core 9/97-10.

Spectral analysis of the $\delta^{18}O_{planktonic}$ curve for core 9-97-10 (see Chapter 3, section 3.4) reveals the nature of the apparently cyclical variations in $\delta^{18}O_{planktonic}$ (Fig. 5.7). This produces peaks at 0.013, 0.0316, 0.0552 and 0.0623 (broadly consistent with the 1: 2.44: 4.348: 4.763 ratio predicted for an orbital pacing of 100kyrs, 41kyrs, 23kyrs and 19kyrs cycles over a 400kyr time period) with the two strongest peaks at 0.013 and 0.0623.

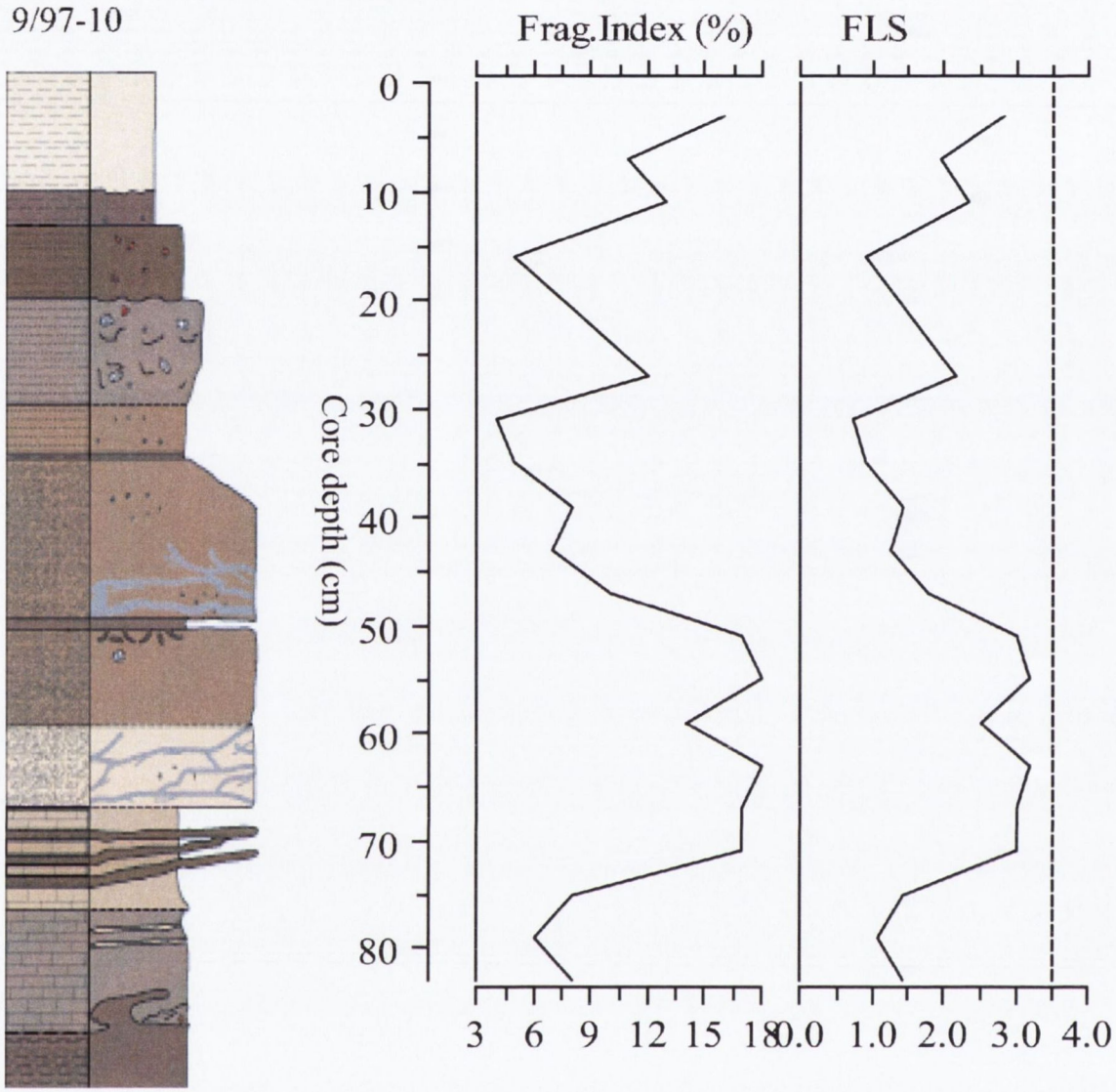

Figure 5.4. Fragmentation indices for the upper 83cm of core 9/97-10. FLS refers to the Le and Shackleton (1992) index.

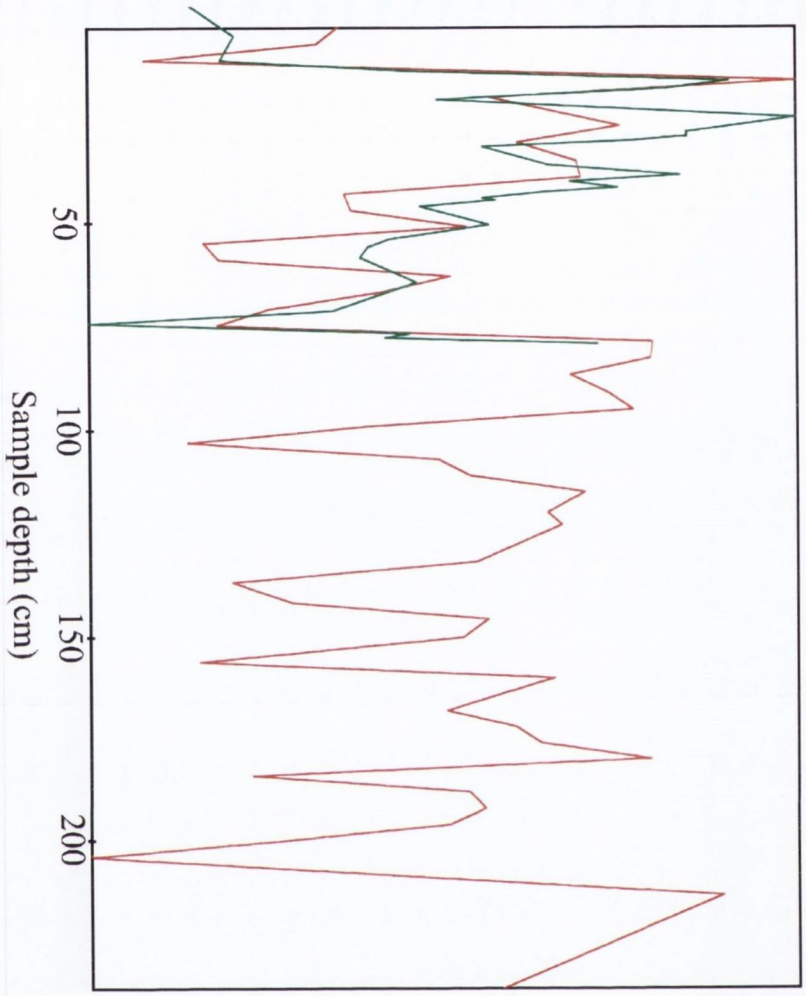

Figure 5.5. Result of overlaying the $\delta^{18}O_{planktonic}$ record from core 9/97-10 from this study (red line) with that from Øvrebø *et al.* (2006) – (green line).

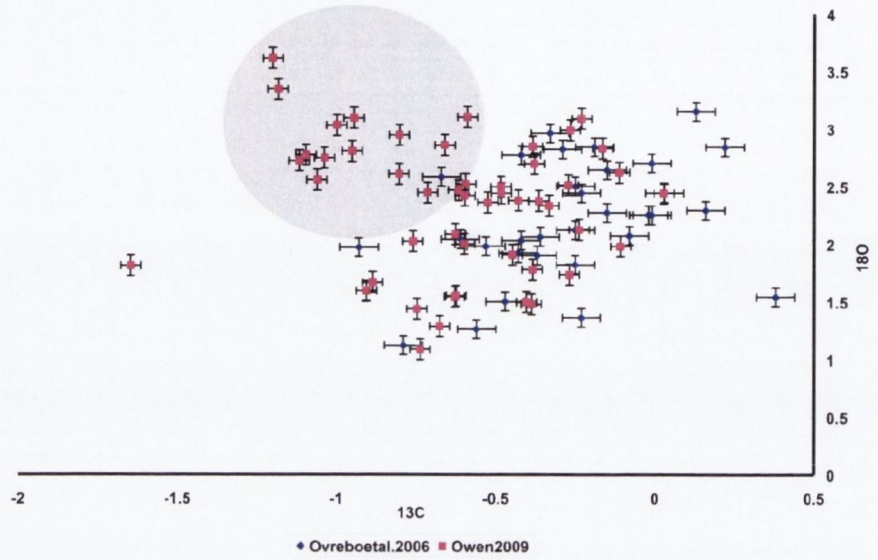

Figure 5.6. Stable isotope data from Øvrebø *et al.* (2006) plotted against data obtained in this study (Owen 2009). Data from this study that plots separately from that of Øvrebø *et al.* (2006) is highlighted by the grey oval.

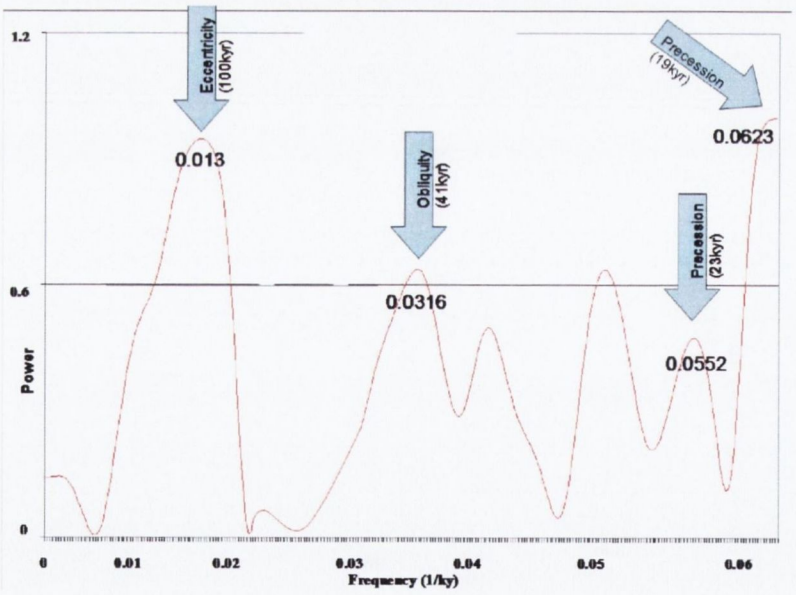

Figure 5.7. Spectral analysis of the $\delta^{18}O_{planktonic}$ curve from core 9/97-10. Note the high power peaks at eccentricity (100kyr) and precession (19kyr) frequencies.

Core 9/97-03

Correlation with ODP 980 suggests that this core preserves a generally low resolution (0-1.1cm / kyr) record (Fig. 5.8a) that extends back to almost 500 kyr B.P. A high resolution (>1 cm / kyr) record between 139-229cm core depth (415-479 kyr B.P.) is also preserved. An hiatus is identified at 125cm core depth (Fig. 5.8b), illustrated by the sharp increase in age versus depth. This hiatus represents a gap of approximately 31 kyrs between 340-371 kyr B.P.

Records of fragmentation for this core (Fig. 5.9) show that preservation is highly variable with no clear link between fragmentation and lithology present. The second largest peak in fragmentation indices is recorded at 125cm core depth, corresponding with the hiatus.

Core 9/97-04

A major hiatus is identified between 38-40cm core depth (Fig. 5.10a), which represents a gap of approximately 50 kyrs. The age of this hiatus is dated between 41-89 kyr B.P, according to the age-depth plot (Fig. 5.10b). The hiatus produces a significantly larger sedimentation rate (>7cm / kyr) for samples at 44-47cm core depth, and an extremely low rate of sedimentation (<0.5cm / kyr) between 38-42cm core depth. This will need to be considered when rates of accumulation of benthic foraminifera are calculated for this core (see Chapter 8). The hiatus is linked to a lithological boundary between 38-42cm core depth (Fig. 5.10a). The boundary is a sharp, irregular contact between two muddy foraminifera sand units, with rip-up mud clasts present in the lower unit (Toms per comm.). An age-depth plot for this core (Fig. 5.10b) suggests that this

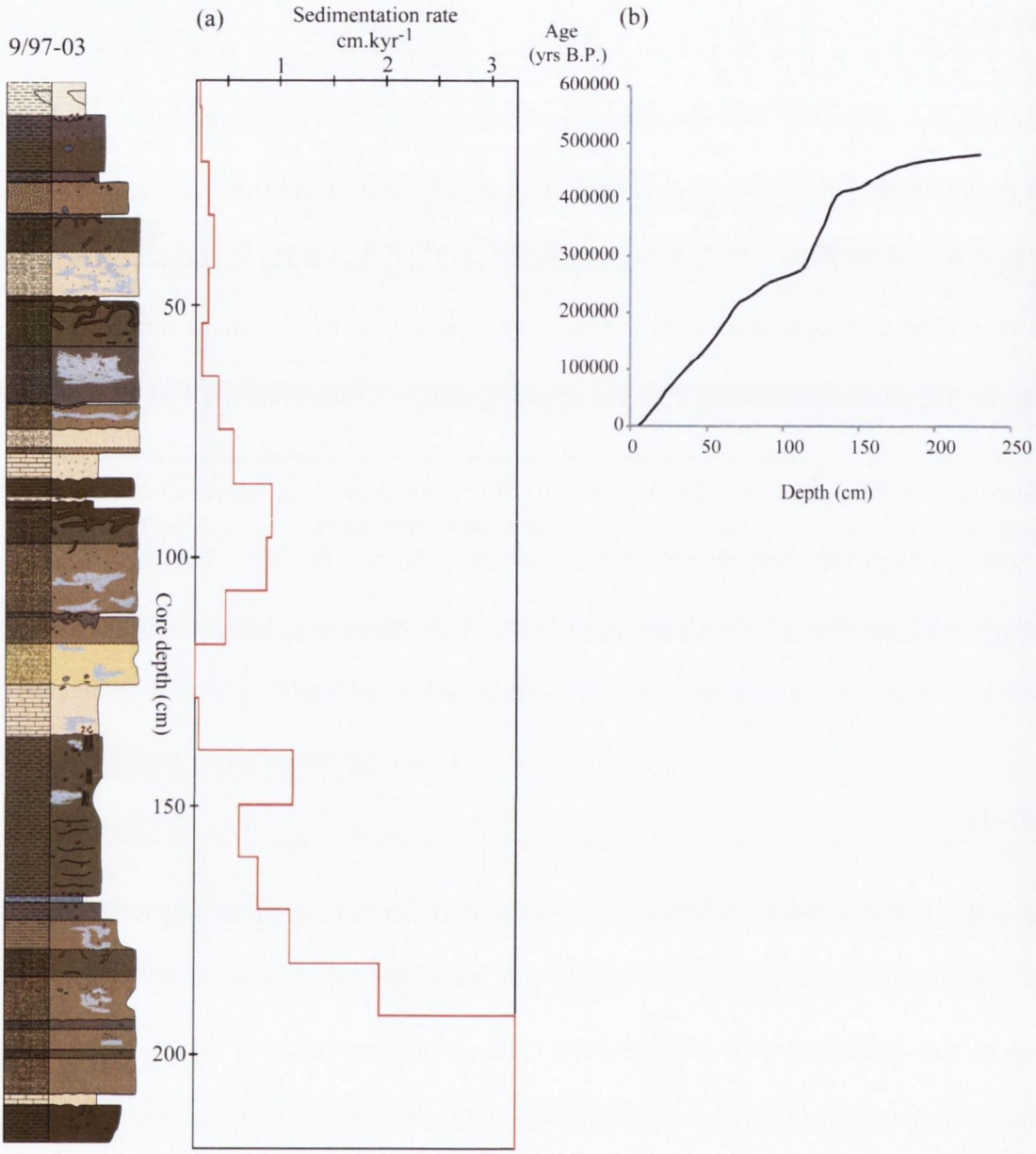

Figure 5.8.(a) Variations in sedimentation rate with depth and (b) age-depth plot for core 9/97-03.

core preserves a relatively high resolution (>1.5cm / kyr) record of the late last glacial – Holocene (0-17 kyr B.P.) and a relatively low resolution (<1cm / kyr) record of MIS 3 to

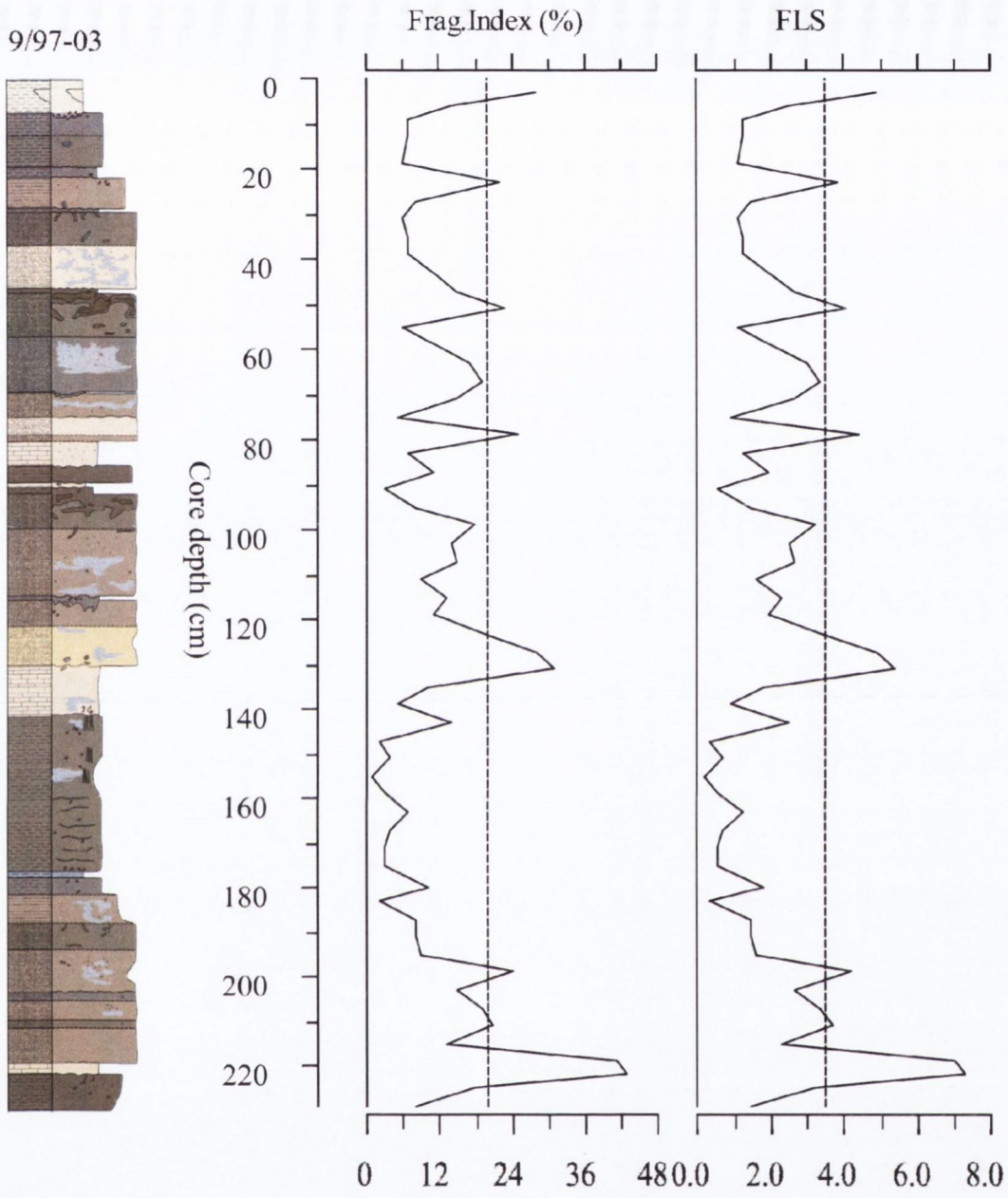

Figure 5.9. Fragmentation indices for the whole of core 9/97-03. FLS refers to the Le and Shackleton (1992) index.

the late last glacial (17-41 kyr B.P.). The record of the early phase of MIS 5 / late phase MIS 6 (115-138 kyr B.P.) appears to be of a relatively moderate resolution (approx. 1cm / kyr).

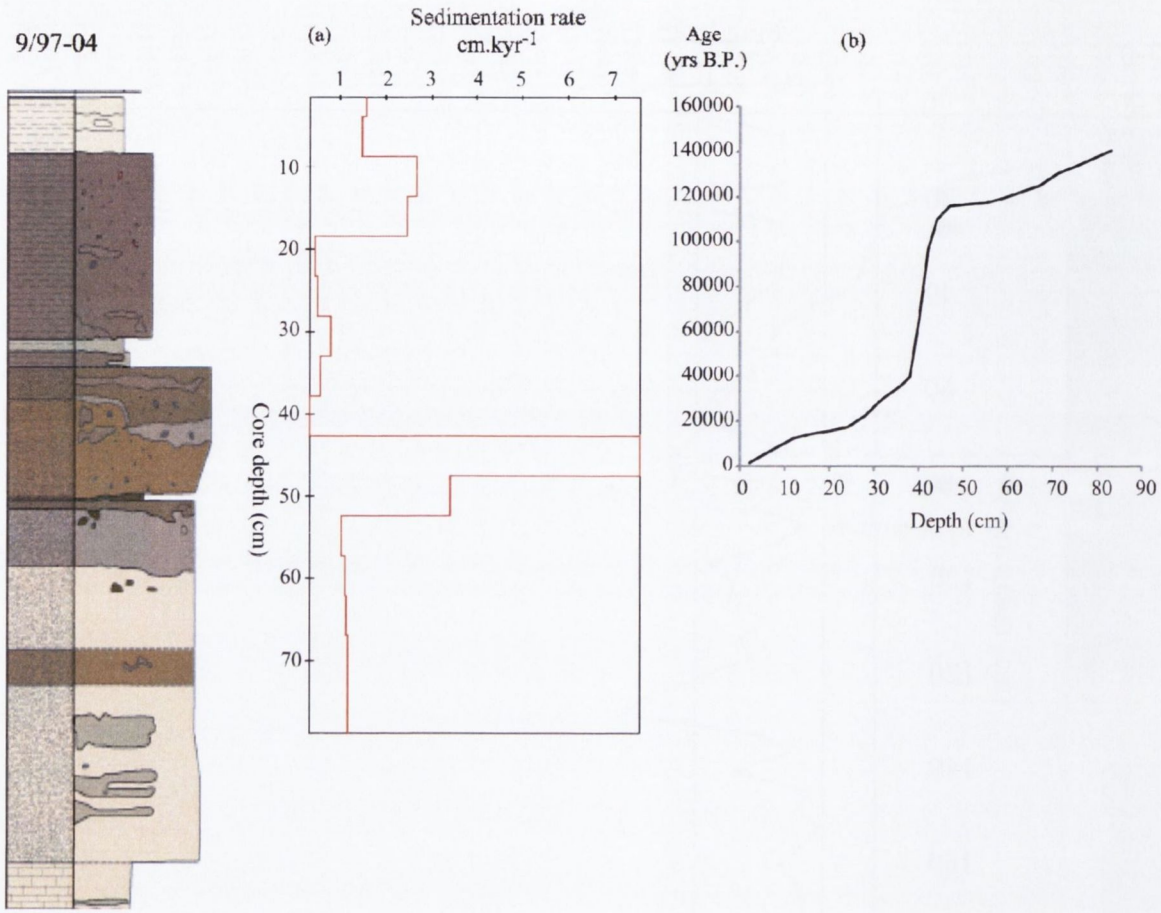

Figure 5.10.(a) Variations in sedimentation rate with depth and (b) age-depth plot for core 9/97-04.

An examination of the downcore fragmentation indices (Fig. 5.11) reveals that no sample exceeds the 20% threshold suggested as the limit above which significant dissolution / post mortem modification of assemblages has probably occurred (Berger 1970). Interglacial samples generally record higher fragmentation indices compared to glacial samples. The hiatus described previously records relatively low fragmentation indices compared to adjacent samples.

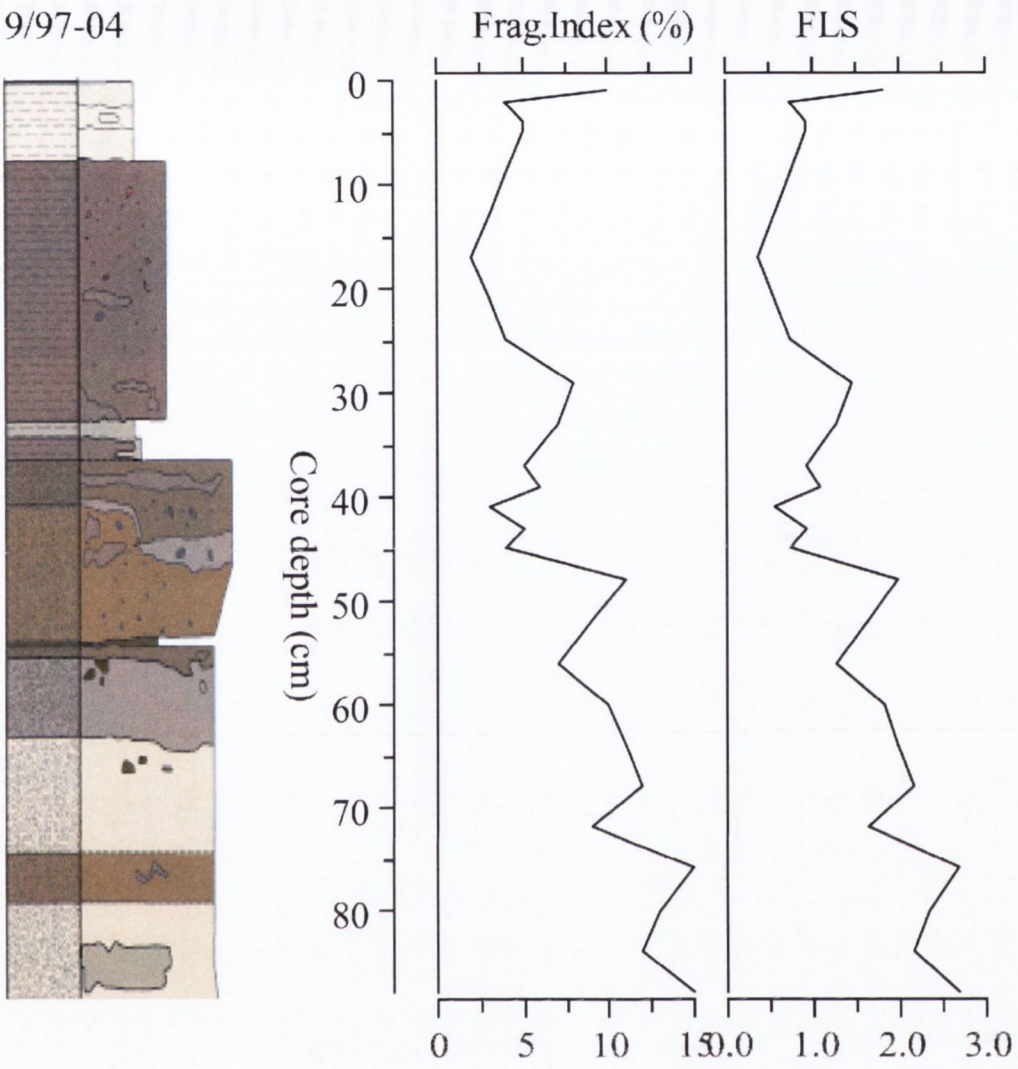

Figure 5.11. Fragmentation indices for the upper 88cm of core 9/97-04. FLS refers to the Le and Shackleton (1992) index.

Core 9/97-14

The calculated sedimentation rates for this core are variable (Fig. 5.12a); with low rates (≤1cm / kyr) between 0-16kyr B.P. and 31-55 kyr B.P. (a hiatus is present in the latter – Fig. 5.12b). Sedimentation rates are relatively high (>1.5cm / kyr) between 16-30 kyr B.P.

and 134-142 kyr B.P. Reservoir ages of the two ^{14}C AMS radiocarbon dates obtained by Toms (pers. comm.) are also calculated (Appendix D).

Plotting fragmentation indices versus depth for this core shows that fragmentation was never greater than 15% (Fig. 5.13). There is a systematic variation in fragmentation with climate, with last glacial samples recording lower fragmentation indices compared to the Holocene and the previous interglacial.

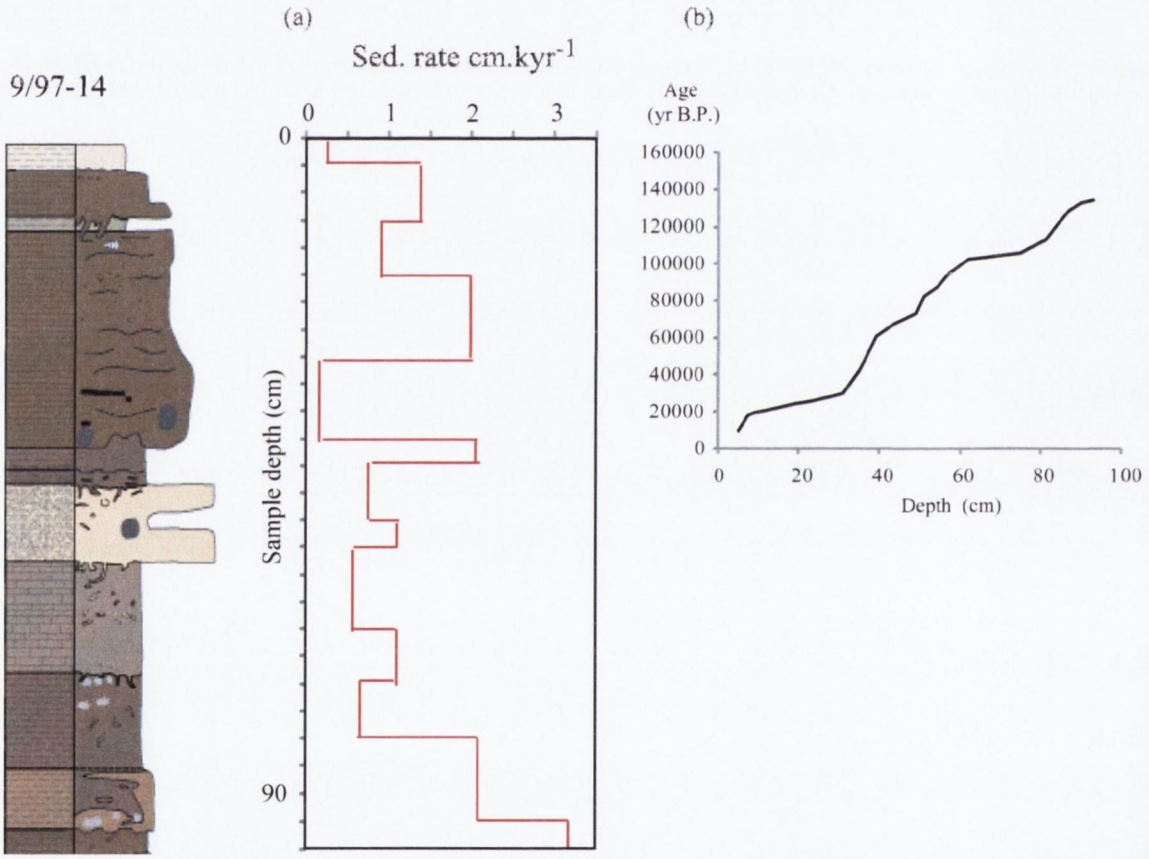

Figure 5.12.(a) Variations in sedimentation rate with depth and (b) age-depth plot for core 9/97-14.

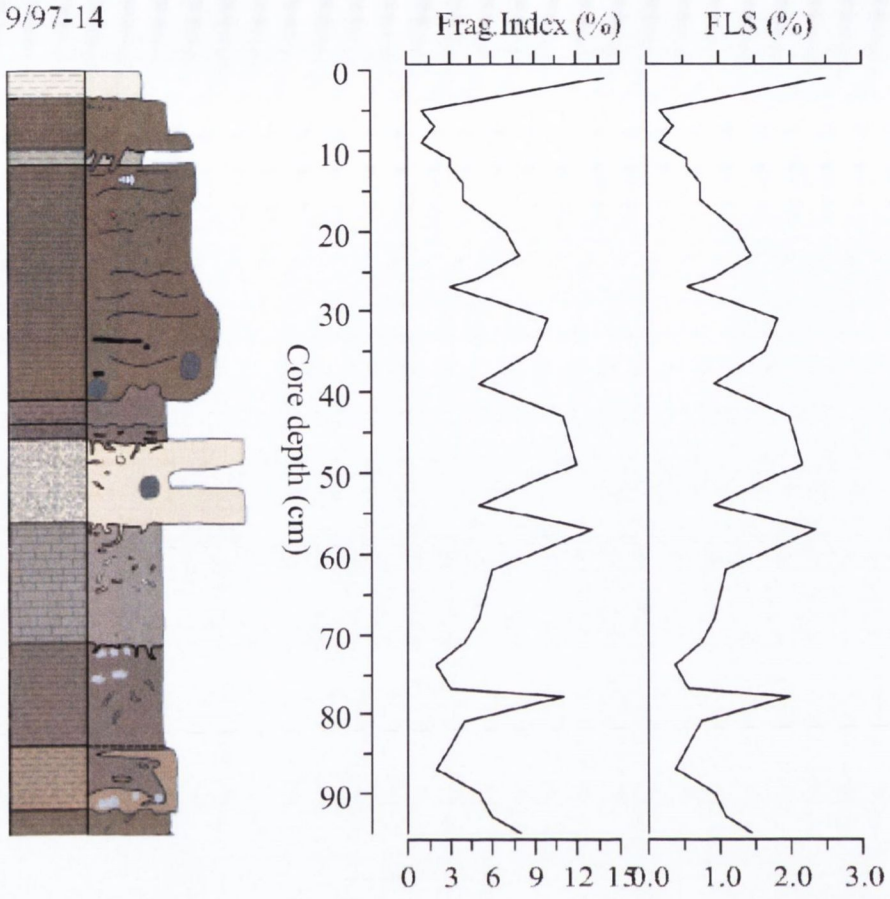

Figure 5.13. Fragmentation indices for the upper 95cm of core 9/97-14. FLS refers to the Le and Shackleton (1992) index.

Core 9/97-08

An examination of the *%N.pachyderma* (sin.) data shows that this core can at least be subdivided (Fig. 5.14) into an initial last glacial unit (0-79cm) followed by a last interglacial section (83-109cm), but developing an internal age model using this method is unlikely to produce a reliable chronology due to the large amount of sediment disturbance. The Holocene

is clearly absent. Fragmentation indices are also generally higher in this core compared to the cores deeper along the slope (Fig. 5.14).

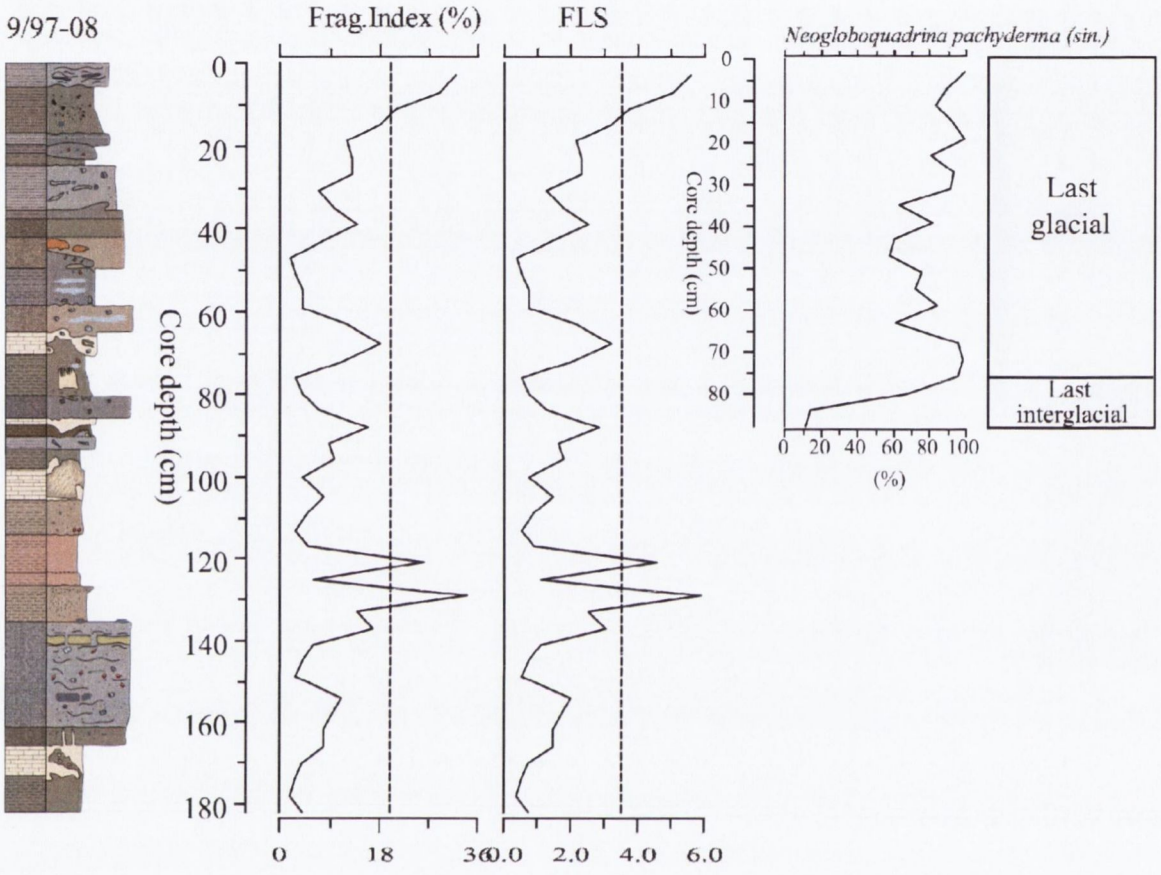

Figure 5.14. Fragmentation indices for the whole of core 9/97-08 and an approximate stratigraphy for the upper 82cm. FLS refers to the Le and Shackleton (1992) index.

Core 9/97-27/2

The relative abundance curves of *%N.pachyderma* (sin.) from the two deeper cores (>2200m water depth) are correlated to the GISP-II oxygen isotope curve (Grootes *et al.* 1993; Grootes and Stuiver 1997). GISP-II is selected for the deeper cores as it provides a high

resolution (sub-millennial scale) record of climatic variation between the present and 100 kyr B.P (see Section 2.3 and Fig. 2.7). The first part of the core (0-94cm) correlates extremely well with the GISP-II data ($r^2 = 0.9026$), lacks any obvious significant hiatuses and provides a high resolution (4-5cm/kyr) record of the early

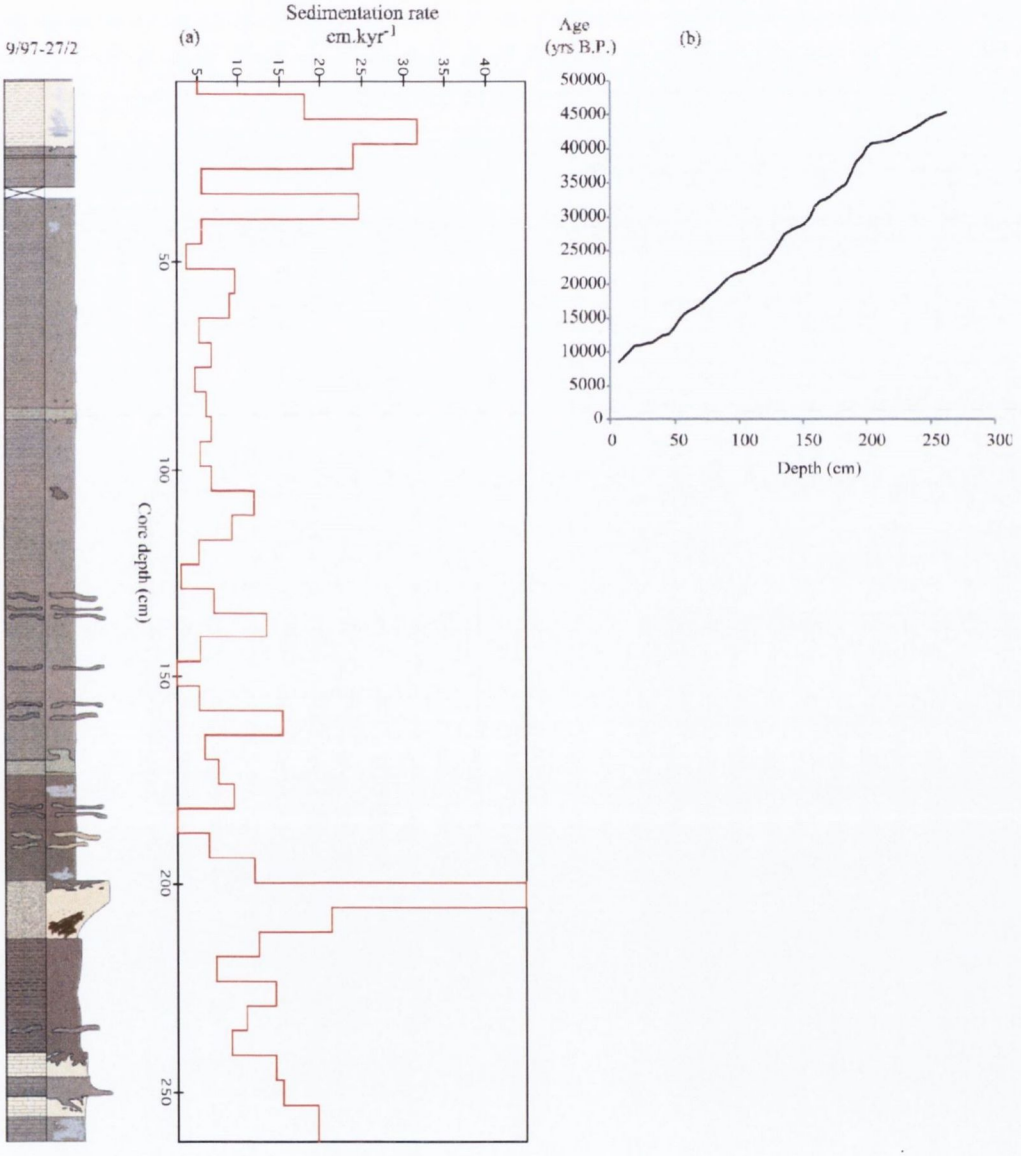

Figure 5.15.(a) Variations in sedimentation rate with depth and (b) age-depth plot for core 9/97-27/2.

Holocene and late last glacial. However, the lower section of the core (94-262cm) is poorly correlated ($r^2 = 0.4201$; Fig. 3.7). Records of stadials at 30kyrs B.P. and 35-

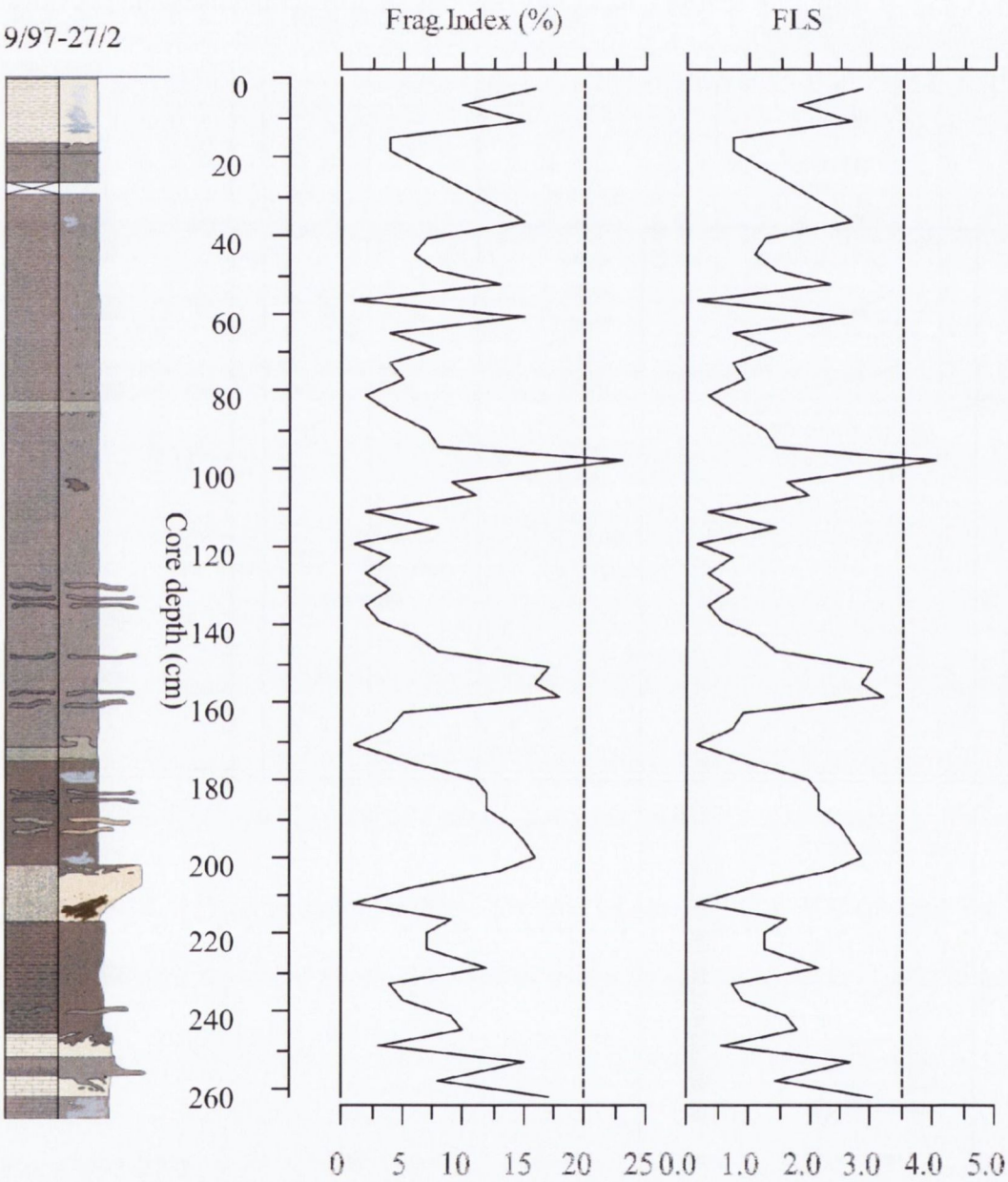

Figure 5.16. Fragmentation indices for the whole of core 9/97-27/2. FLS refers to the Le and Shackleton (1992) index.

41kyrs B.P. appear to be missing from the core. Adjusting parts of the *%N.pachyderma* (sin.) curve with earlier parts of the GISP-II record is possible, but results in unrealistic reservoir ages (approximately 10kyrs). Therefore, the assumption is made that the

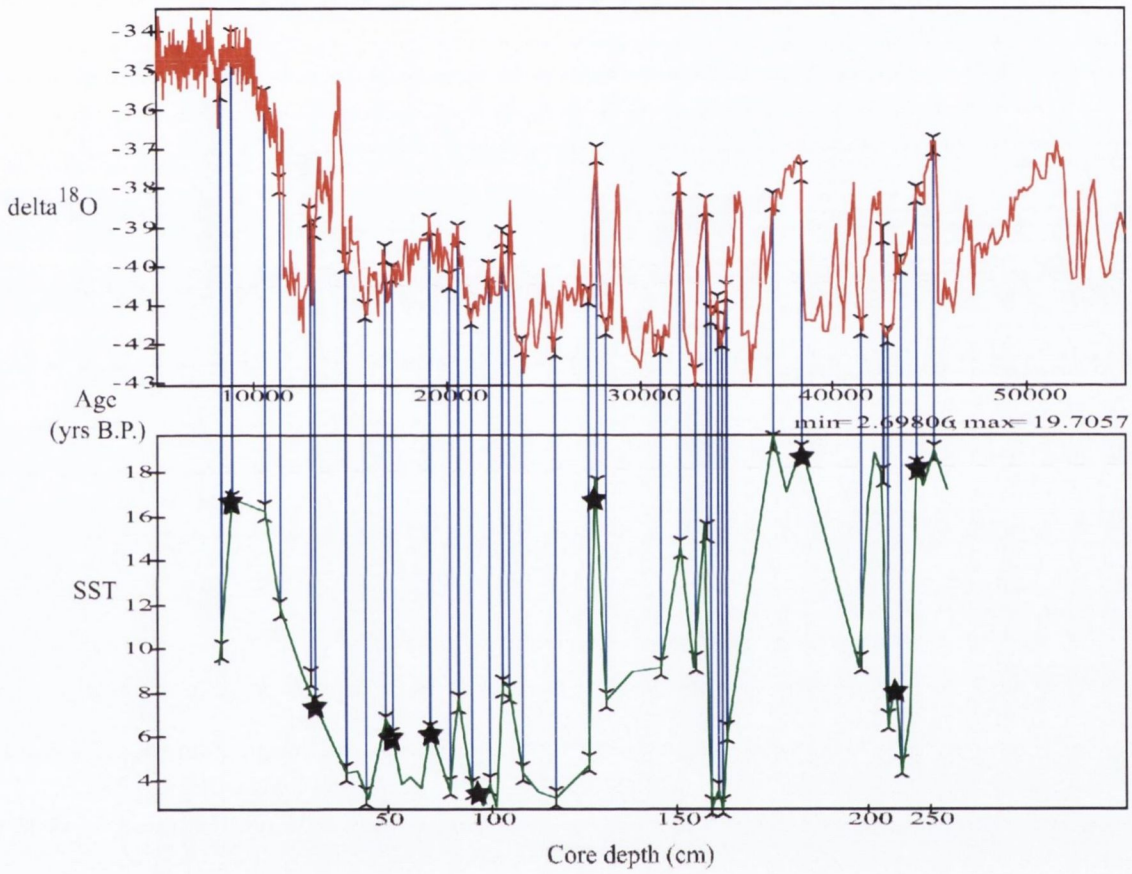

Figure 5.17. Correlation of the MAT reconstructed SSTs for core 9/97-27/2 (green line) with the $\delta^{18}O$ record of GISP-II (red line). Blue lines indicate tie-points, stars denote the positions of ^{14}C AMS radiocarbon dated points.

stadials mentioned are absent from the record, or are being masked by bioturbational mixing or physical reworking incorporating 'warm water' taxa into the stadials. Core depths proposed

for these hiatuses (145cm and 160cm respectively) do not correspond to any obvious lithological boundaries in 9/97-27/2. The overall result of the correlation exercise shows a record that extends back to ~45000 yrs B.P. from the Holocene. Reservoir ages are calculated for the ^{14}C AMS radiocarbon dates obtained by Toms (pers. comm.) following the correlation exercise.

Sedimentation rates (Fig. 5.15a) do appear to vary in line with variations in sedimentology, with lighter coloured units recording higher sedimentation rates (>10cm / kyr) compared to darker coloured units (<10cm / kyr). The gradient of the age-depth plot does not vary significantly (Fig. 5.15b), although some subtle increases in the gradient do occur at 151cm and 180-190cm depth. Plotting fragmentation indices against depth for this core reveals a highly variable preservation state, with no systematic co-variation between fragmentation and lithology (Fig. 5.16). The fragmentation index is quite high (>15% or 3.0) for samples between 145-160cm core depth.

Another correlation is attempted, using the Modern Analogue Technique (MAT) reconstructed sea surface temperatures (SSTs) for core 9/97-27/2 (see Chapter 6). This is also correlated with the GISP-II $\delta^{18}O$ curve, and produces a slightly better overall correlation coefficient (r^2 = 0.603). The amplitude of temperature changes between stadials and interstadials is slightly reduced in some sections, enhancing the correlation (Fig. 5.17), but the absence of the two stadials between approximately 35-42 kyrs B.P. remains problematic.

9/97-20

Core 9/97-20 is also correlated with the GISP-II oxygen isotope record. The linear correlation coefficient is very good ($r^2 = 0.813$). Sedimentation rates are variable, but with an average rate of 3-4cm/kyrs (Fig. 5.18a). Two hiatuses are inferred, one between 12-14.5 kyrs B.P. (at 50cm) and one between 24-25 kyrs B.P. (at 90cm) in this record (Fig. 5.18b). Fragmentation indices (Fig. 5.19) do not co-vary with lithology, but a broad trend of higher fragmentation during the Holocene and during interstadials is recorded.

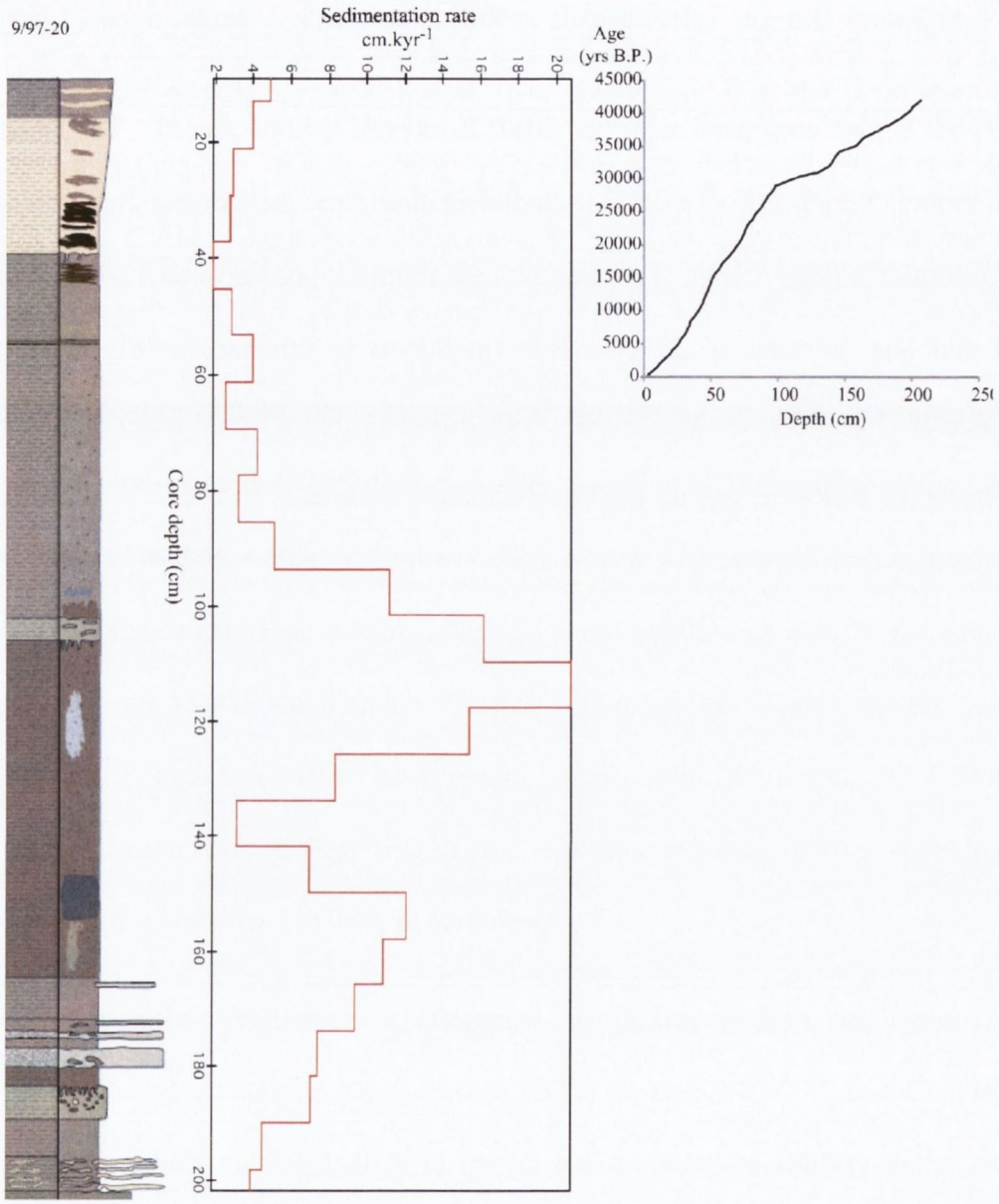

Figure 5.18.(a) Variations in sedimentation rate with depth and (b) age-depth plot for core 9/97-20.

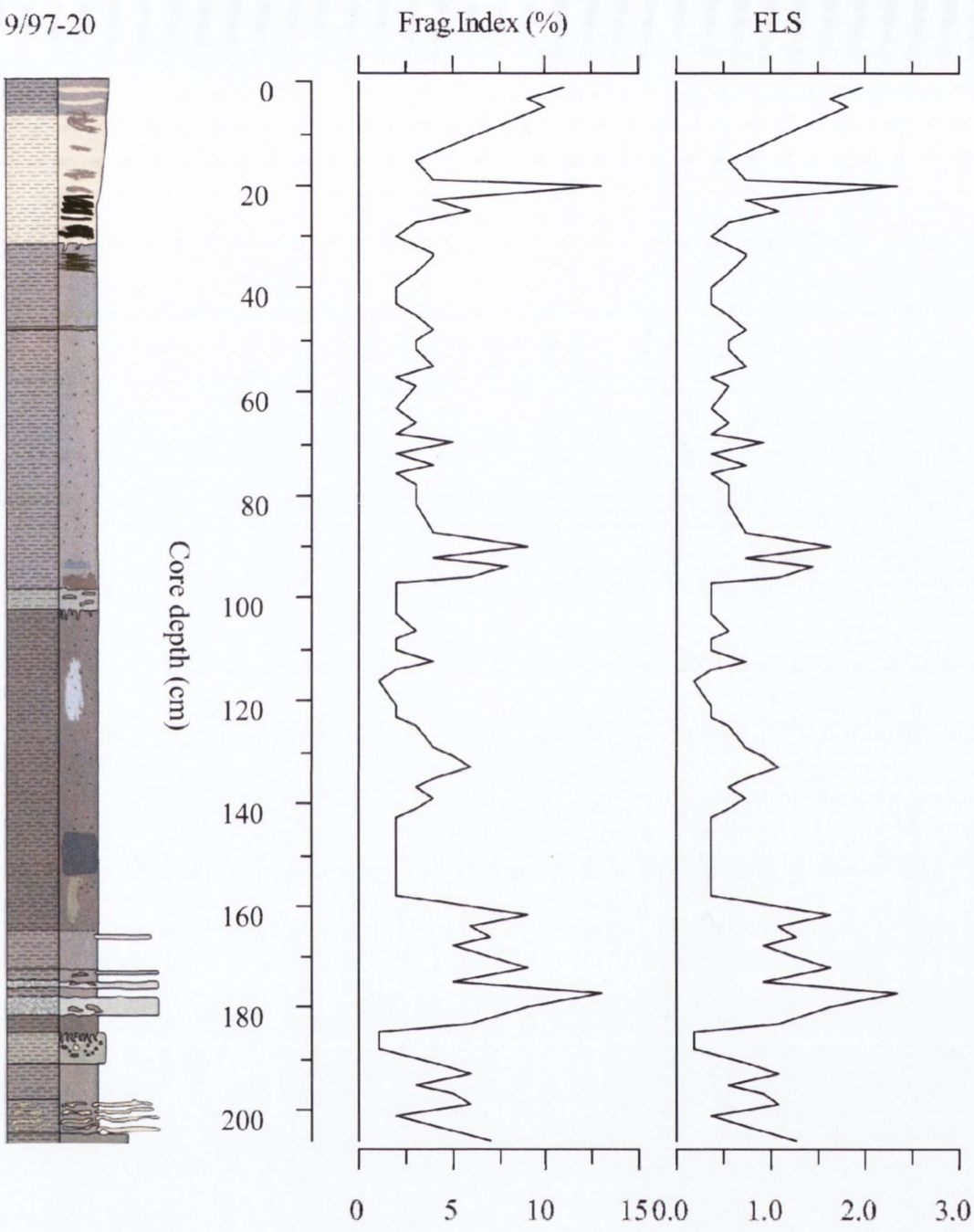

Figure 5.19. Fragmentation indices for the whole of core 9/97-20. FLS refers to the Le and Shackleton (1992) index.

5.3 Discussion

For core 9/97-10, episodes with relatively high rates of sedimentation are not limited to either interglacial (light coloured) or glacial (dark coloured) units. However, the three highest episodes of sedimentation are linked to interglacial deposits. An hiatus is inferred from the results of the correlation and appears to match an appropriate lithological boundary (approx. 30cm core depth). Last interglacial and Holocene samples

record on average higher degrees of fragmentation compared to the last glacial. This could be related to increased bioturbation following increased food supply. Alternatively, this could reflect the increased (during interglacials) influence of bottom current activity, with stronger bottom currents increasing the proportions of test fragmentation. Correlation of the $\delta^{18}O_{planktonic}$ curve from this study (core 9/97-10) with that of Øvrebø *et al.* (2006) reveals similar trends, with lighter values during interglacials and higher values during the last glacial. This should aid correlation between these two discrete portions of the slope, which will be undertaken by Toms (in prep.).

The two strongest peaks from the spectral analysis of the oxygen isotope record for this core indicate that precession and eccentricity cycles may be dominating the orbital pacing. The isotope curve is not a perfect match with the ODP 980 record, which is also supported by the spectral analysis which suggests there is a considerable amount of noise accompanying the orbital pacing. This could be due to the hiatuses and intervals of low sedimentation rate present within the core. Calculated reservoir ages for core 9/97-10 (see Appendix E) suggest that reservoir ages may have been reduced during the last glacial compared to the Holocene, which is contradictory to the general pattern present from other studies. Such a pattern implies

slightly more rapid (by approximately 200 years) atmosphere-ocean exchanges in ^{14}C during the last glacial compared to the Holocene. However, at this stage it is not clear if the last glacial sample used to calculate the reservoir age can be used to extrapolate to the rest of the previous glacial or if it was deposited under unrepresentative oceanographic conditions (e.g. during a Heinrich event).

Cores 9/97-10 and 9/97-03 each provide a record of intermediate depth (approximately 1200-1300m water depth) variations in sedimentation along the western flank of the Porcupine Bank. Each record extends back to Marine Isotope Stage 12 and provides a relatively high resolution record of the transition from Marine Isotope Stage 12 to Stage 11 (Fig. 5.20). The records then diverge, with 9/97-10 containing a relatively poor record between 230-320 kyr B.P. (Marine Isotope Stages 9, 8 and early 7) and core 9/97-03 providing a low resolution record between 250-410 kyr B.P. (Marine Isotope Stages 11, 10, 9 and early 8). The fact that the episodes of low resolution and suspected hiatuses are consistent across the cores (both occur around MISs 9 and 8) suggests that this phase of low resolution records is not core-site specific. Also, this phase appears to start much earlier in core 9/97-03 (MIS 11) but finish later in core 9/97-10 (MIS 7) and each Marine Isotope Stage is still represented (as suggested by the calcareous nannofossil biostratigraphy in core 9/97-10), but not to as high a resolution as the rest of the two records. The combination of factors suggests that this could be caused by a gradual and potentially episodic process of relatively reduced sedimentation rather than one single phase that can be traced between the two cores. Alternatively, this could suggest that the chronologies developed for one or both cores are incorrect, which is more likely in core 9/97-03 which lacks the calcareous nannofossil biostratigraphy of core 9/97-10, although

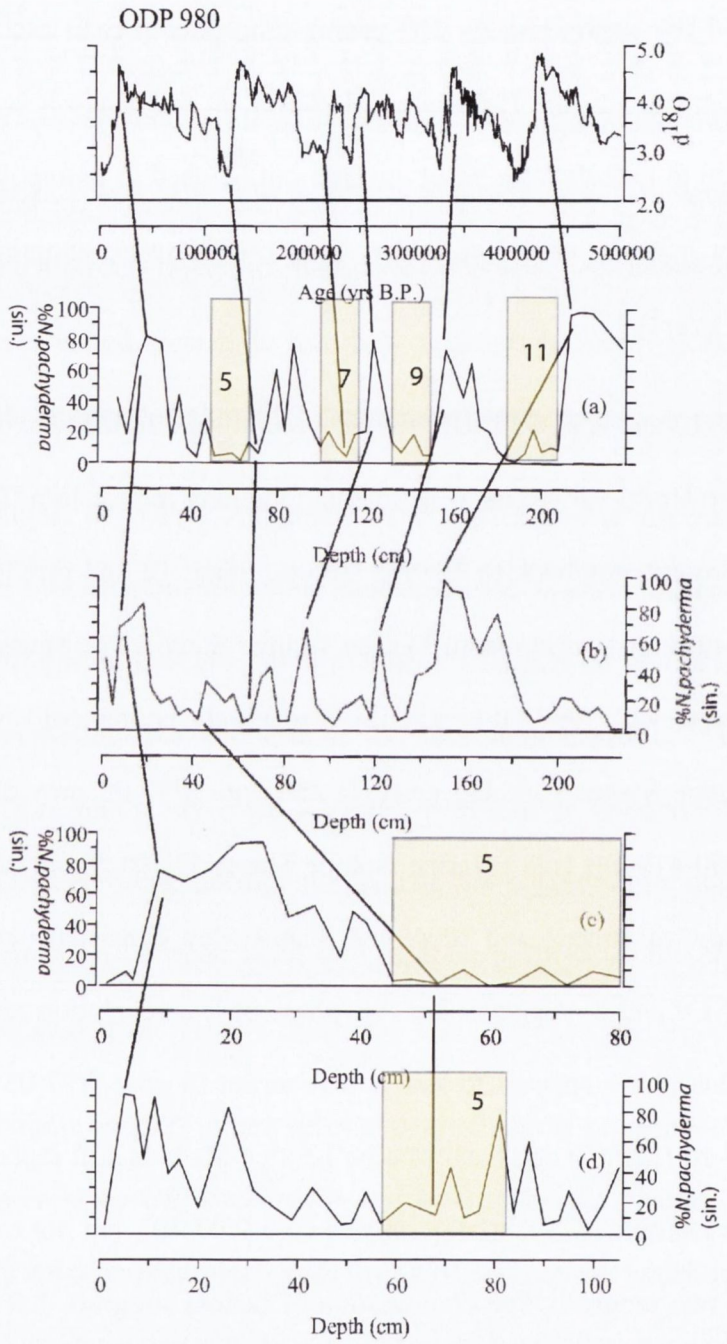

Figure 5.20. Correlation of the $\delta^{18}O$ curve of ODP Site 980 with *%N.pachyderma* (sin.) data from cores (a) 9/97-10, (b) 9/97-03, (c) 9/97-04 and (d) 9/97-14. Yellow shading indicates interglacials (numbered) as suggested by calcareous nannofossil biostratigraphy, with tie-points highlighted.

this interpretation would require an adjustment of almost 100 kyrs in the record of core 9/97-03.

Core 9/97-04 provides an extremely poor record between 120-40 kyr B.P. and core 9/97-14 is missing units deposited between 31-55 kyr B.P. Whether or not this hiatus can be correlated between these two cores is open to debate. Marine isotope stage 3 (30-60kyrs B.P.) is largely absent from two intermediate depth cores (9/97-04 and 9/97-14). In slightly shallower and deeper cores (9/97-10 and 9/97-27/2), this time interval is present, suggesting that the hiatus is localized to a specific depth range (1500-2118m). Most intermediate depth cores examined contained a relatively good resolution record of the transition from the Last Glacial (Marine Isotope Stage 2) to the Holocene (Marine Isotope Stage 1). The exception is core 9/97-14, which contains a large hiatus (approximately 10kyrs) which spans the transition (Termination I) from Marine Isotope Stage 2 to Marine Isotope Stage 1. The lithofacies observed in core 9/97-08 suggest that parts of this core have been heavily remobilised (Toms in prep.). This remobilisation is so extensive that this core cannot be reliably correlated with other cores.

Age model estimates for the two deeper cores examined in detail (9/97-27/2 and 9/97-20) shows that the rate of sedimentation at this depth range (>2500m) was on average 3-4 times greater than higher up on the slope. Core 9/97-27/2 provides a slightly longer record (to approx. 46 kyrs B.P.) than 9/97-20 (to approx. 44 kyrs B.P.). The record between 41-46 kyrs B.P. is excellent in core 9/97-27/2 and has the potential to provide a sub-millenial scale record of climate variations in this region for this time period (Fig. 5.21). The core then provides a moderate record between 35-41 kyrs B.P. (compared to 9/97-20), with the absence of two stadials suggesting that either hiatuses are

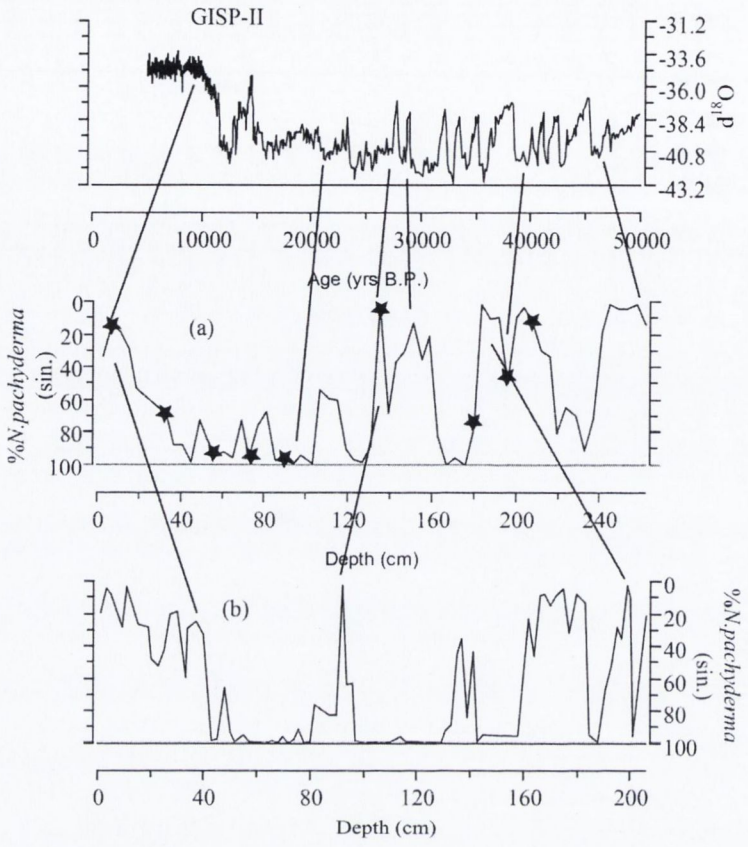

Figure 5.21. Correlation of the GISP-II $\delta^{18}O$ curve with *%N.pachyderma* (sin.) data from cores (a) 9/97-27/2 and (b) 9/97-20. Stars indicate ^{14}C AMS radiocarbon dating points (from Toms pers. comm.), with tie-points indicated.

present or the stadials are being masked. This time interval corresponds with an excellent record in core 9/97-20. Both cores provide high resolution (average 3-5cm/kyrs) records of the late last glacial and early Holocene, although it is slightly better preserved in core 9/97-27/2 (except for the Younger Dryas, which appears to correspond to a break in the core). Core 9/97-20 has a superior record of sedimentation in Marine Isotope Stage 1.

Calculated reservoir ages for radiocarbon dated samples in core 9/97-27/2 generally show a much higher age in last glacial samples compared to Holocene values. Reservoir ages during the last glacial are usually greater than 750 years, implying a much larger atmosphere-ocean off-set in ^{14}C than the Holocene. An exception to this is the sample at 85cm core depth, which records a significantly lower reservoir age (<100 years) compared to adjacent samples, suggesting a significantly lower atmosphere-ocean offset.

The improved correlation coefficient when applying reconstructed SSTs (as opposed to *%N.pachyderma* sin.) is probably due to the expanded range of SSTs covered by the application of multiple species as opposed to this one species (Fig. 3.4). The results of this suggest that correlating reference curves to *%N.pachyderma* (sin.) is less robust than using transfer functions to estimate SSTs for correlation. However (see Chapter 6), there are some problems with the values reconstructed using the MAT method which, once accounted for, could improve the correlation further.

5.4 Comparison with nannofossil biostratigraphy and lithostratigraphy

A nannofossil based biostratigraphic scheme has been developed for Transect 1 (Fig. 5.22) by Toms (in prep.). The scheme is based on changes in the relative abundance of dominant taxa through time which, combined with discrete sampling of presumed interglacial deposits, enables proposed correlations developed by alternative methods (the curve matching outlined above) to be independently tested. This is combined with lithostratigraphic correlation of lithological boundaries to produce the combined down slope nannofossil biostratigraphic and lithostratigraphic scheme (Fig. 5.22) of Toms (in prep.).

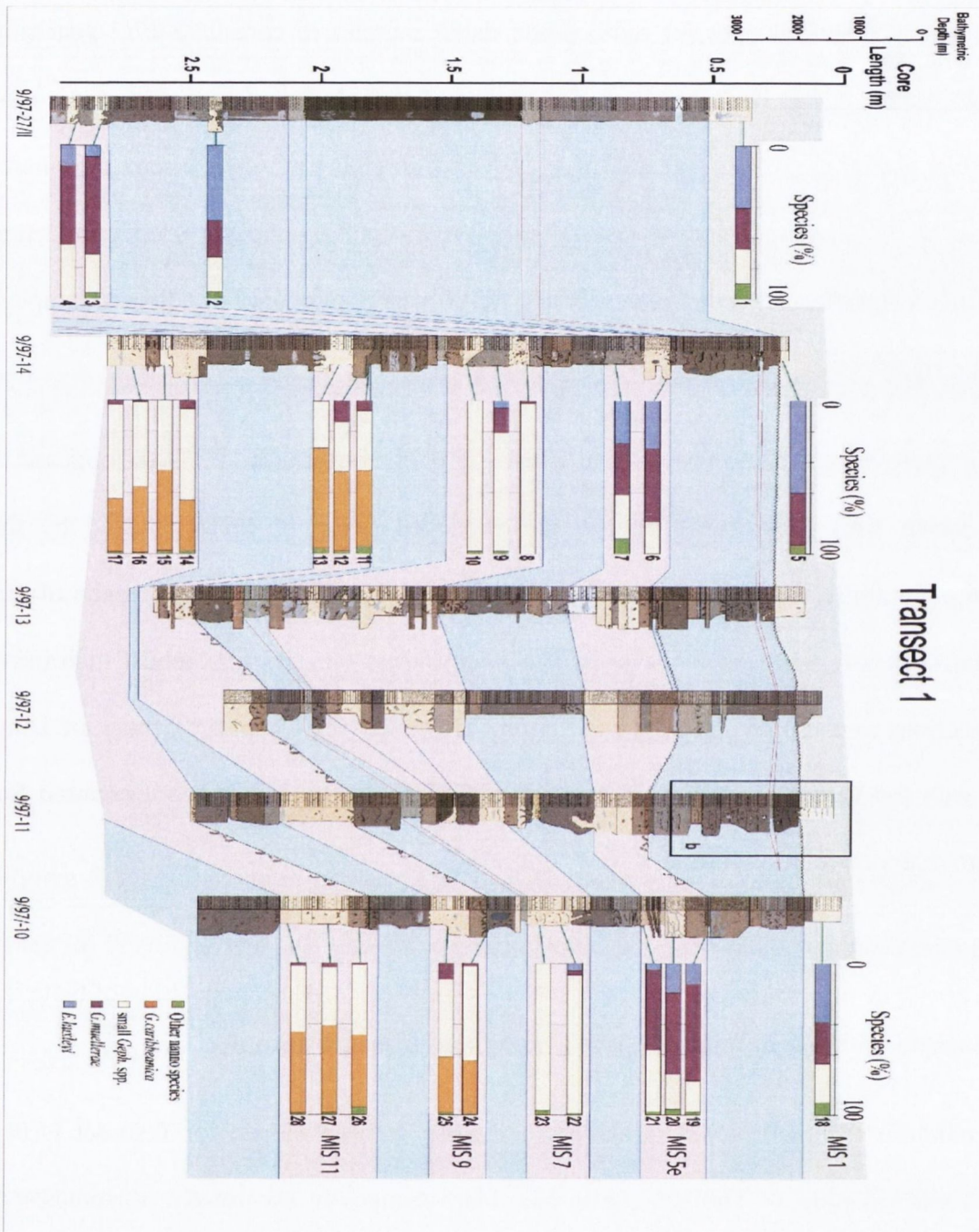

Figure 5.21. Calcareous nannofossil biostratigraphy of cores along Transect 1, modified from Toms (in. prep.). Blue and pink backgrounds indicate glacial and interglacial stages respectively. Coloured bars represent the relative abundance of species of calcareous nannofossil.

The results of the biostratigraphy for core 9/97-10 are in accordance with the record obtained from the correlation of *%N.pachyderma* (sin.) with the oxygen isotope record of ODP site 980. Both independent methods reach the conclusion that this core preserves a record extending back to MIS 12. For core 9/97-14, the position of the previous interglacial as proposed by Toms (in prep.) is in accordance with the results from this study.

However, the stratigraphy proposed by Toms (in prep.) for core 9/97-27/2 is different from that determined by correlation between *%N.pachyderma* (sin.) and the GISP-II oxygen isotope profile. The nannofossil abundance data for the basal units in this core are more compatible with deposition during the last interglacial, where as the *%N.pachyderma* correlation data suggests that this core extends back only as far as ≈45 kyr B.P. For the purposes of this study, the proposal that the base of core 9/97-27/2 represents deposition from the previous interglacial is rejected on the basis that such a proposed hiatus (spanning the interval from approximately 61-100 kyr B.P.) would be obvious from examination of the core (no erosive contact is observed, Toms pers. comm.). As discussed previously, there do appear to be some missing stadials from this record, which could be masked by deposition of material remobilised from higher on the slope. This suggests that this site could be prone to occasional influxes of sediment reworked from adjacent areas. It is more probable, when all of the evidence is considered together, that the base of core 9/97-27/2 was deposited during the last glacial and that the nannofossils have been remobilised from a last interglacial unit perhaps from higher on the slope.

5.5 Summary and conclusions

The results of the age model development process for each core suggest that reliable chronologies may have been developed for each core due to the good agreement between the *%N.pachyderma* (sin.) correlations with reference curves and the alternative methods (calcareous nannofossil biostratigraphy, radiocarbon dating) applied by Toms (in prep.), and that hiatuses and intervals of low sedimentation have been inferred. Calculated sedimentation rates vary in each core and are non-linear. Cores from ≤2118m water depth provide a record of glacial-interglacial variations extending back to Marine Isotope Stage 13, which is perhaps orbitally paced, but is of a relatively low resolution (approximately 2kyr.cm^{-1}). Cores from ≥2118m water depth provide a comparatively higher resolution record (approximately 0.2kyr.cm^{-1}) of the record 0-47 kyr B.P. which shows clear stadial-interstadial variations during MIS 3. Calculated reservoir ages are consistent with those published elsewhere (e.g. Waelbroeck *et al.* 2004; Peck *et al.* 2007) and suggest that reservoir ages increased to greater than 1500 yrs during the last glacial in core 9/97-27/2, with one exception at 85cm core depth. In core 9/97-10, lower reservoir ages are suggested in the last glacial compared to the Holocene. Correlations based on this method are broadly consistent with the correlations suggested by other methods (nannofossil biostratigraphy and lithostratigraphy) although one discrepancy is present in core 9/97-27/2.

Fragmentation indices enable the preservation of each record to be qualified, and this will be useful in later chapters where the preservation of specimens and identification of potential dissolution is important. The results of this chapter will be used in subsequent chapters to provide a temporal framework for variations in SST (Chapter 6), geochemistry (Chapter 7) and assemblages of benthic foraminifera (Chapter 8).

Chapter 6: Planktonic foraminifera

6.1 Introduction

Studies of planktonic foraminifera can provide a large amount of quantitative palaeoceanographic information (e.g. Elderfield and Ganssen 2002; Kucera *et al.* 2005). This chapter focuses on the information derived from examination of assemblages of planktonic foraminifera (see Sections 3.6), particularly reconstructions of seasonal sea surface temperatures (Pflaumann *et al.* 2003) and the potential extent of sea-ice cover over this site (Kucera *et al.* 2005). The aim is to develop an outline of surface ocean conditions through time, which aids the interpretation of assemblages of benthic foraminifera and geochemical data in later chapters (Chapter 7 and 8).

Three distinct transfer function methods are applied to the relative abundance data in Appendix A for six cores, providing a record of sea surface temperature variations that extends back to MIS 13. A sub-millenial scale record of sea surface temperatures is obtained from the deeper (<2200m water depth) cores, with the reliability of the reconstructed values determined by examination of the dissimilarity between fossil and modern assemblages and by comparison with other reconstructions of SST (e.g. Kandiano and Bauch 2003; Peck *et al.* 2008). Composite records for intermediate depth (<2118m water depth) and deeper (>2118m water depth) records are made by splicing records from discrete cores to attempt to create a more complete record of sea surface temperature variations. An alternative proxy (Kucera *et al.* 2005) for sea-ice cover (the percentage of 'sub-polar' species) is also applied to determine the likely presence or absence of perennial sea-ice cover over this site.

6.2 Reliability of SST reconstructions

In order to assess the reliability of the sea surface temperature reconstructions applied to the fossil assemblages, three measures were employed. Firstly, the strength of relationship between observed and estimated sea surface temperatures was calculated to provide an approximate estimate of the predictive strength of each method. Each core reports a correlation coefficient (r^2) of 0.9, suggesting that each technique has an excellent predictive strength. However, the 'gaps' with a relative absence of samples and the minimum / maximum temperature values in each technique will need to be considered when discussing the results. Plotting the estimated values against the observed values (Fig. 6.1) enables scatter in the relationship between observed and predicted SST values to be identified, which shows a very strong linear relationship between the observed and predicted values using MAT (Fig. 6.1) and strong relationships are also present for WAPLS and ML, but these lack the strong linear relationship observed for MAT. WAPLS appears to suffer from poor predictive capability between 7-12°C and ML is poor between 0-5°C. This could be related to the non-normal distribution between *%N.pachyderma* (sin.) and temperature, producing a cold-end tail. Such a phenomenon has been recorded in previous reconstructions (Pflaumann *et al.* 1996; Kucera *et al.* 2005).

Secondly, it is important when attempting to reconstruct SSTs using transfer functions to assess the precision of those reconstructed values. This is achieved by determining the Root Mean Squared Error of Prediction (RMSEP) for each reconstruction. The method estimates the quantity by which extrapolations made for fossil assemblages (and the required ecological parameter) differ from the true values in the modern calibration data set (or the 'goodness of

Core ID		RMSEP (°C) MAT	WAPLS	ML	DC (%)
99710	Summer	0.83	1.32	1.13	9.26
	Winter	0.84	1.35	1.05	9.26
99703	Summer	0.84	1.32	1.13	5.17
	Winter	0.82	1.35	1.05	5.17
99704	Summer	0.84	1.32	1.13	12.50
	Winter	0.83	1.35	1.05	12.50
99714	Summer	0.84	1.32	1.13	8.00
	Winter	0.83	1.34	1.05	8.00
997272	Summer	0.84	1.32	1.13	38.71
	Winter	0.83	1.35	1.05	38.71
99720	Summer	0.84	1.32	1.13	46.91
	Winter	0.83	1.35	2.00	46.91
r^2		0.97	0.96	0.98	

Table 6.1. Root Mean Squared Error of Prediction (RMSEP) values for each transfer function method from each core (bootstrapped average). MAT = Modern Analogue Technique, WAPLS = Weighted averaging, partial least squares and ML = Maximum Likelihood). (Cont.)

Note the relatively high value for the winter SST reconstruction of core 9/97-20 using the Maximum Likelihood method. DC (%) refers to the percentage of (cont.) fossil samples for which a good modern analogue is present in the training set, based on the percentage of samples with a dissimilarity coefficient less than 5%. R squared values (r^2) estimate the predictive strength of each method.

fit' between observed and predicted data). These values are shown in Table 6.1. The highest value is recorded in core 9/97-20 for the reconstruction of winter SSTs using the Maximum Likelihood (ML) algorithm and is almost twice as high as the value recorded for the summer SST from this core. Lowest RMSEP values are obtained using the Modern Analogue Technique (MAT), the highest via the WAPLS (Weighted Average, Partial Least Squares) algorithm. With RMSEP values always below 1°C, MAT produces values with the lowest predicted error. Although MAT has the lowest predicted error, several large outliers are present, suggesting that it could potentially be unstable in some contexts. Also, the MAT curve contains some plateaus, as do the WAPLS and ML curves. For this study, a consistent transfer function with a moderate precision is required to provide reliable estimates that can be compared with other reconstructions.

A strong relationship should be observed between seasonal pairs from the same sample if the reconstruction is producing a linear response to sea surface temperature, which is assessed by scatter plotting the reconstructed summer and winter values against each other and calculating the strength of the linear correlation between the two variables (Fig. 6.2). This is

recorded as r^2, and in each reconstruction performed, this value does not fall below 0.95, suggesting a very strong correlation between each dataset pair assessed.

Calculated dissimilarity coefficients suggest that for intermediate depth cores <15% of fossil samples have good modern analogues in the training dataset. Good analogues are defined as those that are within the 20th percentile of the training set dissimilarities. For this reason, reconstructed SSTs in these cores are applied with caution. For the deeper cores, the percentage of fossil samples with good modern analogues never exceeds 60%, suggesting that SST reconstructions from these cores could be more reliable, but that a large proportion of unreliable values are still present for those techniques that are poor at extrapolating for non-modern analogue samples. As outlined in Chapter 3, the Modern Analogue Technique is particularly poor at extrapolating for fossil samples with no modern analogues, whereas WAPLS does extrapolate species-environment relationships. The lack of good analogues for most of the samples in each core suggests that performing transfer functions to obtain reliable values is futile. However, MAT has been applied in previous studies (e.g. Kandiano and

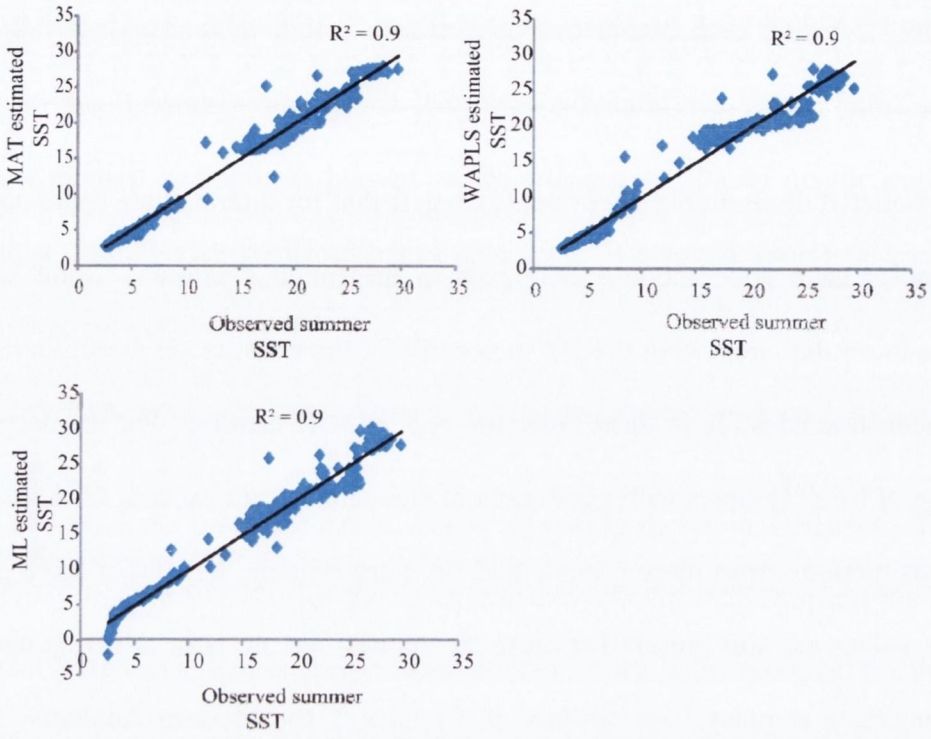

Figure 6.1. Scatter plots showing the relationship between observed SSTs and reconstructed (estimated) values from each transfer function (as calculated from the sample data in core 9/97/10). Note the linear relationship in (a) compared to the relationships in (b) and (c).

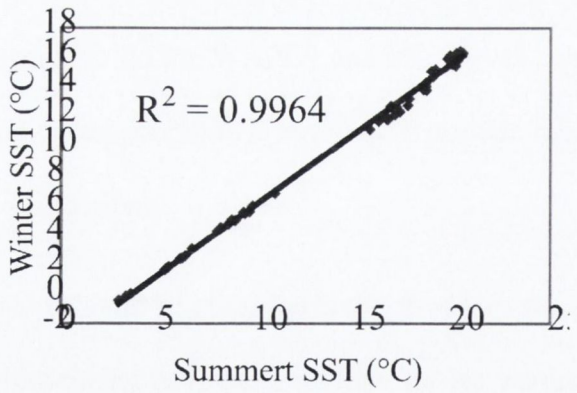

Figure 6.2. Linear relationship between reconstructed summer and winter sea surface temperatures of core 9/97-10 from MAT.

Bauch 2003) in the NE Atlantic Ocean, unlike WAPLS, so are used in this study for comparison with others. Results of ML and WAPLS are described only for cores 9/97-10 and 9/97-20 to provide a comparison of these techniques with MAT at intermediate (<2118m water depth) and deep (>2118m) water depth sites and to highlight the problems of the lack of good modern analogues (in core 9/97-10) and unrealistic values proposed by ML (core 9/97-20).

6.3 Results

6.3.1 Core 9/97-10

The *%N.pachyderma* (sin.) curve suggests that this core potentially provides a record of sea surface temperatures (Figs. 6.3) which extends back to Marine Isotope Stage 12 (Chapter 5; Fig. 5.3). The highest relative abundance of this taxon is recorded between 210-240cm core depths, followed by an interval of low relative abundance at 170-210cm core depth, which corresponds with the highest relative abundance of warm water, oligotrophic taxa. Three intervals of high relative abundance (>40%) are then present (150-170cm, 121cm and 78-90cm), alternating with two intervals of low (<40%) abundance (122-149cm and 91-120cm). This is followed by two intervals of low abundance (30-77cm and 0-15cm), alternating with one interval of high relative abundance (16-29cm). Sub-polar species are present in highest abundance in the core between 30-77cm core depth and the second highest interval (in terms of relative abundance of *%N.pachyderma* (sin.)) is between 16-29cm core depths.

All three transfer function methods (WAPLS, MAT and ML) concur that the assemblages at the base of the core (210-240cm) are characteristic of colder sea surface temperatures (SSTs), with ML recording the lowest SST during this interval (-1.5°C, winter value) at 210-225cm core depth, followed by a glacial termination (205-210cm) and an interglacial episode of warmer SSTs (175-205cm). At the inception of the next glacial episode (sample depth 164-172cm), there is a relatively large difference between the methods in calculating SSTs. MAT data suggests that cooling begins in sample (172cm), rather than in sample (168cm) as suggested by WAPLS or earlier as suggested by ML. With the WAPLS method, a stepwise cooling phase is present (170-180cm). The brief glacial episode, as implied by the cool SSTs (9°C summer), terminates abruptly at sample (156cm) and is followed by a prolonged interglacial episode (100-150cm), which contains one sample with a relatively cool (7°C summer) SST (123cm). This is followed by another termination and glacial episode (70-90cm) before the penultimate interglacial episode is present (30-70cm). There is strong agreement between the methods for the lower part of this interglacial (50-70cm). The upper part of the interglacial (30-50cm) displays clear differences in SST between the methods used. For the last glacial, termination and interglacial episodes, there is good agreement between the two methods. The final sample in the Holocene (3cm) records the highest SST (20.2°C, summer value). This value is 3-4°C warmer than the modern summer SST (16-17°C) according to the data of Pflaumann *et al.* (1996). Seasonal differences (summer temperature minus winter temperature) vary throughout the core, but are generally largest during interglacials (Fig.6.4) and smallest during glacials (>4.2°C and <4.2°C respectively). The average seasonal difference of the modern ocean (3.8°C) is similar to that present in this core (4.2°C), which perhaps suggests that seasonal differences in SST do not

vary significantly through time. Dissimilarity coefficients suggest that only the section between 210-230cm core depths has good modern analogues in the training dataset.

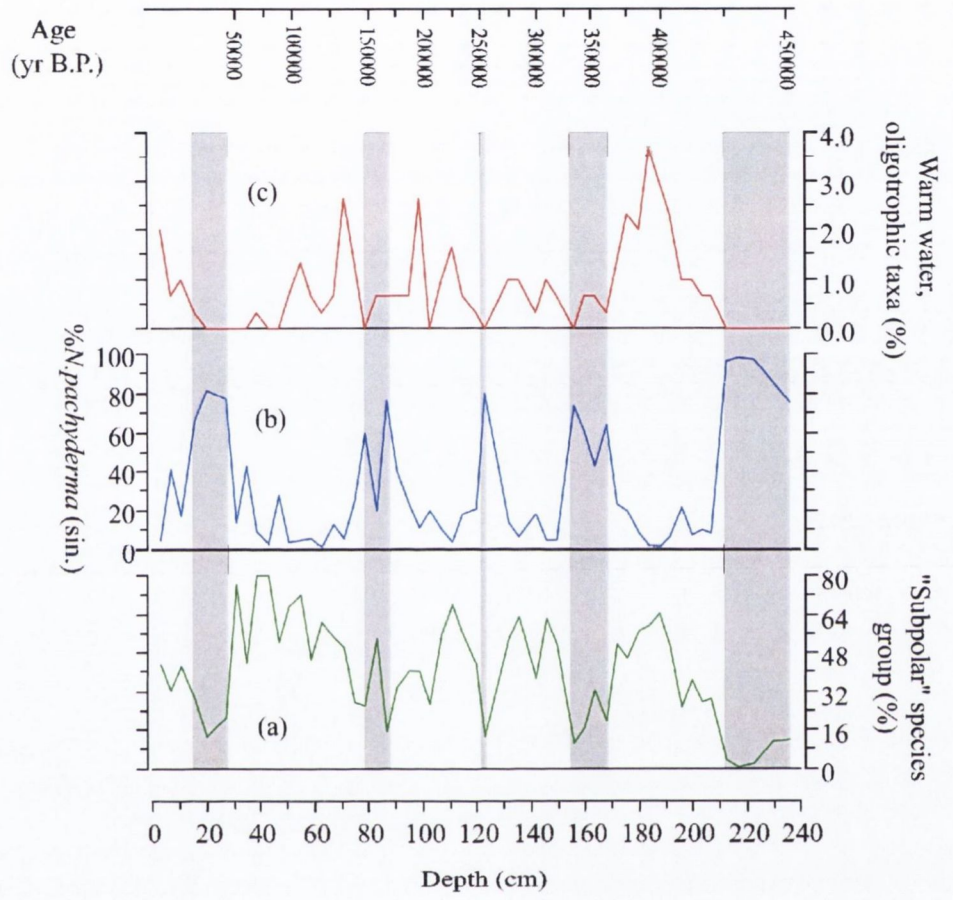

Figure 6.3.(a) Subpolar species group, (b) *%N.pachyderma* (sin.) and (c) abundance of warm water oligotrophic taxa for core 9/97-10. Grey shading highlights intervals where *N.pachyderma* (sin.) is ≥60%.

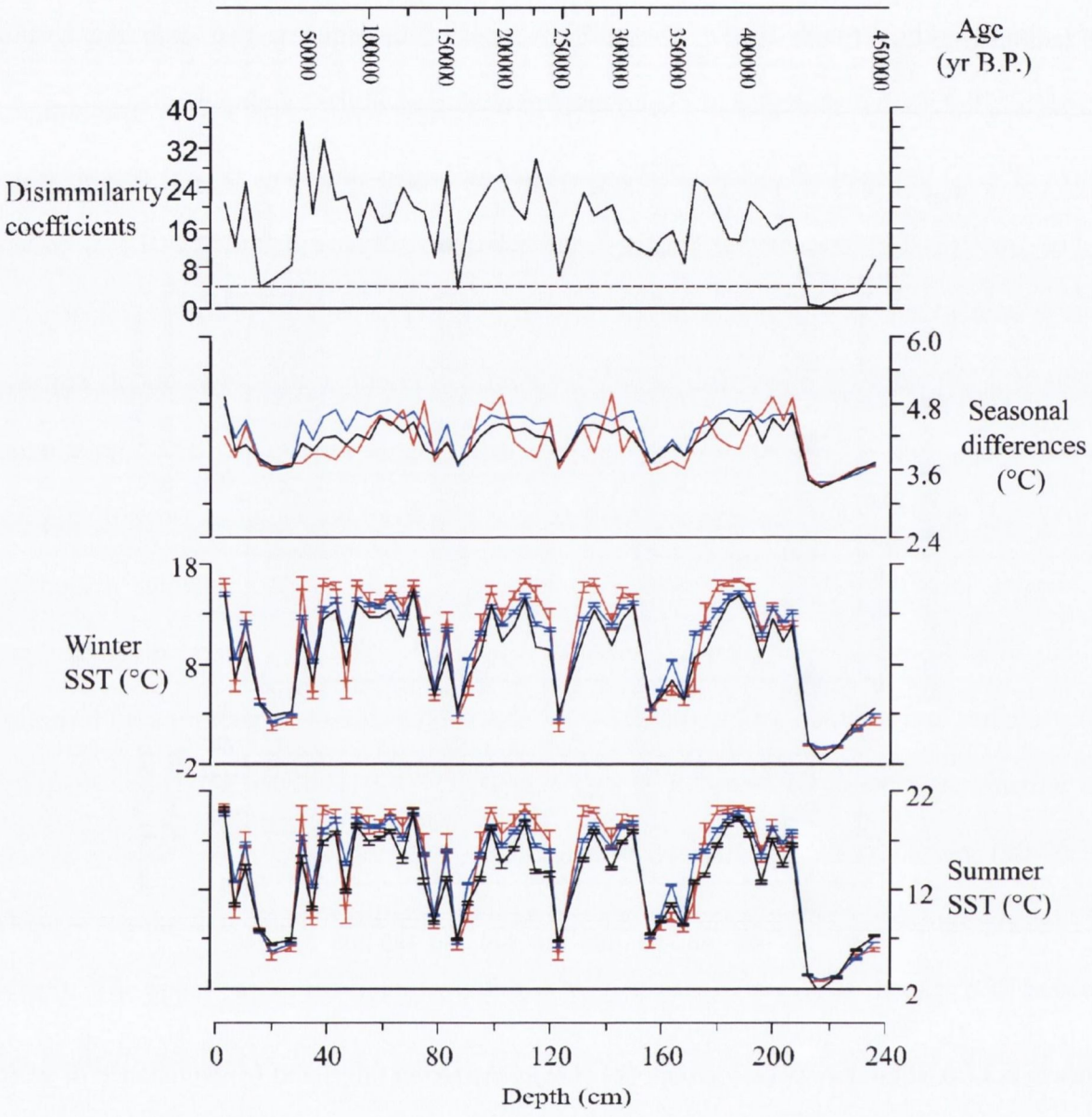

Figure 6.4. Reconstructed summer and winter SSTs and seasonal differences for MAT (red lines), WAPLS (blue lines) and ML (black lines) for core 9/97-10. Dissimilarity coefficients for each sample are presented, with the 20th percentile indicated by the dashed line. The vast majority of samples are above this, suggesting a relative lack of good modern analogues.

6.3.2 Core 9/97-03

The relative abundance of *N.pachyderma* (sin.) alternates between episodes of high (>40%) and low (<40%) relative abundance with an interval of low abundance between 185-223cm and high abundance between 150-184cm, which also records the lowest relative abundance of sub-polar species (Fig. 6.5). These are followed by a record of mostly low relative abundance between 20-149cm, with small short intervals of high abundance at 125, 95 and 75cm core depths. A short interval of high relative abundance is then present between 8-19cm, followed by a low abundance interval between 5-7cm. The relative abundance of warm water, oligotrophic taxa does not display any systematic variation.

The record in core 9/97-03 extends further back in time than that of 9/97-10 (Chapter 5; Fig.5.20) and provides a SST record for MIS 13. The temperature record is similar to that of 9/97-10, with extensive 'warm' periods and relatively shorter 'cold' episodes (Fig. 6.6). An exception is the first cold episode present near the base of the core, which provides an expanded record compared to core 9/97-10. This episode also records the lowest SSTs reconstructed from the core (-0.2 to -0.8°C, winter values). Seasonal differences in SST are generally reduced during cold periods when compared to warmer periods (Fig. 6.6). Average temperatures during the final warm phase are 15°C (summer value), compared to 7°C during the final cold phase, which suggests a temperature drop of 8°C, similar to the value obtained for 9/97-10. Dissimilarity coefficients suggest that only the interval between 150-180cm core depth has good modern analogues.

6.3.3 Core 9/97-04

The *%N.pachyderma* (sin.) curve displays a very clear trend, with two intervals of low relative abundance (45-85cm and 0-5cm) and one interval of high relative abundance (6-44cm), which is the opposite trend to that displayed by the abundance of sub-polar species and warm water oligotrophic species. The sub-polar species group (Fig. 6.7) is always present in percentages greater than 1%. Warm water, oligotrophic taxa were present during the Holocene and last interglacial in moderate abundance. A gradual reduction from 6.5% to 0% is present from the last interglacial to the last glacial in the warm water oligotrophic taxa curve, followed by a

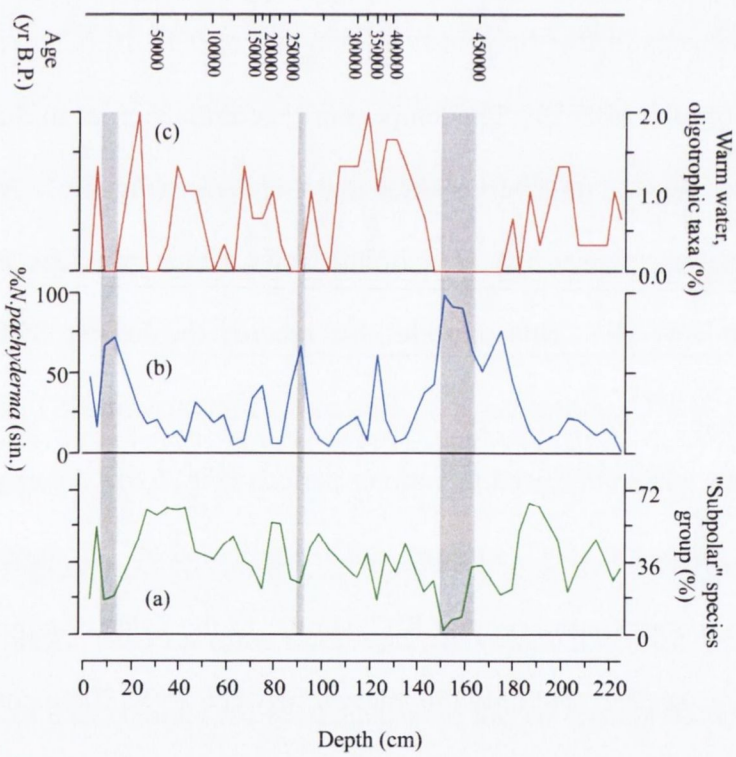

Figure 6.5.(a) Subpolar species group, (b) *%N.pachyderma* (sin.) and (c) abundance of warm water oligotrophic taxa for core 9/97-03. Grey shading highlights intervals where *N.pachyderma* (sin.) is ≥60%.

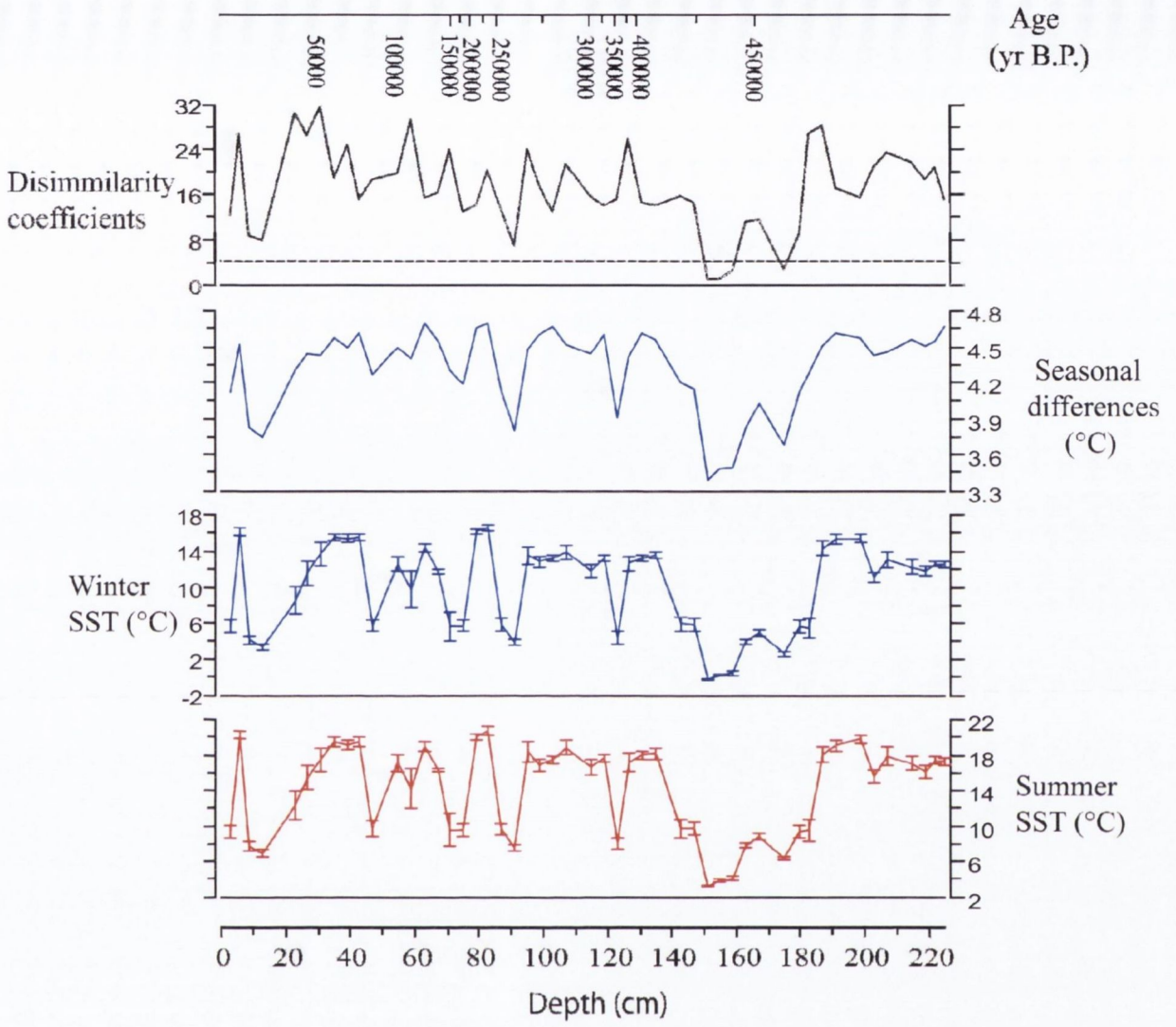

Figure 6.6. Reconstructed summer and winter SSTs and seasonal differences for MAT (red lines), WAPLS (blue lines) and ML (black lines) for core 9/97-03. Dissimilarity coefficients for each sample are presented, with the 20th percentile indicated by the dashed line. The vast majority of samples are above this, suggesting a relative lack of good modern analogues.

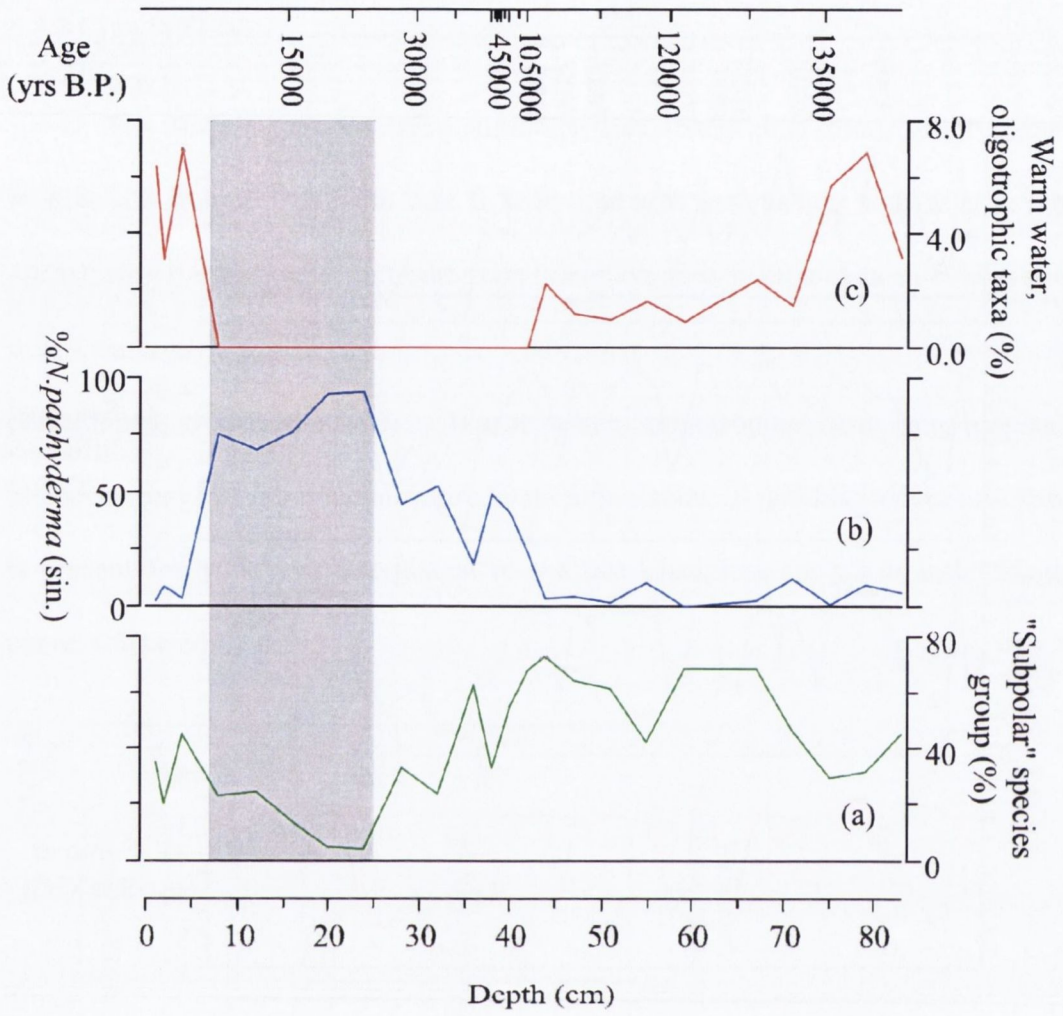

Figure 6.7.(a) Subpolar species group, (b) *%N.pachyderma* (sin.) and (c) abundance of warm water oligotrophic taxa for core 9/97-04. Grey shading highlights intervals where *N.pachyderma* (sin.) is ≥60%.

sharp increase in the Holocene. Reconstructions of SST were made for the upper 85cm of core 9/97-04 (Fig. 6.8). The record begins with a prolonged warm (18-20°C summer) period (84-44cm), followed by a period of high amplitude variations in temperature (44-

26cm). This is followed by a cold (average 8°C) period with very low amplitude variations in SST (26-8cm) and a final warm phase (5-0cm). Seasonal differences in SST are lower during the cold phase and higher during the two warmer phases. Average temperatures for the final warm period are 20°C (summer values) and 7°C for the previous cool period, implying a temperature rise of 13°C, significantly higher than the temperature reduction suggested by other cores. Dissimilarity coefficients indicate that only two samples have good modern analogues.

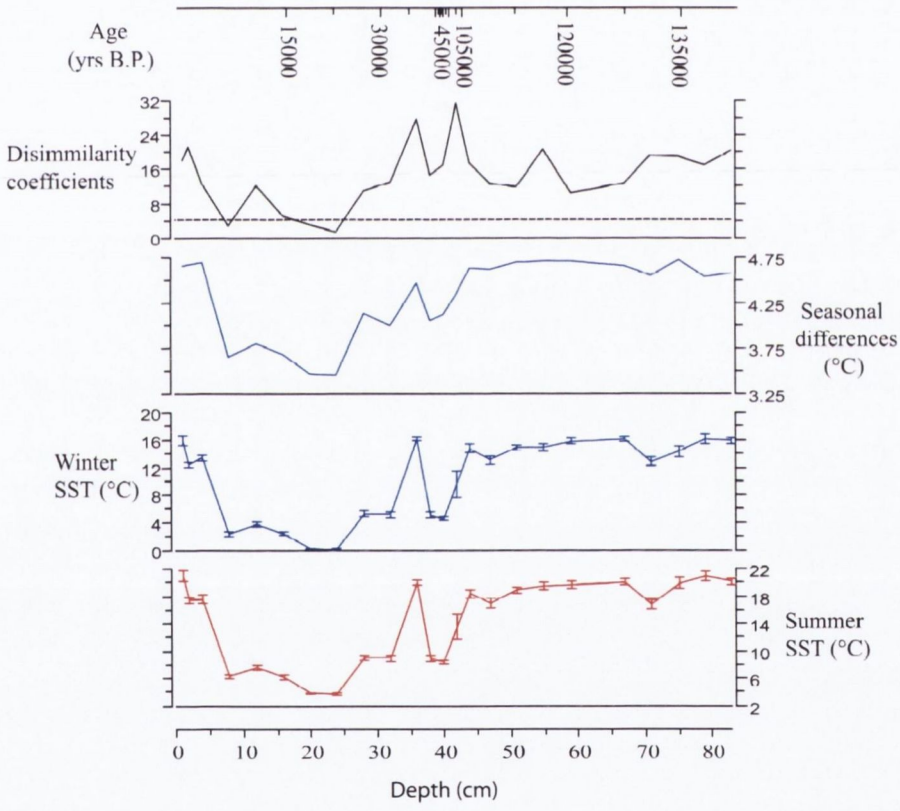

Figure 6.8. Reconstructed summer and winter SSTs and seasonal differences for MAT (red lines), WAPLS (blue lines) and ML (black lines) for core 9/97-04. Dissimilarity coefficients for each sample are presented, with the 20th percentile indicated by the dashed line. The vast majority of samples are above this, suggesting a relative lack of good modern analogues.

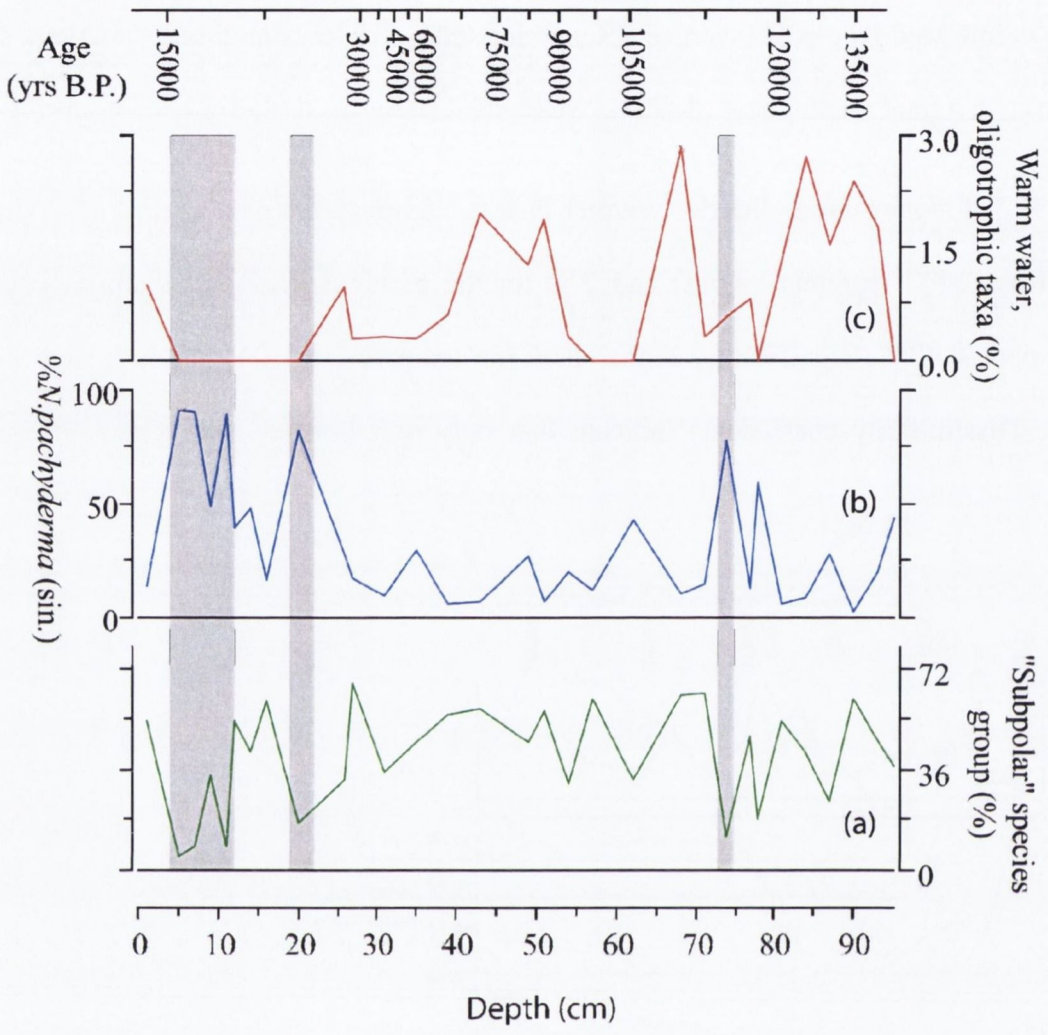

Figure 6.9.(a) Subpolar species group, (b) *%N.pachyderma* (sin.) and (c) abundance of warm water oligotrophic taxa for core 9/97-14. Grey shading highlights intervals where *N.pachyderma* (sin.) is ≥60%.

6.3.4 Core 9/97-14

The *%N.pachyderma* (sin.) varies throughout the core, with four phases of low relative abundance data (80-100cm, 25-75cm, 13-17cm) alternating with three phases of high abundance (76-79cm, 18-24cm and 0-12cm), with the opposite pattern observed in the sub-

polar species and warm water oligotrophic species data (Fig. 6.9). Sub-polar species group are always present in percentages greater than 1%. Sea surface temperatures were reconstructed (Fig. 6.10) for the upper part of core 9/97-14 (0-95cm). The record starts at the base of the core with a short warm (20°C summer) interval (95-80cm), followed by a short

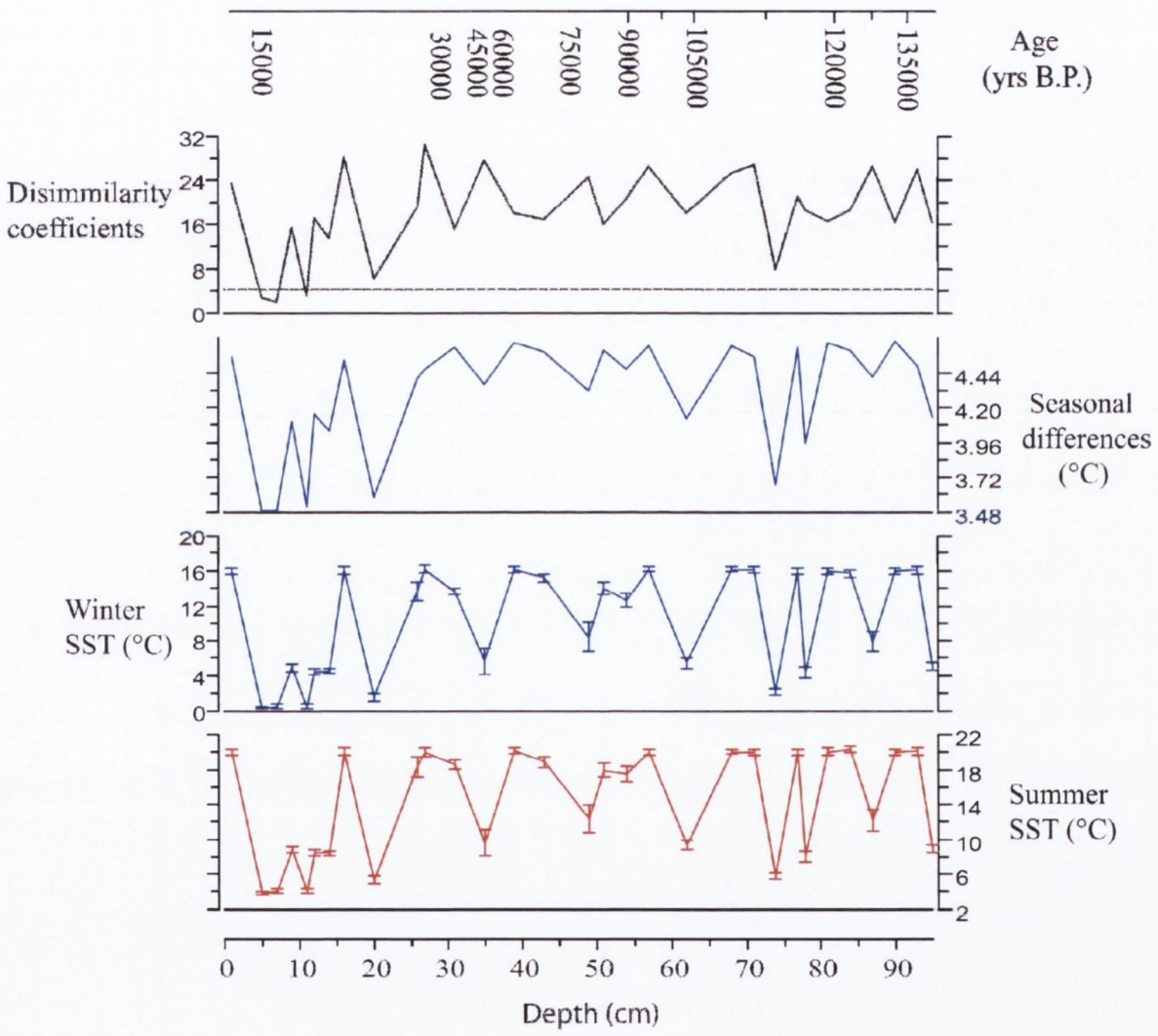

Figure 6.10. Reconstructed summer and winter SSTs and seasonal differences for MAT (red lines), WAPLS (blue lines) and ML (black lines) for core 9/97-14. Dissimilarity coefficients for each sample are presented, with the 20th percentile indicated by the dashed line. The vast majority of samples are above this, suggesting a relative lack of good modern analogues.

cold (14°C summer) interval (78-74cm). There is then a warm (20°C summer) episode (71-25cm), a final cold (6°C summer) episode (20-4cm) and the final warm (20°C summer) period (1-0cm). Seasonal differences in SST do not vary strongly, but are lower during cold phases compared to warm phases. Dissimilarity coefficients suggest that only three samples have good modern analogues in the training dataset.

6.3.5 Composite intermediate (1200-1600m water depth) SST record

A composite record for intermediate depth cores is constructed by splicing (See Section 3.4) the records from three cores: 9/97-04, 9/97-03 and 9/97-10 (Fig. 6.11). The first portion of the composite is derived from 9/97-03 (MIS 12-13), the middle section from 9/97-10 (MIS 5-11) and the final section is from 9/97-04 (MIS 1-4). Interglacials are highlighted by the grey shading. This provides a composite record of SST variations over the last 500kyrs which partially resolves the problem of hiatuses / low resolution records present in each core (see Chapter 5). Temperatures do not appear to fluctuate as strongly during interglacials (i.e. MIS 7, 9) compared to glacials (i.e. MIS 2-4, 6). The results show that MIS 12 and 2 record the lowest SST values and MISs 1 and 11 the highest.

6.3.6 Core 9/97-27/2

The relative abundance of *N.pachyderma* (sin.) varies throughout the core and alternates between intervals of high (>60%) relative abundance (220-240cm, 160-180cm and 30-140cm) and low abundance (240-262cm, 180-220cm, 140-160cm and 0-30cm). Sub-polar

species abundance shows the opposite pattern in terms of high and low relative abundance intervals (Fig. 6.12). The percentage of sub-polar species falls to 0% for two samples between 160-

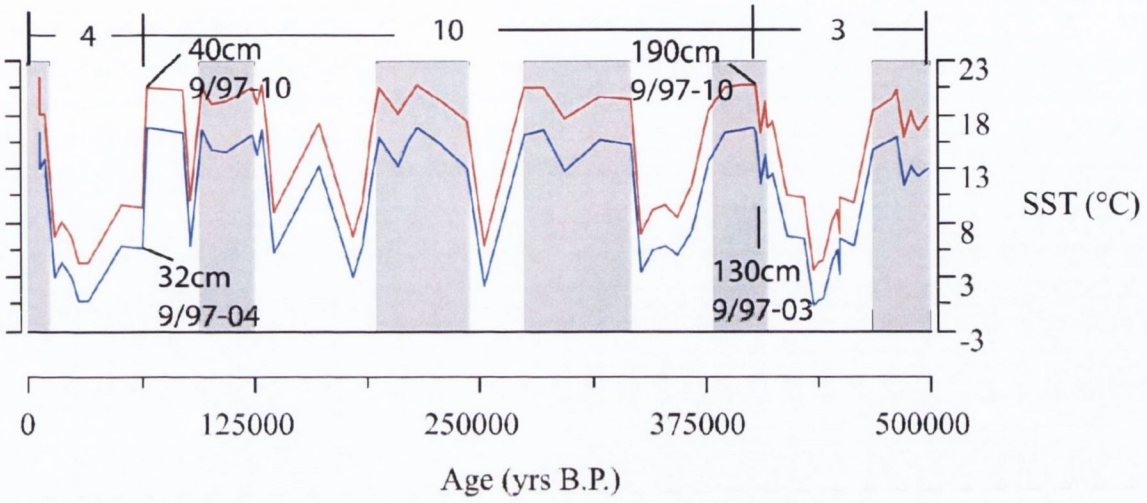

Figure 6.11. Composite MAT derived sea surface temperature record for intermediate depth (1230-2118m water depth) cores. Splicing sections are highlighted (4 = 9/97-04, 10 = 9/97-10 and 3 = 9/97-03). Red line indicates summer values, blue line indicates winter value. Grey shading highlights interglacials.

180cm core depth. Core 9/97-27/2 provides a record extending back to the middle of Marine Isotope Stage 3 (Chapter 5, Fig. 5.15). MAT reconstructions concur that the bottom 140cm of the core are characterised by strongly varying SSTs, followed by a period of weak variation in SSTs until 42cm. A gradual warming is then present, followed by a final warm episode (0-19cm). MAT reconstructions show an average summer temperature in the Holocene of 15°C and 5°C in the last glacial (MIS 2). This implies a temperature rise of 10°C, similar to the result from other cores. Seasonal differences vary throughout the core, but are generally

largest during interglacials / interstadials (Fig. 6.12) and smallest during glacials / stadials. The average seasonal difference of the modern ocean (3.8°C) is similar to that present in this core (Fig. 6.13). No values fall outside two standard deviations from the mean seasonal difference of the modern North Atlantic Ocean. Dissimilarity coefficients indicate that those samples with summer sea surface temperatures less than 6°C do have good modern analogues, but anything that estimates a temperature warmer than this has poor analogues.

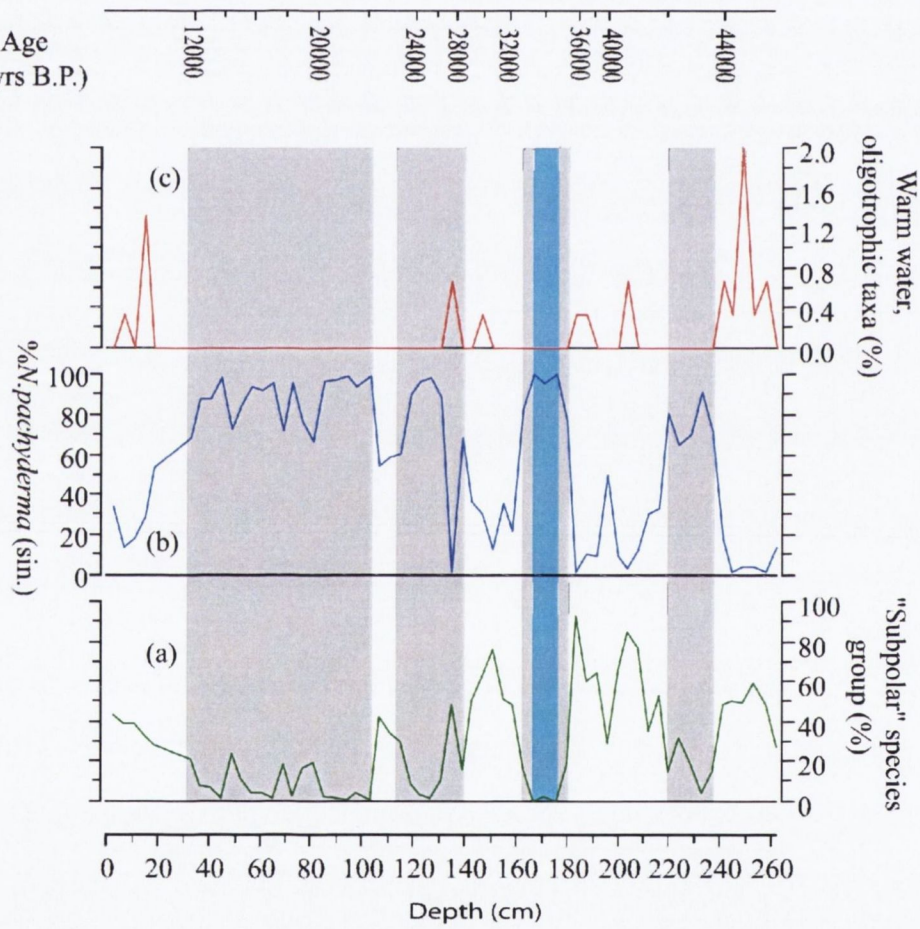

Figure 6.12.(a) Subpolar species group, (b) *%N.pachyderma* (sin.) and (c) abundance of warm water oligotrophic taxa for core 9/97-27/2. Grey shading highlights intervals where *N.pachyderma* (sin.) is ≥60%. Blue shading indicates intervals where sub-polar species group are absent.

6.3.7 Core 9/97-20

The relative abundance of *N.pachyderma* (sin.) varies signifigantly throughout core 9/97-20 (Fig. 6.14) and alternates between episodes of high (>60%) abundance (200cm, 185-190cm, 42-

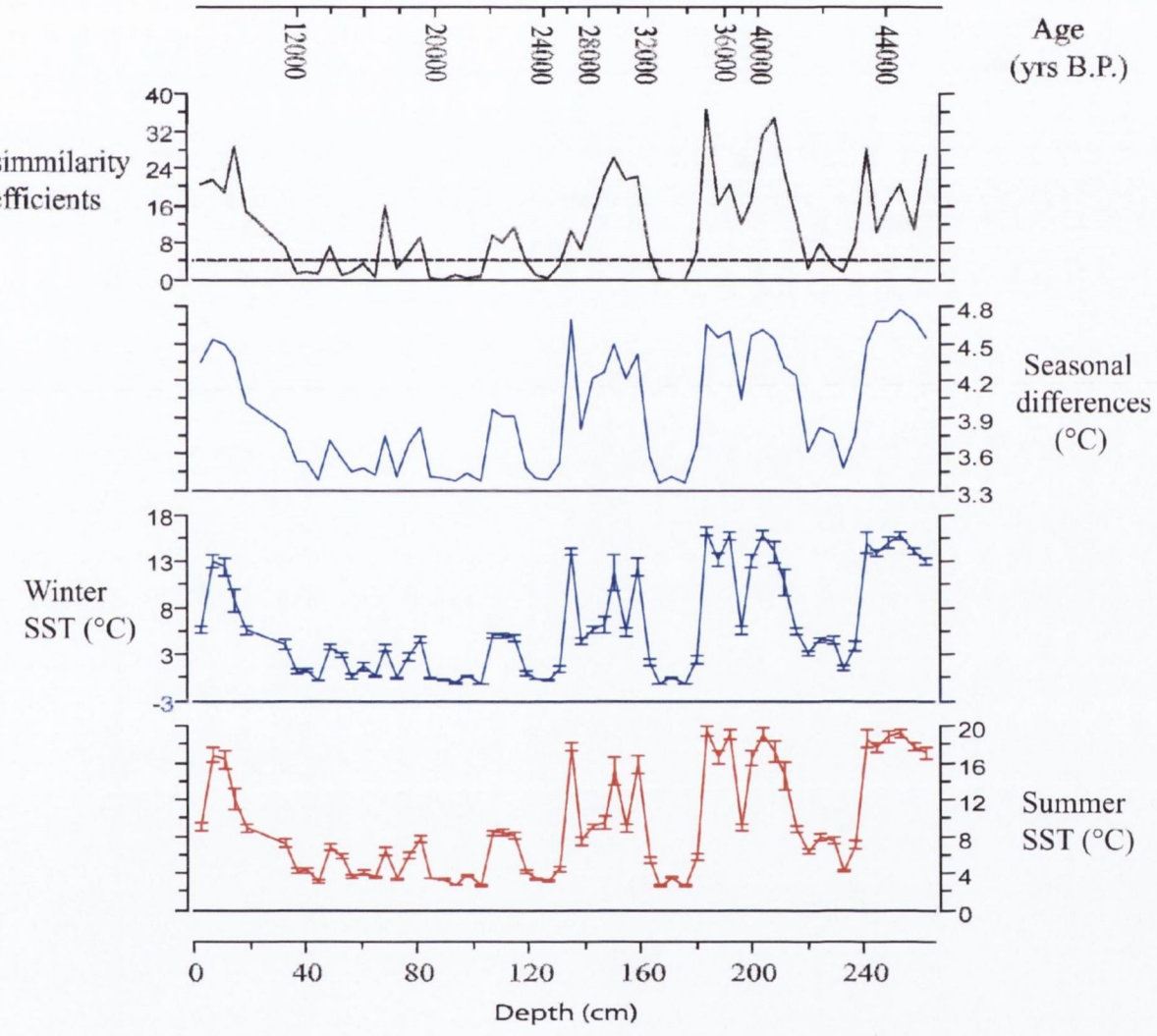

Figure 6.13. Reconstructed summer and winter SSTs and seasonal differences for MAT (red lines), WAPLS (blue lines) and ML (black lines) for core 9/97-27/2. Dissimilarity coefficients for each sample are presented, with the 20th percentile indicated by the dashed line. The majority of samples are above this, suggesting a relative lack of good modern analogues.

160cm) and low (<60%) abundance (202cm, 191-199cm, 161-184cm, 0-41cm). The higher resolution record for 9/97-20 (compared to core 9/97-27/2) suggests that there are three episodes (55-80cm, 100-110cm and 120-130cm core depth) with an absence of sub-polar species during Marine Isotope Stage 2 and one during Marine Isotope Stage 3

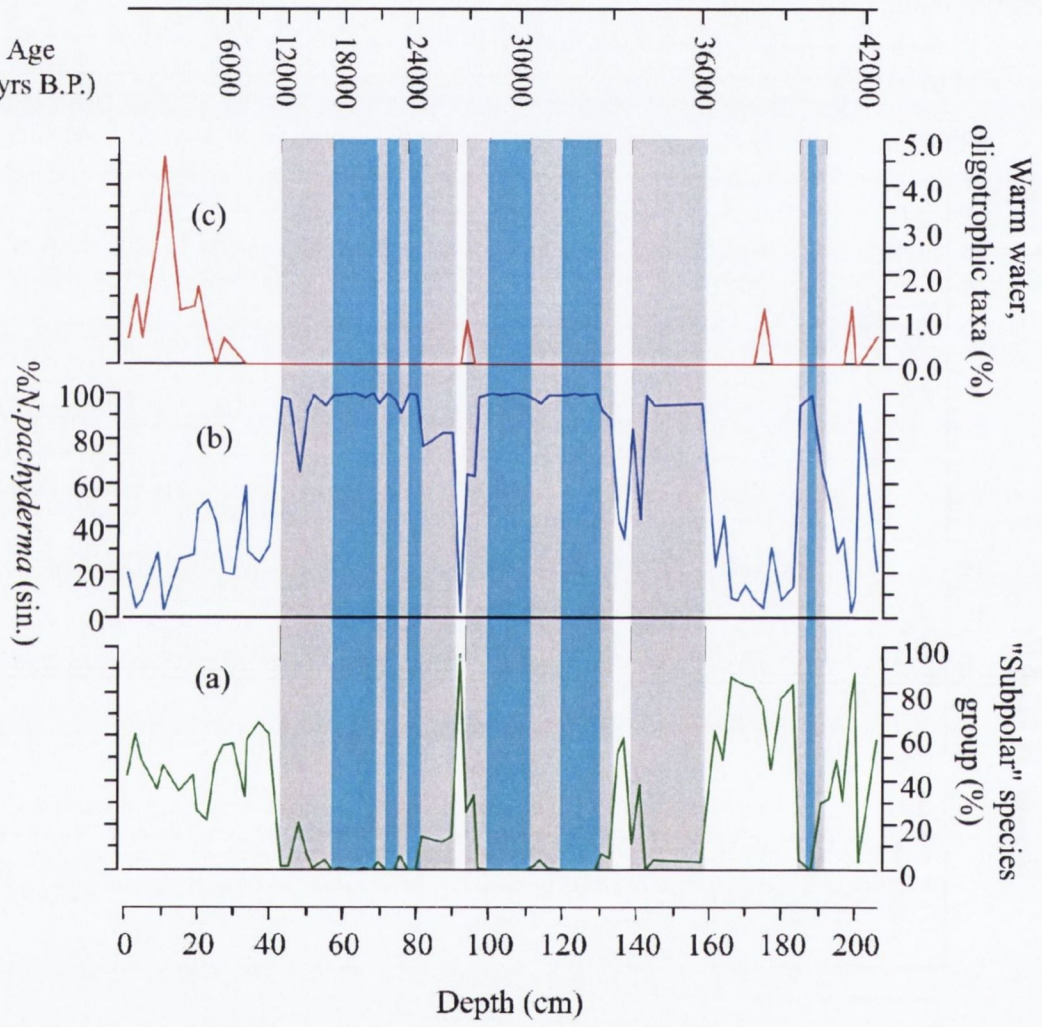

Figure 6.14.(a) Subpolar species group, (b) *%N.pachyderma* (sin.) and (c) abundance of warm water oligotrophic taxa for core 9/97-20. Grey shading highlights intervals where *N.pachyderma* (sin.) is ≥60%. Blue shading indicates intervals where sub-polar species group are absent.

(185-190cm). Each of these episodes is bracketed by periods with a small percentage of sub-polar species.

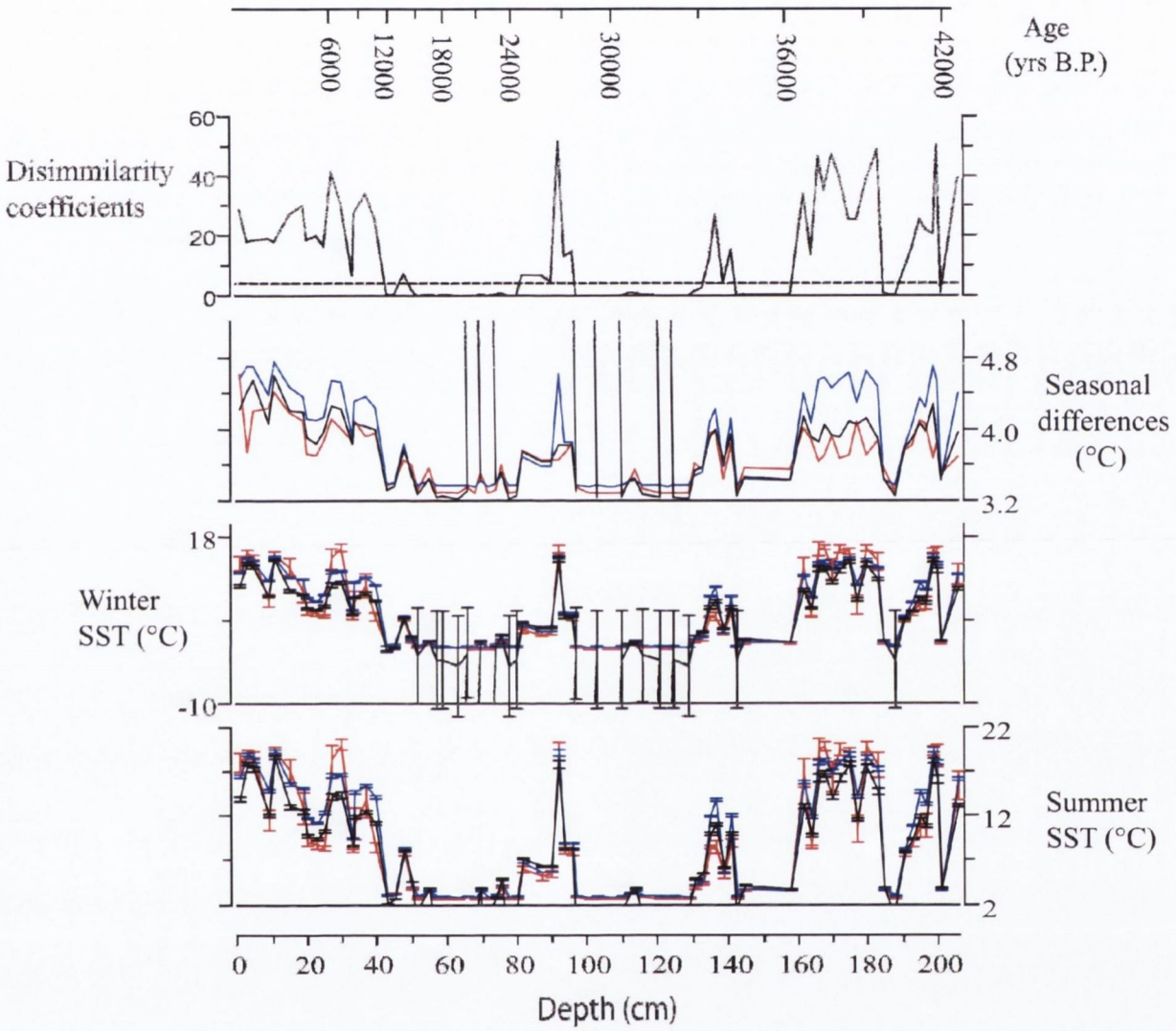

Figure 6.15. Reconstructed summer and winter SSTs and seasonal differences for MAT (red lines), WAPLS (blue lines) and ML (black lines) for core 9/97-20. Dissimilarity coefficients for each sample are presented, with the 20th percentile indicated by the dashed line. The majority of 'cold' samples are below this, suggesting they may have good modern analogues.

As established in the previous chapter (Fig. 5.18), core 9/97-20 provides a much higher resolution record of Marine Isotope Stage 2 than core 9/97-27/2. The pattern of SST variations in this core (Fig. 6.15) is similar to that present in 9/97-27/2 (Fig. 6.15) with the lower 76cm of the core are characterised by high amplitude variations in SST. The following 90cm of the core display consistently low SSTs, with very little variation. A gradual warming trend followed by consistently warm SSTs is present in the top 40cm of the core. Sea surface temperatures are never lower than -0.7°C. Seasonal differences are larger during summer and smaller during winter. Differences between the methods are largest during the warming trend but are otherwise relatively small. Standard deviations are largest during the warming trend and in the warm intervals towards the bottom of the core. Maximum Likelihood reconstructions for this core produce the coldest SSTs (Fig. 6.15). These are the winter SST values (-7 to -8°C), which are much lower than is feasible (-1.8°C is the temperature at which sea-ice formation is initiated). Some of the summer values reconstructed using this method also fall below the -1.8°C minimum. Dissimilarity coefficients suggest that any sample which estimates a summer sea surface temperature greater than 6°C appears to lack a good modern analogue in the training dataset, whereas those that estimate lower temperatures have good analogues.

6.3.8 Composite deep (2000-3200m water depth) SST record

A composite record for deep water sites is constructed by splicing the records of 9/97-27/2 and 9/97-20 (Fig. 6.16). This produces a record with high amplitude variations in SST for MIS 3, followed by consistently low temperature (<10°C summer) values with low

amplitude SST variations for MIS 2. This is followed by a gradual warming phase (Termination I) and a warm phase (average 15°C) with moderate to low amplitude variations in SST (MIS 1).

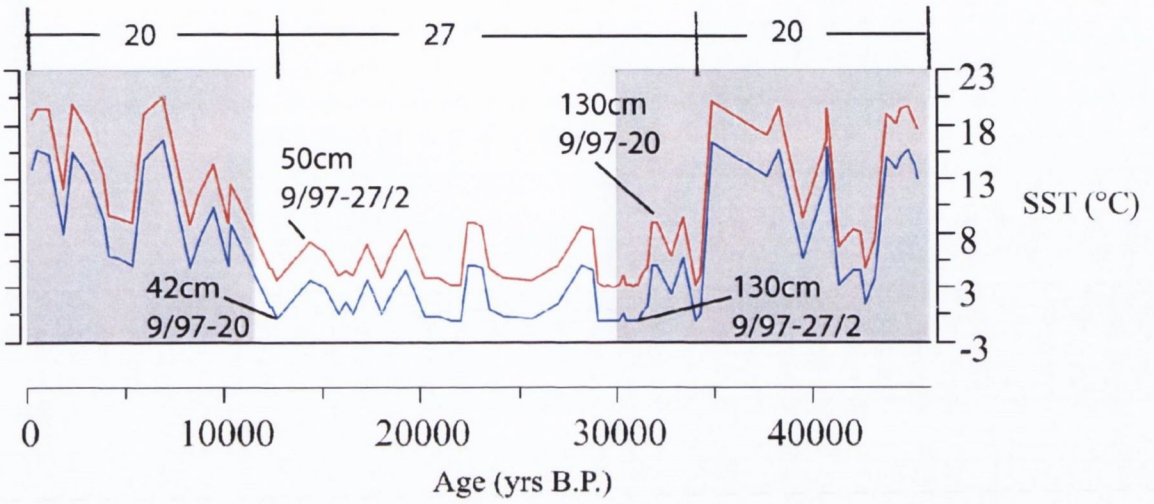

Figure 6.16. Composite MAT derived sea surface temperature record for deep (>2118m water depth) cores. Splicing sections are highlighted (20 = 9/97-20, 27 = 9/97-27/2). Red line indicates summer values, blue line indicates winter value. Grey shading highlights Holocene (left area) and Marine Isotope Stage 3 (right area).

6.4 Discussion

The relative abundance of *N.pachyderma* (sin.) varies significantly in all cores and suggest strong differences in sea surface temperature between glacial-interglacial and stadial-interstadial phases. For the two shallowest cores (9/97-10 and 9/97-03), a record of alternating 'cool' glacial and 'warm' interglacial sea surface conditions are implied by the high and low (respectively) abundance of this species, which extends back to Marine Isotope Stage 13.

Highest abundance of *N.pachyderma* (sin.) occur during MIS 12, implying the coldest sea surface temperatures of the previous 500 kyrs. During MIS 11 the highest relative abundance of warm water oligotrophic taxa is recorded, implying the warmest sea surface conditions of the previous 500 kyrs. For two cores at mid-depth (9/97-04 and 9/97-14) a record of varying sea surface conditions over the previous interglacial, glacial and Holocene is present. Core 9/97-04 presents a relatively straightforward record of changing sea surface conditions, with a phase of warm water conditions for most of the lower portion of the examined core section (last interglacial) followed by a phase of cool surface conditions (last glacial) and then a final warm phase (Holocene). The record of core 9/97-14 is much less straightforward and suggests that cool phases may be relatively short (in terms of cm) compared to warm phases, but that each of these are variable rather than presenting stable surface conditions. In the two deeper cores (9/97-27/2 and 9/97-20), three phases of variation in sea surface conditions is suggested. In both cores, the lower section presents strong variations in sea surface conditions, alternating between phases with no or very few sub-polar species / warm water oligotrophic taxa and phases of very low abundance of *N.pachyderma* (sin.). This is followed by a middle core section with stable and consistently cold sea surface conditions, as implied by the near or total dominance of *N.pachyderma* (sin.) throughout. A final section of warm temperatures is then present, implied by the low relative abundance of *N.pachyderma* (sin.). The abundance of this species appears to dominate the sea surface temperature reconstructions based on transfer functions, with the reconstructed SST curves closely mirroring the *%N.pachyderma* (sin.) curves. Warm water, oligotrophic taxa (McIntyre *et al.* 1972) are present in moderate abundance during all warm phases for all cores and have the highest abundance in intermediate depth ($\leq$2118m water depth) cores during MIS 11 (e.g. Fig. 6.5), implying that

oligotrophic surface conditions prevailed during each interglacial from MIS 11 to 1. This is consistent with an expansion of the sub-tropical gyre with decreasing sea-ice cover and weakening of the sub-polar gyre during interglacials as proposed by Hatun *et al.* (2005).

There is little evidence from examination of the assemblages of planktonic foraminifera (sub-polar species group) in cores 9/97-03, 9/97-10, 9/97-04 and 9/97-14 to support the inference that sea-ice was ever extensive over this locality (e.g. Figs. 6.3-6.10). However, this could be due to the very condensed nature of these records, especially when compared to the deeper cores (see below). Following the SST reconstructions, the only time temperatures are approaching the values low enough for sea-ice development in intermediate depth cores is during MIS 12 in cores 9/97-10 and 9/97-03. However, the sub-polar species data (always greater than 1%) does not support the inference that perennial sea-ice cover occurred.

In the deeper cores, an absence of sub-polar species suggests that episodes of perennial sea-ice cover are present during MIS 3 and 2. In core 9/97-20, these episodes are mostly restricted to MIS 2 and occur in three phases, 55-80cm, 100-110cm and 120-130cm core depth. This suggests that the expansion / contraction of sea-ice during MIS 2 is non-monotonic. A stadial episode at 185-190cm core depth with an absence of sub-polar species is also suggestive of perennial sea-ice cover. Another stadial episode with indications of perennial sea-ice cover is present in core 9/97-27/2 at 165-175cm core depth (33-35 kyr B.P.). An alternative explanation, that the absence of sub-polar taxa indicates the expansion of Arctic Domain water and the associated migration of the polar front (see Chapter 2) as suggested by Scourse *et al.* (2009) is not supported by the recent study by Kucera *et al.* (2005), who identified that Arctic domain water still retains a small but notable percentage of sub-polar

taxa. It remains possible that the polar front did migrate over this site, but using the dominance of *N.pachyderma* (sin.) as a proxy for this may not be appropriate. The absence of this record in shallower cores is probably due to the much higher resolution (0.2kyr.cm^{-1} rather than 2kyr.cm^{-1}) of the deeper cores, which would reduce mixing of cold and warm interval deposits.

There are some substantial differences between the three transfer function methods in terms of the actual values reached following the application of each transfer function. For example, in core 9/97-10 the average difference between winter temperatures derived from MAT and WAPLS is close to 0°C during the winter, but close to 1°C for summer values. The problem of larger differences in reconstructed summer SSTs and during warm periods is also present in core 9/97-20 (Fig. 6.15). This is possibly the result of differences in the two proposed models for the warmer temperature ranges, with MAT proposing a steeper, more linear relationship compared to WAPLS (Fig. 6.1).

Episodes with the largest differences between the three methods appear to be associated with 'transitional' phases between full glacial and full interglacial conditions, possibly due to the poor sample coverage in the modern North Atlantic training dataset over the temperature range 10-15°C, combined with the very different shapes of the three curves during this interval (Fig. 6.1). Also, the high proportions of dissimilar fossil assemblages (compared to modern assemblages) suggest that very few of the fossil samples (from cores ≤2118m water depth) have good modern analogues. This indicates that reconstructed values, particularly in the shallower cores (≤2118m water depth) could be unreliable were the method applied is poor at extrapolating beyond modern analogues.

Another key difference is in the coldest SSTs reconstructed following each method, with SSTs derived from MAT and WAPLS never falling below -0.7°C and those derived from ML never below -8°C. The values from ML are too low to be realistic (no modern SST is lower than ≈-2°C) (Fig. 6.15). Determining accurate SSTs at the colder end of the temperature range is also problematic, due to the dominance of a single species (*N.pachyderma* (sin.)) over a range of temperatures (See Fig. 3.5). The differences in the coldest temperatures recorded between the three methods are due to the different slopes present at the cold temperature range (Fig. 6.1), with a steep relationship between observed and reconstructed values for ML.

High dissimilarity coefficients for each core suggest a lack of good modern analogues for the interglacial and interstadial fossil assemblages in particular. The source of this appears to be primarily linked to the high relative abundance of *G.bulloides* in the fossil assemblages (see Appendix A), compared to the fossil dataset of Pflaumann *et al.* (2003). This suggests that either *G.bulloides* is being preferentially preserved, which seems unlikely when the dissolution series of Hemleben *et al.* (1989), or that another species is under-represented in the fossil assemblages. Either scenario implies significant bioturbational mixing or physical reworking of units may have occurred. As discussed in the previous chapter, most cores record higher fragmentation indices during interglacials and interstadials, which supports the inference that mixing / reworking may have occurred to a greater extent in these units, but this should produce a reduction in *G.bulloides* due to the relative fragility of this taxon (see Chapter 3). Because of the significant problems caused by the absence of good analogues for most of the samples used to reconstruct sea surface temperatures and the other issues with the transfer function method as applied above, it is not appropriate to use the reconstructed values

for further discussion. However, some of the trends that were consistently observed, either in records from more than one core or between different transfer functions, are discussed below.

Reconstructed temperatures in core 9/97-10 are higher in the latter part of MIS 5 (110-95 kyr B.P.) in comparison with the record of ODP 980 by 3-4°C, although this could mostly be explained by limitations in the transfer function methods applied. These samples also record the large differences between the three methods and high dissimilarity coefficients. This interval could be prone to post-depositional modification of assemblages, as suggested by the relatively high fragmentation indices for this interval (see Fig. 5.4). Alternatively, the temperature record proposed by McManus *et al.* (1999) employed *N.pachyderma* (sin.), which is generally a thermocline dwelling taxon rather than a surface dweller (Peck *et al.* 2007), which would also explain the off-set (see below).

The record of temperature variations (not actual values) in cores 9/97-10 and 9/97-03 are consistent with the transfer function based reconstructions of Kandiano and Bauch (2003), although some key differences are evident. Marine Isotope 3, in particular, is very different in this study, recording temperatures equivalent to those of interglacial stages, unlike Kandiano and Bauch (2003) which show a 4-5°C off-set between MIS 3 and previous interglacial temperatures. More than one factor could account for this. It could be due to the low resolution (see Section 5.2) record of this interval in these cores, combined with the apparent gap in predictive capability suggested previously for intermediate (10-15°C) temperatures (Fig. 6.1) and the low percentage of good modern analogues for the fossil assemblages in these cores.

The data from core 9/97-10 suggests that Holocene temperatures averaged 16°C (consistent with modern values; e.g. Pflaumann *et al.* 1996) and late glacial temperatures averaged 7°C, suggesting a warming of 9°C. This is consistent with the findings of previous studies (Kucera *et al.* 2005), who proposed an 11°C warming. The magnitude of cooling is also consistent with that reported in McManus *et al.* (1999), although the temperatures produced in this study are slightly higher (13-14°C summer and 5-6°C winter from McManus *et al.* 1999 compared to 16°C summer and 8°C winter from this study). This is probably because the McManus *et al.* (1999) study used oxygen isotope data from *N.pachyderma* (sin.) to reconstruct SSTs. *Neogloboquadrina pachyderma* (sin.) is not a surface dwelling taxon in the NE Atlantic Ocean, which might explain the consistent off-set in surface temperature estimates.

In core 9/97-27/2, problems with the ML derived SSTs are observed. Several samples at the cold end produce SSTs that are unrealistic (e.g. -7°C), which suggests that this method is not useful when dealing with colder surface conditions. However, it does produce comparable values to the other two methods in the interstadial / Holocene units.

The composite intermediate depth record suggests that the transition from MIS 13 to MIS 12 showed a stepwise cooling trend (cooling interrupted by a short plateau) in cores 9/97-10 and 9/97-03. This is followed by a stepwise warming in the transition from MIS 12 to MIS 11 (although this is only observed in core 9/97-03). Such stepwise cooling and warming trends have been identified in previous reconstructions (based on geochemical data) from other sites for different time intervals (i.e. Coxall *et al.* 2005; Stanford *et al.* 2006; Barker *et al.* 2009). The prevailing hypothesis is that these are caused by instabilities in the Antarctic ice sheet (e.g. Stanford *et al.* 2006), which in turn affects 'deep' water formation in the

Southern Ocean, which impacts on the thermal bipolar seesaw (see Section 2.4). In their high resolution study of the Deep Western Boundary Current during MIS 10-12, Hall and Becker (2006) did not identify such a phenomenon in their reconstruction of current velocities associated with this current. The site of their study (ODP site 1061; 4047m) is perhaps too deep to record this as the primary effects of the bipolar see-saw phenomenon are considered to be present at the surface and at intermediate depths (Rickaby and Elderfield 2005). This could also explain the lack of this phenomenon from the record of NADW circulation proposed by Poli *et al.* (2000). However, as discussed above, the reconstructed values based on transfer functions from intermediate depth cores (≤2118m water depth) need to be regarded with caution. Other data are required to determine whether or not this stepwise warming is an artefact of difficulties with the transfer function method. It is clear that MIS 8 is significantly truncated compared with the record from other sites (i.e. ODP 980). A truncated record for this stage is present in cores 9/97-03 and 9/97-10, suggesting that this is not a core site specific phenomenon and not just due to sampling issues in one core (Fig. 3.1 – large cobble). It could be that this site was particularly prone to sediment starvation during this stage, consistent with the relatively low sedimentation rate present for the early part of MIS 8 in core 9/97-10 in Chapter 5 (Fig. 5.3).

The spliced records of cores 9/97-20 and 9/97-27/2 produce a much higher resolution record of mid MIS 3 to Holocene SSTs compared to the intermediate depth (≤2118m water depth) composite record. Four interstadials and two stadials are present in the composite record during the latter part of MIS 3. The lack of interstadials around 30kyrs B.P. from this record (both 9/97-27/2 and 9/97-20) is probably linked to the intervals of hiatuses / low sedimentation recorded in Chapter 5 for core 9/97-27/2 (Fig. 5.15). An alternative explanation

is that this site was still strongly influenced by local ice-sheets (particularly the British Irish Ice Sheet – BIIS) during this time period and this has minimised the influence of stadial-interstadial variations present in the Greenland Ice Sheet. Some low amplitude variations are present in MIS 2 SST reconstructions with temperatures never exceeding 10°C (summer values). Interstadial 1 from GISP-II is not present in the composite record.

The assemblage based SST reconstructions in this study differ significantly from those of Peck *et al.* (2008), which was based on Mg/Ca values. Their reconstructions suggest that summer sea surface temperatures never fell below 6°C between 8-55 kyr B.P (compared to 2°C in this study, although the sub-polar species component suggests that even this is probably an overestimate). The difference is probably due to the limited temperature range to which the Mg/Ca palaeothermometry method can be accurately applied (e.g. Rosenthal *et al.* 1997; Martin *et al.* 2002). These studies have suggested that applying this method when temperatures are possibly below 5-6°C is inappropriate as the slope of the temperature change with decreasing Mg/Ca values flattens out such that little change in Mg/Ca occurs over a large temperature range (-2 to 6°). This calls into question the author's proposal that this site acted as a potential moisture source for the BIIS and simultaneously ablated the marine ice margin during MIS 3. Alternatively, the relative absence of good modern analogues for some of the samples from deeper (≥2118m water depth) cores could also explain the discrepancy between the two methods. However, the sub-polar species data suggests that SSTs probably were cooler than 6°C, particularly during MIS 2 and MIS 3 stadials.

6.5 Summary and conclusions

The *%N.pachyderma* (sin.) data is a useful qualitative tool for identifying episodes of cool and warm surface water conditions, and appears to have a strong influence on the transfer functions outlined below. Sub-polar species group and warm water oligotrophic taxa appear to vary with the relative abundance of this species, but in an opposite phase. Highest percentages of *N.pachyderma* (sin.) during MIS 12 suggest that this interval experienced the coldest sea surface temperatures of the previous 500 kyrs, with MIS 2 the second coldest. Marine Isotope Stage 11 records the highest percentages of warm water oligotrophic taxa, suggesting the warmest sea surface conditions of the previous 500 kyrs. An absence of sea-ice cover for the intermediate depth (<2118m water depth) record between MIS 13 and 1 is inferred from the continual presence of sub-polar species in all samples, although this is probably an artefact of the low resolution ($2kyr.cm^{-1}$) records available at these depths. Deeper cores (≥2118m water depth) provide a record of stadial-interstadial temperature variations in MIS 3. The absence of sub-polar species during MIS 3 stadials and during MIS 2 is indicative of sea-ice cover during these intervals.

A comparison of modern and fossil assemblages of planktonic foraminifera suggests that most of the samples used in this study have poor modern analogues in the training set of Pflaumann *et al.* (2003). Because many of the samples have poor analogues, reconstructed values are potentially unreliable and should, therefore, be applied with caution. In particular, ML appears to be extremely poor with the coldest intervals of core 9/97-20, proposing sea surface temperatures that are unrealistic. This is also potentially a problem for MAT, which is relatively poor at extrapolating beyond modern analogues. However, the broad trends (glacial-interglacial and stadial interstadial) and their relative duration according the age

models developed in the previous chapter (Chapter 5) should still be accurately determined. Also, for cores with a moderate percentage of good modern analogues (e.g. core 9/97-20) the reliability of the reconstructed values is less of a problem. A lack of good modern analogues, combined with the gap present in plots of observed versus estimated SSTs probably explains the alternation between very cold and very warm temperatures, with very few reconstructed temperatures between 10-15°C. Further work is required to identify the exact cause of the lack of good modern analogues in the modern training set. Some post-mortem modification processes that could alter relative abundance to increase the proportions of *G.bulloides* are considered.

Intermediate depth (≤2118m water depth) cores record the coldest and warmest SSTs during MIS 12 and MIS 11 respectively. A stepwise warming trend is potentially present between these two stages in the reconstruction from core 9/97-03, but this could be an artefact of the problems outlined above. Marine Isotope Stage 8 is relatively truncated in the records from cores 9/97-10 and 9/97-03, consistent with the results of other studies (e.g. McManus *et al.* 1999) and Chapter 5. The Marine Isotope Stage 3 reconstructed temperatures from intermediate depth cores record values equivalent to or higher than those of MIS 5. Finding equivalent temperatures between these two stages is incompatible with the records of other reconstructions (e.g. Kandiano and Bauch 2003) and could also be due to the problems with the transfer fucnction method outlined above. Holocene to last glacial cooling is estimated as between 10-7°C, consistent with the results of other studies (e.g. Kucera *et al.* 2005).

Chapter 7: Geochemistry

7.1 Introduction

This chapter describes the results of the multi-proxy geochemical investigation undertaken on four gravity cores (9/97-10, 9/97-04, 9/97-14 and 9/97-27/2). These cores are selected for this purpose as they are considered to provide a good record of changes in water mass distribution down slope and through time as they are currently located close to boundaries between modern water masses (e.g. Read 2001) and perhaps boundaries of water masses in the past. Cores 9/97-10, 9/97-04 and 9/97-14 provide a low resolution ($2kyr.cm^{-1}$) record that extends back to Marine Isotope Stage 12, although significant hiatuses have been inferred in cores 9/97-04 and 9/97-14, spanning most of MIS 3 (Chapter 5). Core 9/97-27/2 provides a high resolution ($0.2kyr.cm^{-1}$) record that extends back to approximately 46 kyr B.P. The water depths for each core are presented in Table 3.1.

Several proxies and tracers are presented to identify important characteristics of the surface and bottom waters that bathed the western flank of the Porcupine Bank through time (see Table 7.1). Planktonic $\delta^{18}O$ ($\delta^{18}O_{planktonic}$) is chosen primarily as a correlative tool with the profile of Øvrebø *et al.* (2006) (see Chapter 5), but is also used for determining sea surface temperatures (see Chapter 3) using the equation of Bemis *et al.* (1998), providing that the various alternative factors that can also cause variations in $\delta^{18}O_{planktonic}$ (Fig. 3.17) are accounted for. Planktonic $\delta^{13}C$ ($\delta^{13}C_{planktonic}$) can aid this, by identifying samples that formed when the species chosen (*G.bulloides*) was not calcifying at the sea surface. If values are approximately 2‰ lower than at present, then this suggests that the test formed below the thermocline (Berger *et al.* 1988). Sharp negative excursions of lesser magnitude could be

related to reduced stratification of the water column during deglaciations or Heinrich events (e.g. Oppo and Lehman 1993).

In the benthic records, whole core Mg/Ca versus fragmentation indices are used to determine whole core dissolution effects (see Chapter 3) and used in combination with Sr/Ca data from each sample, which is used to identify individual samples that may have undergone selective dissolution (McCorkle *et al.* 1995; Stoll *et al.* 1999). This assumes that Sr/Ca values vary primarily due to changes in dissolution intensity, which may not necessarily be the case (see Section 3.6). Plotting Cd/Ca versus Mn/Ca identifies (or not) if there is a linear correlation between Mn/Ca and Cd/Ca, an indication of preferential enrichement of Cd due to manganese oxide formation. Also, in the literature (e.g. Boyle 1983; Tachikawa and Elderfield 2002), a Mn/Ca value greater than 150μmol/mol is normally suggested as the value above which significant enrichment of manganese (and the trace metals of interest) has occurred due to the formation of manganese oxide test coatings.

Ratios of Ba/Ca are a proxy for refractory nutrient supply (see Fig. 3.13) and provides a useful complementary water mass tracer alongside Cd/Ca ratios, which act as a tracer of labile nutrient distributions (Fig. 3.14). Cd/Ca values are also used to quantify the concentration of phosphorus in bottom waters (Boyle 1992; Bertram *et al.* 1995) and the results of this are described. Reconstructed phosphorus values are combined with benthic $\delta^{13}C$ ($\delta^{13}C_{benthic}$) to determine the relative mixing of water mass end-members, and how this has varied through time (Rickaby and Elderfield 2005; see Fig. 3.15). Benthic carbon isotope ratios also provide information about water column stratification and significant events in the past. Two excellent syntheses of bottom water carbon isotope variations through time have been published (Sarnthein *et al.* 1994; Lynch-Stieglitz *et al.* 2007) and these form the basis of

the comparison with the data presented here (See Chapter 2). Benthic $\delta^{18}O$ ($\delta^{18}O_{benthic}$) also provide information on water mass stratification following conversion into $\delta^{18}O_{sw}$. This requires bottom water temperatures to be estimated, and this is achieved by converting Mg/Ca values into temperatures using the equation of Martin *et al.* (2002). Combining all of these data provides information about the palaeoceanography of the Porcupine Bank region and identifies samples which are likely to provide reliable information. Down slope reconstructions assume that the reconstructed values are representative of the broad trends for each stage. For Marine Isotope Stage 3, the absence of large sections of this stage from cores 9/97-04 and 9/97-14 makes reconstructing water mass distributions for this interval less reliable.

Proxy	**Used to estimate**	**Combined / compared with**	**Reconstructing**
Mn/Ca	Contamination	Cd/Ca	-
Sr/Ca	Dissolution	-	-
Cd/Ca	Phosphorus concentration	$\delta^{13}C_{benthic}$	Water mass flux
Ba/Ca	Refractory nutrients	-	Water mass tracer
Mg/Ca	Bottom water temperature	$\delta^{18}O_{benthic}$	Temp. and stratification
$\delta^{18}O_{sw}$	Bottom water density	-	Stratification
$\delta^{13}C_{benthic}$	Ventilation / productivity	Phosphorus	Water mass flux
$\delta^{18}O_{planktonic}$	Sea surface temperature	$\delta^{13}C_{planktonic}$	Temp. changes
$\delta^{13}C_{planktonic}$	Position in water column	$\delta^{18}O_{planktonic}$	Surface stratification

Table 7.1. Summary of the geochemical proxies examined in this study, their primary utility, what they are combined / compared with to perform reconstructions.

7.2 Planktonic stable isotopes from core 9/97-10

As discussed previously in Chapter 5, the stable isotope data obtained from planktonic foraminifera in core 9/97-10 is a useful correlative tool for this core, but the data can also be applied to examine palaeoceanographic variations through time. A complete downcore planktonic stable isotope record is presented for core 9/97-10 for correlation with the isotope record produced by Øvrebø *et al.* (2006) for core 83/24sc5 (see Section 3.5). The oxygen isotope record is consistent in recording light $\delta^{18}O_{planktonic}$ values implying warm SSTs in lighter coloured interglacial units compared to glacial units. The estimated temperature record is broadly consistent with the SST record provided by the transfer function techniques MAT and WAPLS (Maximum Likelihood (ML) is not applied due to the problems with this method discussed in Chapter 6) for this core (Fig. 7.1). However, there are some important differences. The average interglacial temperature (11-12°C) suggested by the oxygen isotope data is similar to the interglacial winter values suggested by MAT and WAPLS (13-14°C), whereas the glacial values are warmer on average by 3-4°C than the glacial winter values, and are much closer to the glacial summer values suggested by MAT and WAPLS(Fig. 7.1). Another important difference is in the duration of the proposed glacial-interglacial episodes. The oxygen isotope record proposes longer glacial episodes compared to the transfer function method.

Carbon isotope values do not vary significantly or in line with glacial-interglacial variations apart from two relatively strong negative values that are observed in the carbon isotope profile, one at 15cm and another at 142cm.

7.3 Preliminary whole core assessment of geochemical data

A scatter plot of all core fragmentation indices versus Mg/Ca ratios (Fig. 7.2) is used to determine the presence or absence of a dissolution effect on the values recorded. This produces no significant linear correlation (r^2 = 0.00001). A core-by-core comparison of fragmentation versus Mg/Ca data shows that core 9/97-14 has the highest correlation coefficient between the two parameters (r^2 = 0.33). Although this value is not high enough to imply a significant linear correlation for the whole dataset from this core (an r^2 value <0.5 suggests that a correlation between the two variables is less likely), it is relatively high compared to the coefficients of cores 9/97-10 (r^2=0.05), 9/97-04 (r^2=0.05) and 9/97-27/2 (r^2=0.16).

A scatter plot of all-core Cd/Ca values versus Mn/Ca (Fig. 7.3) is presented to identify samples which may have become preferentially enriched in cadmium and barium (but not magnesium, as this is not affected; Martin and Lea 2002) through the formation of manganese oxide coatings (Tachikawa and Elderfield 2002). All of the samples from core 9/97-27/2 are above the suggested threshold value of 150μmol/mol (Fig. 7.3).

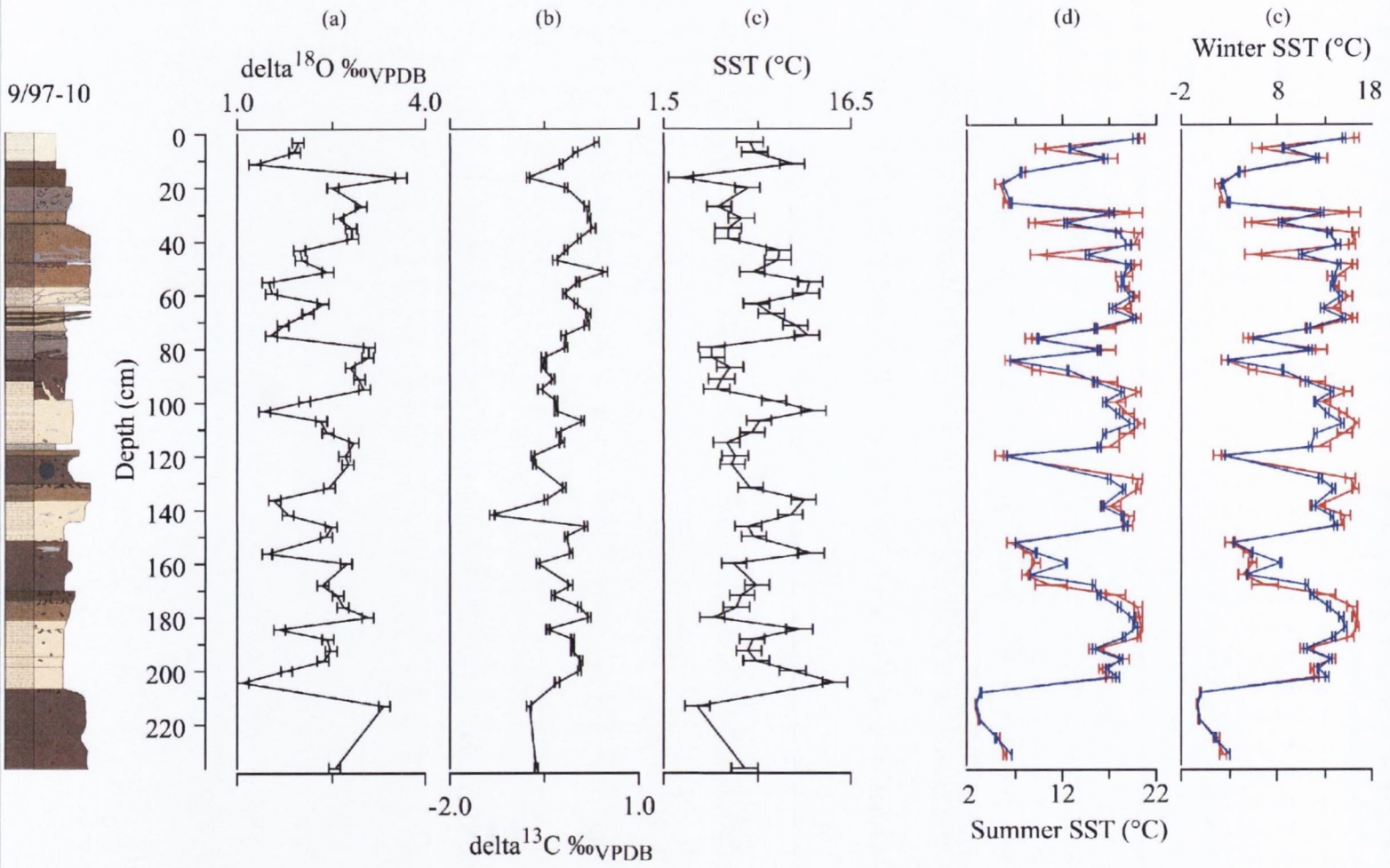

Figure 7.1. Down core (a) delta^{18}Oplanktonic, (b) delta^{13}Cplanktonic, (c) SST derived from delta^{18}Oplanktonic, (d) Summer SST derived from MAT (red line) and WA-PLS (blue line) and (e) Winter SST derived from MAT (red line) and WA-PLS for core 9/97-10.

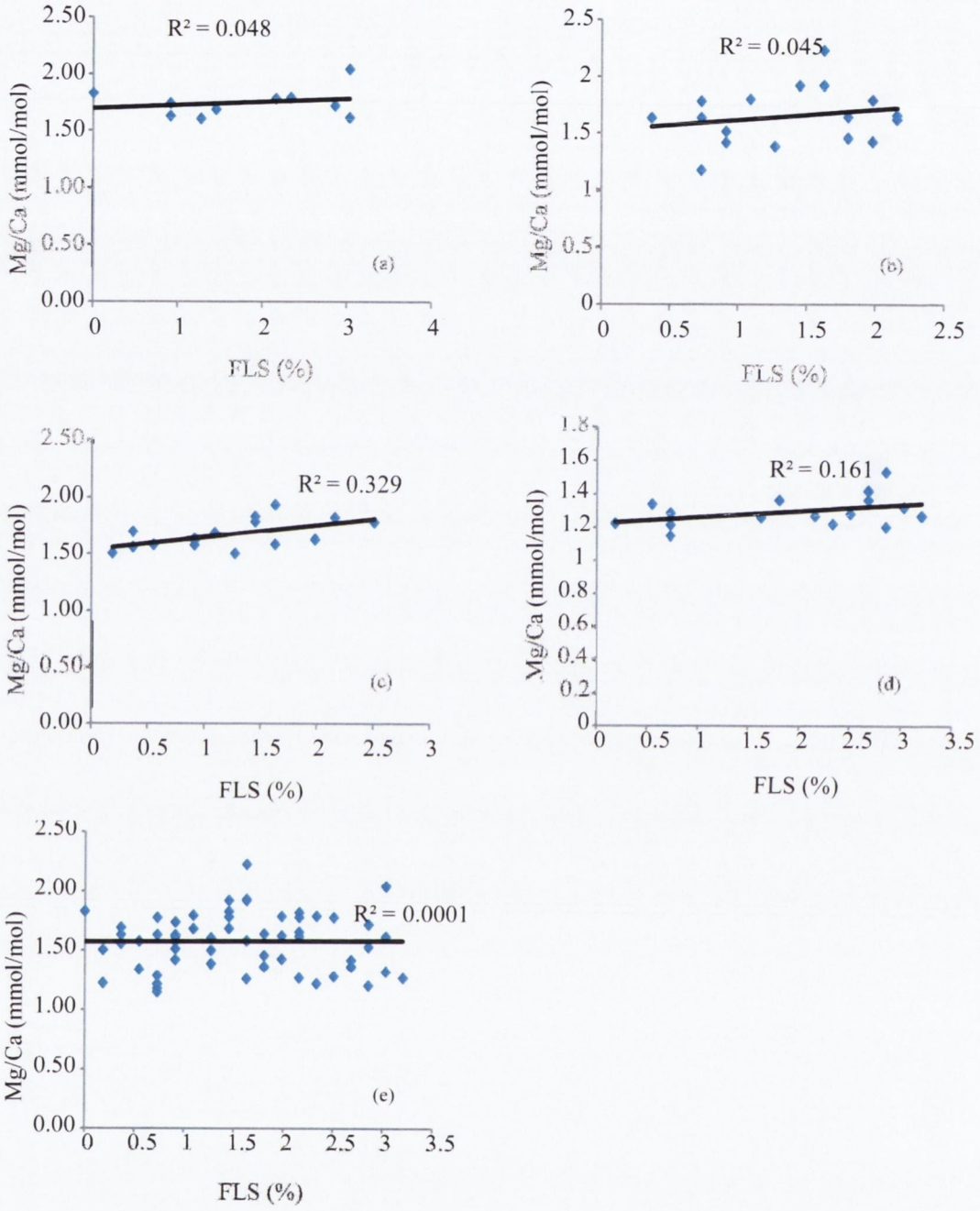

Figure 7.2. Fragmentation index versus Mg/Ca values for cores (a) 9/97-10, (b) 9/97-04, (c) 9/97-14 and (d) 9/97-27/2. The whole core dataset is plotted in (e).

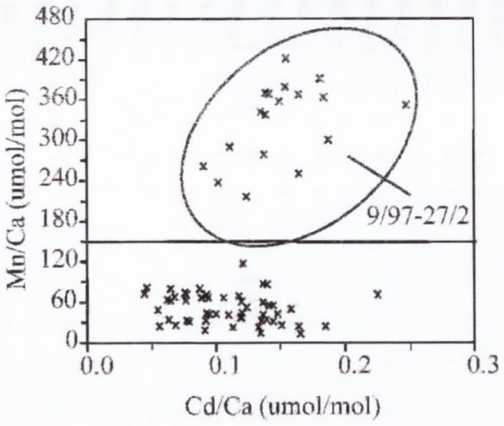

Figure 7.3. Scatter plot of whole core Mn/Ca vs. Cd/Ca values, with all of the samples from core 9/97-27/2 recording concentrations above 150 μmol/mol.

7.4 Results of benthic geochemical analysis

7.4.1 Core 9/97-10

Downcore Sr/Ca ratios vary between 1.36 and 1.48μmol/mol (Fig. 7.4). There are low amplitude variations between 90-27cm, followed by high frequency changes between 27-11cm. The final section (11-0cm) is relatively stable. Samples which are relatively enriched in Ba/Ca are present at 3cm, 20cm, 35cm, 51.5cm and 67.5cm and all values are below 2.5μmol/mol apart from two samples, one at 67cm and one at 35cm. These values are comparable to the results from 117JPC, a similar depth core from the Bahama Banks studied by Hall (2002). Cd/Ca values are usually above 0.09μmol/mol for interglacial deposits and below that value for glacial units and are relatively unstable during the last glacial (Marine Isotope Stages 2 and 3). This instability is also present in the Sr/Ca, Mg/Ca and $\delta^{18}O_{benthic}$ records, but not in the other nutrient proxy records (Ba/Ca and $\delta^{13}C_{benthic}$) although there are

some small scale variations. It is interesting to note that the temperature variations inferred from the Mg/Ca data are out of phase with the temperature

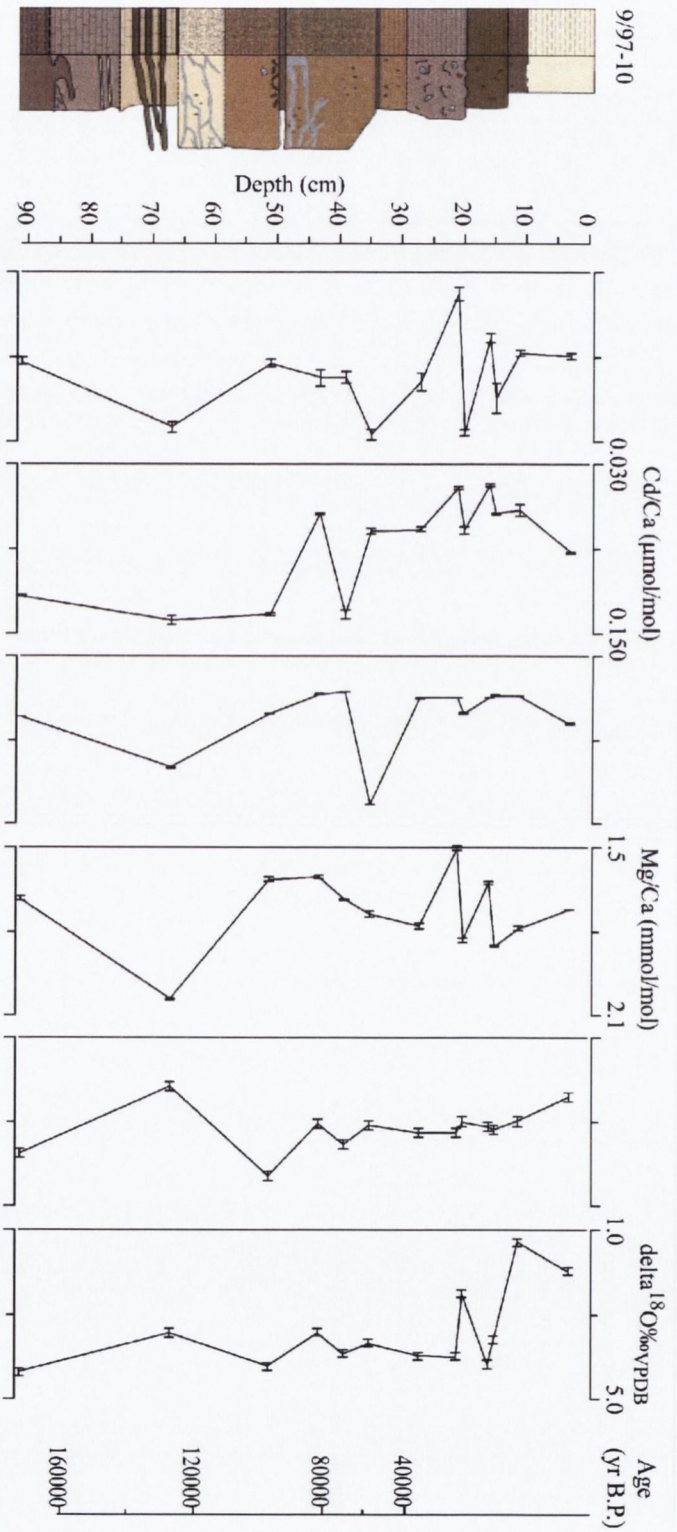

Figure 7.4. Down core multi-element / calcium and stable isotope ratios for core 9/97-10 (1260m water depth).

+ salinity variations (Elderfield and Ganssen 2000) inferred from $\delta^{18}O_{benthic}$. Mg/Ca values vary between 1.5 and 2.1mmol/mol and are generally stable apart from 27-15cm where values vary strongly with a high frequency. Carbon isotope values vary strongly between 91-35cm, followed by a period of relative stability between 35-11cm, with the top sample (3cm) significantly lower than previous values. The apparent stability in carbon isotope values between 21-11cm (19.5-11.5 kyr B.P.) contrasts with the records from other data for this core. Youngest benthic $\delta^{13}C_{benthic}$ values from core 9/97-10 of 1.07‰$_{VPDB}$ compare well with core top values derived from a nearby core site at a similar water depth (1.07‰$_{VPDB}$ at V29–198, 1139m water depth; Oppo and Lehman (1993)). Oxygen isotope ratios are high between the last interglacial and last glacial (91-21cm) and show little variation. Values then vary strongly between 21-15cm before stabilising with lower values at 11cm and 3cm.

7.4.2 Core 9/97-04

Downcore Sr/Ca values do not vary significantly or systematically (Fig. 7.5). The strongest variations are observed between 62-37cm. Cd/Ca values are generally above 0.1 (μmol/mol) for interglacial deposits and below for glacial units. Cd/Ca values are also slightly elevated for Holocene and early Last Interglacial samples. Ba/Ca values are also generally higher and more variable in interglacial deposits compared to glacial units. The values are consistent with the values reported from 117JPC, a similar depth core examined in the western Atlantic by Hall (2002). This trend (higher and more variable interglacial values) is also present in the Mg/Ca and carbon isotope records. A similar trend is also present in the oxygen isotope curve, except that the Holocene values are much lower than

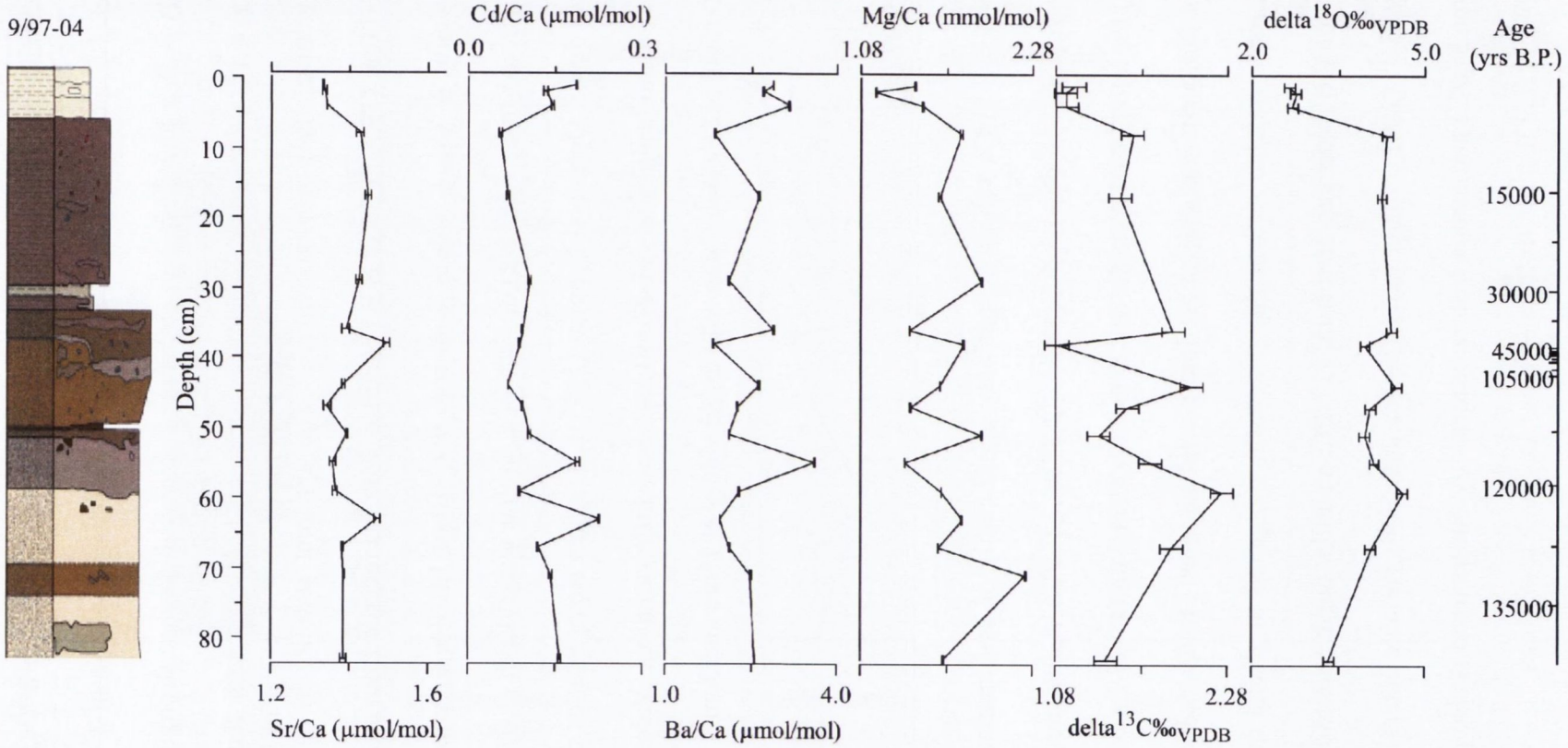

Figure 7.5. Down core multi-element / calcium and stable isotope ratios for core 9/97-04 (1502m water depth).

the rest of the core. Oxygen isotope values are consistently heavy for the last interglacial and last glacial, with lighter values in the Holocene (the same pattern exists in the oxygen isotope profile of core 9/97-10). Carbon isotope values are lower in interglacial units and higher in glacial deposits, with one strong negative carbon isotope excursion at 38cm core depth (41.3 kyr B.P.).

7.4.3 Core 9/97-14

Sr/Ca, Cd/Ca, Mg/Ca and $\delta^{18}O_{benthic}$ each display high levels of variability when followed downcore (Fig. 7.6). Variations observed in the Sr/Ca record appear to lead variations in the Cd/Ca record. Cd/Ca values are generally lower then 0.14 μmol/mol during glacial episodes (with two exceptions) and higher during interglacials. The two exceptions to this are present at 7.5cm and 23cm depth. Ba/Ca values are lower than 2.7 μmol/mol for the last glacial and higher during the interglacials and are largely stable apart from one value at 19cm which is significantly higher than all others in the core. Mg/Ca values are generally higher during interglacials when compared with values from glacial units. There is a slight lead in the twin peaks in bottom water temperature followed by a pair of sand units present in the last interglacial sediments (59-45cm). Carbon isotope values are below 1.1 $‰_{VPDB}$ (Vienna Pee Dee Belemnite) for the lower part of the core (95-53cm) and above 1.1 $‰_{VPDB}$ for the upper part (53-0cm). Oxygen isotope values are more variable during interglacials (particularly the last interglacial) compared to the last glacial. Oxygen isotope values are generally below $4‰_{VPDB}$ during interglacials and higher than this during glacials, although

there are exceptions. The twin lower values observed at 59cm and 51cm are coeval with the twin Mg/Ca peaks discussed previously. Highly variable values are present between 12-1cm.

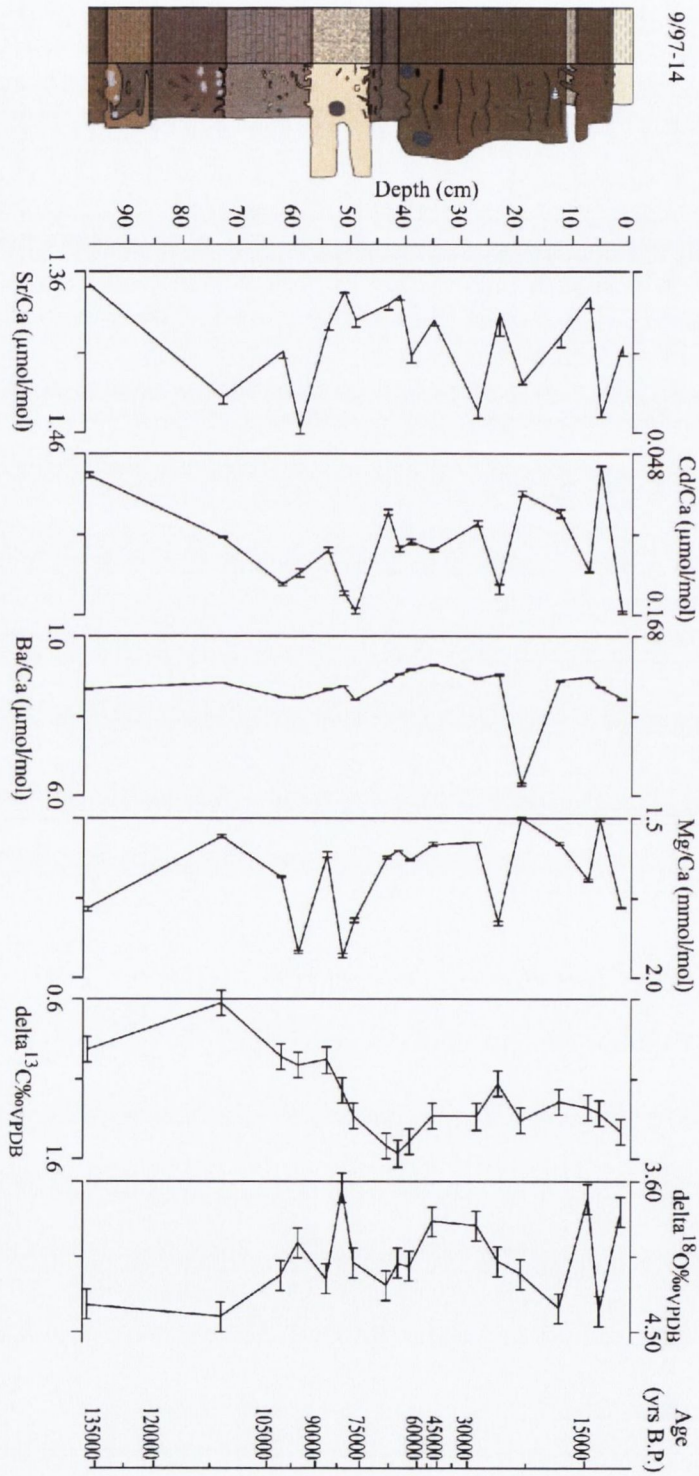

Figure 7.6. Down core multi-element / calcium and stable isotope ratios for core 9/97-14 (2118m water depth).

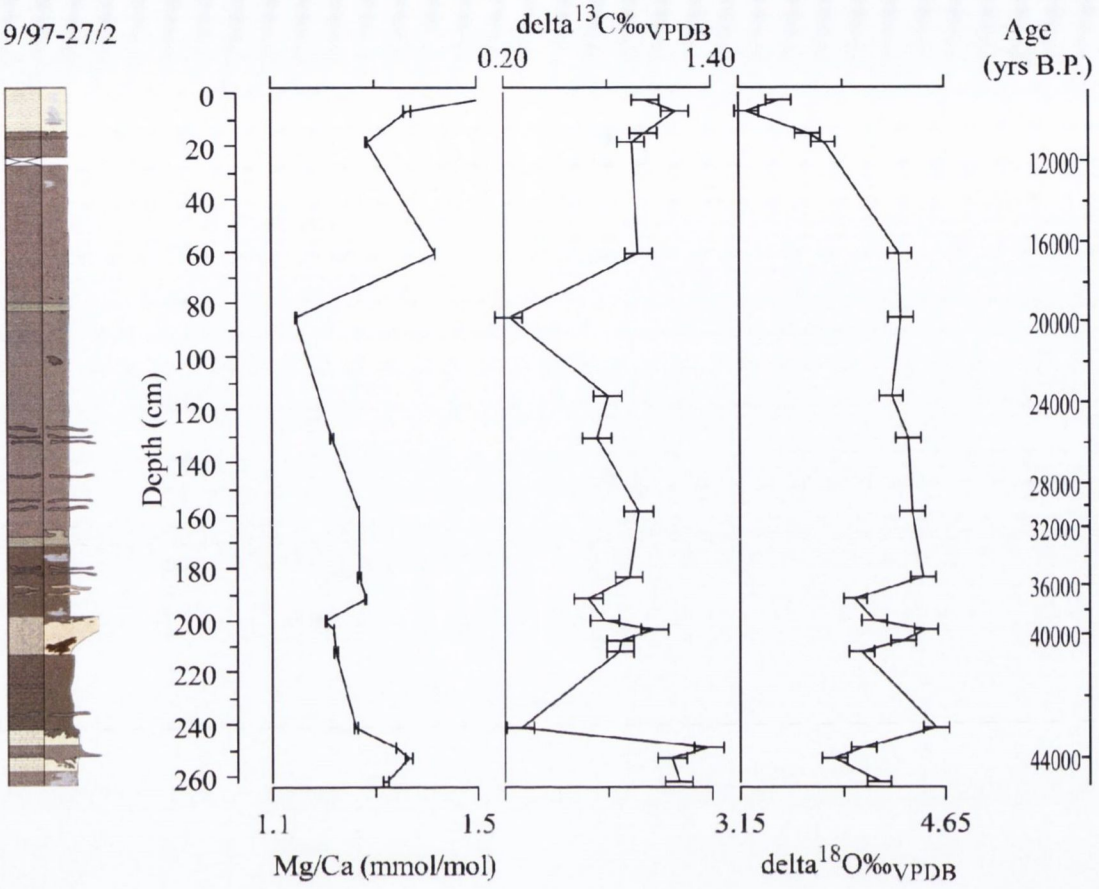

Figure 7.7. Down core multi-element / calcium and stable isotope ratios for core 9/97-27/2 (2756m water depth).

7.4.4 Core 9/97-27/2

The Mg/Ca record is relatively stable with low amplitude variations between 262-192cm (Fig. 7.7). Values are low in samples between 192.5-212.5cm, when compared to the previous interstadial (between 249.5-262.5cm) and the Holocene. The lowest value is recorded at 85cm, followed by strong variations and a final increasing trend in the Holocene (16-0cm). An unusually high (relative to adjacent values) Mg/Ca value is present at 61cm. Carbon isotope values are generally higher than 1 $‰_{VPDB}$ at the top (15-3cm) and bottom

(262-249.5cm) of the core, with lower values for the remainder. Two significantly negative values are present, one at 241.5cm and another at 85cm. The relatively extreme negative carbon isotope values recorded in samples at 85cm and 241.5cm are not linked to any consistent lithofacies (see Fig. 7.7). Oxygen isotope values are relatively variable at the top (19-3cm) and bottom (262-184cm) of the core with minor variations present in the remainder (185-61cm). Oxygen isotope values vary considerably between 262-184cm despite the lack of variation in the Mg/Ca values for this interval.

7.5 Downslope patterns in geochemical data

7.5.1 Mg/Ca (bottom water temperature)

Bottom water temperatures (as estimated from Mg/Ca values) vary between 4-8°C between cores 9/97-10, 9/97-04 and 9/97-14 (Fig. 7.8) and these values are broadly consistent with reconstructed potential temperature values (Read 2001). However, large standard errors (+/- 1.4°C) result from applying the equation of Martin *et al.* (2002). During MIS 5, values are comparable to the Holocene for the core sites above and including 9/97-14 (2118m water depth). Values recorded for the last interglacial in core 9/97-10 (1260m water depth) vary between 6-8°C. Core 9/97-04 (1502m water depth) displays some consistent variation in bottom water temperature between glacial-interglacial episodes. Temperatures are relatively stable during the early part of the last interglacial and are relatively low (>5.1°C). Bottom water temperatures are greater than 6.5°C for the last interglacial in core 9/97-14 and are highly variable.

Values are high for MIS 3 in core 9/97-10 and low in cores 9/97-04 (<6.5°C) and 9/97-14 (<6°C). Bottom water temperatures are highly variable for this interval in core 9/97-27/2. Marine isotope stage 2 values are lower than Holocene values (5°C average temp.) for cores 9/97-04, 9/97-14 and 9/97-27/2, but slightly higher for core 9/97-10 (6.8°C). During MIS 2, values between 20-11.5kyrs B.P. are highly variable (5.2-7.1°C) in core 9/97-10. Temperatures are also variable for cores 9/97-04, 9/97-14 and 9/97-27/2. The coldest bottom water temperature (1.3°C) is recorded at 20kyrs B.P. in core 9/97-27/2.

Holocene temperatures average 6.1-6.7°C between 1260-2118m water depth, and average 2.5°C at 2756m. In core 9/97-10, a clear cooling trend can be observed between 15.8-5.6 kyr B.P. Holocene values are generally low (<5.1°C) in core 9/97-04 and high in core 9/97-14 (>6.5°C). A warming trend is clearly present in the Holocene bottom water temperature reconstruction of core 9/97-27/2.

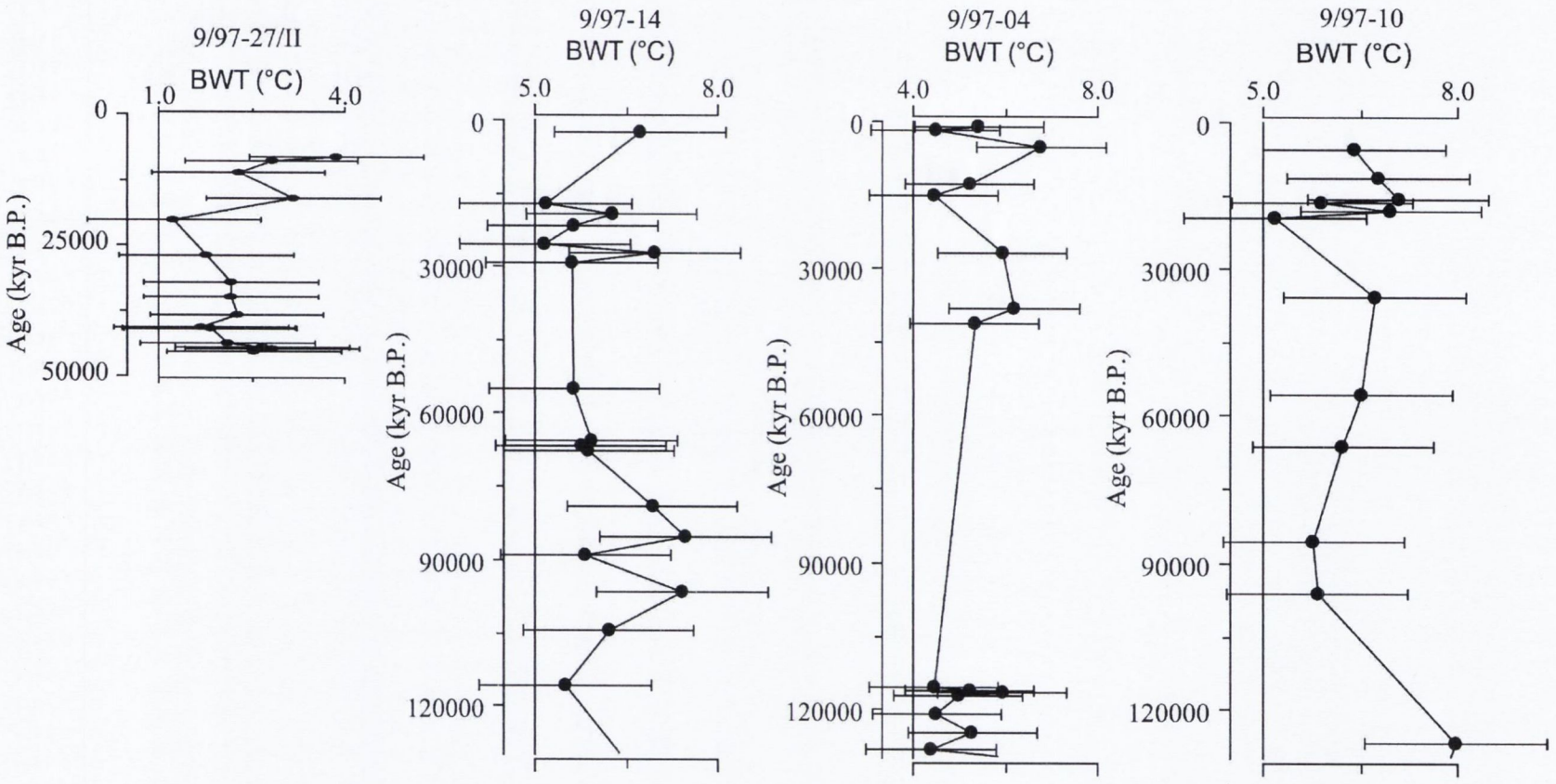

Figure 7.8. Down slope bottom water temperature variations from four cores for the last interglacial to Holocene; 9/97-10 (1260m water depth), 9/97-04 (1502m water depth), 9/97-14 (2118m water depth), 9/97-27/2 (2756m water depth).

7.5.2 Oxygen (seawater density)

Interglacial samples in cores 9/97-10 and 9/97-04 record consistently high (Fig. 7.9) and very similar $\delta^{18}O_{sw}$ values ($\geq 1‰_{VPDB}$). Core 9/97-14 also has high ($\geq 1‰_{VPDB}$) values for the last interglacial. For glacial samples, average values between cores 9/97-10 and 9/97-04 are generally very similar ($\geq 1‰_{VPDB}$), with the exception of one sample at 26.7 kyr B.P. from core 9/97-04. Core 9/97-14 has highly variable $\delta^{18}O_{sw}$ values, whereas core 9/97-27/2 has consistently higher last glacial $\delta^{18}O_{sw}$ values compared to the Holocene (average $0.75‰_{VPDB}$). Comparing Holocene values from cores 9/97-10 (average $-0.5‰_{VPDB}$) and 9/97-04 (average $0.5‰_{VPDB}$) reveals significant stratification in water masses. Stratification is also observed between core 9/97-14 (average $1.3‰_{VPDB}$) and 9/97-27/2 ($-0.25‰_{VPDB}$).

7.5.3 Carbon isotopes (stratification / ventilation)

For core 9/97-10 $\delta^{13}C_{benthic}$ values do not vary significantly, and are all (with 2 exceptions) greater than $1.5‰_{VPDB}$ (Fig. 7.10). Glacial values, even during MIS 3 and between the last glacial maximum and the start of the Holocene display little variation around $1.5‰_{VPDB}$. The Holocene sample is lower than the glacial values ($1.07‰_{VPDB}$). Core 9/97-04 displays clear glacial-interglacial variations in carbon isotope value. Last interglacial values are generally greater than $1.6‰_{VPDB}$, Holocene values are approximately $1.1‰_{VPDB}$, with glacial values averaging $1.6‰_{VPDB}$. Holocene $\delta^{13}C_{benthic}$ values for the cores above 2100m are consistent with Sarnthein *et al.* (1994), all values are greater than $1.1‰_{VPDB}$. Last interglacial values for core 9/97-14 are lower than $1.01‰_{VPDB}$. Core 9/97-14 also has a relatively stable carbon isotope record for the Holocene and last glacial, with values between $1.1\text{-}1.6‰_{VPDB}$. Core

9/97-27/2 displays consistent variation between Holocene / interstadial and glacial / stadial carbon isotope values.

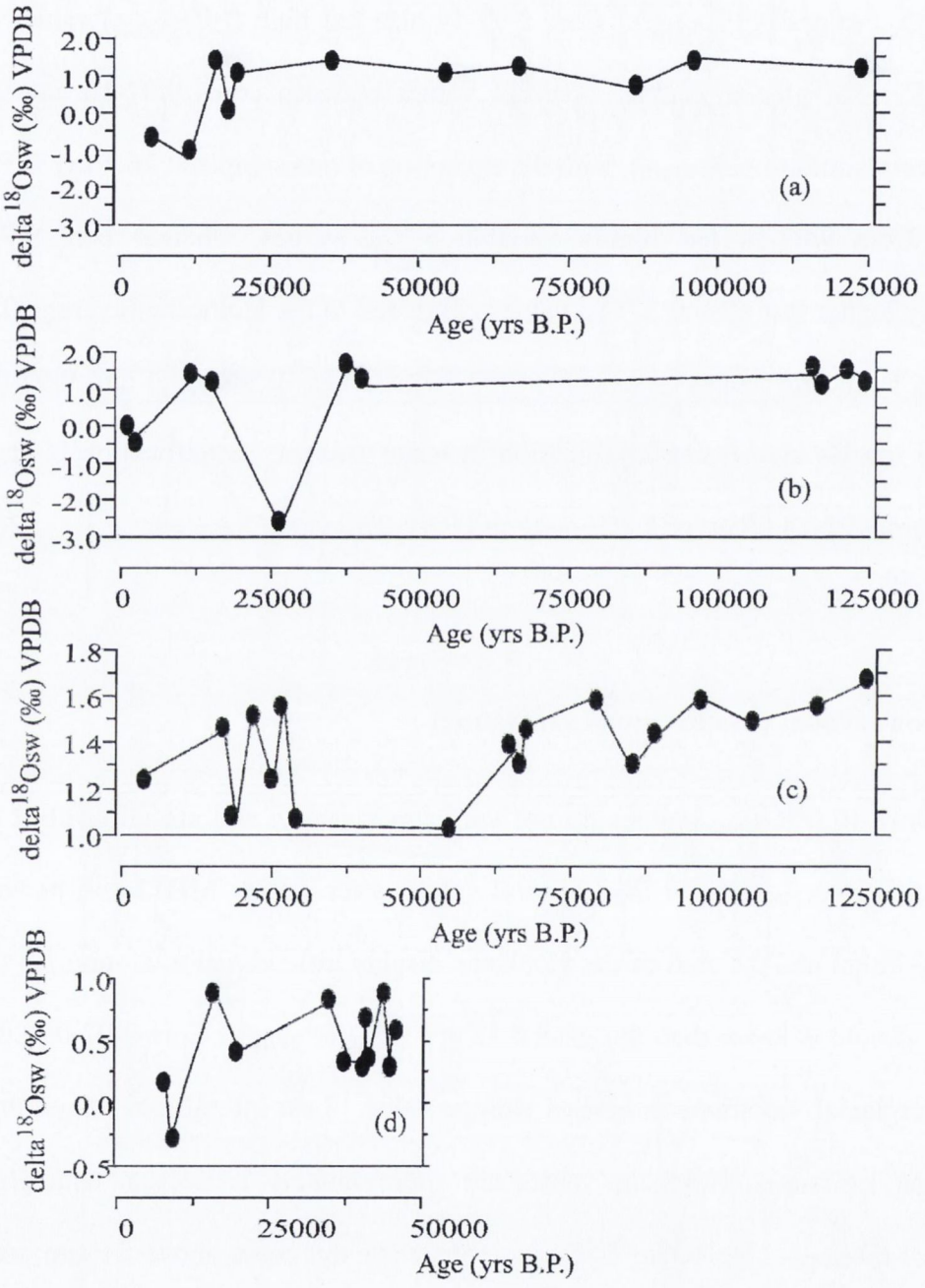

Figure 7.9. Reconstructed $\delta^{18}O_{sw}$ values for cores (a) 9/97-10 (1260m water depth), (b) 9/97-04 (1502m water depth), (c) 9/97-14 (2118m water depth) and (d) 9/97-27/2 (2756m water depth) for the time interval 0-125 kyr B.P.

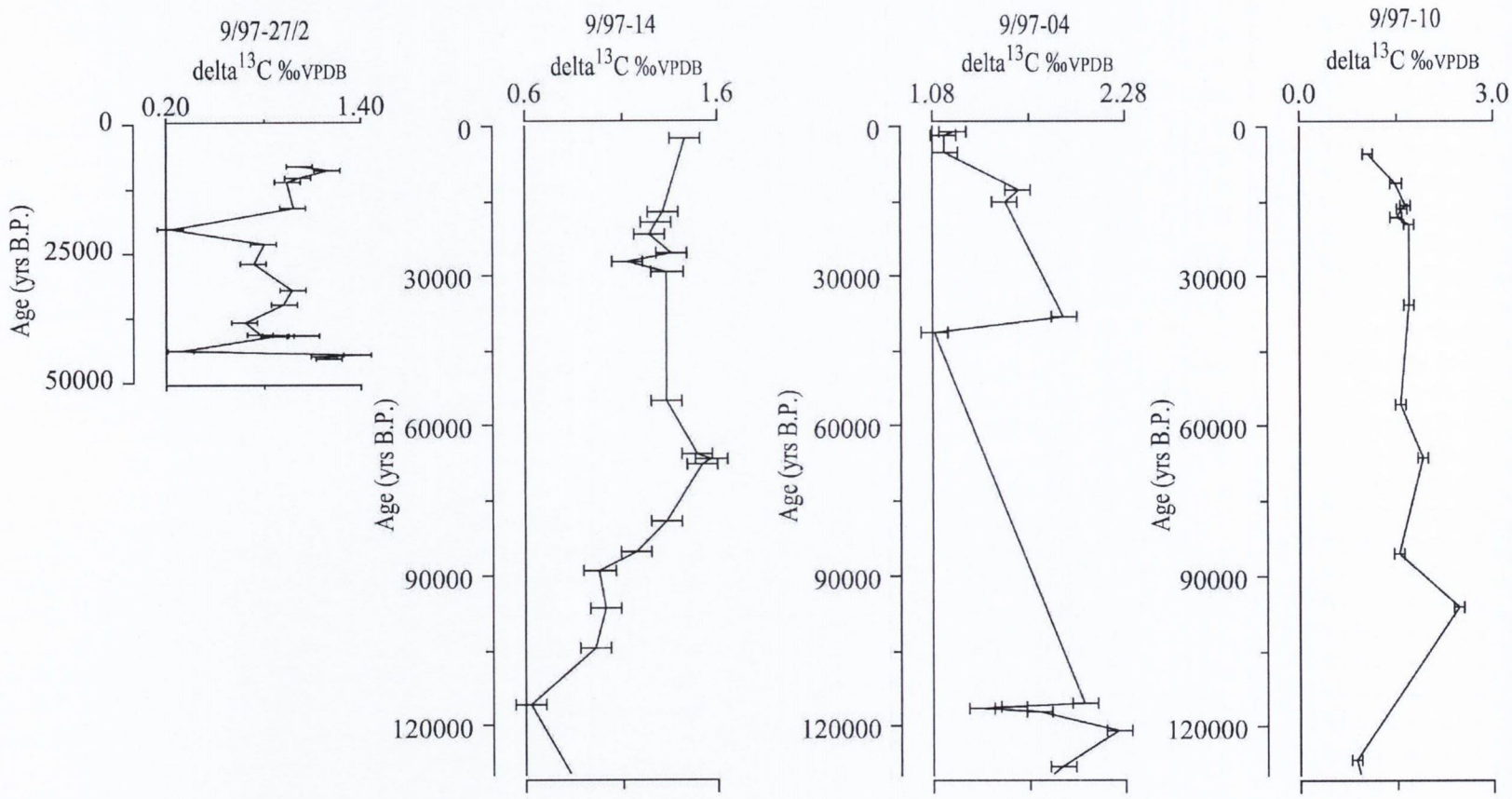

Figure 7.10. Down slope carbon isotope ratios from four cores for the last interglacial to Holocene; 9/97-10 (1260m water depth), 9/97-04 (1502m water depth), 9/97-14 (2118m water depth), 9/97-27/2 (2756m water depth).

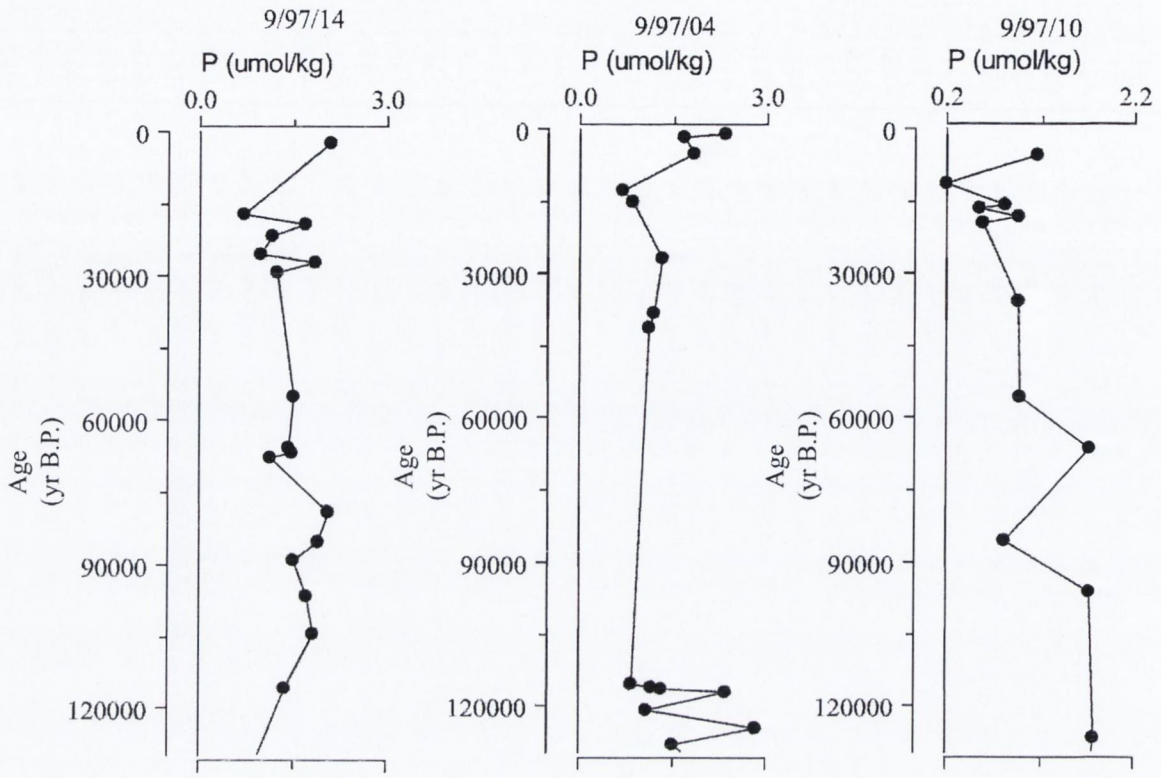

Figure 7.11. Down slope reconstructed phosphorus concentrations from three cores for the last interglacial to Holocene; 9/97-10 (1260m water depth), 9/97-04 (1502m water depth), 9/97-14 (2118m water depth).

7.5.4 Phosphorus concentrations

Reconstructed phosphorus concentrations (Fig. 7.11) in core 9/97-10 are high for the last interglacial (>1.5µmol/kg) and low for the last glacial and Holocene (<1µmol/kg). Phosphorus concentrations for the last interglacial are also relatively stable (+/- 0.05µmol/kg). There is a slight increase in phosphorus concentration between the last glacial and Holocene (increasing to 1.16µmol/kg). Core 9/97-04 displays clear changes in phosphorus concentrations which are consistent with glacial-interglacial variations. Values are highly variable in the early part of the last interglacial. Values are consistently low during the last

glacial (<1.5µmol/kg) and high (>1.5µmol/kg) during the Holocene. The data for the Holocene and last glacial from both cores are broadly consistent with previous water mass reconstructions for this region (i.e. Sarnthein *et al.* 1994; Rickaby and Elderfield 2005; Lynch-

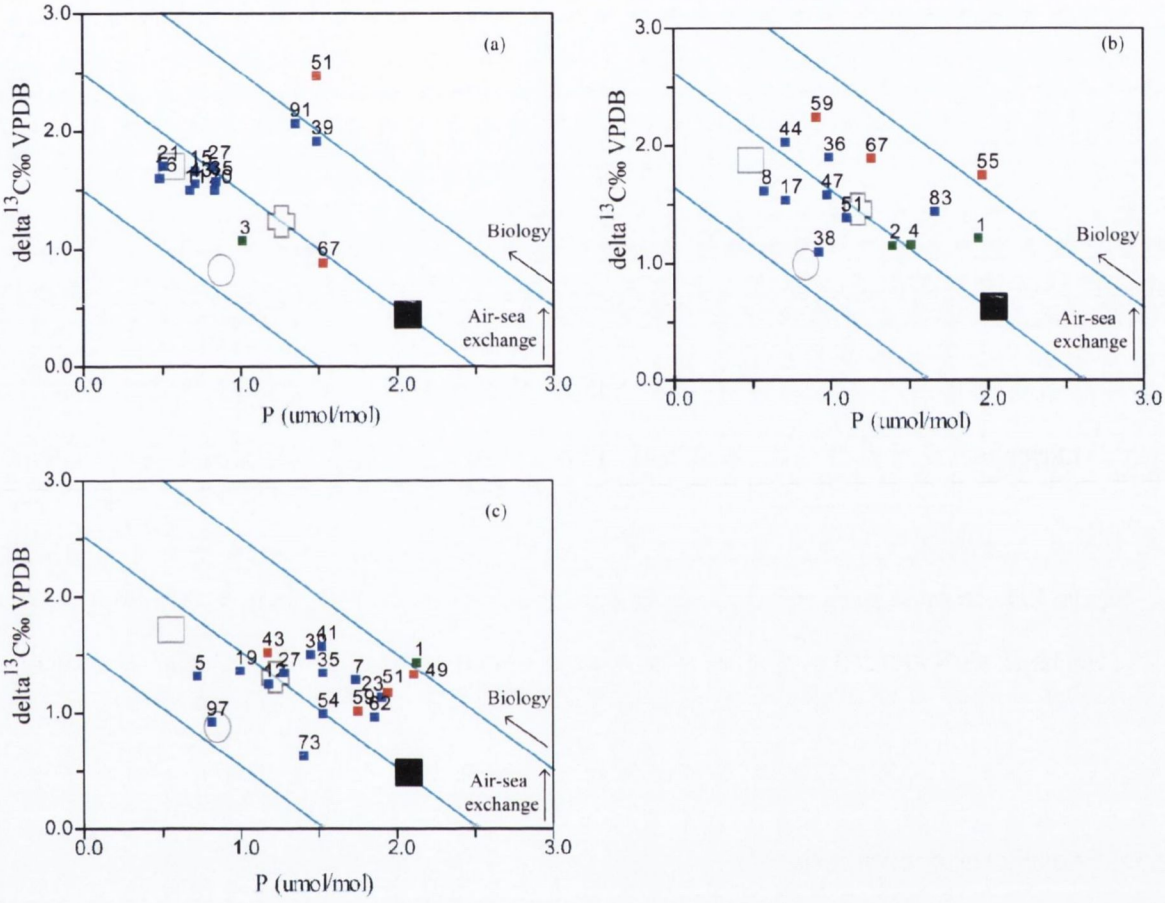

Figure 7.12. Plots of reconstructed phosphorus concentrations versus $\delta^{13}C_{benthic}$ for cores (a) 9/97-10, (b) 9/97-04 and (c) 9/97-14. End-member compositions are derived following the methodology of Rickaby and Elderfield (2005). Open square = GNAIW, open circle = MOW (Mediterranean Outflow Water), open cross = NADW, full square = AABW. Green dots refer to Holocene samples, blue dots to last glacial samples and red dots to last interglacial samples. Samples which are removed vertically along the air-sea exchange parameter are considered to be mixed with AAIW.

Stieglitz *et al.* 2007). Phosphorus concentrations of bottom water masses varied significantly through time in core 9/97-14. There is no consistent glacial-interglacial variation in values, as relatively high values are present in both glacial and interglacial samples. The values do not vary significantly and average at 1.5μmol/kg. These values can be combined with $\delta^{13}C_{benthic}$ to determine water mass influence (Fig. 7.12).

7.6 Discussion

7.6.1 Planktonic geochemical analysis

The planktonic oxygen isotope record is a useful correlative tool (see Chapter 5). These data also provide some information about the temperature of the surface ocean through time. This temperature record is broadly consistent with the SST record provided by transfer function techniques in showing higher temperatures in lighter coloured units (Chapter 6). However, there are some important differences. In the current interglacial, *G.bulloides* is most productive in this part of the NE Atlantic during the spring (Schiebel *et al.* 1997; Ganssen and Kroon 2000) and this is broadly consistent with the results presented here from the $\delta^{18}O_{planktonic}$ record which suggest the temperature of calcification is lower than the reconstructed summer values. Comparison with the MAT and WAPLS values for the last glacial, however, imply that this might not always have been the case, and suggests that during glacial episodes *G.bulloides* was more productive during the summer. This could be related to a glacial reduction / absence of the spring bloom that is currently observed at this locality (e.g. Gooday and Hughes 2002) which is when *G.bulloides* is more productive (e.g. Schiebel *et al.* 1997). The season of maximum production could have shifted to later in the year, perhaps when sea

surface temperatures are high enough to increase stratification of the water column, concentrating nutrients at the thermocline and supporting the growth of *G.bulloides*. This potentially has profound implications for SST reconstructions based on geochemical studies and modern analogue studies of planktonic foraminifera (and maybe other groups) and perhaps suggests that some of the large SST variations implied for periods in Earth's history (Pflaumann *et al.* 2003; Kucera *et al.* 2005) are potentially under-estimated if authors make the assumption that they are comparing temperature records from the same season. However, problems with the values reconstructed via MAT due to the lack of good modern analogues for the fossil assemblages (see Chapter 6) suggest that this may not be the case. WAPLS should cope better with no analogue samples as it is able to extrapolate relationships between species and parameters, but this presents similar values to MAT.

Another important difference is in the duration of the proposed glacial-interglacial episodes. The oxygen isotope record proposes longer glacial episodes compared to the transfer function method. This could be due to a number of factors. The first set assume that the transfer function method is over-estimating the SSTs due to post-mortem modification of the planktonic assemblages; (1) preferential dissolution of 'cold' taxa (i.e. *N.pachyderma* (sin.)), (2) preferential winnowing out of 'cold' taxa. The second set assume that there are errors associated with estimating SSTs using $\delta^{18}O_{planktonic}$ from *G.bulloides*; (1) *G.bulloides* does not always record surface temperature values, (2) variations in global ice volume are not sufficiently accounted for when calculating SSTs. *Neogloboquadrina pachyderma* (sin.), the coldest taxon, is significantly less susceptible to dissolution compared to 'warmer' taxa (Hemleben *et al.* 1989 and see Fig. 3.3), which would produce colder rather than warmer SSTs via the transfer function method if dissolution were a significant factor. If *G.bulloides* was not

recording sea surface values and instead reflected values recorded at depth, then those values would also be lower, not higher as seawater cools with depth. The effect of varying global ice volume on $\delta^{18}O_{sw}$ has been estimated specifically for this region in a recent publication (Elderfield and Ganssen 2000) but uncertainties in SST estimates derived from Mg/Ca data could also be a problem. Preferential winnowing out of the 'colder' taxa (particularly *N.pachyderma* sin.) as a mechanism of post-mortem modification of assemblages could potentially explain discrepancies between the SST records from geochemical and transfer function estimates by producing the warm estimates from the transfer function methods. However, problems identified in the determination of absolute temperature values via the transfer function methods (discussed further in Chapter 6) could also explain this discrepancy, particularly when the gaps in observed versus reconstructed values for each method is considered (Fig. 6.1).

The lack of strong systematic variations in carbon isotope values corresponding with the changes in oxygen isotope values implies that the species chosen (*G.bulloides*) is consistently recording values from the same water depth (See Fig. 3.18, Chapter 3), which is likely to be the upper (0-60m) part of the water column (Schiebel *et al.* 1997). Strongly negative values of approximately 0.5‰$_{VPDB}$ are generally associated with significantly increased organic matter oxidation which adds net ^{12}C to dissolved inorganic carbon (DIC) in the surface ocean. One of the strong negative values observed in the record (at 15cm) is associated with the termination of the last glacial (16.4 kyr B.P.). A similar phenomenon of negative carbon isotope excursions linked to deglaciation has been observed in previous studies from the southern hemisphere (Spero and Lea 2002). The authors linked the carbon isotope minimum events to a breakdown in surface water stratification in the Southern Ocean.

A similar excursion has also been observed in intermediate depth benthic records from the NE Atlantic region (Knutz *et al.* 2002; Hall *et al.* 2006; Peck *et al.* 2007) and are associated with H1 (Heinrich event 1). This interpretation (that this excursion is related to H1) is consistent with the findings of Peck *et al.* (2007), who observed the negative isotope excursion in their intermediate depth benthic data at approximately 16 kyr B.P., after H1 (dated at 16.8 kyr B.P. in their study). Although these excursions are off-set by 0.4 kyr, given age uncertainties they are consistent with each other.

The earlier negative excursion (at 142cm) is also potentially the result of an event similar to H1, with perhaps a strong reduction in surface stratification leading to an increase in organic matter oxidation at the sea surface. This is potentially the first record of a Heinrich-like event associated with Marine Isotope Stage 8 and the volume of the excursion suggests that this event had a larger impact on surface ocean productivity than H1, with a slightly larger scale negative excursion in $\delta^{13}C_{benthic}$. However, an examination of the IRD (ice-rafted debris) content from this sample and adjacent samples is necessary before this can be definitively assigned to a Heinrich-like event. Although a large cobble (Fig. 3.1) is present in the core directly above this sample point, this could be reworked from an adjacent site. Another possibility is that the carbon isotope excursion is caused by methane hydrate destabilisation, a large increase in productivity, or sample dissolution. Locating this in another core (ideally from a different locality) is required before the nature of this excursion can be described further.

7.6.2 Assessment of geochemical data

Comparing the correlation coefficients for each core Mg/Ca versus fragmentation index suggests that fragmentation (and, therefore, dissolution) is having a stronger impact on some of the Mg/Ca ratios in 9/97-14 due to the higher correlation coefficient. Because Mg-rich calcite is more soluble than pure calcite, this would lead to depletion in Mg concentrations in the test and the values obtained following analysis. This would produce lower bottom water temperature estimates for some samples in this core (McCorkle *et al.* 1995), but comparing the data between cores (see Figs. 7.4-7.7) shows that there are no evident offsets. For the other cores, there is no evidence of any dissolution effect on the trace metal data from the fragmentation indices.

No linear correlation is observed between all core Cd/Ca and Mn/Ca values (Fig. 7.3). However, all of the samples from core 9/97-27/2 contain Mn/Ca values greater than 150μmol/mol and therefore can not be used to reliably determine bottom water Cd/Ca and Ba/Ca values. As all of the samples from core 9/97-27/2 contain high concentrations of Mn, this suggests that they formed under dysoxic conditions (Boyle 1983). The finding of consistently dysoxic sediments is not suggested by modelling studies of the modern continental slope in this region (Read 2001). The model produced by Read (2001), based on data from a grid of CTD transects, suggests that dissolved oxygen never falls below 5ml/l in the modern Porcupine Bank / Rockall Trough region. This suggests this could be a localised phenomenon, perhaps related to local topography, which is too small in scale to be observed in the modelled reconstruction of modern water mass distributions.

Examination of the Sr/Ca data in core 9/97-10 leads to the interpretation that the sample at 21cm (with the most depleted Sr/Ca value) has potentially undergone some selective dissolution. As mentioned previously, an examination of whole core fragmentation index versus Mg/Ca values shows that no dissolution effect is evident. However, any significance applied to this data point must be considerate of the possibility that this sample has undergone selective dissolution. Also, if selective dissolution has occurred, this could itself be due to a particular oceanographic event (e.g. Heinrich event – see Section 2.7) or process (influx of Southern Component Water which is more corrosive).

Sr/Ca values are never evidently depleted in core 9/97-04, suggesting that selective dissolution is unlikely to have affected any of the samples, which is in agreement with the data from the fragmentation index / Mg/Ca plots (Fig. 7.2). In core 9/97-14, two samples (49cm and 41cm) in particular have depleted Sr/Ca and Mg/Ca values, consistent with selective dissolution occurring (McCorkle *et al.* 1995). There are other samples with depleted Sr/Ca values, but these are not paired with depleted Mg/Ca (which would be expected if selective dissolution were occurring) so a dissolution effect can probably be ruled out for those sample points. The suggestion that some samples in this core are affected by selective dissolution is also suggested by the comparison of Mg/Ca values and fragmentation index data (Fig. 7.2).

7.6.3 Water masses and their structure

The warm bottom water temperatures present for the last interglacial derived from Mg/Ca values are comparable to modern values (Read 2001). The similar values in all cores above 2118m during the last interglacial imply that little thermal stratification existed.

However, clear differences in early last interglacial values are present, with core 9/97-10 recording slightly warmer temperatures. It is therefore possible that some minor thermal stratification was present at the start of this episode.

The colder and more stable temperatures present in MIS 3 in three cores contrasts with the highly variable MIS 2 from these cores (9/97-10, 9/97-04 and 9/97-14). It is generally expected that MIS 3 would display a higher degree of variability compared to MIS 2, according to the GISP-II record (Grootes and Stuiver 1997). However, changes in water mass configuration, which are potentially evident in other data from this study during MIS 3 in core 9/97-27/2, would not necessarily produce variations in bottom water temperature. Also, the large standard errors associated with the reconstructed temperatures complicates the interpretation of actual values and the lack of large parts of MIS 3 in cores 9/97-04 and 9/97-14 could also result in the suggestion that bottom water temperatures are stable during this interval. The cooler bottom water temperatures for MIS 2 compared to MIS 3 and the Holocene obtained in core 9/97-27/2 are in accordance with the findings of Martin *et al.* (2002), who reported lower temperatures (relative to the Holocene and MIS 3) for their site in the Eastern Tropical Atlantic. Although the temperature changes reported here (approx. 0.8°C reduction from Holocene to Last Glacial) are slightly less than the 2°C cooling anticipated from Labeyrie *et al.* (1987) and Martin *et al.* (2002), this is potentially explained by increased mixing with GNAIW at this shallower site, although the problem of large standard errors is also present. The Holocene temperatures above 2118m are consistent with the reconstructed potential temperature estimates for the modern ocean (Read 2001). The similarity in Holocene values above 2118m water depth suggests that there may be little or no thermal stratification.

A lack of any significant systematic variation in $\delta^{18}O_{benthic}$ values in core 9/97-10 between the last interglacial and the last glacial implies that there could be little change in bottom water density through time. It is expected that during interglacials bottom waters will be less dense than during glacials (reflecting warmer temperatures). This discrepancy could be related to the influence of AAIW over this site during the last interglacial (as suggested by other data), with high Cd/Ca values corresponding with higher oxygen isotope ratios suggesting that AAIW during the last glacial may have been as dense as GNAIW or NADW. It could be that the variations in recorded $\delta^{18}O_{benthic}$ from core 9/97-10 between 11-21cm reflect density contrasts, which has been shown to also have a significant effect on Cd/Ca ratios preserved in benthic foraminifera (Tachikawa and Elderfield 2002). However, changes in density need to be quite substantial in order to significantly alter Cd/Ca values (Boyle 1992; Bertram *et al.* 1995; Tachikawa and Elderfield 2002). It is possible that this is indicative of the transient influx of SCW (Southern Component Water), possibly AAIW although this is inconsistent with the stable and positive ($\geq$1.5‰$_{VPDB}$) carbon isotope values, which instead suggest that this site was continually bathed in GNAIW. This probably reflects the different behaviours of the two tracers, with Cd reflecting micronutrient distributions (particularly phosphorus) and $\delta^{13}C_{benthic}$ capable of being fractionated following biological uptake. The contrast between non-conservative and conservative water mass tracers suggests that the rapid ventilation of the intermediate NE Atlantic Ocean during this interval is masking (in the carbon isotope record) the incursions of SCW implied by the varying Cd/Ca ratios. Alternatively, dissolution could be causing the variation in Cd/Ca values (especially the sample at 21cm core depth), but this should also affect $\delta^{13}C_{benthic}$ values, according to

McCorkle *et al.* (1995). Also, dissolution (if present) could be caused by an increase in mixing with SCW.

The consistently heavy values in $\delta^{18}O_{benthic}$ present between the last interglacial and last glacial in core 9/97-04 contrasts with the strongly varying Mg/Ca values. This implies that another component in the $\delta^{18}O_{benthic}$ signal (such as salinity) could be varying simultaneously with temperature to produce an oxygen isotope profile with only small scale variations through time. Lighter oxygen isotope values for the Holocene are concurrent with low Mg/Ca values, suggesting lower temperatures could be causing the reduction in oxygen isotope ratios.

Twin Mg/Ca peaks in core 9/97-14 appear to precede the two sand layers by approximately 10 kyr according to the age model, although the temporal constraints for this time period are relatively poor due to a lack of absolute dating. Changes present in $\delta^{13}C_{benthic}$ data perhaps reflect varying ventilation rates, with last interglacial to Holocene values indicative of relatively rapid ventilation under the influence of GNAIW and earlier values suggesting a strong AABW influence. This is in contrast to the more variable Cd/Ca record discussed previously. The highly variable $\delta^{18}O_{benthic}$ values recorded in the top part of the core (0-12cm) appear to suggest very variable oceanographic conditions, possibly associated with the switch from the interglacial to glacial to modern modes of water mass distribution, although two relatively low Sr/Ca values are present in this interval. This variation is also possibly caused by dissolution.

The similar $\delta^{18}O_{sw}$ values present in cores 9/97-10 and 9/97-04 suggest a lack of significant stratification between these cores during the last interglacial. This is consistent

with the $\delta^{13}C_{benthic}$ / Phosphorus data (see below), which shows that the influence of AAIW is more episodic in core 9/97-10 compared to core 9/97-04 (where an AAIW signal is consistently observed in the samples from the last interglacial). High values in core 9/97-14 also imply a lack of significant stratification of bottom water masses down to a water depth of at least 2118m.

The highly variable $\delta^{18}O_{sw}$ values recorded in core 9/97-14 for the last glacial perhaps reflect the proximity of this core to a boundary between GNAIW and AABW (Bertram *et al.* 1995), as each of these water masses expanded in response to climatic variations at each pole. However, dissolution of these samples could also be causing this variation, although this interpretation is not supported by the Sr/Ca data. Similar values present in cores 9/97-10 and 9/97-04 for the last glacial imply very weak stratification, consistent with the carbon isotope data which suggest that both sites were well ventilated by GNAIW. The values for these cores are different from the values in core 9/97-27/2, consistent with this site experiencing a strong influence from a water mass with a different density (e.g. GAABW). Reconstructed Holocene $\delta^{18}O_{sw}$ values for all cores are dissimilar so are compatible with modern observations of a highly stratified water column along the slope edge at this locality (Read 2001).

Last interglacial $\delta^{13}C_{benthic}$ values for core 9/97-10 are greater than 1.5‰$_{VPDB}$, implying a strong NADW influence based on the reconstruction of Lynch-Stieglitz *et al.* (2007). A strong NADW influence can also be inferred for core 9/97-04, although a high SCW signal is evident from the data in core 9/97-14. This suggests a similar water mass distribution to the last glacial model proposed by Lynch-Stieglitz *et al.* (2007), with little or no evidence of SCW presence at sites above 2000m. However, a comparison with phosphorus concentrations is necessary to validate this interpretation as more than one factor can influence carbon isotope

values (Broecker and Peng 1982; Curry and Lohmann 1982; Michel 1991 and see Fig. 3.19) and carbon isotope values $\geq 1.5‰_{VPDB}$ are not inconsistent with strong mixing with AAIW. The high values for MIS 3 to MIS 2 are indicative of a consistently well-ventilated GNAIW signal in cores 9/97-10, 9/97-04 and 9/97-14. In core 9/97-27/2 higher $\delta^{13}C_{benthic}$ values during MIS 3 interstadials suggest a GNAIW expansion to this depth (2756m). However, this could also be due to increased productivity. Comparison with BFAR (see Chapters 8 and 9) is required to test this. During MIS 2, $\delta^{13}C_{benthic}$ values are lower, indicative of SCW dominance (probably GAABW) over this site, which is consistent with the models produced by Sarnthein *et al.* (1994) and Lynch-Stieglitz *et al.* (2007), although the expansion of GNAIW during MIS 3 interstadials is not evident from the study by Sarnthein *et al.* (1994). This is probably because their time slice reconstruction ends 30 kyr B.P. and the proposed MIS 3 expansion of GNAIW is first observed in this study earlier at 43-44 kyr B.P. For the Holocene, $\delta^{13}C_{benthic}$ values are slightly lower in cores 9/97-10 and 9/97-04, implying perhaps a stronger SCW influence (probably AAIW). Values are similar to last glacial values in core 9/97-14, suggesting a continued NCW influence (probably NADW). The influence of NADW is also present in the carbon isotope values recorded from the Holocene of core 9/97-27/2. This is consistent with modern water mass distributions implied by carbon isotope profiles (Sarnthein *et al.* 1994; Lynch-Stieglitz *et al.* 2007) and modern oceanographic data (Read 2001).

The greater than $1‰_{VPDB}$ $\delta^{13}C_{benthic}$ values present in core 9/97-27/2 are suggestive of a NADW (North Atlantic Deep Water) signal (or the glacial equivalent) and the lower values of AABW influence (Lynch-Stieglitz *et al.* 2007), although without concurrent Cd/Ca data, it is not possible to distinguish between a productivity and water mass change. A higher than $1‰_{VPDB}$ $\delta^{13}C_{benthic}$ value recorded in the sample at 204.5cm depth could suggest a brief

episode of greatly enhanced productivity. An absence of clear co-variation of Mg/Ca and $\delta^{18}O_{benthic}$ between 262-184cm implies that the temperature of the bottom water does not vary significantly (as Mg/Ca does not vary significantly), and that either global ice volume or salinity instead varied significantly (Elderfield and Ganssen 2000). Little variation in bottom water parameters is suggested by a lack of variation between 185-61cm. Both the Mg/Ca (higher values relative to the glacial) and $\delta^{18}O_{benthic}$ (lighter values relative to the glacial) data for the Holocene in core 9/97-27/2 are consistent with increased bottom water temperatures (compared to the last glacial).

A negative carbon isotope excursion in the sample at 85cm (20 kyr B.P.) in core 9/97-27/2 is of a similar magnitude (approx. 0.5‰) to that present in the record of Peck *et al.* (2007) so is potentially the result of a Heinrich-like event. However, it does not appear to be coeval with any of the Heinrich events from the record of Peck *et al.* (2007). The scale of the two (85cm, 20 kyr B.P. and 241cm, 43.8 kyr B.P.) negative 'excursions' (both values approx. $0.5‰_{VPDB}$) are similar to the two strong negative values of Peck *et al.* (2007), which are associated with Heinrich events (H1, 16.8 kyr B.P. and H4, 39 kyr B.P.). This potentially leads to the conclusion that the age model proposed for 9/97-27/2 is incorrect as the negative excursions are off-set temporally. However, the record from Peck *et al.* (2007) is considered to be bathed in GNAIW at this time, whereas this site is probably bathed in GAABW according to the reconstructions of Sarnthein *et al.* (1994) and Lynch-Stieglitz *et al.* (2007)(Fig. 7.7). The age off-set between the negative carbon isotope excursions possibly reflects the difference in ventilation rates between the two water masses. If these excursions are linked, then the negative excursions recorded in GAABW appear to precede the excursions in GNAIW by approximately 4kyrs in each case. Alternatively, the strong negative excursions

could be due to dissolution (McCorkle et al. 1995), although this should also affect the Mg/Ca and $\delta^{18}O_{benthic}$ data, which does not appear to be the case when examining these proxies. Even if the excursion is caused by dissolution, this does not rule out the possibility that the dissolution is due to a Heinrich event.

The plot of $\delta^{13}C_{benthic}$ versus phosphorus values in core 9/97-10 reveals that the AAIW signal (Fig. 7.12) is strongest in one sample from the last interglacial (51cm). Data from most glacial samples shows that GNAIW dominated the last glacial over this core site. The position of the 3cm data point compared to values at 11cm and 15cm suggest that a change in the source region for NCW (GNAIW / NADW) may have occurred between the last glacial and the Holocene, possibly combined with some slight mixing with SCW or MOW.

A plot of $\delta^{13}C_{benthic}$ versus reconstructed phosphorus concentrations from core 9/97-04 reveals a strong AAIW influence for five samples (1cm, 55cm, 59cm, 67cm and 83cm) with the rest indicative of GNAIW and AABW influence. This is consistent with the interpretations made previously from Ba/Ca data regarding the stronger influence of SCW during interglacials over this core site. Differences in the plots of samples 8cm, 17cm and 38cm potentially reflects a switch in the source region for NCW during the last glacial, or mixing with MOW. Last glacial values for core 9/97-04 imply GNAIW ventilated this portion of the slope.

There are slight variations in the relative influence of SCW versus NCW apparent in the plot of P / $\delta^{13}C_{benthic}$ data (Fig. 7.12) for core 9/97-14 but these are not entirely consistent with glacial-interglacial variations. A few samples suggest an influence of AAIW (or AABW) but these are not limited to either glacials or interglacials. The plot of data suggests a

relatively weaker influence of GNAIW compared with the two other sites. This inability to clearly distinguish a glacial-interglacial SCW versus NCW variability probably reflects the fact that this core is currently bathed in North Atlantic Deep Water (NADW; Read 2001) but is close to the boundary with AABW or AAIW and was probably at the boundary between water masses during the last glacial (Lynch-Stieglitz *et al.* 2007). Further evidence that a site at approximately 2000m water depth is at the boundary between water masses during the last glacial is also recorded by Bertram *et al.* (1995). Samples at 73cm and 97cm core depth suggest mixing with MOW has occurred.

7.6.4 Nutrients

Phosphorus values are highly variable between 11.5-19.5 kyr B.P in core 9/97-10. Such apparent instability in reconstructed phosphorus concentrations has not been observed without co-eval variations in carbon isotope values (see Rickaby and Elderfield 2005, Fig. 3). The planktonic carbon isotope profile produced for this core (see above) displays some evidence of apparent instability in surface productivity (with one strong negative value observed at 15cm). However, any changes in surface productivity would presumably also have an impact on $\delta^{13}C_{benthic}$ as this is also affected by productivity (Fig. 3.19). As no evidence of this is present in the benthic data it is unlikely that surface productivity is varying strongly enough to significantly change the benthic geochemical environment. However, the interval is co-eval with a strong negative excursion in the benthic carbon isotope profile of core 9/97-27/2 (85cm, 20 kyrs B.P.) which is potentially linked to the H1 excursion from Peck *et al.* (2007). These data are interesting as they clearly show a moderate degree of variability

in the phosphorus concentration of bottom waters at this site preceding the H1 event (dated at 16.4 kyr B.P.; Peck *et al.* 2007) which was not observed in the record of NEAP4A (Rickaby and Elderfield 2005). Dissolution could also be causing this instability (especially for the sample at 21cm core depth), but the dissolution itself (if present) could be caused by the same mechanism. In cores 9/97-04 and 9/97-14, phosphorus concentrations are relatively increased during interglacials and reduced during the previous glacial, implying an increase in SCW influence during interglacials compared to glacials.

Three of the samples from core 9/97-10 that are enriched in Ba/Ca from core 9/97-10 (3cm, 51.5cm and 67.5cm) are from interglacials and suggest an increase in refractory nutrient content (See Section 2.7) so could be due to the influence of the southern sourced AAIW (Antarctic Intermediate Water). A sample at 35cm records a very high value (3.65µmol/mol), which could also be due to the precipitation of inorganic barite, although it is below the recommended cut-off value of 4µmol/mol (Hall 2002). The slightly elevated value at 20cm is coeval with an increase in Cd/Ca, both of which imply an increase in mixing with AAIW.

Higher Ba/Ca values are an indicator of increased refractory nutrient input and the data presented for core 9/97-04 indicate that interglacials experienced increased refractory nutrient input compared to glacial episodes. This is consistent with the interpretation of the glacial units as being deposited under the influence of a strong NCW (Northern Component Water), most likely GNAIW (Glacial North Atlantic Intermediate Water). According to this data, 9/97-04 was bathed in a water mass with a strong SCW (Southern Component Water) signature (probably AAIW) during interglacials. The values from 1-4cm show a gradual increase in Cd/Ca ratios, suggesting that the influence of AAIW is increasing through time during the Holocene.

Cd/Ca data from core 9/97-14 record high values which suggests that interglacial units are deposited under a stronger influence of SCW compared to glacial units (possibly AAIW or AABW), although the potential dissolution highlighted above during this interval could be complicating this signal. Two glacial peaks in Cd/Ca correspond with slight reductions in $\delta^{13}C_{benthic}$ (particularly the peak at 23cm), which implies a stronger influence of SCW. The short durations of these strong peaks (less than 4 kyr as suggested by the age model for this core) suggesting that these could be transient incursions of AABW (Antarctic Bottom Water). These peaks in Cd/Ca could be linked to the negative excursions in $\delta^{13}C$ from Peck *et al.* (2007) at 18.8 kyr and 25 kyr B.P., preceding each by 1-2 kyr according the age model developed for this core.

The Ba/Ca record of core 9/97-14 records high values during interglacials, which implies that refractory nutrient supply is higher during interglacials compared to glacial episodes (Fig 7.6). An exception to this is present at 19cm, which recorded a value of 5.66μmol/mol. This is higher than the 4 μmol/mol suggested by Hall (2002) as the value above which significant sedimentary barite formation could have occurred.

7.7 Summary

Comparison of the sea surface temperature estimates derived from $\delta^{18}O_{planktonic}$ and the MAT/WAPLS methods (see Chapter 6) for core 9/97-10 suggests that the season during which *G.bulloides* is most productive (currently the spring) switches to the summer during glacials. This interpretation, if valid, has significant implications for other studies which use planktonic foraminifera to reconstruct sea surface temperatures. However, the discrepancies between the

two records could be due to post-mortem modification of assemblages or the lack of good modern analogues for the transfer function technique (see Chapter 6).

A Heinrich-like event is potentially present in the MIS 8 sediments examined from core 9/97-10. A relatively strong negative carbon isotope excursion is then followed 2-3cm later by the deposition of a large cobble (Fig. 3.1), which is potentially the first evidence of a Heinrich-like event occurring prior to MIS 3. More detailed analysis is required to determine the exact nature of this excursion, however.

Important links between negative carbon isotope excursions present in this study and those from other studies (Rickaby and Elderfield 2005; Peck *et al.* 2007) are recorded. A strong negative carbon isotope excursion is present at 15cm core depth in the planktonic record which is related to Heinrich event 1. In core 9/97-04, a negative carbon isotope excursion is present, dated at 41.3kyr B.P., but the proximity of this sample to a hiatus suggests that this could be caused by reworking from an adjacent, much older unit. Core 9/97-14 records two negative carbon isotope shifts that coincide with increases in Cd/Ca, dated at 19 kyr and 27 kyr B.P. respectively. These suggest that AABW expanded briefly twice during the last glacial, in both cases preceding a Heinrich event (H2 and H1 respectively) by 2-2.5 kyr B.P. Low Sr/Ca values could suggest that these samples have undergone selective dissolution, but this could also itself be an indication of an increased flux of AABW. The presence of negative carbon isotope excursions in core 9/97-27/2 (2756m) which are volumetrically identical to those observed by Peck *et al.* (2007) in core MD01-2461 (1153m) which are linked to Heinrich events H1 and H4 and the apparent preceding of the AABW (this study) signal versus GNAIW signal (Peck *et al.* 2007) suggests that Heinrich events in the North East Atlantic are potentially preceded by similar events in the Southern Ocean. This is

perhaps further evidence of the bi-polar see-saw (Broecker 1998; Severinghaus 2009), with climatic oscillations in the northern and southern hemispheres linked via MOC. The results here suggest that Heinrich events H1 and H4 are preceded by events in the southern hemisphere.

No strong linear correlations are present between Mg/Ca and fragmentation index data, although core 9/97-14 does present a higher correlation coefficient compared to the other cores. Examination of Sr/Ca data suggests that some samples in core 9/97-14 could have undergone selective dissolution. No strong linear correlation exists between Cd/Ca and Mn/Ca values, although all of the samples from core 9/97-27/2 present Mn/Ca values greater than 150μmol/mol.

Time slice reconstructions of water mass distributions, stratification and refractory nutrient supply are made for four time slices, with the assumption that the reconstructed values reflect the broad trends during these time slices. These are: the last interglacial (MIS 5: 90-125 kyr B.P.), Marine isotope stage 3 (30-60 kyr B.P.), Marine isotope stage 2 (11.5-30 kyr B.P.) and the Holocene (11.5-0 kyr B.P.). These are based on the data discussed previously and show clear differences in each stage in terms of reconstructed oceanography. For MIS 3, the generalized reconstructions are less certain due to the absence of large parts of this stage from cores 9/97-04 and 9/97-14 (see Chapter 5). For the last interglacial (MIS 5) there is a clear stratification in water mass distribution along the slope, although the stratification is relatively weak and frequent mixing probably occurred (Fig. 7.13). A strong AAIW signal is present in the two shallowest cores and refractory nutrient supply is relatively increased at all core sites compared to last glacial and even Holocene values, suggesting a strong influence of SCW across the whole of the slope between at least 1260-2118m water depth. The absence of

a NCW influence is perhaps further confirmation of the absence of LSW formation (Hillaire-Marcel *et al.* 2001) during MIS 5. This has important implications, considering the role SCW (and, in particular, AAIW) is considered to play in stabilising northern hemisphere climate via a salinity feedback (Lassen *et al.* 2002; Rickaby and Elderfield 2005).

During Marine Isotope Stage 3, GNAIW dominates the signal in the two shallowest cores, with data from 9/97-14 and 9/97-27/2 suggesting a switching in dominance between AABW / GNAIW flux (Fig. 7.13). Refractory nutrient supply is relatively reduced higher up on the slope and the benthic environment is dysoxic around the core site of 9/97-27/2.

During Marine Isotope Stage 2, GNAIW strongly dominates the signal in cores 9/97-04 and 9/97-14 (Fig. 7.14). It is also strong in core 9/97-10, although apparent instability in the phosphorus concentration at this site suggests that the transient incursion of SCW (most likely AAIW) could have occurred more than once during this interval, although the possible presence of dissolution could also explain this trend (the dissolution itself could also be caused by SCW influence). Refractory nutrient supply was relatively reduced compared to the Holocene in all cores except for 9/97-10 where it varied during this interval. The benthic environment surrounding core site 9/97-27/2 remained dysoxic.

Reconstructed Holocene values for most parameters are compatible with modern values obtained from oceanographic studies (Read 2001) and core top studies (Boyle 1992; Oppo and Lehman 1993; Bertram *et al.* 1995; Hall 2002; Martin *et al.* 2002). The reconstruction reveals a clearly and strongly stratified water mass distribution with a clear AAIW influence in cores 9/97-04 and 9/97-14 (Fig. 7.14). Refractory nutrient supply is increased in cores 9/97-10, 9/97-04 and 9/97-14, consistent with a strong SCW influence. The

benthic environment surrounding core site 9/97-27/2 is still dysoxic and the carbon isotope data suggest a strong NADW influence, consistent with other reconstructions (e.g. Sarnthein *et al.* 1994; Lynch-Stieglitz *et al.* 2007). The result of plotting $\delta^{13}C_{benthic}$ versus phosphorus for the Holocene value in core 9/97-10 suggests that mixing with MOW has occurred.

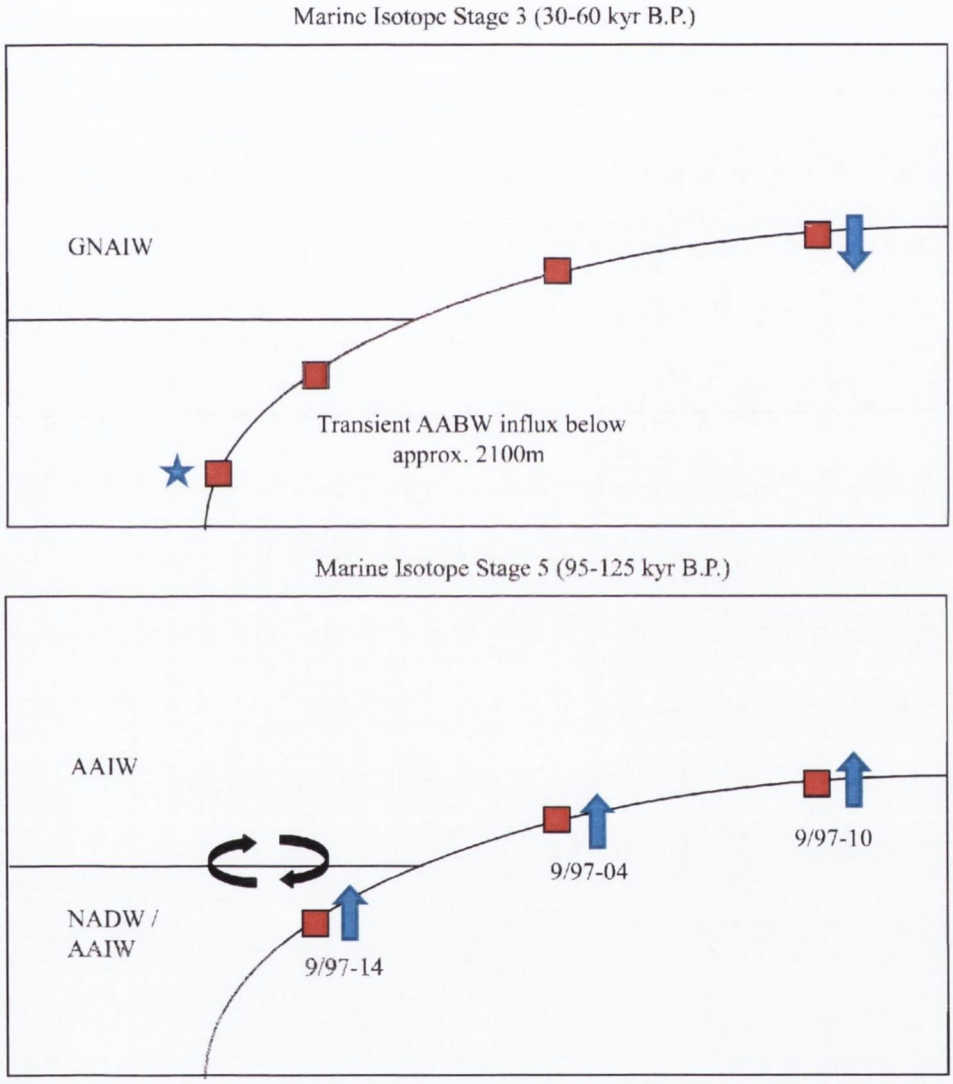

Figure 7.13. Water mass stratification reconstructions along the slope for two time periods; the last interglacial (95-125 kyr B.P.) and Marine Isotope Stage 3 (30-60 kyr B.P.). Blue arrows indicate the relative increase or decrease in refractory nutrient supply and blue stars indicate bottom water dysoxia. Curved arrows indicate mixing of water masses.

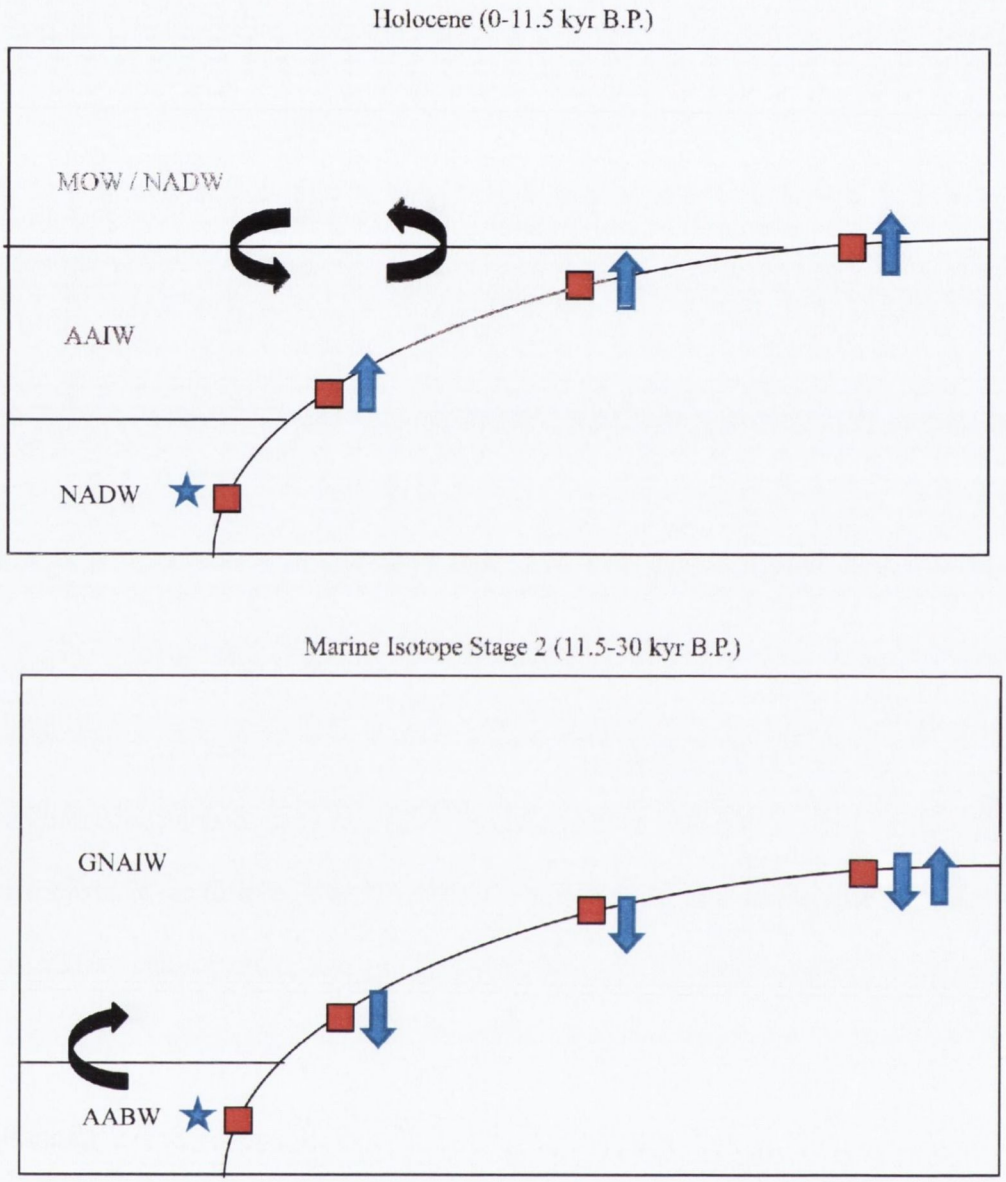

Figure 7.14. Water mass stratification reconstructions along the slope for two time periods; the Marine Isotope Stage 2 (11.5-30 kyr B.P.) and the Holocene (0-11.5 kyr B.P.). Blue arrows indicate the relative increase or decrease in refractory nutrient supply and blue stars indicate bottom water dysoxia. Curved arrows indicate mixing of water masses.

Chapter 8 – Benthic foraminifera

8.1 Introduction

The distribution of the fifteen most abundant species is described for the larger size fraction (250-500μm), with the distribution of the four most abundant species described from the smaller size fraction (63-250μm). Ecological preferences of these species are outlined in Chapters 2 and 3. The main focus is on species distributions along a depth transect (cores 9/97-08, 9/97-10, 9/97-04, 9/97-14 and 9/97-27/2), with along slope distributions of the large size fraction also considered (9/97-03 and 9/97-10; 9/97-27/2 and 9/97-20). Cluster and DCA (Chapter 3) are used to assess sample similarities in terms of assemblage compositions, particularly in relation to down slope, along slope similarities and the similarities between the different size fractions examined. Principle components analysis is used to determine the key species causing dissimilarity between samples and to then use the proposed ecological preferences of those key species (see Chapters 2 and 3) to infer the ecological parameter causing dissimilarity.

The abundance of benthic foraminifera (>150μm) in the sediment, or BFAR (Benthic Foraminifera Accumulation Rate) has been linked to the amount of food supply (or flux rates) to the seafloor (Herguera and Berger 1991; Wollenberg and Mackensen 1998; Wollenberg and Kuhnt 2000; Altenbach and Struck 2001). Nees *et al.* (1997) identified a peak in BFAR between 9-12 kyr B.P. migrating along a north-south transect of the North Atlantic Ocean (Fig. 2.14). They observed that the peak in BFAR was progressively younger with increasing latitude, and this was attributed to the northward migration of the polar front during the last deglaciation. BFARs are calculated as described in Chapter 3, using the age models and

variable sedimentation rates outlined in Chapter 5, unlike the linear sedimentation rate applied by Herguera and Berger (1991) and Nees *et al.* (1997). This removes the assumption that sedimentation rates do not change through time, an assumption that would clearly be false (see Chapter 5) for these cores whilst recognising that any errors in the variable sedimentation rates will propagate through to the BFAR. For core 9/97-08, the number of specimens per gram of dry sediment is calculated but developing a reliable age model for the core is not possible due to the large amount of disturbance evident from examination of the sedimentology (see Chapter 5). Instead, a linear sedimentation rate of 0.75 cm/kyr (the average sedimentation rate calculated for core 9/97-10) is applied.

This proxy of flux rates enables the identification of samples in each core which are deposited during episodes of enhanced productivity, as well as determining if flux rates towards the bottom of the slope are on average different at corresponding time intervals than higher on the slope. It is important to compare this proxy with proxies for dissolution (i.e. the fragmentation index – see Chapters 3 and 5). As most benthic foraminifera use calcite to compose their tests, dissolution would have a clear impact on the concentration of benthic foraminifera.

8.2 Results

8.2.1 Core 9/97-08

8.2.1.1 Large size fraction (250-500μm)

Paired cluster and detrended correspondence analysis of samples from the upper 80cm of core 9/97-08 produces three distinct cluster groups (LFAZ 08-I to III; Fig. 8.1). The groups are linked to distinct lithofacies. LFAZ 08-III is recorded in lithofacies CO-1 (nannofossil ooze) and CO-2 (clay-rich nannofossil ooze). This group is dominated by *Cibicides kullenbergi* (up to 20%), *Melonis barleeanum* (25%) and *Sigmoilopsis schlumbergeri* (20%). LFAZ 08-II is present in two lithofacies; SM and FS-2. This cluster group is dominated by *Uvigerina peregrina* (50%). LFAZ-08-I is linked to lithofacies BM. This cluster group is dominated by *Cibicides wuellerstorfi* (25%), *C.kullenbergi* (45%) and *U.peregrina* (20%).

8.2.1.2 Small size fraction (63-250μm)

The lower section of the core (65-80cm; Fig. 8.2) is characterised by a low abundance of *Cassidulina laevigata* (<20%), *Epistominella exigua* (<10%) and *Triffarina angulosa* (<15%). Samples between 25-65cm contain a high abundance of *T.angulosa* (≥20%), with episodic increases in the abundance of *C.laevigata*. The upper section of the core (0-25cm) contains a relatively high abundance of *Alabaminella weddellensis* (>2%), *C.laevigata* (>24%) and *E.exigua* (>7.5%), with a low relative abundance of *T.angulosa* (<10%).

8.2.1.3 BFAR

A linear sedimentation rate is used to calculate BFAR for core 9/97-08 (Fig. 8.1). Low accumulation rates are recorded at the base of the core (174-182cm) and high BFARs are present in the lower part of the core (92-170cm). A trough in values is then present (47.5-88cm) followed by a short peak (39-43cm). This is then followed by another trough (3-35cm). There is no obvious link between variations in BFAR and sedimentology in this core.

8.2.2 Core 9/97-10

8.2.2.1 Large size fraction (250-500μm)

Paired cluster and detrended correspondence analysis of samples from the upper 83cm of core 9/97-10 produces five distinct cluster groups (LFAZ 10-I to V; Fig. 8.3). Each faunal group corresponds to a distinct lithofacies, as proposed by Toms (in prep.). LFAZ 10-V is present in lithofacies BM (hemipelagic brown mud) and is dominated by *C.wuellerstorfi* (up to 20%), *Rupertina stabilis* (17%) and *Karerriella bradyi* (14%). LFAZ 10-IV is linked to a mixture of lithofacies; FS1 (foraminifera sand) and CO-1 (nannofossil ooze). This cluster group is dominated by *S.schlumbergeri* (32%), *K.bradyi* (32%) and *M.barleeanum* (20%). LFAZ 10-III is present in lithofacies FS-2 (muddy foraminifera sand) and is dominated by *C.wuellerstorfi* (30%) and *M.barleeanum* (20%). LFAZ 10-II is linked to two lithofacies; BM and SM (brown sandy mud). This cluster group is dominated by *R.stabilis* (32%), *C.kullenbergi* (30%) and *C.wuellerstorfi* (30%). LFAZ 10-I is present in lithofacies CM (calcareous mud) and is dominated by *C.wuellerstorfi* (30%), *M.barleeanum* (32%) and *S.schlumbergeri* (20%).

8.2.2.2 Small size fraction (63-250μm)

Alabaminella weddellensis is entirely absent from this core in the small size fraction (Fig. 8.4). The lower section of the core (70-85cm) contains a high relative abundance of *Cassidulina laevigata* (>40%). *Triffarina anguloa* has a high relative abundance (≥10%) in assemblages between 50-70cm core depth. *Cassidulina laevigata* dominates (≥40%) assemblages between 15-57cm, but episodic occurrences of *E.exigua* are also present.

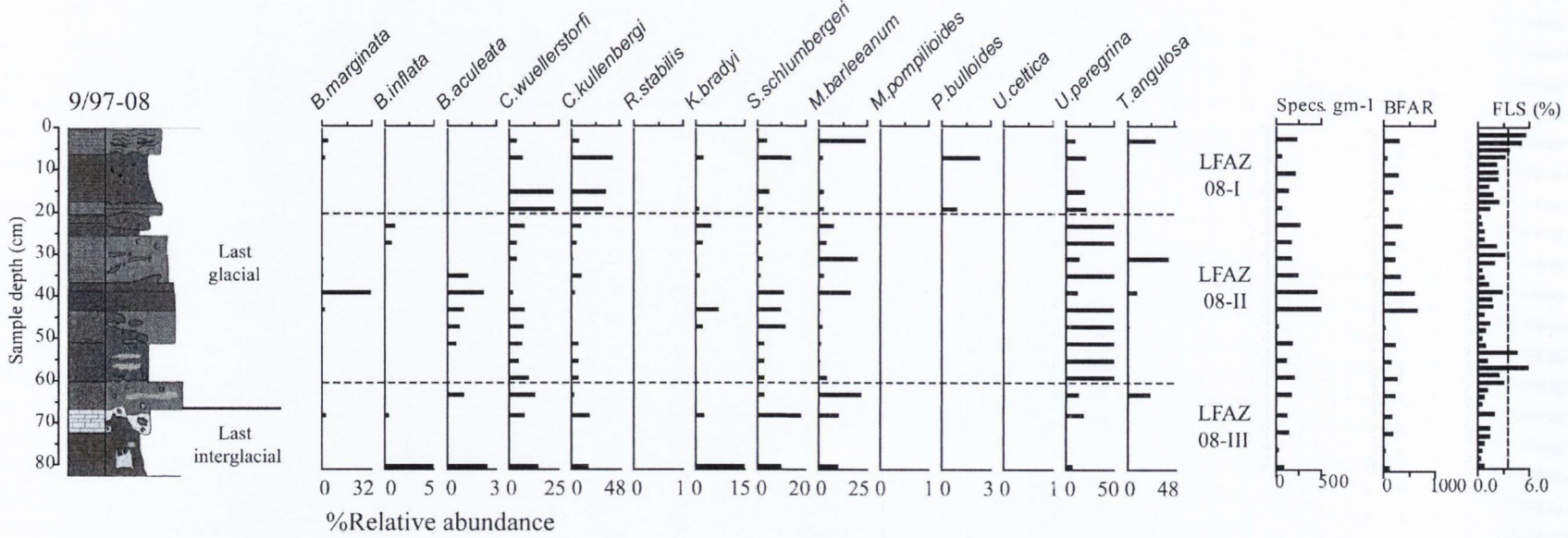

Figure 8.1. Down core distribution of taxa and lithofacies assemblage zones (LFAZ) from the 250-500μm size fraction (9/97-08). Also BFAR and fragmentation data.

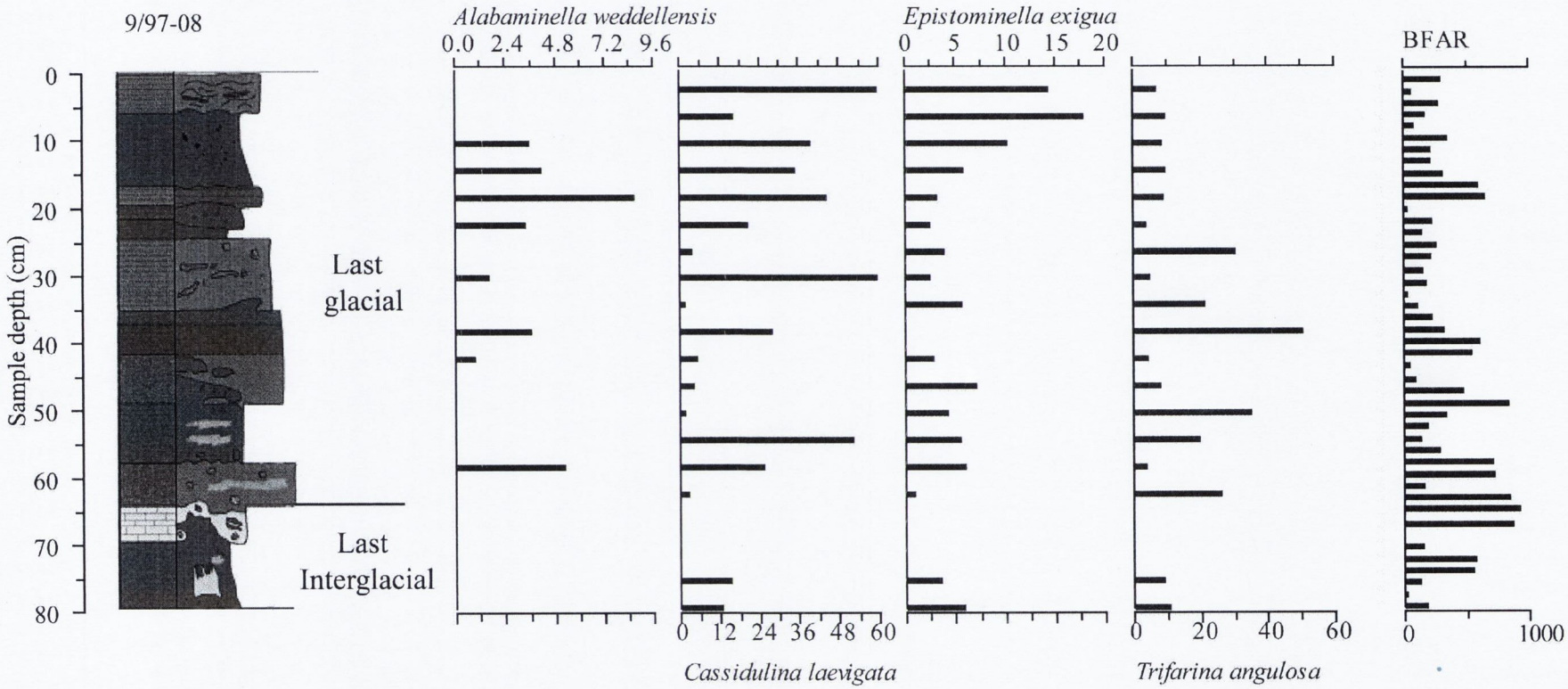

Figure 8.2. Down core distribution of taxa from the 63-250μm size fraction (9/97-08). Also BFAR and fragmentation data.

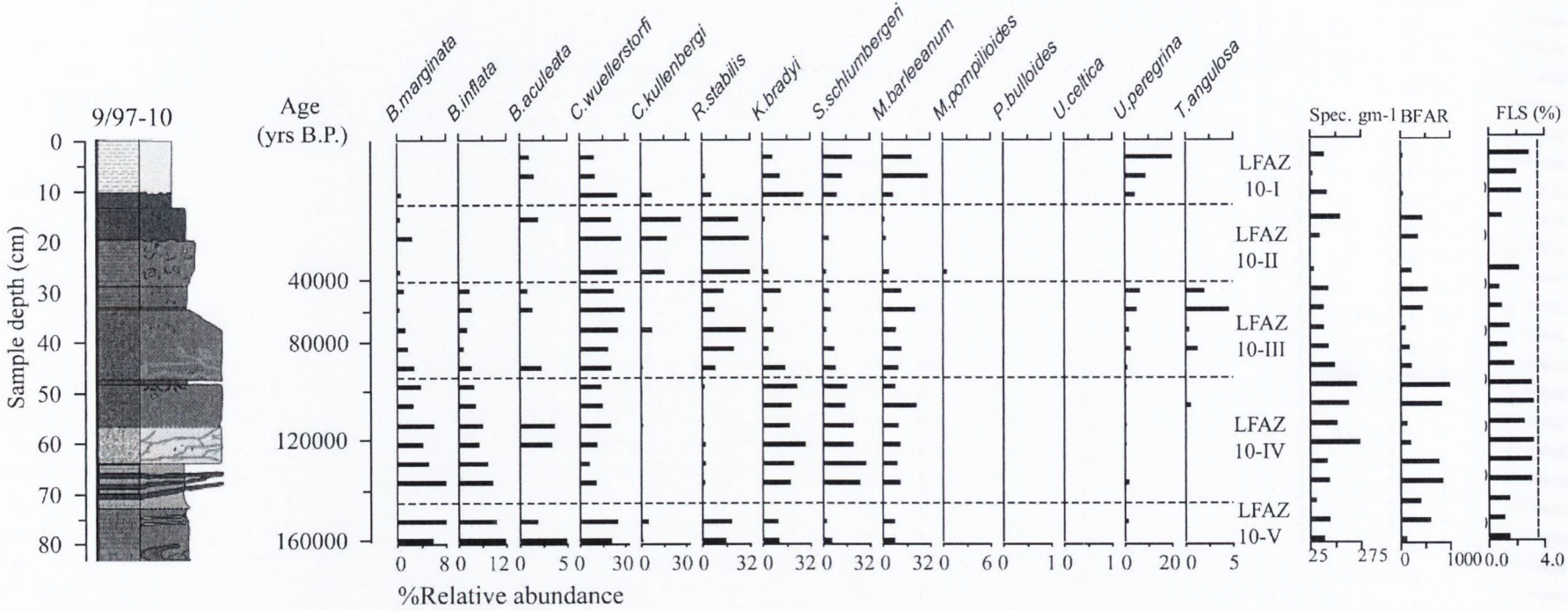

Figure 8.3. Down core distribution of taxa and lithofacies assemblage zones (LFAZ) from the 250-500μm size fraction (9/97-10). Also BFAR and fragmentation data.

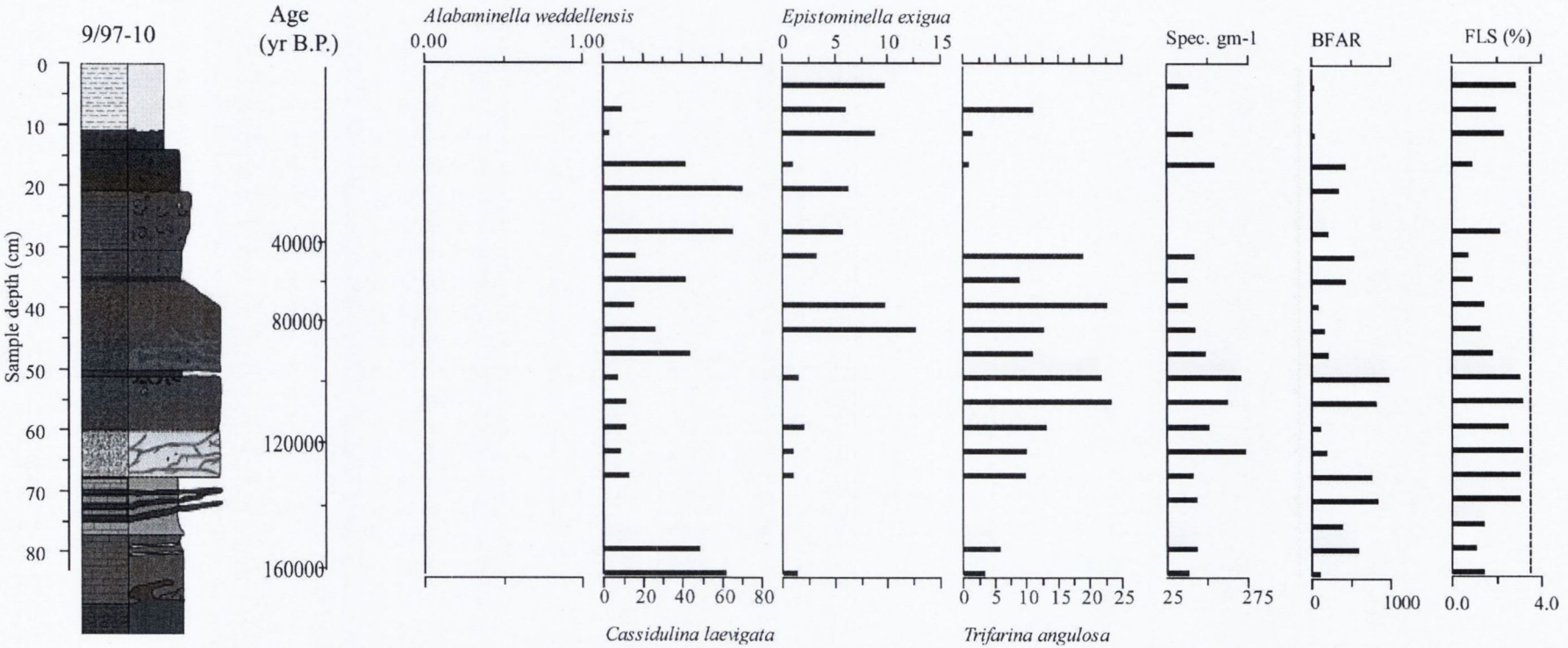

Figure 8.4. Down core distribution of taxa from the 63-250μm size fraction (9/97-10). Also BFAR and fragmentation data.

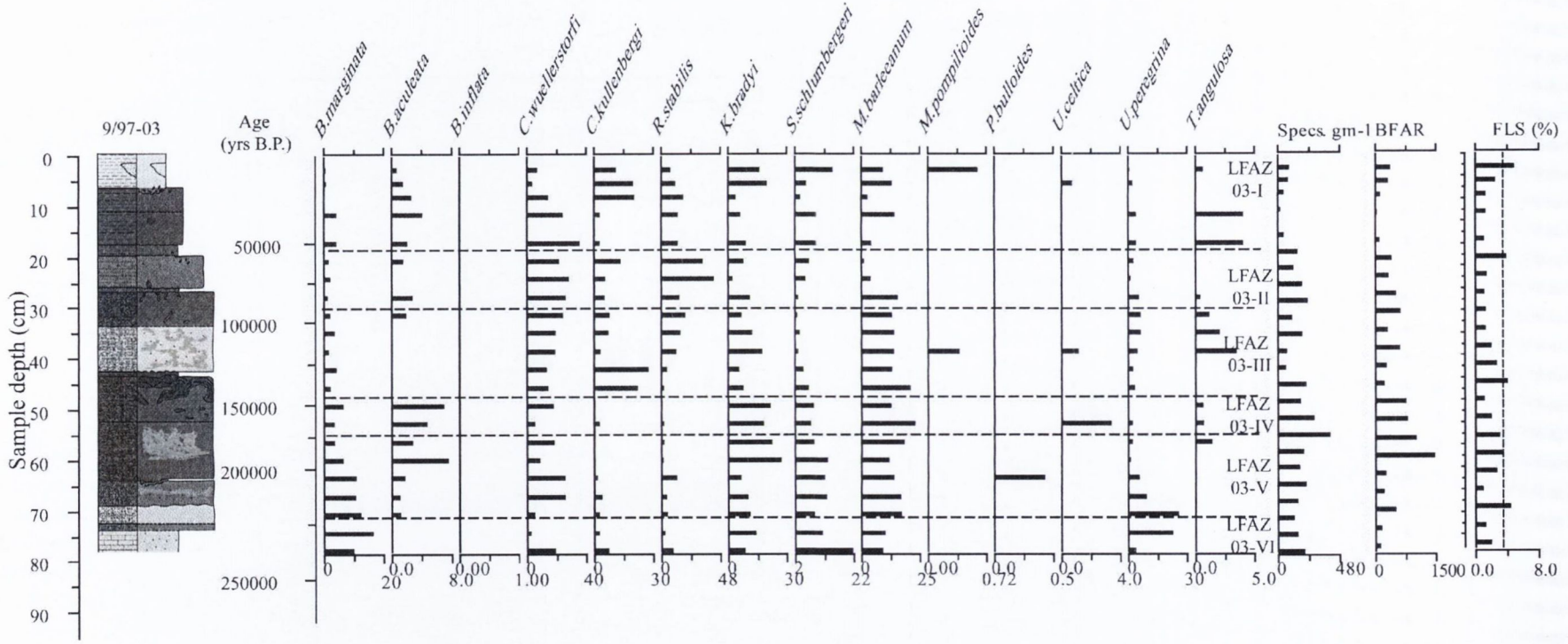

Figure 8.5. Down core distribution of taxa and lithofacies assemblage zones (LFAZ) from the 250-500μm size fraction (9/97-03).

Also BFAR and fragmentation data.

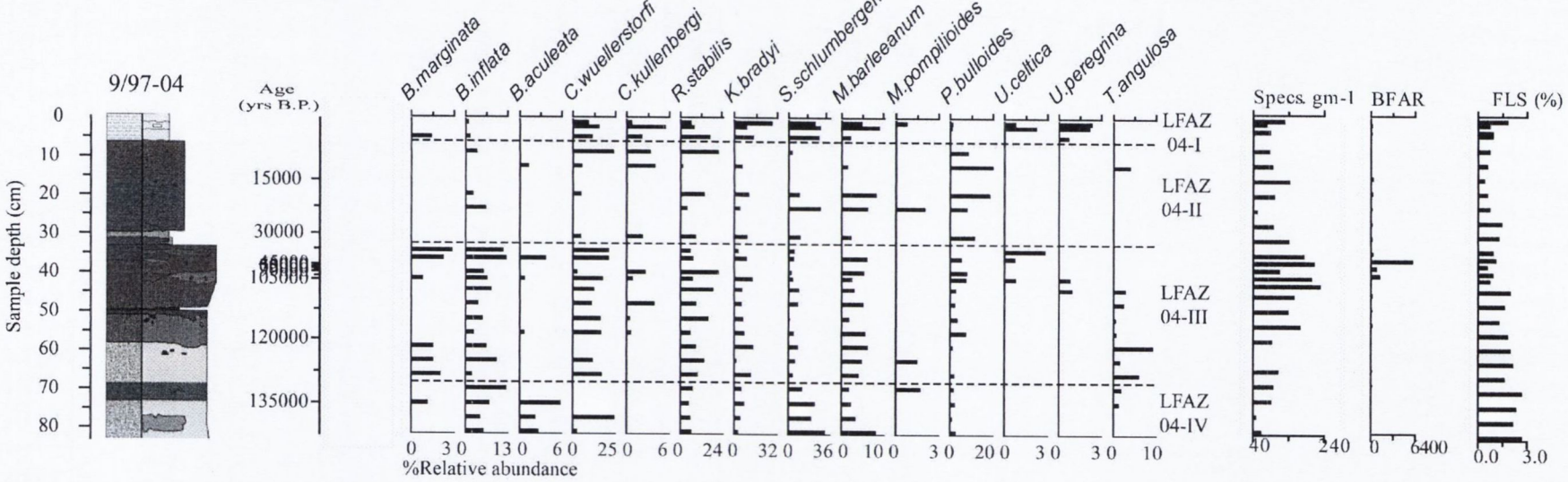

Figure 8.6. Down core distribution of taxa and lithofacies assemblage zones (LFAZ) from the 250-500μm size fraction (9/97-04). Also BFAR and fragmentation data.

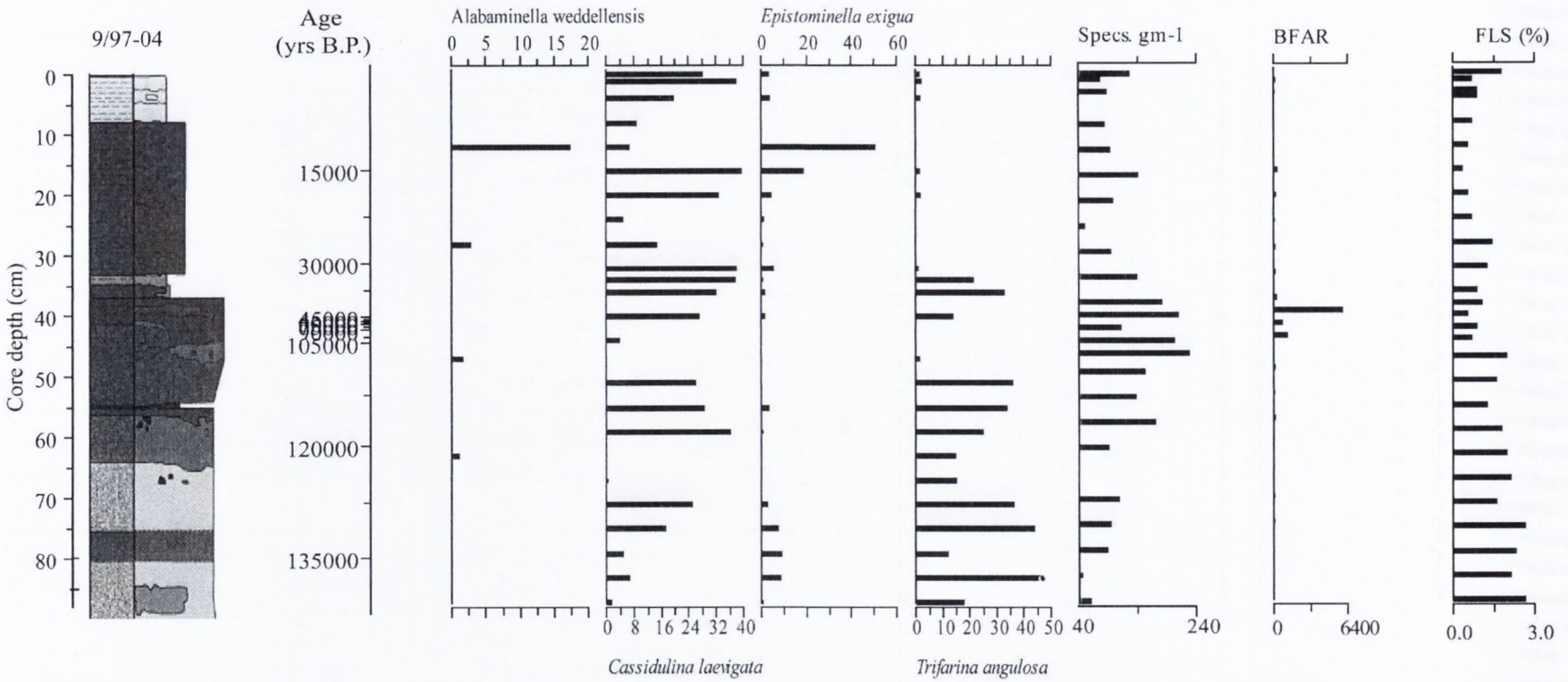

Figure 8.7. Down core distribution of taxa from the 63-250μm size fraction (9/97-04). Also BFAR and fragmentation data.

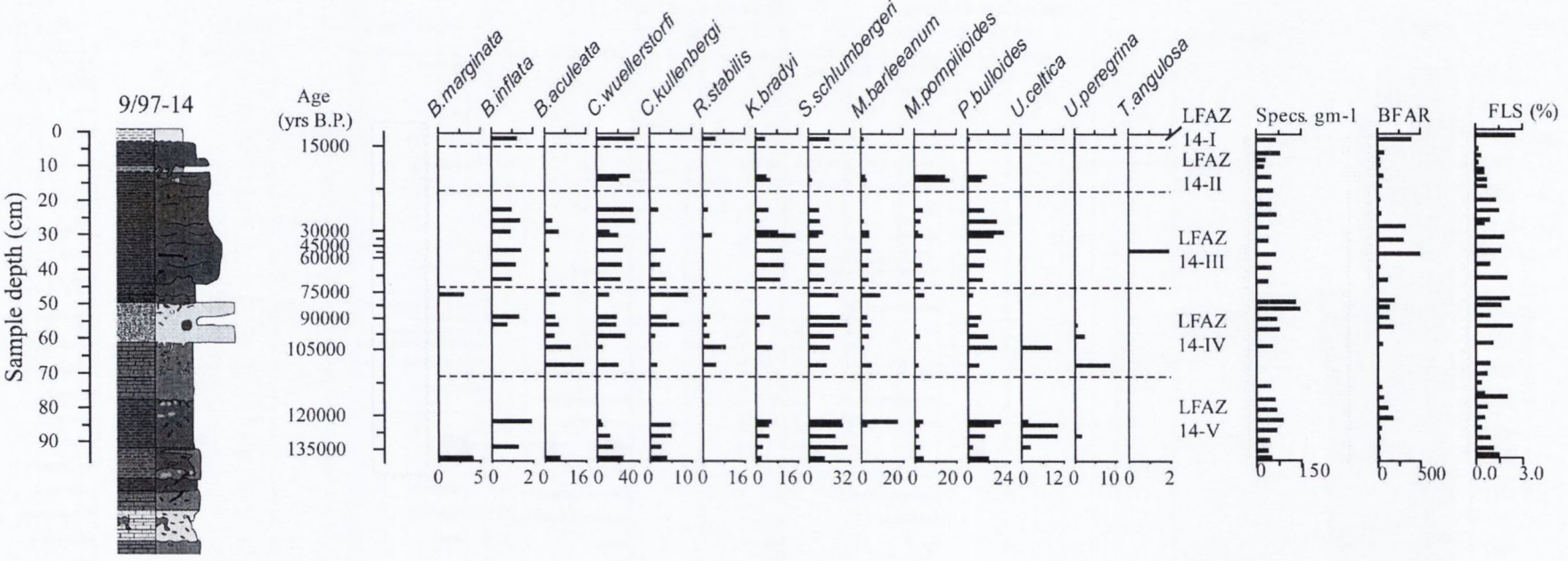

Figure 8.8. Down core distribution of taxa and lithofacies assemblage zones (LFAZ) from the 250-500μm size fraction (9/97-14).

Also BFAR and fragmentation data.

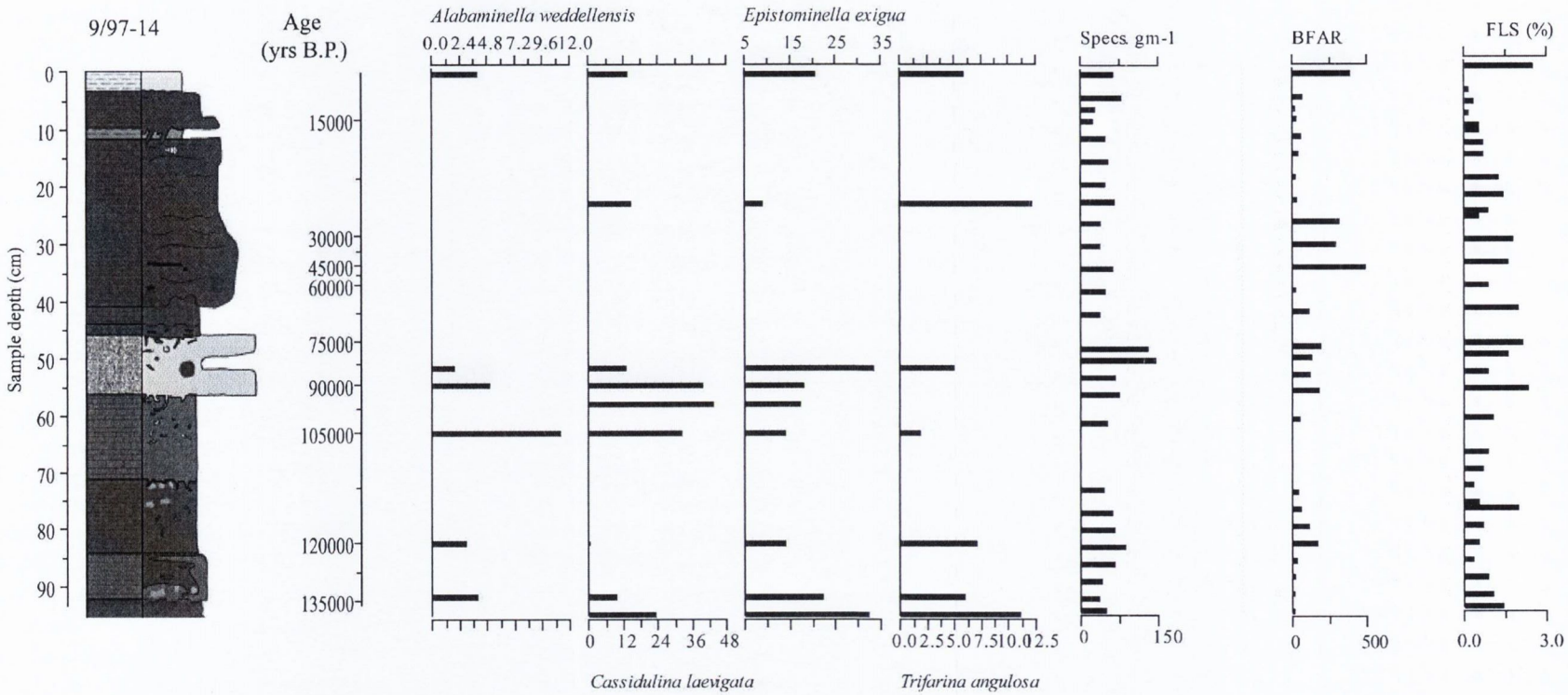

Figure 8.9. Down core distribution of taxa from the 63-250μm size fraction (9/97-14). Also BFAR and fragmentation data.

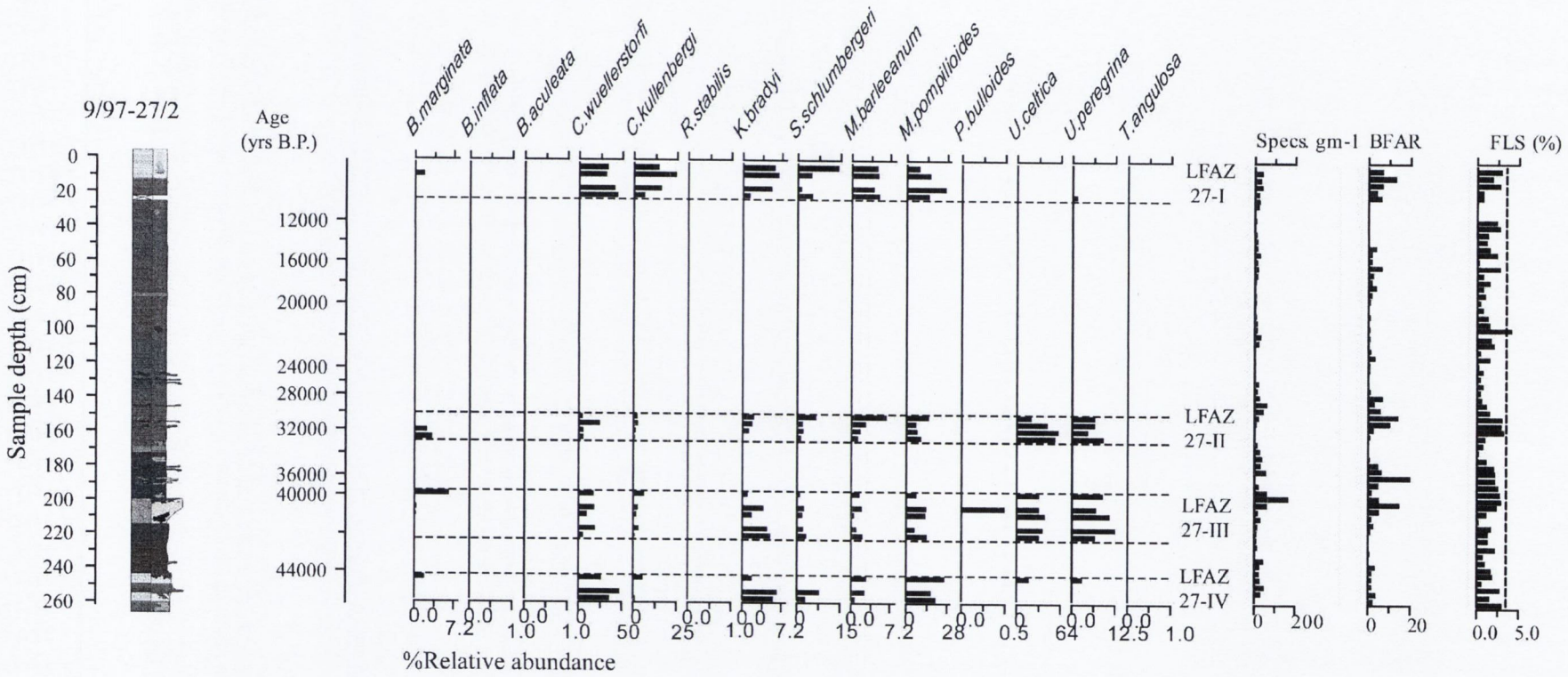

Figure 8.10. Down core distribution of taxa and lithofacies assemblage zones (LFAZ) from the 250-500μm size fraction (9/97-27/2). Also BFAR and fragmentation data.

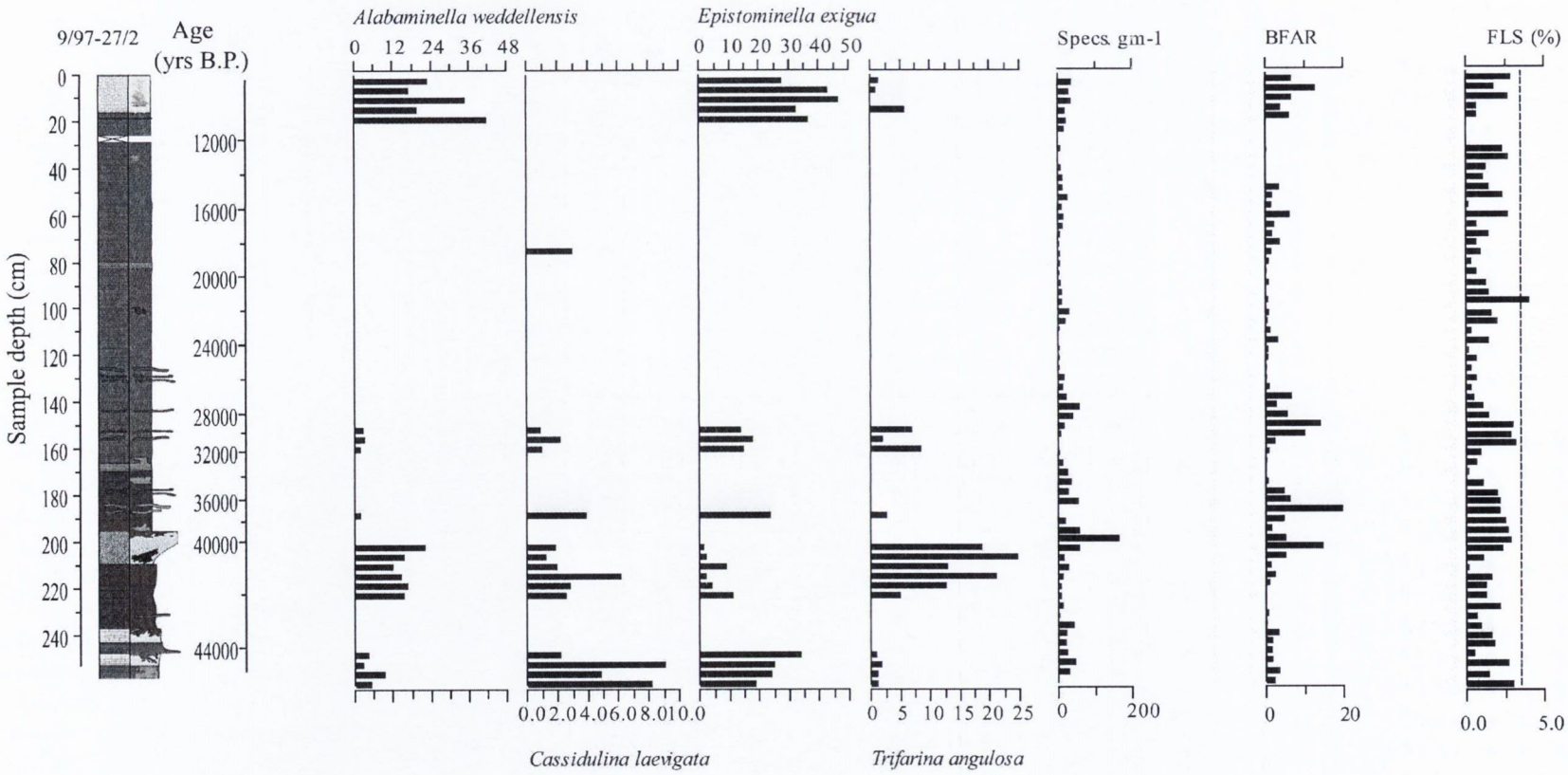

Figure 8.11. Down core distribution of taxa from the 63-250μm size fraction (9/97-27/2). Also BFAR and fragmentation data.

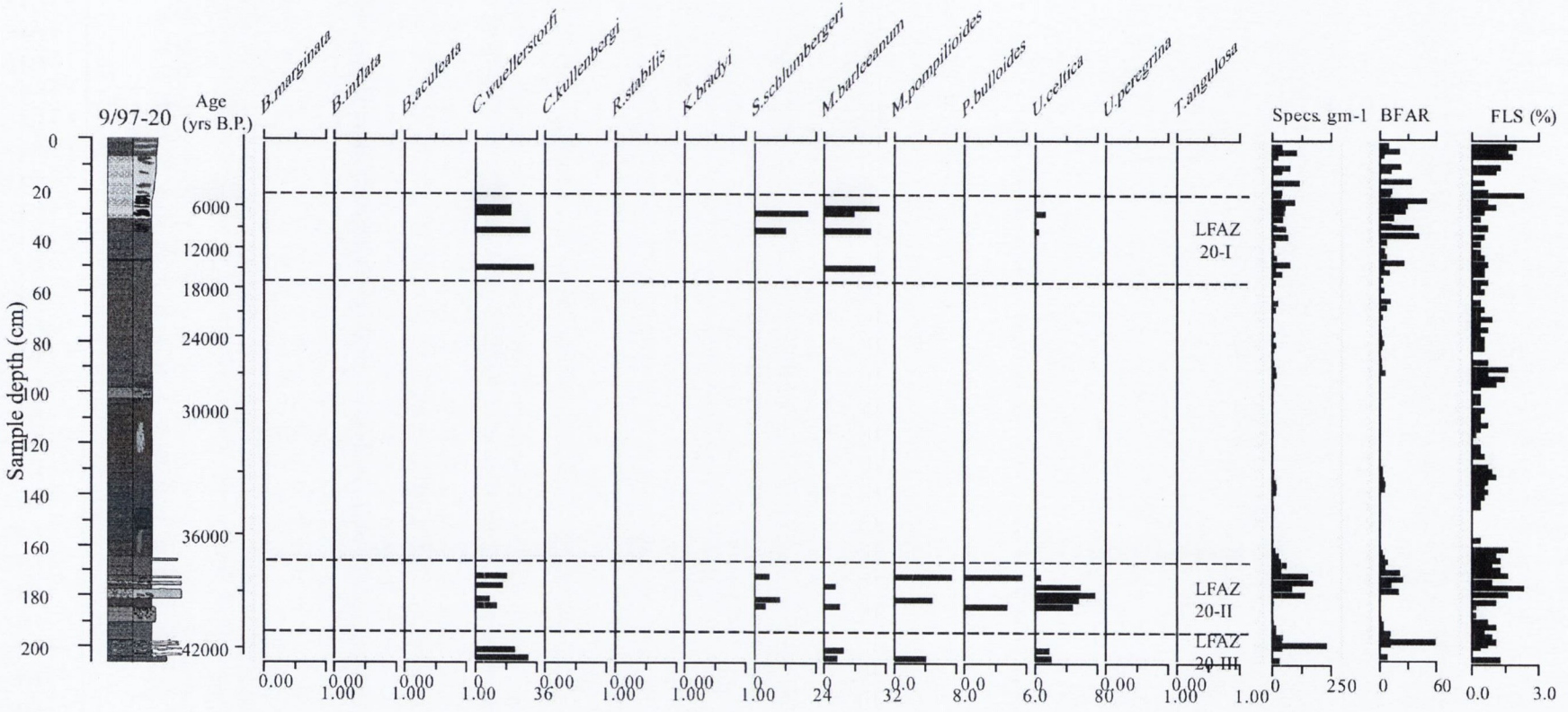

Figure 8.12. Down core distribution of taxa and lithofacies assemblage zones (LFAZ) from the 250-500μm size fraction (9/97-20). Also BFAR and fragmentation data.

Epistominella exigua has a relatively high abundance (≥7.5%) in the uppermost section of the core (0-15cm).

8.2.2.3 BFAR

The sample at 83cm in core 9/97-10 (Fig. 8.3) records a low BFAR (107 specimens/cm^2/kyr). Samples between 67.5-79.5cm record above average BFARs (average for core = 365 specimens/cm^2/kyr), followed by a low accumulation rate interval between 59.5-63.5cm. A period of high accumulation is then present between 51.5-55.5cm, followed by two troughs (39-47cm and 3-11cm) adjacent to a moderate peak in accumulation rates (16-35cm). The variations in BFAR appear to be independent of variations in sedimentology.

8.2.3 9/97-03

8.2.3.1 Large size fraction (250-500μm)

Paired cluster and detrended correspondence analysis of assemblage data from core 9/97-03 produces six cluster groups (LFAZ 03-I to VI; Fig. 8.5). Cluster groups do not always correspond to a specific lithofacies in this core. LFAZ 03-VI is located between 71-87cm and is dominated by *C.kullenbergi*, *K.bradyi*, *Quinqueloculina seminulum* and *R.stabilis*. LFAZ 03-V is recorded between 55-67cm and contains *C.wuellerstorfi*, *K.bradyi*, *M.barleeanum* and *S.schlumbergeri* in high relative abundance. This group occurs exclusively within the foraminifera sand (FS) lithofacies. LFAZ 03-IV is present between 47-51cm and contains high proportions of *C.kullenbergi*, *C.wuellerstorfi* and *M.barleeanum*. LFAZ 03-III is located

between 31-43cm and is dominated by *C.wuellerstorfi*, *R.stabilis*, *K.bradyi* and *M.barleeanum*. This cluster group is limited to the foraminifera sand lithofacies (FS). LFAZ 03-II is recorded between 23-27cm and contain *C.wuellerstorfi* and *R.stabilis* in high relative abundance. This group is located within the BM/SM lithofacies group only. LFAZ 03-I is present between 3-21cm and contains high proportions of *C.kullenbergi*, *R.stabilis*, *S.schlumbergeri* and *K.bradyi*. This group is primarily located in the calcareous mud (CM) lithofacies, although it does extend into the underlying BM/SM lithofacies as well.

8.2.3.2 BFAR

Benthic foraminifera accumulation rates in core 9/97-03 (Fig. 8.5) are generally comparable to those in core 9/97-10 (average value = 409 specimens/cm^2/kyr). The BFAR values between 71 and 95cm are low. An interval of relatively enhanced BFAR is recorded between 55 and 67cm and appears to correlate well with a muddy foraminifera sand unit. Between 23-43cm an interval of moderate accumulation rates is observed and this also co-varies with the sedimentology as the next interval (9-19cm) contains relatively low BFARs but also a slightly higher proportion of mud. The top part of the core (3-6cm) records slightly elevated accumulation rates compared to the previous interval.

8.2.4 Core 9/97-04

8.2.4.1 Large size fraction (250-500µm)

Paired cluster and detrended correspondence analysis of samples from the upper 84cm of core 9/97-04 produces four distinct cluster groups (LFAZ 04-I to IV; Fig. 8.6). Each cluster group is linked to a distinct lithofacies. LFAZ 04-IV is present is lithofacies FS 1. This group is dominated by *S.schlumbergeri* (up to 38%), *R.stabilis* (8%) and *Gyroidina soldanii* (11%). LFAZ 04-III is recorded in lithofacies FS (1 and 2). This group is dominated by *C.wuellerstorfi* (25%) and *R.stabilis* (24%). LFAZ 04-II is linked to lithofacies SM and is dominated by the following taxa; *K.bradyi* (10%), *S.schlumbergeri* (38%) and *Pullenia bulloides* (20%). LFAZ 04-I is observed in lithofacies CM. This group contains high percentages of *C.wuellerstorfi* (14%), *R.stabilis* (20%) and *S.schlumbergeri* (38%).

8.2.4.2 Small size fraction (63-250μm)

Cassidulina laevigata occurs in relatively high abundance (≥16%) throughout this core (Fig. 8.7). *Triffarina angulosa* has a high abundance (>10%) in the lower part of the core (35-90cm). Two species (*A.weddellensis* and *E.exigua*) have a peak in abundance (17% and 50% respectively) between 10-15cm core depth. *C.laevigata* are abundant during the early phase of MIS 2 with a strong peak (12cm core depth, 13.5 kyr B.P.) in abundance for *E.exigua* (small fraction) that characterises the latest part of this stage.

8.2.4.3 BFAR

The record of accumulation of benthic foraminifera in core 9/97-04 (Fig. 8.6) displays three samples which suggest an episode of significantly enhanced BFAR (38-42cm). However, this interval also coincides with a significant hiatus in the sedimentological record (see Chapter 5). Excluding these three samples, the other values are always below 350

specimens/cm^2/kyr and average 126 specimens/cm^2/kyr. Values are initially below this average value for the bottom part of the core (59-83cm) and are above average for most of the rest of the core (16-55cm). Values are then highly variable between 1-12cm. There is no observable link between BFAR and the alternation of lighter and darker coloured sedimentary units in this core.

8.2.5 Core 9/97-14

8.2.5.1 Large size fraction (250-500μm)

Paired cluster and detrended correspondence analysis of samples from the upper 93cm of core 9/97-14 produces five distinct cluster groups (LFAZ 14-I to V; Fig. 8.8). Each cluster group is linked to a distinct lithofacies. LFAZ 14-V is present in lithofacies BM and is dominated by *S.schlumbergeri* (up to 32%) and *P.bulloides* (24%). LFAZ 14-IV is linked to lithofacies FS-1 and CO-1 and contains high percentages of *S.schlumbergeri* (32%) and *C.wuellerstorfi* (25%). LFAZ 14-III is recorded in lithofacies FS-2. This group is dominated by *C.wuellerstorfi* (40%), *S.schlumbergeri* (16%) and *P.bulloides* (24%). LFAZ 14-II is present in lithofacies BM and contains high percentages of the following taxa; *C.wuellerstorfi* (40%) and *M.pompilioides* (20%). LFAZ 14-I is linked to lithofacies CM and is dominated by *C.wuellerstorfi* (40%) and *S.schlumbergeri* (16%).

8.2.5.2 Small size fraction (63-250μm)

Each sample that contains a sufficient number of species to produce reliable estimates of relative abundance records very little change in the percentage of each of the dominant species (Fig. 8.9). The lower section of the core (80-95cm) records a relatively low abundance for *A.weddellensis* (<4%) and *C.laevigata* (≥8%) and a relatively high abundance for *E.exigua* (≥14%) and *T.angulosa* (>6%). The section between 50-65cm records a relatively low abundance for *T.angulosa* (<5%) and a relatively high abundance for the other three species (*A.weddellensis*, >4%; *C.laevigata*, 24%; *E.exigua*, >15%). At 21cm, an absence of *A.weddellensis* is present and the sample at 1cm core depth records relatively moderate percentages for each species (*A.weddellensis*, >3.6%; *C.laevigata*, >12%; *E.exigua*, >20%; *T.angulosa*, >5%).

8.2.5.3 BFAR

Accumulation rates for core 9/97-14 (Fig. 8.8) are, on average, much lower than those present higher up on the slope (average value = 119 specimens/cm^2/kyr). Values are low for the initial interval (62-96cm), followed by an episode of moderately enhanced BFAR between 43-57cm. Two peaks in BFAR are then present (27-35cm and 1cm) either side of a trough (5-23cm). No consistent co-variation between BFAR and sedimentology is observed, although it does appear that units with a higher mud content tend to correspond with the lowest BFARs in the core.

8.2.6 Core 9/97-27/II

8.2.6.1 Large size fraction (250-500μm)

Paired cluster and detrended correspondence analysis of samples from the whole of core 9/97-27/II produces four distinct cluster groups (LFAZ 27-I to IV; Fig. 8.10). Linking each faunal group to a facies is difficult in this core, due to the relatively high number of samples that contain insufficient specimens to be included in the analysis. LFAZ 27-IV is recorded in lithofacies CO (calcareous ooze). This group is dominated by *C.wuellerstorfi* (up to 50%) and *M.pompilioides* (28%). LFAZ 27-III is present in two lithofacies; FS-2 (muddy foraminifera sand) and BM. This cluster group contains high percentages of *Uvigerina celtica* (40%), *M.pompilioides* (15%) and *C.wuellerstorfi* (25%). LFAZ 27-II is linked to lithofacies BM and is dominated by *U.celtica* (64%), *M.pompilioides* (14%) and *C.wuellerstorfi* (25%). LFAZ 27-I is present in lithofacies CM and is dominated by *C.wuellerstorfi* (50%), *M.pompilioides* (28%) and *C.kullenbergi* (25%).

8.2.6.2 Small size fraction (63-250μm)

The lower section (240-260cm) of the core (Fig. 8.11) contains a high relative abundance of *C.laevigata* (>2%) and *E.exigua* (>15%). The section between 190-220cm core depth contains a high relative abundance of *A.weddellensis* (>12%), *C.laevigata* (≥2%), and *T.angulosa* (>12%). Between 145-155cm, *E.exigua* and *T.angulosa* record relative high abundance (>15% and >5% respectively). In the uppermost section (0-20cm core depth), *A.weddellensis* and *E.exigua* dominate assemblages (≥15% and >25% respectively).

8.2.6.3 BFAR

Accumulation rates of benthic foraminifera are significantly lower for core 9/97-27/2 (Fig. 8.10) than for any discussed previously (average value = 3 specimens/cm^2/kyr). Values are initially low for the first interval (212.5-262cm), followed by two large peaks (200.5-208.5cm and 180-192cm). A third peak is then observed (139.5-155.5cm) following a short trough (159.5-176cm). A prolonged interval of very low accumulation rates is then recorded between 33-135cm, with a slight increase in BFAR present during this interval (49-73cm). A strong peak in BFAR is then recorded for the top part of the core (3-19cm). No link between BFAR and sedimentology is present in this core.

8.2.7 9/97-20

8.2.7.1 Large size fraction (250-500μm)

Paired cluster and detrended correspondence analysis of assemblage data from core 9/97-20 produces three cluster groups (LFAZ 20-I to III; Fig. 8.12). LFAZ 20-III is located between 197.5-200cm and contains *C.wuellerstorfi* and *U.celtica* in high relative abundance. This group is strongly linked to the intercalated foraminifera sands lithofacies. LFAZ 20-II is present between 172-180cm and contains high proportions of *U.celtica*. This group is also linked to the intercalated foraminifera sands lithofacies (but a separate unit). LFAZ 20-I is recorded between 25.5-48cm and is dominated by *C.wuellerstorfi*, *M.barleeanum* and *E.exigua*.

8.2.7.2 BFAR

The average accumulation rate for core 9/97-20 (Fig. 8.12) is 8 specimens/cm^2/kyr. Two peaks in BFAR are present at the bottom of the core (168.5-206.5cm). For most of the rest of the core, very low values are recorded (68.5-166.5cm). This is followed by an interval of gradually increasing and highly variable values (23-66.5cm). BFAR then gradually decreases towards the top of the core (1.5-20.5cm). No consistent co-variation is observed between lithology and BFAR.

8.3 Temporal variations in assemblage

8.3.1 Last interglacial

Inter core correlation of last interglacial samples shows that the assemblages of benthic foraminifera vary strongly with depth. Shallower depth cores (9/97-08, 9/97-10 and 9/97-04) are dominated by *M.barleeanum* and *S.schlumbergeri* with low to moderate percentages of *C.wuellerstorfi*. *Cibicides kullenbergi* is only present in relatively high numbers in 9/97-08, the shallowest core. *Bullimina inflata* increases in relative abundance with increasing depth to a peak in core 9/97-04. The deepest core (9/97-14) contains higher percentages of *C.wuellerstorfi* as well as *P.bulloides* and *M.pompilioides*. *Melonis barleeanum* displays a distinctive dip in abundance (Figs. 8.3 and 8.6) in the two intermediate cores (9/97-04 and 9/97-14). This is in contrast to *R.stabilis*, which peaks in abundance at intermediate depths (Figs 8.3 and 8.6).

8.3.2 Last glacial

Inter core correlations of the last glacial show that there are very strong variations in assemblages of benthic foraminifera with depth. Shallow cores (9/97-08 and 9/97-10) contain a high relative abundance of Cibicidids (*C.wuellerstorfi* and *C.kullenbergi*) and *U.peregrina*. The highest abundance of *R.stabilis* occurs in two intermediate cores (9/97-10 and 9/97-04). Core 9/97-04 is very distinctive (Fig. 8.6), dominated by *K.bradyi* and *S.schlumbergeri* and contains the only significant occurrence of *B.inflata*. *Pullenia bulloides* has a high relative abundance in two cores, 9/97-04 and 9/97-14. Deeper cores (9/97-14 and 9/97-27/2) contain a high relative abundance of *C.wuellerstorfi*, *M.pompilioides* and *U.celtica*.

8.3.3 Holocene

Inter core correlation Holocene samples shows that there are strong variations in assemblages of benthic foraminifera with depth. However, all cores have a high relative abundance of *C.wuellerstorfi* and *S.schlumbergeri*. The shallowest core containing this interval (9/97-10) also contains *M.barleeanum* and *U.peregrina* in high relative abundance. *Rupertina stabilis* has a peak in relative abundance at intermediate depths (9/97-04 and 9/97-14). The deepest core with this interval (9/97-27/2) contains high percentages of *M.pompilioides*, and also displays a peak in *C.kullenbergi*. Buliminids are entirely absent, as is *U.celtica*.

8.3.4 BFAR and diversity variations through time

When calculated BFARs are plotted against fragmentation indices for all cores (Fig. 8.13) no linear correlation is present ($r^2 = 0.08$). This is also the case when BFARs are plotted against the fragmentation index for individual cores (max $r^2 = 0.2$, core 9/97-14). For cores 9/97-10, 9/97-04 and 9/97-14, BFAR is generally lower during MIS 5 (Fig. 8.14) and MIS 4 compared with during MIS 3 (with two exceptions in core 9/97-10), although large gaps are present in the MIS 3 records of cores 9/97-04 and 9/97-14. Accumulation rates are high during MIS 3 but variable in 9/97-27/2 and 9/97-20 and low during MIS 2 at all depths. For MIS 1, the three deeper cores (9/97-14, 9/97-27/2 and 9/97-20) each display elevated BFARs, but this pattern is not present in the two higher cores (9/97-10 and 9/97-04).

A mid depth diversity maximum (Fig. 8.15) is present in core 9/97-04 for each time interval. The maximum is most pronounced during the last glacial. In the Holocene, the diversity maximum is still present, but diversity varies less strongly between all depths. This corresponded with a down slope productivity gradient, with higher flux rates (inferred from higher BFARs) on the higher portions of the slope (Fig. 8.14) and lower flux rates on the lower portions of the slope. This productivity gradient is also apparently consistent through time (Fig. 8.14).

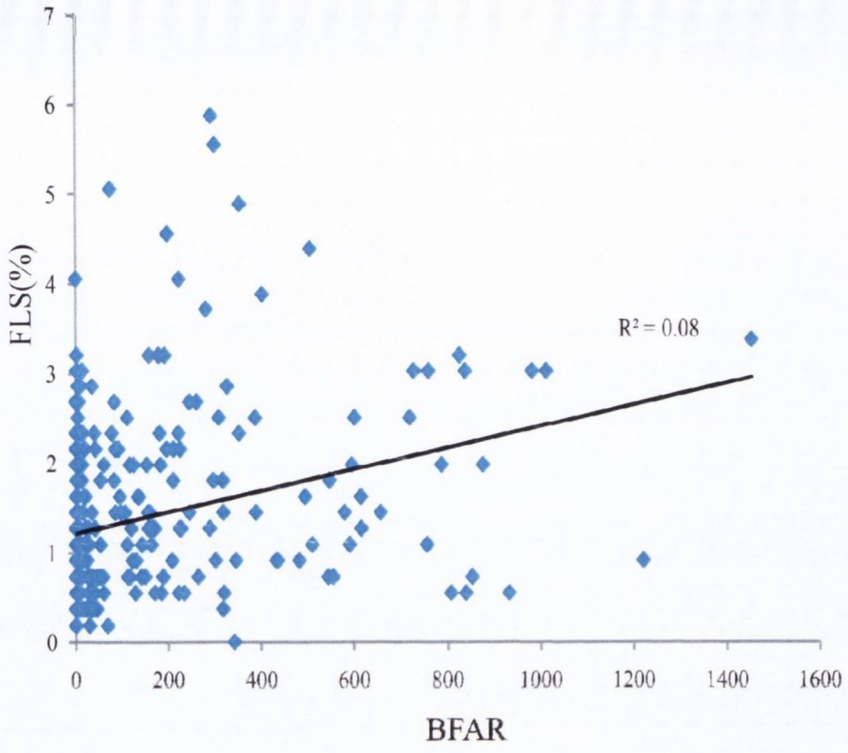

Figure 8.13. Scatter plot of all core BFAR data versus fragmentation index.

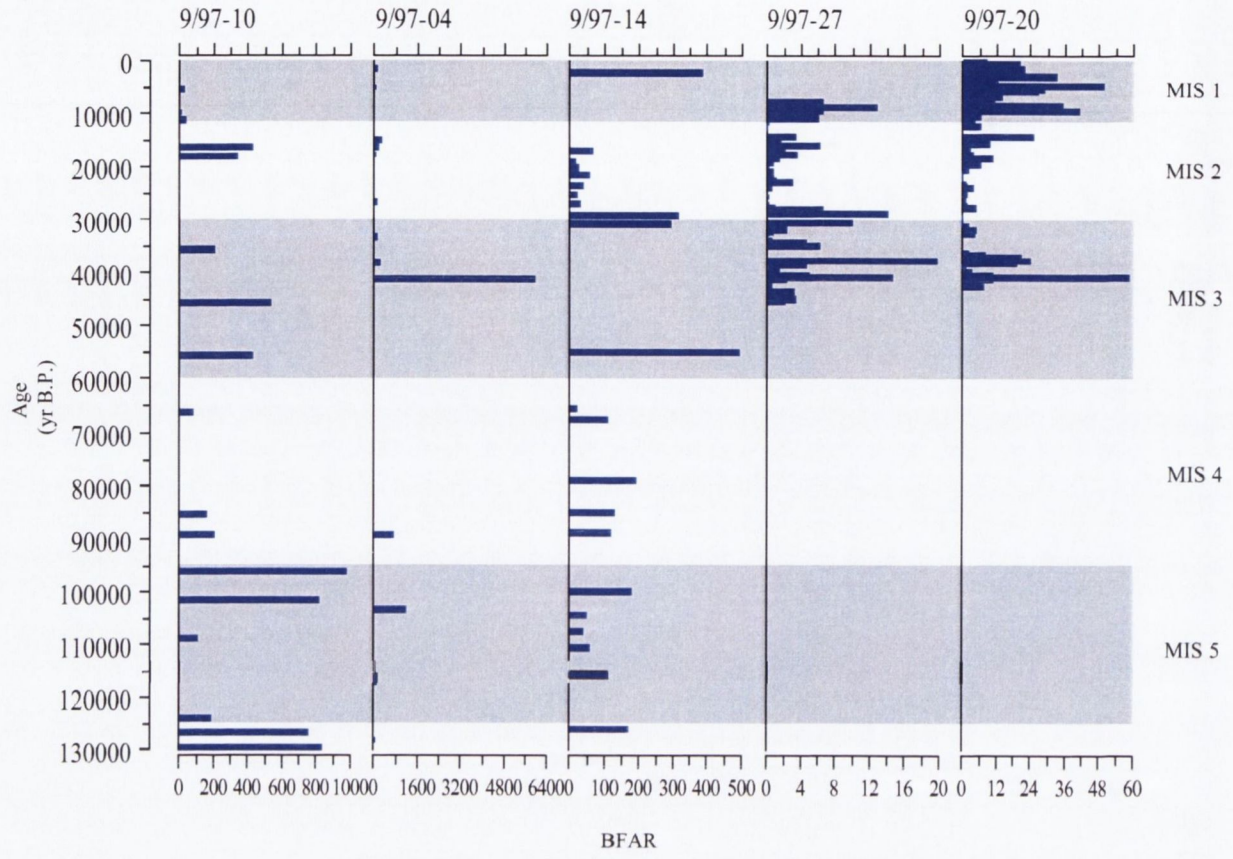

Figure 8.14. Variation of BFAR through time down slope for cores 9/97-10 (1260m water depth), 9/97-04 (1502m water depth), 9/97-14 (2118m water depth), 9/97-27/2 (2756m water depth) and 9/97-20 (3073m water depth).

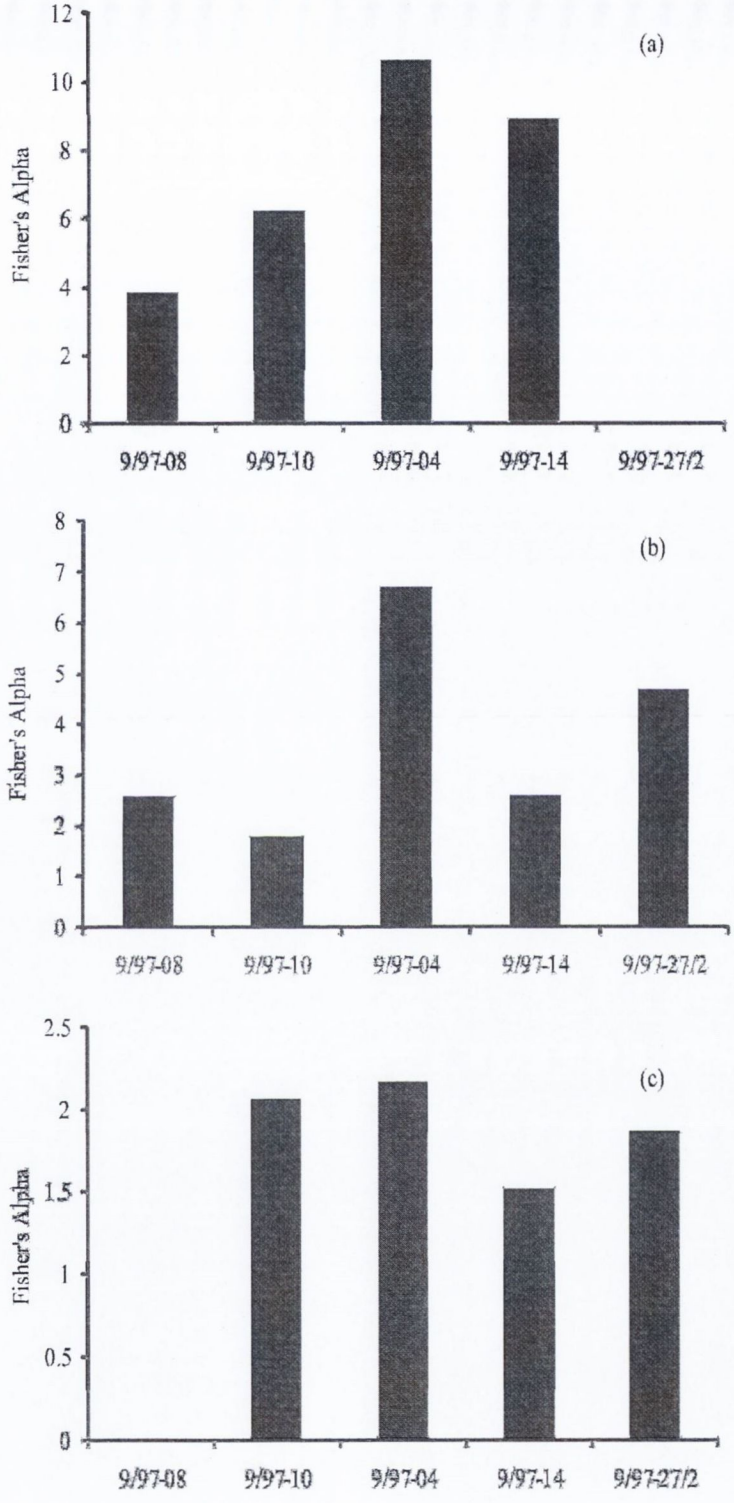

Figure 8.15. Fisher's Alpha diversity index for each interval; (a) Last interglacial, (b) Last glacial, (c) Holocene.

8.4 Statistical analysis of assemblage data

8.4.1 Whole dataset cluster analysis

Cluster analysis of the whole dataset (Fig. 8.16) shows that inter-core clustering of samples is less prevalent than intra-core clustering. In particular, samples from cores 9/97-08 and 9/97-27/2 tend to contain the most distinct faunal assemblages. The exception is the sample at 80cm core depth in 9/97-08, which clusters with samples from core 9/97-10. Some samples from the three middle cores along the depth transect (9/97-10, 9/97-04 and 9/97-14) tend to cluster closer to each other than to samples from the shallowest and deepest cores (as suggested by PCA, see below). In particular, samples from MIS 5 and MIS 3 (highlighted by the red squares, Fig 8.16) foraminifera sand units from cores 9/97-10 and 9/97-04 tend to cluster together quite strongly. Two samples from core 9/97-14 (11cm and 12.5cm) cluster with samples from MIS 1 in core 9/97-27/2. This could suggest a short-lived episode of environmental uniformity between these two sites, although the age model data for core 9/97-14 suggests that the samples at 11cm and 12.5cm are much older (approx. 21 kyr B.P.) than the Holocene samples in 9/97-27/2. The overall pattern though suggests that there are very strong inter-core differences in assemblage.

8.4.2 Cluster analysis of along slope cores

Unconstrained cluster analysis is performed on assemblage data from each sample for cores 9/97-10 and 9/97-03 (Fig. 8.17). Two cluster group pairs are identified; Pair X and Pair Y (Fig. 8.18). Each pair of cluster groups is co-eval, with Pair X mainly consisting of late glacial / Termination I sediments and Pair Y representing the last interglacial. Assemblages in

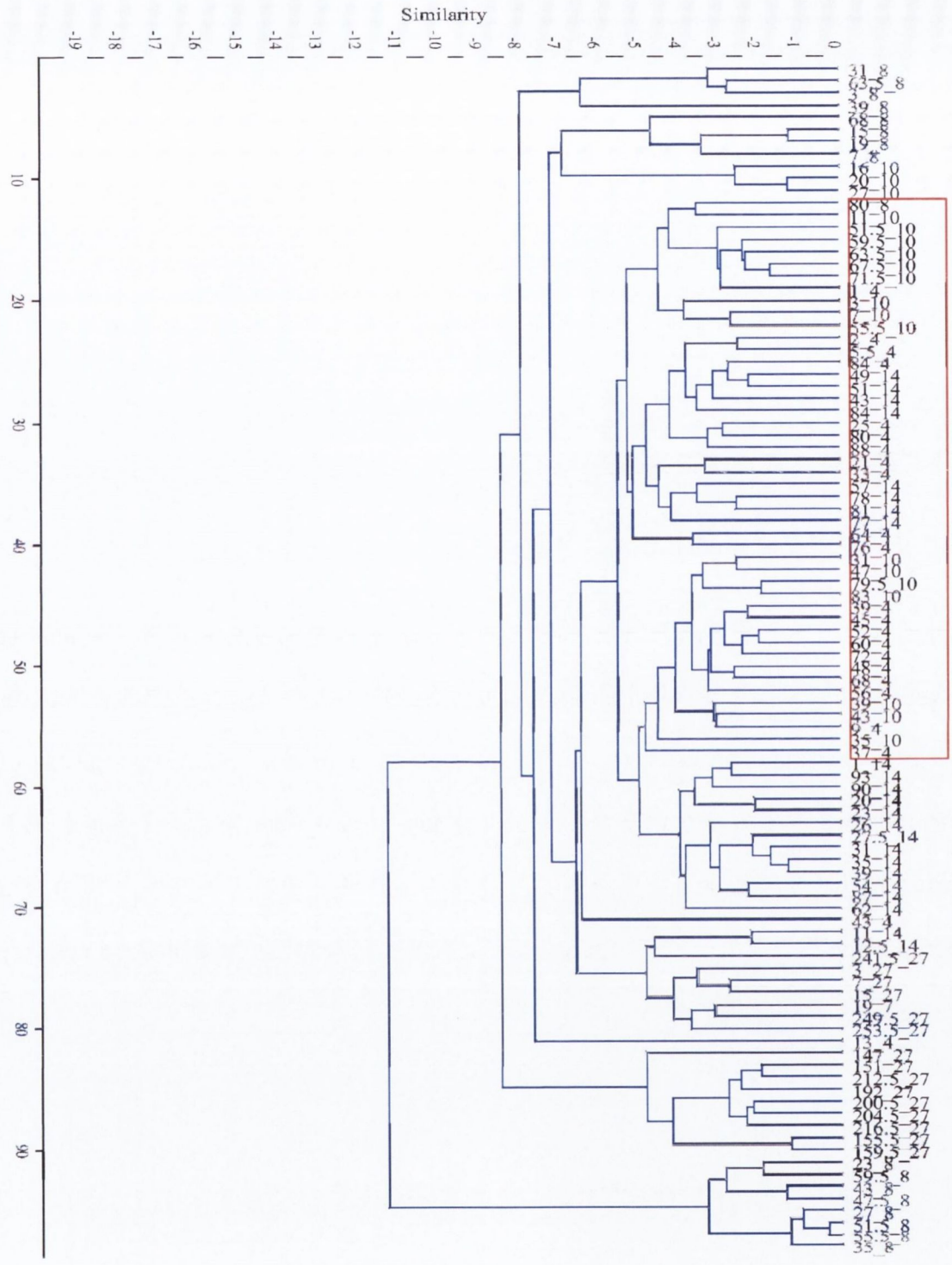

Figure 8.16. Whole dataset cluster analysis for the larger size fraction (250-500µm). Samples ending in _8 are from core 9/97-08, ending in _10 from core 9/97-10 etc. Inter-core clustering is highlighted by the red square.

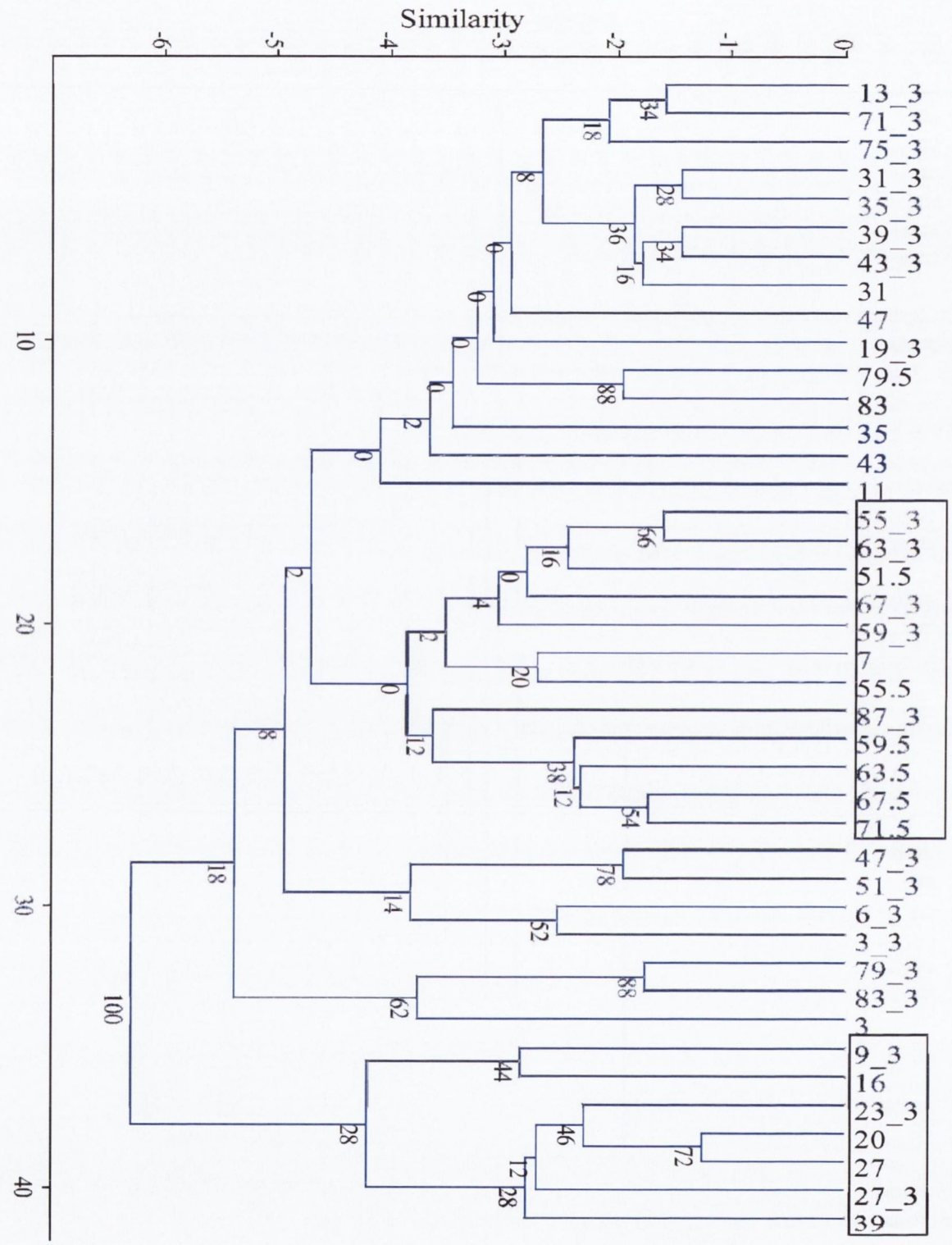

Figure 8.17. Cluster analysis (bootstrapped) of the larger size fraction (250-500µm) for cores 9/97-10 and 9/97-03 (ending in _3).

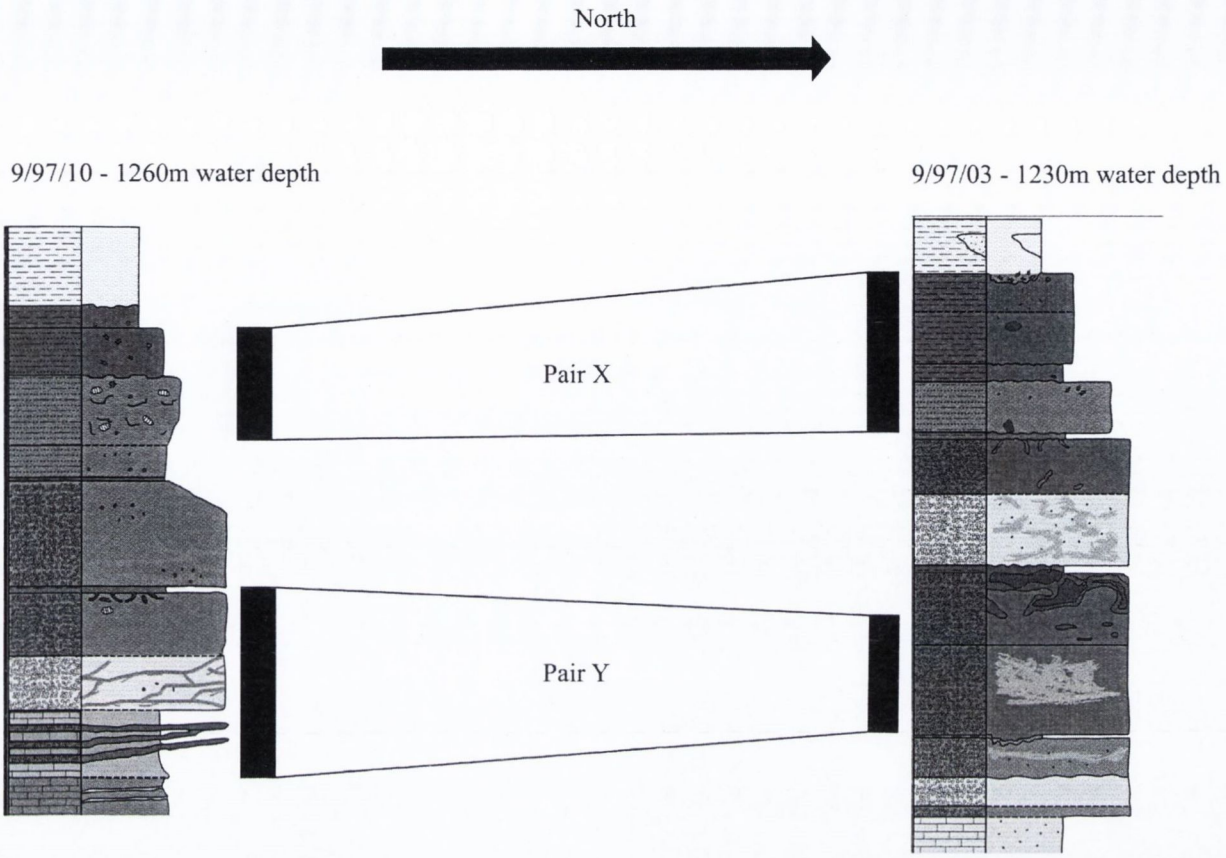

Figure 8.18. Position in cores 9/97-10 and 9/97-03 of cluster pairs X and Y from the larger size fraction (250-500μm).

Pair X samples contain *Cibicides wuellerstorfi* and *Rupertina stabilis* in high relative abundance and are linked to lithofacies BM/SM. The assemblages in the Pair Y cluster groups are characterized by a high abundance of the following taxa; *Sigmoilopsis schlumbergeri*, *Karerriella bradyi*, *Melonis barleeanum* and *Cibicides wuellerstorfi*. An initial examination of the grain size data from core 9/97-10 for the last interglacial reveals that most units are extremely well sorted (Fig. 9.9). However, the high degree of sorting present in the last interglacial units is not present in the late glacial sediments.

Unconstrained cluster analysis is also performed on assemblage data from each sample for cores 9/97-20 and 9/97-27/2 (Fig. 8.19). One pair of cluster groups is identified using this method (Pair Z; Fig. 8.20). This pair is time transgressive, with the samples in core 9/97-20 deposited 37-38 kyr B.P. and the samples in core 9/97-27/2 deposited 30-32 kyr B.P according

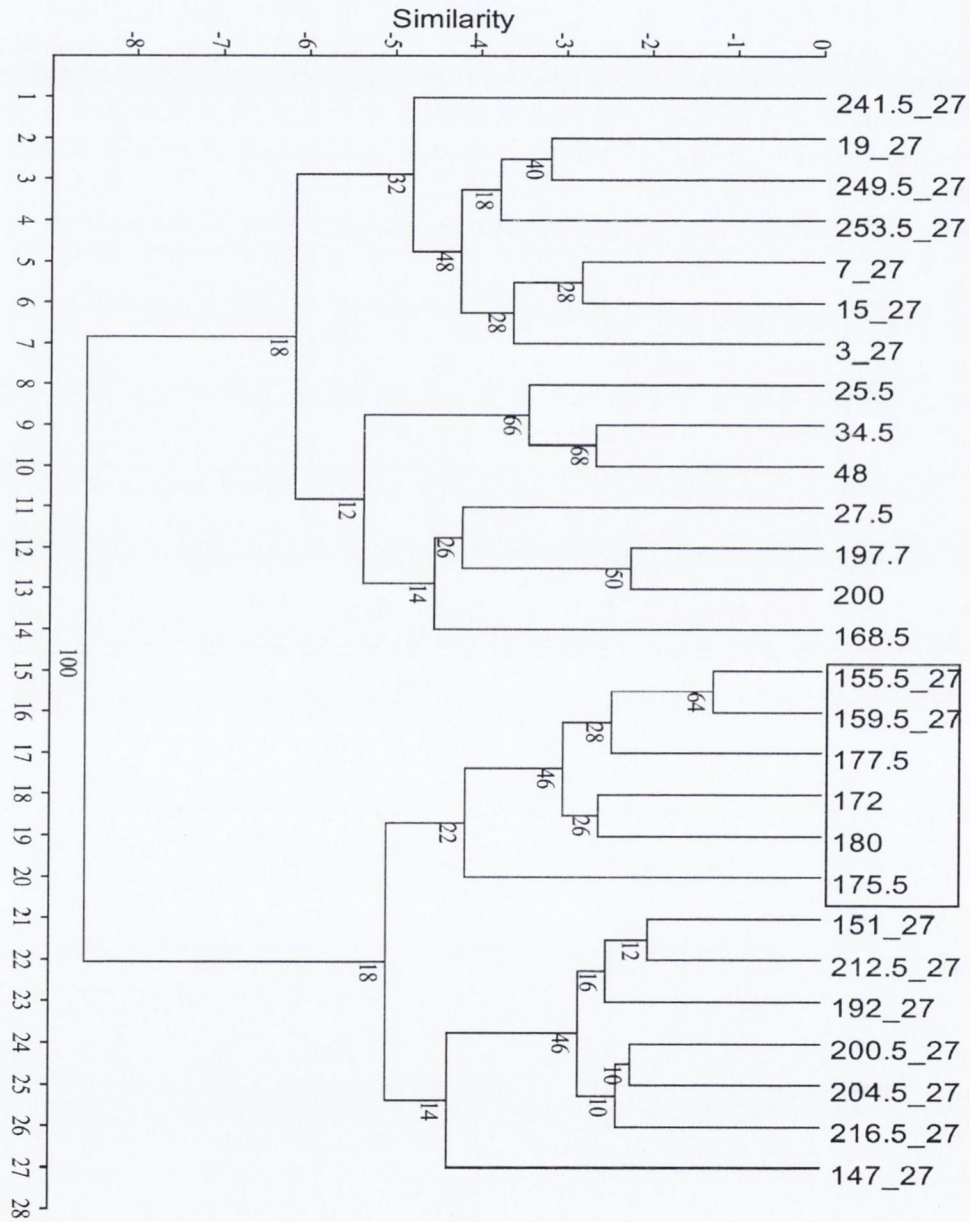

Figure 8.19. Results of cluster analysis of the larger size fraction (250-500µm) for cores 9/97-27/2 (ending in _27) and 9/97-20.

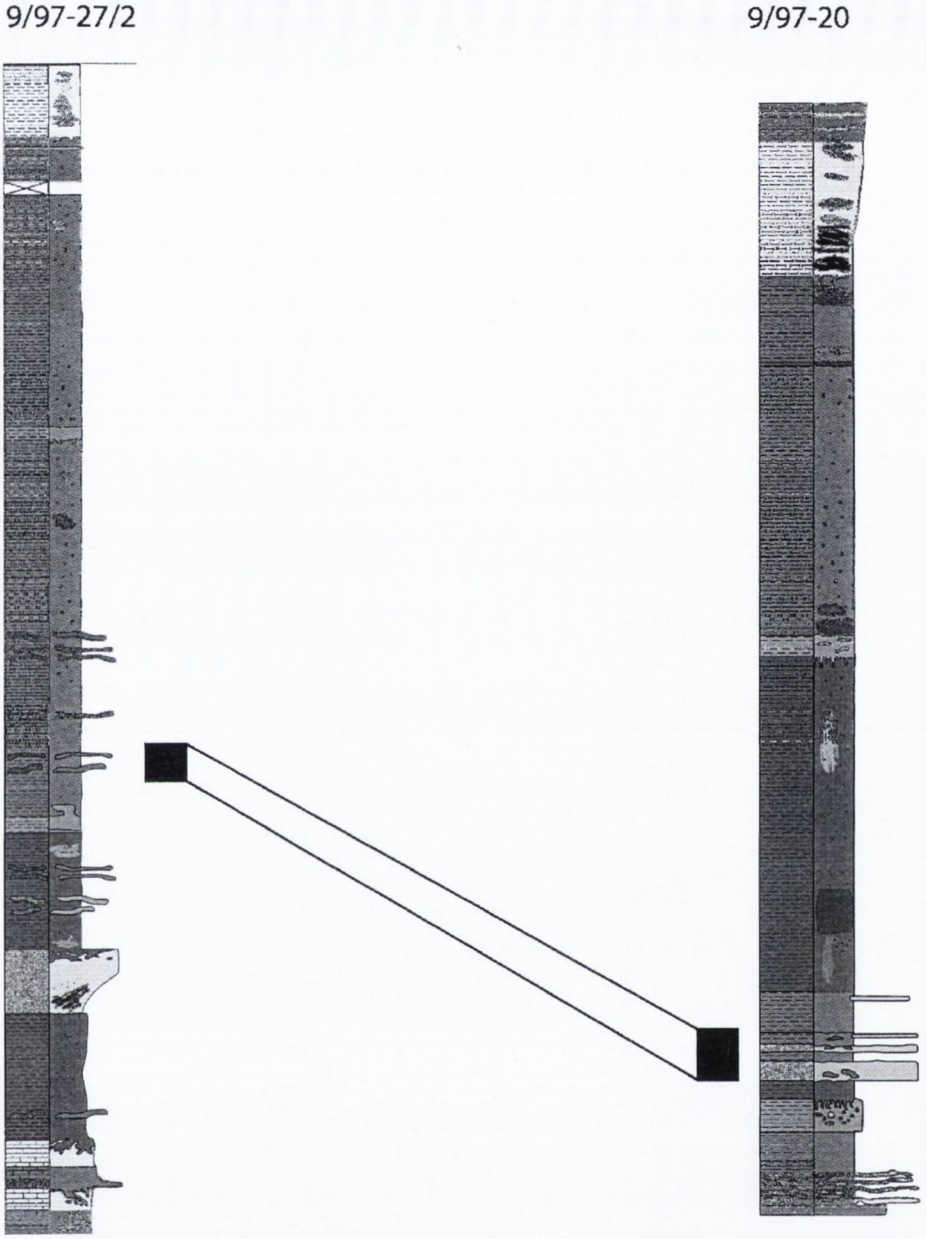

Figure 8.20. Position in cores 9/97-27/2 and 9/97-20 of cluster pair Z from the larger size fraction (250-500μm).

to the age models developed in Chapter 5. This represents a time difference of 5-8 kyr. Samples from this pair of cluster groups contain *U.celtica* in very high abundance. In both

cores, these samples are linked to the intercalated foraminifera sands lithofacies (Fig. 8.17). An examination of the grain size data for this interval in core 9/97-27/2 reveals a slightly larger sand component to the grain size distribution when compared to samples above and below (Fig. 8.17).

8.4.3 Principal components analysis of the whole dataset

Principal components analysis of the whole dataset shows almost all of the data points from core 9/97-08 aligned away from the rest of the dataset along the component 1 axis (Fig. 8.21a). This is primarily due to the high proportions of *U.peregrina*, which are dominating most of these assemblages, particularly the samples from LFAZ 08-II, with the samples from LFAZ 08-I and LFAZ 08-III containing higher percentages of other taxa. Samples containing high proportions of the following taxa; *C.wuellerstorfi*, *S.schlumbergeri*, *R.stabilis* and *K.bradyi*, are aligned opposite to *U.peregrina* along the component 1 axis. These represent the majority of samples from this dataset. The contrast between assemblages containing *U.celtica* in high abundance (generally from core 9/97-27/2) and those that do not is displayed along the component 2 axis. The component 3 axis (Fig. 8.21b) places a large number of the last interglacial and Holocene samples (aligned with *S.schlumbergeri*) towards the bottom and the last glacial samples towards the top (aligned with *C.wuellerstorfi* and *M.pompilioides*). Plotting component 4 against component 3 (Fig. 8.21c) a lot of the samples higher up on the component 4 axis are from the three shallowest cores (9/97-08, 10 and 04), with those at the lower end from the deepest sites. Principal component scores for each sample for the four

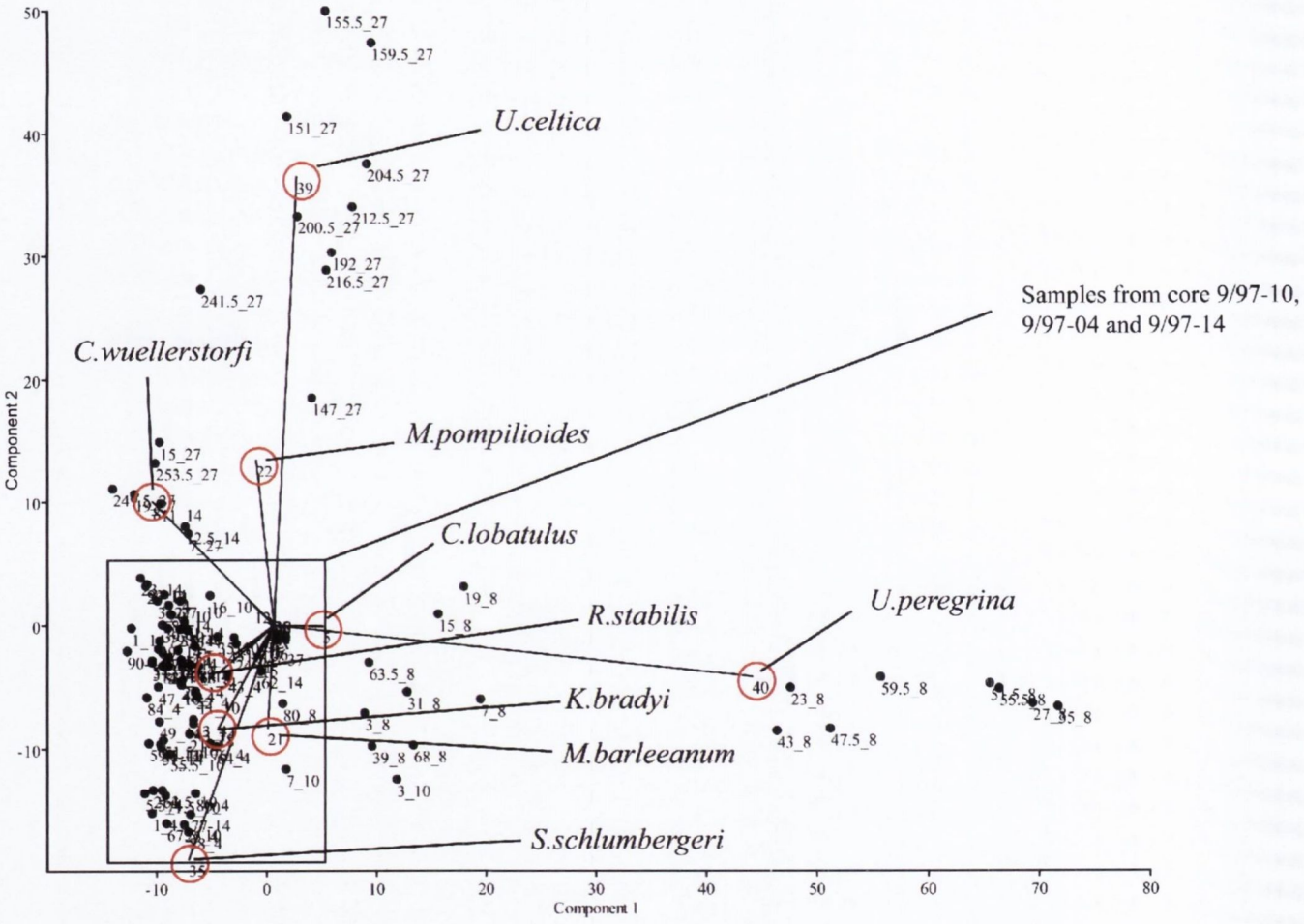

Figure 8.21a. Principle components analysis (component 1 versus component 2) of the whole large size fraction (250-500µm) dataset, with important taxa highlighted. Samples ending in _8 are from core 9/97-08, ending in _10 from core 9/97-10 etc.

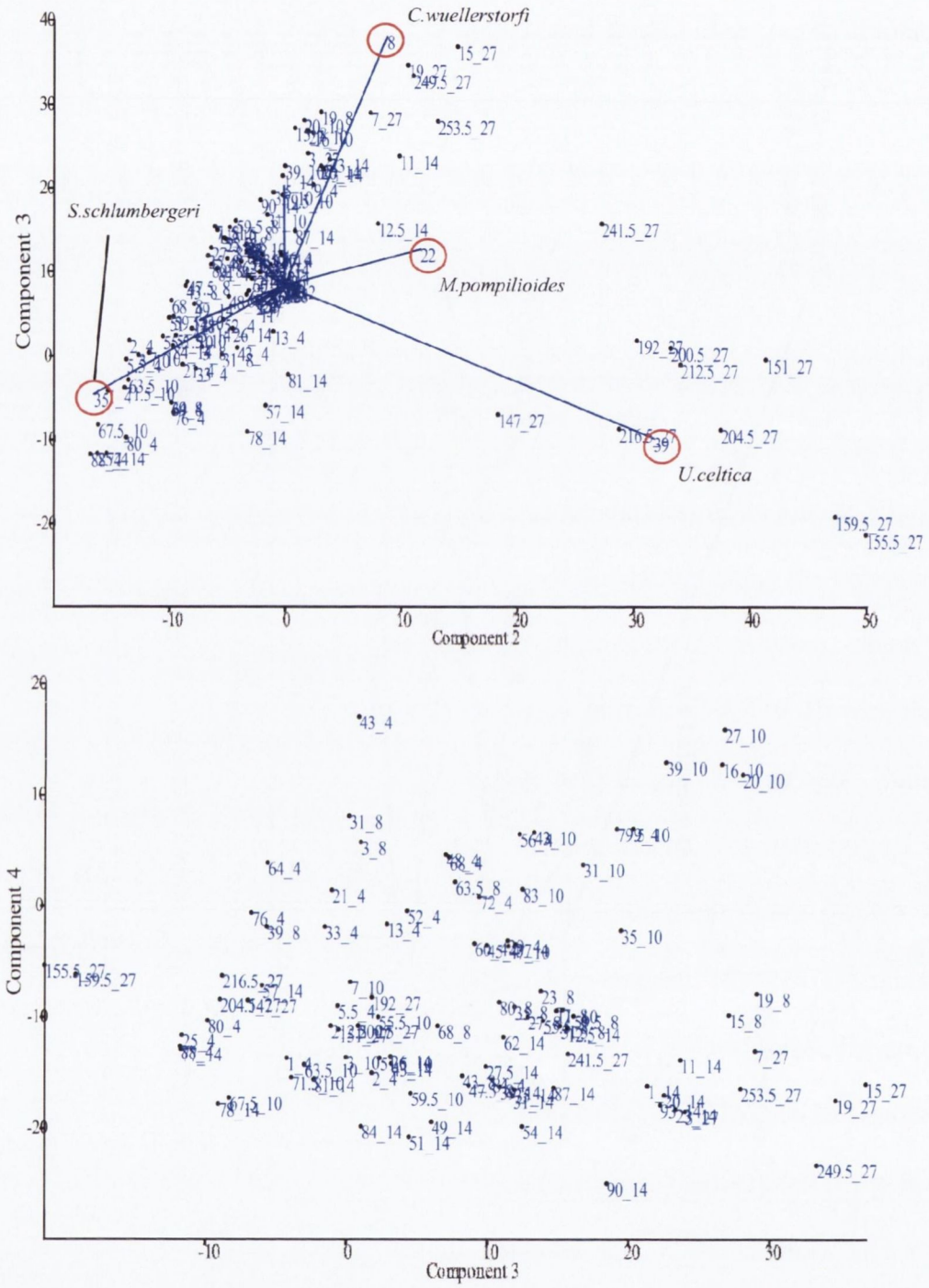

Figure 8.21a and b. Principle components analysis (component 2 versus component 3, top graph; component 3 versus component 4, bottom graph) of the whole large size fraction (250-500µm) dataset. Samples ending in _8 are from core 9/97-08, ending in _10 from core 9/97-10 etc. Important taxa are highlighted.

components are given in Appendix F and eigenvalues for each component (1-4) are presented in Table 8.1.

Component	Eigenvalue	%Variance
1	372.58	32.20
2	188.30	16.27
3	149.45	12.91
4	85.53	7.39

Table 8.1. Eigenvalues and the percentage variance for each principal component.

8.4.4 Principal components analysis of individual cores

Principal components analysis of the samples from core 9/97-08 (Fig. 8.22a) shows that *U.peregrina* is strongly orientated away from *C.kullenbergi*, *C.wuellerstorfi*, *M.barleeanum* and *Trifarina angulosa* along the component 1 axis. *Cibicides kullenbergi* and *C.wuellerstorfi* are orientated away from *T.angulosa* and *M.barleeanum* along the component 2 axis. For core 9/97-10, PCA of the samples (Fig. 8.22b) shows *R.stabilis*, *C.wuellerstorfi* and *C.kullenbergi* orientated away from *K.bradyi* and *S.schlumbergeri* along the component 1 axis. *Melonis barleeanum*, *U.peregrina* and *Hoeglundia elegans* are orientated away from these two groups along the component 2 axis.

Principal components analysis of the samples from core 9/97-04 (Fig. 8.22c) shows *S.schlumbergeri* strongly orientated away from *C.wuellerstorfi*, *R.stabilis* and *P.bulloides* along the component 1 axis. *Cibicides wuellerstorfi* and *R.stabilis* are orientated away from

P.bulloides along the component 2 axis. For core 9/97-14, PCA of the samples (Fig. 8.22d) shows *C.wuellerstorfi* strongly orientated away from *S.schlumbergeri* along the component 1 axis. *P.bulloides*, *K.bradyi* and *Melonis pompilioides* are orientated away from *C.wuellerstorfi* and *S.schlumbergeri* along the component 2 axis. Principal components analysis of the samples from core 9/97-27/2 (Fig. 8.22e) shows *C.wuellerstorfi* (and also *C.kullenbergi* and *M.pompilioides*) orientated away from *U.celtica* along the component 1

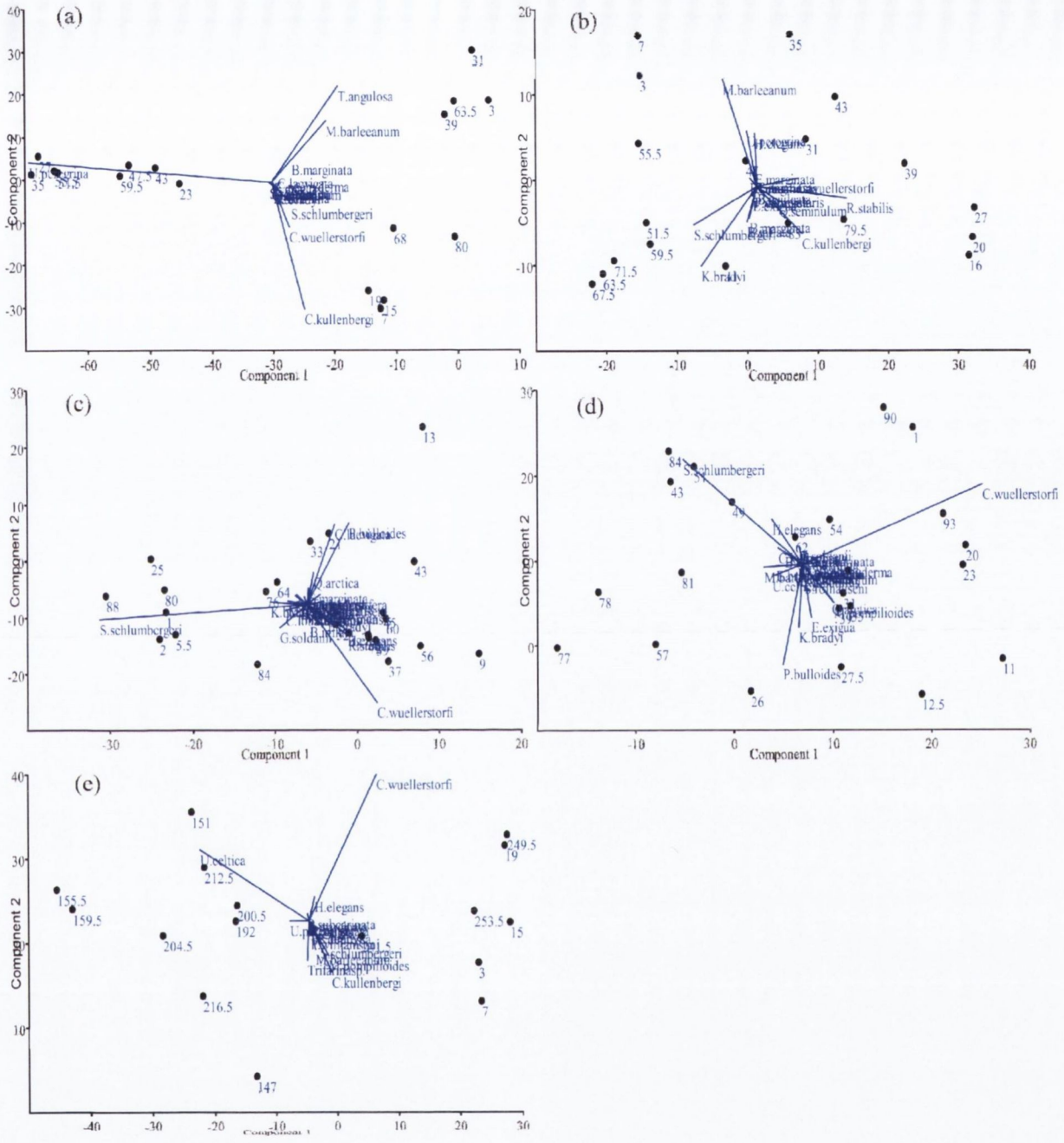

Figure 8.22. Principle components analysis of large size fraction data (250-500µm) of samples from cores 9/97-08 (a), 9/97-10 (b), 9/97-04 (c), 9/97-14 (d), 9/97-27/2 (e).

axis. *C.wuellerstorfi* and *U.celtica* are orientated away from *C.kullenbergi* and *M.pompilioides* along the component 2 axis.

8.4.5 Detrended correspondence analysis of time interval data

Detrended correspondence analysis of the samples from each time interval (Holocene, Last Glacial and Last Interglacial) shows that Holocene assemblages are relatively discrete (i.e. occupy different ordination space) for each core (Fig. 8.23). For the Last Glacial and Last Interglacial assemblages some samples from three cores (9/97/10, 9/97/04 and 9/97/14) occupy similar ordination space and appear to be linked to the foraminifera sand (FS) lithofacies in each core. This is also present when applying unconstrained cluster analysis to the whole dataset (Fig. 8.16) and perhaps suggests that there is some minor down slope movement of sediment within this lithofacies (although the assemblages in core 9/97/27/2 are still clearly distinct). Alternatively, it could represent environmental uniformity between each of the three cores for this time period.

8.4.6 Cluster analysis of the small size fraction (63-250μm)

Cluster analysis results for each core display a less clear link between assemblages of benthic foraminifera and lithofacies (Fig. 8.24), compared to the results for the larger size fraction. Some apparent lithofacies-assemblages links are present. The cluster group between 11-19cm is linked to lithofacies group BM/SM in core 9/97-08. In core 9/97-10, the cluster group between 51.5-67.5cm is linked exclusively to foraminifera sands deposited during the

last interglacial (Fig. 8.24). For core 9/97-04, the cluster group recorded between 1-5.5cm is linked to the Holocene CM lithofacies.

Core 9/97-27/2 is an exception in that each cluster group is linked to a lithofacies. The cluster group recorded between 241.5-253.5cm is linked to the lithofacies CO at the base of the core. The group present at 196.5-216.5cm core depth is primarily recorded in lithofacies FS. Between 147-155.5cm, this cluster group is linked to the intercalated foraminifera sand layers recorded during this interval. The cluster group between 3-19cm is linked to the Holocene lithofacies CM.

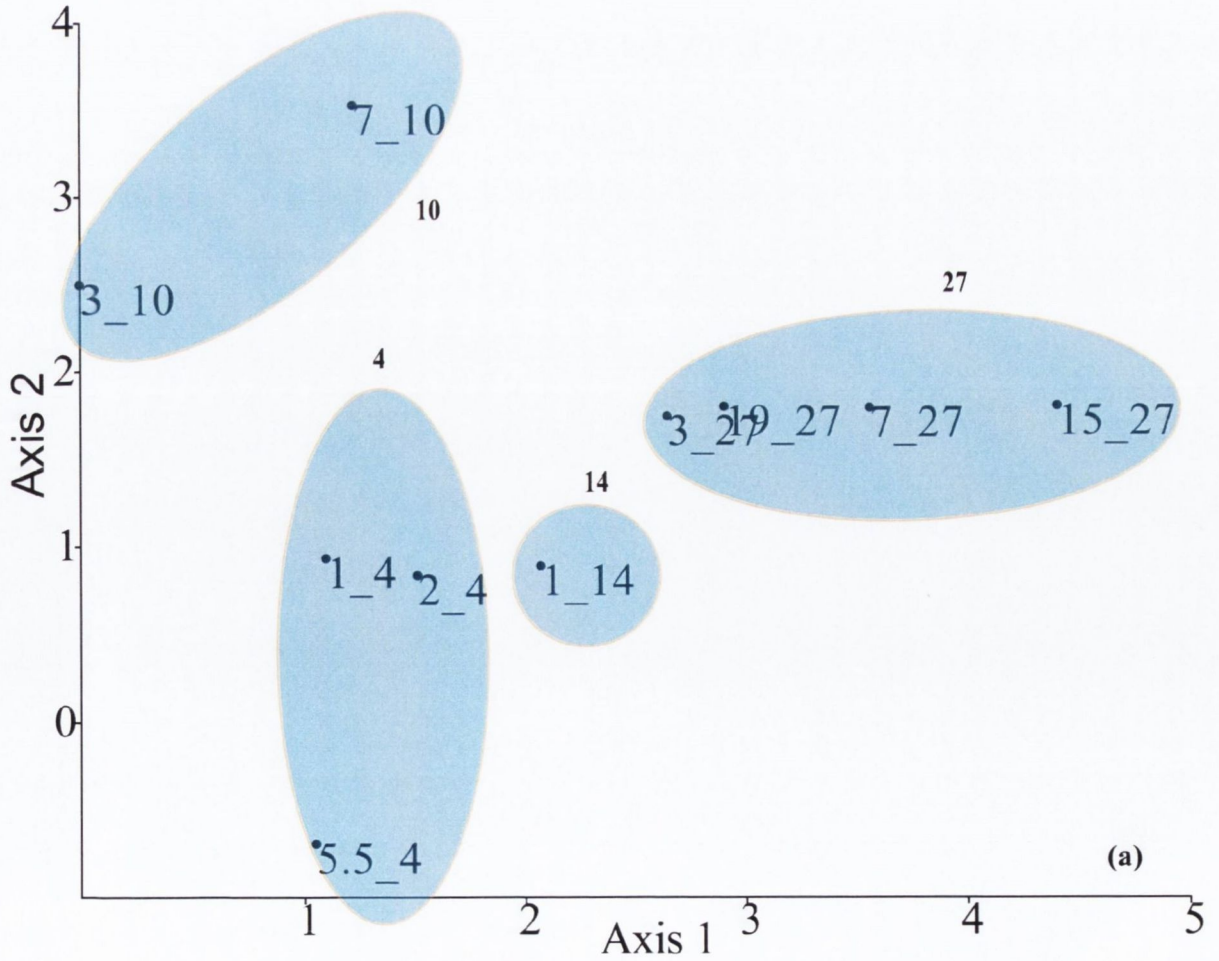

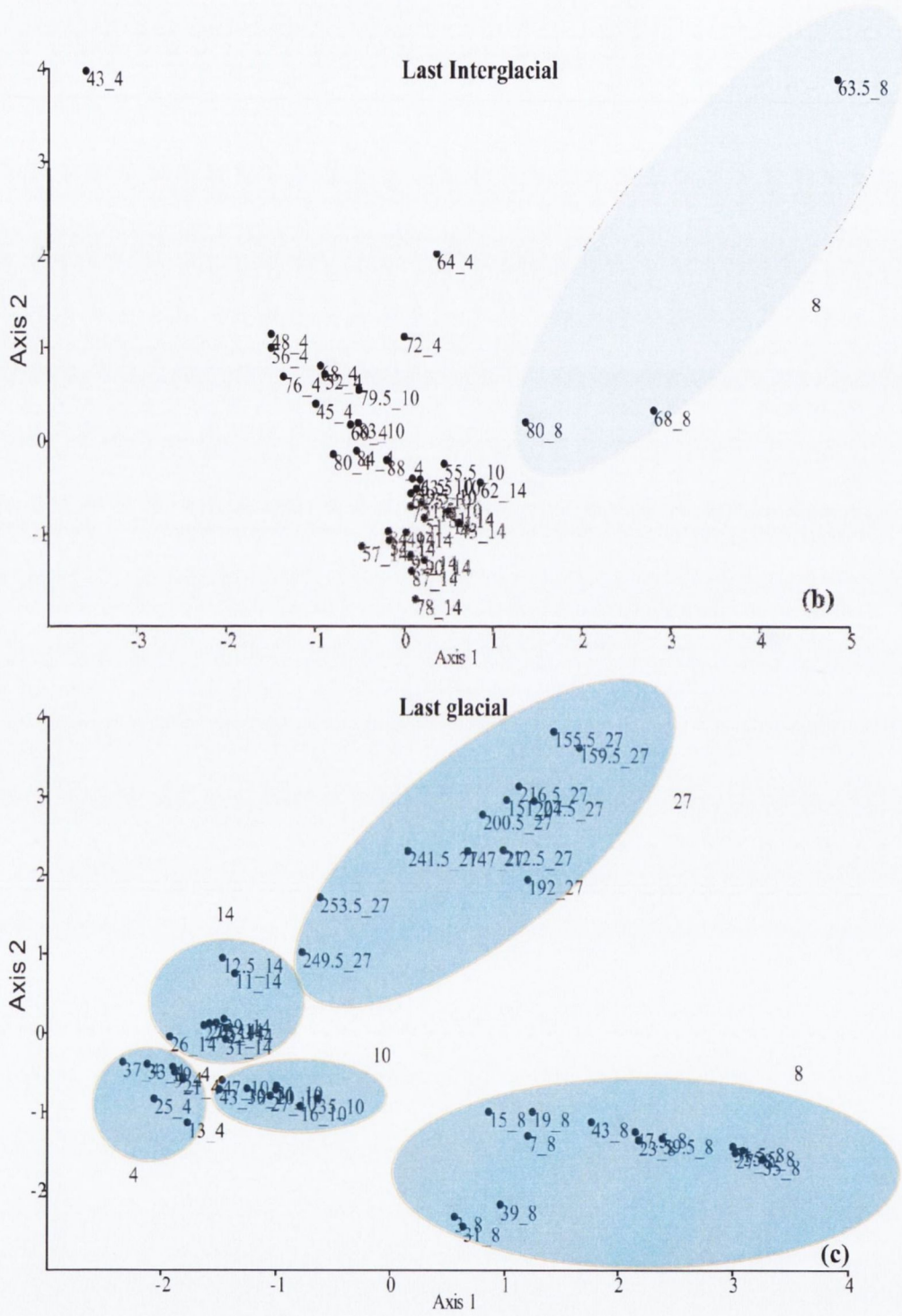

Figure 8.23. Detrended correspondence analysis of large size fraction data (250-500µm) of samples from different time slices; (a) Holocene, (b) Last glacial and (c) Last interglacial. Samples ending in _8 are from core 9/97-08, ending in _10 from core 9/97-10 etc.

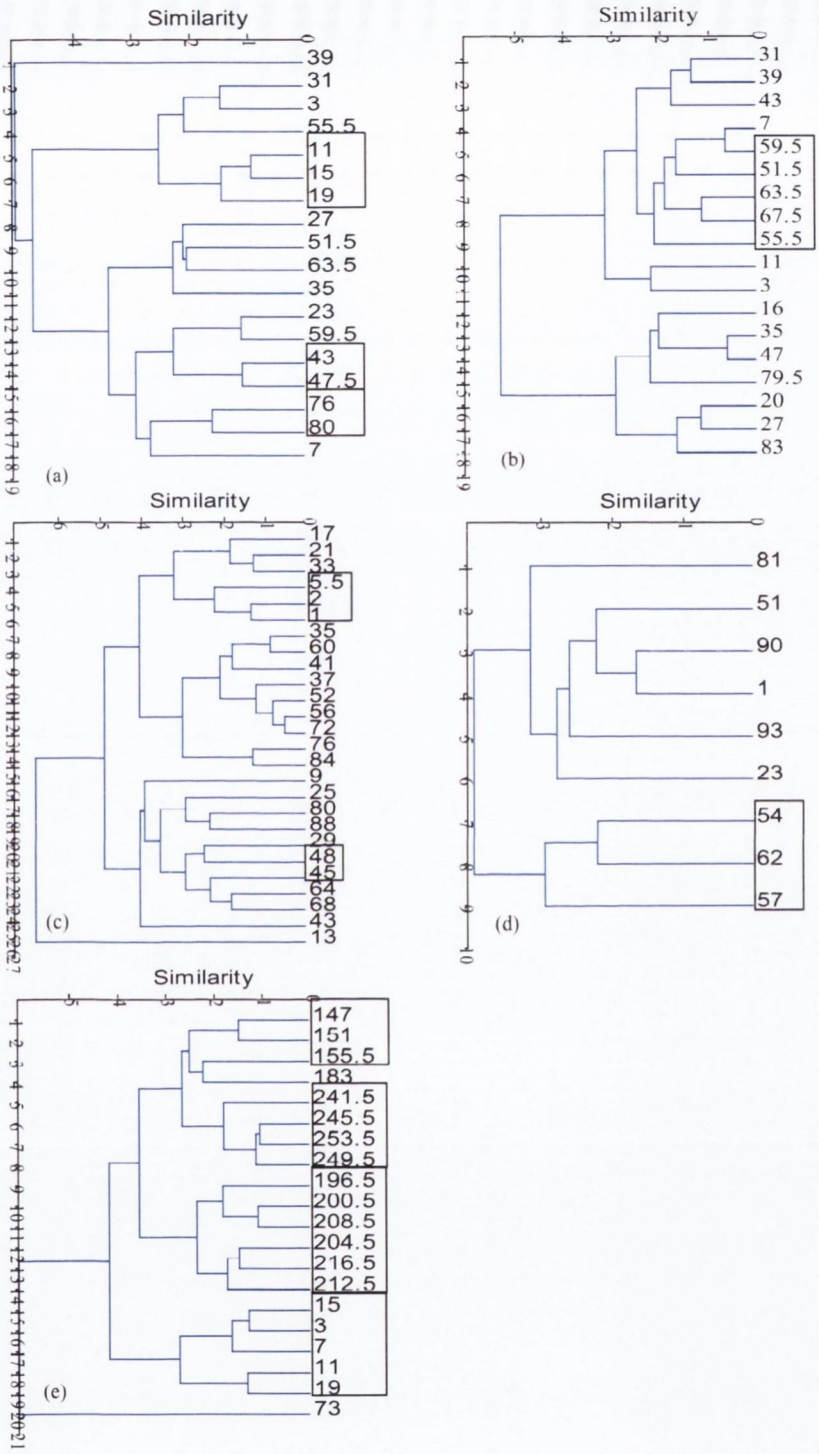

Figure 8.24. Cluster analysis of the small size fraction data (63-250µm) for cores (a) 9/97-08, (b) 9/97-10, (c) 9/97-04, (d) 9/97-14 and (e) 9/97-27/2.

8.4.7 Principal components analysis of the whole small size fraction dataset (63-250μm)

Principal components analysis of the whole small size fraction dataset shows that the inter-core variability is significantly reduced when compared to the larger size fraction. There is no clear separation of any of the cores (Fig. 8.25). However, there is a general trend with the samples from cores 9/97-27/2 and 9/97-14 aligned towards the lower ends of the two component axes, away from the other core data. This contrasts with the PCA of the large size fraction data, which shows a clear separation of cores 9/97-08 and 9/97-27/2.

8.4.8 Detrended correspondence analysis of large and small size fraction data

There is a clear separation between size fractions in terms of assemblage compositions present in the DCA plot for all cores except 9/97-04. This core does show a few of the smaller size fraction samples occupying a similar ordination space to the larger fraction data (Fig. 8.26) Also, uniquely, the large and small size fraction assemblages are very similar for the sample at 43cm core depth.

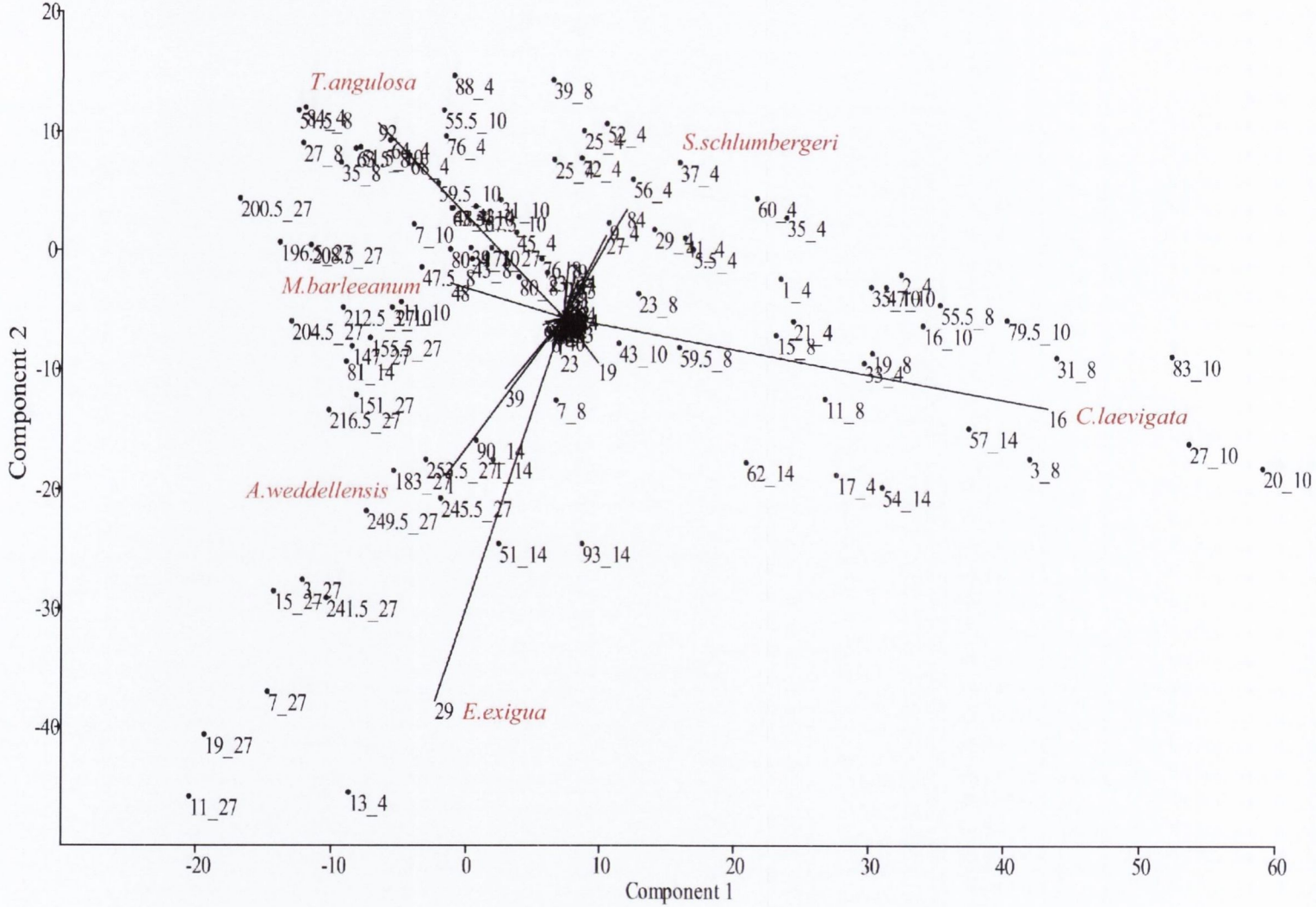

Figure 8.25. Principle components analysis of the whole small size fraction (63-250μm) dataset. Samples ending in _8 are from core 9/97-08, ending in _10 from core 9/97-10 etc.

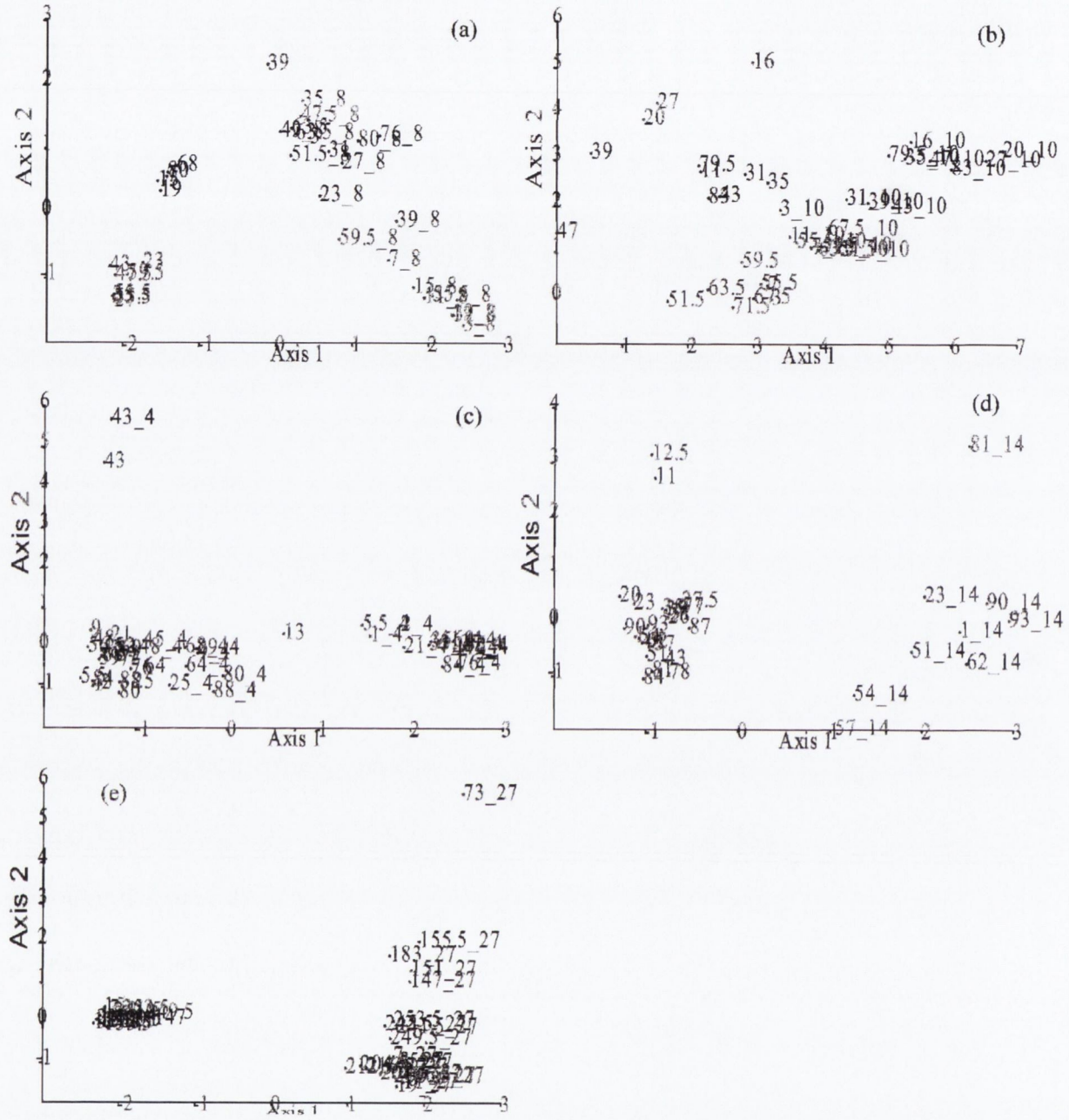

Figure 8.26. Detrended correspondence analysis of the small (63-250μm) and large (250-500 μm) size fraction data for cores (a) 9/97-08, (b) 9/97-10, (c) 9/97-04, (d) 9/97-14 and 9/97-27/2. Samples ending with the core label (e.g. _8 for core 9/97-08) are from the small size fraction.

8.5 Discussion

8.5.1 Last Interglacial

The last interglacial contains high relative percentages of *C.wuellerstorfi, K.bradyi* and *S.schlumbergeri*, suggestive of oligotrophic conditions as none of these taxa have ever been linked to high levels of nutrient supply (i.e. Altenbach *et al.* 1999). The high relative abundance of *M.barleeanum*, *U.peregrina* and *B.inflata* on the higher portions of the slope is consistent with slightly elevated productivity (and possibly reduced oxygenation of sediments; Fontanier *et al.* 2002), which perhaps has a slight seasonal or bloom related component, suggested by the high proportions of *U.peregrina* in 9/97-08. At intermediate depths (core 9/97-04 – Fig. 8.5), a peak in *R.stabilis* implies that this could be the point on the slope where lateral currents with a consistent nutrient supply are most common (Linke 1992). Low proportions of Melonids and Uvigerinids also imply that productivity is reduced but consistent (or less seasonally influenced) compared to higher on the slope (Fariddudin and Loubere 1997). The high relative abundance of *M.barleeanum* (Farridudin and Loubere 1997) during MIS 5 in core 9/97-10 is suggestive of enhanced productivity relative to the last glacial (as also suggested by the BFAR record, Fig. 8.2).

Data for the last interglacial from core 9/97-04 are consistent with the interpretation of this interval in core 9/97-10, implying a period of enhanced productivity. The addition of *R.stabilis* in high abundance during this interval suggests that either the seasonality in food supply for this interval is absent / reduced or that overall flux rates are reduced sufficiently to enable this taxon to out-compete others in core 9/97-04 (or a combination of the two – Linke 1992). Last interglacial assemblages are more diverse in core 9/97-14 in terms of dominant

taxa than glacial assemblages and are consistent with the interpretation of this interval in cores 9/97-10 and 9/97-04 in suggesting enhanced productivity. The presence of *R.stabilis* and the Uvigerinids both in high relative abundance in the same samples (57-62cm) implies that this unit could represent a mixed assemblage as *R.stabilis* requires low but consistent levels of food supply (Linke 1992), unlike Uvigerinids, which require the opposite (Altenbach *et al.* 1999; Fontanier *et al.* 2006; Schönfeld 2006), as reflected in the opposing PCA plots of these two species (Fig. 8.21a).

This interval displays a clear diversity maximum at mid-depth (core 9/97-04, 1502m water depth), with a consistent down slope decrease in productivity implied by the decreasing accumulation of benthic foraminifera with increasing depth (Fig. 8.14). Following the dynamic equilibrium model of Huston (1979), this implies that where productivity appears to be decreasing down slope, environmental stability is increasing and vice versa.

8.5.2 Last glacial

This time interval contains high proportions of *C.wuellerstorfi*, *U.celtica* and *U.peregrina* (in the deepest and shallowest cores, respectively). The high abundance of Uvigerinids (during MIS 3 only in core 9/97-27/2) suggests that the deepest and shallowest cores are characterized by strongly seasonal, bloom related productivity (Fontanier *et al.* 2002).

Cibicides wuellerstorfi, *S.schlumbergeri* and *R.stabilis* dominate the assemblages at intermediate depths, suggesting low productivity, oligotrophic conditions (Linke 1992; Altenbach *et al.* 1999). An apparent 'Uvigerinid exclusion zone' (in the >250μm size

fraction) is present at intermediate depths during this interval (Figs. 8.4-8.7). It could be due to strong lateral current transport of nutrients, with this parameter favouring epifaunal taxa such as *C.wuellerstorfi* and *R.stabilis*. This interpretation, however, is not supported by the grain size data (Fig. 9.9), which suggests that bottom currents are less vigorous during the deposition of the late last glacial (due to the high mud / clay content). It is more likely that the seasonal bloom of phytoplankton did not occur during this interval, favouring less opportunistic taxa, which could imply that the cessation of the spring bloom is necessary for bottom currents to become the primary (or at least an important) factor controlling populations of benthic foraminifera. The absence of *U.celtica* above LFAZ-II suggests that a collapse of the phytoplankton spring bloom would have occurred after the deposition of LFAZ 27-II in core 9/97-27/2 but before the deposition of the Holocene (as the spring bloom is present today). The high relative abundance of *P.bulloides* in two intermediate cores (Figs. 8.5 and 8.6) suggests there was very low productivity (Altenbach *et al.* 1999) at this depth (~1500-2000m).

Marine Isotope Stage 3 samples from core 9/97-14 contain *C.wuellerstorfi* in high relative abundance. This perhaps suggests a period of moderate bottom currents (as *C.wuellerstorfi* is an epifaunal taxon; Lutze and Thiel 1989) combined with low productivity (Altenbach *et al.* 1999; Schönfeld 2002). The absence of *R.stabilis* from this interval could potentially be related to productivity. Linke (1992) demonstrated that this species requires a constant food supply to maintain a relatively high ATP content (153 +/- ng ATP ind.$^{-1}$). As this species is only present in this core when other taxa indicate relatively enhanced productivity (Fig. 8.8) this suggests that the base-line value required to support *R.stabilis* is

perhaps only achieved during interglacials / high productivity events at this water depth (2118m).

The large numbers of *U.celtica* during MIS 3 and early MIS 2 in core 9/97-27/2 are indicative of a bloom related productivity regime (Fontanier *et al.* 2002). Two large peaks in BFAR are present in core 9/97-27/2 at 204.5cm and 188.5cm (40.8 and 37.7 kyr B.P.). Temporally, these appear to straddle H4 in the record produced by Peck *et al.* (2007). The peaks do not correspond with a sharp change in sedimentation rate. An increase in productivity either side of H4 is not present in the record of Peck *et al.* (2007). These peaks are broadly co-eval with two strong negative carbon isotope excursion recorded in the Santa Barbara Basin by Kennett *et al.* (2000). These negative excursions have been linked to methane hydrate destabilisation, and the data shown here could indicate that this had an impact at the Porcupine Bank. If methane hydrate destabilisation did occur, this could explain the large increase in productivity. When methane hydrates become destabilised, large amounts of isotopically light carbon are released into the atmosphere. Air-sea exchanges cause this light carbon to be incorporated into surface waters where phytoplankton (which preferentially utilise ^{12}C over ^{13}C) populations increase significantly. The phytoplankton are then exported to the sea-floor and are consumed by opportunistic benthic taxa that are adapted to exploit phytoplankton blooms (*U.celtica*). It is important to note though that the process of enhanced productivity as observed in this case does not necessarily require a methane hydrate destabilisation to have occurred. Also, the interpretation of methane hydrate release in this case has been challenged (Cannariato and Stott 2004). An alternative explanation is that this unit has been transported down slope, although this explanation is not favoured as the species composition is similar to adjacent samples and, as shown in Figure 8.10, cluster separately

from units studied higher up on the slope. This interpretation is also not supported by the fragmentation indices for these samples, which should be higher if down slope transport has occurred.

A dominance of epifaunal taxa during MIS 2 in core 9/97-10 and reduced abundance of *E.exigua* (small fraction) compared to MIS 3 is consistent with the hypothesis that this interval is under conditions of low food supply with a low seasonal component. The epifaunal taxa are also possibly exploiting pebbles deposited during the termination of the last glaciation to elevate their position above the sediment-water interface (Lutze and Thiel 1989; Linke 1992). A high abundance of *C.laevigata* (small) suggests that although food supply is relatively reduced compared to other time intervals it may not be extremely low (de Stigter *et al.* 1998; Austin and Evans 2000). *Cibicides kullenbergi*, in particular, has a high relative abundance during this interval, with a peak in abundance in the sample at 15cm core depth. There have been some suggestions that *C.kullenbergi* displays an affinity for Mediterranean Outflow Water (Murray 1991), which would explain the high abundance of this taxon in this sample if MOW influence can be detected.

The early phase of MIS2 in core 9/97-04 is dominated by *M.barleeanum* and *C.laevigata* (small fraction) with a moderate abundance of *R.stabilis* which suggests high flux rates for this interval (Farridudin and Loubere 1997; Austin and Evans 2000) but perhaps an absence of seasonality due to the lack of Uvigerinids and presence of *R.stabilis*. The latest phase of MIS 2 in this core is characterized by a very strong peak in the relative abundance of *E.exigua* (small fraction). During MIS 2, a high abundance of *C.wuellerstorfi* is recorded and is perhaps an indication of reduced productivity and perhaps enhanced bottom current activity for this interval in core 9/97-14. As *E.exigua* is almost entirely absent during this interval

(except for the sample at 23cm core depth), this suggests an absence of a seasonal phytoplankton bloom except at 23cm core depth (Thomas *et al.* 1995).

Unlike the study by Nees *et al.* (1997) no peak in BFAR is present for the interval mentioned (9-12.5 kyr B.P.) in any of these cores, which the authors related to an export productivity belt at the sea-ice edge that gradually retreated during Termination I, which is probably due to differences in the methodologies used between the study by Nees *et al.* (1997) and this study. One of the problems with assuming a linear sedimentation rate is the assumption that rates of sediment accumulation do not vary with time. This assumption was made by Nees *et al.* (1997) and their data shows a gradually retreating peak in BFAR along a South to North transect in the sub-polar North Atlantic Ocean (Fig. 2.14). By using a linear sedimentation rate (rather than calculating and applying a true rate of sedimentation) it is not possible to say for certain that a true peak in the accumulation rate of benthic foraminifera has occurred as it remains possible that for this interval (12.5-9 kyr B.P.), sedimentation was instead significantly reduced (see, for example, the peak in BFAR in Fig. 8.6). There is also no mention of whether or not a dissolution effect has been accounted for. Both of these factors are likely to have a significant impact on calculating accurate BFARs and are more likely to be manifest during transitions between different climatic states (i.e. glacial-interglacial transitions) or associated with hiatuses. The interpretation is that the results of the Nees *et al.* (1997) study could be due to an artefact of the method used. Alternatively, the polar front possibly did not extend this far south during the last deglaciation, although this seems unlikely based on the proposed southern most extent of the polar front suggested by Nees *et al.* (1997). Another explanation for the absence of the peak, that it is missed due to

the sampling resolution employed over this interval is perhaps unlikely also due to the relatively good record of this interval preserved in core 9/97-20 (see Chapter 5).

8.5.3 Holocene

This interval contains high proportions of *C.wuellerstorfi* and *S.schlumbergeri* at all depths, implying oligotrophic, low productivity conditions (Altenbach *et al.* 1999). The two shallowest cores with this interval (9/97-10 and 9/97-04) also contain moderate percentages of *U.peregrina* and *M.barleeanum* which implies a seasonal component to the annual food supply (Fariddudin and Loubere 1997; Schönfeld 2006) or perhaps slight mixing of assemblages. The deeper cores (9/97-14 and 9/97-27/2) lack moderate percentages of *U.peregrina* and *M.barleeanum.*

For Holocene samples in core 9/97-10, the high relative abundance of *M.barleeanum*, *U.peregrina*, *E.exigua* (small fraction) and *C.wuellerstorfi* suggests that food supply is high or has a very strong seasonal component (Thomas *et al.* 1995; Farridudin and Loubere 1997; Schönfeld 2006) or that this is an apparently mixed assemblage (due to the abundance of *C.wuellerstorfi*). As the BFAR for this interval is relatively low (Fig. 8.3), it is more likely that a strong seasonality in food supply is prevalent during the Holocene at this site. This interpretation makes sense when modern observations of a seasonal phytoplankton bloom during the spring (Gooday 1988) are considered. Holocene samples from core 9/97-04 record a moderate to high relative abundance for most taxa highlighted in Figs. 8.6 and 8.7 (with the exception of *E.exigua*, small fraction). This suggests a highly variable (or strongly mixed) signal in terms of bottom water currents and productivity.

The Holocene assemblage is diverse in core 9/97-14, with epifaunal taxa (*R.stabilis* and *C.wuellerstorfi*) abundant in the larger size fraction and *C.laevigata* and *E.exigua* abundant in the smaller fraction. This suggests a slight increase in productivity compared to the last glacial (Austin and Evans 2000). The high relative abundance of *E.exigua* implies that the seasonal phytoplankton bloom prevalent in this region today (Gooday 1988) is influencing benthic assemblages here.

Holocene samples contain high proportions of *C.kullenbergi*, *C.wuellerstorfi*, *M.barleeanum*, *A.weddellensis* (small fraction) and *E.exigua* (small fraction) in core 9/97-27/2. Uvigerinids are absent from these samples. The high abundance of *E.exigua* and *A.weddellensis* (small fraction) suggests that the seasonal phytoplankton bloom that is currently present over this part of the NE Atlantic Ocean is affecting assemblages here (Thomas *et al.* 1995). The absence of Uvigerinids (particularly *U.celtica*) could be related to an absence of the highly unstable food supply discussed previously for MIS 3. *Melonis barleeanum* is also indicative of enhanced productivity (Farridudin and Loubere 1997), although the large numbers of *C.wuellerstorfi* suggest that this enhancement is probably not very large (Altenbach *et al.* 1999). This is consistent with the BFAR data, which shows that BFAR was lower during the Holocene than during the MIS 3 interstadial high productivity spikes (Fig. 8.10).

8.5.4 Synthesis across time

Whole dataset PCA reveals that four components are responsible for the majority of the variation in assemblages (Table 8.1). Two of these components (component 1 and

component 2) are probably related to the same parameter (strong seasonality / instability in food supply) as they are both related to the dominance of Uvigerinids. Separation of the two species along the slope, with *U.peregrina* dominating assemblages high on the slope (819m water depth) and *U.celtica* dominating assemblages on the lower portions of the slope (2756m water depth) could be related to base-line productivity values. *Uvigerina peregrina* is present in the samples examined from core 9/97-27/2, but it appears to be out-competed by *U.celtica* which is usually more abundant. Component 3 appears to be related to variations through time, with last glacial samples located higher on this axis compared to samples from the previous interglacial and the Holocene. This variable could perhaps be related to the volume of food supply when the strong seasonal supply is absent or suppressed (during parts of the last glacial). Component 4 appears to be related to variations with depth for the three intermediate depth cores (9/97-10, 9/97-04 and 9/97-14). The samples are aligned with the shallower samples (9/97-10 and 9/97/08) towards the bottom and the deeper samples (9/97-14 and 9/97-27/2) towards the top. This could reflect the non-seasonal productivity gradient related to depth.

In intermediate depth cores (9/97-10, 9/97-04 and 9/97-14), it appears that the primary factor controlling the relative abundance of taxa is different from that present at the shallowest and deepest sites, which is also suggested in the PCA analysis of the assemblages (Fig. 8.22). In 9/97-08 and 9/97-27/2, the Uvigerinids are aligned opposite to *C.wuellerstorfi*, *C.kullenbergi* and *S.schlumbergeri* along the component 1 axis, possibly relating to strong seasonality in food supply (Schönfeld 2006). This is different in cores 9/97-10, 9/97-04 and 9/97-14 where *C.wuellerstorfi* and *S.schlumbergeri* are aligned in opposite directions along the component 1 axis, which could be related to constant lateral currents, which favour

elevated epifaunal taxa such as *C.wuellerstorfi* and *R.stabilis* (Schönfeld 2002). These currents could be a dominant factor controlling populations of benthic foraminifera during the last glacial, but absent or less significant in controlling assemblages during interglacials where seasonal productivity becomes more significant.

The depth down the slope in which the position of highest relative abundance of *R.stabilis* appears varies between cores 9/97-04 and 9/97-10 with apparent climate change (glacial-interglacial variations). During the last interglacial, this taxon is most abundant in 9/97-04 (1502m water depth), before peaking in abundance in both 9/97-04 and 9/97-10 (1260m water depth) during Marine Isotope Stage 3 (although MIS 3 is truncated in core 9/97-04). The species is then most abundant in 9/97-10 during the last glacial (MIS 2) before switching back to recording a maximum occurrence in core 9/97-04 during the Holocene. Because *R.stabilis* relies upon consistent nutrient supply throughout the year provided by lateral advection (Linke 1992) it is reasonable to suggest that the species is shifting position up and down the transect to follow a particular bottom current. This is consistent with the proposals of Øvrebø *et al.* (2006) for a shifting current position with changing climate (see Fig. 2.17). Alternatively, this could be due to the species requiring a base level of productivity (Linke 1992). Previous studies have also proposed a link between sandy, bottom current winnowed units and 'epibenthic' foraminifera (i.e. Schönfeld 1997, 2002). An alternative explanation is that this species is being redistributed down slope, but this interpretation is not supported by the strong differences in inter-core clustering.

Following the assemblages of core 9/97-27/2 through time shows that the dominant species do not change (*C.wuellerstorfi*, *M.pompilioides* and *U.celtica*) which suggests that this is a very stable environment. Samples from core 9/97-14 are almost always dominated by

either *C.wuellerstorfi* or *S.schlumbergeri,* again potentially implying some stability in environment across lithofacies. This is consistent with the findings of Øvrebø *et al.* (2006) who observed a reduction in the frequency of erosive contacts with depth along the slope and with the bottom current measurements of Dickson and McCave (1986), which showed higher-energy, more erosive bottom current velocities are prevalent on the higher portion of the slope. This perhaps supports the hypothesis of increasing environmental stability with depth.

There is a clear trend of decreasing average BFAR with depth present in these cores. Core 9/97-10 (1260m water depth) records average values 3-4 times greater than those present in core 9/9714 (2118m water depth). Core 9/97-14 records (on average) values approximately 40 times greater than values present in core 9/97-27/2 (approx. 2800m water depth), which implies a much sharper productivity gradient between the mid and lower slope (2118-2756m water depth) compared with the upper and mid slope (1260-2118m water depth). If the different sedimentation rates are accounted for (average = 1cm/kyr for $\leq$2118m water depth and 10cm/kyr for $\geq$2118m water depth, so a 10 times increase in sedimentation rate) then the remainder (3-4 times) is explained by a near linear decrease in the accumulation of benthic foraminifera with depth. This implies a similar gradient in BFAR between the mid to lower slope and upper to mid slope.

When traced down slope each facies consistently displays a mid slope diversity (based on Fisher's Alpha Index) maximum located in core 9/97-04 (Fig. 8.15). This phenomenon has been observed at other locations (Sanders 1968; Patterson and Lambshead 1995), and is perhaps best explained by the dynamic equilibrium model of species diversity (Huston 1979). The dynamic equilibrium model predicts that species diversity is controlled by a combination of resource supply and the rate of habitat disturbance, with the intersection

between these two factors producing maximum diversity (Fig. 8.27), which is consistent with the disturbed sediments observed in core 9/97-08 (Fig. 8.1) and the lack of graded beds or sharp contacts in 9/97-27/2 (Fig. 8.10). This produces a down slope stability gradient with low stability near the top and high stability in the deeper environment. As the diversity maximum is consistently recorded in the same core (9/97-04), this implies that the down slope environmental stability gradient also does not alter through time. Productivity has the opposite pattern (Fig. 8.14), with higher productivity higher up on the slope, and lower productivity lower down. Sediment characteristics (particularly modal grain size and sorting) could also have an influence on species diversity along this transect (Etter and Grassle 1992), but this is potentially linked to both stability and productivity. Variations in stability (e.g. current velocity) can alter grain size distributions (Hjulström 1939) by winnowing out finer material in an unstable environment or enabling finer particles to be deposited in calm environments. Productivity also has the potential to influence sediment grain size, as enhanced surface productivity leads to the production of more benthic foraminifera >150μm in size (Herguera and Berger 1991), for example.

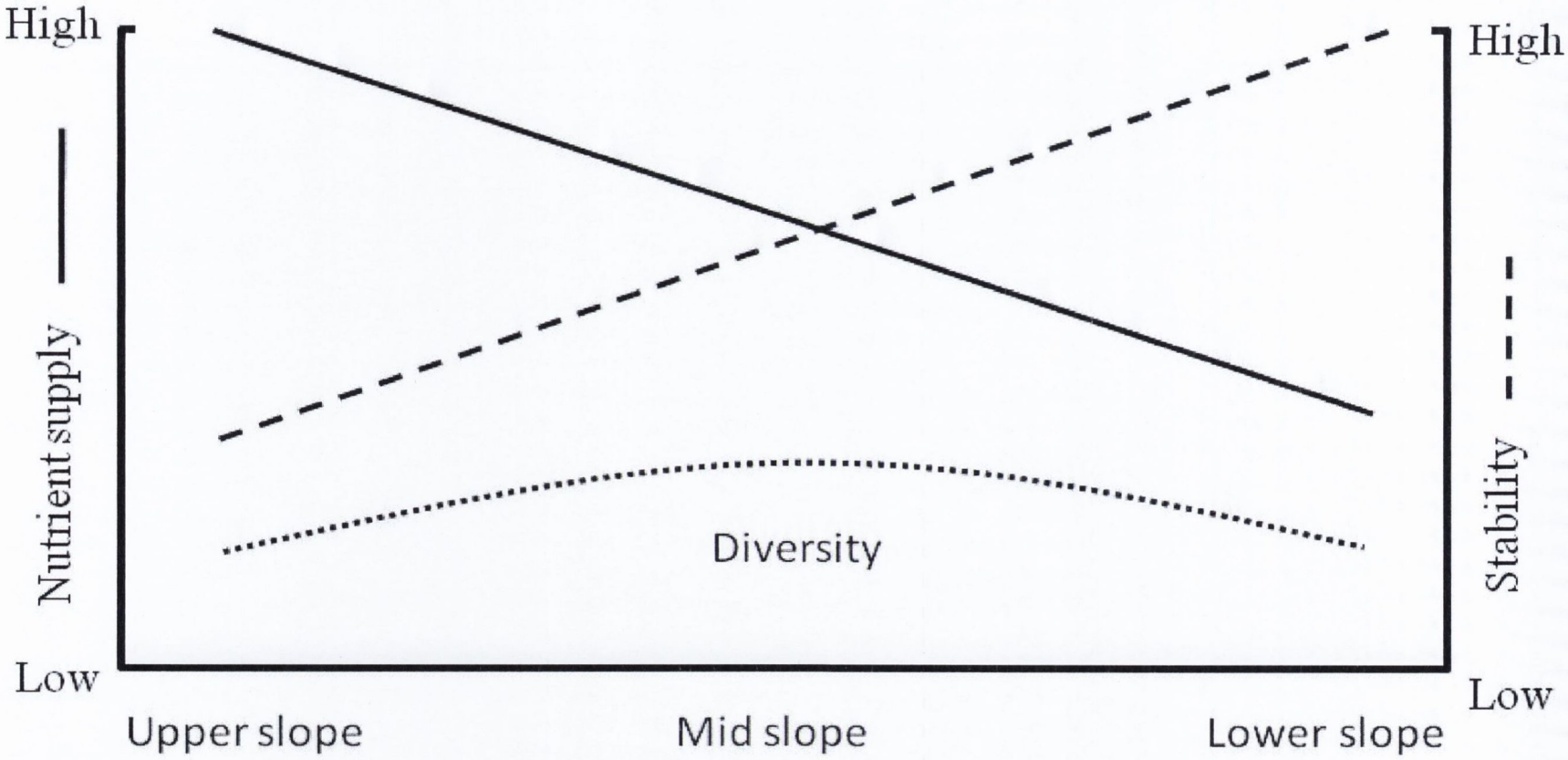

Figure 8.27. Mid slope diversity maximum produced by dynamic equilibrium of benthic foraminifera populations with nutrient supply and environmental stability.

8.5.5 Correlations across the slope

Pair X is a co-eval late glacial unit with similar lithofacies deposited during this interval in each core (lithofacies BM/SM). Units in cores 9/97-10 and 9/97-03 contain a high percentage of mud and clay and are, therefore, unlikely to have been deposited under the influence of strong bottom currents. The unit does contain *Cibicides wuellerstorfi*, *Cibicides kullenbergi* and *Rupertina stabilis* (all epifaunal taxa) in high relative abundance. *Rupertina stabilis* is indicative of low but continuous food supply throughout the year, combined with consistent bottom currents (Linke 1992). This is broadly consistent with the BFAR data for both cores, which show relatively suppressed flux rates for this interval, and the high relative abundance of *C.wuellerstorfi* (Altenbach *et al.* 1999). The low abundance / absence of *Epistominella exigua* from all samples during this interval support the inference that the seasonal phytodetritus supply characteristic of the modern NE Atlantic Ocean is possibly largely absent (Gooday 1988; Gooday and Hughes 2002).

Pair Y is a co-eval last interglacial unit with some similar lithofacies (FS) deposited during this interval in each core (9/97-10 and 9/97-03). The high degree of grain sorting (Fig. 9.9) implies that bottom currents could be winnowing out the finer material. The assemblages remain similar in core 9/97-10, despite the clear variations in BFAR present, which suggests that flux rates are not the main variable controlling populations of benthic foraminifera during this interval. However, flux rates do appear to have a secondary control on assemblages, with baseline flux rates too high (or probably too episodic) to support populations of *Rupertina stabilis* (Linke 1992), but sufficient for *Melonis barleeanum*, which is known to prefer areas of enhanced productivity (Fariddudin and Loubere 1997). The comparatively high proportions of *Epistominella exigua* (a seasonal "phytodetritus" indicator species (Gooday 1988; Turley *et al.*

1993; Thomas *et al.* 1995)) support the interpretation that flux rates were mostly episodic rather than continuous throughout the year during the last interglacial.

Pair Z is possibly indicative of down slope transport of sediment in cores 9/97-27/2 and 9/97-20. Samples 155.5cm and 159.5cm (9/97-27/2) cluster separately from the rest of the samples in this core (Fig. 8.20), which is shown in both cluster analysis and DCA plots for this core. These samples also record relatively high fragmentation indices, another indication of potential reworking of sediments. A similar pattern is present for the samples between 172.5-180cm in core 9/97-20, which suggests that this unit is potentially the result of down slope remobilisation, with material from a common original unit (and possibly species content) being deposited at both sites. The data perhaps implies that the high abundance of *U.celtica* (which is not present in such high abundance in the rest of the samples in core 9/97-20 but is present in other samples from core 9/97-27/2) recorded in core 9/97-20 is an artefact of this down slope transport. This interpretation also has potential implications for the age models of these cores, possibly explaining the relatively low correlation coefficient between GISP-II and core 9/97-27/2 for the lower part of this core (See Chapter 5).

8.5.6 Smaller size fraction (63-250μm)

The lack of clear, intra-core lithofacies group-cluster group linkages suggests that the smaller size fraction (63-250μm) is more prone to vertical mixing than the larger size fraction (250-500μm) where clear lithofacies-cluster group links are present. Some evidence that smaller particles are more prone to mixing when bioturbation occurs is available (Bard *et al.* 2001) and bioturbation is clearly evident on some of these cores (e.g. Figs. 8.1 and 8.3; Toms

in prep.). It is therefore probable that bioturbation is causing the smaller size fraction of benthic foraminifera to be mixed between different lithofacies. Alternatively, down slope transport of the smaller size fraction could be mixing species across different stages. It is likely that a combination of these mechanisms is responsible.

As the lithofacies group-cluster group links present for the larger size fraction are retained in the smaller size fraction for core 9/97-27/2, this implies that bioturbation (or downcore mixing) either does not occur or is relatively shallow.

Because it is not possible to separate the cores using either PCA or DCA based on the smaller size fraction assemblages (as it is for the larger size fraction) this suggests that down slope transport of the smaller benthic foraminifera may be occurring. This is possibly linked to bottom current activity, with the smaller fraction being preferentially winnowed out of the sediment and redistributed down slope via Ekman transport (perhaps within the benthic boundary layer; Dickson and McCave 1986) as bottom currents pass along the slope axis. The main bottom current driving this is likely to be located higher up on the slope, as the deeper cores (9/97-14 and 9/97-27/2) can still be separated out to some extent in ordination space (Fig. 8.25). An alternative hypothesis (that the distribution of taxa is driven by down slope remobilisation) is not supported by the lithological evidence, which shows little evidence of down slope transport of sediments (except in core 9/97-08). This hypothesis is also not supported by the fragmentation indices (which should be higher if down slope transport is occurring) or the larger size fraction assemblage data, which should also be affected to some extent.

The presence of *Cassidulina laevigata* aligned opposite to *Epistominella exigua* along the component 1 axis (Fig. 8.25), with *C.laevigata* associated with the higher portion of the slope (<2000m water depth) and *E.exigua* abundant in samples from the lower slope region (>2500m water depth) is consistent with the observations of Austin and Evans (2000). Their study showed a *C.laevigata* dominated assemblage group on the higher portion of the continental slope south of Iceland. This assemblage group was linked to a region of high productivity, with the *E.exigua* group linked to low productivity (but with a stronger seasonality). It is reasonable to assume that a similar trend is occurring along the depth transect examined in this study, with productivity decreasing with depth. This finding also correlates well with the proposed down slope productivity gradient inferred from BFARs (Fig. 8.14). It is interesting that this broad pattern of down slope species distribution is apparently still retained in this transect, despite some evidence that down slope remobilization of the smaller size fraction could be occurring. It could be linked to the dysoxia present at core site 9/97-27/2 (Chapter 7), which perhaps favours *E.exigua*. However, this would not prevent large numbers of *C.laevigata* being transported down slope. It could be due to a physical oceanographic barrier being present between core sites 9/97-14 and 9/97-27/2, such as an intermediate nepheloid layer (Dickson and McCave 1986), which would transport material away from the slope and into the water column and disperse the material over a wide area (White *et al.* 2005). These tend to form due to internal wave activity (Cacchione and Drake 1986). Internal waves are formed at the boundary between two water masses with different densities (Stow *et al.* 1998). Core site 9/97-14 is currently bathed in AAIW and core site 9/97-27/2 is bathed in NADW (Read 2001). If internal waves / nepheloid layer formation are responsible for creating a physical barrier between core sites, this could perhaps also partly

explain the DCA results of the large size fraction. This shows samples from the last glacial and last interglacial occupying similar ordination space, unlike the pattern for Holocene samples which display stronger inter-core separation.

The DCA plots show very discrete assemblages for each size fraction from each sample (Fig. 8.26). Also, the smaller size fraction data points are usually sparsely distributed compared to the tightly clustered larger size fraction data. The analysis also reveals a down slope increase in the density of clustering of the larger size fraction. Pairing between the larger and smaller size fractions of the sample at 43cm core depth in 9/97-04 appears to be linked to a unique occurrence of a high relative abundance of the taxon *Hormosina globulifera*. The ecological preferences of this taxon are relatively unknown as it is usually a minor component of the faunal assemblage and has therefore received little attention. It is not possible to comment upon why this species would occur in such high relative abundance in this particular sample. Equally, in core 9/97-14, the isolation of samples 11cm and 12.5cm appears to be linked to a high relative abundance of the species *Quinqueloculina arctica*. The ecological preferences of this species are also poorly defined.

8.6 Summary

The contourite deposits on the western flank of the Porcupine Bank contain diverse populations of benthic foraminifera that vary, both temporally and spatially. A few species from the >250μm size fraction appear to be restricted to portions of the slope (e.g. *Melonis pompilioides* >1500m water depth, *Rupertina stabilis* <2200m water depth and *Uvigerina*

celtica >1500m water depth), but most do not appear to be depth restricted in all facies (in particular, *S.schlumbergeri* and *C.wuellerstorfi*).

Whole dataset cluster analysis of the larger size fractions shows that assemblages in cores 9/97-08 and 9/97-27/2 are very different from those in cores 9/97-10, 9/97-04 and 9/97-14. Some inter-core clustering of samples during MIS 5 and MIS 3 is clearly evident, and this is also suggested by whole dataset DCA. Principle components analysis of all cores shows that four components explain two thirds (67%) of the variation in assemblage. These appear to be linked to presence / absence of seasonality or instability in food supply (components 1 and 2), food supply variations through time (component 2) and food supply changes with depth (component 4).

Last interglacial faunal assemblages and BFAR from all cores suggest that this interval mostly experienced oligotrophic productivity which was relatively enhanced compared to MIS 2. During MIS 3 in core 9/97-27/2 the accumulation of benthic foraminifera shows that some peaks appear to be associated with Heinrich events. Two peaks in BFAR are associated with H4 in the record of Peck *et al.* (2007), with peaks occurring either side of the event. It is possible that these are linked to episodes of methane hydrate instability, as identified by Kennett *et al.* (2000), but this is not conclusively proven. Faunal evidence suggests that there is an absence of the spring bloom during the last glacial (MIS 2). Taxa with a preference for spring bloom conditions (Uvigerinids, *Epistominella exigua*) are absent from parts of the last glacial and BFARs are significantly reduced for each core during this interval. No peak in BFAR is present between 9-12 kyr B.P., despite a good record of this interval preserved in the two deeper cores (9/97-27/2 and 9/97-20). This could be due to problems with the method applied by Nees *et al.* (1997), which assumed a linear sedimentation rate in each of the cores

examined in their study. Holocene assemblages from all cores imply that oligotrophic conditions prevail, but a seasonal spring bloom probably occurs, consistent with modern observations for this region (e.g. Gooday 1988).

The depth position of the highest relative abundance of *R.stabilis* appears to vary between cores 9/97-04 and 9/97-10 through time. During the last interglacial, this taxon is most abundant in 9/97-04, before peaking in abundance in both 9/97-04 and 9/97-10 in the latter stage of the last interglacial. The species is then most abundant in 9/97-10 during the last glacial before switching back to 9/97-04 in the Holocene. This is possibly due to variations in the strength and / or positioning of a stable bottom current, as suggested by Øvrebø *et al.* (2006).

Fisher's Alpha plots along depth transects for each time interval reveal a mid slope diversity maximum that is perhaps best explained by the dynamic equilibrium model of species diversity. This is supported by an inferred decrease in organic matter flux to the seafloor and an increase in environmental stability with distance down slope (inferred from sedimentology). The intersection between these two points could be producing the observed diversity maximum. The fact that the depth of this maximum does not shift during either glacial or interglacial depositional regimes implies that the environmental stability gradient does not alter through time.

It is possible to correlate cluster groups along slope, and this suggests that a time transgressive units is present between cores 9/97-20 and 9/97-27/2. This could explain the poor correlation coefficient for the lower part of core 9/97-27/2 in Chapter 5.

Cluster analysis of the smaller size fraction (63-250μm) reveals intra-core clustering that cannot be linked to individual lithofacies, unlike the larger size fraction. Preferential mixing of smaller foraminifera compared to larger foraminifera could perhaps explain this (Bard 2001). An exception to this is core 9/97-27/2, where a clear link between cluster groups and lithofacies is present. This is probably related to the dysoxia suggested for this core site in Chapter 7, which could limit the depth of burrowing of bioturbating organisms.

Nepheloid layers / internal waves have the potential to provide a physical barrier between core sites, and potentially explain the strong inter-core separation of assemblages revealed by cluster analysis and DCA, which could also explain the apparently greater degree of separation between cores in terms of assemblage composition during interglacials compared to glacial. During interglacials, there is a clear stratification of water masses (Chapter 7 and Read 2001), unlike during the last glacial where one water mass (GNAIW) dominates over all core sites (Chapter 7). This removes the interfaces between the different water masses that are necessary to generate internal waves / nepheloid layers and promotes environmental uniformity between the core sites. It is not clear if the proposed removal of these physical barriers enables certain species to expand their bathymetric ranges or if they are transported down slope. The generally relatively low fragmentation indices for the last glacial suggest that down slope transportation is the least likely mechanism.

9.1 Integrity of the record

Age models and taphonomic inferences developed for each of the six cores examined in this study show that the integrity of the record is variable. Core 9/97-08 contains sedimentological evidence of remobilization (Toms pers. comm.), although examination of the planktonic foraminifera records shows (via examination of *%N.pachyderma* (sin.)) some consistency in terms of cold and warm phases are preserved which suggests that a rough stratigraphy is still present in the upper part of the core. Cores at intermediate water depths (1230-2118m) preserve a relatively (compared to lower on the slope) low resolution (approx. 2kyr.cm^{-1}) record of glacial-interglacial climate variations (as suggested by *%N.pachyderma* sin.) with some apparent hiatuses present (particularly during Marine Isotope Stage 3 in cores 9/97-04 and 9/97-14). The relatively large (approximately 40-50 kyrs duration) hiatus in core 9/97-04 is linked to a sharp contact in the sedimentological record and causes problems for BFAR calculations (Fig. 8.6). Deeper cores (>2118m water depth) appear to contain a high-resolution (sub-millennial scale, approx. 0.2kyr/cm^{-1}) record extending back to approximately 45 kyr B.P. These deeper cores appear to suffer from some minor disturbance, particularly during MIS 3 where correlation with a reference curve becomes more problematic.

A pair of correlatable cluster groups are present in the two deeper cores, within the problematic (with regards to correlation of core 9/97-27/2) interval (Fig. 8.20). The time-transgressive nature of this correlatable unit could suggest that this is evidence of down slope remobilization of sediment. This interpretation is perhaps supported by the relatively poor clustering of the benthic foraminifera assemblages from these units within each individual

core and the relatively high fragmentation indices for this unit. If down slope remobilization has occurred, this could explain the poor correlation of this section of core 9/97-27/2 (see Chapter 5), perhaps by introducing 'warm water' taxa into the planktonic foraminiferal assemblages and therefore altering the original *%N.pachyderma* (sin.) data. An alternative explanation, that these units represent environmental uniformity, seems less likely as both units record relatively high fragmentation indices and, especially for core 9/97-20, contain a relatively distinctive fauna compared to adjacent units. The result of the transfer function analyses for these units reveals very high dissimilarity coefficients, which suggests that they both lack good modern analogues in the training dataset and that they may have undergone post-mortem modification. Each core presents a variable sedimentation rate which does not display any clear co-variation with lithofacies. Although in core 9/97-10 some interglacials record relatively high sedimentation rates compared to glacials (see Fig. 5.3), this pattern is not observed throughout the whole core and is not present deeper down the slope in cores 9/97-20 (Fig. 5.18) and 9/97-27/2 (Fig. 5.15).

For some cores, the combination of high sedimentation rates and sampling has produced a highly resolved (approximately 200 yr.cm-1) record of high frequency SST variability during MIS 3. These variations occur with a frequency of 3-4 kyrs in cores 9/97-27/2 and 9/97-20 and are too high a frequency to be recorded in the low resolution records higher on the slope (2cm .kyr^{-1}, sampling every 4cm), although some variation in SST is still preserved (e.g. Fig. 6.4). Reconstructed summer SSTs for this stage in core 9/97-27/2 show temperatures varying quasi-cyclically between an interstadial average of 17-18°C to a stadial average of 3-7°C within 3-4 kyrs (as suggested by ^{14}C AMS radiocarbon dating), consistent with the Dansgaard-Oeschger cycles associated with GI-8 and 12 in Scourse *et al.* (2009).

Evidence from examination of the assemblages of benthic foraminifera shows that some assemblage groups can be correlated along the slope (Fig. 8.18) and down slope (Fig. 8.16). Assemblage groups from MIS 3 and the last interglacial in core 9/97-10 (1260m water depth), 9/97-03 (1230m water depth) and 9/97-04 (1502m water depth) contain similar species compositions, unlike last glacial and Holocene assemblage groups, which display a comparatively spatially restricted distribution. One explanation for this could be that conditions across this section of the slope are relatively uniform during the last interglacial and MIS 3, expanding the range at which the key species in the assemblage groups can occupy successfully. Alternatively, this could reflect down slope transport of sediments (and foraminifera) which is redistributing specimens across a wider area, perhaps due to the influence of stronger bottom currents. The grain size distribution curve produced for one of these cores (9/97-10 – see below) by Toms (in prep.) shows that sediment grains are uni-modal, well sorted and sand dominated. This could be an indication of grain size sorting via bottom current activity, with high velocity currents winnowing out the finer material. Ekman divergence resulting from this could then cause the down and along slope redistribution of foraminifera. However, it is important to note that the sediment samples that were prepared for grain size studies were not de-calcified (acid leached) prior to analysis. As increased productivity could also feasibly produce foraminiferal sand units that are well-sorted, it is not possible to determine absolutely that bottom current activity has increased based on these data.

Fragmentation indices suggest that fragmentation of foraminiferal tests is more frequent during interglacials and interstadials compared to glacials and stadials. This pattern of improved preservation during glacials compared to interglacials has been observed in other localities (e.g. the Nordic Seas; Helmke and Bauch, 2002) and has led to the suggestion that

this is caused by enhanced productivity, which causes dissolution due to increased acidification of the benthic environment following aerobic respiration. Increased aerobic respiration increases the concentration of CO^2 in the sediments, acidifying pore waters and dissolving foraminiferal tests. An alternative explanation is that interglacial seawaters are perhaps more acidic than glacial seawaters due to increased atmospheric CO^2, which increases ocean acidification following air-sea exchange (Barker and Elderfield 2002). Although this is potentially a problem for geochemical studies, careful sample selection (e.g. only picking 'glassy' specimens; Sexton *et al.* 2006) should avoid this. For assemblage studies, this is perhaps more of a problem, and could partially explain the lack of good modern analogues for sea surface temperature estimates via transfer functions (see Chapter 6), following the dissolution series (see Fig. 3.3) of Hemleben *et al.* (1989). However, many of the planktonic assemblages from interglacial units contain high percentages of *G.bulloides* (see Appendix A), which is considered to be more susceptible to dissolution compared to other taxa (e.g. *N.pachyderma* sin.). Assuming the dissolution series proposed by Hemleben *et al.* (1989) is correct, if dissolution were influencing assemblages, an increased concentration of *G.bulloides* is unlikely. It could be that although dissolution is increased relative to glacials, it is not strong enough to alter assemblages of foraminifera significantly.

Sr/Ca data are used as a proxy for selective dissolution of individual samples, as they have been shown to co-vary with carbonate ion concentration (Stoll *et al.* 1999). Based on this assumption, data from core 9/97-14 suggest that some samples have undergone selective dissolution, as evidenced by depleted Sr/Ca values. Selective dissolution is a problem for estimating reliable bottom water temperatures from Mg/Ca values and determining phosphorus concentrations from Cd/Ca. The occurrence of selective dissolution could be due

to the expansion of colder, more corrosive Southern Component Water (particularly AABW). However, this should also produce a dissolution signal in the deeper cores (9/97-27/2 and 9/97-20), which is not evident.

Examination of benthic foraminifera cluster grouping differences between a smaller (63-250μm) and larger (250-500μm) size fraction suggests that smaller size fraction foraminiferal assemblages are much more mixed, both within cores and between different core sites. However, the shallowest and deepest cores are relatively distinctive in terms of assemblages of foraminifera in both size fractions. The cluster grouping differences between the two size fractions make sense in light of the study by Bard (2001). This study proposed that smaller sized particles are preferentially prone to vertical mixing in a core compared to larger sized particles, which would explain the lack of clear lithofacies related cluster groups in the smaller size fraction (as opposed to the larger size fraction). Another potential explanation is that bottom current activity is preferentially winnowing the smaller size fraction and redistributing the tests across the transect area. Grain size data for glacial sediments in core 9/97-10 (see below) shows very poor particle sorting which suggests that bottom currents may not have been very strong on this part of the slope during this interval, which implies that physical bottom current reworking is not as significant as vertical mixing. A combination of these two mechanisms therefore remains possible. Also, any interpretations based on examination of small sized particles (Bard 2001) should perhaps be regarded with caution, as the analysis presented in this study shows that smaller particles may be more prone to mixing. The presence of clear core depth related cluster groups in core 9/97-27/2 suggests that the finer particle mixing that may be present higher on the slope is relatively absent at this site. This potentially suggests that bioturbation is limited (in terms of depth of burrows). A

restriction of bioturbation could be due to a lack of food, but as productivity (inferred from BFAR) is potentially very high during some interstadials (Fig. 8.11), this seems unlikely. Another possibility is that bioturbation is limited by oxygen depletion.

Mn/Ca data for core 9/97-27/2 show that every sample contains an Mn/Ca concentration greater than 150μmol/mol. When foraminiferal tests record Mn/Ca values this high, this suggests that foraminiferal test coatings of manganese oxide have formed. As shown by Boyle (1983), manganese oxide coatings form under dysoxic conditions. The data in this case suggest that dysoxic conditions have been present over this core site throughout the depositional history of this core. As Boyle (1983) also showed, manganese oxide coatings can cause preferential enrichment of some of the trace metals of interest (particularly barium and cadmium), which makes the application of these two to palaeoceanographic studies over this core site impractical. The dysoxia suggested by the Mn/Ca data is not suggested by the modeled data by Read (2001). It is probable that the resolution of the model produced by Read (2001) may be too coarse to detect dysoxia if it is localized to the core site and immediate area. Alternatively, problems with obtaining surface sediments from gravity coring could result in the loss of uppermost Holocene sediments, which could be well oxygenated in accordance with the model. However, it seems unlikely that a core site that displays persistent dysoxia from approximately 45 kyr B.P. to the Recent would switch to being well oxygenated at the present day.

The consistent manganese enrichment is indicative of continuous oxygen depletion over 9/97-27/2, despite clear changes in sedimentology and assemblages of benthic foraminifera (including a presumably healthy infaunal component – see Chapter 8). This suggests that very little particle reworking has occurred in this core, particularly via

bioturbation by macrobenthos (Aller 1990) and suggests that although oxygen must be present to support some of the species of benthic foraminifera which live at depth in the sediment (e.g. *M.barleeanum*; Jorissen *et al.* 1998) the oxygen is probably very quickly utilized and could potentially be a limiting factor on populations of foraminifera.

9.2 Inferences from assemblage / geochemical data

The general pattern of warmer interglacial episodes alternating with colder glacial episodes over the last 500 kyrs (McManus *et al.* 1999; Kandiano and Bauch 2003) is preserved in the cores at intermediate water depths (particularly at approx. 1100-1300m water depth). This is reflected in the sedimentology with alternations of lighter and darker coloured units (Figs. 5.3 and 5.8) and in the reconstructed sea surface temperatures for these cores (Figs. 6.4, 6.6 and 7.1). Close coupling between variations in sedimentology and variations in climate appears to be restricted to this part of the slope, with cores higher and lower on the slope recording strong variations in SST which are not always reflected in the lithostratigraphy. The result of spectral analysis of the oxygen isotope profile for core 9/97-10, demonstrate that the cycles of glacial-interglacial climate change present in this core are orbitally paced (see Fig. 5.7). Within this general glacial-interglacial pattern, smaller scale processes and events have been identified.

Sea surface temperatures have been reconstructed using transfer functions applied to fossil assemblages of planktonic foraminifera, and (in core 9/97-10) these generally conform with those obtained from transformation of oxygen isotope ratios. Both records are consistent in recording the coldest and warmest SSTs during MIS 12 and 11 respectively. These

intervals also record relatively high sedimentation rates in cores 9/97-10 and 9/97-03. A lack of foraminiferal accumulation rate data during this interval means it is not possible to determine if this is due to increased pelagic production or terrigenous input.

Apparent stability in SSTs (estimated from transfer functions) during MIS 5 coincides with the increased influence of AAIW (Fig. 7.12) in cores 9/97-10 and 9/97-04 inferred from paired $\delta^{13}C_{benthic}$ and phosphorus data. This contrasts with the MIS 3 records in these cores, where unstable SSTs correspond with an overall dominance of GNAIW inferred from the $\delta^{13}C_{benthic}$ / phosphorus plots, which suggests that AAIW may be responsible for stabilizing North Atlantic sea surface temperatures. However, MIS 2 SSTs are also apparently stable in both cores, despite the clear dominance of GNAIW, and Holocene SSTs are relatively unstable despite an AAIW signal being detected in cores 9/97-04 and 9/97-14. It seems more reasonable to propose, based on these data, that when AAIW or GNAIW flux crosses a threshold value, this results in relative stability in SSTs. It is necessary to consider though that the actual reconstructed SSTs are perhaps unreliable due to the lack of good modern analogues of the preserved assemblages and hence the apparent stability may in fact indicate a lack of transfer function sensitivity to sea surface temperature change. Also, due to proximity to the BIIS (see Chapter 2), this could be causing stability in SSTs during MIS 2, which might not be present at other sites in the North Atlantic, perhaps via expansion of the ice sheet margin close to this site and imprinting a regional signal on this record.

Last interglacial assemblages of benthic foraminifera suggest that oligotrophic conditions prevailed (see Chapter 8) and unconstrained cluster analysis of the whole dataset shows that inter-core clustering is common during this interval at intermediate depths (1230-1502m water depth). Also, as discussed above, the results of geochemical studies show that a

strong AAIW influence was present over these core sites. A potential link between the dominance of AAIW and increased environmental uniformity between core sites at intermediate depths could be proposed on this basis. Perhaps the absence of water mass stratification between these core sites facilitates improved oceanographic mixing, perhaps via deep convective mixing (Holliday *et al.* 2000) or eddy stirring (Sherwin *et al.* 1999) between these sites. This potentially leads to the interpretation that an AAIW assemblage group could be proposed for the last interglacial. However, the conditions that could be causing environmental uniformity between the core sites are probably due to other factors, such as increased productivity (see Fig 8.14) which increases the bathymetric range of some taxa, e.g. *Rupertina stabilis*. The expansion of AAIW during this interval as well is more likely to be coincidental, as water masses have been demonstrated to have a negligible influence on assemblages of benthic foraminifera (Jorissen *et al.* 2007). However, it also remains possible that properties of certain water masses (e.g. refractory / labile nutrient input, alkalinity etc.) could also impact on assemblages of benthic foraminifera, if not as the primary factor.

Marine Isotope Stage 3 is characterized by stadial-interstadial variations in SST and benthic foraminifera (assemblages and accumulation rates) in cores 9/97-27/2 and 9/97-20. Assemblages of benthic foraminifera are highly variable in terms of specimen abundance (not species content) in the deeper cores (9/97-27/2 and 9/97-20) during MIS 3. Interstadial sediments contained relatively large numbers of benthic foraminifera (usually dominated by *U.celtica*) where as stadials are usually relatively barren of benthic taxa (Fig. 8.10). Assemblages higher on the slope do not display this level of variability and instead appear homogenized, and can even be correlated down slope (Fig. 8.16). No assemblages higher on the slope than 2756m contain assemblages with *U.celtica* as the dominant taxon or are

significantly similar to the interstadial assemblages in terms of species composition (Figs. 8.16 and 8.21a). As the species content also does not change significantly during MIS 3 in both 9/97-27/2 and 9/97-20 this suggests that the interstadials may not be artifacts of down slope remobilization of sediment. The dominance of *U.celtica* is indicative of an unstable but occasionally very high flux rate regime (e.g. Fontanier *et al.* 2002; Fontanier *et al.* 2006). This feature of MIS 3 productivity is observed for the duration of this stage in core 9/97-27/2.

Opportunistic taxa (*U.celtica* and *E.exigua*) are abundant during interstadials but relatively absent during stadials in these deeper cores, apparently exploiting the intermittent food supply and phytodetritus deposition that occurs during this interval. A strong negative carbon isotope excursion is present at 43.8 kyr B.P., and appears to pre-date H4 in the record of Peck *et al.* (2007) by approximately 4kyr B.P. Two peaks in BFAR in core 9/97-27/2 (at 85 and 241cm core depth) follow this and are associated with variable benthic carbon isotope values and SSTs (Fig. 9.1). The peaks are rapid (constrained to occurring within 1 kyr) and imply greatly enhanced productivity (approximately 5-7 times higher compared with adjacent sample values). The lower peak (40.3 kyr B.P.) precedes H4 (as dated by Peck *et al.* (2007)) and the second (37.7 kyr B.P.) follows it, although the second peak could be due to the relatively low sedimentation rate at this point (Fig. 5.15). Comparison of the benthic foraminifera preserved during this interval with those from shallower cores (Fig. 8.16) shows that the assemblages within the peaks are more similar to adjacent samples within the core than they are to assemblages higher up on the slope. This appears to rule out down slope transport as a causal mechanism for the deposition of these peaks. It seems more likely that this is a record of one (possibly two) peaks in productivity (BFAR) which are perhaps related to a Heinrich event. An alternative explanation could be inferred from examination of the

grain size data (Fig. 9.2), which shows that the sediments associated with the lower peak are well-sorted sands and implies that these peaks in BFAR are caused by winnowing of sediments due to enhanced bottom current activity, which would concentrate benthic foraminifera and increase BFAR, provided that the age model developed for this core does not detect this and account for it. However, as mentioned previously, the samples used for grain size study were not acid leached prior to analysis so it is not possible to determine if the grain size sorting is a productivity signal or due to winnowing of the sediment.

Marine isotope stage 3 records enhanced productivity at all depths relative to MISs 4 and 2 (Fig. 8.14). In the deeper cores (9/97-27/2 and 9/97-20) BFAR is highly variable, consistent with the SST data in suggesting that episodes of sea-ice cover alternate rapidly with periods which potentially experienced ice free conditions (Fig. 6.13 and 6.15). Ice free conditions would enable surface productivity to reach levels comparable to modern values, either via reduced stratification of the upper water column or by enabling phytoplankton to utilize sunlight. Sea-ice cover would suppress productivity by preventing phytoplankton blooms. However, this pattern is potentially complicated by the incorporation of reworked units into the core (Chapter 8).

In core 9/97-04, Marine Isotope Stage 3 is significantly truncated (See Fig. 5.10). Samples from this interval contain abundant *C.wuellerstorfi* and *C.laevigata* (small fraction) and a relatively strong negative $\delta^{13}C_{benthic}$ value (38cm core depth, approximately 41.3 kyr B.P.) is present. The negative benthic carbon isotope value is broadly co-eval with H4 in the record of Peck *et al.* (2007), although the signal in this core appears to pre-date theirs slightly by 1-2 kyrs. However, this sample is adjacent to a major hiatus (see Fig. 5.10) in the sedimentological record, which could cause material from a significantly older time interval

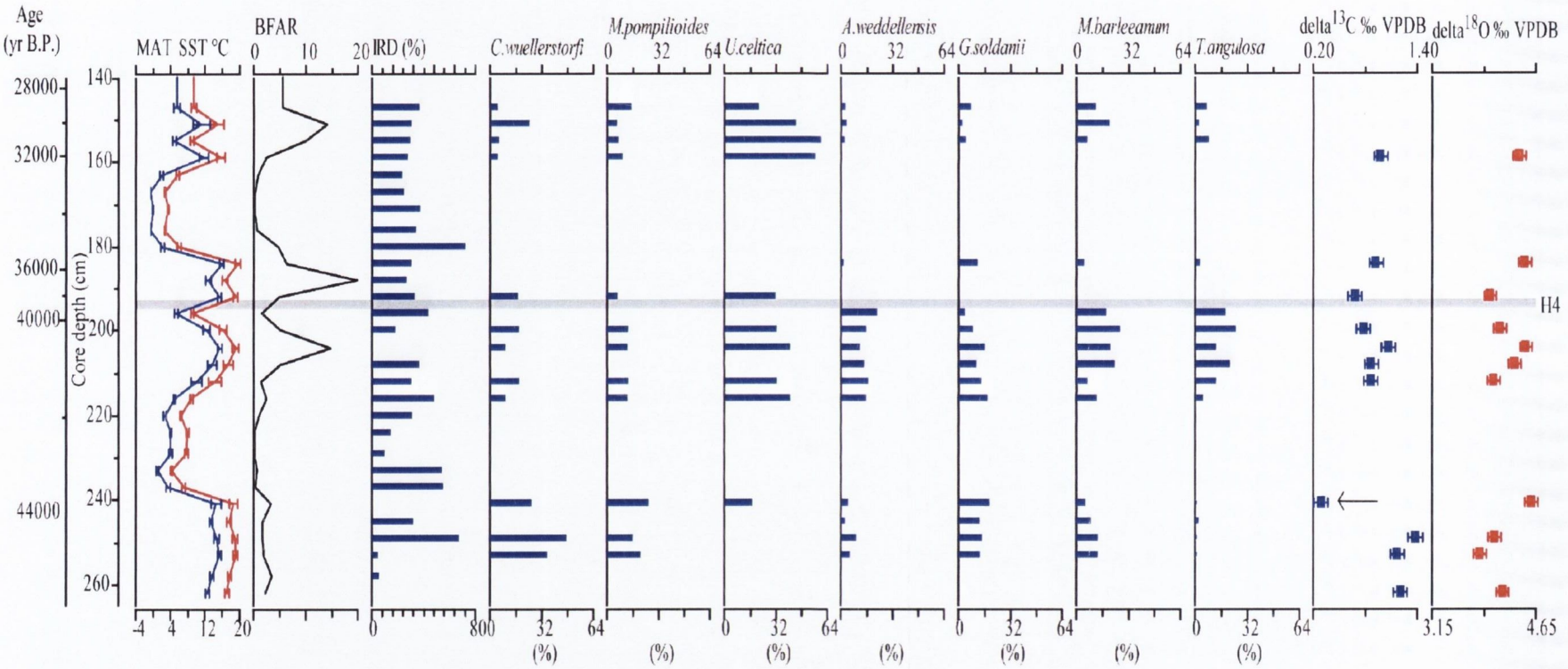

Figure 9.1. Multi-proxy record of MIS 3 in core 9/97-27/2. Note the strong negative delta^{13}C value (arrow) approximately 4kyrs before H4 (as dated by Peck *et al.* 2007 - grey band). For MAT SST, red line = summer values, blue line = winter values. IRD (%) is the percentage of IRD grains in the greater than 150 micron size fraction, courtesy of Toms (in prep.).

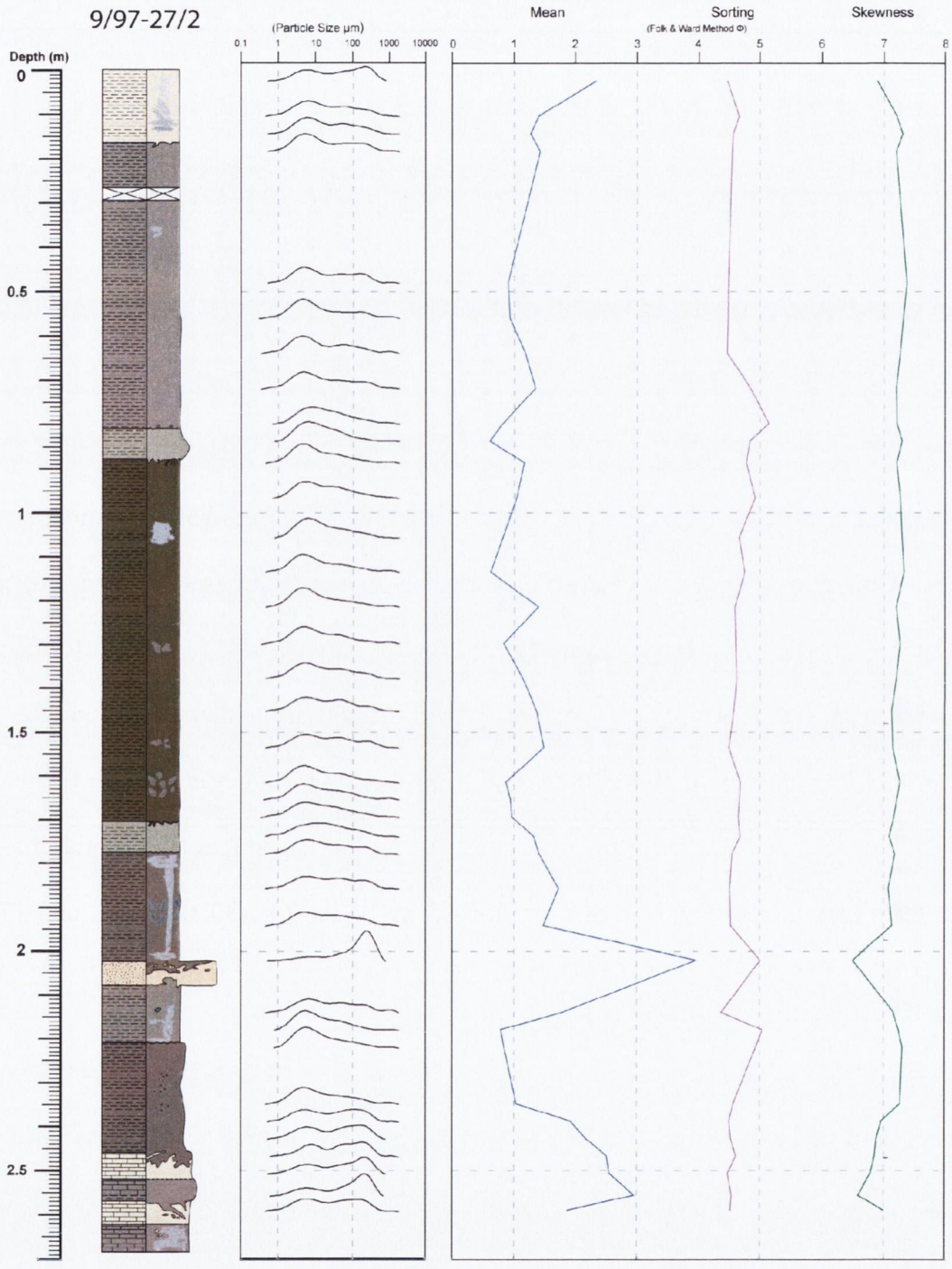

Figure 9.2. Results of particle size analysis results for core 9/97-27/2, courtesy of Toms (in prep.).

(e.g. the previous interglacial) to become incorporated into the MIS 3. Any data obtained from samples at or adjacent to this hiatus are therefore unreliable due to the potential for significant reworking.

Examination of benthic foraminifera during MIS 2 suggests that none of the species indicative of spring bloom deposition (Uvigerinids and *E.exigua*) are present in the deeper cores. This leads to the interpretation that the phytoplankton spring bloom currently present in this part of the NE Atlantic Ocean was absent during this stage. This assumes that these key species have not been removed by post-mortem modification of assemblages (or perhaps dysoxia / anaoxia). Such an interpretation conforms with evidence from examination of assemblages of planktonic foraminifera, which lack sub-polar species (see Section 3.6) and suggests that sea-ice may have formed over this site (Kucera *et al.* 2005). Sea-ice formation would reduce surface productivity by limiting phytoplankton from acquiring sunlight for photosynthesis. Reduced productivity during this stage is also suggested by the relatively reduced BFARs for this interval in all cores (Fig. 8.14). Three main stages of potential sea-ice development are identified in core 9/97-20 at 30-31.5 kyr B.P., 29.1-30.3kyr B.P. and 17.3-25kyr B.P.

The high abundance of 'low productivity', epifaunal taxa, combined with the absence of *E.exigua* (small fraction) during MIS 2 in core 9/97-10 supports the proposed sea-ice cover, which would suppress productivity and, during episodes of perennial sea-ice cover, shut off the seasonal phytoplankton bloom. Marine Isotope Stage 2 assemblages of benthic foraminifera from core 9/97-04 are dominated by *Melonis barleeanum*, *Sigmoilopsis schlumbergeri* and *Pullenia bulloides*. This is a mixed assemblage, containing taxa associated with relatively enhanced productivity (e.g. *Melonis barleeanum*; Farriduddin and Loubere

1997) and reduced productivity (*Pullenia bulloides*; Altenbach *et al.* 1999). Core 9/97-27/2 is relatively barren of benthic foraminifera during MIS 2 (numbers are not sufficient for cluster analysis, in most samples $n < 40$). This is consistent with a shut-down in surface productivity.

Marine Isotope Stage 2 also contains few samples with sufficient numbers of benthic foraminifera (minimum 40 specimens) for reliable estimates of relative abundance in core 9/97-27/2, despite no significant difference in sedimentation rates (see Chapter 5). This is possibly also the result of the perennial / seasonal sea-ice cover suggested for this interval (Fig. 6.14), which would reduce surface productivity. The high Mn/Ca values in this core provide an alternative explanation; that bottom water oxygen content was significantly reduced (see above), which could also limit the number of benthic foraminifera. However, as all samples from this core have high Mn/Ca values this would be expected to affect the whole core (i.e. MIS 3 as well), not just this interval. The carbon isotope record for this interval implies that the site was possibly continually bathed in the glacial equivalent of AABW (see Fig. 7.7), but bottom waters by themselves do not exert a great influence on assemblages of benthic foraminifera (Jorissen *et al.* 2007).

The sample at 23cm core depth in core 9/97-14 corresponds with a slight negative excursion in the benthic $\delta^{13}C_{benthic}$. An isolated occurrence of *E.exigua* is also present in this sample, which suggests that the seasonal phytoplankton bloom is present temporarily during MIS 2. Alternatively, the relatively depleted Sr/Ca value recorded in this sample suggests that it could have undergone dissolution (Fig. 7.6). The sample also records high Cd/Ca and Mg/Ca values, which should also be relatively depleted if selective dissolution has occurred (McCorkle *et al.* 1995). This suggests that dissolution may not have occurred in this sample, or that it is not strong enough to significantly alter geochemical records. The high Cd/Ca

value, combined with low carbon isotope values suggests that this sample could be recording an expansion of AABW (Fig. 7.6). This expansion of AABW occurs at 27kyr B.P. and precedes H2, as dated by Peck *et al.* (2007), by approximately 2.5kyrs. Another sample with low carbon isotope values and increased Cd/Ca suggesting expansion of AABW flux is also present in this core at 19kyr B.P., preceding H1 (as dated by Peck *et al.* 2007) by approximately 2kyrs. No peak in *E.exigua* is recorded in this sample.

As discussed in Section 7.6, the sample at 15cm (16.4 kyr B.P.) core depth in 9/97-10 recorded a low planktonic carbon isotope value which is potentially linked to a breakdown in surface ocean stratification during Termination 1 / H1 as it is co-eval (within dating uncertainties) to H1 (16.8 kyr B.P.) as dated by Peck *et al.* (2007) . A co-eval increase in the relative abundance of *C.kullenbergi* in this sample, could suggest that the influence of MOW has increased over this core site relative to adjacent samples (see Section 2.4). This interpretation is not supported by examination of the geochemical data for this sample (Fig. 7.12), which suggests that a strong GNAIW influence is present. *Cibicides kullenbergi* has also been linked to high velocity bottom currents (Rasmussen *et al.* 2002), but this interpretation is not supported by the grain size data for this interval which shows that the sediments consist mainly of poorly sorted muds, implying low velocity bottom currents (see below). It is not possible, based on this data, to determine the ecological preferences of this taxon.

Holocene sea surface temperatures are warmer than glacial (MIS 2 and 3) SSTs. Average SSTs for the Holocene differ in the records of intermediate depth and deeper depth sites (Figs. 6.11 and 6.16). The composite intermediate depth record suggests that SSTs were on average 19°C during the summer, compared with 15.5°C from the composite deep site

record. This discrepancy is probably due to the low resolution of the intermediate depth sites, with warm water taxa becoming incorporated into assemblages that were originally deposited under cooler SSTs following bioturbation. An average summer SST of 15.5°C reconstructed from deeper sites (9/97-27/2 and 9/97-20) is compatible with modern oceanographic observations for this region (Pflaumann *et al.* 1996) and from previous reconstructions from a nearby locality (Kandiano and Bauch 2003). An average seasonal difference in SST of 4.0-4.2°C is also broadly comparable to the modern average seasonal difference in SST (3.8°C) for the whole North Atlantic Ocean, with the slight increase from the average probably due to the location of this study area at temperate latitudes (which experiences larger seasonal differences in SST than the polar or tropical regions).

The Holocene $\delta^{18}O_{sw}$ values in cores 9/97-10 and 9/97-04 are similar (0.0 to -0.1‰$_{VPDB}$) suggesting limited stratification between 9/97-10 and 9/97-04. Core 9/97-14 records a very different $\delta^{18}O_{sw}$ value (1.24‰ VPDB) for the Holocene. This suggests that this site is flushed by a water mass with a very distinctive density. Other data ($\delta^{13}C$ / phosphorus) points to this site being bathed in AAIW during the Holocene, consistent with modern observations (Read 2001). There are two possible explanations for the distinctive $\delta^{18}O_{sw}$ value in the Holocene of core 9/97-14. The first is that this core site is located at a depth that currently experiences relatively rapid geostrophic current velocity (see Fig. 2.1; Chapter 2). This significantly increased geostrophic current velocity is translated into a denser $\delta^{18}O_{sw}$ value (or higher salinity), following the transformation of Lynch-Stieglitz *et al.* (1999). The salinity difference suggested by this is approximately 2‰, which is probably unrealistic given the salinity profile estimated for this region by Read (2001) which shows salinity varying by at most 1‰ in the modern NE Atlantic Ocean. Alternatively, selective dissolution of

foraminifera could preferentially reduce the Mg content of calcite tests (McCorkle *et al.* 1995), which would suggest colder bottom waters and therefore higher density $\delta^{18}O_{sw}$.

Assemblages of benthic foraminifera display a clear bathymetry related pattern of distribution. Assemblages at 1260m water depth (core 9/97-10) are dominated by *C.wuellerstorfi*, *K.bradyi*, *S.schlumbergeri*, *M.barleeanum* and *E.exigua* (small fraction). At 1502m water depth, samples contain a similar faunal assemblage, only with abundant *R.stabilis*, *C.kullenbergi* and *C.laevigata* (small fraction) in addition to the taxa dominating at 1260m water depth. *Cibicides wuellerstorfi*, *R.stabilis*, *K.bradyi*, *S.schlumbergeri* and *E.exigua* (small fraction) dominate assemblages at 2118m water depth. At 2756m water depth, *C.wuellerstorfi*, *C.kullenbergi*, *K.bradyi*, *S.schlumbergeri*, *M.barleeanum*, *M.pompilioides*, *A.weddellensis* (small fraction) and *E.exigua* (small fraction) are the dominant taxa. The relative dominance of *C.wuellerstorfi*, *S.schlumbergeri* and *K.bradyi* at all depths is indicative of a generally oligotrophic productivity regime, perhaps with some bottom current influence at sites between 1502-2118m water depth suggested by the large epifaunal component (*R.stabilis* and *C.wuellerstorfi*). The high abundance of *M.barleeanum* and *E.exigua* (small fraction) is compatible with the modern observation of a seasonal phytoplankton bloom in surface waters leading to the deposition of a spring a 'phytodetritus layer' (Gooday 1988; Thomas *et al.* 1995).

9.3 Wider implications

9.3.1 Pre-MIS 5

The observation of a step-wise warming in the transition from Marine Isotope Stage 12 to 11 in the reconstructed sea surface temperature (SST) record preserved in core 9/97-03 (Fig. 6.6) suggests that the bipolar seesaw mechanism proposed by Broecker (1998) did affect North Atlantic SSTs during this glacial termination (Fig. 9.3; Section 2.4). As this phenomenon is not recorded in the deeper water profiles of other studies (Poli *et al.* 2000; Hall and Becker 2006) this could have only affected surficial and, possibly, intermediate depth circulation. However, closer inspection of the benthic $\delta^{18}O_c$ record produced by Poli *et al.* (2000) for ODP site 1063 (4595m water depth) shows a strong, short-lived increase in $\delta^{18}O_c$ during the transition from MIS 12 to MIS 11 (Fig. 9.3). Although this is not remarked upon in the publication, it could be related to the step-wise warming observed in the SST data. More work is required to determine if this stepwise warming did occur or whether this is an artifact of the transfer function methods applied (see sections 6.2 and 6.4 – discussion of reliability of absolute values obtained via transfer functions). A comparative study, perhaps using an independent proxy to verify this, is required.

The record of relatively high sedimentation rates during MIS 11 and 12 in cores 9/97-10 and 9/97-03 (Figs. 5.3 and 5.8) could be due to enhanced pelagic production. A lack of faunal accumulation rate data for this interval makes it impossible to determine this based on currently available data. However, that interpretation would make sense in light of the proposals of Barker *et al.* (2006), who suggested that pelagic production increased significantly during this interval in response to enhanced atmospheric carbon dioxide levels

(see Section 2.3). Alternatively this could be due to enhanced sediment focusing by currents onto this portion of slope during this interval. Testing this hypothesis should be relatively straightforward, only requiring the acquisition of accumulation rate data for fauna and sediments during this interval and comparing the two to determine which has increased. An examination of fragmentation / corrosion would also be necessary to determine the taphonomic effects during this interval and improve accumulation rate reliability.

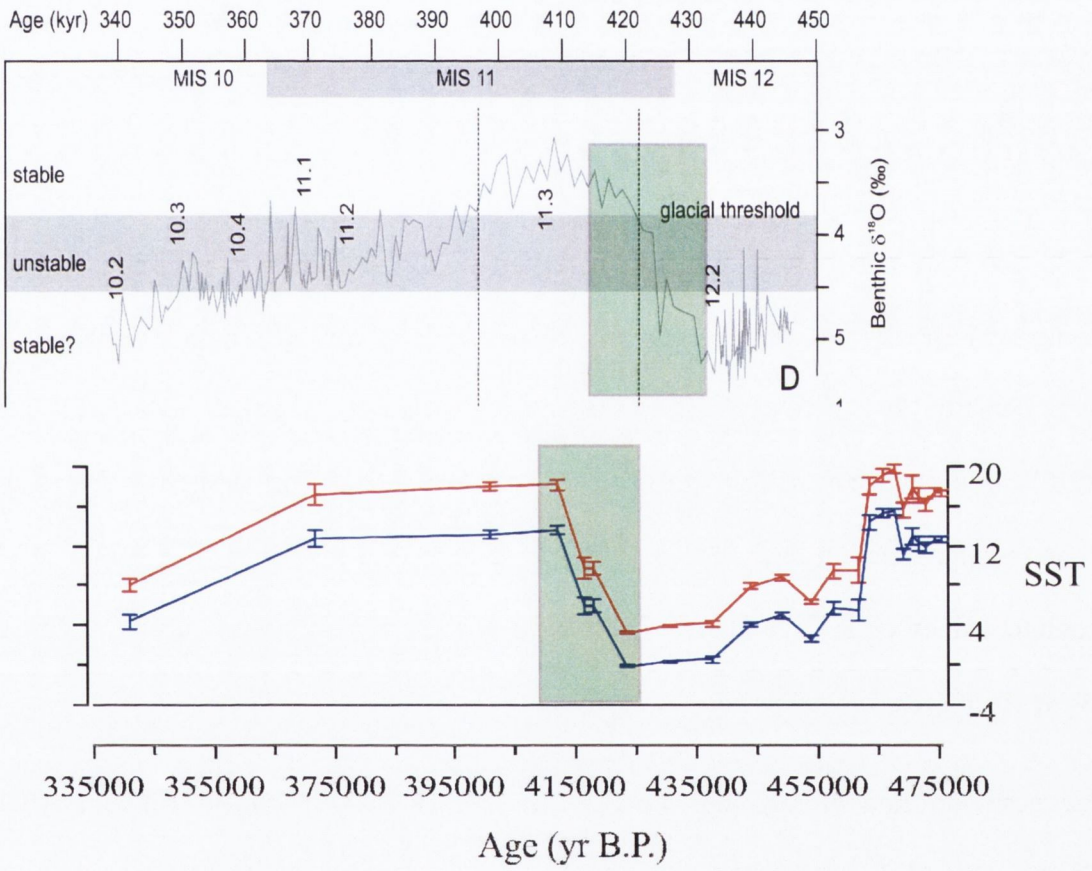

Figure 9.3. Comparison of MAT derived SST summer values from the composite SST record of Chapter 6 with the benthic $\delta^{18}O$ record of Poli *et al.* (2000) for MIS 11-13 (10.2, 10.3 etc. refer to sub-stages of each marine isotope stage). Note the step-wise increase in the SST values at the termination of the MIS 12 glacial in the composite SST record.

A possible Heinrich-like event is recorded in MIS 8 in core 9/97-10 (Fig. 7.1), characterized by a relatively strong (>0.5‰$_{VPDB}$) planktonic negative carbon isotope excursion preceding the deposition of IRD (ice-rafted detritus) (Fig. 3.1). The relative timing of these two events is consistent with more recent Heinrich events from MIS 2 (see below), which show a strong negative carbon isotope excursion preceding the deposition of IRD (e.g. Peck *et al.* 2007). Absolute dating of these two peaks (how close they are to each other temporally) is less well defined and would require further research to determine reliable ages for these two peaks. Also, the carbon isotope excursion could be caused by a range of alternative mechanisms (e.g. dissolution, methane hydrate release) and the cobble (Fig. 3.1) could be reworked. Finding a similar interval in other cores is required and a provenance study of the IRD recovered would also be of interest to determine the source region for this.

9.3.2 AAIW / GNAIW climate stability

The last interglacial (MIS 5) is recorded by relatively warm SSTs, with the planktonic oxygen isotope record suggesting they may have been even higher than Holocene values (see Fig. 7.1). There is no evidence of sea-ice cover and reconstructed values for the composite record (Fig. 6.11) show that sea surface temperatures are relatively stable (19-21°C summer, 15-17°C winter) compared to MIS 3. The appearance of stable sea surface temperatures could result from mixing of the sediments for this interval (either from the actions of bottom currents or bioturbation), with cold phases mixing with warm phases to produce a consistent planktonic faunal assemblage throughout (which would produce similar SST values following the application of a transfer function or modern analogue method). A lack of good modern analogues for most of the fossil assemblages suggests that this is a possibility. A less stable

record of SSTs for MIS 5 is suggested by the oxygen isotope data (Fig. 7.1) and other reconstructions (e.g. Kandiano and Bauch 2003).

This stage also displays a similar water mass configuration to the Holocene (Fig. 7.13), with a stratified water column incorporating NADW (North Atlantic Deep Water) and AAIW (Antarctic Intermediate Water). All three sites at intermediate water depths (1260-2118m water depth) record an increase (relative to glacial values) in refractory nutrient content and SCW (Southern Component Water) influence following increases in Ba/Ca (refractory nutrients) and Cd/Ca (phosphorus/ labile nutrients) respectively. Comparable $\delta^{18}O_{sw}$ values at each water depth (Fig. 7.9) suggest that mixing between these sites could be quite strong. Combined phosphorus and $\delta^{13}C_{benthic}$ data also suggest that a stronger influence of SCW is present at site 9/97-10 during the last interglacial than during the Holocene (Fig. 7.12) which implies that AAIW may have been more vertically expansive along the slope during MIS 5 compared to the modern distribution of this water mass (Fig. 7.14). This finding, coupled with the stable SST values proposed above, is consistent with the hypotheses of Lassen *et al.* (2002) and Rickaby and Elderfield (2005) that interglacial climate is stabilized by a strong AAIW / AABW (Antarctic Bottom Water) influence (see Section 2.4) over atlantic meridional overturning circulation (AMOC) via a salinity feedback. In order to determine a density contrast between AAIW / NADW material from this interval that was bathed in predominantly NADW is necessary. This could potentially be provided by a core adjacent to (or at a similar water depth to) 9/97-27/2, but which provides a record extending back further in time.

The apparent absence of AAIW during a phase of climate variability (MIS 3) is further support of the hypothesis that AAIW stabilizes northern hemisphere climate (Lassen *et al.* 2002) as SSTs are highly variable during this interval. However, as discussed above, the MIS

3 record in these intermediate depth cores is poorly preserved or absent. The benthic $\delta^{18}O$ values for this stage also alternate around 3.8‰$_{VPDB}$ and are all greater than 3.5‰$_{VPDB}$ (Fig. 7.7) in core 9/97-27/2. These values are significant as they have been suggested as a 'threshold' value, above which a stable glacial climate will occur and below which a stable interglacial climate will prevail (McManus *et al.* 1999; Hall and Becker 2006). Values will be highly unstable if they are close to the threshold. The results from this core show that 3.8‰ is the more accurate value. The strong variations in $\delta^{18}O_{benthic}$ suggest that ice sheets are highly unstable during this period, producing rapid, millennial scale oscillations between periods of large-scale iceberg discharges and periods of cooling.

Sea surface temperature reconstructions in cores 9/97-10 and 9/97-03 reveal MIS 2 achieved the second lowest temperatures of the previous 500 kyrs (Figs. 6.4 and 6.6). In the deeper core record (9/97-27/2 and 9/97-20) Marine Isotope Stage 2 (MIS 2) is characterized by very low and relatively (compared to MIS 3) stable SSTs. These stable SSTs correspond with the strongest GNAIW signals in cores 9/97-10 and 9/97-04 (Fig. 7.12). When this is considered along with the dominance of AAIW / stability of SSTs during the previous interglacial (see above), this implies that glacial-interglacial climate stability coincides with the flux of each of these water masses crossing a particular threshold value (Fig. 9.4). The interpretation that a strong GNAIW flux can stabilize SSTs is perhaps incompatible with the suggestion by Rickaby and Elderfield (2005) that a strong AAIW flux is required for stability. Also, Heinrich events occur during this interval (see below), which imply that stability has not been achieved. However, this is compatible with the suggestions of McManus *et al.* (1999) and Hall and Becker (2006) that when ice volume crosses a threshold value, stability will occur. The data presented here suggests that the concept of AAIW stabilizing interglacial

climate is correct, but that GNAIW flux is more important during glacials and does result in overall stability. However, problems with the acquisition of reliable SST values via MAT and the lack of a good MIS 3 record at intermediate water depths suggest that further work is necessary to investigate this.

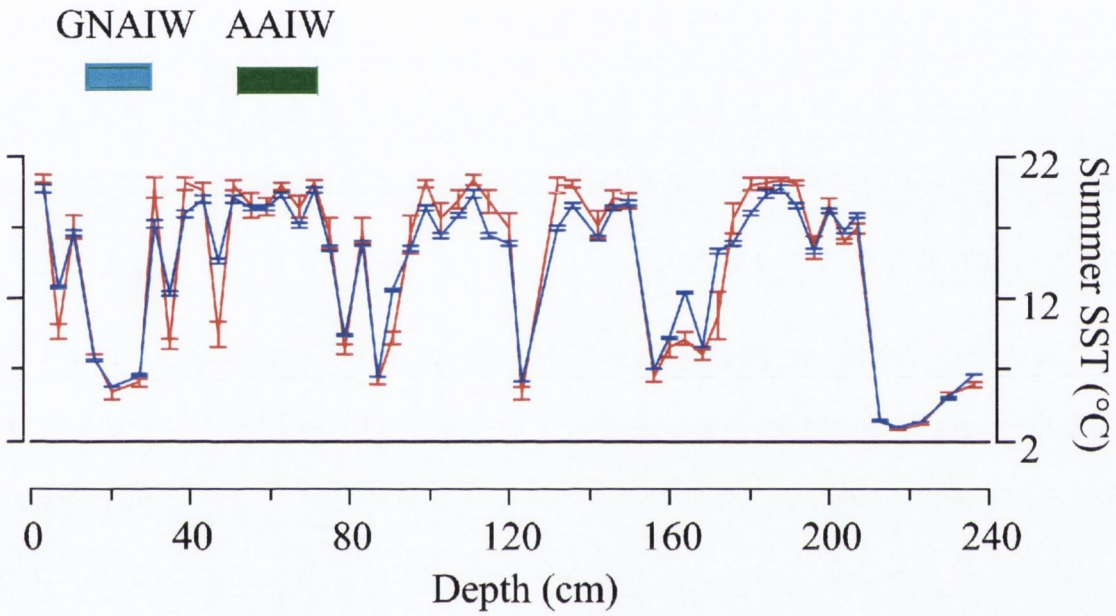

Figure 9.4. Stability of SSTs (MAT derived from core 9/97-10, red line = summer values, blue line = winter values) and the maximum fluxes of AAIW / GNAIW during MIS 5 and MIS 2 respectively according to benthic geochemistry.

9.3.3 Distribution of benthic foraminifera

Cluster and principal components analysis (PCA) including data from all cores shows that there are very clear differences in assemblages with depth (Figs. 8.16, 8.21 and 8.23). However, there is some inter-core clustering of samples from this stage. These appear to be

linked to the foraminifera sand units deposited during the last interglacial at intermediate depths (cores 9/97-10, 9/97-04). The cluster group of benthic foraminifera associated with (part of) the FS lithofacies in core 9/97-10 can also be correlated along slope into core 9/97-03 (Fig. 8.18 and Fig. 9.5). As this unit in core 9/97-10 records very well sorted sands following particle size analysis (Fig. 9.6), it is arguable that bottom current activity has become so intense at this stage, that even benthic foraminifera from the >250μm size fraction are being re-distributed to a detectable degree. The species present in the correlated cluster groups from

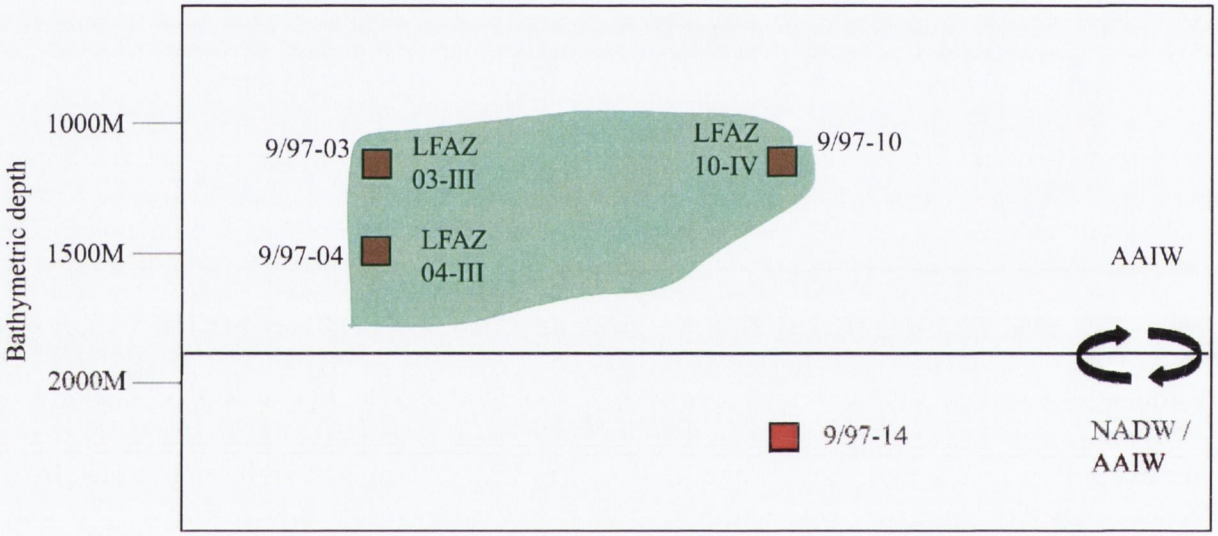

Figure 9.5. Correlation of lithofacies assemblage zone groups from cores 9/97-10, 9/97-03 and 9/97-04 during MIS 5. Note the position of a potential boundary between cores 9/97-04 and 9/97-14 which corresponds to the AAIW / NADW boundary proposed by benthic geochemistry.

cores 9/97-10 and 9/97-03 do not suggest any specialist adaptation to exploit these enhanced bottom currents, however. The dominant taxa are *S.schlumbergeri*, *K.bradyi*, *M.barleeanum*

and *C.wuellerstorfi*. Apart from *C.wuellerstorfi* (which is notoriously cosmopolitan; Schwager 2006), none of these taxa has displayed an elevated 'epifaunal' mode of life or adaptation to areas of enhanced bottom current activity. A problem with using the particle size data, in the form it is currently, as a qualitative proxy for bottom current activity is that the samples used to acquire these data were not decalcified prior to analysis. It is not possible, therefore, to determine if the variations in particle size sorting are due to bottom current activity alone, or if there is also a strong biological signal which is masking / enhancing this. Due to the relative absence of species which, at other localities (e.g. Schönfeld 2002), have displayed an affinity for strong bottom current activity, it is probably more plausible that this well-sorted foraminiferal sand unit was deposited under enhanced productivity, rather than enhanced bottom currents.

A relative absence of water mass stratification could promote environmental uniformity between core sites due to the removal of physical oceanographic barriers (e.g. nepheloid layers / internal waves) and improved mixing. Combined with relative stability in the surface ocean suggested by SST data and enhanced productivity inferred from BFAR, this could enable some species to expand their distribution over a wider area, both bathymetrically and along the slope. This could perhaps explain why assemblage groups between 1230-2118m water depth are more similar during the last interglacial compared to Holocene and some last glacial assemblages (Fig. 8.16). Alternatively, this similarity could be due to post-mortem modification of assemblages, an interpretation which is supported by relatively high fragmentation indices during this interval in most cores and by the well-sorted sands suggested by examination of grain size data.

An alternative explanation for the absence of strong bottom current adapted species is that productivity is too high or too episodic to give a competitive advantage to taxa adapted to exploit bottom currents. There is some evidence for pulsed food supply in the high numbers of *Melonis barleeanum* and the moderate percentages of *E.exigua* (small fraction). The accumulation rate of benthic foraminifera is also comparatively high within this unit (Fig. 8.3). It remains possible that food supply is so high as to make the strength of bottom currents relatively meaningless in terms of controlling populations of benthic foraminifera during this stage.

A study of the next unit above, which is another very well sorted foraminifera sand deposit (Fig. 9.6) but with a lower benthic foraminifera accumulation rate (BFAR), shows higher percentages of *Rupertina stabilis* and *C.wuellerstorfi* together with reduced percentages of *K.bradyi* and *S.schlumbergeri*. The degree of grain sorting is identical to that of the unit below yet the species composition has clearly changed. The accumulation rate of benthic foraminifera is the main parameter that is lower within this unit (Fig. 8.3) which potentially leads to the conclusion that only when productivity is below a certain threshold value does bottom current strength become an important factor in controlling populations of benthic foraminifera. Examination of the next unit above this in core 9/97-10 shows that this unit is also dominated by large proportions of *R.stabilis* and *C.wuellerstorfi*. This unit is a poorly sorted glacial deposit. It is clear that bottom current strength is either not strong enough or consistent enough to produce a significant effect on assemblages of benthic foraminifera. The amount and consistency (+/- quality) of food is the primary parameter controlling species relative abundance through time. The proposal that in this study area, productivity needs to fall below a threshold value before bottom current activity can significantly affect assemblages

of benthic foraminifera is an extension of the proposal by Schönfeld (2002) who observed an elevated epifaunal group that was associated with bottom current activity on the Portuguese continental margin, but did not consider the impact of varying productivity.

An estimation of Fisher's Alpha diversity index versus depth for the previous interglacial, MIS 2 and the Holocene reveals a strong mid-slope diversity maximum located at 1502m water depth in core 9/97-04 (Fig. 8.15). Combined with the reduced productivity with increasing depth inferred by BFAR data (Fig. 8.14) this could suggest that a dynamic equilibrium between food supply and environmental stability is controlling species diversity down slope. It is not possible to determine the position of the diversity maximum along the slope during this stage, as the MIS 3 record is largely absent from intermediate depth sites (in particular, cores 9/97-04 and 9/97-14). This is perhaps further evidence of the downslope increase in environmental stability as the deeper cores (9/97-27/2 and 9/97-20) preserve relatively undisturbed records from MIS 3 to the Holocene. This is supported by an interpreted decrease in organic matter flux to the seafloor and an increase in environmental stability with distance down slope (inferred from sedimentology). The intersection between these two points could be producing the observed diversity maximum. The fact that the depth of this maximum does not shift during glacial or interglacial periods suggests the down slope environmental stability gradient does not alter through time.

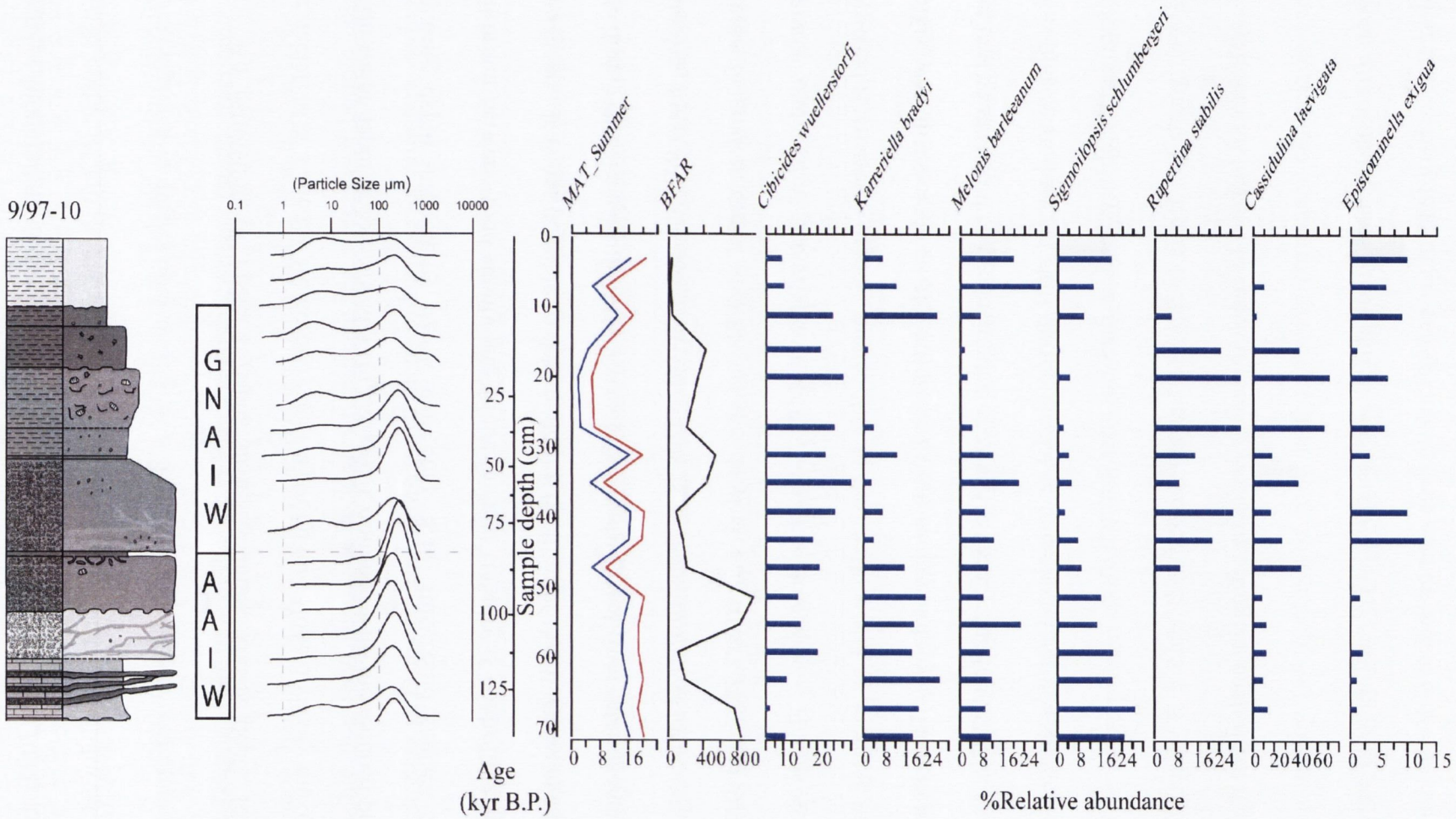

Figure 9.6. Comparison of benthic foraminifera relative abundance with particle size data (courtesy of Toms in prep.), SSTs (red line = summer values, blue line = winter values), BFAR and overall water mass influence in core 9/97-10.

9.3.4 Records of Heinrich events

Stadial-interstadial variations in SST correspond roughly with variations in benthic $\delta^{13}C$, implying GNAIW (Glacial North Atlantic Intermediate Water) expansion-contraction over site 9/97-27/2. However, the comparatively low resolution $\delta^{13}C$ record makes a determination of relative ages for the expansion-contraction of GNAIW versus stadial-interstadial surface variations impractical. A strong negative value in $\delta^{13}C$ present at 43.8 kyr B.P. is volumetrically identical to the negative benthic isotope excursion recorded by Peck *et al.* (2007) at 39 kyr B.P and related to Heinrich event 4. As 9/97-27/2 was probably bathed in GAABW (Glacial Antarctic Bottom Water) according to the reconstruction of Lynch-Stieglitz *et al.* (2007), this suggests that this is could be a record of a similar event in the Southern Ocean that preceded H4 in the northern hemisphere by approximately 4 kyrs. Core 9/97-27/2 records a 5-7 fold increase in BFAR either side of H4, as dated by Peck *et al.* (2007), as well as warm SSTs. The species composition does not alter. This phenomenon has not been recorded previously from other localities in the NE Atlantic Ocean (Baas *et al.* 1998; Peck *et al.* 2007) although this could be because BFAR is not normally calculated as any productivity variations are likely to show up in the carbon isotope profiles that are usually acquired for this type of research. A summary of the record of Heinrich event 4 as recorded in core 9/97-27/2 is presented in Figure 9.1. In core 9/97-27/2, two peaks in BFAR (mostly *Uvigerina celtica*) are present at 40.8 and 37.7kyr B.P, which occur before and after Heinrich event 4 (H4) as dated by Peck *et al.* (2007). These peaks are potentially linked to a pair of strong negative carbon isotope excursions in the Santa Barbara Basin, which were considered to result from methane hydrate destabilization (Kennett *et al.* 2000), although this interpretation has been subsequently challenged (Carriato and Stott 2003). They could also be due to the migration of

a frontal system over this core site, perhaps the Polar Front as proposed by Nees *et al.* (1997) and Scourse *et al.* (2009). This would explain the increase in BFAR, as the polar front is associated with significantly enhanced productivity (Nees *et al.* 1997) and perhaps also ties in with the proposed Dansgaard-Oeschger climate variations in the migration of this front proposed by Scourse *et al.* (2009), with the polar front migrating southwards over this site once (see Fig. 2.12), causing the earlier BFAR peak, H4 occurring, then the polar front migrating northwards over the site and causing the second BFAR peak (Fig. 9.7).

The probable record of H4 from MIS 3 and Heinrich events 1 (H1) and 2 (H2) from MIS 2 leads to the obvious problem of the absence of Heinrich event 3 (H3) from the record of 9/97-27/2. One possible explanation is that the sampling resolution employed for this time period was too low, and the record of this Heinrich event has been missed. Heinrich event 1 is associated with a 'grey band' (80-85cm core depth) in core 9/97-27/2, and there is another 'grey band' at 165cm (Fig. 7.7), dated at 32 kyr B.P. The second grey band contains a large peak in IRD (approx. 90% of the >150μm size fraction) according to Toms (in prep.) and could be a sedimentological expression of H3. The IRD peak is followed by a rapid incursion of warm water taxa, consistent with the concept that this Heinrich event occurs at the termination of a stadial and is immediately followed by a rapid SST rise (Scourse *et al.* 2009). However, this interpretation is not compatible with the IRD record of Peck *et al.* (2007), which shows that this Heinrich event recorded no peak in IRD in the adjacent Porcupine Seabight, although that study used accumulation rates of IRD, unlike this data which is the percentage of the >150μm size fraction that is IRD (Toms pers. comm.).

Benthic phosphorus / $\delta^{13}C$ data from three intermediate sites (1260-2118m water depth) are unanimous in recording a clear GNAIW signal throughout MIS 2 (Fig. 7.12), although the

record for core 9/97-14 is more variable. Benthic $\delta^{13}C$ from core 9/97-27/II is relatively low (<1.0‰$_{VPDB}$) throughout stage 2, and implies that GAABW continually bathed this core site (Lynch-Stieglitz *et al.* 2007). Data from core 9/97-14 (Fig. 9.8) suggests that GAABW may have episodically increased in volume to mix with the GNAIW that flushed this site (Fig. 7.6). The data presented here suggests that the volumetric flux of GAABW at this site never reached 1502m water depth and that the maximum flux was located between 1502-2118m water depth. This is in agreement with the reconstruction of Lynch-Stieglitz *et al.* (2007) for the Last Glacial Maximum (LGM). This study perhaps goes a little further, in showing that the volume of GAABW fluctuated above and below 2118m water depth (core 9/97-14) during stage 2. The data suggests that GAABW flux increased above 2118m only twice during MIS 2; at 19 and 27 kyr B.P. However, both of the samples that record increased Cd/Ca (and therefore, seawater phosphorus) also record low Sr/Ca values from a core that displays some evidence of a dissolution influence (Fig. 7.6). This interpretation is therefore applied with caution, but this apparent dissolution effect could also be due to the increased GAABW component, as AABW is less alkaline than NADW (Read 2001). Also, dissolution should also cause low Cd/Ca values, not relatively high values (McCorkle *et al.* 1995). Similar $\delta^{18}O_{sw}$ values recorded in cores 9/97-10 and 9/97-04 for this stage (Fig. 7.9) show that stratification is weak or absent between sites 9/97-10 and 9/97-04 during MIS 2. Density contrasts are apparent between cores 9/97-14 and 9/97-27/2, except at 19 and 27 kyr B.P., where two strong negative $\delta^{18}O_{sw}$ values are observed which significantly reduces stratification between these two sites, giving them comparable values during episodes where GAABW appears to have increased in volume (see above).

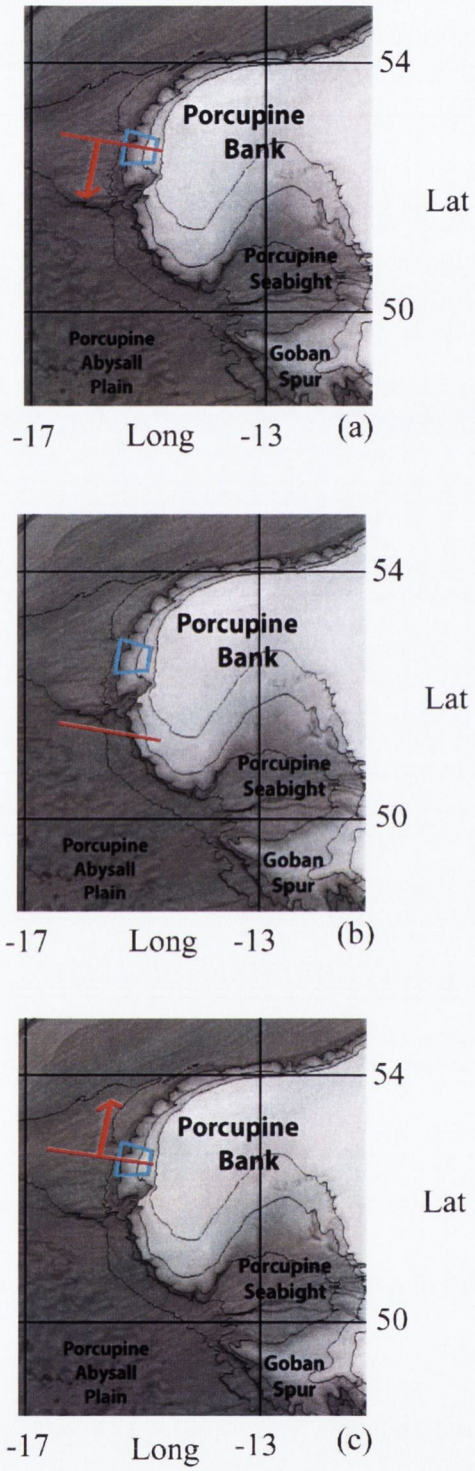

Figure 9.7. Migration of the polar front (red line) over this study area at (a) 40.8 kyr B.P. (BFAR peak 1), (b) 39 kyr B.P. (Heinrich event 4 as dated by Peck *et al.* 2007) and (c) 37.7kyr B.P. (BFAR peak 2). Map courtesy of Toms (in prep.).

Evidence of carbon isotope excursions linked to the last termination / H1 can be found in two cores (9/97-10 and 9/97-27/2). For core 9/97-10, a strong negative carbon isotope excursion is present in the planktonic carbon isotope record at 15cm core depth (16.4 kyr B.P.). This is contemporaneous (within dating uncertainties) with the record of H1 (16.8 kyr B.P.) from the record of Peck *et al.* (2007) from the adjacent Porcupine Seabight. A similar negative carbon isotope excursion is present in the benthic carbon isotope record for core 9/97-27/2 at 85cm core depth (20 kyr B.P.). The fact that the deep record appears to lead the shallow / intermediate record is probably explained by the water mass distribution at this time, with the higher sites (including 9/97-10) flushed by GNAIW, and the deeper site (9/97-27/2) bathed in GAABW. The observation of the SCW signal 'leading' the Northern Component Water (NCW) signal is explained by the bi-polar seesaw hypothesis, first proposed by Broecker (1998) which proposes that disruption to deep-intermediate water formation in the southern ocean leads to disruption in North Atlantic / Arctic Ocean deep water formation via a negative salinity feedback.

9.3.5 MIS 2 – Sea ice

Examination of the planktonic faunal assemblage in core 9/97-27/2 reveals a near absence of sub-polar taxa 42-44 kyr B.P. and a total absence 32-35 kyr B.P (Fig. 6.12) which suggests a stadial producing seasonal sea-ice cover over this site 42-44 kyr B.P., followed by a stadial producing perennial sea-ice cover 32-35 kyr B.P. (Kucera *et al.* 2005). These stadials also record extremely low BFARs, consistent with the hypothesis that sea-ice is covering the

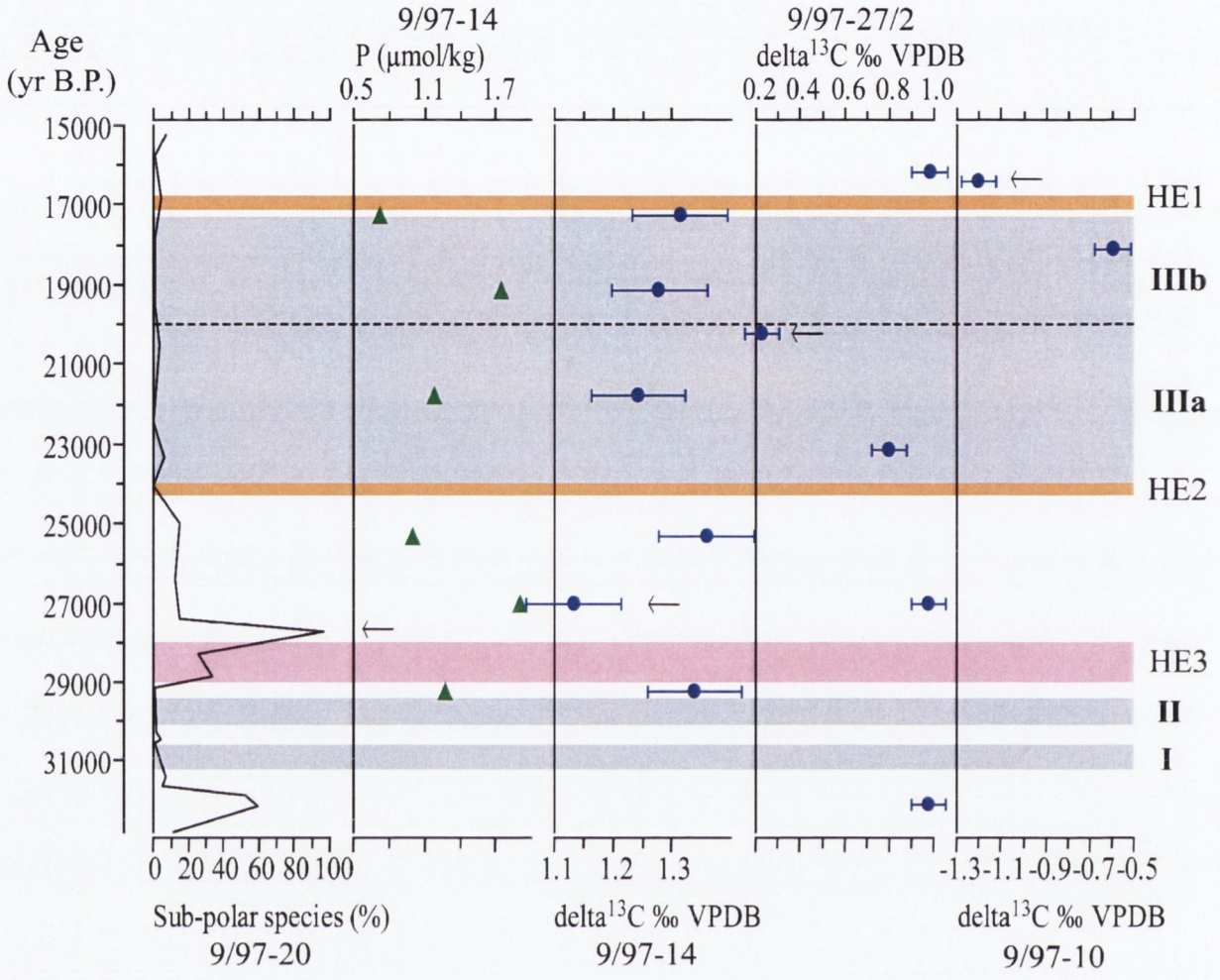

Figure 9.8. Comparison of geochemical proxy data from three cores (9/97-10, 9/97-14 and 9/97-27/2) with Heinrich events (as dated by Peck *et al.* 2007, pink and orange shading) and the three phases (I-IIIa and b) of perennial sea-ice development (grey shading), as suggested by the planktonic foraminifera assemblages data of core 9/97-20.

site and disrupting surface productivity. There is some evidence from onshore records that the western sector of the Irish Ice Sheet was (at times during MIS 3) as extensive or possibly even more extensive than during the LGM (Bowen *et al.* 2002). However, the onshore record of

pre-LGM ice sheet evolution is largely poorly constrained temporally, particularly for the west coast of Ireland (McCabe *et al.* 2007).

Subtle differences between the GISP-II ice core record and the record for core 9/97-27/2 could be due to the influence of the British Irish Ice Sheet which, it has been proposed, did not at all times vary in synch with the Greenland Ice Sheet (Hubbard *et al.* 2009). For instance, the age model proposed for core 9/97-20 (Fig. 5.18) suggests that high amplitude variations in SST ended prior to 30 kyr B.P., where as the GISP-II record has these continuing beyond 30 kyr B.P. and finishing at 27.5 kyr B.P. This could be because the sampling resolution employed in core 9/97-20 is too low and the post 30 kyr B.P. interstadials have been missed. Alternatively, this could reflect differences in the timing of expansion of the BIIS at the MIS 2 / MIS 3 boundary compared to the Greenland Ice Sheet. The $\delta^{18}O_{benthic}$ record from this time interval in 9/97-27/2 is not of a high enough resolution during or after this transition to help resolve this problem by providing data on ice volume changes. The transition from MIS 3 into MIS 2 is fairly abrupt in core 9/97-20 (Fig. 5.18) and appears to be co-eval with the maximum extent of the British Irish Ice Sheet (BIIS) as proposed by Wilson *et al.* (2001).

There are conflicting interpretations of this stage in terms of sea-ice cover from this study. One core (9/97-27/2) records a minor sub-polar component in the planktonic faunal assemblage throughout this stage, which suggests that seasonal sea-ice cover prevailed, with no perennial sea-ice (Fig. 6.12). The record from another core (9/97-20) suggests that sea-ice cover was perennial over this area, with three main phases of perennial cover separated by phases of seasonal sea-ice cover (Fig. 6.14). As examined in Section 5.2, core 9/97-20 probably provides a slightly higher resolution record of stage 2. It is therefore more probable that this core provides a more accurate record of sea-ice cover compared to 9/97-27/2. It is

likely that core 9/97-27/2 has undergone some minor mixing via bioturbation, with sub-polar taxa becoming incorporated into deposits that originally only contained polar taxa. This mixing does not appear to have occurred in core 9/97-20 as bioturbation is unlikely to produce monospecific assemblages of *N.pachyderma* (sin.). Alternatively, core 9/97-20 could have undergone more severe dissolution, preferentially removing the sub-polar species according to the dissolution series of Hemleben *et al.* (1989). This interpretation is not supported by the SST reconstructions from these cores, which suggest that SSTs were too warm for sea-ice to form during this interval (Figs. 6.13 and 6.15). However, as mentioned in Chapter 6, the modern training dataset used in this study (Pflaumann *et al.* 2003) does not contain samples from areas that experience perennial sea-ice cover.

The notion of seasonal sea-ice cover over this site is a contradiction of the reconstructions produced by CLIMAP (CLIMAP 1981) and GLAMAP (Pflaumann *et al.* 2003). In their reconstructions, reviewed in Meland *et al.* (2005), the margin of seasonal sea-ice is further to the north. However, it should be noted that the sites used in the reconstructions did not include any that were as proximal to the BIIS (British Irish Ice Sheet) as the sites used in this study. The time interval during which sea-ice cover occurred (17.8-31.4 kyr B.P.) is broadly equivalent to the phases of maximum ice sheet advance on the Hebrides shelf margin (16-30 kyr B.P.) recorded by Knutz *et al.* (2001) and Wilson *et al.* (2001). This is also co-eval with the Glenavy Stadial from the Irish onshore record (Jones and Keen 1993; McCabe 1987; Richter *et al.* 2001). It is plausible that due to proximity to a large ice sheet (Boulton *et al.* 1985, 1991; Lambeck 1995; Knight 2006; Cofaigh and Evans 2007; Fretwell *et al.* 2008) and, aided by Taylor column formation trapping cold water above the Porcupine Bank (Martin and Drucker 1997; White *et al.* 1998), that sea-ice could have

formed and been retained over this area during the last glacial (approx. 16-30 kyr B.P.). This inferred sea-ice formation also has implications for the albedo effect in this part of the NE Atlantic Ocean during this interval, which would impact on climate models for the LGM.

Another important finding is that the proposed episode of sea-ice cover is not as straightforward as a simple, monotonic 'one advance and one retreat' and instead displays some variation in the development of perennial versus seasonal sea ice. Examination of the sub-polar taxon content of planktonic foraminifera from this time interval in core 9/97-20 (Fig. 6.14) suggests that there were three main phases of perennial sea-ice development during MIS 2 (Fig. 9.8). These occurred at 30.7-31.5 kyr B.P. (Phase I), 29.1-30.3 kyr B.P. (Phase II) and a final phase 17.3-25 kyr B.P. (Phase III). The final phase can be further subdivided into a variable sub-phase between 20-25 kyr B.P. (Phase IIIb) and a consistent sub-phase between 17.3-20 kyr B.P (Phase IIIa). After 17.3 kyr B.P., no evidence of perennial sea-ice development is observed. This is compatible with the repeated drumlinisation observed in the Irish onshore record of western Ireland dated at this time (McCabe *et al.* 1986; McCabe *et al.* 1998) which suggests a continual discharge from the BIIS rather than an increase in volume. These phases of perennial sea-ice development are co-eval with the Glenavy stadial from Irish onshore records (Coxon 2001) but perhaps suggests that this stadial could in fact represent three sub-divisions. Interestingly, the start of Phase III is preceded (by approximately 2kyrs) by an expansion of GAABW as recorded in core 9/97-14 (Fig. 9.8) and a Heinrich event (H2), as dated by Peck *et al.* (2007).

Evidence of suppressed flux rates in all cores is evident from examination of the BFAR of each core (Fig. 8.14). This suggests a reduction in productivity at all sites relative to MIS 3 and MIS 1 (except for core 9/97-10, which displays the opposite trend). This is consistent

with the proposed sea-ice cover for this stage, with sea-ice shutting off surface production by denying phytoplankton access to sunlight.

9.3.6 Holocene MOW signal

A reconstruction of Holocene bottom water mass distributions along the slope reveals a similar distribution to that observed at present (Read 2001). The presence of NADW at 2756m water depth, with AAIW present above this at 2118m and 1502m water depth is consistent with the current mode of water mass circulation adjacent to Porcupine Bank (Read 2001). The observation of the Holocene sample from core 9/97-10 (Fig. 9.9) at 1260m water depth (Fig. 7.12) displaying a $\delta^{13}C$ / phosphorus signal indicative of NADW with a slight MOW (Mediterranean Outflow Water) mixed component is a slight deviation from modern observations. Mediterranean Outflow Water can currently be detected only as far north as 53°N in the NE Atlantic Ocean. At this latitude, MOW currently shoals to the surface and becomes incorporated into northwardly advecting surface currents (New and Smythe-Wright 2001). This could suggest that MOW developed a higher density component during the early-mid Holocene. Moderate coeval negative carbon and oxygen isotope excursions are observed in the benthic data of Voelker *et al.* (2006) at approximately 8 kyr B.P (Fig. 9.10). This perhaps leads to the interpretation that the mode of deep water formation in the Mediterranean (in particular, the Gulf of Lions) switched from winter time cooling / convection to buoyancy loss via brine formation (Dokken and Jansen 1999; Labeyrie *et al.* 2005). This produced an intensification or displacement in the flow path of MOW (or perhaps both), enabling the signature for this water mass to be detected at this depth, this far north (although still mixed

with NADW +/- AAIW). As this is based on only one sample from this study, however, further research is required to test this hypothesis.

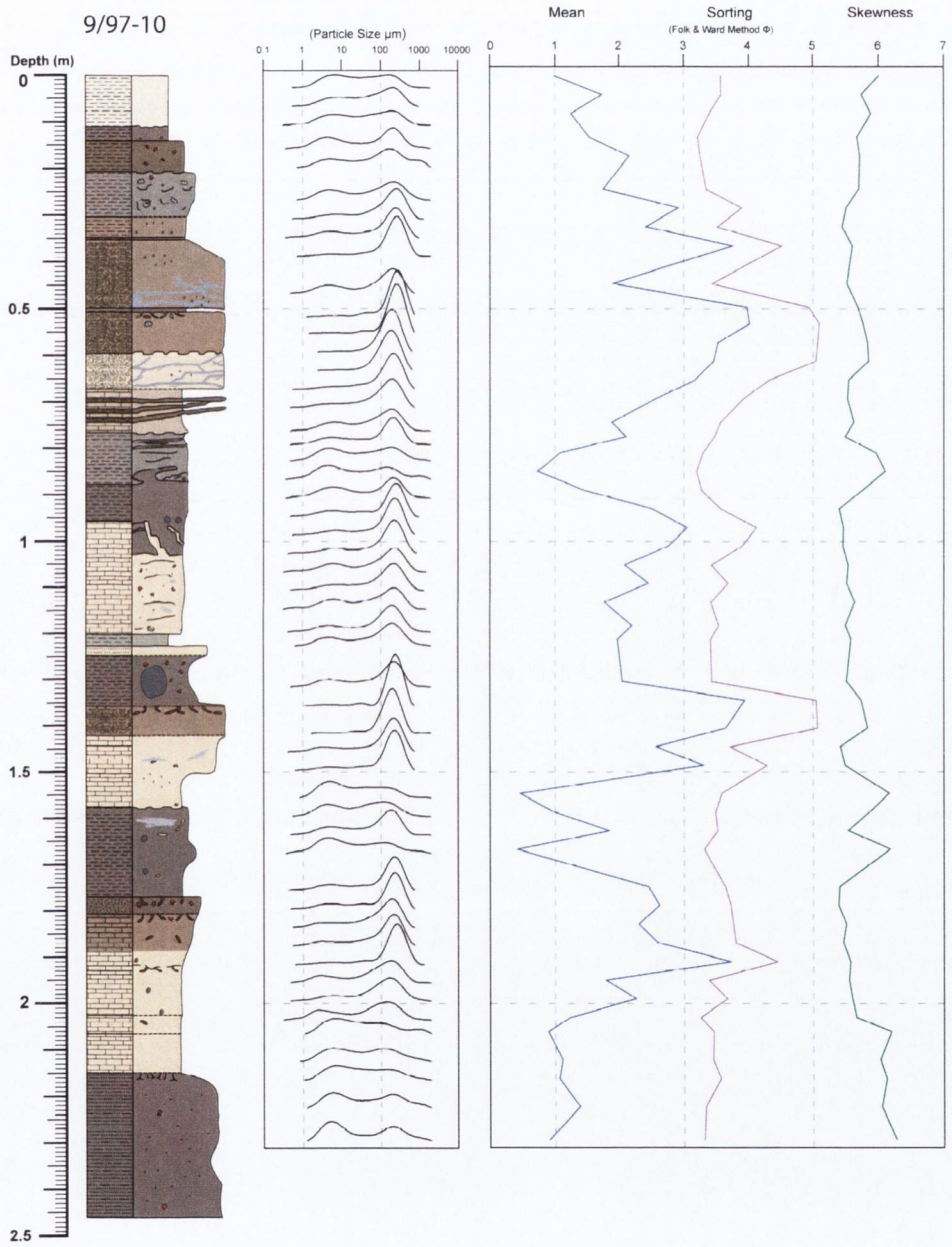

Figure 9.9. Particle size analysis results for core 9/97-10, courtesy of Toms (in prep.).

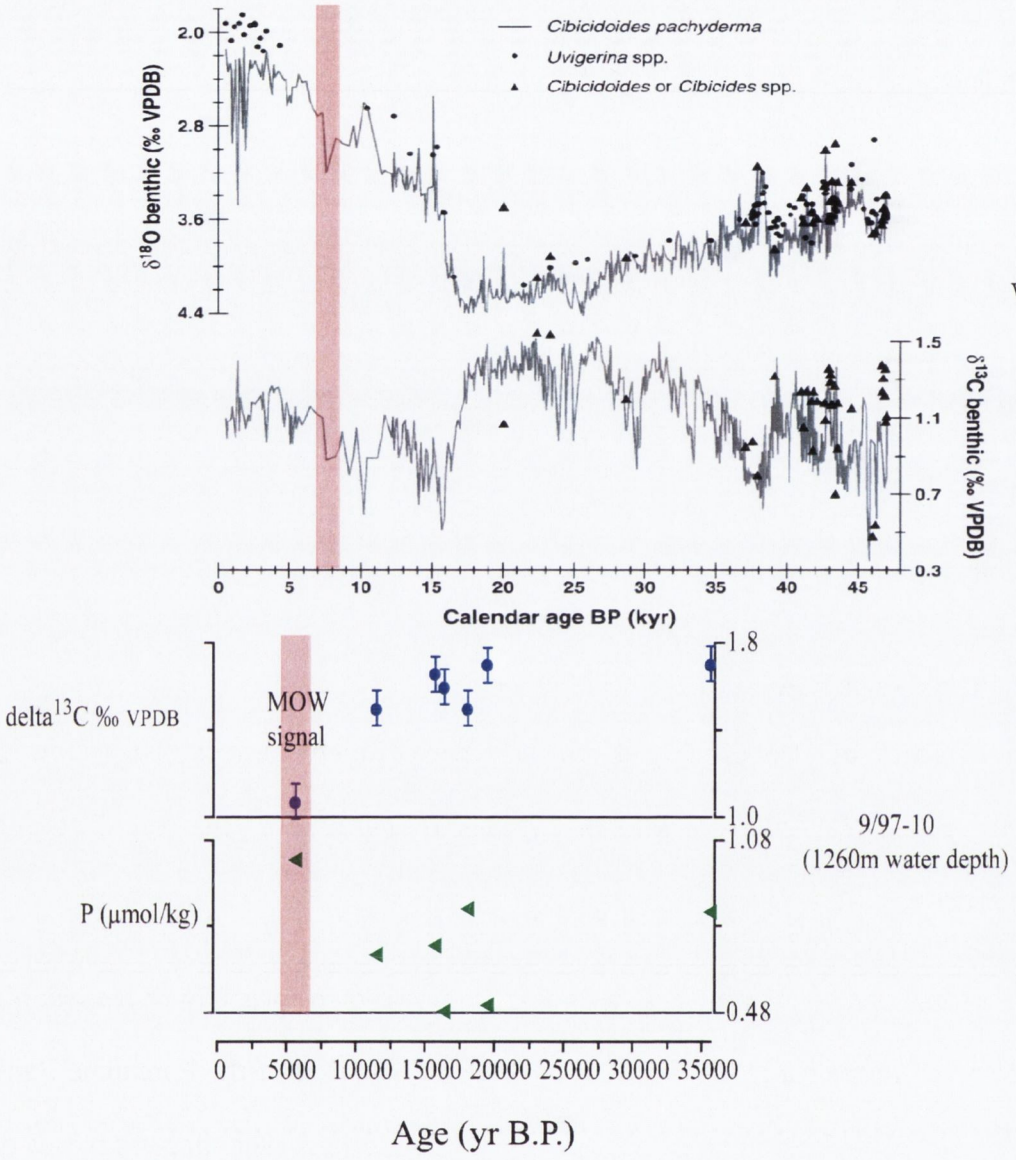

Figure 9.10. Record of benthic $\delta^{13}C$ and $\delta^{18}O$ from the Gulf of Cadiz (Voelker *et al.* 2006) and the benthic record of phosphorus concentrations and $\delta^{13}C$ in core 9/97-10. The sample which records the influence of MOW is highlighted.

Chapter 10

10.1 Outline

This chapter completes the thesis by summarizing the extent to which the research questions outlined in Chapter 1 have been addressed. This uses the results and interpretations described in previous chapters to directly answer the questions raised. Areas of potential future research which are considered to be most promising given the results of this thesis are then presented.

10.2 Addressing the research questions

10.2.1. Is there evidence of physical (e.g. bottom-current sorting/winnowing, inclusion of allochthonous material) and / or chemical (e.g. dissolution) taphonomic processes distorting any original climate records?

The project has successfully established a taxonomic scheme for study of the benthic foraminifera preserved in the contourite deposits on the western slope of the Porcupine Bank (Chapter 4). Sixty-five species of benthic foraminifera are described, including diagnoses of species to increase understanding of key differences between taxa. This expands on the taxonomy of Jones (1984) for Porcupine Bank foraminifera and includes the description of a new species, *Fissurina porcupinensis* sp. nov. Achieving this objective has provided a framework for describing the special and temporal variations in the distribution of each species.

The results of DCA of assemblages of benthic foraminifera (see Chapter 8) from the large size fraction (≥250μm) suggest that bottom current related mixing of assemblages

between cores may be more prevalent during interglacials, relative to glacials (see Fig. 8.23). Size fraction sorting of benthic foraminifera is also apparent, with the larger size fraction producing strong inter-core differences in assemblage through time unlike the smaller size fraction (63-250μm) which shows that inter-core assemblages are much more similar in composition, although this is not restricted to interglacials. This is observed when comparing the strong relationship between lithostratigraphy and assemblage groups for the large size fraction, compared to the weak relationship for the smaller size fraction. In the larger size fraction, stratigraphically adjacent samples cluster together when comparing assemblage compositions and the cluster groups formed are directly comparable to lithofacies (Figure 3.19). This is not present in the smaller size fraction, although a broader pattern is observed involving the species *Cassidulina laevigata* and *Epistominella exigua*. *C.laevigata* is associated with the shallower portions of the slope (<2000m water depth) with *E.exigua* dominant in deeper sections (>2500m water depth), a relationship observed in a previous NE Atlantic study (Austin and Evans 2000.) which is expressed following PCA. Although this depth related distribution pattern is observed, the clear link with lithofacies is not present in the smaller size fraction, suggesting significantly enhanced mixing of assemblages.

Through a detailed assessment of the integrity of the gravity cored record along a depth transect on the western margin of the Porcupine Bank, it has been possible to highlight which samples / sedimentary units are likely to have undergone taphonomic processes that render them inappropriate for use in palaeoceanographic studies. However, comparison of *%N.pachyderma* (sin.) curves to reference curves suggests that a coherent stratigraphy is present in most cores examined between 1230-3073m water depth, although some relatively large hiatuses have been identified in some cores (see Chapter 5). The nature of the preserved

stratigraphy appears to vary with depth, with cores shallower than 2200m water depth preserving a relatively low resolution (2kyr.cm^{-1}) record of glacial-interglacial variations extending back as far as Marine Isotope Stage 13, with relatively high resolution records of MIS 11 and 12 also preserved. Cores deeper than 2200m water depth appear to preserve a high resolution (200yr.cm^{-1}) record from approximately 47 kyr B.P. to the Holocene. An apparently coherent stratigraphy that can be traced down slope lends itself to comparison of a multi-proxy record at different water depths through time.

An absence of similarity between modern assemblages of planktonic foraminifera and those preserved in most of these cores (see Chapter 6) clearly suggests that post-mortem distortion of planktonic assemblages may have occurred. The distortion is specifically related to a relatively high proportion of *G.bulloides* which is not present in modern assemblages. This suggests either that *G.bulloides* is preferentially preserved or that other species are underrepresented. It is unlikely that *G.bulloides* would be preferentially preserved as it produces a delicate test (see Fig. 3.3). Alternatively, this could be linked to surface ocean conditions, with a continental margin setting producing a higher proportion of the species *G.bulloides*, which is known to thrive in settings where primary productivity is enhanced (Kucera 2007).

Chemical taphonomic processes, as suggested by fragmentation indices and a potential geochemical proxy, also appear to influence the multi-proxy record. Fragmentation indices (a proxy of dissolution intensity) vary in accordance with glacial-interglacial climate variations as suggested by *%N.pachyderma* (sin.), with a higher dissolution intensity present during interglacials relative to glacials. This pattern is observed in all cores at all depths along the depth transect. The geochemical proxy (Sr/Ca values) appears to vary less systematically and

does not display a clear glacial-interglacial pattern. This proxy appears to be more responsive to episodes of abrupt climate change, such as potential Heinrich events or the termination of glacial episodes. High Mn/Ca values throughout one core (9/97-27/2) indicate dysoxic conditions persisted between approximately 46 kyr B.P. and the Holocene at this core site.

10.2.2. Do indicators of preservation potential vary systematically either within cores or down slope?

There are clear glacial-interglacial variations in some indicators of preservation potential. Fragmentation indices are higher during interglacials relative to glacials in all cores, suggesting a higher dissolution intensity during interglacials. DCA and cluster analysis of assemblages of benthic foraminifera shows that last interglacial samples from intermediate depth cores (9/97-10, 9/97-04 and 9/97-14) are quite similar. This is potentially evidence of enhanced bottom current activity causing mixing of assemblages during this interval. However, it could also reflect increased environmental uniformity between these sites caused by the strong influence of AAIW (see below). Evidence of increased mixing of assemblages during interglacials is also suggested by planktonic foraminifera. No good modern analogues exist for interglacial / interstadial populations, with slightly better analogues for glacial assemblages.

Attempted correlation of the cores used in this study with those from other areas, combined with taphonomic information derived from the fragmentation of foraminifera (Chapter 5), assessment of the degree of similarity between modern and fossil assemblages of planktonic foraminifera (Chapter 6), geochemical proxies of selective dissolution and post-depositional chemical alteration of foraminiferal test coatings (Chapter 7) and comparison of

cluster grouping between different size fractions of benthic foraminifera (Chapter 8) has revealed that several factors exist to complicate the preserved record. These are: hiatuses / low rates of sedimentation; a lack of good modern analogues for most planktonic assemblages; intervals of apparent selective dissolution and post-mortem modification of test geochemistry and; preferential mixing and possible redistribution of smaller sized particles over larger sized particles. However, by identifying where these taphonomic features occur and how they are likely to alter the original data, it is still possible to obtain some palaeoceanographic information from these deposits, even if actual sea surface temperature values cannot be reliably obtained via transfer function methods.

10.2.3. What were the surface oceanographic conditions under which these deposits formed?

Despite the apparent imprint of taphonomic processes at this site, several significant surface oceanographic events and processes can be detected. The problems highlighted above with respect to the reliability of the reconstructed sea surface temperature values (Chapter 6) due to an apparent lack of similarity between modern and fossil assemblages of planktonic foraminifera are substantial. However, every core still records relatively higher sea surface temperatures (summer and winter) during proposed interglacials / interstadials compared with glacials / stadials, with the last glacial approximately 9°C cooler than the mid-late Holocene, comparable to other studies (e.g. Kucera *et al.* 2005). This pattern is also present when oxygen isotope ratios are used to reconstruct sea surface temperatures, although different values between those derived from this method and the transfer function method are observed. Oxygen isotope derived values are usually closer to winter values derived from MAT or WAPLS during interglacials, but closer to summer values during glacials. This potentially

suggests that *G.bulloides*, the species used to obtain oxygen isotope values, switches between a winter/spring season of maximum production during interglacials and a summer season of maximum production during glacials. This could have significant implications for other studies that use *G.bulloides* to reconstruct sea surface temperatures. However, the problems highlighted above with regard to the lack of good modern analogues for most fossil samples during interglacials show that further research using fossil samples with better modern analogues is required to examine this issue.

The apparent expansion of perennial sea-ice formation over the Porcupine Bank area, as suggested by the absence of the sub-polar species group during the last glacial (Chapter 6), appears to coincide with the proposed maximum extent of the British Irish Ice Sheet (16-27 kyr B.P.), with implications for increased albedo effect during this interval. This also impacts on benthic productivity (Chapter 8), shutting down the seasonal phytoplankton bloom characteristic of the present day NE Atlantic Ocean. The results of this study suggest that sea-ice cover was present during three stages during Marine Isotope Stage 2; 30.7-31.5 kyr B.P. (Phase I), 29.1-30.3 kyr B.P. (Phase II) and a final phase 17.3-25 kyr B.P. (Phase III) and one stage during Marine Isotope Stage 3 (32-35 kyr B.P.).

10.2.4. How did the influence of Southern Component Water in this region vary between the Last Interglacial and the Holocene?

Data from the last interglacial indicate that Antarctic Intermediate Water has a strong influence between 1260-2118m water depth. During the last glacial, Glacial North Atlantic Intermediate Water dominates the geochemical signal down to 2118m water depth, except for

two episodes preceding Heinrich events (see below). Holocene data indicate a stratified water column similar in composition to that suggested by modern observations, with North Atlantic Deep Water present below approximately >2100m water depth and Antarctic Intermediate Water above this. The effect of glacial-interglacial variations on water mass flux and the resulting effect on sea surface temperatures can also be inferred from geochemical analysis and suggest that when Glacial North Atlantic Intermediate Water / Antarctic Intermediate Water flux crosses a threshold value in glacials / interglacials (respectively), this appears to result in stable SSTs in the North Atlantic region. Warm, stable SSTs as suggested by MAT correspond with a strong AAIW signal at all depths during the previous interglacial, whereas cold, stable SSTs correspond with a strong GNAIW signal at all sites down to approximately 2500m water depth. However, when the influence of either of these water masses is reduced (during the Holocene or MIS 3 where a good record exists) highly variable SSTs are recorded. It is important to consider the problem highlighted previously with respect to the lack of good modern analogues for the fossil assemblages of planktonic foraminifera when using the resulting SST values. The suggested increase in Mediterranean Outflow Water influence during the mid Holocene in core 9/97-10 is different from modern observations which show that MOW does not flow (as a discrete and discernable water mass) this far north in the NE Atlantic Ocean.

Heinrich events also impact on the palaeoceanography of this site with an increase in AABW flux potentially present 2-2.5 kyrs before two Heinrich events (H1 and H2) suggested for core 9/97-14. In a deeper core (9/97-27/2), strong negative carbon isotope excursions are observed and appear to precede two Heinrich events (H4 and H1). The observation of sites presumably bathed in SCW recording a negative isotope excursion (or an increase in SCW

flux) that precedes northern hemisphere Heinrich events suggest that events in the Southern Ocean are potentially preceding events in the Nordic Seas.

10.2.5. How does productivity vary through both time and space at this site?

A response to productivity variations is apparent when the known ecological preferences of certain benthic foraminiferid taxa are considered. This (in more than one way) appears to exert overwhelmingly the biggest influence on species distributions on the slope for the larger size fraction. The strong alignment of Uvigerinid species with components 1 and 2 following principal components analysis suggests that seasonality of food supply causes the strongest variation in assemblages. This is followed by glacial-interglacial variations in productivity (Component 3) and then depth-related variations in productivity (Component 4).

During the previous interglacial, *S.schlumbergeri, C.wuellerstorfi* and *M.barleeanum* are the most abundant species at intermediate depth sites, suggesting a lack of seasonality but slightly elevated levels of productivity, relative to the last glacial. Early last glacial (Marine Isotope Stage 3) assemblages are similar but contain a higher proportion of *U.peregrina* and lower abundance of *S.schlumbergeri*, which suggests some seasonality in food supply, similar to that indicated by Holocene assemblages. Late last glacial assemblages do not contain any *U.peregrina* which perhaps suggests a link to the sea-ice cover suggested above, which prevents seasonal phytoplankton blooms occurring during this time.

Accumulation rates of benthic foraminifera indicate that interglacials / interstadials record higher productivity relative to glacials / stadials regardless of water depth. A lack of correlation between fragmentation indices and BFAR suggests that dissolution is not

significantly influencing BFAR. Also, shallower sites record higher accumulation rates when compared to deeper sites. This pattern is consistently observed in most samples for all cores. Sedimentological evidence indicates that environmental stability may be increasing down slope, with less frequent erosive surfaces observed in deeper cores compared to shallower cores. This is potentially interacting with the down slope decrease in productivity to produce a mid-slope diversity maximum.

For the smaller size fraction, mixing both within and between cores appear to be more prevalent and suggest that proxy data based on small particle size data should be treated with caution.

10.2.6. Did the core of a bottom current vary in strength and positioning along the slope following glacial-interglacial climate variations, as proposed by Øvrebø *et al.* (2006)?

Following a previous examination of the contourite units preserved on the Porcupine Bank, Øvrebø *et al.* (2006) proposed that the core of a bottom current varied in strength and positioning along the slope, with increased strength and shallower water depth during interglacials. The results of this thesis do lend some support to this proposal, with evidence of increased mixing of assemblages during interglacials, perhaps with material advecting down slope due to Ekman divergence from a north or southward migrating bottom current. Also, the position of maximum abundance of one species, *Rupertina stabilis*, appears to migrate up and down the slope. As this species is known to rely on lateral currents with a consistent nutrient supply, this species is most probably following a region with a consistent, strong bottom current. There is some evidence to suggest enhanced bottom current activity was present

during the last interglacial relative to the last glacial and Holocene. However, it is not clear if the core of a bottom current migrated up and down slope in response to interglacial / glacial variations, although the migration of *R.stabilis* does potentially support this proposal.

10.3 Recommendations for further research

This study only examined seven gravity cores out of a total of eighty seven available from this study area kept at the Petroleum Affairs Division's (PAD) core store in Sandyford Industrial Estate, Dublin, as well as numerous piston cores and box cores stored at Nederlands Instituut voor Onderzoek der Zee (NIOZ), which should provide plenty of source material for future studies that expand on this research. Although many of these will not be suitable for palaeoceanographic research due to poor recovery, some (especially the long piston cores and the box core samples) could have the potential to provide higher resolution records of key intervals, or extend our understanding of palaeoceanographic processes further back in time. Based on this available dataset and the key findings of this research, the following areas of future research are recommended:

1. Examination of the modern benthic foraminifera from box core samples

Our current understanding of the ecology of several key species from this locality is currently poor. This site presents an ideal opportunity to examine the relative abundance of living benthic foraminifera in relation to a range of environmental parameters (e.g. grain size and sorting, surface productivity, flux rates, organic matter quality, seasonality of food supply,

bottom current strength, water column stratification). This would greatly enhance the application of benthic foraminifera to palaeocological reconstructions. For example, a study of living and fossil *Rupertina stabilis* would test the suitability of this species to geochemical studies as an alternative to *Cibicides wuellerstorfi* in regions where this species is relatively rare. Box core samples stored at NIOZ contain rose Bengal stained benthic foraminifera, so these could be related to the oceanographic conditions at the time these samples were recovered. This would significantly improve our understanding of the spatial distribution of benthic foraminifera in these deposits.

2. Higher resolution study of Heinrich event 4 from this area (ENAM core)

This study revealed apparent increases in productivity (inferred from BFAR) preceding and following Heinrich Event 4, a phenomenon not observed from other localities (e.g. Peck *et al.* 2007), but which could potentially be linked to the migration of the polar front over this core site during Dansgaard-Oeschger oscillations (Nees *et al.* 1997; Scourse *et al.* 2009). A higher resolution study of this in one (or ideally more) of the deeper water piston and gravity cores could investigate this further and explore the nature of the increased export production that presumably caused these peaks in BFAR. In particular, a high resolution planktonic (surface dwelling *G.bulloides* and deeper dwelling *N.pachyderma* sin.) geochemical study over this interval should reveal key information regarding changes in surface productivity and stratification. Paired with high resolution benthic $\delta^{13}C$ and faunal studies, as well as examination of IRD and available XRF data should better constrain the relative timing of the different processes operating during this interval, as well as identifying the potential role of the British Irish Ice Sheet.

3. Higher resolution study of the previous interglacial – last interglacial stability vs. influence of AAIW.

This project has highlighted the necessity of a higher resolution study of the last interglacial, particularly in relation to the relative distributions of different water masses through time. The data from this study suggests that at intermediate water depths (1250-2200m) during the previous interglacial an increased AAIW flux was detected in the Porcupine Bank region compared to today. Does an increase of an AAIW signal in the Porcupine Bank area and adjacent regions coincide with relatively stable SSTs and northern hemisphere climate in general (or does it lead / lag)? Although this study explored this, the low resolution of the cores examined at intermediate depths makes determinations of SST stability or otherwise impractical due to potential mixing effects. Cores from other sites at intermediate depths have the potential to record higher resolution records of the previous interglacial that may not suffer from mixing to such a degree. What is the threshold of volumetric flux of AAIW above which northern hemisphere climate is stabilized?

4. Multi-proxy (+/-) higher resolution examination of MIS 12, the MIS 12 / MIS 11 transition and MIS 11.

Marine Isotope Stage 11 has been suggested as an analogue for our current interglacial (Dickson *et al.* 2009). This stage is also part of the Mid-Brunhes Dissolution Interval (Droxler *et al.* 1990), a time where pelagic production increased dramatically and dissolution in deep and intermediate water depths increased globally (Barker *et al.* 2006). Examination of this interval, in light of current proposed effects of increased atmospheric CO^2 on oceanic acidification is recommended, particularly to provide information on the water mass distribution during this interval to examine the role of ocean circulation. However, as this

stage is part of a dissolution interval, carbonate based geochemical proxies are probably impractical. Perhaps the application of neodymium isotopes would be more appropriate for this as these can be measured on fish teeth which are composed of apatite and, therefore, less prone to dissolution than calcite. Marine Isotope Stage 12 is the 'coldest' glacial of the previous 500 kyr and a high resolution examination of this stage and the termination of it is feasible using the material examined in this project.

5. Holocene study – presence of MOW following the 8.2ka event – paired Cd/Ca and $\delta^{13}C$

Numerous cores recovered from this region contain Holocene sediments. A high resolution record of Holocene deposition at intermediate depths (approximately 1100-1300m water depth) has the potential to better constrain (and confirm) the increased flux of MOW during the mid Holocene. Identification of a potential MOW influence over this site should lead to a re-examination of MOW records from the Gulf of Cadiz / Portuguese continental margin to explore the cause of this.

References

Aller, R.C., 1990. Bioturbation and manganese cycling in hemipelagic sediments. *Philosophical Transactions of the Royal Society, London A*, 331, 51-68.

Altenbach, A.V., and Struck,U., 2001. On the coherence of organic carbon flux and benthic foraminiferal biomass. *Journal of Foraminiferal Research*, 31(2), 79-85.

Altenbach, A.V., Pflaumann, U., Schiebel, R., Thies, A., Timm, S. and Trauth, M., 1999. Scaling percentages and distributional patterns of benthic foraminifera with flux rates of organic carbon. *Journal of Foraminiferal Research*, 29(3): 173-185.

Andrews, J.T., Domack, E.W., Cunningham, W.L., Leventer, A., Licht, K.J., Jull, A.J.T., DeMaster, D.J., and Jennings, A.E., 1999. Problems and possible solutions concerning radiocarbon dating of surface marine sediments, Ross Sea, Antarctica. *Quaternary Research*, 52(2), 206-216.

Austin, W.E.N., and Evans, J.R., 1999. North East Benthic foraminifera taxonomy database. NEAPACC Data CD-ROM dataset, available from the British Ocean Sediment Core Repository, Southampton, SO14 3ZH, United Kingdom.

Austin, W.E.N. and Evans, J.R., 2000. NE Atlantic benthic foraminifera: modern distribution patterns and palaeoecological significance. *Journal of the Geological Society, London*, 157: 679-691.

Baas, J.H., Schönfeld, J., and Zahn, R., 1998. Mid-depth oxygen draw down during Heinrich events: evidence from benthic foraminiferal community structure, trace fossil tiering and benthic δ13C at the Portuguese Margin. *Marine Geology*, 152, 25-55.

Bandy, O.L., 1960. The geologic significance of coiling ratios in the foraminifer *Globigerina pachyderma* (Ehrenberg). *Journal of Paleontology*, 34, 671-681.

Bard, E., 2001. Palaeoceanographic implications of the difference in deep sea sediment mixing between large and fine particles. *Paleoceanography*, 16: 235-239.

Bard, E., Arnold, M., Maurice, P., Duprat, J., Moyes, J., and Duplessy, J.C., 1987. Retreat velocity of the North-Atlantic polar front during the last deglaciation determined by ^{14}C accelerator mass spectrometry. *Nature,* 328, 791-794.

Baringer, M.O., and Price, J.F., 1999. A review of the physical oceanography of the Mediterranean outflow. *Marine Geology*, 155, 63-82.

Barker, R.W., 1960. Taxonomic notes on the species figured by H. B. Brady in his report on the foraminifera dredged by H. M. S. Challenger during the years 1873-1876. *Society of Economical Petrology and Mineralogy, Special Publication,* 29, pp. 238.

Barker, S., Elderfield, H., 2002. Foraminiferal calcification response to glacial-interglacial changes in atmospheric CO^2. *Science*, 297, 833–836.

Barker, S., Cacho, I., Benway, H., and Tachikawa, K., 2005. Planktonic foraminiferal Mg/Ca as a proxy for past oceanic temperatures: a methodological overview and data compilation for the Last Glacial Maximum. *Quaternary Science Reviews*, 24, 821-834.

Barker, S., Archer, D., Booth, L., Elderfield, H., Henderiks, J., and Rickaby, R.E.M., 2006. Globally increased pelagic carbonate production during the Mid-Brunhes dissolution interval and the CO_2 paradox of MIS 11. *Quaternary Science Reviews*, 25, 3278-3293.

Barker, S., Diz, P., Vautravers, M.J., Pike, J., Knorr, G., Hall, I.R., and Broecker, W.S., 2009. Interhemispheric Atlantic seesaw response during the last deglaciation. *Nature*, 457, 1097-1101.

Bassinot, F.C., 2007. Oxygen isotope stratigraphy of the oceans. In: Elias, S.A., (eds.), *Encyclopaedia of Quaternary Science*, 1740-1748. Elsevier, Oxford.

Bauch, D., Darling, K., Simstich, J., Bauch, H.A., Erienkeuser, H., and Kroon, D., 2003. Palaeoceanographic implications of genetic variation in living North Atlantic *Neogloboquadrina pachyderma*. *Nature*, 242, 299-302.

Bauch, H.A., Erlenkeuser, H., Bauch, D., Mueller-Lupp, T., and Taldenkova, E., 2004. Stable oxygen and carbon isotopes in modern benthic foraminifera from the Laptev Sea shelf: implications for restructuring proglacial and profluvial environments in the Arctic. *Marine Micropalaeontology*, 51, 285-300.

Bemis, B.E., Spero, H.J., Bijma, J., and Lea, D.W., 1998. Reevaluation of the oxygen isotopic composition of planktonic foraminifera: Experimental results and revised paleotemperature equations. *Paleoceanography*, 13, 150–160.

Berger, W.H., 1970. Planktonic foraminifera: selective solution and the lysocline. *Marine Geology*, 8, 111-138.

Berger, W.H., and Piper, D.J.W., 1972. Planktonic foraminifera: Differential settling, dissolution and redeposition. *Limnology and Oceanography*, 17, 275-287.

Berger, W.H., and Vincent, E., 1986. Deep-sea carbonates: Reading the carbon-isotope signal. *Geologische Rundschau*, 75(1), 249-269.

Berger, W.H., Fischer, K., Lai, C., and Wu., G., 1988. Ocean carbon flux: global maps of primary production and export production. In: Agegian, C.R., (eds.) *Biogeochemical cycling and fluxes between the deep euphotic zone and other oceanic realms.* NOAA National Undersea Research Program, Research Reports, 88(1), 131-176.

Bernhard, J.M., and Alve, E., 1996. Survival, ATP pool, and ultrastructural characterization of benthic foraminifera from Drammensfjord (Norway): response to anoxia. *Marine Micropaleontology*, 28, 5-17.

Bersch, M., 1995. On the circulation of the northeastern Atlantic Ocean. *Deep-Sea research I*, 42(9), 1583-1607.

Bertram, C.J., Elderfield, H., Shackleton, N.J., and MacDonald, J.A., 1995. Cadmium/calcium and carbon isotope reconstructions of the glacial northeast Atlantic Ocean. *Paleoceanography*, 10(3), 563-578.

Bickert, T., and Wefer, G., 1999. South Atlantic and benthic foraminifer d13C-deviations: Implications for reconstructing the Late Quaternary deep-water circulation. *Deep-Sea Research*, 46, 437-452.

Birks, H.J.B., 1992. Some reflections on the application of numerical methods in Quaternary palaeoecology. University of Joensuu Publication, Karelian Institute, 102, 7-20.

Birks, H.J.B., 1995. Quantitative palaeoenvironmental reconstructions. In: Maddy, D., and Brew, J., (eds.), *Statistical modelling of Quaternary science data*, Technical Guide No. 5: Quaternary Research Association, Cambridge, 161-236.

Bishop, J.K.B., 1988. The barite-opal-organic carbon association in oceanic particulate matter. *Nature,* 332, 341-343.

Bond, G.C., Lotti, R., 1995. Iceberg Discharges into the North Atlantic on Millennial Time Scales During the Last Glaciation. *Science,* 267(5200), 1005.

Bond, G.C., Heinrich, H., Broecker, W.S., Labeyrie, L., McManus, J.F., Andrews, J.T., Huson, S., Jantschik, R., Clasen, S., Simet, C., Tedesco, K., Klas, M., Bonani, G., Ivy, S., 1992. Evidence for massive discharges of icebergs into the North Atlantic ocean during the last glacial period. *Nature*, 360(6401), 245-249.

Bond, G.C., Broecker, W., Johnsen, S., McManus, J., Labeyrie, L., Jouzel, J., and Bonani, G., 1993. Correlations between climate records from North Atlantic sediments and Greenland ice. *Nature*, 365, 143-147.

Bond, G.C., Showers, W., Elliot, M., Evans, M., Lotti, R., Hajdas, I., Bonani, G., and Johnson, S., 1999. The North Atlantic's 1-2 kyr climate rhythm: relation to Heinrich events, Dansgaard/Oeschger cycles and the Little IceAge. *Mechanisms of Global Climate Change at Millennial Time Scales*, Geophysical Monograph 112, American Geophysical Union, 35-57.

Boulton, G.S., Smith, G.S., Jones, A.J., and Newsome, J., 1985. Glacial geology and glaciology of the last mid-latitude ice sheets. Journal of the Geological Society, London, 142, 447-474.

Boulton, G.S., Peacock, J.D., and Sutherland, D.G., 1991. Quaternary. In: *The Geology of Scotland*, Craig G.Y., (eds.). Special Publication, Geological Society of London: London, 503–544.

Bowen, D.Q., Phillips, F.M., McCabe, A.M., Knutz, P.C., Sykes, G.A., 2002. New data for the Last Glacial Maximum in Great Britain and Ireland. *Quaternary Science Reviews*, 21, 89–101.

Boyle, E.A., 1983. Manganese carbonate overgrowths on foraminifera tests. *Geochimica et Cosmochimica Acta*, 47: 1815-1819.

Boyle, E.A., 1988. Cadmium: chemical tracer of deep-water paleoceanography. *Paleoceanography* 3: 471-490.

Boyle, E.A., 1992. Cadmium and δ13C paleochemical ocean distributions during the stage 2 glacial maximum, *Annual Review Earth and Planetary Science Letters*, 20, 245-287.

Boyle, E.A., and Keigwin, L.D., 1985. Comparison of Atlantic and Pacific paleochemical records for the last 215,000 years: changes in deep ocean circulation and chemical inventories. *Earth and Planetary Science Letters*, 76, 135-150.

Brady, H.B., 1884. Report on the Foraminifera dredged by H.M.S Challenger during the years 1873-1876. In: Murray, J., (ed.) *Report on the Scientific results of the Voyage of H.M.S. Challenger during the years 1873-1876, Zoology*, 9: 814 pp.

Braun, H., Christl, M., Rahmstorf, S., Ganopolski, A., Mangini, A., Kubatzki, C., Roth, K., and Kromer, B., 2005. Solar forcing of abrupt glacial climate change in a coupled climate system model. *Nature*, 438, 208-211.

Broecker, W. S., 1991. The great ocean conveyor. *Oceanography*, 4, 79-89.

Broecker, W.S., 1998. Paleocean circulation during the last deglaciation: A bipolar seesaw? *Paleoceanography*, 13, 119-121.

Broecker, W.S., and Clark, E., 2001. Glacial-to-Holocene redistribution of carbonate ion in the deep sea. *Science,* 294, 2152-2154.

Broecker, W.S., Andree, M., Bonani, G., Wolfli, W., Oeschger, H., Klas, M., 1988. Can the Greenland climatic jumps be identified in records from ocean and land? *Quaternary Research*, 30(1), 1-6.

Bryan, S. P., and Marchitto, T.M., 2008. The Mg/Ca - temperature proxy in benthic foraminifera: New calibrations from the Florida Straits and a hypothesis regarding Mg/Li. *Paleoceanography*, 23(2), PA2220, doi:10.1029/2007PA001553, 2008.

Buchner, P., 1940. Die Lagenen des Golfes von Neapel und der marinen Ablagerungen auf Ischia (Beitrage zur Naturgeschichte der Insel Ischia 1): Nova Acta Leopoldina, Abhandlungen def Kaiserlich Leopoldinisch-carolinisch deutschen Akademie der Naturforscher, new series, Y. 9(62), 364-560.

Cacchione, D.A., and Drake, D.E., 1986. Nepheloid layers and internal waves over continental shelves and slopes. *Geo-Marine Letters*, 6, 147–152.

Cacho, I., Grimalt, J.O., Pelejero, C., Canals, M., Sierro, F.J., Flores, J.A., and Shackleton, N., 1999. Dansgaard-Oeschger and Heinrich event imprints in Alboran Sea paleotemperatures. *Paleoceanography,* 14, 698-705.

Cannariato, K., and Stott, L.D., 2004. High-resolution bulk organic carbon $d^{13}C$ values argue against brief catastrophic releases of sedimentary methane to the surface waters of Santa Barbara Basin. *Geochemistry, Geophysics, Geosystems*, 5(5), Q05007, doi:10.1029/2003GC000600.

Carpenter, W.B., Jefreys, J.G., Thomson, W., 1870. Preliminary report of the scientific exploration of the deep sea in HM surveying-vessel Porcupine, during the summer of 1862.

Proceedings of the Royal Society of London, 18, 397-453.

Chan, L.H., Drummond, D., Edmond, J.M., and Grant, B., 1977. On the barium data from the Atlantic GEOSECS expedition. *Deep-Sea Research,* 24, 613-649.

Chapman, M.R., and Maslin, M.A., 1999. Low-latitude forcing of meridional temperature and salinity gradients in the subpolar North Atlantic and the growth of glacial ice sheets. Geology, 27(10), 875-878.

Chappell, J., and Shackleton, N.J., 1986. Oxygen isotopes and sea level. *Nature*, 324, 137-140.

Clark, P.U., Pisias, N.G., Stocker, T.F., and Weaver, A.J., 2002. The role of the thermohaline circulation in abrupt climate change. *Nature*, 415, 863-869.

Clark, J., McCabe, A.M., Schnabel, C., Clark, P.U., McCarron, S., Freeman, S.P.H.T., Maden, C., and Xu, S., 2009. Cosmogenic 10Be chronology of the last deglaciation of western Ireland, and implications for sensitivity of the Irish Ice Sheet to climate change. *GSA Bulletin*, 121, 3-16.

Claussen, M., Brovkin, V., Ganopolski, A., Kubatzki, C., and Petoukhov V., 2003. Climate change in northern Africa: The past is not the future. *Climate Change*, 57(1-2), 99-118.

Cleveringa, P., Meijer, T., van Leeuwen, R.J.W., de Wolf, H., Pouwer, R., Lissenberg T., and Burger, A.W., 2000. The Eemian stratotype locality at Amersfoort in the central Netherlands: a re-evaluation of old and new data. *Geologie en Mijnbouw / Netherlands Journal of Geosciences*, 79, 197-216.

CLIMAP, Climate: Long-Range Investigation, Mapping, and Prediction Project Members, 1976. The surface of the Ice Age Earth. *Science*, 191, 1131-1137.

CLIMAP, Climate: Long-Range Investigation, Mapping, and Prediction Project Members, 1981. Seasonal reconstructions of the Earth's surface at the Last Glacial Maximum. *Geological Society of American Map Chart Series MC*, 36, 1-18.

Cobb, K.M., Charles, C.D., Cheng, H., and Edwards, R.L., 2003. El Niño/Southern Oscillation and tropical Pacific climate during the last millennium. *Nature*, 424, 271-276.

Coles, G.P., Ainsworth, N.R., Whaley, R.C., and Jones, R.W., 1996. Foraminifera and Ostracoda from Quateranry carbonate mounds associated with gas seepage in the Porcupine Basin, Offshore Western Ireland. *Revista Española de Micropaleontología*, 28(2), 113-151.

Cook, E.R., d'Arrigo, R.D., and Briffa, K.R., 1998. The North Atlantic Oscillation and its expression in circum-Atlantic tree-ring chronologies from North America and Europe. *The Holocene,* 8(1), 9-17.

Corliss, B.H., and Chen, C., 1988. Morphotype patterns of Norwegian Sea deep-sea benthic foraminifera and ecological implications. *Geology*, 16, 716-719.

Coxall, H.K., Wilson, P.A., Pälike, H., Lear, C.H., and Backman, J., 2005. Rapid stepwise onset of Antarctic glaciations and deeper calcite compensation in the Pacific Ocean. *Nature*, 433, 53-57.

Coxon, P., 2001. Cenozoic: Tertiary and Quaternary (until 10 000 years before present). In: Holland, C.E., (eds.), *The Geology of Ireland*. Dunedin Academic Press, Edinburgh, 387-427.

Crowley, T.J., 1985. Late Quaternary carbonate changes in the North Atlantic and Atlantic/Pacific comparisons. In: Sundquist, E., Broecker, W.S., (eds.), *The Carbon Cycle and Atmospheric CO2: Natural Variations Archean to Present,* Geophysical Monograph Series, AGU, Washington DC, 271–284.

Currie, L.A., Klouda, G.A., Benner, B.A., and Garrity, K., 1999. Isotopic and molecular fractionation in combustion; Three Routes to Molecular Marker Validation, Including Direct Molecular `Dating' (GC/AMS). *Atmospheric Environment*, 33, 2789-2806.

Cushman, J.A., 1911. A monograph of the foraminifera of the North Pacific Ocean, Part II: Textulariidae. *Bulletin of the United State National Museum*, 71(2), 1-156.

Cushman, J.A., 1923. Foraminifera of the Atlantic Ocean. *Bulletin of the United States National Museum*, 228 pp.

Cushman, J.A., 1940. Foraminifera: Their classification and economic use (3rd ed.), Harvard University Press, Cambridge (Massachusetts), pp. 275.

Dansgaard, W., Johnsen, S.J., Clausen, H.B., Dahl-Jensen, D., Gundestrup, N.S., Hammer, C.U., Hvidberg, C.S., Steffensen, J.P., Sveinbjornsdottir, A.E., Jouzel, J., Bond, G., 1993. Evidence for general instability of past climate from a 250-kyr ice-core record. *Nature*, 364, 218–220.

Darling, K.F., Wade, C.M., Stewart, I., Kroon, D., Dingle, R., and Leigh Brown, A.J., 2000. Molecular evidence for genetic mixing of Arctic and Antarctic subpolar populations of planktonic foraminifers. *Nature*, 405: 43- 47.

Darling, K.F., Kucera, M., Pudsey, C., and Wade, C., 2004. Molecular evidence links cryptic diversification in polar planktonic protists to Quaternary climate dynamics. *Proceedings of the National Academy of Science*, 101(20): 7657-7662.

Davies, S.M., Branch, N.P., Lowe, J.J., and Turney, C.S.M., 2002. Towards a European tephrochronological framework for Termination 1 and the early Holocene. *Philosophical Transactions of the Royal Society of London,* Series A, 360, 767-802.

Delaney, M.L., Be, A.W.H., and Boyle E.A., 1985. Li, Sr, Mg, and Na in foraminiferal calcite shells from laboratory culture, sediment traps, and sediment cores. *Geochimica et Cosmochimica Acta*, 49, 1327-1341.

Dickens, G.R., O'Neill, J.R., Rea, D.K., and Owen, R.M., 1995. Dissociation of oceanic methane hydrate as a cause of the carbon isotope excursion at the end of the Paleocene. *Paleoceanography*, 10(6), 965–971.

Dickson, R.R. and McCave, I.N., 1986. Nepheloid layers on the continental slope west of Porcupine Bank. *Deep-Sea Research*, 33: 791-818.

Dickson, R., Lazier, J., Meincke, J., Rhines, P., and Swift, J., 1996. Long-term coordinated changes in the convective activity of the North Atlantic. *Progress in Oceanography*, 38, 241-295.

Dickson, A.J., Austin, W.E.N., Hall, I.R., Maslin, M.A., and Kucera, M., 2008. Centennial-scale evolution of Dansgaard-Oeschger events in the northeast Atlantic Ocean between 39.5 and 56.5 ka B.P. *Paleoceanography*, 23, PA3206, doi:10.1029/2008PA001595.

Dickson, A.J., Beer, C.J., Dempsey, C., Maslin, M.A., Bendle, J.A., McClymont, E.L., and Pancost, R.D., 2009. Oceanic forcing of the Marine Isotope Stage 11 interglacial. *Nature geosciences*, 2, 428-433.

Dokken, T.M., and Nisancioglu, K.M., 2004. Palaeoclimatology: fresh angle on the polar seesaw. *Nature*, 430, 842-843.

Donner, J., 1995. The quaternary history of Scandinavia. Cambridge University Press, UK, pp. 200.

Droxler, A.W., Haddad, G.A., Mucciarone, D.A., Cullen, J.L., 1990. Pliocene–Pleistocene aragonite cyclic variations in holes 714A and 716B (The Maldives) compared with hole 633A (The Bahamas): records of climate-induced CaCO3 preservation at intermediate depths. *Proceedings of the Ocean Drilling Program, Scientific Results*, 115, 539–567.

Droxler, A.W., Ferro, E.C., Mucciarone, D.A., Haddad, G.A., 1997. The marine carbonate system during oxygen isotope stage 11 (423–362 ka): a case of basin-to-shelf and/or basin-to-basin carbonate fractionation? *EOS, Transactions of the American Geophysical Union*, 78, S179.

Earland, A., 1936. Foraminifera. Part IV. Additional records from the Weddell Sea sector from material obtained by the S.Y. Scotis. *Discovery reports*, 13, 76 pp.

Elderfield, H., Bertram, C.J., and Erez, J., 1996. A biomineralization model for the incorporation of trace elements into foraminiferal calcium carbonate. *Earth and Planetary Science Letters*, 142, 409-423.

Elderfield, H., and Ganssen, G., 2000. Past temperature and $\delta^{18}O$ of surface ocean waters inferred from foraminiferal Mg/Ca ratios. *Nature*, 405, 442-445.

Emiliani, C., 1955. Pleistocene temperatures. *Journal of Geology*, 63, 538-78.

Emiliani, C., 1972. Quaternary paleotemperatures and the duration of the high temperature intervals. *Science*, 178, 398-401.

EPICA community members, 2004. Eight glacial cycles from an Antarctic ice core. *Nature*, 429, 623–628.

EPICA community members, 2006. One-to-one coupling of glacial climate variability in Greenland and Antarctica. *Nature*, 444, 195-198.

Ericson, D.B., 1959, Coiling direction of *Globigerina pachyderma* as a climatic index. *Science*, 130, 219-220.

Etter, R.J. and Grassle, F.J., 1992. Patterns of species diversity in the deep sea as a function of sediment particle size diversity. *Nature*, 360: 576-578.

Fairbanks, R.G., Mortlock, R.A., Chiu, T.C., Cao, L., Kaplan, A., Guilderson, T.P., Fairbanks T.W., and Bloom, A.L., 2005. Marine Radiocarbon Calibration Curve Spanning 10,000 to 50,000 Years B.P. Based on Paired $^{230}Th/^{234}U/^{238}U$ and ^{14}C Dates on Pristine Corals. *Quaternary Science Reviews*, 24, 1781-1796.

Fariduddin, M. and Loubere, P., 1997. The surface ocean productivity response of deeper water benthic foraminifera in the Atlantic Ocean. *Marine Micropalaeontology*, 32: 289-310.

Fatela, F., and Taborda, R., 2002. Confidence limits of species proportions in microfossil assemblages. *Marine Micropaleontology*, 45: 169-174.

Faugères, J.C.and Stow, D.A.V., 1993. Bottom-Controlled Sedimentation: A Synthesis of the Contourite Problem. *Sedimentary Geology*, 82, 287–297.

Feyling-Hansen, R.W., 1964. Foraminifera in Late Quaternary deposits from the Oslofjord area. *Norges Geologiske Undersökelse*, 225, 383 pp.

Fluckiger, J., Knutti, R., and White, J.W.C., 2006. Oceanic processes as potential trigger and amplifying mechanisms for Heinrich events. *Paleoceanography*, 21, PA2014, doi:10.1029/2005PA001204.

Fontanier, C., Jorissen, F.J., Licari, L., Alexandre, A., Anschutz, P. and Carbonel, P., 2002. Live benthic foraminiferal faunas from the Bay of Biscay: faunal density, composition, and microhabitats. *Deep-Sea Research, Part I*, 49: 751-785.

Fontanier, C., Jorissen, F.J., David, C., Anschutz, P., Chaillou, G., Lafon, V., 2003. Seasonal and interannual variability of benthic foraminiferal faunas at a 550 m depth in the Bay of Biscay. *Deep-Sea Research I*, 50, 457-494.

Fontanier, C., Jorissen, F.J., Anschutz, P., and Chaillou, G., 2006. Seasonal variability of foraminiferal faunas at 1000m depth in the Bay of Biscay. *Journal of Foraminiferal Research*, 36, 61-76.

Fretwell, P.T., Smith, D.E., and Harrison, S., 2008. The Last Glacial Maximum British–Irish Ice Sheet: a reconstruction using digital terrain mapping. *Journal of Quaternary Science*, 23(3), 241-248.

Galloway, J. J., and Wissler, S. G., 1927. Pleistocene foraminifera from the Lomita Quarry, Palos Verdes Hills, California. *Journal of Paleontology*, 1, 35-87.

Ganssen, G.M., and Kroon, D., 2000. The isotopic signature of planktonic foraminifera from NE Atlantic surface sediments: implications for the reconstruction of past oceanic conditions. *Journal of the Geological Society, London*, 157, 693-699.

Genty, D., Blamart, D., Ouahdi, R., Gilmour, M., Baker, A., Jouzel, J., and Van-Exter, S., 2003. Precise dating of Dansgaard–Oeschger climate oscillations in western Europe from stalagmite data. *Nature*, 421, 833-837.

Gersonde, R., Crosta, X., Abelman, A., Armand, L.K., 2005. Sea-surface temperature and sea ice distribution of the Southern Ocean at the EPILOG Last Glacial Maximum: A circum-Antarctic view based on siliceous microfossil records. *Quaternary Science Reviews*, 24, 869-896.

Gibbard, P.L., 2003. Definition of the Middle-Upper Pleistocene boundary. *Global and Planetary Change*, 36, 201-208.

Gibbard, P.L., Head, M.J., Walker, M.J.C., and The Subcommision on Quaternary Stratigraphy, 2009. Formal ratification of the Quaternary System / Period and the Pleistocene Series/Epoch with a base at 2.58 Ma. Journal of Quaternary Science, DOI: 10.1002/jqs.1338.

Gooday, A. J., 1986a. Meiofaunal foraminiferans from the bathyal Porcupine Seabight (Northeast Atlantic): size structure, standing stock, taxonomic composition, species diversity and vertical distribution in the sediment. *Deep Sea Research*, 33, 1345–1373.

Gooday, A. J., 1986b. Soft-shelled foraminifera in meiofauna samples from the bathyal northeast Atlantic. *Sarsia*, 71, 275–287.

Gooday, A.J., 1988. A response by benthic foraminifera to the deposition of phytodetritus in the deep sea. *Nature*, 332, 70-73.

Gooday, A. J., 1999. Biodiversity of Foraminifera and other protists in the deep-sea: scales and patterns. *Belgian Journal of Zoology*, 129, 61–80.

Gooday, A.J. and Lambshead, P.J.D., 1989. Influence of seasonally deposited phytodetritus on benthic foraminiferal populations in the bathyal northeast Atlantic: The species response. *Marine Ecology Progress Series*, 58: 53-67.

Gooday, A.J., and Hughes, J.A., 2002. Foraminifera associated with phytodetritus deposits at a bathyal site in the northern Rockall Trough (NE Atlantic): seasonal contrasts and a comparison of stained and dead assemblages. *Marine Micropalaeontology*, 46, 83-110.

Gooday, A. J., Carstens, M., and Thiel, H., 1995. Micro-and nano-foraminifera from abyssal Northeast Atlantic sediments: A preliminary report. *International Revue ges Hydrobiologie*, 80, 361–383.

Gooday, A. J., Bett, B.J., Shires, R., and Lambshead, P.J.D., 1998. Deep-sea benthic foraminiferal species diversity in the NE Atlantic and NW Arabian Sea: a synthesis. *Deep Sea Research II*, 45, 165–201.

Green, O.R., 2001. A Manual of Practical Laboratory and Field Techniques in Palaeobiology. Kluwer Academic Publishers. 538 pages.

Greig-Smith, P., 1983. Quantitative plant ecology. Third edition. Blackwell, London.

Grootes, P.M., and Stuiver, M., 1997. Oxygen 18/16 variability in Greenland snow and ice with 10^3 to 10^5-year time resolution. *Journal of Geophysical Research*, 102:26455-26470.

Grootes, P.M., Stuiver, M., White, J.W.C., Johnsen, S.J., and Jouzel, J., 1993. Comparison of oxygen isotope records from the GISP2 and GRIP Greenland ice cores. *Nature*, 366, 552–554.

Grousset, F.E., Pujol, C., Labeyrie, L., Auffret, G., and Boelaert, A., 2000. Were the North Atlantic Heinrich events triggered by the behavior of the European ice sheets? *Geology*, 28, 123–126.

Guichard, S., Jorissen, F.J. and Peypouquet, J.P., 1999. Late Quaternary benthic foraminiferal records testifying lateral variability of the Cape Blanc upwelling signal. *Comptes Rendus de l'Academie de Sciences, Paris.* Sciences de la Terre et des Planetes, 329, 295-301.

Guiot, J., and de Vernal, A., 2007. Transfer functions: Methods for quantitative palaeoceanography based on microfossils. In: Developments in Marine Geology 1: Proxies in Late Cenozoic paleoceanography. Hillaire-Marcel, C., and De Vernal, A., (eds.), Elsevier, Amsterdam, The Netherlands. 523-563.

Gustafsson, M., and Nordberg, K., 2001. Living (stained) benthic foraminiferal response to primary production and hydrography in the deepest part of the Gullmar Fjord, Swedish

west coast, with comparisons to Höglund's 1927 material. *Journal of Foraminiferal Research*, 31, 2-11.

Gwiazda, R. H., Hemming, S.R., and Broecker, W.S., 1996. Provenance of icebergs during Heinrich event 3 and the contrast to their sources during other Heinrich episodes.

Paleoceanography, 11(4), 371–378.

Hall, J.M., 2002. Barium and lithium in foraminifera: Glacial-interglacial changes in the north atlantic. Unpublished PhD Thesis, Louisiana State University.

Hall, I.R., and Becker, J., 2006. Deep Western Boundary Current variability in the subtropical northwest Atlantic Ocean during marine isotope stages 12–10. *Geochemistry, Geophysics, Geosystems*, 8(6): doi:10.1029/2006GC001518.

Hall, J.M., and Chan, L.H., 2003. Li/Ca in multiple species of benthic and planktonic foraminifera: Thermocline and glacial-interglacial changes. *Geochimica et Cosmochimica Acta*, 68, 529-545.

Hall, J.M., and Chan, L.H., 2004. Ba/Ca in *Neogloboquadrina pachyderma* as an indicator of meltwater discharge into the western Arctic Ocean. *Paleoceanography* 19(1), PA1017, 10.1029/2003PA000910.

Hall, I.R., Moran, S.B., Zahn, R., Knutz, P.C., Shen, C-C., and Edwards, R.L., 2006. Accelerated draw-down of meridional overturning in the late-glacial Atlantic triggered by transient pre-H event freshwater perturbation. *Geophysical Research Letters*. 33, L16616, doi:10.1029/2006GL026239.

Harlof, J., and Mackensen, A., 1997. Recent benthic foraminiferal associations and ecology of the Scotia Sea and Argentine Basin. *Marine Micropaleontology*, 31, 1-29.

Hátún, H., Sandø, A.B., Drange, H., Hansen, B., and Valdimarsson, H., 2005. Influence of the Atlantic subpolar gyre on the thermohaline circulation. *Science*, 309, 1841-1844.

Hawley, N., 2004. Response of the benthic nepheloid layer to near-inertial internal waves in southern Lake Michigan. *Journal of Geophyical Research*, 109, C04007, doi:10.1029/2003JC002128.

Hays, J.D., Imbrie, J., and Shackleton, N.J., 1976. Variations in the Earth's Orbit: Pacemaker of the Ice Ages. *Science*, 194(4207), 1121-1132.

Heinrich, H., 1988. Origin and consequences of cyclic ice rafting in the Northeast Atlantic Ocean during the past 130,000 years. *Quaternary Research*, 29, 142-152.

Heinrich, R., Baumann, K.H., Huber, R., Meggers, H., 2002. Carbonate preservation records of the past 3Myr in the Norwegian-Greenland Sea and the northern North Atlantic: implications for the history of NADW production. *Marine Geology*, 184, 17–39.

Hemleben, C., Spindler, M., and Anderson, O.R., 1989. Modern Planktonic Foraminifera. Springer-Verlag, New York, 363 pp.

Herguera, J.C. and Berger, W.H., 1991. Palaeoproductivity: glacial to postglacial change in the western equatorial Pacific, from benthic foraminifera. *Geology*, 19: 1173-1176.

Hermelin, J.O.R. and Scott, D.B., 1985. Recent benthic foraminifera from the central North Atlantic. *Micropaleontology*, 31 (3): 199-220.

Hester, K., and Boyle E.A., 1982. Water chemistry control of the cadmium content of some recent benthic foraminifera. *Nature*, 298, 260-262.

Hieftje, G., Huang, M., Lehn, S., Warner, K., Gamez, G., Ray, S., and Leach, A., 2002. Toward a fuller understanding of analytical atomic spectrometry. *Analytical Sciences*. 18: 1185-1189.

Higgins, S.M., Jenkins, C.J., Morin, P., Ito, E., Kamp, B., Yu-Chung, C.J., Lee, J., Rao, A., Leigh, J., Johnson, A., and Renambot, L., 2006. An update on CoreWall Tool Suite development: An integrated approach for data discovery, description, visualization and correlation. American Geophysical Union, Fall Meeting 2006, Abstract number: N13C-1174.

Hill, M.O., and Gauch, H.G., 1980. Detrended Correspondence analysis: an improved ordination technique. *Vegetatio,* 42, 47-58.

Hillaire-Marcel, C., de Vernal, A., Bilodeau, G., and Weaver, A.J., 2001. Absence of deep-water formation in the Labrador Sea during the last interglacial period. *Nature*, 410, 1073-1077.

Hjulstrøm, F., 1939. Transportation of debris by moving water. In: Trask, P.D., eds., Recent Marine Sediments; A Symposium. Tulsa, Oklahoma, American Association of Petroleum Geologists, 5-31.

Hoddell, D.A., Charles, C.D., Ninnemann, U.S., 2000. Comparison of interglacial stages in the South Atlantic sector of the southern ocean for the past 450 kyr: implifications for Marine Isotope Stage (MIS) 11. *Global Planetary Change*, 24, 7–26.

Holliday, N.P., Pollard, R.T., Read, J.F., and Leach, H., 2000. Water mass properties and fluxes in the Rockall Trough, 1975-1998. *Deep-Sea Research I*, 40, 1521-1527.

Horton, B.P., and Edwards, R.J., 2005. Quantifying Holocene sea-level change using intertidal foraminifera: lessons from the British Isles. Cushman Foundation for Foraminiferal Research, Special Publication, 40, 97 pp.

Hubbard, A., Bradwell, T., Golledge, N., Hall, A., Patton, H., Sugden, D., Cooper, R., and Stocker, M., 2009. Dynamic cycles, ice streams and their impact on the extent, chronology and deglaciation of the British–Irish ice sheet. *Quaternary Science Reviews*, 28, 758-776.

Hughen, K.A., Southon, J.R., Lehman, S.J., and Overpeck, J.T., 2000. Synchronous radiocarbon and climate shifts during the last deglaciation. *Science*, 290(5498), 1951-1954.

Hurrell, J.W., 1995. Decadal trends in the North Atlantic Oscillation: Regional temperatures and precipitation. *Science*, 269(5224), 676-679.

Huston, M., 1979. A general hypothesis of species diversity. *American Naturalist*, 113(1): 81-101.

Hutson, W.H., 1980. The Aghulas current during the Late Pleistocene: Analysis of modern faunal analogs. *Science*, 207, 64-66.

Huybers, P., 2009. Antarctica's Orbital Beat. *Science*, 325, 1085.

Imbrie, J.D., and Kipp, N.G., 1971. A new micropaleontological method for quantitive paleoclimatology: Applicaton to a late Pleistocene Caribbean core. In: Turekian, K.K., (eds.) *The Late Cenozoic glacial ages*. Yale University Press, New Haven, USA, 71-181.

Imbrie, J., Hays, J.D., Martinson, D.G., McIntyre, M., Mix, A.C., Morley, J.J., Paces, N.G., Prell, W.L., and Shackleton, N.J., 1984. The orbital theory of Pleistocene climate: support from a revised chronology of the marine $\delta^{18}O$ record. In: *Milankovitch and climate*, part 1. Edited by A., Berger *et al.*, pp. 269-305.

Jacquet, S.H.M., Dehairs, F., Cardinal, D., Navez, J., and Delille, B., 2005. Barium distribution across the Southern Ocean frontal system in the Crozet-Kerguelen Basin. *Marine Chemistry*, 95, 149-162.

Johnson, R.G., 1997. Climate control requires a dam at the Strait of Gibraltar. *Eos Transactions*, AGU, 78(27), 280-281.

Jones, R.W., 1984a. Late Quaternary benthonic foraminifera from deep water sites in the North East Atlantic and Arctic Oceans. Unpublished PhD Thesis, University College of Wales, Aberystwyth.

Jones, R.W., 1984b. Revised classification of the Unilocular Nodosariida and Buliminida (Foraminifera). *Revista Española Micropalaeontologia,* 6, 91-160.

Jones, R.W., 1994. The Challenger Foraminifera. Oxford University Press, Oxford, pp. 149.

Jorissen, F.J. and Wittling, I., 1999. Ecological evidence from taphonomical studies; living-dead comparisons of benthic foraminiferal faunas off Cape Blanc (NW Africa). *Palaeogeography, Palaeoclimatology, Palaeoecology*, 149, 151-170.

Jorissen, F.J., De Stigter, H.C. and Widmark, J.G.V, 1995. A conceptual model explaining benthic foraminiferal microhabitats. *Marine Micropalaeontology*, 26: 3-15.

Juggins, S., 2003. C2 software for ecological and palaeoecological data analysis and visualization, User Guide Version 1.3, 69 pp.

Kandiano, E.S., and Bauch, H.A., 2003. Surface ocean temperatures in the north-east Atlantic during the last 500 000 years: evidence from foraminiferal census data. *Terra Nova*, 15(4), 265-271.

Kandiano, E.S., and Bauch, H.A., 2007. Phase relationship and surface water mass change in the Northeast Atlantic during Marine Isotope Stage 11 (MIS 11). *Quaternary Research*, 68(3), 445-455.

Kaiho, K., 1994. Benthic foraminiferal dissolved-oxygen index and dissolved-oxygen levels in the modern ocean. *Geology*, 22(8), 719-722.

Kanfoush, S.L., Hodell, D.A., Charles, C.D., Guilderson, T.P., Mortyn, P.G., and Ninnemann, U.S., 2000. Millennial-Scale Instability of the Antarctic Ice Sheet During the Last Glaciation. *Science*, 288(5472), 1815-1819.

Kennett, J.P., and Srinivasan, M.R., 1983. Neogene planktonic foraminifera: a phylogenetic atlas. Hutchinson Ross, Stroudsburg, P.A.

Kennett, J.P., Cannariato, K.G., and Hendy, I.L., and Behl, R.J., 2000. Carbon isotopic evidence for methane hydrate instability during Quaternary interstadials. *Science*, 288(5463), 128-133.

Kennett, J.P., Cannariato, K.G., and Hendy, I.L., and Behl, R.J., 2003. Methane Hydrates in Quaternary climate change: the clathrate gun hypothesis, American Geophysical Union, Washington DC, USA, pp. 216.

Knight, J., 2006. Sub-ice shelf deposition during the late Devensian glaciation in western Ireland. *Marine Geology*, 235, 229-240.

Knutz, P.C., Jones, E.J.W., Austin, W.E.N., and van Weering, T.C.E., 2001. Glacimarine slope sedimentation, contourite drifts and bottom current pathways on the Barra Fan, UK North Atlantic margin. *Marine Geology*, 188, 129-146.

Knutz, P.C., Hall, I.R., Zahn, R., Rasmussen, T.L., Kuijpers, A., Moros, M., and Shackleton, N.J., 2002. Multidecadal ocean variability and NW European ice sheet surges during the last deglaciation, *Geochemistry, Geophysics, Geosystems,* 3.

Knutz, P.C., Zahn, R., and Hall, I.R., 2007. Centennial-scale variability of the British Ice Sheet: Implications for climate forcing and Atlantic meridional overturning circulation during the last deglaciation. *Paleoceanography*, 22, PA1207, doi: 10.1029/2006PA001298.

Koç, N., Jansen, E., and Haflidason, H., 1993. Palaeoceanographic reconstructions of surface ocean conditions in the Greenland, Iceland and Norwegian seas through the last 14ka based on diatoms. *Quaternary Science Reviews*, 12, 115-140.

Kucera, M., 2007. Planktonic foraminifera as tracers of past oceanic conditions. In: Developments in Marine Geology 1: Proxies in Late Cenozoic paleoceanography. Hillaire-Marcel, C., and De Vernal, A., (eds.), Elsevier, Amsterdam, The Netherlands. 213-262.

Kucera, M., and Darling, K.F., 2002. Cryptic species of planktonic foraminifera: their effect on paleoceanographic reconstructions. *Philosophical Transactions of the Royal Society of London,* A, 360: 695-718.

Kucera, M., Weinelt, M., Kiefer, T., Pflaumann, U., Hayes, A., Martin Weinelt, M., Chen, M-T., Mix, A.C., Barrow, T.T., Cortijo, E., Duprat, J., Juggin, S., and Waelbroeck, C., 2005. Reconstruction of sea-surface temperatures from assemblages of planktonic foraminifera: multi-technique approach based on geographically constrained calibration data sets and its application to glacial Atlantic and Pacific Oceans. *Quaternary Science Reviews*. 24, 951-998.

Kuhnt, W., Hess, S. and Jian, Z., 1999. Quantitative composition of benthic foraminiferal assemblages as a proxy indicator for organic carbon flux rates in the South China Sea. In: Sarnthein, M. and Wang, P. X., (eds.), *Response of West Pacific Marginal Seas to Global Climate Change. Marine Geology*, 156: 123-157.

Labeyrie, L.D., Duplessy, J-C., and Blanc, P.L., 1987. Variations in mode of formation and temperature of oceanic deep waters over the past 125,000 years. *Nature*, 327, 477-483.

Lacan, F., Francois, R., Ji, Y., and Sherrell, R.M., 2006. Cadmium isotopic composition in the ocean. *Geochimica et Cosmochimica Acta*, 70(20), 5104-5118.

Lassen, S., Kuijpers, A., Kunzendorf H., Lindgren, H., Heinemeier, J., Jansen, E., and Knudsen, K.L., 2002. Intermediate water signal leads surface water response during Northeast Atlantic deglaciation. *Global and Planetary Change*, 32, 111-125.

Le, J., and Shackleton, N.J., 1992. Carbonate dissolution fluctuations in the Western Equatorial Pacific during the Late Quaternary. *Paleoceanography*, 7(1), 21–42.

Lea, D.W., and Boyle, E.A., 1989. Barium content of benthic foraminifera controlled by bottom water composition. *Nature,* 338, 751-753.

Lear, C.H., Elderfield, H., and Wilson, P.A., 2000. Cenozoic deep-sea temperatures and global ice volumes from Mg/Ca in benthic foraminiferal calcite. *Science*, 287, 269-272.

Legendre, P., and Gallagher, E., 2001. Ecologically meaningful transformations for ordination of species data. *Oecologia*, 129: 271-280.

Linke, P., 1992. Metabolic adaptations of deep-sea benthic foraminifera to seasonally varying food input. *Marine Ecology Progress Series*. 81: 51-63.

Linke, P. and Lutze, G.F., 1993. Microhabitat preferences of benthic foraminifera: A static concept or a dynamic adaptation to optimise food acquisition? *Marine Micropaleontology*, 20: 215-233.

Lisiecki, L.E., and Raymo, M.E., 2005. A Pliocene-Pleistocene stack of 57 globally distributed benthic $\delta^{18}O$ records. *Paleoceanography*, 20, PA1003, doi:10.1029/2004PA001071.

Loeblich, A.R., and Tappan, H., 1953. Studies of Arctic foraminifera. *Smithsonian Miscellaneous Collections*, 121, 150 pp.

Longet, D., and Pawlowski, J., 2007. Higher-level phylogeny of foraminifera inferred from the RNA polymerase II (RPB1) gene. *European Journal of Protistology*, 43, 171-177.

Loubere, P., 1991. Deep-sea foraminiferal assemblage response to a surface ocean productivity gradient: A test. *Paleoceanography*, 6: 193-204.

Loutre, M.F., and Berger, A., 2003. Stage 11 as an analogue for the present interglacial. *Global and Planetary Change*, 36(3), 209-217.

Lukashina, N.P., 1983. Distribution of recent bottom foraminifers in the north-eastern Atlantic. *Oceanology*, 23, 100-105.

Lukashina, N. P., 1988a. Benthic foraminifera communities and water masses of the North Atlantic and the Norway-Greenland Basin. *Oceanology*, 28, 612–617.

Lukashina, N. P., 1988b. Distribution patterns of benthic foraminifera in the North Atlantic. *Oceanology*, 28, 492–497.

Lutze, G.F., and Thiel, H., 1989. Epibenthic foraminifera from elevated habitats: *Cibicidoides wuellerstorfi* and *Planulina ariminensis*. *Journal of Foraminiferal Research*, 19: 153-158.

Lynch-Stieglitz, J. and Fairbanks, R.G., 1994. A conservative tracer for glacial ocean circulation from carbon isotope and palaeo-nutrient measurements in benthic foraminifera. *Nature*, 369, 308-310.

Lynch-Stieglitz, J., Fairbanks, R.G., and Charles, C.D., 1994. Glacial-interglacial history of Antarctic Intermediate Water: Relative strengths of Antarctic vs. Indian Ocean sources. *Paleoceanography*, 9, 7-29.

Lynch-Stieglitz, J., Stocker, T.F., Broecker W.S., and Fairbanks, R.G., 1995. The influence of air-sea exchange on d13C of SCO2 in the surface ocean: Observations and Modeling. *Global Biogeochemical Cycles*, 9, 653-665.

Lynch-Stieglitz, J., Adkins, J.F., Curry, W.B., Dokken, T., Hall, I.R., Herguera, J.C., Hirschi, J.J-.M., Ivanova, E.V., Kissel, C., Marchal, O., Marchitto, T.M., McCave, N., McManus, J.M., Mulitza, J.F., Ninnemann, U., Peeters, F., Yu, E-.F., and Zahn, R., 2007. Atlantic meridional overturning circulation during the Last Glacial Maximum. *Science*. 316: 66-69.

Manighetti, B., McCave, I.N., Maslin, M., and Shackleton, N.J., 1995. Chronology for Climate Change: Developing Age Models for the Biogeochemical Ocean Flux Study Cores. *Paleoceanography*, 10(3), 513–525.

Marchitto, T. M., 2004. Lack of a significant temperature influence on the incorporation of Cd into benthic foraminiferal tests. *Geochemistry, Geophysics, Geosystems*, 5(10), Q10D11, doi:10.1029/2004GC000753, 2004.

Marchitto, T. M., Oppo, D.W., and Curry, W.B., 2002. Paired benthic foraminiferal Cd/Ca and Zn/Ca evidence for a greatly increased presence of Southern Ocean Water in the glacial North Atlantic. *Paleoceanography*, 17(3), 1038, doi:10.1029/2000PA000598.

Martin, S., and Drucker, R., 1997. The effect of possible Taylor columns on the summer ice retreatin the Chukchi Sea. *Journal of Geophysical Research*, 102(5), 473-482.

Martin, P.A., and Lea, D.W., 2002. A simple evaluation of cleaning procedures on fossil benthic foraminiferal Mg/Ca and Sr/Ca. *Geochemistry, Geophysics, Geosystems*, 3, doi: 2002GC000280.

Martin, P.A., Lea, D.W., Mashiotta, T.A., Papenfuss, T., and Sarnthein, M., 1999. Variation of foraminiferal Sr/Ca over Quaternary glacial-interglacial cycles: Evidence for changes in mean ocean Sr/Ca? *Geochemistry, Geophysics, Geosystems*, 1, Paper number: 1999GC000006.

Martin, P.A., Lea, D.W., Rosenthal, Y., Shackleton, N.J., Sarnthein, M., and Papenfuss, T., 2002. Quaternary deep sea temperature histories derived from benthic foraminiferal Mg/Ca. *Earth and Planetary Science Letters*, 198, 193-209.

Maslin, M., Seidov, D., Lowe, J., 2001. Synthesis of the nature and causes of rapid climate transitions during the Quaternary. *Geophysical monograph,* 126, 9–52.

MacAyeal, D.R., 1993. Binge/purge oscillations of the Laurentide Ice Sheet as a cause of the North Atlantic's Heinrich events. *Paleoceanography*, 8, 775–784.

McCabe, A.M., 1987. Quaternary deposits and glacial stratigraphy in Ireland. *Quaternary Science Reviews*, 6, 259–299.

McCabe, A.M., Knight, J., and McCarron, S., 1998. Evidence for Heinrich 1 in the British Isles. *Journal of Quaternary Science*, 13, 549–568.

McCartney, M.S. and Mauritzen, C., 2001. On the origin of the warm inflow to the Nordic Seas. *Progress in Oceanography*, 51: 125-214.

McCave, I.N., Manighetti, B., and Robinson, S.G., 1995. Sortable silt and fine sediment size / composition slicing: parameters for palaeocurrent speed and palaeoceanography. *Paleoceanography*, 10(3), 593-610.

McCorkle, D.C., Martin, P.A., Lea, D.W., and Klinkhammer G.P., 1995. Evidence of a dissolution effect on benthic foraminiferal shell chemistry: $\delta^{13}C$, Cd/Ca, Ba/Ca and Sr/Ca results from the Ontong Java Plateau. *Paleoceanography*, 10(4), 699-714.

McCulloch, I.J., 1977. *Qualitative observations on recent foraminiferal tests. Parts 1-3 with emphasis on the eastern Pacific.* Los Angeles, University of South Carolina, Los Angeles.

McIntyre, A., Ruddiman, W.F., and Jantzen, R., 1972. Southward penetrations of the North Atlantic Polar Front; faunal and floral evidence of large-scale surface water mass movements over the last 225,000 years. *Deep-Sea Research*, 19, 61-77.

McManus, J.F., Oppo, D.W., and Cullen, J.L., 1999. A 0.5 million year record of millennial-scale climate variability in the North Atlantic. *Science*, 283(5404), 971-975.

McManus, J.F., Francois, R., Gherardi, J.M., Keigwin, L.D., and Brown-Leger, S., 2004. Collapse and rapid resumption of Atlantic meridional circulation linked to deglacial climate changes. *Nature*, 428, 834-837.

Meincke, J., 1986. Convection in the oceanic waters west of Britain. *Proceedings of the Royal Society of Edinburgh*, 88B, 127-139.

Meland, M.Y., Jansen, E., and Elderfield, H., 2005. Constraints on SST estimates for the northern North Atlantic/Nordic Seas during the LGM. *Quaternary Science Reviews*, 24, 835-852.

Morey, A.E., Mix, A.C., and Pisias, N.G., 2005. Planktonic foraminiferal assemblages preserved in surface sediments correspond to multiple environment variables. *Quaternary Science Reviews*, 24, 925-950.

Moros, M., Kuijpers, A., Snowball, I., Lassen, S., Backstrom, D., Gingele, F., and McManus, J., 2002. Were glacial iceberg surges in the North Atlantic triggered by climatic warming? *Marine Geology*, 192(4), 393–417.

Morris, P.H., Payne, S.N.J., and Richards, D.J.P., 1999. Micropalaeontological biostratigraphy of the Magnus Sandstone Member (Kimmeridgian-Early Volgian), Magnus Field, UK North Sea. In: Jones, R.W., and Simmonds, M.D., (eds.) *Biostratigraphy in production and development geology*. Geological Society Special Publication, pp. 309.

Murray, J.W., 1971. *An atlas of British recent foraminiferids.* London, Heinemann Educational Books, 244 pp.

Murray, J.W., 1991. Ecology and palaeoecology of benthic foraminifera. Longman Scientific and Technical, New York, USA. pp. 397.

Murray, J. W., Weston, J.F., Haddon, C.A., and Powell, A.D.J., 1986. Miocene to Recent bottom water masses of the Northeast Atlantic: an analysis of benthic Foraminifera. *Geological Society Special Publication*, 21, 219–230.

Nees, S., Altenbach, A.V., Kassens, H., and Thiede, J., 1997. High-resolution record of foraminiferal response to Late Quaternary sea-ice retreat in the Norwegian-Greenland sea. *Geology*, 25(7): 659-662.

New, A.L., and Smythe-Wright, D., 2001. Aspects of the circulation in the Rockall Trough. *Continental Shelf Research*, 21, 777-810.

New, A.L., Barnard, S., Herrmann, P., and Molines, J.M., 2001. On the origin and pathways of the saline inflow to the Nordic Seas: insights from models. *Progress in Oceanography*, 48, 255-287.

O´Cofaigh, C., and Evans, D.J.A., 2007. Radiocarbon constraints on the age of the maximum advance of the British–Irish Ice Sheet in the Celtic Sea. *Quaternary Science Reviews,* 26, 1197–1203.

Okushi, K., Thomas, E., and Kawahata, H., 2000. Abyssal benthic foraminifera from the North-western Pacific (Shatsky Rise) during the last 289 kyr. *Marine Micropalaeontology*, 38, 119-147.

d'Orbigny, A., 1826. Tableau méthodique de la classe des Céphalopodes. *Annales des Sciences Naturelles,* 7: 245-314.

Oppo, D.W., and Fairbanks, R.G., 1987. Variability in the deep and intermediate water circulation of the Atlantic Ocean during the past 25,000 years: Northern Hemisphere modulation of the Southern Ocean. *Earth and Planetary Science Letters*, 86, 1-15.

Oppo, D.W., and Lehman, S.J., 1993. Mid-depth circulation of the subpolar North Atlantic during the Last Glacial Maximum. *Science*, 259(5098), 1148-1152.

Øvrebø, L.K., 2005. Spatial and temporal variations in sedimentary slope processes along the margins of the Rockall Trough, offshore west Ireland. Unpublished PhD Thesis, University College Dublin, Ireland.

Øvrebø, L.K., Haughton, P.D.W. and Shannon, P.M., 2006. A record of fluctuating bottom currents on the slopes west of the Porcupine Bank, offshore Ireland – implications for Late Quaternary climate forcing. *Marine Geology*, 225(1-4): 279-309.

Paillard, D., Labeyrie, L., and Yiou, P., 1996. Macintosh program performs time-series analysis. *EOS*, 77, 239.

Parker, W.K., and Jones, T.R., 1865. On some foraminifera from the North Atlantic and Arctic Oceans, including Davis Straits and Baffin's Bay. *Royal Society of London, Philosophical Transactions, 155,* 325-441.

Patterson, G.L.J. and Lambshead, P.J.D., 1995. Bathymetric patterns of polychaete diversity in the Rockall Trough, northeast Atlantic. *Deep Sea Research part I: Oceanographic research papers*, 42 (7): 1199-1214.

Peck, V. L., Hall, I.R., Zahn, R., Elderfield, H., Grousset, F.E., and Scourse, J.D., 2006. High resolution evidence for linkages between European ice sheet instability and Atlantic meridional overturning circulation. *Earth and Planetary Science Letters*, 243, 476–488.

Peck, V.L., Hall, I.R., Zahn, R., and Scourse, J.D., 2007. Progressive reduction in NE Atlantic intermediate water ventilation prior to Heinrich events: Response to NW European ice sheet instabilities? *Geochemistry, geophysics, geosystems*, 8(1), doi:10.1029/2006GC001321.

Peck, V.L., Hall, I.R., Zahn, R., and Elderfield, H., 2008. Millennial-scale surface and subsurface paleothermometry from the northeast Atlantic, 55–8 ka BP. *Paleoceanography*, 23, PA3221, doi:10.1029/2008PA001631.

Peterson, L.C., Haug, G.H, Hughen, K.A., and Röhl U., 2000. Rapid changes in the hydrologic cycle of the tropical Atlantic during the last glacial. *Science*, 290, 1947-1950.

Petit, J.R., Jouzel, J., Raynaud, D., Barkov, N.I., Barnola, J.M., Basile, I., Bender, M., Chappellaz, J., Davis, M., Delaygue, G., Delmotte, M., Kotlyakov, V.M., Legrand, M., Lipenkov, V.Y., Lorius, L., PÉpin, L., Ritz, C., Saltzman, E., and Stievenard, M., 1999.

Climate and atmospheric history of the past 420,000 years from the Vostok ice core, Antarctica. *Nature*, 399, 429-436.

Pflaumann, U., Duprat, J., Pujol, C., and Labeyrie, L.D., 1996. SIMMAX: A modern analogue technique to deduce Atlantic sea surface temperatures from planktonic foraminifera in deep-sea sediments. *Paleoceanography*, 11(1): 15-35.

Pflaumann, U., Sarnthein, M., Chapman, M.R., d'Abreu, L., Funnell, B., Huels, M., Kiefer, T., Maslin, M., Schulz, H., Swallow, J., van Kreveld, S., Vautravers, M., Vogelsang, E., and Weinelt, M., 2003. Glacial North Atlantic sea-surface conditions reconstructed by GLAMAP 2000. *Paleoceanography.* 18, 1065.

Phleger, F.B., Parker, F.L. and Peirson, J.F., 1953. North Atlantic foraminifera. *Reports of the Swedish Deep-Sea exhibition 1947-1948. Sediment cores from the North Atlantic Ocean.* Pettersson, H., (ed.), Vol. 7.

Poli, M.S., Thunnell, R.C., and Rio, D., 2000. Millennial-scale changes in North Atlantic Deep Water circulation during marine isotope stages 11 and 12: Linkage to Antarctic climate. *Geology*, 28(9): 807-810.

Prell, W.L., 1985. The stability of low-latitude sea-surface temperatures, an evaluation of the CLIMAP reconstruction with emphasis on the positive SST anomalies. Report number TR 025. US Department of Energy, Washington DC, USA.

Puig, P., Palanques, A., Guillén, J., and El Khatab, M., 2004. Role of internal waves in the generation of nepheloid layers on the northwestern Alboran slope: Implications for continental margin shaping. Journal of Geophysical Research, 109, C09011, doi:10.1029/2004JC002394.

Rasmussen, T.L., Thomsen, E., Troelstra, S.R., Kuijpers, A. and Prins, M.A., 2002. Millenial-scale glacial variability versus Holocene stability: changes in planktic and benthic foraminifera faunas and ocean circulation in the North Atlantic during the last 60 000 years. *Marine micropalaeontology*, 47(1-2): 143-176.

Rahmstorf, S., 1997. Influence of Mediterranean Outflow on climate. EOS, 79(24).

Rahmstorf, S., 2003. Thermohaline circulation: The current climate. *Nature*, 421, 699.

Rahmstorf, S., 2006. Testing climate reconstructions. *Science*, 312, 1872.

Rathburn, A.E., Corliss, B.H., Tappa, K.D., and Lohmann, K.C., 1996. Comparisons of the Ecology and Stable Isotopic Compositions of Living (Stained) Deep-Sea Benthic Foraminifera from the Sulu and South China Seas. *Deep-Sea Research*, 43(10), 1617-1646.

Ravelo, A.C., and Hillaire-Marcel, C., 2007. The use of oxygen and carbon isotopes of foraminifera in palaeoceanography. In: Developments in Marine Geology 1: Proxies in Late Cenozoic paleoceanography. Hillaire-Marcel, C., and De Vernal, A., (eds.), Elsevier, Amsterdam, The Netherlands, 735-764.

Raymo, M.E., Oppo, D.W., and Curry, W.B., 1997. The mid-Pleistocene climate transition: A deep sea carbon isotopic perspective. *Paleoceanography*, 12(4), 546-559.

Raymo, M.E., Oppo, D.W., Flower, B.P., Hoddell, D.A., McManus, J., Venz, K.A., Kleiven, K.F., and McIntyre, K., 2004. Stability of North Atlantic water masses in face of pronounced natural climate variability. *Paleoceanography*, 19, PA2008, doi: 10.1029/2003PA000921.

Read, J.F., 2001. CONVEX-91: water masses and circulation of the Northeast Atlantic subpolar gyre. *Progress in oceanography*. 48: 461-510.

Reid, J.L., 1979. On the contribution of the Mediterranean Sea outflow to the Norwegian-Greenland Sea. *Deep-Sea Research*, 26, 1199–1223.

Richter, T.O., Lassen, S., van Weering, T.C.E., and de Haas, H., 2001. Magnetic susceptibility patterns and provenance of ice-rafted material at Feni Drift, Rockall Trough: implications for the history of the British–Irish ice sheet. *Marine Geology*, 173, 37–54.

Rickaby, R.E.M., and Elderfield, H., 2005. Evidence from the high-latitude North Atlantic for variations in Antarctic Intermediate Water flow during the last deglaciation. *Geochemistry, Geophysics, Geosystems*. 6(5): Q05001, doi:10.1029/2004GC000858.

Ridgwell, A.J., Watson, A.J., and Raymo, M.E., 1999. Is the spectral signature of the 100 kyr glacial cycle consistent with a Milankovitch origin? *Paleoceanography*, 14, 437-440.

Roche, D., Paillard, D., and Cortijo, E., 2004. Duration and iceberg volume of Heinrich event 4 from isotope modelling study. *Nature,* 432, 379–382.

Rosenthal, Y., Boyle, E.A., and Slowey, N., 1997. Temperature control on the incorporation of magnesium, strontium, fluorine, and cadmium into benthic foraminiferal shells from Little Bahama Bank: Prospects for thermocline paleoceanography. *Geochimica et Cosmochimica Acta*, 61, 3633-3643.

Ruddiman, W.F., 1977. North Atlantic Ice-Rafting: A Major Change at 75,000 Years Before the Present. *Science*, 196(4295), 1208-1211.

Ruddiman, W.F., 2006. Orbital changes and climate. *Quaternary Science Reviews*, 25, 3092-3112.

Sabin, A.L., and Pisias, N.G., 1996. Sea Surface Temperature Changes in the Northeastern Pacific Ocean during the Past 20,000 Years and Their Relationship to Climate Change in Northwestern North America. *Quaternary Research*, 46(1), 48-61.

Sachs, H.M., Webb, T., and Clark, D.R., 1977. Palaeoecological transfer functions. *Annual Review of Earth and Planetary Sciences*, 5, 159-178.

Sanders, H.L., 1968. Marine benthic diversity: a comparative study. *American Naturalist.* 102: 243–282.

Sarnthein, M., Winn, K., Jung, S.J.A., Duplessy, J-C., Labeyrie, L., Erlenkeuser, H., and Ganssen, G., 1994. Changes in east Atlantic deepwater circulation over the last 30,000 years: eight time slice reconstructions. *Paleoceanography*, 9(2), 209-267.

Sarnthein, M., Stattegger, K., Dreger, D., Erlenkeuser, H., Grootes, P., Haupt, B., Jung, S., Kiefer, T., Kuhnt, W., Pflaumann, U., Schäfer -Neth, C., Schulz, H., Schulz, M., Seidov, D., Simstich, J., van Kreveld, S., Alfane, S., Vogelsang, E., Völker, A., Weinelt, M., 2001. Fundamental modes and abrupt changes in North Atlantic circulation and climate over the last 60 ky - Concepts, reconstruction, and numerical modelling. In: Schäfer, P., *et al.* (eds.), *The northern North Atlantic: A changing environment*, Springer Verlag, 365-410.

Schiebel, R., Bijma, J., and Hemleben, C., 1997. Population dynamics of the planktic foraminifer *Globigerina bulloides* from the eastern North Atlantic. *Deep Sea Research I*, 44(9), 1701-1713, doi:10.1016/S0967-0637(97)00036-8.

Schlumberger, C., 1891. Revision des Biloculines des grands fonds. *Memoires de* la *Societe. Zoologique,. France,* 4, 542-579.

Schmiedl, G., and Mackensen, A., 1997. Late Quaternary paleoproductivity and deep water circulation in the eastern South Altantic Ocean: Evidence from benthic foraminifera. *Palaeogeography, Palaeoclimatology, Palaeoecology*, 130(1-4), 43-80.

Schmittner, A., Saenko, O.A., and Weaver, A.J., 2003. Coupling of the hemispheres in observations and simulations of glacial climate change. *Quaternary Science Reviews*, 22, 659-671.

Schnitker, D., 1994. Deep-sea benthic foraminifers: Food and bottom water masses. In: Zahn, R., Pederson, T.F., Kaminski, M.A. and Labeyrie, L., (eds.). *Carbon cycling in the Glacial Ocean: Constraints on the ocean's role in global change.* New York, Springer-Verlag, 539-554.

Schönfeld, J., 1997. The impact of the Mediterranean Outflow Water (MOW) on benthic foraminiferal assemblages and surface sediments at the southern Portuguese continental margin. *Marine Micropaleontology*, 29: 211-236.

Schönfeld, J., 2002. A new benthic foraminiferal proxy for near-bottom current velocities in the Gulf of Cadiz, northeastern Atlantic Ocean. *Deep-Sea Research I*, 49: 1853-1875.

Schönfeld, J., 2006. Taxonomy and distribution of the *Uvigerina peregina* plexus in the tropical to Northeastern Atlantic. *Journal of Foraminiferal Research*, 36 (4), 355-367.

Schrag, D.P., and Linsley, B.K., 2002. Paleoclimate: Corals, chemistry, and climate. *Science*, 296, 277-278.

Schwager, C., 1866. Fossile Foraminiferen von Kar Nikobar, Reise der Oesterreichischen Fregatte Novara um Erde in den Jahren 1857, 1858, 1859 unten den Befehlen des Commodore B. Von Wuellerstorf-Urbair. Geologischer Theil, *Geologische Beobachtung no. 2, Palaeontologische Mittheilung*, 2(1): 187-268.

Schweiger, M., 2006. Evolution and molecular phylogeny of *Cibicides* and *Uvigerina* (Rotaliida, Foraminifera). Geologica Ultraiectina, PhD Thesis, Universiteit Utrecht, 168 pp.

Scourse, J. D., Hall, I.R., McCave, I.N., Young, J.R., and Sugdon, C., 2000. The origin of Heinrich layers: Evidence from H2 for European precursor events. *Earth and Planetary Science Letters*, 182, 187–195.

Scourse, J.D., Haapaniemi, A.I., Colmenero-Hidalgo, E., Peck, V.L., Hall, I.R., Austin, W.E.N., Knutz, P., and Zahn, R., 2009. Growth, dynamics and deglaciation of the last British–Irish ice sheet: the deep-sea ice-rafted detritus record. Quaternary Science Reviews, in press, doi:10.1016/j.quascirev.2009.08.009.

Seguenza, G., 1862. Dei terreni Terziani del distretto di Messina; Parte 2. Descrizione dei foraminiferi monotalamici delle marne mioceniche del Distretto di Messina: T. Capra, Messina, 84 pp.

Seidov, D., and Maslin, M., 1999. North Atlantic Deep Water Circulation Collapse During Heinrich Events. *Geology*, 27(1), 23-26.

Seidov, D., and Maslin, M., 2001. Atlantic ocean heat piracy and the bipolar climate see-saw during Heinrich and Dansgaard-Oeschger events. *Journal of Quaternary Science,* 16(4), 321–328.

Sepulchre, P., Ramstein, G., Kageyama, M., Vanhaeren, M., Krinner, G., Sánchez-Goñi, M.F., and d'Errico, F., 2007. H4 abrupt event and late Neanderthal presence in Iberia. *Earth and Planetary Science Letters*, 258, 283–292.

Severinghaus, J.P., 2009. Southern See Saw Seen. *Nature,* 457, 1093.

Sexton, P.F., P.A. Wilson, and P.N. Pearson 2006. Microstructural and geochemical perspectives on planktic foraminiferal preservation: "Glassy" versus "Frosty". *Geochemistry, Geophysics, Geosystems.* 7, Q12P19, doi:10.1029/2006GC001291.

Shackleton, N.J., 1973. Attainment of isotopic equilibrium between ocean water and the benthonic foraminifera genus *Uvigerina*: Isotopic changes in the ocean during the last glacial: *in* Colloques Internationaux du C.N.R.S. No. 219. Les methodes quantitative d'etude des variations du climat au cours du Pleistocene, p. 203–209.

Shackleton, N.J., 1977. The oxygen isotope stratigraphic record of the late Pleistocene. In: *The Changing Environmental Conditions in Great Britain and Ireland during the Devensian (last) Cold Stage*, a meeting for discussion organised by G.F. Mitchell and R.G. West. Philosophical Transactions of the Royal Society, B, 280, 169-179.

Shackleton, N. J., 1987. The carbon isotope history of the Cenozoic. In: Brooks, J., and Fleet, A. J., (eds.), *Petroleum Source Rocks,* Oxford (Blackwell), 427-438.

Shackleton, N.J., and Opdyke, N.D., 1973. Oxygen isotope and paleomagnetic stratigraphy of equatorial Pacific Core V28-238: oxygen isotope temperatures and ice volume on a 105 year and 106 year scale. *Quaternary Research*, 3, 39-55.

Shackleton, N.J., Berger, A., and Peltier, W.R., 1990. An alternative astronomical calibration of the lower Pleistocene timescale based on ODP site 677. *Transactions of the Royal Society of Edinburgh, Earth Sciences*, 81, 251-261.

Shannon, P.M., O'Reilly, B.M., Readman, P.W., Jacob, A.W.B., and Kenyon, N., 2001. Slope failure features on the margins of the Rockall Trough. *Geological Society London, Special Publications*, 188, 455-464.

Sherwin, T.J., Turrell, W.R., Jeans, D.R.G., and Dye, S., 1999. Eddies and a mesoscale deflection of the slope current in the Faroe-Shetland Channel. Deep-Sea Research I, 46(3), 415-438

Siddall, M., 2005. The riddle of the sediments, *Nature*, 437, 39-41.

Sierro, F.J., Flores, J.A., and Baraza, J., 1999. Late glacial to recent palaeoenvironmental changes in the Gulf of Cadiz and formation of sandy contourite layers. *Marine Geology*, 155, 157-172.

Smart, C.W., and Gooday, A.J., 1997. Recent benthic foraminifera in the abyssal northeast Atlantic Ocean: relation to phytodetritus inputs. *Journal of Foraminiferal Research*, 27, 85-92.

Spero, H.J., and Lea, D.W., 1996. Experimental determination of intraspecific stable isotope variability in *Globigerina bulloides*: Implications for paleoceanographic reconstructions. *Marine Micropaleontology*, 28: 231-246.

Spero, H.J., and Lea, D.W., 2002. The cause of carbon isotope minimum events on glacial terminations, *Science,* 296, 522–525.

Spero, H.J., Bijma, J., Lea, D.W., and Bemis, B.E., 1997. Effect of seawater carbonate concentration on planktonic foraminiferal carbon and oxygen isotopes. *Nature* 390: 497-500.

Stanford, J.D., Rohling, E.J., Hunter, S.E., Roberts, A.P., Rasmussen, S.O., Bard, E., McManus, J., and Fairbanks, R.G., 2006. Timing of meltwater pulse 1a and climate responses to meltwater injections. *Paleoceanography*, 21, PA4103, doi:10.1029/2006PA001340.

Stocker, T.F., 1998. The seesaw effect. *Science,* 282(5386), 61–62.

De Stigter, H.C., Jorissen, F.J. and Van der Zwaan, G.J., 1998. Bathymetric distribution and microhabitat partitioning of live (Rose Bengal stained) benthic foraminifera along a shelf to deep sea transect in the Southern Adriatic Sea. *Journal of Foraminiferal Research*, 28, 40-65.

Stocker, T.F., and Johnsen, S.J., 2003. A minimum model for the bipolar seesaw. *Paleoceanography,* 18, 1087, doi: 10.1029/2003PA000920.

Stoll, H.M., Schrag, D.P., and Clemens S.C., 1999. Are seawater Sr/Ca variations preserved in Quaternary foraminifera? *Geochimica et Cosmochimica Acta.* 63(21), 3535-3547.

Stow, D.A.V., Faugeres, J.C., Viana, A., and Gonthier, E., 1998. Fossil contourites: a critical review. *Sedimentary Geology*, 115, 3-31.

Struck, U., 1992. Zur Paläo-Öokologie benthischer Foraminiferen im Europäischen Nordmeer während der letzten 600 000 Jahre. *Bereich Sonderforschungsbereich*, 313(38), 1-129. Universität Kiel, Germany.

Tachikawa, K., and Elderfield, H., 2002. Microhabitat effects on Cd/Ca and δ13C of benthic foraminifera. *Earth and Planetary Science Letters*, 202, 607-624.

Thomas, E., Booth, L., Maslin, M. and Shackleton, N.J., 1995. Northeastern Atlantic benthic foraminifera during the last 45,000 years: changes in productivity seen from the bottom up. *Paleoceanography*, 10 (3): 545-562.

Thomson, J., Brown, L., Nixon, S., Cook, G.T., and MacKenzie, A.B., 2000. Bioturbation and Holocene sediment accumulation fluxes in the north-east Atlantic Ocean (Benthic Boundary Layer experiment sites). *Marine Geology*, 169, 21-39.

Thornalley, D.J.R., Elderfield, H., and McCave, I.N., 2009. Holocene oscillations in temperature and salinity of the surface subpolar North Atlantic. *Nature*, 457, 711-714.

Toms, L., (in prep.). Late Quaternary stratigraphy and sediment distribution on current-swept slopes of the west Porcupine Bank, offshore Ireland. Unpublished PhD thesis, University College Dublin, Ireland.

Turley, C.M., Gooday, A., and Green, J.C., 1993. Maintenance of abyssal benthic foraminifera under high pressure and low temperature: Some preliminary results. *Deep Sea Research*, 40A: 643-652.

Tziperman, E., Raymo, M.E., Huybers, P., and Wunsch, C., 2006. Consequences of pacing the Pleistocene 100 kyr ice ages by nonlinear phase locking to Milankovitch forcing. *Paleoceanography*, 21, PA4206, doi:10.1029/2005PA001241.

Van der Zwann, G.J., Duijnstee, I.A.P., Den Dulk, M., Ernst, S.R., Jannik, N.T. and Kouwenhoven, T.J., 1999. Benthic foraminifers: proxies or problems? A review of paleoecological concepts. *Earth Science Reviews*, 46: 213-236.

Venz, K.A., Hodell, D.A., Stanton, C., and Warnke, D.A., 1999. A 1.0 Myr record of Glacial North Atlantic Intermediate Water variability from ODP site 982 in the northeast Atlantic. *Paleoceanography*, 14, 42–52.

de Vernal, A., Eynaud, F., Henry, M., Hillaire-Marcel, C., Londeix, L., Mangin, S., Matthiessen, J., Marret, F., Radi, T., Rochon, A., Solignac, S., and Turon, J.L., 2005. Reconstruction of sea-surface conditions at middle to high latitudes of the Northern Hemisphere during the Last Glacial Maximum (LGM) based on dinoflagellate cyst assemblages. *Quaternary Science Reviews*, 24, 897-924.

Viana, A.R., Faugeres, J.-C., and Stow, D.A.V., 1998. Bottom current controlled sand deposits: a review from modem shallow and deep water environments. In: Stow, D.A.V., Faugeres, J.-C., (Eds.), Contourites, Turbidites and Process Interaction. *Sedimentary Geology*, 115, 53-80.

Viana, A.R., and Rebesco, M., 2007. The economic and palaeoceanographic significance of contourite deposits. *Geological Society (London) Special Publication*, 276, pp. 343.

Vidal, L., Labeyrie, L., Cortijo, E., Arnold, M., Duplessy, J.C., Michel, E., Becque, S., and van Weering, T.C.E., 1997. Evidence for changes in the North Atlantic Deep Water

linked to meltwater surges during the Heinrich events. *Earth and Planetary Science Letters*, 146, 13–27.

Voelker, A.H.L., 2003. Global distribution of centennial-scale records for Marine Isotope Stage (MIS) 3: a database. *Quaternary Science Reviews,* 21, 1185–1212.

Voelker, A. H. L., Sarnthein, M., Grootes, P.M., Erlenkeuser, H., Laj, C., Mazaud, A., Nadeau, M.J., and Schleicher, M., 1998. Correlation of marine C-14 ages from the Nordic seas with the GISP2 isotope record: Implications for C-14 calibration beyond 25 kyr BP. *Radiocarbon*, 40, 517–534.

Voelker, A.H.L., Lebreiro, S., Schoenfeld, J., Cacho, I., Erlenkeuser, H., and Abrantes, F., 2006. Mediterranean Outflow Strengthening during Northern Hemisphere Coolings: A salt source for the glacial Atlantic? *Earth and Planetary Science Letters*, 245(1-2), 39–55.

Waelbroeck, C., Duplessy, J.C., Michel, E., Labeyrie, L., Paillard, D., and Duprat, J., 2004. The timing of the last deglaciation in North Atlantic climate records. *Nature*, 412, 724-727.

Walker, M., Johnsen, S., Rasmussen, S.O., Popp, T., Steffensen, J.-P., Gibbard, P., Hoek, W., Lowe, J., Andrews, J., Bjorck, S., Cwynar, L.C., Hughen, K., Kershaw, P., Kromer, B., Litt, T., Lowe, D. J., Nakagawa, T., Newnham, R., and Schwander, J., 2009. Formal definition and dating of the GSSP (Global Stratotype Section and Point) for the base of the Holocene using the Greenland NGRIP ice core, and selected auxiliary records. *Journal of Quaternary Science*, 24, 3–17.

Weston, J.F., 1985. Comparison between recent benthic foraminiferal faunas of the Porcupine Seabight and Western Approaches continental slope. *Journal of Micropalaeontology*, 4, 165-183.

Weston, J.F., and Murray, J.W., 1984. Benthic foraminifera as deep-sea water-mass indicators. In: Oertli, H.J. (eds.), *Benthos '83*, 2nd International Symposium on benthic foraminifera, Pau, 605-610.

White, M. and Bowyer, P., 1997. The shelf-edge current north-west of Ireland. *Annales Geophysicae*, 15: 1076-1083.

White, M., Mohn, C. and Orren, M.J., 1998. Nutrient distributions across the Porcupine Bank. *ICES Journal of Marine Science*, 55: 1082-1094.

White, M., Mohn, C., de Stigter, H., and Mottram, G., 2005. Deep water coral development as a function of hydrodynamics and surface productivity around the submarine banks of the Rockall Trough, NE Atlantic. *In: Cold-water corals and Ecosystems,* Roberts (Eds.), Springer, 503-514.

Williams, M., Haywood, A.M., Vautravers, M., Sellwood, B.W., Hillenbrand, C.D., Wilkinson, I.P., and Miller, C.G., 2007. Relative effect of taphonomy on calcification temperature estimates from fossil planktonic foraminifera. *Geobios*, 40(6), 861-874.

Williamson, W.C., 1858. *On the Recent foraminifera of Great Britain.* Ray society.

Wilson, J.B., 1982. Cenozoic benthonic Foraminifera from the Irish continental margin, N. Atlantic. Unpublished M.Sc. Dissertation. University of Aberystwyth, Wales.

Wilson, L.J., Austin, W.E.N., and Jansen, E., 2001. The last British Ice Sheet: growth, maximum extent and deglaciation. *Polar Research*, 21(2), 243-250.

Wollenburg, J.E., and Mackensen, A., 1998. Living benthic foraminifers from the central Arctic Ocean: faunal composition, standing stock and diversity. *Marine Micropaleontology*, 34, 153–185.

Wollenberg, J.E., and Kuhnt, W., 2000. The response of benthic foraminifers to carbon flux and primary production in the Arctic Ocean. *Marine Micropalaeontology*, 40, 189-231.

Wunsch, C., 2003. Greenland—Antarctic phase relations and millennial time-scale climate fluctuations in the Greenland ice-cores. *Quaternary Science Reviews*, 22, 1631-1646.

Yin, J.H., and Battisti, D.S., 2001. The importance of tropical sea surface temperature patterns in simulations of Last Glacial Maximum climate. *Journal of Climate*, 14, 565-581.

Yoder, J. A., Ackleson, S.G., Barber, R.T., Flament, P., and Balch, W.M., 1994. A line in the sea. *Nature*, 371, 689–692.

Yu, J.M., Day, J., Greaves, M., and Elderfield, H., 2005. Determination of multiple element/calcium ratios in foraminiferal calcite by quadrupole ICP-MS. *Geochemistry, Geophysics, Geosystems*, 6, Q09P01 10.1029/2005GC000964.

Zahn, R., Schonfeld, J., Kudrass, H., Park, M., Erlenkeuser, H., and Grootes, P., 1997. Thermohaline instability in the North Atlantic during meltwater events: Stable isotope and ice rafted detritus records from core SO75-26KL, Portuguese margin. *Paleoceanography*, 12(5), 696–710.

Appendix A - Planktonic foraminifera assemblage data

Core 9/97-08
Relative abundance - Planktonic foraminifera >150um

Sample depth (cm)	3	7	11	15	19	23	27	31	35	39	43	47.5	51.5	55.5	59.5
Globigerina bulloides	0.67	9.33	7.33	4.33	0.00	9.00	4.00	4.67	27.33	10.67	12.33	20.67	14.00	13.33	7.67
Turborotalita quinqueloba	0.00	1.00	1.00	1.00	0.33	2.00	0.33	0.67	1.00	0.67	4.67	2.33	1.33	4.33	0.67
Orbulina universa	0.00	0.00	0.00	0.00	0.00	0.00	0.00	0.00	0.00	0.00	0.00	0.00	0.00	0.00	0.00
Neogloboquadrina pachyderma (sin.)	99.00	89.67	83.33	92.00	99.33	80.33	93.33	91.00	62.67	81.00	60.00	57.33	75.00	72.00	84.00
Neogloboquadrina pachyderma (dext.)	0.00	0.00	2.67	0.00	0.00	4.00	2.33	2.33	9.00	7.00	18.67	14.67	7.33	7.67	3.67
Globigerinoides ruber	0.00	0.00	0.00	0.00	0.33	0.00	0.00	0.00	0.00	0.00	0.33	0.00	0.00	0.00	0.00
Globorotalia scitula	0.33	0.00	5.67	2.67	0.00	0.67	0.00	1.33	0.00	0.67	0.33	2.67	2.33	2.67	0.00
Globorotalia inflata	0.00	0.00	0.00	0.00	0.00	4.00	0.00	0.00	0.00	0.00	5.33	2.00	0.00	0.00	4.00
Globorotalia truncatulinoides	0.00	0.00	0.00	0.00	0.00	0.00	0.00	0.00	0.00	0.00	0.33	0.00	0.00	0.00	0.00
Globorotalia hirsuta	0.00	0.00	0.00	0.00	0.00	0.00	0.00	0.00	0.00	0.00	1.33	0.33	0.00	0.00	0.00
Globigerinoides sacculifer	0.00	0.00	0.00	0.00	0.00	0.00	0.00	0.00	0.00	0.00	0.00	0.00	0.00	0.00	0.00
Neogloboquadrina duertrei	0.00	0.00	0.00	0.00	0.00	0.00	0.00	0.00	0.00	0.00	0.00	0.00	0.00	0.00	0.00
Hastigerinella digitata	0.00	0.00	0.00	0.00	0.00	0.00	0.00	0.00	0.00	0.00	0.00	0.00	0.00	0.00	0.00
Globigerina rubescens	0.00	0.00	0.00	0.00	0.00	0.00	0.00	0.00	0.00	0.00	0.00	0.00	0.00	0.00	0.00
Globorotalia crassaformis	0.00	0.00	0.00	0.00	0.00	0.00	0.00	0.00	0.00	0.00	0.00	0.00	0.00	0.00	0.00
Hastigerina pelagica	0.00	0.00	0.00	0.00	0.00	0.00	0.00	0.00	0.00	0.00	0.00	0.00	0.00	0.00	0.00
Globigerinoides conglobatus	0.00	0.00	0.00	0.00	0.00	0.00	0.00	0.00	0.00	0.00	0.00	0.00	0.00	0.00	0.00
Globigerina glutinata	0.00	0.00	0.00	0.00	0.00	0.00	0.00	0.00	0.00	0.00	0.33	0.00	0.00	0.00	0.00
Globigerina calida	0.00	0.00	0.00	0.00	0.00	0.00	0.00	0.00	0.00	0.00	0.00	0.00	0.00	0.00	0.00
Orbulina sp. A	0.00	0.00	0.00	0.00	0.00	0.00	0.00	0.00	0.00	0.00	0.00	0.00	0.00	0.00	0.00
Globorotalia tumida	0.00	0.00	0.00	0.00	0.00	0.00	0.00	0.00	0.00	0.00	0.00	0.00	0.00	0.00	0.00
Globierinella siphonifera	0.00	0.00	0.00	0.00	0.00	0.00	0.00	0.00	0.00	0.00	0.00	0.00	0.00	0.00	0.00
Globoturborotalita tenella	0.00	0.00	0.00	0.00	0.00	0.00	0.00	0.00	0.00	0.00	0.00	0.00	0.00	0.00	0.00
Orbulina bilobata	0.00	0.00	0.00	0.00	0.00	0.00	0.00	0.00	0.00	0.00	0.00	0.00	0.00	0.00	0.00

Appendix A - Planktonic foraminifera assemblage data

Core 9/97-08
Relative abundance - Planktonic foraminifera >150um

Sample depth (cm)	63.5	68	72	76	80	84	88	92	96.5	100.5	105	109	113	117.5	121.5
Globigerina bulloides	29.00	2.33	2.00	2.67	14.67	30.67	35.33	34.67	36.33	35.33	28.33	56.33	42.33	45.67	2.33
Turborotalita quinqueloba	0.00	0.33	0.00	0.00	3.67	1.00	9.00	6.33	2.33	3.00	4.33	7.67	2.33	2.33	0.33
Orbulina universa	0.00	0.00	0.00	0.00	0.00	2.67	0.00	0.00	0.33	0.00	1.00	0.00	0.00	0.67	0.00
Neogloboquadrina pachyderma (sin.)	60.67	95.67	98.00	95.33	67.00	14.00	11.33	21.67	25.67	30.33	16.33	20.00	52.67	46.00	96.33
Neogloboquadrina pachyderma (dext.)	9.33	0.67	0.00	2.00	12.33	19.00	24.00	26.00	19.00	17.00	37.00	10.67	0.67	3.00	1.00
Globigerinoides ruber	0.00	0.00	0.00	0.00	0.00	1.33	1.33	0.00	0.00	0.00	1.00	0.67	0.00	0.00	0.00
Globorotalia scitula	1.00	1.00	0.00	0.00	2.33	4.00	4.00	1.00	0.00	2.33	0.33	3.67	0.33	1.33	0.00
Globorotalia inflata	0.00	0.00	0.00	0.00	0.00	23.00	12.67	10.33	11.33	11.33	9.67	1.00	1.67	1.00	0.00
Globorotalia truncatulinoides	0.00	0.00	0.00	0.00	0.00	2.00	1.00	0.00	2.67	0.00	1.00	0.00	0.00	0.00	0.00
Globorotalia hirsuta	0.00	0.00	0.00	0.00	0.00	0.00	0.00	0.00	1.00	0.67	0.33	0.00	0.00	0.00	0.00
Globigerinoides sacculifer	0.00	0.00	0.00	0.00	0.00	0.33	0.33	0.00	0.00	0.00	0.00	0.00	0.00	0.00	0.00
Neogloboquadrina duertrei	0.00	0.00	0.00	0.00	0.00	0.00	0.00	0.00	0.00	0.00	0.00	0.00	0.00	0.00	0.00
Hastigerinella digitata	0.00	0.00	0.00	0.00	0.00	0.00	0.00	0.00	0.00	0.00	0.00	0.00	0.00	0.00	0.00
Globigerina rubescens	0.00	0.00	0.00	0.00	0.00	0.00	0.00	0.00	0.00	0.00	0.00	0.00	0.00	0.00	0.00
Globorotalia crassaformis	0.00	0.00	0.00	0.00	0.00	0.00	0.00	0.00	0.00	0.00	0.00	0.00	0.00	0.00	0.00
Hastigerina pelagica	0.00	0.00	0.00	0.00	0.00	0.00	0.00	0.00	0.00	0.00	0.00	0.00	0.00	0.00	0.00
Globigerinoides conglobatus	0.00	0.00	0.00	0.00	0.00	0.00	0.00	0.00	0.00	0.00	0.00	0.00	0.00	0.00	0.00
Globigerina glutinata	0.00	0.00	0.00	0.00	0.00	0.67	0.67	0.00	0.67	0.00	0.00	0.00	0.00	0.00	0.00
Globigerina calida	0.00	0.00	0.00	0.00	0.00	0.00	0.00	0.00	0.00	0.00	0.00	0.00	0.00	0.00	0.00
Orbulina sp. A	0.00	0.00	0.00	0.00	0.00	0.00	0.00	0.00	0.00	0.00	0.00	0.00	0.00	0.00	0.00
Globorotalia tumida	0.00	0.00	0.00	0.00	0.00	0.00	0.00	0.00	0.00	0.00	0.00	0.00	0.00	0.00	0.00
Globierinella siphonifera	0.00	0.00	0.00	0.00	0.00	1.00	0.00	0.00	0.67	0.00	0.67	0.00	0.00	0.00	0.00
Globoturborotalita tenella	0.00	0.00	0.00	0.00	0.00	0.33	0.00	0.00	0.00	0.00	0.00	0.00	0.00	0.00	0.00
Orbulina bilobata	0.00	0.00	0.00	0.00	0.00	0.00	0.33	0.00	0.00	0.00	0.00	0.00	0.00	0.00	0.00

Appendix A - Planktonic foraminifera assemblage data

Core 9/97-08
Relative abundance - Planktonic foraminifera >150um

Sample depth (cm)	125.5	129.5	133.5	137.5	141.5	145.5	149.5	154	162	166	170	174	178	182
Globigerina bulloides	4.00	29.33	44.00	10.67	27.00	39.67	59.67	22.67	45.00	18.67	2.33	57.00	2.33	29.00
Turborotalita quinqueloba	1.00	1.00	0.33	4.67	2.00	6.00	4.00	6.00	2.00	2.00	1.00	7.33	0.33	4.33
Orbulina universa	0.00	0.00	2.00	1.00	2.67	5.33	1.33	0.67	6.00	0.00	4.00	0.00	0.00	0.00
Neogloboquadrina pachyderma (sin.)	83.33	42.00	3.67	71.67	23.00	13.00	15.67	58.67	9.33	43.33	60.67	10.67	97.00	32.00
Neogloboquadrina pachyderma (dext.)	10.67	18.00	24.00	5.67	25.00	27.33	11.00	6.33	13.33	9.00	14.00	21.33	0.33	10.67
Globigerinoides ruber	0.00	0.00	1.00	0.00	0.00	2.00	0.00	0.00	0.00	0.00	0.33	0.00	0.00	0.00
Globorotalia scitula	1.00	0.67	2.33	0.33	0.67	2.00	0.00	1.00	6.00	2.33	2.00	2.33	0.00	2.00
Globorotalia inflata	0.00	9.00	17.33	5.67	17.33	0.00	7.33	4.33	12.67	24.33	11.00	0.00	0.00	21.00
Globorotalia truncatulinoides	0.00	0.00	2.33	0.00	0.00	1.00	0.67	0.00	3.00	0.33	0.67	0.33	0.00	1.00
Globorotalia hirsuta	0.00	0.00	2.00	0.33	2.33	0.67	0.33	0.33	0.00	0.00	4.00	1.00	0.00	0.00
Globigerinoides sacculifer	0.00	0.00	0.00	0.00	0.00	0.00	0.00	0.00	0.00	0.00	0.00	0.00	0.00	0.00
Neogloboquadrina duertrei	0.00	0.00	0.00	0.00	0.00	0.00	0.00	0.00	0.00	0.00	0.00	0.00	0.00	0.00
Hastigerinella digitata	0.00	0.00	0.00	0.00	0.00	0.00	0.00	0.00	0.00	0.00	0.00	0.00	0.00	0.00
Globigerina rubescens	0.00	0.00	0.00	0.00	0.00	0.00	0.00	0.00	0.00	0.00	0.00	0.00	0.00	0.00
Globorotalia crassaformis	0.00	0.00	0.00	0.00	0.00	0.00	0.00	0.00	0.00	0.00	0.00	0.00	0.00	0.00
Hastigerina pelagica	0.00	0.00	0.00	0.00	0.00	0.00	0.00	0.00	0.00	0.00	0.00	0.00	0.00	0.00
Globigerinoides conglobatus	0.00	0.00	0.00	0.00	0.00	0.00	0.00	0.00	0.00	0.00	0.00	0.00	0.00	0.00
Globigerina glutinata	0.00	0.00	0.67	0.00	0.00	0.00	0.00	0.00	1.33	0.00	0.00	0.00	0.00	0.00
Globigerina calida	0.00	0.00	0.00	0.00	0.00	0.00	0.00	0.00	0.00	0.00	0.00	0.00	0.00	0.00
Orbulina sp. A	0.00	0.00	0.00	0.00	0.00	0.00	0.00	0.00	0.00	0.00	0.00	0.00	0.00	0.00
Globorotalia tumida	0.00	0.00	0.00	0.00	0.00	0.00	0.00	0.00	0.00	0.00	0.00	0.00	0.00	0.00
Globierinella siphonifera	0.00	0.00	0.33	0.00	0.00	1.00	0.00	0.00	0.67	0.00	0.00	0.00	0.00	0.00
Globoturborotalita tenella	0.00	0.00	0.00	0.00	0.00	2.00	0.00	0.00	0.00	0.00	0.00	0.00	0.00	0.00
Orbulina bilobata	0.00	0.00	0.00	0.00	0.00	0.00	0.00	0.00	0.67	0.00	0.00	0.00	0.00	0.00

Appendix A - Planktonic foraminifera assemblage data

Core 9/97-10
Relative abundance - Planktonic foraminifera >150um

Sample depth (cm)	3	7	11	16	20	27	31	35	39	43	47	51.5	55.5	59.5	63.5
Globigerina bulloides	41.00	29.67	38.67	17.67	13.00	20.00	75.67	43.67	78.00	75.67	46.00	66.33	58.67	38.00	51.33
Turborotalita quinqueloba	2.33	2.00	3.67	11.00	0.67	1.00	0.67	0.33	2.00	4.00	5.67	0.67	9.00	7.00	9.00
Orbulina universa	1.00	0.67	1.00	0.00	0.00	0.00	0.00	0.00	0.00	0.00	0.00	0.33	0.00	0.33	0.00
Neogloboquadrina pachyderma (sin.)	5.67	41.33	17.67	66.67	81.67	77.33	14.33	43.33	10.00	3.33	28.00	4.00	5.67	6.00	1.67
Neogloboquadrina pachyderma (dext.)	13.00	11.67	23.33	2.67	2.00	0.33	3.00	5.33	1.33	6.67	9.33	14.33	8.33	27.00	13.33
Globigerinoides ruber	0.00	0.00	0.00	0.00	0.00	0.00	0.00	0.00	0.00	0.00	0.00	0.00	0.33	0.00	0.33
Globorotalia scitula	0.67	2.67	2.00	1.33	0.33	0.33	1.33	0.33	0.00	0.00	0.33	1.33	1.67	3.33	3.00
Globorotalia inflata	27.00	9.00	9.00	0.00	2.33	0.67	5.00	6.33	8.00	8.67	8.00	11.67	8.00	14.33	17.33
Globorotalia truncatulinoides	3.33	1.00	1.67	0.00	0.00	0.00	0.00	0.00	0.00	0.33	1.33	0.67	0.67	2.00	2.67
Globorotalia hirsuta	4.00	1.00	1.33	0.00	0.00	0.33	0.00	0.67	0.00	1.00	0.33	0.00	0.33	1.00	0.33
Globigerinoides sacculifer	1.00	0.00	0.00	0.00	0.00	0.00	0.00	0.00	0.00	0.00	0.00	0.33	0.00	0.33	0.00
Neogloboquadrina duertrei	0.00	0.00	0.00	0.00	0.00	0.00	0.00	0.00	0.00	0.00	0.00	0.00	0.00	0.00	0.00
Hastigerinella digitata	0.00	0.00	0.00	0.00	0.00	0.00	0.00	0.00	0.00	0.00	0.00	0.00	0.00	0.00	0.00
Globigerina rubescens	0.00	0.00	0.00	0.00	0.00	0.00	0.00	0.00	0.00	0.00	0.00	0.00	0.00	0.00	0.00
Globorotalia crassaformis	0.00	0.00	0.00	0.00	0.00	0.00	0.00	0.00	0.00	0.00	0.00	0.00	1.00	0.00	0.00
Hastigerina pelagica	0.00	0.00	0.00	0.00	0.00	0.00	0.00	0.00	0.00	0.00	0.00	0.00	0.00	0.00	0.00
Globigerinoides conglobatus	0.00	0.00	0.00	0.33	0.00	0.00	0.00	0.00	0.33	0.00	0.00	0.00	1.00	0.00	0.00
Globigerina glutinata	0.00	0.67	0.00	0.33	0.00	0.00	0.00	0.00	0.00	0.00	0.67	0.00	4.33	0.00	0.33
Globigerina calida	0.00	0.00	0.67	0.00	0.00	0.00	0.00	0.00	0.33	0.33	0.00	0.33	0.00	0.67	0.33
Orbulina sp. A	0.00	0.00	0.00	0.00	0.00	0.00	0.00	0.00	0.00	0.00	0.00	0.00	0.00	0.00	0.00
Globorotalia tumida	0.00	0.00	0.00	0.00	0.00	0.00	0.00	0.00	0.00	0.00	0.00	0.00	1.00	0.00	0.00
Globierinella siphonifera	1.00	0.33	0.67	0.00	0.00	0.00	0.00	0.00	0.00	0.00	0.33	0.00	0.00	0.00	0.00
Globoturborotalita tenella	0.00	0.00	0.33	0.00	0.00	0.00	0.00	0.00	0.00	0.00	0.00	0.00	0.00	0.00	0.33
Indet.	0.00	0.00	0.00	0.00	0.00	0.00	0.00	0.00	0.00	0.00	0.00	0.00	0.00	0.00	0.00

Appendix A - Planktonic foraminifera assemblage data

Core 9/97-10
Relative abundance - Planktonic foraminifera >150um

Sample depth (cm)	67.5	71.5	75.5	79.5	83	87	91	95	99	103	107	111
Globigerina bulloides	45.67	48.67	23.67	23.00	50.33	11.67	29.00	34.33	37.33	24.67	51.33	63.67
Turborotalita quinqueloba	8.00	1.33	3.67	3.33	3.33	3.67	5.33	6.33	3.33	2.00	4.33	4.00
Orbulina universa	0.67	2.33	0.67	0.00	0.67	0.33	0.67	0.00	2.67	0.00	0.00	0.00
Neogloboquadrina pachyderma (sin.)	13.33	6.00	25.00	60.00	20.33	76.67	40.67	23.33	11.00	20.00	10.67	4.33
Neogloboquadrina pachyderma (dext.)	16.33	10.00	27.67	7.67	18.33	4.67	11.00	16.33	14.33	28.33	17.67	8.33
Globigerinoides ruber	0.00	0.33	0.33	0.00	0.00	0.33	0.00	0.67	0.00	0.00	1.00	1.33
Globorotalia scitula	0.67	1.33	1.67	0.00	0.67	0.33	0.67	1.33	1.33	1.33	2.67	0.67
Globorotalia inflata	11.33	21.67	10.33	5.33	6.00	2.33	10.67	16.33	26.33	20.00	9.33	11.33
Globorotalia truncatulinoides	1.67	6.33	6.33	0.33	0.00	0.00	0.00	0.33	2.33	2.00	2.00	3.67
Globorotalia hirsuta	1.00	1.33	0.00	0.00	0.33	0.00	0.00	0.00	0.00	1.67	0.33	0.00
Globigerinoides sacculifer	0.00	0.00	0.33	0.00	0.00	0.00	0.00	0.00	0.00	0.00	0.00	0.33
Neogloboquadrina duertrei	0.00	0.00	0.00	0.00	0.00	0.00	0.00	0.00	0.00	0.00	0.00	0.00
Hastigerinella digitata	0.00	0.00	0.00	0.00	0.00	0.00	0.00	0.00	0.00	0.00	0.00	0.00
Globigerina rubescens	0.00	0.00	0.00	0.00	0.00	0.00	0.00	0.00	0.00	0.00	0.00	0.00
Globorotalia crassaformis	0.00	0.00	0.00	0.00	0.00	0.00	0.67	0.33	1.00	0.00	0.00	0.00
Hastigerina pelagica	0.00	0.00	0.00	0.00	0.00	0.00	0.00	0.00	0.33	0.00	0.00	0.00
Globigerinoides conglobatus	0.00	0.00	0.00	0.00	0.00	0.00	0.00	0.00	0.00	0.00	0.00	0.00
Globigerina glutinata	0.67	0.33	0.33	0.00	0.00	0.00	0.00	0.00	0.00	0.00	0.00	0.00
Globigerina calida	0.00	0.00	0.00	0.00	0.00	0.00	1.00	0.00	0.00	0.00	0.00	0.00
Orbulina sp. A	0.00	0.00	0.00	0.00	0.00	0.00	0.00	0.00	0.00	0.00	0.00	0.00
Globorotalia tumida	0.00	0.00	0.00	0.00	0.00	0.00	0.00	0.00	0.00	0.00	0.00	0.00
Globierinella siphonifera	0.33	0.00	0.00	0.00	0.00	0.00	0.33	0.33	0.00	0.00	0.67	2.00
Globoturborotalita tenella	0.33	0.00	0.00	0.33	0.00	0.00	0.00	0.00	0.00	0.00	0.00	0.33
Indet.	1.00	0.33	0.00	0.00	0.00	0.00	0.00	0.33	0.00	0.00	0.00	0.00

Appendix A - Planktonic foraminifera assemblage data

Core 9/97-10
Relative abundance - Planktonic foraminifera >150um

Sample depth (cm)	115	120	123	132	136	142	146	150	156	160	164	168	172
Globigerina bulloides	50.33	39.33	12.33	47.67	61.00	34.00	57.00	48.67	6.67	12.67	30.00	15.00	43.33
Turborotalita quinqueloba	5.33	3.67	1.00	6.00	1.67	3.33	4.67	2.67	3.67	4.33	2.33	4.67	7.67
Orbulina universa	0.33	0.00	0.00	0.67	0.67	0.33	1.00	0.33	0.00	0.67	0.33	0.33	0.33
Neogloboquadrina pachyderma (sin.)	18.33	20.67	80.00	14.33	7.00	18.33	5.33	5.33	73.33	60.33	42.67	64.33	23.67
Neogloboquadrina pachyderma (dext.)	12.33	18.67	2.00	16.00	10.33	26.33	19.00	22.67	9.33	11.67	10.33	6.00	10.33
Globigerinoides ruber	0.33	0.33	0.00	0.33	0.00	0.00	0.00	0.00	0.00	0.00	0.00	0.00	0.33
Globorotalia scitula	1.00	4.33	0.33	0.67	4.67	3.00	2.00	0.67	1.00	0.00	2.67	0.67	1.00
Globorotalia inflata	9.33	11.67	4.33	13.67	13.33	13.00	10.33	13.33	5.67	10.00	9.67	9.00	9.33
Globorotalia truncatulinoides	0.67	0.00	0.00	0.00	0.33	1.00	0.00	0.33	0.33	0.00	0.00	0.00	1.33
Globorotalia hirsuta	0.33	0.33	0.00	0.33	0.33	0.00	0.00	1.33	0.00	0.00	0.00	0.00	0.00
Globigerinoides sacculifer	0.00	0.00	0.00	0.00	0.33	0.00	0.00	0.00	0.00	0.00	0.33	0.00	0.00
Neogloboquadrina duertrei	0.00	0.00	0.00	0.00	0.00	0.00	0.00	0.67	0.00	0.00	0.00	0.00	0.00
Hastigerinella digitata	0.00	0.00	0.00	0.00	0.00	0.00	0.00	0.00	0.00	0.00	0.00	0.00	0.00
Globigerina rubescens	0.00	0.00	0.00	0.00	0.00	0.00	0.00	0.67	0.00	0.00	0.00	0.00	0.00
Globorotalia crassaformis	0.00	0.00	0.00	0.00	0.00	0.00	0.00	1.00	0.00	0.00	0.00	0.00	0.33
Hastigerina pelagica	0.00	0.00	0.00	0.00	0.00	0.00	0.00	0.67	0.00	0.00	0.00	0.00	0.00
Globigerinoides conglobatus	0.00	0.00	0.00	0.00	0.00	0.00	0.00	0.33	0.00	0.00	0.00	0.00	0.67
Globigerina glutinata	0.00	0.33	0.00	0.00	0.00	0.00	0.33	0.67	0.00	0.00	0.00	0.00	1.00
Globigerina calida	0.00	0.67	0.00	0.33	0.33	0.33	0.00	0.33	0.00	0.00	0.00	0.00	0.00
Orbulina sp. A	0.00	0.00	0.00	0.00	0.00	0.00	0.00	0.33	0.00	0.00	0.00	0.00	0.00
Globorotalia tumida	0.00	0.00	0.00	0.00	0.00	0.00	0.00	0.00	0.00	0.00	0.00	0.00	0.00
Globierinella siphonifera	1.67	0.00	0.00	0.00	0.00	0.33	0.33	0.00	0.00	0.00	1.67	0.00	0.00
Globoturborotalita tenella	0.00	0.00	0.00	0.00	0.00	0.00	0.00	0.00	0.00	0.33	0.00	0.00	0.00
Indet.	0.00	0.00	0.00	0.00	0.00	0.67	0.00	0.00	0.00	0.00	0.00	0.00	0.33

Appendix A - Planktonic foraminifera assemblage data

Core 9/97-10
Relative abundance - Planktonic foraminifera >150um

Sample depth (cm)	176	180	184	188	192	196	200	204	207	213	217	223	230	236
Globigerina bulloides	40.33	49.33	54.67	62.33	44.33	22.00	30.67	17.00	23.00	3.33	1.00	2.33	7.67	5.33
Turborotalita quinqueloba	5.33	7.00	4.67	1.67	6.67	3.67	5.33	10.00	5.67	0.00	0.00	0.00	3.33	7.00
Orbulina universa	1.33	1.67	3.33	3.00	2.33	1.00	0.33	0.33	0.33	0.00	0.00	0.00	0.00	0.00
Neogloboquadrina pachyderma (sin.)	20.33	8.67	3.00	2.00	7.00	22.00	7.67	10.33	8.67	96.33	98.67	97.00	85.67	75.33
Neogloboquadrina pachyderma (dext.)	19.67	15.33	11.67	10.00	16.00	38.67	34.67	48.67	40.00	0.33	0.33	0.00	2.00	5.00
Globigerinoides ruber	0.33	0.33	0.00	0.00	0.00	0.00	0.33	0.00	0.00	0.00	0.00	0.00	0.00	0.00
Globorotalia scitula	0.33	1.00	1.67	1.67	2.33	2.33	2.00	3.00	3.00	0.00	0.00	0.33	0.00	0.00
Globorotalia inflata	10.33	15.00	18.67	15.00	18.33	9.00	14.00	8.67	14.67	0.00	0.00	0.33	0.67	6.00
Globorotalia truncatulinoides	0.00	0.33	0.67	1.67	1.33	0.00	2.33	0.33	2.33	0.00	0.00	0.00	0.67	1.00
Globorotalia hirsuta	0.00	0.00	0.33	0.00	0.67	1.00	0.00	0.00	0.33	0.00	0.00	0.00	0.00	0.33
Globigerinoides sacculifer	0.33	0.00	0.33	0.00	0.00	0.00	0.33	0.33	0.33	0.00	0.00	0.00	0.00	0.00
Neogloboquadrina duertrei	0.00	0.00	0.00	0.00	0.00	0.00	0.00	0.00	0.00	0.00	0.00	0.00	0.00	0.00
Hastigerinella digitata	0.00	0.00	0.00	0.00	0.00	0.00	0.00	0.00	0.00	0.00	0.00	0.00	0.00	0.00
Globigerina rubescens	0.00	0.00	0.00	0.00	0.00	0.00	0.00	0.00	0.00	0.00	0.00	0.00	0.00	0.00
Globorotalia crassaformis	0.33	0.00	0.00	0.00	0.00	0.00	0.00	0.00	0.00	0.00	0.00	0.00	0.00	0.00
Hastigerina pelagica	0.00	0.00	0.00	0.00	0.00	0.00	0.00	0.00	0.00	0.00	0.00	0.00	0.00	0.00
Globigerinoides conglobatus	0.33	0.00	0.00	0.00	0.00	0.00	0.00	0.00	0.00	0.00	0.00	0.00	0.00	0.00
Globigerina glutinata	0.00	0.67	0.33	0.67	0.00	0.00	0.67	0.33	0.67	0.00	0.00	0.00	0.00	0.00
Globigerina calida	0.33	0.00	0.00	0.00	0.33	0.33	0.67	0.67	0.00	0.00	0.00	0.00	0.00	0.00
Orbulina sp. A	0.33	0.00	0.00	0.00	0.00	0.00	0.00	0.00	0.00	0.00	0.00	0.00	0.00	0.00
Globorotalia tumida	0.00	0.00	0.00	0.00	0.00	0.00	0.00	0.00	0.00	0.00	0.00	0.00	0.00	0.00
Globierinella siphonifera	0.33	0.67	0.67	2.00	0.33	0.00	0.67	0.33	0.67	0.00	0.00	0.00	0.00	0.00
Globoturborotalita tenella	0.00	0.00	0.00	0.00	0.33	0.00	0.33	0.00	0.00	0.00	0.00	0.00	0.00	0.00
Indet.	0.00	0.00	0.00	0.00	0.00	0.00	0.00	0.00	0.00	0.00	0.00	0.00	0.00	0.00

Appendix A - Planktonic foraminifera assemblage data

Core 9/97-03
Relative abundance - Planktonic foraminifera >150um

Sample depth (cm)	3	6	9	13	23	27	31	35	39	43
Globigerina bulloides	14.67	49.33	14.33	17.33	46.33	59.67	56.67	59.67	59.00	61.00
Turborotalita quinqueloba	3.33	4.33	3.00	2.00	1.33	2.33	2.67	3.67	3.33	1.67
Orbulina universa	0.00	0.00	0.00	0.00	0.00	0.00	0.00	0.00	0.00	0.00
Neogloboquadrina pachyderma (sin.	47.00	17.00	67.00	72.00	27.00	18.00	21.00	10.00	14.00	7.00
Neogloboquadrina pachyderma (dex	26.33	9.67	5.33	2.33	19.00	16.00	10.67	13.67	14.67	17.00
Globigerinoides ruber	0.00	1.33	0.00	0.00	1.67	0.00	0.00	0.33	0.33	0.67
Globorotalia scitula	2.00	2.33	4.33	1.33	3.00	3.67	1.33	0.33	0.33	1.00
Globorotalia inflata	5.00	12.33	6.00	5.00	0.67	0.33	7.33	11.67	6.67	10.67
Globorotalia truncatulinoides	0.33	0.00	0.00	0.00	0.00	0.00	0.00	0.67	0.00	0.00
Globorotalia hirsuta	1.00	1.67	0.00	0.00	0.00	0.00	0.00	0.00	0.00	0.00
Globigerinoides sacculifer	0.00	0.00	0.00	0.00	0.00	0.00	0.00	0.00	0.00	0.00
Neogloboquadrina duertrei	0.00	0.00	0.00	0.00	0.00	0.00	0.00	0.00	0.00	0.00
Hastigerinella digitata	0.00	0.00	0.00	0.00	0.00	0.00	0.00	0.00	0.00	0.00
Globigerina rubescens	0.00	0.00	0.00	0.00	0.00	0.00	0.00	0.00	0.00	0.00
Globorotalia crassaformis	0.00	0.33	0.00	0.00	0.00	0.00	0.00	0.00	0.00	0.00
Hastigerina pelagica	0.00	0.00	0.00	0.00	0.00	0.00	0.00	0.00	0.00	0.00
Globigerinoides conglobatus	0.00	0.00	0.00	0.00	0.00	0.00	0.00	0.00	0.00	0.00
Globigerina glutinata	0.00	0.00	0.00	0.00	0.00	0.00	0.00	0.00	0.00	0.00
Globigerina calida	0.33	1.33	0.00	0.00	0.33	0.00	0.33	0.00	0.00	0.00
Orbulina sp. A	0.00	0.00	0.00	0.00	0.00	0.00	0.00	0.00	0.00	0.00
Globorotalia tumida	0.00	0.00	0.00	0.00	0.00	0.00	0.00	0.00	0.00	0.00
Globierinella siphonifera	0.00	0.33	0.00	0.00	0.33	0.00	0.00	0.00	0.67	0.67
Globoturborotalita tenella	0.00	0.00	0.00	0.00	0.33	0.00	0.00	0.00	1.00	0.33
Orbulina bilobata	0.00	0.00	0.00	0.00	0.00	0.00	0.00	0.00	0.00	0.00

Appendix A - Planktonic foraminifera assemblage data

Core 9/97-03
Relative abundance - Planktonic foraminifera >150um

Sample depth (cm)	47	55	59	63	67	71	75	79	83	87
Globigerina bulloides	36.67	34.00	39.00	42.67	25.33	34.33	19.00	54.33	50.33	23.00
Turborotalita quinqueloba	4.33	3.67	5.33	6.33	11.33	0.00	3.33	1.33	4.33	4.67
Orbulina universa	0.00	0.00	0.33	0.00	0.33	0.67	0.67	0.00	0.33	0.00
Neogloboquadrina pachyderma (sin.	32.00	19.00	24.00	5.00	8.00	34.00	42.00	6.00	6.33	42.00
Neogloboquadrina pachyderma (dex	18.00	30.00	12.33	24.67	36.67	13.00	19.00	11.33	6.67	23.33
Globigerinoides ruber	0.00	0.00	0.00	0.00	0.67	0.00	0.00	0.33	0.00	0.00
Globorotalia scitula	1.00	2.33	0.00	1.67	2.33	0.67	0.00	4.33	4.00	2.67
Globorotalia inflata	6.33	10.00	15.00	17.00	7.33	12.67	15.00	20.00	25.00	3.00
Globorotalia truncatulinoides	0.00	0.67	3.00	0.67	1.67	1.00	0.67	0.67	2.00	0.00
Globorotalia hirsuta	0.00	0.33	0.33	0.67	0.33	1.67	0.33	0.00	0.33	0.00
Globigerinoides sacculifer	0.00	0.00	0.00	0.00	0.33	0.00	0.00	0.67	0.00	0.00
Neogloboquadrina duertrei	0.00	0.00	0.00	0.00	0.00	0.00	0.00	0.00	0.00	0.00
Hastigerinella digitata	0.00	0.00	0.00	0.00	0.00	0.00	0.00	0.00	0.00	0.00
Globigerina rubescens	0.00	0.00	0.00	0.00	0.00	0.00	0.00	0.00	0.00	0.00
Globorotalia crassaformis	0.00	0.00	0.00	0.00	0.00	0.00	0.00	0.00	0.00	0.00
Hastigerina pelagica	0.00	0.00	0.00	0.00	0.00	0.00	0.00	0.00	0.00	0.00
Globigerinoides conglobatus	0.00	0.00	0.00	0.00	0.00	0.00	0.00	0.00	0.00	0.00
Globigerina glutinata	0.00	0.00	0.00	0.00	0.33	0.00	0.00	0.00	0.33	0.00
Globigerina calida	0.00	0.00	0.00	0.00	0.67	0.00	0.00	0.00	0.33	0.33
Orbulina sp. A	0.00	0.00	0.00	0.00	0.00	0.00	0.00	0.00	0.00	0.00
Globorotalia tumida	0.00	0.00	0.00	0.00	0.00	0.00	0.00	0.00	0.00	0.00
Globierinella siphonifera	0.67	0.00	0.67	1.33	4.67	2.00	0.00	1.00	0.00	1.00
Globoturborotalita tenella	1.00	0.00	0.00	0.00	0.00	0.00	0.00	0.00	0.00	0.00
Orbulina bilobata	0.00	0.00	0.00	0.00	0.00	0.00	0.00	0.00	0.00	0.00

Appendix A - Planktonic foraminifera assemblage data

Core 9/97-03
Relative abundance - Planktonic foraminifera >150um

Sample depth (cm)	91	95	99	103	107	115	119	123	127	131
Globigerina bulloides	24.33	40.67	46.00	33.33	35.00	23.00	36.00	16.33	39.33	29.00
Turborotalita quinqueloba	1.00	2.67	4.00	9.00	2.67	4.33	4.33	1.00	1.00	2.33
Orbulina universa	0.00	0.67	0.33	0.00	0.33	0.67	1.00	1.00	1.33	0.67
Neogloboquadrina pachyderma (sin.	67.00	18.00	9.00	4.00	15.00	23.00	8.00	61.00	21.00	7.00
Neogloboquadrina pachyderma (dex	5.33	20.67	26.67	40.00	24.33	31.67	41.33	12.33	25.67	43.33
Globigerinoides ruber	0.00	0.33	0.00	0.00	1.00	0.67	1.00	0.00	0.33	1.00
Globorotalia scitula	0.67	3.33	6.67	3.67	4.00	1.33	4.00	1.00	1.33	3.67
Globorotalia inflata	1.33	11.33	5.00	7.67	14.00	11.33	4.00	7.00	7.33	10.33
Globorotalia truncatulinoides	0.00	0.67	0.00	1.00	0.33	0.00	0.00	0.00	0.67	1.00
Globorotalia hirsuta	0.00	0.00	0.00	0.33	0.00	1.00	0.33	0.00	0.00	0.00
Globigerinoides sacculifer	0.00	0.00	0.00	0.00	0.00	0.00	0.00	0.00	0.00	0.00
Neogloboquadrina duertrei	0.00	0.00	0.00	0.00	0.00	0.00	0.00	0.00	0.00	0.00
Hastigerinella digitata	0.00	0.00	0.00	0.00	0.00	0.00	0.00	0.00	0.00	0.00
Globigerina rubescens	0.00	0.00	0.00	0.00	0.00	0.00	0.00	0.00	0.00	0.00
Globorotalia crassaformis	0.00	0.00	0.00	0.00	0.00	0.00	0.00	0.00	0.00	0.00
Hastigerina pelagica	0.00	0.00	0.00	0.00	0.00	0.00	0.00	0.00	0.00	0.00
Globigerinoides conglobatus	0.00	0.00	0.00	0.00	0.00	0.00	0.00	0.00	0.00	0.00
Globigerina glutinata	0.00	0.00	0.33	0.00	0.00	0.67	0.00	0.00	0.00	0.00
Globigerina calida	0.33	0.67	1.33	0.33	0.67	0.67	0.00	0.00	0.67	0.00
Orbulina sp. A	0.00	0.00	0.00	0.00	0.00	0.00	0.00	0.00	0.00	0.00
Globorotalia tumida	0.00	0.00	0.00	0.00	0.00	0.00	0.00	0.00	0.00	0.00
Globierinella siphonifera	0.00	1.00	0.67	0.67	2.67	1.67	0.00	0.00	1.00	1.67
Globoturborotalita tenella	0.00	0.00	0.00	0.00	0.00	0.00	0.00	0.00	0.00	0.00
Orbulina bilobata	0.00	0.00	0.00	0.00	0.00	0.00	0.00	0.00	0.00	0.00

Appendix A - Planktonic foraminifera assemblage data

Core 9/97-03
Relative abundance - Planktonic foraminifera >150um

Sample depth (cm)	135	143	147	151	155	159	163	167	175	180	183	187
Globigerina bulloides	41.00	10.67	17.00	1.67	6.67	7.67	31.00	32.00	14.67	18.33	51.33	62.67
Turborotalita quinqueloba	4.33	10.33	9.67	0.33	0.33	0.67	3.00	2.67	5.33	4.67	0.33	3.00
Orbulina universa	0.00	0.00	0.00	0.00	0.00	0.00	0.00	0.00	0.00	0.67	0.00	1.00
Neogloboquadrina pachyderma (sin.)	10.00	38.00	43.00	98.00	91.00	90.00	64.00	51.00	76.00	45.00	31.00	14.00
Neogloboquadrina pachyderma (dext.)	31.33	31.00	20.00	0.00	2.00	1.00	0.67	5.67	2.00	17.67	12.67	12.00
Globigerinoides ruber	1.33	0.67	0.00	0.00	0.00	0.00	0.00	0.00	0.00	0.00	0.00	0.00
Globorotalia scitula	0.67	1.67	0.00	0.00	0.00	0.00	0.00	1.33	0.33	5.67	1.67	2.33
Globorotalia inflata	9.00	7.33	10.33	0.00	0.00	0.67	1.33	7.33	1.67	7.33	3.00	5.00
Globorotalia truncatulinoides	0.67	0.33	0.00	0.00	0.00	0.00	0.00	0.00	0.00	0.67	0.00	0.00
Globorotalia hirsuta	0.00	0.00	0.00	0.00	0.00	0.00	0.00	0.00	0.00	0.00	0.00	0.00
Globigerinoides sacculifer	0.00	0.00	0.00	0.00	0.00	0.00	0.00	0.00	0.00	0.00	0.00	0.00
Neogloboquadrina duertrei	0.00	0.00	0.00	0.00	0.00	0.00	0.00	0.00	0.00	0.00	0.00	0.00
Hastigerinella digitata	0.00	0.00	0.00	0.00	0.00	0.00	0.00	0.00	0.00	0.00	0.00	0.00
Globigerina rubescens	0.00	0.00	0.00	0.00	0.00	0.00	0.00	0.00	0.00	0.00	0.00	0.00
Globorotalia crassaformis	0.00	0.00	0.00	0.00	0.00	0.00	0.00	0.00	0.00	0.00	0.00	0.00
Hastigerina pelagica	0.00	0.00	0.00	0.00	0.00	0.00	0.00	0.00	0.00	0.00	0.00	0.00
Globigerinoides conglobatus	0.00	0.00	0.00	0.00	0.00	0.00	0.00	0.00	0.00	0.00	0.00	0.00
Globigerina glutinata	0.00	0.00	0.00	0.00	0.00	0.00	0.00	0.00	0.00	0.00	0.00	0.00
Globigerina calida	0.67	0.00	0.00	0.00	0.00	0.00	0.00	0.00	0.00	0.00	0.00	0.00
Orbulina sp. A	0.00	0.00	0.00	0.00	0.00	0.00	0.00	0.00	0.00	0.00	0.00	0.00
Globorotalia tumida	0.00	0.00	0.00	0.00	0.00	0.00	0.00	0.00	0.00	0.00	0.00	0.00
Globierinella siphonifera	1.00	0.00	0.00	0.00	0.00	0.00	0.00	0.00	0.00	0.00	0.00	0.00
Globoturborotalita tenella	0.00	0.00	0.00	0.00	0.00	0.00	0.00	0.00	0.00	0.00	0.00	0.00
Orbulina bilobata	0.00	0.00	0.00	0.00	0.00	0.00	0.00	0.00	0.00	0.00	0.00	0.00

Appendix A - Planktonic foraminifera assemblage data

Core 9/97-03
Relative abundance - Planktonic foraminifera >150um

Sample depth (cm)	191	199	203	207	215	219	222	225
Globigerina bulloides	61.00	46.00	17.33	31.67	38.33	29.33	22.33	25.00
Turborotalita quinqueloba	2.67	1.00	4.00	2.33	9.33	6.67	4.67	8.00
Orbulina universa	0.00	0.00	0.00	0.33	0.00	0.33	1.00	0.00
Neogloboquadrina pachyderma (sin.)	6.00	12.00	22.00	21.00	11.00	16.00	11.00	2.00
Neogloboquadrina pachyderma (dext	17.00	23.67	41.33	26.67	22.00	36.33	45.00	45.00
Globigerinoides ruber	0.33	1.33	0.33	0.00	0.33	0.00	0.00	0.67
Globorotalia scitula	2.33	1.00	4.00	1.00	4.00	2.33	2.00	3.33
Globorotalia inflata	7.67	14.00	5.33	14.00	12.67	7.67	9.33	11.00
Globorotalia truncatulinoides	1.67	0.00	1.33	2.33	0.00	0.67	0.67	0.67
Globorotalia hirsuta	0.33	0.33	1.00	0.00	0.00	0.00	0.00	0.00
Globigerinoides sacculifer	0.00	0.00	0.33	0.00	0.00	0.00	0.00	0.00
Neogloboquadrina duertrei	0.00	0.00	0.00	0.00	0.00	0.00	0.00	0.00
Hastigerinella digitata	0.00	0.00	0.00	0.00	0.00	0.00	0.00	0.00
Globigerina rubescens	0.00	0.00	0.00	0.00	0.00	0.00	0.00	0.00
Globorotalia crassaformis	0.00	0.00	0.00	0.00	0.00	0.00	0.00	0.00
Hastigerina pelagica	0.00	0.00	0.00	0.00	0.00	0.00	0.00	0.00
Globigerinoides conglobatus	0.00	0.00	0.00	0.00	0.00	0.00	0.00	0.00
Globigerina glutinata	0.00	0.00	0.00	0.00	0.00	0.00	0.00	0.00
Globigerina calida	0.00	0.00	0.67	0.00	0.00	0.00	0.00	0.67
Orbulina sp. A	0.00	0.00	0.00	0.00	0.00	0.00	0.00	0.00
Globorotalia tumida	0.00	0.00	0.00	0.00	0.00	0.00	0.00	0.00
Globierinella siphonifera	1.00	0.67	1.67	0.33	2.33	0.67	4.00	3.67
Globoturborotalita tenella	0.00	0.00	0.67	0.00	0.00	0.00	0.00	0.00
Orbulina bilobata	0.00	0.00	0.00	0.00	0.00	0.00	0.00	0.00

Appendix A - Planktonic foraminifera assemblage data

Core 9/97-04
Relative abundance - Planktonic foraminifera >150um

Sample depth (cm)	1	2	4	8	12	16	20	24	28	32	36	38	40	42	44
Globigerina bulloides	30.81	17.56	41.52	5.86	21.11	11.78	3.92	3.99	29.11	17.89	63.09	31.45	53.97	66.12	69.87
Turborotalita quinqueloba	2.93	2.27	3.51	17.24	3.81	2.23	0.98	0.00	1.90	6.07	0.00	1.89	1.32	0.65	1.92
Orbulina universa	1.96	1.70	5.26	0.00	0.00	0.00	0.00	0.00	0.00	0.00	0.00	0.00	0.00	0.00	0.64
Neogloboquadrina pachyderma (sin.)	2.20	9.07	3.22	75.17	68.17	76.43	92.81	93.69	44.94	52.40	18.30	48.74	41.06	24.10	3.85
Neogloboquadrina pachyderma (dext.)	19.56	47.59	29.53	1.72	0.00	7.01	0.00	1.00	11.71	20.13	7.89	10.69	2.65	7.17	17.31
Globigerinoides ruber	1.96	0.57	0.88	0.00	0.00	0.00	0.00	0.00	0.00	0.00	0.00	0.00	0.00	0.00	0.32
Globorotalia scitula	6.60	3.40	1.17	0.00	0.69	0.00	0.00	0.00	0.63	0.00	0.00	0.00	0.00	0.00	0.00
Globorotalia inflata	20.54	11.61	9.36	0.00	6.23	2.55	2.29	1.33	8.54	3.51	10.73	7.23	0.99	0.98	2.24
Globorotalia truncatulinoides	5.62	1.13	0.88	0.00	0.00	0.00	0.00	0.00	0.00	0.00	0.00	0.00	0.00	0.00	0.00
Globorotalia hirsuta	0.98	2.27	2.34	0.00	0.00	0.00	0.00	0.00	0.95	0.00	0.00	0.00	0.00	0.00	0.96
Globigerinoides sacculifer	1.96	0.57	0.58	0.00	0.00	0.00	0.00	0.00	0.00	0.00	0.00	0.00	0.00	0.00	0.64
Neogloboquadrina duertrei	0.00	0.00	0.00	0.00	0.00	0.00	0.00	0.00	0.00	0.00	0.00	0.00	0.00	0.00	0.00
Hastigerinella digitata	0.00	0.00	0.00	0.00	0.00	0.00	0.00	0.00	0.00	0.00	0.00	0.00	0.00	0.00	0.00
Globigerina rubescens	0.00	0.00	0.00	0.00	0.00	0.00	0.00	0.00	0.00	0.00	0.00	0.00	0.00	0.00	0.00
Globorotalia crassaformis	0.00	0.00	0.00	0.00	0.00	0.00	0.00	0.00	0.00	0.00	0.00	0.00	0.00	0.00	0.00
Hastigerina pelagica	0.00	0.00	0.00	0.00	0.00	0.00	0.00	0.00	0.00	0.00	0.00	0.00	0.00	0.00	0.00
Globigerinoides conglobatus	0.00	0.00	0.00	0.00	0.00	0.00	0.00	0.00	0.00	0.00	0.00	0.00	0.00	0.00	0.00
Globigerina glutinata	1.96	0.57	0.29	0.00	0.00	0.00	0.00	0.00	2.22	0.00	0.00	0.00	0.00	0.98	0.96
Globigerina calida	1.71	0.57	0.29	0.00	0.00	0.00	0.00	0.00	0.00	0.00	0.00	0.00	0.00	0.00	0.32
Orbulina sp. A	0.00	0.00	0.00	0.00	0.00	0.00	0.00	0.00	0.00	0.00	0.00	0.00	0.00	0.00	0.00
Globorotalia tumida	0.00	0.00	0.00	0.00	0.00	0.00	0.00	0.00	0.00	0.00	0.00	0.00	0.00	0.00	0.00
Globierinella siphonifera	0.73	0.85	0.88	0.00	0.00	0.00	0.00	0.00	0.00	0.00	0.00	0.00	0.00	0.00	0.32
Globoturborotalita tenella	0.49	0.28	0.29	0.00	0.00	0.00	0.00	0.00	0.00	0.00	0.00	0.00	0.00	0.00	0.64
Orbulina bilobata	0.00	0.00	0.00	0.00	0.00	0.00	0.00	0.00	0.00	0.00	0.00	0.00	0.00	0.00	0.00
Indet.	0.00	0.00	0.00	0.00	0.00	0.00	0.00	0.00	0.00	0.00	0.00	0.00	0.00	0.00	0.00

Appendix A - Planktonic foraminifera assemblage data

Core 9/97-04
Relative abundance - Planktonic foraminifera >150um

Sample depth (cm)	47	51	55	59	67	71	75	79	83
Globigerina bulloides	57.57	57.84	40.33	67.30	66.16	41.44	25.16	29.26	41.86
Turborotalita quinqueloba	6.82	3.59	1.63	1.27	2.13	5.11	3.82	2.04	2.62
Orbulina universa	0.30	0.98	0.23	0.63	0.30	0.60	1.27	0.51	0.00
Neogloboquadrina pachyderma (sin.)	4.75	1.96	10.96	0.32	2.74	12.61	1.27	9.67	6.40
Neogloboquadrina pachyderma (dext.)	19.58	21.57	21.45	15.87	12.20	28.53	19.11	23.92	18.02
Globigerinoides ruber	0.30	0.00	0.47	0.00	0.30	0.00	1.27	1.27	0.87
Globorotalia scitula	1.48	0.33	5.13	1.27	0.61	1.50	12.42	3.31	3.78
Globorotalia inflata	6.82	13.73	12.12	12.06	10.98	5.11	21.34	19.85	12.50
Globorotalia truncatulinoides	0.00	0.00	0.47	0.32	0.30	0.60	4.46	0.76	6.69
Globorotalia hirsuta	0.00	0.00	4.66	0.00	0.91	1.20	1.91	1.02	1.16
Globigerinoides sacculifer	0.30	0.00	0.47	0.32	1.52	0.30	2.55	4.58	1.74
Neogloboquadrina duertrei	0.00	0.00	0.00	0.00	0.00	0.00	0.00	0.00	0.00
Hastigerinella digitata	0.00	0.00	0.00	0.00	0.00	0.00	0.00	0.00	0.00
Globigerina rubescens	0.00	0.00	0.00	0.00	0.00	0.00	0.00	0.00	0.00
Globorotalia crassaformis	0.00	0.00	0.00	0.00	0.00	0.00	0.00	0.00	0.00
Hastigerina pelagica	0.00	0.00	0.00	0.00	0.00	0.00	0.00	0.00	0.00
Globigerinoides conglobatus	0.00	0.00	0.00	0.00	0.00	0.00	0.00	0.00	0.00
Globigerina glutinata	0.30	0.00	0.47	0.00	0.30	0.30	0.96	0.51	0.58
Globigerina calida	0.89	0.00	0.70	0.00	0.30	0.90	2.55	0.76	1.16
Orbulina sp. A	0.00	0.00	0.00	0.00	0.00	0.00	0.00	0.00	0.00
Globorotalia tumida	0.00	0.00	0.00	0.00	0.00	0.00	0.00	0.00	0.00
Globierinella siphonifera	0.59	0.00	0.47	0.63	0.91	1.20	1.27	2.04	2.03
Globoturborotalita tenella	0.30	0.00	0.47	0.00	0.30	0.60	0.64	0.51	0.58
Orbulina bilobata	0.00	0.00	0.00	0.00	0.00	0.00	0.00	0.00	0.00
Indet.	0.00	0.00	0.00	0.00	0.00	0.00	0.00	0.00	0.00

Appendix A - Planktonic foraminifera assemblage data

Core 9/97-14
Relative abundance - Planktonic foraminifera >150um

Sample depth (cm)	1	5	7.5	9	12	15	19	23	27	31	35	39	43	49	51	54
Globigerina bulloides	49.87	5.23	7.67	32.07	8.20	52.94	41.67	58.86	16.00	31.49	66.26	33.33	44.84	51.38	55.41	43.49
Turborotalita quinqueloba	3.50	0.00	1.00	1.90	0.00	0.98	0.89	2.29	1.33	1.30	1.22	1.98	0.88	4.28	1.31	2.22
Orbulina universa	0.27	0.00	0.00	0.00	0.00	0.00	0.00	0.00	0.00	0.32	0.30	0.00	0.29	0.61	0.33	0.00
Neogloboquadrina pachyderma (sin.)	5.789	91.18	90.67	48.91	89.18	39.22	48.51	16.57	82.67	28.25	17.33	9.24	29.79	6.42	7.21	27.62
Neogloboquadrina pachyderma (dext.)	17.25	0.33	0.67	4.62	0.33	3.92	6.55	6.29	0.00	19.16	6.69	42.24	7.96	13.15	20.00	18.10
Globigerinoides ruber	0.54	0.00	0.00	0.00	0.00	0.00	0.00	0.00	0.00	0.00	0.00	0.00	0.00	0.00	0.66	0.63
Globorotalia scitula	3.23	0.65	0.00	4.62	0.00	0.65	0.00	3.14	0.00	1.30	0.91	1.32	5.01	2.14	2.62	0.95
Globorotalia inflata	14.70	2.61	0.00	6.79	2.30	2.29	2.38	12.00	0.00	16.56	7.29	9.90	9.73	16.51	5.57	3.81
Globorotalia truncatulinoides	2.16	0.00	0.00	0.00	0.00	0.00	0.00	0.00	0.00	0.00	0.00	0.99	0.59	3.67	0.98	0.95
Globorotalia hirsuta	1.08	0.00	0.00	1.09	0.00	0.00	0.00	0.86	0.00	0.97	0.00	0.33	0.88	0.61	0.98	0.63
Globigerinoides sacculifer	0.54	0.00	0.00	0.00	0.00	0.00	0.00	0.00	0.00	0.65	0.00	0.33	0.00	0.00	0.66	0.32
Neogloboquadrina duertrei	0.00	0.00	0.00	0.00	0.00	0.00	0.00	0.00	0.00	0.00	0.00	0.00	0.00	0.00	0.00	0.00
Hastigerinella digitata	0.00	0.00	0.00	0.00	0.00	0.00	0.00	0.00	0.00	0.00	0.00	0.00	0.00	0.00	0.00	0.00
Globigerina rubescens	0.00	0.00	0.00	0.00	0.00	0.00	0.00	0.00	0.00	0.00	0.00	0.00	0.00	0.00	0.00	0.00
Globorotalia crassaformis	0.00	0.00	0.00	0.00	0.00	0.00	0.00	0.00	0.00	0.00	0.00	0.00	0.00	0.00	0.00	0.00
Hastigerina pelagica	0.00	0.00	0.00	0.00	0.00	0.00	0.00	0.00	0.00	0.00	0.00	0.00	0.00	0.00	0.00	0.00
Globigerinoides conglobatus	0.00	0.00	0.00	0.00	0.00	0.00	0.00	0.00	0.00	0.00	0.00	0.00	0.00	0.00	0.00	0.00
Globigerina glutinata	0.27	0.00	0.00	0.00	0.00	0.00	0.00	0.00	0.00	0.00	0.00	0.33	0.00	0.31	0.98	0.32
Globigerina calida	0.54	0.00	0.00	0.00	0.00	0.00	0.00	0.00	0.00	0.00	0.00	0.00	0.00	0.31	0.98	0.32
Orbulina sp. A	0.00	0.00	0.00	0.00	0.00	0.00	0.00	0.00	0.00	0.00	0.00	0.00	0.00	0.00	0.00	0.00
Globorotalia tumida	0.00	0.00	0.00	0.00	0.00	0.00	0.00	0.00	0.00	0.00	0.00	0.00	0.00	0.00	0.00	0.00
Globierinella siphonifera	0.27	0.00	0.00	0.00	0.00	0.00	0.00	0.00	0.00	0.00	0.00	0.00	0.00	0.61	1.97	0.32
Globoturborotalita tenella	0.00	0.00	0.00	0.00	0.00	0.00	0.00	0.00	0.00	0.00	0.00	0.00	0.00	0.00	0.33	0.32
Orbulina bilobata	0.00	0.00	0.00	0.00	0.00	0.00	0.00	0.00	0.00	0.00	0.00	0.00	0.00	0.00	0.00	0.00
Indet.	0.00	0.00	0.00	0.00	0.00	0.00	0.00	0.00	0.00	0.00	0.00	0.00	0.00	0.00	0.00	0.00

Appendix A - Planktonic foraminifera assemblage data

Core 9/97-14
Relative abundance - Planktonic foraminifera >150um

Sample depth (cm)	57	62	75	78	81	84	87	90	93	96	106	114	120	129.5	133
Globigerina bulloides	49.22	28.99	57.86	31.60	61.83	62.54	10.06	45.90	17.86	49.87	40.54	16.21	57.31	45.27	36.31
Turborotalita quinqueloba	7.21	2.28	4.01	0.65	0.95	1.30	2.07	1.91	0.65	3.50	1.89	8.26	3.58	0.89	1.19
Orbulina universa	0.63	0.00	0.00	0.00	2.21	0.33	0.59	0.27	0.00	0.27	1.08	0.61	0.90	0.59	0.00
Neogloboquadrina pachyderma (sin.)	6.90	20.20	12.37	43.32	10.73	15.31	78.11	13.39	59.74	6.47	9.19	28.13	2.39	19.82	43.75
Neogloboquadrina pachyderma (dext.)	19.75	31.92	2.68	20.85	5.36	6.84	3.25	11.48	7.47	17.25	20.00	19.88	12.84	11.24	9.52
Globigerinoides ruber	0.00	0.00	0.00	0.00	0.00	0.00	0.00	0.00	0.00	0.54	0.27	0.00	0.60	0.00	0.00
Globorotalia scitula	2.19	2.61	0.67	0.98	2.21	1.30	0.89	2.46	0.65	3.23	2.43	0.00	3.58	2.07	2.38
Globorotalia inflata	10.03	12.70	21.07	2.61	13.25	10.75	4.14	22.95	13.64	14.02	16.76	18.96	11.04	15.38	6.85
Globorotalia truncatulinoides	0.63	0.98	0.00	0.00	0.63	0.33	0.59	0.00	0.00	2.16	3.78	4.28	3.58	0.59	0.00
Globorotalia hirsuta	0.00	0.00	1.34	0.00	2.21	1.30	0.30	1.09	0.00	1.08	1.08	2.75	0.90	1.18	0.00
Globigerinoides sacculifer	0.94	0.33	0.00	0.00	0.63	0.00	0.00	0.55	0.00	0.54	1.35	0.92	0.60	0.89	0.00
Neogloboquadrina duertrei	0.00	0.00	0.00	0.00	0.00	0.00	0.00	0.00	0.00	0.00	0.00	0.00	0.00	0.00	0.00
Hastigerinella digitata	0.00	0.00	0.00	0.00	0.00	0.00	0.00	0.00	0.00	0.00	0.00	0.00	0.00	0.00	0.00
Globigerina rubescens	0.00	0.00	0.00	0.00	0.00	0.00	0.00	0.00	0.00	0.00	0.00	0.00	0.00	0.00	0.00
Globorotalia crassaformis	0.00	0.00	0.00	0.00	0.00	0.00	0.00	0.00	0.00	0.00	0.00	0.00	0.00	0.00	0.00
Hastigerina pelagica	0.00	0.00	0.00	0.00	0.00	0.00	0.00	0.00	0.00	0.00	0.00	0.00	0.00	0.00	0.00
Globigerinoides conglobatus	0.00	0.00	0.00	0.00	0.00	0.00	0.00	0.00	0.00	0.00	0.00	0.00	0.00	0.00	0.00
Globigerina glutinata	0.63	0.00	0.00	0.00	0.00	0.00	0.00	0.00	0.00	0.27	0.00	0.00	0.60	0.89	0.00
Globigerina calida	0.94	0.00	0.00	0.00	0.00	0.00	0.00	0.00	0.00	0.54	0.00	0.00	0.90	0.59	0.00
Orbulina sp. A	0.00	0.00	0.00	0.00	0.00	0.00	0.00	0.00	0.00	0.00	0.00	0.00	0.00	0.00	0.00
Globorotalia tumida	0.00	0.00	0.00	0.00	0.00	0.00	0.00	0.00	0.00	0.00	0.00	0.00	0.00	0.00	0.00
Globierinella siphonifera	0.63	0.00	0.00	0.00	0.00	0.00	0.00	0.00	0.00	0.27	1.62	0.00	0.90	0.30	0.00
Globoturborotalita tenella	0.31	0.00	0.00	0.00	0.00	0.00	0.00	0.00	0.00	0.00	0.00	0.00	0.30	0.30	0.00
Orbulina bilobata	0.00	0.00	0.00	0.00	0.00	0.00	0.00	0.00	0.00	0.00	0.00	0.00	0.00	0.00	0.00
Indet.	0.00	0.00	0.00	0.00	0.00	0.00	0.00	0.00	0.00	0.00	0.00	0.00	0.00	0.00	0.00

Appendix A - Planktonic foraminifera assemblage data

Core 9/97-27/2
Relative abundance - Planktonic foraminifera >150um

Sample depth (cm)	3	7	11	15	19	33	37	41	45	49	53	57	61	65	69
Globigerina bulloides	38.33	33.00	34.00	30.00	26.33	20.00	8.33	7.33	2.00	13.00	7.33	4.00	3.00	1.33	18.67
Turborotalita quinqueloba	5.00	6.00	5.33	2.33	2.33	1.67	0.00	0.00	0.00	10.67	4.33	0.33	1.00	0.67	0.00
Orbulina universa	0.00	0.00	0.00	1.33	0.00	0.00	0.00	0.00	0.00	0.00	0.00	0.00	0.00	0.00	0.00
Neogloboquadrina pachyderma (sin.)	34.00	14.33	18.67	29.00	53.33	68.67	88.00	87.67	98.00	73.00	84.33	93.67	92.00	95.33	72.33
Neogloboquadrina pachyderma (dext.)	8.00	30.67	25.67	32.33	6.00	5.33	1.67	3.00	0.00	0.00	2.67	0.67	0.00	2.00	0.00
Globigerinoides ruber	0.00	0.00	0.00	0.00	0.00	0.00	0.00	0.00	0.00	0.00	0.00	0.00	0.00	0.00	0.00
Globorotalia scitula	3.67	3.67	4.33	2.33	1.00	0.00	0.00	0.67	0.00	3.33	1.33	1.33	2.67	0.67	9.00
Globorotalia inflata	4.33	7.67	8.33	0.00	11.00	4.33	2.00	1.33	0.00	0.00	0.00	0.00	1.33	0.00	0.00
Globorotalia truncatulinoides	2.67	1.67	2.00	0.00	0.00	0.00	0.00	0.00	0.00	0.00	0.00	0.00	0.00	0.00	0.00
Globorotalia hirsuta	4.00	1.00	0.67	2.67	0.00	0.00	0.00	0.00	0.00	0.00	0.00	0.00	0.00	0.00	0.00
Globigerinoides sacculifer	0.00	0.33	0.00	0.00	0.00	0.00	0.00	0.00	0.00	0.00	0.00	0.00	0.00	0.00	0.00
Neogloboquadrina duertrei	0.00	0.00	0.00	0.00	0.00	0.00	0.00	0.00	0.00	0.00	0.00	0.00	0.00	0.00	0.00
Hastigerinella digitata	0.00	0.00	0.00	0.00	0.00	0.00	0.00	0.00	0.00	0.00	0.00	0.00	0.00	0.00	0.00
Globigerina rubescens	0.00	0.00	0.00	0.00	0.00	0.00	0.00	0.00	0.00	0.00	0.00	0.00	0.00	0.00	0.00
Globorotalia crassaformis	0.00	0.00	0.00	0.00	0.00	0.00	0.00	0.00	0.00	0.00	0.00	0.00	0.00	0.00	0.00
Hastigerina pelagica	0.00	0.00	0.00	0.00	0.00	0.00	0.00	0.00	0.00	0.00	0.00	0.00	0.00	0.00	0.00
Globigerinoides conglobatus	0.00	0.00	0.00	0.00	0.00	0.00	0.00	0.00	0.00	0.00	0.00	0.00	0.00	0.00	0.00
Globigerina glutinata	0.00	0.00	0.00	0.00	0.00	0.00	0.00	0.00	0.00	0.00	0.00	0.00	0.00	0.00	0.00
Globigerina calida	0.00	0.67	1.00	0.00	0.00	0.00	0.00	0.00	0.00	0.00	0.00	0.00	0.00	0.00	0.00
Orbulina sp. A	0.00	0.00	0.00	0.00	0.00	0.00	0.00	0.00	0.00	0.00	0.00	0.00	0.00	0.00	0.00
Globorotalia tumida	0.00	0.00	0.00	0.00	0.00	0.00	0.00	0.00	0.00	0.00	0.00	0.00	0.00	0.00	0.00
Globierinella siphonifera	0.00	0.33	0.00	0.00	0.00	0.00	0.00	0.00	0.00	0.00	0.00	0.00	0.00	0.00	0.00
Globoturborotalita tenella	0.00	0.67	0.00	0.00	0.00	0.00	0.00	0.00	0.00	0.00	0.00	0.00	0.00	0.00	0.00
Orbulina bilobata	0.00	0.00	0.00	0.00	0.00	0.00	0.00	0.00	0.00	0.00	0.00	0.00	0.00	0.00	0.00
Indet.	0.00	0.00	0.00	0.00	0.00	0.00	0.00	0.00	0.00	0.00	0.00	0.00	0.00	0.00	0.00

Appendix A - Planktonic foraminifera assemblage data

Core 9/97-27/2
Relative abundance - Planktonic foraminifera >150um

Sample depth (cm)	73	77	81	85	90	94	98	103	107	111	115	119	123	127	131.5
Globigerina bulloides	3.00	16.00	18.33	3.00	1.67	1.00	2.67	0.67	36.67	31.00	29.67	8.00	1.33	1.00	9.67
Turborotalita quinqueloba	0.00	0.67	1.33	0.00	0.33	0.00	2.00	0.00	5.67	3.33	0.67	0.67	2.00	0.33	1.00
Orbulina universa	0.00	0.00	0.00	0.00	0.00	0.00	0.00	0.00	0.00	0.00	0.00	0.00	0.00	0.00	0.00
Neogloboquadrina pachyderma (sin.)	96.00	76.00	67.00	96.33	97.33	99.00	94.00	99.33	54.33	59.00	60.33	90.67	96.67	98.00	88.33
Neogloboquadrina pachyderma (dext.)	0.00	6.00	8.00	0.67	0.67	0.00	1.33	0.00	0.00	2.33	4.33	0.00	0.00	0.67	0.00
Globigerinoides ruber	0.00	0.00	0.00	0.00	0.00	0.00	0.00	0.00	0.00	0.00	0.00	0.00	0.00	0.00	0.00
Globorotalia scitula	1.00	0.00	5.33	0.00	0.00	0.00	0.00	0.00	2.33	2.00	2.67	0.33	0.00	0.00	0.67
Globorotalia inflata	0.00	1.33	0.00	0.00	0.00	0.00	0.00	0.00	1.00	2.33	2.00	0.33	0.00	0.00	0.33
Globorotalia truncatulinoides	0.00	0.00	0.00	0.00	0.00	0.00	0.00	0.00	0.00	0.00	0.00	0.00	0.00	0.00	0.00
Globorotalia hirsuta	0.00	0.00	0.00	0.00	0.00	0.00	0.00	0.00	0.00	0.00	0.33	0.00	0.00	0.00	0.00
Globigerinoides sacculifer	0.00	0.00	0.00	0.00	0.00	0.00	0.00	0.00	0.00	0.00	0.00	0.00	0.00	0.00	0.00
Neogloboquadrina duertrei	0.00	0.00	0.00	0.00	0.00	0.00	0.00	0.00	0.00	0.00	0.00	0.00	0.00	0.00	0.00
Hastigerinella digitata	0.00	0.00	0.00	0.00	0.00	0.00	0.00	0.00	0.00	0.00	0.00	0.00	0.00	0.00	0.00
Globigerina rubescens	0.00	0.00	0.00	0.00	0.00	0.00	0.00	0.00	0.00	0.00	0.00	0.00	0.00	0.00	0.00
Globorotalia crassaformis	0.00	0.00	0.00	0.00	0.00	0.00	0.00	0.00	0.00	0.00	0.00	0.00	0.00	0.00	0.00
Hastigerina pelagica	0.00	0.00	0.00	0.00	0.00	0.00	0.00	0.00	0.00	0.00	0.00	0.00	0.00	0.00	0.00
Globigerinoides conglobatus	0.00	0.00	0.00	0.00	0.00	0.00	0.00	0.00	0.00	0.00	0.00	0.00	0.00	0.00	0.00
Globigerina glutinata	0.00	0.00	0.00	0.00	0.00	0.00	0.00	0.00	0.00	0.00	0.00	0.00	0.00	0.00	0.00
Globigerina calida	0.00	0.00	0.00	0.00	0.00	0.00	0.00	0.00	0.00	0.00	0.00	0.00	0.00	0.00	0.00
Orbulina sp. A	0.00	0.00	0.00	0.00	0.00	0.00	0.00	0.00	0.00	0.00	0.00	0.00	0.00	0.00	0.00
Globorotalia tumida	0.00	0.00	0.00	0.00	0.00	0.00	0.00	0.00	0.00	0.00	0.00	0.00	0.00	0.00	0.00
Globierinella siphonifera	0.00	0.00	0.00	0.00	0.00	0.00	0.00	0.00	0.00	0.00	0.00	0.00	0.00	0.00	0.00
Globoturborotalita tenella	0.00	0.00	0.00	0.00	0.00	0.00	0.00	0.00	0.00	0.00	0.00	0.00	0.00	0.00	0.00
Orbulina bilobata	0.00	0.00	0.00	0.00	0.00	0.00	0.00	0.00	0.00	0.00	0.00	0.00	0.00	0.00	0.00
Indet.	0.00	0.00	0.00	0.00	0.00	0.00	0.00	0.00	0.00	0.00	0.00	0.00	0.00	0.00	0.00

Appendix A - Planktonic foraminifera assemblage data

Core 9/97-27/2
Relative abundance - Planktonic foraminifera >150um

Sample depth (cm)	135	139.5	143	147	151	155.5	159.5	163.5	167.5	171.5	176	180	184	188
Globigerina bulloides	46.00	11.67	46.33	60.67	66.67	50.67	43.67	15.67	0.33	2.33	0.00	18.33	91.67	57.67
Turborotalita quinqueloba	3.00	4.00	4.00	2.33	9.00	0.67	4.67	1.00	0.00	0.67	0.00	0.67	1.00	2.33
Orbulina universa	0.00	0.00	0.00	0.00	0.00	0.00	0.00	0.00	0.00	0.00	0.00	0.00	0.33	0.00
Neogloboquadrina pachyderma (sin.)	1.67	68.33	37.00	30.33	13.00	35.67	21.67	82.33	99.67	96.00	100.00	77.33	1.33	10.67
Neogloboquadrina pachyderma (dext.)	31.67	13.00	5.67	4.33	6.00	10.67	25.00	0.00	0.00	1.00	0.00	2.33	2.67	21.67
Globigerinoides ruber	0.33	0.00	0.00	0.33	0.00	0.00	0.00	0.00	0.00	0.00	0.00	0.00	0.00	0.33
Globorotalia scitula	5.67	1.67	1.67	1.00	2.33	1.00	2.00	0.33	0.00	0.00	0.00	0.33	0.67	1.67
Globorotalia inflata	7.33	1.00	4.67	0.67	2.00	2.33	3.00	0.67	0.00	0.00	0.00	1.00	2.33	4.00
Globorotalia truncatulinoides	2.33	0.00	0.00	0.00	0.00	0.00	0.00	0.00	0.00	0.00	0.00	0.00	0.00	0.00
Globorotalia hirsuta	0.67	0.33	0.33	0.00	0.00	0.00	0.00	0.00	0.00	0.00	0.00	0.00	0.00	0.33
Globigerinoides sacculifer	0.33	0.00	0.00	0.00	0.00	0.00	0.00	0.00	0.00	0.00	0.00	0.00	0.00	0.00
Neogloboquadrina duertrei	0.00	0.00	0.00	0.00	0.00	0.00	0.00	0.00	0.00	0.00	0.00	0.00	0.00	0.00
Hastigerinella digitata	0.00	0.00	0.00	0.00	0.00	0.00	0.00	0.00	0.00	0.00	0.00	0.00	0.00	0.00
Globigerina rubescens	0.00	0.00	0.00	0.00	0.00	0.00	0.00	0.00	0.00	0.00	0.00	0.00	0.00	0.00
Globorotalia crassaformis	0.00	0.00	0.00	0.00	0.00	0.00	0.00	0.00	0.00	0.00	0.00	0.00	0.00	0.00
Hastigerina pelagica	0.00	0.00	0.00	0.00	0.00	0.00	0.00	0.00	0.00	0.00	0.00	0.00	0.00	0.00
Globigerinoides conglobatus	0.00	0.00	0.00	0.00	0.00	0.00	0.00	0.00	0.00	0.00	0.00	0.00	0.00	0.00
Globigerina glutinata	0.00	0.00	0.00	0.00	0.67	0.00	0.00	0.00	0.00	0.00	0.00	0.00	0.00	0.33
Globigerina calida	0.33	0.00	0.33	0.00	0.33	0.00	0.00	0.00	0.00	0.00	0.00	0.00	0.00	0.00
Orbulina sp. A	0.00	0.00	0.00	0.00	0.00	0.00	0.00	0.00	0.00	0.00	0.00	0.00	0.00	0.00
Globorotalia tumida	0.00	0.00	0.00	0.00	0.00	0.00	0.00	0.00	0.00	0.00	0.00	0.00	0.00	0.00
Globierinella siphonifera	0.67	0.00	0.00	0.00	0.00	0.00	0.00	0.00	0.00	0.00	0.00	0.00	0.00	1.00
Globoturborotalita tenella	0.00	0.00	0.00	0.33	0.00	0.00	0.00	0.00	0.00	0.00	0.00	0.00	0.00	0.00
Orbulina bilobata	0.00	0.00	0.00	0.00	0.00	0.00	0.00	0.00	0.00	0.00	0.00	0.00	0.00	0.00
Indet.	0.00	0.00	0.00	0.00	0.00	0.00	0.00	0.00	0.00	0.00	0.00	0.00	0.00	0.00

Appendix A - Planktonic foraminifera assemblage data

Core 9/97-27/2
Relative abundance - Planktonic foraminifera >150um

Sample depth (cm)	192	196.5	200.5	204.5	208.5	212.5	216.5	220.5	224.5	229.5	233.5	237.5	241.5	245.5	249.5
Globigerina bulloides	61.00	26.00	59.00	82.00	72.33	35.00	44.00	11.00	29.33	12.00	4.00	14.67	46.00	40.67	41.67
Turborotalita quinqueloba	3.00	3.00	7.33	2.67	4.33	0.00	9.00	4.33	2.67	7.00	0.67	0.67	2.67	9.67	8.00
Orbulina universa	0.00	0.00	0.00	0.00	0.00	0.00	0.00	0.00	0.00	0.00	0.00	0.00	0.67	0.00	1.00
Neogloboquadrina pachyderma (sin.)	9.33	50.00	9.67	3.67	12.00	30.33	33.33	80.67	65.00	70.00	91.00	71.67	18.67	2.00	4.33
Neogloboquadrina pachyderma (dext.)	14.67	16.00	20.67	7.67	6.67	29.33	9.67	2.67	2.00	8.33	3.00	9.33	12.67	34.67	21.67
Globigerinoides ruber	0.00	0.00	0.00	0.67	0.00	0.00	0.00	0.00	0.00	0.00	0.00	0.00	0.00	0.00	1.00
Globorotalia scitula	2.33	1.00	0.67	1.00	1.00	2.00	2.67	0.33	0.33	1.33	1.00	1.00	4.00	4.00	4.67
Globorotalia inflata	8.67	4.00	0.67	0.67	3.33	3.33	1.00	1.00	0.67	1.33	0.33	2.67	13.67	6.00	12.67
Globorotalia truncatulinoides	0.00	0.00	0.00	0.33	0.00	0.00	0.00	0.00	0.00	0.00	0.00	0.00	0.67	0.67	0.67
Globorotalia hirsuta	0.33	0.00	0.67	0.33	0.33	0.00	0.33	0.00	0.00	0.00	0.00	0.00	0.33	0.33	1.33
Globigerinoides sacculifer	0.00	0.00	0.00	0.00	0.00	0.00	0.00	0.00	0.00	0.00	0.00	0.00	0.00	0.33	0.00
Neogloboquadrina duertrei	0.00	0.00	0.00	0.00	0.00	0.00	0.00	0.00	0.00	0.00	0.00	0.00	0.00	0.00	0.00
Hastigerinella digitata	0.00	0.00	0.00	0.00	0.00	0.00	0.00	0.00	0.00	0.00	0.00	0.00	0.00	0.00	0.00
Globigerina rubescens	0.00	0.00	0.00	0.00	0.00	0.00	0.00	0.00	0.00	0.00	0.00	0.00	0.00	0.00	0.00
Globorotalia crassaformis	0.00	0.00	0.00	0.00	0.00	0.00	0.00	0.00	0.00	0.00	0.00	0.00	0.00	0.00	0.00
Hastigerina pelagica	0.00	0.00	0.00	0.00	0.00	0.00	0.00	0.00	0.00	0.00	0.00	0.00	0.00	0.00	0.00
Globigerinoides conglobatus	0.00	0.00	0.00	0.00	0.00	0.00	0.00	0.00	0.00	0.00	0.00	0.00	0.00	0.00	0.00
Globigerina glutinata	0.67	0.00	0.33	0.00	0.00	0.00	0.00	0.00	0.00	0.00	0.00	0.00	0.33	0.33	0.00
Globigerina calida	0.00	0.00	0.33	0.33	0.00	0.00	0.00	0.00	0.00	0.00	0.00	0.00	0.33	0.33	0.67
Orbulina sp. A	0.00	0.00	0.00	0.00	0.00	0.00	0.00	0.00	0.00	0.00	0.00	0.00	0.00	0.00	0.00
Globorotalia tumida	0.00	0.00	0.00	0.00	0.00	0.00	0.00	0.00	0.00	0.00	0.00	0.00	0.00	0.00	0.00
Globierinella siphonifera	0.00	0.00	0.67	0.67	0.00	0.00	0.00	0.00	0.00	0.00	0.00	0.00	0.00	1.00	2.00
Globoturborotalita tenella	0.00	0.00	0.00	0.00	0.00	0.00	0.00	0.00	0.00	0.00	0.00	0.00	0.00	0.00	0.33
Orbulina bilobata	0.00	0.00	0.00	0.00	0.00	0.00	0.00	0.00	0.00	0.00	0.00	0.00	0.00	0.00	0.00
Indet.	0.00	0.00	0.00	0.00	0.00	0.00	0.00	0.00	0.00	0.00	0.00	0.00	0.00	0.00	0.00

Appendix A - Planktonic foraminifera assemblage data

Core 9/97-27/2
Relative abundance - Planktonic foraminifera >150um

Sample depth (cm)	253.5	258.5	262
Globigerina bulloides	57.00	45.33	24.67
Turborotalita quinqueloba	2.67	3.00	2.33
Orbulina universa	0.00	0.00	0.00
Neogloboquadrina pachyderma (sin.)	4.00	1.67	14.00
Neogloboquadrina pachyderma (dext.)	17.00	32.33	51.00
Globigerinoides ruber	0.33	0.33	0.00
Globorotalia scitula	4.33	5.67	3.00
Globorotalia inflata	8.33	7.33	2.67
Globorotalia truncatulinoides	1.33	2.33	1.67
Globorotalia hirsuta	4.00	0.67	0.67
Globigerinoides sacculifer	0.00	0.33	0.00
Neogloboquadrina duertrei	0.00	0.00	0.00
Hastigerinella digitata	0.00	0.00	0.00
Globigerina rubescens	0.00	0.00	0.00
Globorotalia crassaformis	0.00	0.00	0.00
Hastigerina pelagica	0.00	0.00	0.00
Globigerinoides conglobatus	0.00	0.00	0.00
Globigerina glutinata	0.00	0.00	0.00
Globigerina calida	0.67	0.33	0.00
Orbulina sp. A	0.00	0.00	0.00
Globorotalia tumida	0.00	0.00	0.00
Globierinella siphonifera	0.00	0.67	0.00
Globoturborotalita tenella	0.33	0.00	0.00
Orbulina bilobata	0.00	0.00	0.00
Indet.	0.00	0.00	0.00

Appendix A - Planktonic foraminifera assemblage data

Core 9/97-20
Relative abundance - Planktonic foraminifera >150um

Sample depth (cm)	1.5	3	5.5	9	11.5	15	19	20.5	23	25.5	27.5	30.5	33
Globigerina bulloides	41.21	58.44	48.28	33.67	45.65	35.76	42.86	26.29	21.23	46.18	54.93	54.90	30.16
Turborotalita quinqueloba	1.15	2.50	1.15	2.33	0.82	0.00	0.00	0.00	0.92	1.59	1.19	1.63	2.22
Orbulina universa	0.58	0.94	0.57	3.00	4.08	1.21	1.30	1.71	0.62	0.00	0.60	0.33	0.00
Neogloboquadrina pachyderma (sin.)	19.88	4.38	8.05	28.67	3.80	26.36	28.25	48.00	52.31	42.68	20.60	18.95	59.05
Neogloboquadrina pachyderma (dext.)	16.71	16.88	21.55	15.67	21.47	11.52	7.79	9.71	6.46	1.91	1.49	6.86	6.67
Globigerinoides ruber	0.00	0.63	0.00	0.00	0.54	0.00	0.00	0.00	0.00	0.00	0.00	0.00	0.00
Globorotalia scitula	5.76	4.38	5.75	5.33	8.15	6.36	6.82	4.00	4.92	1.91	5.97	2.61	0.32
Globorotalia inflata	12.39	8.75	12.36	9.33	13.04	16.06	12.34	8.00	9.54	5.73	12.84	12.09	1.59
Globorotalia truncatulinoides	0.00	0.94	0.00	0.67	0.27	0.61	0.65	0.86	1.85	0.00	0.00	0.65	0.00
Globorotalia hirsuta	2.31	2.19	2.30	1.33	2.17	2.12	0.00	1.43	2.15	0.00	2.39	1.96	0.00
Globigerinoides sacculifer	0.00	0.00	0.00	0.00	0.00	0.00	0.00	0.00	0.00	0.00	0.00	0.00	0.00
Neogloboquadrina duertrei	0.00	0.00	0.00	0.00	0.00	0.00	0.00	0.00	0.00	0.00	0.00	0.00	0.00
Hastigerinella digitata	0.00	0.00	0.00	0.00	0.00	0.00	0.00	0.00	0.00	0.00	0.00	0.00	0.00
Globigerina rubescens	0.00	0.00	0.00	0.00	0.00	0.00	0.00	0.00	0.00	0.00	0.00	0.00	0.00
Globorotalia crassaformis	0.00	0.00	0.00	0.00	0.00	0.00	0.00	0.00	0.00	0.00	0.00	0.00	0.00
Hastigerina pelagica	0.00	0.00	0.00	0.00	0.00	0.00	0.00	0.00	0.00	0.00	0.00	0.00	0.00
Globigerinoides conglobatus	0.00	0.00	0.00	0.00	0.00	0.00	0.00	0.00	0.00	0.00	0.00	0.00	0.00
Globigerina glutinata	0.00	0.00	0.00	0.00	0.00	0.00	0.00	0.00	0.00	0.00	0.00	0.00	0.00
Globigerina calida	0.00	0.00	0.00	0.00	0.00	0.00	0.00	0.00	0.00	0.00	0.00	0.00	0.00
Orbulina sp. A	0.00	0.00	0.00	0.00	0.00	0.00	0.00	0.00	0.00	0.00	0.00	0.00	0.00
Globorotalia tumida	0.00	0.00	0.00	0.00	0.00	0.00	0.00	0.00	0.00	0.00	0.00	0.00	0.00
Globierinella siphonifera	0.00	0.00	0.00	0.00	0.00	0.00	0.00	0.00	0.00	0.00	0.00	0.00	0.00
Globoturborotalita tenella	0.00	0.00	0.00	0.00	0.00	0.00	0.00	0.00	0.00	0.00	0.00	0.00	0.00
Orbulina bilobata	0.00	0.00	0.00	0.00	0.00	0.00	0.00	0.00	0.00	0.00	0.00	0.00	0.00

Appendix A - Planktonic foraminifera assemblage data

Core 9/97-20
Relative abundance - Planktonic foraminifera >150um

Sample depth (cm)	34.5	37	40.5	43.5	45	48	50.5	52	55.5	57.5	59.5	63	66.5
Globigerina bulloides	57.62	65.90	60.71	1.33	1.33	19.16	6.67	0.67	3.33	0.00	0.67	0.00	0.67
Turborotalita quinqueloba	0.99	0.66	0.00	0.00	0.00	1.95	0.00	0.00	0.67	0.00	0.00	0.00	0.33
Orbulina universa	0.00	0.00	0.00	0.00	0.00	0.00	0.00	0.00	0.00	0.00	0.00	0.00	0.00
Neogloboquadrina pachyderma (sin.)	29.47	24.59	32.79	98.33	97.67	65.26	92.67	99.00	95.00	99.33	99.33	99.67	98.67
Neogloboquadrina pachyderma (dext.)	4.64	2.95	3.25	0.33	1.00	9.09	0.67	0.33	1.00	0.67	0.00	0.33	0.33
Globigerinoides ruber	0.00	0.00	0.00	0.00	0.00	0.00	0.00	0.00	0.00	0.00	0.00	0.00	0.00
Globorotalia scitula	0.66	2.62	1.30	0.00	0.00	2.60	0.00	0.00	0.00	0.00	0.00	0.00	0.00
Globorotalia inflata	6.62	3.28	1.95	0.00	0.00	1.30	0.00	0.00	0.00	0.00	0.00	0.00	0.00
Globorotalia truncatulinoides	0.00	0.00	0.00	0.00	0.00	0.65	0.00	0.00	0.00	0.00	0.00	0.00	0.00
Globorotalia hirsuta	0.00	0.00	0.00	0.00	0.00	0.00	0.00	0.00	0.00	0.00	0.00	0.00	0.00
Globigerinoides sacculifer	0.00	0.00	0.00	0.00	0.00	0.00	0.00	0.00	0.00	0.00	0.00	0.00	0.00
Neogloboquadrina duertrei	0.00	0.00	0.00	0.00	0.00	0.00	0.00	0.00	0.00	0.00	0.00	0.00	0.00
Hastigerinella digitata	0.00	0.00	0.00	0.00	0.00	0.00	0.00	0.00	0.00	0.00	0.00	0.00	0.00
Globigerina rubescens	0.00	0.00	0.00	0.00	0.00	0.00	0.00	0.00	0.00	0.00	0.00	0.00	0.00
Globorotalia crassaformis	0.00	0.00	0.00	0.00	0.00	0.00	0.00	0.00	0.00	0.00	0.00	0.00	0.00
Hastigerina pelagica	0.00	0.00	0.00	0.00	0.00	0.00	0.00	0.00	0.00	0.00	0.00	0.00	0.00
Globigerinoides conglobatus	0.00	0.00	0.00	0.00	0.00	0.00	0.00	0.00	0.00	0.00	0.00	0.00	0.00
Globigerina glutinata	0.00	0.00	0.00	0.00	0.00	0.00	0.00	0.00	0.00	0.00	0.00	0.00	0.00
Globigerina calida	0.00	0.00	0.00	0.00	0.00	0.00	0.00	0.00	0.00	0.00	0.00	0.00	0.00
Orbulina sp. A	0.00	0.00	0.00	0.00	0.00	0.00	0.00	0.00	0.00	0.00	0.00	0.00	0.00
Globorotalia tumida	0.00	0.00	0.00	0.00	0.00	0.00	0.00	0.00	0.00	0.00	0.00	0.00	0.00
Globierinella siphonifera	0.00	0.00	0.00	0.00	0.00	0.00	0.00	0.00	0.00	0.00	0.00	0.00	0.00
Globoturborotalita tenella	0.00	0.00	0.00	0.00	0.00	0.00	0.00	0.00	0.00	0.00	0.00	0.00	0.00
Orbulina bilobata	0.00	0.00	0.00	0.00	0.00	0.00	0.00	0.00	0.00	0.00	0.00	0.00	0.00

Appendix A - Planktonic foraminifera assemblage data

Core 9/97-20
Relative abundance - Planktonic foraminifera >150um

Sample depth (cm)	68.5	70.5	72.5	74.5	76.5	78.5	80.5	82	87	90.5	92.5	94.5	96.5
Globigerina bulloides	0.00	3.32	0.00	0.33	6.62	0.00	0.33	13.21	12.14	13.97	96.67	25.73	33.67
Turborotalita quinqueloba	0.00	0.00	0.00	0.00	0.00	0.00	0.00	1.57	0.32	0.63	0.00	0.00	0.00
Orbulina universa	0.00	0.00	0.00	0.00	0.00	0.00	0.00	0.00	0.00	0.00	0.00	0.98	0.00
Neogloboquadrina pachyderma (sin.)	100.00	95.35	100.00	97.67	91.39	99.67	99.33	76.42	82.43	82.54	2.67	63.84	63.00
Neogloboquadrina pachyderma (dext.)	0.00	1.33	0.00	1.33	1.99	0.33	0.33	4.72	5.11	2.54	0.67	4.56	2.33
Globigerinoides ruber	0.00	0.00	0.00	0.00	0.00	0.00	0.00	0.00	0.00	0.00	0.00	0.00	0.00
Globorotalia scitula	0.00	0.00	0.00	0.00	0.00	0.00	0.00	0.00	0.00	0.32	0.00	2.28	0.00
Globorotalia inflata	0.00	0.00	0.00	0.67	0.00	0.00	0.00	4.09	0.00	0.00	0.00	2.61	1.00
Globorotalia truncatulinoides	0.00	0.00	0.00	0.00	0.00	0.00	0.00	0.00	0.00	0.00	0.00	0.00	0.00
Globorotalia hirsuta	0.00	0.00	0.00	0.00	0.00	0.00	0.00	0.00	0.00	0.00	0.00	0.00	0.00
Globigerinoides sacculifer	0.00	0.00	0.00	0.00	0.00	0.00	0.00	0.00	0.00	0.00	0.00	0.00	0.00
Neogloboquadrina duertrei	0.00	0.00	0.00	0.00	0.00	0.00	0.00	0.00	0.00	0.00	0.00	0.00	0.00
Hastigerinella digitata	0.00	0.00	0.00	0.00	0.00	0.00	0.00	0.00	0.00	0.00	0.00	0.00	0.00
Globigerina rubescens	0.00	0.00	0.00	0.00	0.00	0.00	0.00	0.00	0.00	0.00	0.00	0.00	0.00
Globorotalia crassaformis	0.00	0.00	0.00	0.00	0.00	0.00	0.00	0.00	0.00	0.00	0.00	0.00	0.00
Hastigerina pelagica	0.00	0.00	0.00	0.00	0.00	0.00	0.00	0.00	0.00	0.00	0.00	0.00	0.00
Globigerinoides conglobatus	0.00	0.00	0.00	0.00	0.00	0.00	0.00	0.00	0.00	0.00	0.00	0.00	0.00
Globigerina glutinata	0.00	0.00	0.00	0.00	0.00	0.00	0.00	0.00	0.00	0.00	0.00	0.00	0.00
Globigerina calida	0.00	0.00	0.00	0.00	0.00	0.00	0.00	0.00	0.00	0.00	0.00	0.00	0.00
Orbulina sp. A	0.00	0.00	0.00	0.00	0.00	0.00	0.00	0.00	0.00	0.00	0.00	0.00	0.00
Globorotalia tumida	0.00	0.00	0.00	0.00	0.00	0.00	0.00	0.00	0.00	0.00	0.00	0.00	0.00
Globierinella siphonifera	0.00	0.00	0.00	0.00	0.00	0.00	0.00	0.00	0.00	0.00	0.00	0.00	0.00
Globoturborotalita tenella	0.00	0.00	0.00	0.00	0.00	0.00	0.00	0.00	0.00	0.00	0.00	0.00	0.00
Orbulina bilobata	0.00	0.00	0.00	0.00	0.00	0.00	0.00	0.00	0.00	0.00	0.00	0.00	0.00

Appendix A - Planktonic foraminifera assemblage data

Core 9/97-20
Relative abundance - Planktonic foraminifera >150um

Sample depth (cm)	97.5	101	103.5	106.5	108.5	110.5	112.5	114.5	116.5	121	123.5	125.5	129.5
Globigerina bulloides	0.67	0.00	0.00	0.00	0.00	0.00	1.00	4.00	0.33	0.00	0.00	0.00	0.00
Turborotalita quinqueloba	0.00	0.00	0.00	0.00	0.00	0.00	0.33	0.00	0.33	0.00	0.00	0.00	0.00
Orbulina universa	0.00	0.00	0.00	0.00	0.00	0.00	0.00	0.00	0.00	0.00	0.00	0.00	0.00
Neogloboquadrina pachyderma (sin.)	98.67	100.00	99.33	100.00	100.00	99.33	97.00	95.33	99.00	99.33	100.00	99.33	99.67
Neogloboquadrina pachyderma (dext.)	0.67	0.00	0.67	0.00	0.00	0.67	0.67	0.67	0.33	0.67	0.00	0.67	0.33
Globigerinoides ruber	0.00	0.00	0.00	0.00	0.00	0.00	0.00	0.00	0.00	0.00	0.00	0.00	0.00
Globorotalia scitula	0.00	0.00	0.00	0.00	0.00	0.00	0.33	0.00	0.00	0.00	0.00	0.00	0.00
Globorotalia inflata	0.00	0.00	0.00	0.00	0.00	0.00	0.67	0.00	0.00	0.00	0.00	0.00	0.00
Globorotalia truncatulinoides	0.00	0.00	0.00	0.00	0.00	0.00	0.00	0.00	0.00	0.00	0.00	0.00	0.00
Globorotalia hirsuta	0.00	0.00	0.00	0.00	0.00	0.00	0.00	0.00	0.00	0.00	0.00	0.00	0.00
Globigerinoides sacculifer	0.00	0.00	0.00	0.00	0.00	0.00	0.00	0.00	0.00	0.00	0.00	0.00	0.00
Neogloboquadrina duertrei	0.00	0.00	0.00	0.00	0.00	0.00	0.00	0.00	0.00	0.00	0.00	0.00	0.00
Hastigerinella digitata	0.00	0.00	0.00	0.00	0.00	0.00	0.00	0.00	0.00	0.00	0.00	0.00	0.00
Globigerina rubescens	0.00	0.00	0.00	0.00	0.00	0.00	0.00	0.00	0.00	0.00	0.00	0.00	0.00
Globorotalia crassaformis	0.00	0.00	0.00	0.00	0.00	0.00	0.00	0.00	0.00	0.00	0.00	0.00	0.00
Hastigerina pelagica	0.00	0.00	0.00	0.00	0.00	0.00	0.00	0.00	0.00	0.00	0.00	0.00	0.00
Globigerinoides conglobatus	0.00	0.00	0.00	0.00	0.00	0.00	0.00	0.00	0.00	0.00	0.00	0.00	0.00
Globigerina glutinata	0.00	0.00	0.00	0.00	0.00	0.00	0.00	0.00	0.00	0.00	0.00	0.00	0.00
Globigerina calida	0.00	0.00	0.00	0.00	0.00	0.00	0.00	0.00	0.00	0.00	0.00	0.00	0.00
Orbulina sp. A	0.00	0.00	0.00	0.00	0.00	0.00	0.00	0.00	0.00	0.00	0.00	0.00	0.00
Globorotalia tumida	0.00	0.00	0.00	0.00	0.00	0.00	0.00	0.00	0.00	0.00	0.00	0.00	0.00
Globierinella siphonifera	0.00	0.00	0.00	0.00	0.00	0.00	0.00	0.00	0.00	0.00	0.00	0.00	0.00
Globoturborotalita tenella	0.00	0.00	0.00	0.00	0.00	0.00	0.00	0.00	0.00	0.00	0.00	0.00	0.00
Orbulina bilobata	0.00	0.00	0.00	0.00	0.00	0.00	0.00	0.00	0.00	0.00	0.00	0.00	0.00

Appendix A - Planktonic foraminifera assemblage data

Core 9/97-20
Relative abundance - Planktonic foraminifera >150um

Sample depth (cm)	131.5	133.5	135.5	137.5	139.5	141.5	143.5	145.5	158	162.5	164.5	166.5	168.5
Globigerina bulloides	6.64	4.67	49.33	59.24	10.49	36.67	0.33	4.65	3.67	62.13	48.33	86.73	83.00
Turborotalita quinqueloba	0.00	1.00	2.67	0.00	0.66	1.00	0.00	0.00	0.00	1.00	1.33	0.00	2.00
Orbulina universa	0.00	0.00	0.00	0.00	0.00	0.00	0.00	0.00	0.00	0.00	0.00	0.00	0.00
Neogloboquadrina pachyderma (sin.)	91.69	89.33	44.00	35.03	83.93	43.67	99.33	94.35	95.67	22.59	45.67	9.06	7.67
Neogloboquadrina pachyderma (dext.)	1.33	5.00	4.00	1.91	2.62	13.00	0.33	1.00	0.67	6.64	3.33	3.24	2.33
Globigerinoides ruber	0.00	0.00	0.00	0.00	0.00	0.00	0.00	0.00	0.00	0.00	0.00	0.00	0.00
Globorotalia scitula	0.00	0.33	0.00	0.00	1.97	2.67	0.00	0.00	0.00	0.00	0.00	0.65	0.33
Globorotalia inflata	0.33	0.67	0.00	3.82	0.33	3.00	0.00	0.00	0.00	7.64	1.33	0.32	4.67
Globorotalia truncatulinoides	0.00	0.00	0.00	0.00	0.00	0.00	0.00	0.00	0.00	0.00	0.00	0.00	0.00
Globorotalia hirsuta	0.00	0.00	0.00	0.00	0.00	0.00	0.00	0.00	0.00	0.00	0.00	0.00	0.00
Globigerinoides sacculifer	0.00	0.00	0.00	0.00	0.00	0.00	0.00	0.00	0.00	0.00	0.00	0.00	0.00
Neogloboquadrina duertrei	0.00	0.00	0.00	0.00	0.00	0.00	0.00	0.00	0.00	0.00	0.00	0.00	0.00
Hastigerinella digitata	0.00	0.00	0.00	0.00	0.00	0.00	0.00	0.00	0.00	0.00	0.00	0.00	0.00
Globigerina rubescens	0.00	0.00	0.00	0.00	0.00	0.00	0.00	0.00	0.00	0.00	0.00	0.00	0.00
Globorotalia crassaformis	0.00	0.00	0.00	0.00	0.00	0.00	0.00	0.00	0.00	0.00	0.00	0.00	0.00
Hastigerina pelagica	0.00	0.00	0.00	0.00	0.00	0.00	0.00	0.00	0.00	0.00	0.00	0.00	0.00
Globigerinoides conglobatus	0.00	0.00	0.00	0.00	0.00	0.00	0.00	0.00	0.00	0.00	0.00	0.00	0.00
Globigerina glutinata	0.00	0.00	0.00	0.00	0.00	0.00	0.00	0.00	0.00	0.00	0.00	0.00	0.00
Globigerina calida	0.00	0.00	0.00	0.00	0.00	0.00	0.00	0.00	0.00	0.00	0.00	0.00	0.00
Orbulina sp. A	0.00	0.00	0.00	0.00	0.00	0.00	0.00	0.00	0.00	0.00	0.00	0.00	0.00
Globorotalia tumida	0.00	0.00	0.00	0.00	0.00	0.00	0.00	0.00	0.00	0.00	0.00	0.00	0.00
Globierinella siphonifera	0.00	0.00	0.00	0.00	0.00	0.00	0.00	0.00	0.00	0.00	0.00	0.00	0.00
Globoturborotalita tenella	0.00	0.00	0.00	0.00	0.00	0.00	0.00	0.00	0.00	0.00	0.00	0.00	0.00
Orbulina bilobata	0.00	0.00	0.00	0.00	0.00	0.00	0.00	0.00	0.00	0.00	0.00	0.00	0.00

Appendix A - Planktonic foraminifera assemblage data

Core 9/97-20
Relative abundance - Planktonic foraminifera >150um

Sample depth (cm)	170.5	172	175.5	177.5	180	183	185.5	188	191.5	193.5	195.5	197.5	199.5
Globigerina bulloides	81.67	82.62	73.52	44.95	76.33	82.67	4.32	0.33	28.81	31.68	47.51	31.33	73.48
Turborotalita quinqueloba	1.33	0.00	0.00	0.00	0.33	0.67	0.00	0.00	1.32	0.00	1.99	0.00	2.24
Orbulina universa	0.00	0.00	1.25	0.00	0.00	0.00	0.00	0.00	0.00	0.00	0.00	0.00	0.64
Neogloboquadrina pachyderma (sin.)	15.33	9.18	4.36	31.92	8.00	13.67	95.02	99.33	66.56	52.15	28.57	35.67	2.24
Neogloboquadrina pachyderma (dext.)	1.67	5.90	12.15	14.98	4.33	2.67	0.66	0.33	3.31	7.92	12.29	29.00	9.58
Globigerinoides ruber	0.00	0.00	0.00	0.00	0.00	0.00	0.00	0.00	0.00	0.00	0.00	0.00	0.64
Globorotalia scitula	0.00	0.98	3.74	1.30	4.00	0.00	0.00	0.00	0.00	2.64	2.66	0.00	2.56
Globorotalia inflata	0.00	1.31	4.36	6.84	3.33	0.33	0.00	0.00	0.00	4.95	6.64	4.00	6.07
Globorotalia truncatulinoides	0.00	0.00	0.62	0.00	1.00	0.00	0.00	0.00	0.00	0.00	0.00	0.00	0.64
Globorotalia hirsuta	0.00	0.00	0.00	0.00	2.67	0.00	0.00	0.00	0.00	0.66	0.33	0.00	1.92
Globigerinoides sacculifer	0.00	0.00	0.00	0.00	0.00	0.00	0.00	0.00	0.00	0.00	0.00	0.00	0.00
Neogloboquadrina duertrei	0.00	0.00	0.00	0.00	0.00	0.00	0.00	0.00	0.00	0.00	0.00	0.00	0.00
Hastigerinella digitata	0.00	0.00	0.00	0.00	0.00	0.00	0.00	0.00	0.00	0.00	0.00	0.00	0.00
Globigerina rubescens	0.00	0.00	0.00	0.00	0.00	0.00	0.00	0.00	0.00	0.00	0.00	0.00	0.00
Globorotalia crassaformis	0.00	0.00	0.00	0.00	0.00	0.00	0.00	0.00	0.00	0.00	0.00	0.00	0.00
Hastigerina pelagica	0.00	0.00	0.00	0.00	0.00	0.00	0.00	0.00	0.00	0.00	0.00	0.00	0.00
Globigerinoides conglobatus	0.00	0.00	0.00	0.00	0.00	0.00	0.00	0.00	0.00	0.00	0.00	0.00	0.00
Globigerina glutinata	0.00	0.00	0.00	0.00	0.00	0.00	0.00	0.00	0.00	0.00	0.00	0.00	0.00
Globigerina calida	0.00	0.00	0.00	0.00	0.00	0.00	0.00	0.00	0.00	0.00	0.00	0.00	0.00
Orbulina sp. A	0.00	0.00	0.00	0.00	0.00	0.00	0.00	0.00	0.00	0.00	0.00	0.00	0.00
Globorotalia tumida	0.00	0.00	0.00	0.00	0.00	0.00	0.00	0.00	0.00	0.00	0.00	0.00	0.00
Globierinella siphonifera	0.00	0.00	0.00	0.00	0.00	0.00	0.00	0.00	0.00	0.00	0.00	0.00	0.00
Globoturborotalita tenella	0.00	0.00	0.00	0.00	0.00	0.00	0.00	0.00	0.00	0.00	0.00	0.00	0.00
Orbulina bilobata	0.00	0.00	0.00	0.00	0.00	0.00	0.00	0.00	0.00	0.00	0.00	0.00	0.00

Appendix A - Planktonic foraminifera assemblage data

Core 9/97-20
Relative abundance - Planktonic foraminifera >150um

Sample depth (cm)	200	201	206.5
Globigerina bulloides	88.03	3.32	58.13
Turborotalita quinqueloba	0.32	0.00	0.00
Orbulina universa	0.00	0.00	0.63
Neogloboquadrina pachyderma (sin.)	9.39	95.35	21.25
Neogloboquadrina pachyderma (dext.)	1.29	1.00	10.63
Globigerinoides ruber	0.00	0.00	0.00
Globorotalia scitula	0.65	0.33	5.31
Globorotalia inflata	0.32	0.00	2.50
Globorotalia truncatulinoides	0.00	0.00	1.56
Globorotalia hirsuta	0.00	0.00	0.00
Globigerinoides sacculifer	0.00	0.00	0.00
Neogloboquadrina duertrei	0.00	0.00	0.00
Hastigerinella digitata	0.00	0.00	0.00
Globigerina rubescens	0.00	0.00	0.00
Globorotalia crassaformis	0.00	0.00	0.00
Hastigerina pelagica	0.00	0.00	0.00
Globigerinoides conglobatus	0.00	0.00	0.00
Globigerina glutinata	0.00	0.00	0.00
Globigerina calida	0.00	0.00	0.00
Orbulina sp. A	0.00	0.00	0.00
Globorotalia tumida	0.00	0.00	0.00
Globierinella siphonifera	0.00	0.00	0.00
Globoturborotalita tenella	0.00	0.00	0.00
Orbulina bilobata	0.00	0.00	0.00

Appendix B - Benthic foraminifera assemblage data

Core 9/97/08
Relative abundance - Benthic foraminifera 500-250um

Sample depth (cm)	3	7	15	19	23	27	31	35	39	43	47.5
Alabaminella weddellensis	0.00	0.00	0.00	0.00	0.00	0.00	0.00	0.00	0.00	0.00	0.00
Amphycorina scalaris	0.00	0.00	0.00	0.00	0.00	0.00	0.00	0.00	0.00	0.00	0.00
Astacolus hyalacrulus	0.00	0.00	2.48	0.97	0.00	0.00	0.00	0.00	0.00	0.00	0.00
Astacolus sp.	0.00	0.00	0.00	0.00	0.00	0.00	0.00	0.00	0.00	0.00	0.00
Bolivina albatrossi	0.00	0.00	0.00	0.00	0.00	0.00	0.00	0.00	0.00	0.00	0.00
Bolivina pseduopunctata	0.00	0.00	0.00	0.00	0.00	0.00	0.00	0.00	0.00	0.00	0.00
Bolivina sp.	0.00	0.00	0.00	0.00	0.00	0.00	0.00	0.00	0.00	0.00	0.00
Bolivina spinescens	0.00	0.00	0.00	0.00	0.00	0.00	0.00	0.00	0.00	0.00	0.00
Bolivina subspinescens	1.00	0.00	0.00	0.97	0.00	0.00	2.00	0.00	0.00	0.00	0.00
Brizalina cf. robusta	0.00	0.00	0.00	0.00	0.00	0.00	0.00	0.00	0.00	0.00	0.00
Brizalina variabilis	0.00	0.00	0.00	0.00	0.00	0.00	0.00	0.00	0.00	0.00	0.00
Bulimina aculeata	0.00	0.00	0.00	0.00	0.00	0.00	0.00	1.29	2.25	1.01	0.77
Bullimina cf. gibba	0.00	0.00	0.00	0.00	0.00	0.00	0.00	0.00	0.00	0.00	0.00
Bulimina inflata	0.00	0.00	0.00	0.00	1.09	0.69	0.00	0.00	0.00	0.00	0.00
Bullimina marginata	4.00	2.33	0.00	0.49	0.00	0.00	1.00	1.29	31.46	2.02	0.00
Cassidulina laevigata	4.00	0.00	0.00	0.00	1.23	0.00	5.00	0.00	0.00	0.00	0.00
Cassidulina obtusa	0.00	0.00	0.00	0.00	0.00	0.00	0.00	0.00	0.00	0.00	0.00
Chilostomella oolina	0.00	0.00	0.00	0.00	0.00	0.00	0.00	0.00	0.00	0.00	0.00
Cibicides kullenbergi	8.00	41.86	34.78	32.52	10.63	4.83	2.00	10.30	3.37	0.00	0.00
Cibicides lobatulus	1.00	0.00	2.48	1.46	2.18	1.38	0.00	2.58	0.00	0.00	0.00
Cibicides pachyderma	0.00	0.00	0.00	0.00	0.00	0.00	0.00	0.00	0.00	0.00	0.00
Cibicides sp.	0.00	0.00	0.00	0.00	0.00	0.00	0.00	0.00	0.00	0.00	0.00
Cibicides wuellerstorfi	4.00	6.98	22.36	23.30	7.90	4.14	4.00	0.64	2.25	8.08	7.67
Cyclammina pusilla	0.00	0.00	0.00	0.00	0.00	0.00	0.00	0.00	0.00	0.00	0.00
Dentalina communis	0.00	0.00	0.00	0.00	0.00	0.00	0.00	0.00	0.00	0.00	0.00
Dentalina sp.	0.00	0.00	0.00	0.00	0.00	0.00	0.00	0.00	0.00	0.00	0.00
Eggerella bradyi	0.00	0.00	0.00	0.00	0.00	0.00	0.00	0.00	0.00	0.00	0.00
Ehrenbergina serrata	0.00	0.00	0.00	0.00	0.00	0.00	1.00	0.00	1.12	0.00	0.00
Epistominella exigua	3.00	0.00	0.00	0.00	1.91	1.38	4.00	0.00	2.25	0.00	0.26
Eponides pusillus	0.00	0.00	0.00	0.00	0.00	0.00	0.00	0.00	0.00	0.00	0.00
Fissurina marginata	1.00	0.00	0.00	0.00	0.00	0.00	0.00	0.00	0.00	0.00	0.00
Fissurina orbignyana	0.00	0.00	0.00	0.00	0.00	0.00	1.00	0.00	0.00	0.00	0.00
Fissurina porcupinensis	0.00	0.00	0.62	1.46	1.77	0.69	0.00	0.64	0.00	0.00	0.00

Appendix B - Benthic foraminifera assemblage data

Core 9/97/08
Relative abundance - Benthic foraminifera 500-250um

Sample depth (cm)	3	7	15	19	23	27	31	35	39	43	47.5
Fissurina varioperforata	0.00	0.00	0.00	0.00	0.00	0.00	0.00	0.00	0.00	0.00	0.00
Fursenkoina complanata	0.00	0.00	0.00	0.00	0.00	0.00	0.00	0.00	0.00	0.00	0.00
Gavelinopsis lobatus	0.00	0.00	0.00	0.00	0.00	0.00	0.00	0.00	0.00	0.00	0.00
Globobulimina auriculata	0.00	0.00	0.00	0.00	0.00	0.00	0.00	0.00	0.00	0.00	0.00
Globobullimina affinis	0.00	0.00	0.00	0.00	0.00	0.00	0.00	0.00	0.00	0.00	0.00
Gyroidina soldanii	0.00	0.00	0.00	0.00	0.00	0.00	0.00	0.00	0.00	0.00	0.00
Hoeglundia elegans	0.00	2.33	0.00	0.00	0.00	0.00	0.00	0.00	0.00	3.03	3.84
Hormosina globulifera	0.00	0.00	0.00	0.00	0.00	0.00	0.00	0.00	0.00	0.00	0.00
Indeterminate	0.00	0.00	0.00	0.00	0.00	0.00	0.00	0.00	0.00	0.00	0.00
Karreriella bradyi	0.00	2.33	0.00	0.97	4.63	2.07	0.00	1.29	0.00	7.07	2.05
Lagena cf. acuticosta	0.00	0.00	0.00	0.00	0.00	0.00	0.00	0.00	0.00	0.00	0.00
Lagena cf. interrupta	0.00	0.00	0.00	0.00	0.00	0.00	1.00	0.00	0.00	0.00	0.00
Lagena semistriata	0.00	0.00	0.00	0.00	0.00	0.00	0.00	0.00	0.00	0.00	0.00
Lagena sulcata	2.00	0.00	0.00	0.00	0.00	0.00	0.00	0.00	1.12	1.01	0.26
Melonis barleeanum	24.00	2.33	2.48	2.43	7.77	4.14	20.00	2.58	16.85	1.01	2.05
Melonis pompilioides	0.00	0.00	0.00	0.00	0.00	0.00	0.00	0.00	0.00	0.00	0.00
Nodosaria sp.	0.00	0.00	0.00	0.00	0.00	0.00	0.00	0.00	0.00	0.00	0.00
Nonionella auricula	0.00	0.00	0.00	0.00	0.00	0.00	0.00	0.00	0.00	0.00	0.00
Nonionella turgida	0.00	0.00	0.00	0.00	0.00	0.00	0.00	0.00	0.00	0.00	0.00
Nummoloculina irregularis	0.00	0.00	0.00	0.00	0.00	0.00	0.00	0.00	0.00	0.00	0.00
Oolina apiopleura	0.00	0.00	0.00	0.00	0.00	0.00	0.00	0.00	0.00	0.00	0.00
Oolina heronalleni	0.00	0.00	0.00	0.00	0.00	0.00	0.00	0.00	0.00	0.00	0.00
Oolina hexagona	0.00	2.33	2.48	0.49	0.00	0.00	0.00	0.00	0.00	0.00	0.00
Oolina intercalata	0.00	0.00	0.00	0.00	0.00	0.00	0.00	0.00	0.00	0.00	0.00
Oolina melo	0.00	0.00	0.00	0.00	0.00	0.00	0.00	0.00	0.00	0.00	0.00
Oolina squamosa	1.00	0.00	0.00	0.00	0.00	0.00	0.00	0.00	0.00	0.00	0.00
Oridorsalis umbonatus	0.00	0.00	0.00	0.00	0.00	0.00	0.00	0.00	0.00	0.00	0.00
Pseudofissurina mccullocha	0.00	0.00	0.00	0.00	0.00	0.00	0.00	0.00	0.00	0.00	0.00
Pseudosolenina borealis	0.00	0.00	0.00	0.00	0.00	0.00	0.00	0.00	0.00	0.00	0.00
Pullenia bulloides	0.00	2.33	0.00	0.97	0.00	0.00	0.00	0.00	0.00	0.00	0.00
Pullenia subcarinata	1.00	0.00	0.00	0.00	0.00	0.00	0.00	0.00	2.25	0.00	0.26
Pyrgo depressa	0.00	0.00	0.00	0.00	0.00	0.00	0.00	0.00	0.00	0.00	0.00
Pyrgo lacernula	0.00	0.00	0.00	0.00	0.00	0.00	0.00	0.00	0.00	0.00	0.00

Appendix B - Benthic foraminifera assemblage data

Core 9/97/08
Relative abundance - Benthic foraminifera 500-250um

Sample depth (cm)	3	7	15	19	23	27	31	35	39	43	47.5
Pyrgo murrhina	0.00	2.33	4.97	3.40	0.00	0.00	0.00	0.00	0.00	1.01	2.30
Pyrgo oblonga	0.00	0.00	0.00	0.00	0.00	0.00	0.00	0.00	0.00	0.00	0.00
Pyrgo rotalia	0.00	0.00	0.00	0.00	0.00	0.00	0.00	0.00	0.00	0.00	0.00
Pyrgo sarsi	0.00	0.00	0.00	0.00	0.00	0.00	0.00	0.00	0.00	0.00	0.00
Pyrgo serrata	0.00	0.00	0.00	0.00	0.00	0.00	0.00	0.00	0.00	0.00	0.00
Pyrgo sp.	0.00	0.00	0.00	0.00	0.00	0.00	0.00	0.00	0.00	0.00	0.00
Pyrgo williamsoni	0.00	0.00	0.00	0.97	1.09	0.00	1.00	0.00	0.00	0.00	0.00
Quinqueloculina arctica	0.00	0.00	0.00	0.00	0.00	0.00	0.00	0.00	0.00	0.00	0.00
Quinqueloculina bicornis	0.00	0.00	0.00	0.00	0.00	0.00	0.00	0.00	0.00	0.00	0.00
Quinqueloculina cliarensis	0.00	0.00	0.00	0.00	0.00	0.00	0.00	0.00	0.00	0.00	0.00
Quinqueloculina elongata	0.00	0.00	0.00	0.00	0.00	0.00	0.00	0.00	0.00	0.00	0.00
Quinqueloculina lata	2.00	0.00	0.00	0.00	0.00	0.00	0.00	0.00	0.00	0.00	0.00
Quinqueloculina seminulum	0.00	0.00	2.48	3.40	0.95	0.69	0.00	1.29	3.37	2.02	0.77
Quinqueloculina sp.	0.00	0.00	0.00	0.00	0.00	0.00	0.00	0.00	0.00	0.00	0.00
Quinqueloculina stalkeri	0.00	0.00	0.00	0.00	0.00	0.00	0.00	0.00	0.00	0.00	0.00
Quinqueloculina striata	0.00	0.00	0.00	0.00	0.00	0.00	0.00	0.00	0.00	0.00	0.00
Rupertina stabilis	0.00	0.00	0.00	0.00	0.00	0.00	0.00	0.00	0.00	0.00	0.00
Sigmoilopsis schlumbergeri	4.00	13.95	4.97	2.43	1.77	1.38	2.00	1.50	11.24	10.10	11.76
Siphotextularia rolhauseni	0.00	0.00	0.00	0.00	0.00	0.69	0.00	0.00	0.00	6.06	5.12
Solenina radiata	0.00	0.00	0.00	0.00	0.00	0.00	0.00	0.00	0.00	0.00	0.00
Spiroloculina limbata	0.00	0.00	0.00	0.00	0.00	0.00	0.00	0.00	0.00	0.00	0.00
Spiroloculina rotunda	1.00	0.00	0.00	0.00	0.00	0.00	0.00	0.00	0.00	0.00	0.00
Stainforthia (Fursenkoina) f	0.00	0.00	0.00	0.00	0.00	0.00	0.00	0.00	0.00	0.00	0.00
Stainforthia loeblichi	0.00	0.00	0.00	0.00	0.00	0.00	0.00	0.00	0.00	0.00	0.00
Stainforthia schreibersiana	0.00	0.00	0.00	0.00	0.00	0.00	0.00	0.00	0.00	0.00	0.00
Trifarina angulosa	29.00	0.00	0.00	0.49	0.82	0.69	42.00	0.00	10.11	0.00	1.53
Trifarina bradyi	0.00	0.00	0.00	0.00	0.00	0.00	0.00	0.00	0.00	0.00	0.77
Trifarina sp.	0.00	0.00	0.00	0.00	0.00	0.00	0.00	0.00	0.00	0.00	0.00
Triloculina tricarinata	0.00	0.00	0.00	0.00	0.00	0.00	0.00	0.00	0.00	0.00	0.00
Uvigerina celtica	0.00	0.00	0.00	0.00	0.00	0.00	0.00	0.00	0.00	0.00	0.00
Uvigerina cf. pigmea	0.00	0.00	0.00	0.00	0.00	0.00	0.00	0.00	0.00	0.00	0.00
Uvigerina peregrina	10.00	20.93	19.88	21.84	52.72	75.17	14.00	75.97	12.36	54.55	59.08
Virgulina advena	0.00	0.00	0.00	0.00	0.00	0.00	0.00	0.00	0.00	0.00	0.00

Appendix B - Benthic foraminifera assemblage data

Core 9/97/08
Relative abundance - Benthic foraminifera 500-250um

Sample depth (cm)	51.5	55.5	59.5	63.5	68	80
Alabaminella weddellensis	0.00	0.00	0.00	0.00	0.00	0.00
Amphycorina scalaris	0.00	0.00	0.00	0.00	0.00	0.00
Astacolus hyalacrulus	0.00	0.00	0.00	0.00	0.00	0.00
Astacolus sp.	0.00	0.00	0.00	0.00	0.00	0.00
Bolivina albatrossi	0.00	0.00	0.00	0.00	0.00	0.00
Bolivina pseduopunctata	0.00	0.00	0.00	2.00	0.00	0.00
Bolivina sp.	0.00	0.00	0.00	0.00	0.00	0.00
Bolivina spinescens	0.00	0.00	0.00	0.00	0.00	0.00
Bolivina subspinescens	0.00	0.00	0.00	2.00	0.00	0.00
Brizalina cf. robusta	0.00	0.00	0.00	0.00	0.00	0.00
Brizalina variabilis	0.00	0.00	0.00	0.00	0.00	0.00
Bulimina aculeata	0.56	0.00	0.00	1.00	0.00	2.48
Bullimina cf. gibba	0.00	0.00	0.00	0.00	0.00	0.00
Bulimina inflata	0.00	0.00	0.00	0.00	0.44	4.97
Bullimina marginata	0.00	0.00	0.00	0.00	2.62	0.00
Cassidulina laevigata	0.00	0.00	0.00	1.00	0.00	0.00
Cassidulina obtusa	0.00	0.00	0.00	0.00	0.00	0.00
Chilostomella oolina	0.00	0.00	0.00	0.00	0.00	0.00
Cibicides kullenbergi	6.67	6.80	7.19	3.00	18.34	17.39
Cibicides lobatulus	2.22	2.91	1.44	0.00	0.00	0.00
Cibicides pachyderma	0.00	0.00	0.29	8.00	0.00	0.00
Cibicides sp.	0.00	0.00	0.00	0.00	0.00	0.00
Cibicides wuellerstorfi	6.67	4.85	10.06	13.00	7.86	14.91
Cyclammina pusilla	0.00	0.00	0.00	0.00	0.00	0.00
Dentalina communis	0.00	0.00	0.00	0.00	0.00	0.00
Dentalina sp.	0.00	0.00	0.00	0.00	0.00	0.00
Eggerella bradyi	0.00	0.00	0.00	0.00	0.00	0.00
Ehrenbergina serrata	0.00	0.00	0.00	0.00	0.00	0.00
Epistominella exigua	0.28	0.00	1.08	0.00	0.00	0.62
Eponides pusillus	0.00	0.00	1.08	0.00	0.00	0.00
Fissurina marginata	0.56	0.97	0.00	1.00	0.00	0.00
Fissurina orbignyana	0.00	0.00	0.00	0.00	0.00	0.00
Fissurina porcupinensis	0.00	0.00	0.14	0.00	0.00	0.00

Appendix B - Benthic foraminifera assemblage data

Core 9/97/08
Relative abundance - Benthic foraminifera 500-250um

Sample depth (cm)	51.5	55.5	59.5	63.5	68	80
Fissurina varioperforata	0.00	0.00	0.00	0.00	0.00	0.00
Fursenkoina complanata	0.00	0.00	0.00	0.00	0.00	0.00
Gavelinopsis lobatus	0.00	0.00	0.00	0.00	0.00	0.00
Globobulimina auriculata	0.00	0.00	0.00	0.00	0.00	0.00
Globobullimina affinis	0.00	0.00	0.00	0.00	0.00	0.00
Gyroidina soldanii	0.00	0.00	0.00	0.00	0.00	0.00
Hoeglundia elegans	0.83	0.97	0.00	0.00	5.24	2.48
Hormosina globulifera	0.00	0.00	0.00	0.00	0.00	0.00
Indeterminate	0.00	0.00	0.00	0.00	0.00	0.00
Karreriella bradyi	0.00	0.00	0.00	0.00	2.62	14.91
Lagena cf. acuticosta	0.00	0.00	0.00	0.00	0.00	0.00
Lagena cf. interrupta	0.00	0.00	0.00	0.00	0.00	0.00
Lagena semistriata	0.00	0.00	0.00	0.00	0.00	0.00
Lagena sulcata	0.28	0.00	1.08	0.00	2.62	0.00
Melonis barleeanum	1.39	0.97	4.31	22.00	10.48	9.94
Melonis pompilioides	0.00	0.00	0.00	0.00	0.00	0.00
Nodosaria sp.	0.00	0.00	0.00	0.00	0.00	0.00
Nonionella auricula	0.00	0.00	0.00	0.00	0.00	0.00
Nonionella turgida	0.00	0.00	0.00	0.00	0.00	0.00
Nummoloculina irregularis	0.00	0.00	0.00	0.00	0.00	0.00
Oolina apiopleura	0.00	0.00	0.00	0.00	0.00	0.00
Oolina heronalleni	0.00	0.00	0.00	0.00	0.00	0.00
Oolina hexagona	0.00	0.00	0.00	0.00	0.00	0.00
Oolina intercalata	0.00	0.00	0.00	0.00	0.00	0.00
Oolina melo	0.00	0.00	0.00	0.00	0.00	0.00
Oolina squamosa	0.00	0.00	0.00	0.00	0.00	0.00
Oridorsalis umbonatus	0.00	0.00	0.00	0.00	0.00	0.00
Pseudofissurina mccullochae	0.00	0.00	0.00	0.00	0.00	0.00
Pseudosolenina borealis	0.00	0.00	0.00	0.00	0.00	0.00
Pullenia bulloides	0.00	0.00	0.00	0.00	0.00	0.00
Pullenia subcarinata	0.00	0.00	0.00	3.00	0.00	0.00
Pyrgo depressa	0.00	0.00	0.00	0.00	0.00	0.00
Pyrgo lacernula	0.00	0.00	0.00	0.00	0.00	0.00

Appendix B - Benthic foraminifera assemblage data

Core 9/97/08
Relative abundance - Benthic foraminifera 500-250um

Sample depth (cm)	51.5	55.5	59.5	63.5	68	80
Pyrgo murrhina	1.39	0.97	1.44	0.00	0.00	0.00
Pyrgo oblonga	0.00	0.00	0.00	0.00	0.00	0.00
Pyrgo rotalia	0.00	0.00	0.00	0.00	0.00	0.00
Pyrgo sarsi	0.00	0.00	0.00	0.00	0.00	0.00
Pyrgo serrata	0.00	0.00	0.00	0.00	0.00	0.00
Pyrgo sp.	0.00	0.00	0.00	0.00	0.00	0.00
Pyrgo williamsoni	0.00	0.00	0.00	2.00	0.00	0.00
Quinqueloculina arctica	0.00	0.00	0.00	0.00	0.00	0.00
Quinqueloculina bicornis	0.00	0.00	0.00	1.00	0.00	0.00
Quinqueloculina cliarensis	0.00	0.00	0.00	0.00	0.00	0.00
Quinqueloculina elongata	0.00	0.00	0.00	0.00	0.00	0.00
Quinqueloculina lata	0.00	0.00	0.00	2.00	0.00	0.00
Quinqueloculina seminulum	1.67	1.94	2.88	0.00	5.24	0.62
Quinqueloculina sp.	0.00	0.00	0.00	0.00	0.00	0.00
Quinqueloculina stalkeri	0.00	0.00	0.00	0.00	0.00	0.00
Quinqueloculina striata	0.56	0.97	0.00	0.00	0.00	4.97
Rupertina stabilis	0.00	0.00	0.00	0.00	0.00	0.00
Sigmoilopsis schlumbergeri	2.78	2.91	2.88	3.00	18.34	9.94
Siphotextularia rolhauseni	0.00	0.00	0.00	0.00	0.00	4.97
Solenina radiata	0.00	0.00	0.00	0.00	0.00	0.00
Spiroloculina limbata	0.00	0.00	0.00	0.00	0.00	0.00
Spiroloculina rotunda	0.28	0.97	0.00	0.00	0.00	2.48
Stainforthia (Fursenkoina) fusiform	0.00	0.00	0.00	0.00	0.00	0.00
Stainforthia loeblichi	0.00	0.00	0.00	0.00	0.00	0.00
Stainforthia schreibersiana	0.00	0.00	0.00	0.00	0.00	0.00
Trifarina angulosa	0.00	0.00	0.00	23.00	0.00	0.00
Trifarina bradyi	0.00	0.00	0.00	0.00	0.00	0.00
Trifarina sp.	0.00	0.00	0.00	0.00	0.00	0.00
Triloculina tricarinata	0.00	0.00	0.00	0.00	0.00	0.00
Uvigerina celtica	0.00	0.00	0.00	0.00	0.00	0.00
Uvigerina cf. pigmea	0.00	0.00	0.00	0.00	0.00	0.00
Uvigerina peregrina	71.39	71.84	61.83	13.00	18.34	7.45
Virgulina advena	0.00	0.00	0.00	0.00	0.00	0.00

Appendix B - Benthic foraminifera assemblage data

Core 9/97/10
Relative abundance - Benthic foraminifera 500-250um

Sample depth (cm)	3	7	11	16	20	27	31	35	39	43	47	51.5
Alabaminella weddellensis	0.00	0.00	0.00	0.00	0.00	0.00	0.00	0.00	0.00	0.00	0.00	0.00
Amphycorina scalaris	0.00	0.00	0.00	0.00	0.00	0.00	0.00	0.00	0.00	0.00	0.00	0.00
Astacolus hyalacrulus	0.00	0.00	0.00	0.00	0.00	0.00	0.00	0.00	0.00	0.00	0.00	0.00
Astacolus sp.	0.00	0.00	0.00	0.00	0.00	0.00	0.00	0.00	0.00	0.00	0.00	0.00
Bolivina albatrossi	0.00	0.00	0.00	0.00	0.00	0.00	0.00	0.00	0.00	0.00	0.00	0.00
Bolivina pseduopunctata	0.00	0.00	0.00	0.00	0.00	0.00	0.00	0.00	0.00	0.00	0.00	0.00
Bolivina sp.	0.00	0.00	0.00	0.00	0.00	0.00	0.00	0.00	0.00	0.00	0.00	0.00
Bolivina spinescens	0.00	0.00	0.00	0.00	0.00	0.00	0.00	0.00	0.00	0.00	0.00	0.00
Bolivina subspinescens	0.00	0.00	0.00	0.00	0.00	0.00	0.00	0.00	0.00	0.00	0.00	0.00
Brizalina cf. robusta	0.00	0.00	0.00	0.00	0.00	0.00	0.00	0.00	0.00	0.00	0.00	0.00
Brizalina variabilis	0.00	0.00	0.00	0.00	0.00	0.00	0.00	0.00	0.00	0.00	0.00	0.00
Bulimina aculeata	1.00	1.51	0.00	1.99	0.00	0.00	0.78	1.37	0.00	0.00	2.30	0.00
Bullimina cf. gibba	0.00	0.00	0.00	0.00	0.83	0.00	0.00	0.00	0.00	0.00	0.00	0.00
Bulimina inflata	0.00	0.00	0.00	0.00	0.00	0.00	2.73	3.20	2.12	1.24	3.23	3.87
Bullimina marginata	0.00	0.00	0.74	0.50	2.50	0.53	1.17	0.46	1.41	1.86	2.76	3.87
Cassidulina laevigata	0.00	0.00	0.00	0.50	0.00	0.00	0.00	0.00	0.35	0.00	0.00	0.00
Cassidulina obtusa	0.00	0.00	0.00	0.00	0.00	0.00	0.00	0.00	0.00	0.00	0.46	0.00
Chilostomella oolina	0.00	0.00	0.00	0.00	0.00	0.00	0.00	0.00	0.00	0.00	0.00	0.00
Cibicides kullenbergi	0.00	0.00	7.41	26.37	17.50	15.87	0.00	0.00	7.07	0.00	0.92	0.00
Cibicides lobatulus	0.00	0.00	0.74	0.50	0.83	0.53	0.00	0.00	0.35	0.62	0.00	0.00
Cibicides pachyderma	0.00	0.00	1.48	0.00	0.00	0.00	0.00	0.00	0.00	0.00	0.00	0.00
Cibicides sp.	0.00	0.00	0.00	0.00	0.00	0.00	0.00	0.00	0.00	0.00	0.00	0.00
Cibicides wuellerstorfi	9.45	10.05	24.44	20.90	27.50	24.87	22.27	29.68	25.09	18.63	20.74	14.19
Cyclammina pusilla	0.00	0.00	0.00	0.00	0.00	1.59	0.00	0.00	1.06	0.00	0.00	0.00
Dentalina communis	0.00	0.00	0.00	0.00	0.00	0.00	0.00	0.00	0.00	0.00	0.00	0.00
Dentalina sp.	0.00	0.00	0.00	0.00	0.00	0.00	0.00	0.00	0.00	0.00	0.00	0.00
Eggerella bradyi	0.00	0.00	0.00	0.00	0.00	0.00	0.00	0.00	0.00	0.00	0.00	0.00
Ehrenbergina serrata	0.00	0.00	0.00	0.00	0.00	0.00	0.00	0.00	0.35	0.00	0.46	2.58
Epistominella exigua	1.99	0.00	0.00	0.00	0.00	0.53	0.00	0.00	2.12	4.97	0.00	5.16
Eponides pusillus	0.00	0.00	0.00	0.00	0.00	0.00	0.00	0.00	0.00	0.00	0.00	0.00
Fissurina marginata	1.49	5.03	0.74	0.50	1.67	0.00	2.73	4.11	0.35	0.62	0.00	1.29
Fissurina orbignyana	2.49	1.01	0.00	0.00	0.00	0.00	0.39	0.00	0.00	0.00	0.00	0.00
Fissurina porcupinensis	0.00	0.00	0.00	0.00	0.00	0.00	0.00	0.00	0.35	0.62	0.00	0.00

Appendix B - Benthic foraminifera assemblage data

Core 9/97/10
Relative abundance - Benthic foraminifera 500-250um

Sample depth (cm)	3	7	11	16	20	27	31	35	39	43	47	51.5
Alabaminella weddellensis	0.00	0.00	0.00	0.00	0.00	0.00	0.00	0.00	0.00	0.00	0.00	0.00
Amphycorina scalaris	0.00	0.00	0.00	0.00	0.00	0.00	0.00	0.00	0.00	0.00	0.00	0.00
Astacolus hyalacrulus	0.00	0.00	0.00	0.00	0.00	0.00	0.00	0.00	0.00	0.00	0.00	0.00
Astacolus sp.	0.00	0.00	0.00	0.00	0.00	0.00	0.00	0.00	0.00	0.00	0.00	0.00
Bolivina albatrossi	0.00	0.00	0.00	0.00	0.00	0.00	0.00	0.00	0.00	0.00	0.00	0.00
Bolivina pseduopunctata	0.00	0.00	0.00	0.00	0.00	0.00	0.00	0.00	0.00	0.00	0.00	0.00
Bolivina sp.	0.00	0.00	0.00	0.00	0.00	0.00	0.00	0.00	0.00	0.00	0.00	0.00
Bolivina spinescens	0.00	0.00	0.00	0.00	0.00	0.00	0.00	0.00	0.00	0.00	0.00	0.00
Bolivina subspinescens	0.00	0.00	0.00	0.00	0.00	0.00	0.00	0.00	0.00	0.00	0.00	0.00
Brizalina cf. robusta	0.00	0.00	0.00	0.00	0.00	0.00	0.00	0.00	0.00	0.00	0.00	0.00
Brizalina variabilis	0.00	0.00	0.00	0.00	0.00	0.00	0.00	0.00	0.00	0.00	0.00	0.00
Bulimina aculeata	1.00	1.51	0.00	1.99	0.00	0.00	0.78	1.37	0.00	0.00	2.30	0.00
Bullimina cf. gibba	0.00	0.00	0.00	0.00	0.83	0.00	0.00	0.00	0.00	0.00	0.00	0.00
Bulimina inflata	0.00	0.00	0.00	0.00	0.00	0.00	2.73	3.20	2.12	1.24	3.23	3.87
Bullimina marginata	0.00	0.00	0.74	0.50	2.50	0.53	1.17	0.46	1.41	1.86	2.76	3.87
Cassidulina laevigata	0.00	0.00	0.00	0.50	0.00	0.00	0.00	0.00	0.35	0.00	0.00	0.00
Cassidulina obtusa	0.00	0.00	0.00	0.00	0.00	0.00	0.00	0.00	0.00	0.00	0.46	0.00
Chilostomella oolina	0.00	0.00	0.00	0.00	0.00	0.00	0.00	0.00	0.00	0.00	0.00	0.00
Cibicides kullenbergi	0.00	0.00	7.41	26.37	17.50	15.87	0.00	0.00	7.07	0.00	0.92	0.00
Cibicides lobatulus	0.00	0.00	0.74	0.50	0.83	0.53	0.00	0.00	0.35	0.62	0.00	0.00
Cibicides pachyderma	0.00	0.00	1.48	0.00	0.00	0.00	0.00	0.00	0.00	0.00	0.00	0.00
Cibicides sp.	0.00	0.00	0.00	0.00	0.00	0.00	0.00	0.00	0.00	0.00	0.00	0.00
Cibicides wuellerstorfi	9.45	10.05	24.44	20.90	27.50	24.87	22.27	29.68	25.09	18.63	20.74	14.19
Cyclammina pusilla	0.00	0.00	0.00	0.00	0.00	1.59	0.00	0.00	1.06	0.00	0.00	0.00
Dentalina communis	0.00	0.00	0.00	0.00	0.00	0.00	0.00	0.00	0.00	0.00	0.00	0.00
Dentalina sp.	0.00	0.00	0.00	0.00	0.00	0.00	0.00	0.00	0.00	0.00	0.00	0.00
Eggerella bradyi	0.00	0.00	0.00	0.00	0.00	0.00	0.00	0.00	0.00	0.00	0.00	0.00
Ehrenbergina serrata	0.00	0.00	0.00	0.00	0.00	0.00	0.00	0.00	0.35	0.00	0.46	2.58
Epistominella exigua	1.99	0.00	0.00	0.00	0.00	0.53	0.00	0.00	2.12	4.97	0.00	5.16
Eponides pusillus	0.00	0.00	0.00	0.00	0.00	0.00	0.00	0.00	0.00	0.00	0.00	0.00
Fissurina marginata	1.49	5.03	0.74	0.50	1.67	0.00	2.73	4.11	0.35	0.62	0.00	1.29
Fissurina orbignyana	2.49	1.01	0.00	0.00	0.00	0.00	0.39	0.00	0.00	0.00	0.00	0.00
Fissurina porcupinensis	0.00	0.00	0.00	0.00	0.00	0.00	0.00	0.00	0.35	0.62	0.00	0.00

Appendix B - Benthic foraminifera assemblage data

Core 9/97/10
Relative abundance - Benthic foraminifera 500-250um

Sample depth (cm)	3	7	11	16	20	27	31	35	39	43	47	51.5
Pyrgo murrhina	5.97	1.01	0.00	0.00	0.00	0.00	0.00	2.28	0.35	1.24	0.92	2.58
Pyrgo oblonga	0.00	0.00	0.00	0.00	0.00	0.00	0.00	0.00	0.00	0.00	0.00	0.00
Pyrgo rotalia	0.00	0.00	0.00	0.00	0.00	0.00	0.00	0.00	0.00	0.00	0.00	0.00
Pyrgo sarsi	0.00	0.00	0.00	0.00	0.00	0.00	0.00	0.00	0.00	0.00	0.00	0.00
Pyrgo serrata	0.00	0.00	0.00	0.00	0.00	0.00	0.00	0.00	0.00	0.00	0.00	0.00
Pyrgo sp.	0.00	0.00	0.00	0.00	0.00	0.00	0.00	0.00	0.00	0.00	0.00	0.00
Pyrgo williamsoni	0.00	0.00	0.00	0.00	0.00	0.00	0.00	0.00	0.00	0.00	0.00	0.00
Quinqueloculina arctica	0.00	0.00	0.00	0.00	0.00	0.00	0.00	0.00	0.00	0.00	0.00	0.00
Quinqueloculina bicornis	0.00	0.00	0.00	0.00	0.00	0.00	0.00	0.00	0.00	0.00	0.00	0.00
Quinqueloculina cliarensis	0.00	0.00	0.00	0.00	0.00	0.00	0.00	0.00	0.00	0.00	0.00	0.00
Quinqueloculina elongata	0.00	0.00	0.00	0.00	0.00	0.00	0.00	0.00	0.00	0.00	0.00	0.00
Quinqueloculina lata	0.00	0.00	0.00	0.00	3.33	0.00	0.00	0.00	0.00	0.62	0.00	0.00
Quinqueloculina seminulum	0.00	1.01	5.93	13.43	5.83	10.05	6.64	3.20	1.77	4.35	4.15	0.65
Quinqueloculina sp.	0.00	0.00	0.00	0.00	0.00	0.00	0.00	0.00	0.00	0.00	0.00	0.00
Quinqueloculina stalkeri	0.00	2.01	5.93	24.38	31.67	31.75	14.84	8.68	28.98	21.12	9.22	1.94
Quinqueloculina striata	0.00	0.00	0.00	0.00	0.00	0.00	0.00	0.00	0.00	0.00	0.00	0.00
Rupertina stabilis	0.00	0.00	0.00	0.00	0.00	0.00	0.00	0.00	0.00	0.00	0.00	0.00
Sigmoilopsis schlumbergeri	19.90	13.07	9.63	0.50	4.17	2.12	3.91	5.02	2.47	7.45	8.76	16.13
Siphotextularia rolhauseni	0.00	0.00	0.00	0.00	0.00	0.00	0.00	0.00	0.00	0.00	0.00	0.00
Solenina radiata	0.00	0.00	0.00	0.00	0.00	0.00	0.00	0.00	0.00	0.00	0.00	0.00
Spiroloculina limbata	0.00	0.00	0.00	0.00	0.00	0.00	0.00	0.00	0.00	0.00	0.00	0.00
Spiroloculina rotunda	0.00	1.01	1.48	0.00	0.00	0.00	0.00	0.00	0.00	0.00	0.00	0.65
Stainforthia (Fursenkoina) fusiform	0.00	0.00	0.00	0.00	0.00	0.00	0.00	0.00	0.00	0.00	0.00	0.00
Stainforthia loeblichi	0.00	0.00	0.00	0.00	0.00	0.00	0.00	0.00	0.00	0.00	0.00	0.00
Stainforthia schreibersiana	0.00	0.00	0.00	0.00	0.00	0.00	0.00	0.00	0.00	0.00	0.00	0.00
Trifarina angulosa	0.00	0.00	0.00	0.00	0.00	0.00	1.95	4.57	0.35	1.24	0.00	0.00
Trifarina bradyi	0.00	0.00	0.00	0.00	0.00	0.00	0.00	0.00	0.00	0.00	0.00	0.00
Trifarina sp.	0.00	0.00	0.00	0.00	0.00	0.00	0.00	0.00	0.00	0.00	0.00	0.00
Triloculina tricarinata	0.00	0.00	0.00	0.00	0.00	0.00	0.00	0.00	0.00	0.00	0.00	0.00
Uvigerina celtica	0.00	0.00	0.00	0.00	0.00	0.00	0.00	0.00	0.00	0.00	0.00	0.00
Uvigerina cf. pigmea	0.00	0.00	0.00	0.00	0.00	0.00	0.00	0.00	0.00	0.00	0.00	0.00
Uvigerina peregrina	19.90	9.05	4.44	0.00	0.00	0.00	6.25	5.02	1.77	2.48	0.92	0.65
Virgulina advena	0.00	0.00	0.00	0.00	0.00	0.00	0.00	0.00	0.00	0.00	0.00	0.00

Appendix B - Benthic foraminifera assemblage data

Core 9/97/10
Relative abundance - Benthic foraminifera 500-250um

Sample depth (cm)	55.5	59.5	63.5	67.5	71.5	79.5	83
Alabaminella weddellensis	0.00	0.00	0.00	0.00	0.00	0.00	0.00
Amphycorina scalaris	0.00	0.00	0.00	1.03	0.00	0.00	0.00
Astacolus hyalacrulus	0.00	0.00	0.00	0.00	0.00	0.00	0.00
Astacolus sp.	0.00	0.00	0.00	0.00	0.00	0.00	0.00
Bolivina albatrossi	0.00	0.00	0.00	0.00	0.00	0.00	0.00
Bolivina pseduopunctata	0.00	0.00	0.00	0.00	0.00	0.00	0.00
Bolivina sp.	0.00	0.00	0.00	0.00	0.00	0.00	0.00
Bolivina spinescens	0.00	0.00	0.00	0.00	0.00	0.00	0.00
Bolivina subspinescens	0.00	0.00	0.00	0.00	0.00	0.00	0.00
Brizalina cf. robusta	0.00	0.00	0.00	0.00	0.00	0.00	0.00
Brizalina variabilis	0.00	0.00	0.00	0.00	0.00	0.00	0.00
Bulimina aculeata	0.00	3.64	3.40	0.00	0.00	1.90	4.95
Bullimina cf. gibba	0.00	0.00	0.00	0.00	0.00	0.00	0.00
Bulimina inflata	4.21	6.06	5.11	7.22	8.65	9.49	11.88
Bullimina marginata	2.63	6.06	4.26	5.15	8.65	9.49	5.94
Cassidulina laevigata	0.00	0.00	0.00	0.00	0.00	0.00	0.00
Cassidulina obtusa	0.00	0.00	0.00	0.00	0.00	0.00	0.00
Chilostomella oolina	0.00	0.00	0.00	0.00	0.00	0.00	0.00
Cibicides kullenbergi	0.00	1.21	0.00	0.00	0.00	4.43	0.99
Cibicides lobatulus	1.58	1.21	0.43	2.06	0.00	0.63	0.00
Cibicides pachyderma	0.00	0.00	0.00	0.00	0.00	1.90	0.00
Cibicides sp.	0.00	0.00	0.00	0.00	0.00	0.00	0.00
Cibicides wuellerstorfi	15.26	20.00	11.06	6.19	10.58	24.68	20.79
Cyclammina pusilla	0.00	0.00	0.00	0.00	0.00	0.00	0.00
Dentalina communis	0.00	0.00	0.00	0.00	0.00	0.00	0.00
Dentalina sp.	0.00	0.00	0.00	0.00	0.00	0.00	0.00
Eggerella bradyi	0.00	0.00	0.00	0.00	0.00	0.00	0.00
Ehrenbergina serrata	0.00	0.61	0.43	1.03	0.96	0.00	1.98
Epistominella exigua	0.00	4.85	0.00	5.15	1.92	0.00	4.95
Eponides pusillus	0.00	0.00	0.00	0.00	0.00	0.00	0.00
Fissurina marginata	0.53	0.00	0.85	2.06	0.96	3.80	1.98
Fissurina orbignyana	0.53	0.00	0.00	0.00	0.00	0.00	0.00
Fissurina porcupinensis	0.53	0.61	0.43	0.00	0.00	0.00	0.00

Appendix B - Benthic foraminifera assemblage data

Core 9/97/10
Relative abundance - Benthic foraminifera 500-250um

Sample depth (cm)	**55.5**	**59.5**	**63.5**	**67.5**	**71.5**	**79.5**	**83**
Fissurina varioperforata	0.00	0.00	0.00	0.00	0.00	0.00	0.00
Fursenkoina complanata	0.00	0.00	0.00	0.00	0.00	0.00	0.00
Gavelinopsis lobatus	0.00	0.00	0.00	0.00	0.00	0.00	0.00
Globobulimina auriculata	0.00	0.00	0.00	0.00	0.00	0.00	0.00
Globobullimina affinis	0.00	0.00	0.00	0.00	0.00	0.00	0.00
Gyroidina soldanii	0.00	0.00	0.00	0.00	0.00	0.00	0.00
Hoeglundia elegans	6.32	3.64	2.13	0.00	0.00	0.00	1.98
Hormosina globulifera	0.00	0.00	0.00	0.00	0.00	0.00	0.00
Indeterminate	0.00	0.00	0.00	0.00	0.00	0.00	0.00
Karreriella bradyi	18.95	18.18	28.51	20.62	18.27	10.13	10.89
Lagena cf. acuticosta	0.00	0.00	0.00	0.00	0.00	0.00	0.00
Lagena cf. interrupta	0.00	0.00	0.00	0.00	0.00	0.00	0.00
Lagena semistriata	0.00	0.00	0.00	0.00	0.00	0.00	0.00
Lagena sulcata	0.53	0.00	0.85	3.09	0.00	0.00	0.99
Melonis barleeanum	22.63	10.91	11.91	9.28	11.54	7.59	7.92
Melonis pompilioides	0.00	0.00	0.00	0.00	0.00	0.00	0.00
Nodosaria sp.	0.00	0.00	0.00	0.00	0.00	0.00	0.00
Nonionella auricula	0.00	0.00	0.00	0.00	0.00	0.00	0.00
Nonionella turgida	0.00	0.00	0.00	0.00	0.00	0.00	0.00
Nummoloculina irregularis	0.00	0.00	0.00	0.00	0.00	0.00	0.00
Oolina apiopleura	0.00	0.00	0.00	0.00	0.00	0.00	0.00
Oolina heronalleni	0.00	0.00	0.00	0.00	0.00	0.00	0.00
Oolina hexagona	0.00	0.00	0.00	0.00	0.00	0.00	0.00
Oolina intercalata	0.00	0.00	0.00	0.00	0.00	0.00	0.00
Oolina melo	0.00	0.00	0.00	0.00	0.00	0.00	0.99
Oolina squamosa	0.00	0.00	0.00	0.00	0.00	0.63	0.00
Oridorsalis umbonatus	0.00	0.00	0.00	0.00	0.00	0.00	0.00
Pseudofissurina mccullochae	0.00	0.00	0.00	0.00	0.00	0.00	0.00
Pseudosolenina borealis	0.00	0.00	0.00	0.00	0.00	0.00	0.00
Pullenia bulloides	0.00	0.00	0.00	0.00	0.00	0.00	0.00
Pullenia subcarinata	5.26	0.61	4.68	0.00	1.92	0.63	0.99
Pyrgo depressa	1.05	0.00	0.85	0.00	5.77	0.00	0.00
Pyrgo lacernula	0.00	0.00	0.00	0.00	0.00	0.00	0.00

Appendix B - Benthic foraminifera assemblage data

Core 9/97/10
Relative abundance - Benthic foraminifera 500-250um

Sample depth (cm)	55.5	59.5	63.5	67.5	71.5	79.5	83
Pyrgo murrhina	0.00	0.00	0.00	0.00	0.00	1.27	0.00
Pyrgo oblonga	0.00	0.00	0.00	0.00	0.00	0.00	0.00
Pyrgo rotalia	0.00	0.00	0.00	0.00	0.00	0.00	0.00
Pyrgo sarsi	0.00	0.00	0.00	0.00	0.00	0.00	0.00
Pyrgo serrata	0.00	0.00	0.00	0.00	0.00	0.00	0.00
Pyrgo sp.	0.00	0.00	0.00	0.00	0.00	0.00	0.00
Pyrgo williamsoni	0.00	0.00	0.00	1.03	0.00	0.00	0.00
Quinqueloculina arctica	0.00	0.00	0.00	0.00	0.00	0.00	0.00
Quinqueloculina bicornis	0.00	0.00	0.00	0.00	0.00	0.00	0.00
Quinqueloculina cliarensis	0.00	0.00	0.00	0.00	0.00	0.00	0.00
Quinqueloculina elongata	0.00	0.00	0.00	0.00	0.00	0.00	0.00
Quinqueloculina lata	0.00	0.00	0.00	0.00	0.00	0.00	0.00
Quinqueloculina seminulum	1.05	0.00	0.85	1.03	0.00	0.00	0.99
Quinqueloculina sp.	0.00	0.00	0.00	0.00	0.00	0.00	0.00
Quinqueloculina stalkeri	0.53	1.21	2.13	2.06	1.92	19.62	15.84
Quinqueloculina striata	0.00	0.00	0.00	0.00	0.00	0.00	0.00
Rupertina stabilis	0.00	0.00	0.00	0.00	0.00	0.00	0.00
Sigmoilopsis schlumbergeri	14.74	20.61	20.43	28.87	25.00	2.53	5.94
Siphotextularia rolhauseni	0.00	0.00	0.00	0.00	0.00	0.00	0.00
Solenina radiata	0.00	0.00	0.00	0.00	0.00	0.00	0.00
Spiroloculina limbata	0.00	0.00	0.00	0.00	0.00	0.00	0.00
Spiroloculina rotunda	1.58	0.00	0.85	1.03	1.92	0.00	0.00
Stainforthia (Fursenkoina) fusiform	0.00	0.00	0.00	0.00	0.00	0.00	0.00
Stainforthia loeblichi	0.00	0.00	0.00	0.00	0.00	0.00	0.00
Stainforthia schreibersiana	0.00	0.00	0.00	0.00	0.00	0.00	0.00
Trifarina angulosa	0.53	0.00	0.00	0.00	0.00	0.00	0.00
Trifarina bradyi	1.05	0.00	0.00	0.00	0.00	0.00	0.00
Trifarina sp.	0.00	0.00	0.00	0.00	0.00	0.00	0.00
Triloculina tricarinata	0.00	0.00	0.00	0.00	0.00	0.00	0.00
Uvigerina celtica	0.00	0.00	0.00	0.00	0.00	0.00	0.00
Uvigerina cf. pigmea	0.00	0.00	0.00	0.00	0.00	0.00	0.00
Uvigerina peregrina	0.53	0.61	0.85	0.00	1.92	1.27	0.00
Virgulina advena	0.00	0.00	0.00	0.00	0.00	0.00	0.00

Appendix B - Benthic foraminifera assemblage data

Core 9/97-03
Relative abundance - Benthic foraminifera 500-250um

Sample depth (cm)	3	6	9	13	19	23	27	31	35	39	43	47	51	55	59	63
Bullimina aculeata	0.61	1.45	2.56	4.04	2.02	1.55	0.00	2.70	1.92	0.00	0.00	0.00	0.00	6.92	4.70	2.78
Bullimina inflata	0.00	0.00	0.00	0.00	0.00	0.00	0.00	0.00	0.00	0.00	0.00	0.00	0.00	0.00	0.00	0.00
Bullimina marginata	0.61	0.72	0.00	4.04	4.04	1.55	2.19	1.16	1.92	3.55	1.53	4.07	2.20	6.29	3.36	3.47
Cassidulina laevigata	0.00	0.00	0.00	0.00	0.00	0.00	0.00	0.00	0.38	0.00	0.38	0.00	0.00	0.00	0.00	0.00
Cibicides kullenbergi	11.04	19.57	20.51	3.03	3.03	13.40	5.46	5.02	7.66	7.11	3.05	27.64	21.98	0.00	2.68	0.00
Cibicides lobatulus	6.13	5.80	1.28	1.01	1.01	4.12	0.00	0.39	0.38	2.03	3.05	0.00	0.00	1.89	7.38	2.78
Cibicides pachyderma	0.00	0.00	0.00	0.00	0.00	0.00	0.00	0.00	0.00	0.00	0.00	0.00	0.00	0.00	0.00	0.00
Cibicides wuellerstorfi	6.75	3.62	14.10	24.24	35.35	21.65	28.42	25.87	24.14	19.29	18.70	13.01	14.29	17.61	5.37	18.06
Cyclammina pusilla	0.00	0.00	5.13	0.00	0.00	0.52	0.00	0.39	0.00	0.00	0.00	0.00	0.00	0.00	0.00	0.00
Dentalina communis	0.00	0.00	0.00	0.00	0.00	0.00	0.00	0.00	0.00	0.00	0.00	0.00	0.00	0.00	0.00	0.00
Eggerella bradyi	0.00	0.00	0.00	0.00	0.00	0.00	0.00	0.00	0.00	0.00	0.00	0.00	0.00	0.00	0.00	0.00
Epistominella exigua	3.68	3.62	0.00	1.01	0.00	2.58	1.64	5.41	1.53	2.54	4.58	2.44	0.00	6.29	8.72	10.42
Fissurina marginata	1.84	0.00	0.00	1.01	0.00	1.55	0.00	0.00	0.00	0.00	0.76	1.63	2.20	1.89	2.01	0.00
Fissurina porcupinensis	0.61	0.00	0.00	0.00	0.00	0.00	0.00	0.00	0.00	0.00	0.00	0.00	0.00	0.00	0.00	0.00
Gyroidina soldanii	3.07	0.72	0.00	1.01	1.01	0.00	0.00	0.77	2.30	0.00	1.53	0.81	1.10	1.26	0.00	0.00
Hoeglundia elegans	4.29	0.72	0.00	4.04	4.04	0.00	1.64	3.47	4.98	6.60	3.82	8.94	4.40	6.92	6.04	6.94
Hormosina globulifera	0.00	0.00	0.00	0.00	0.00	0.00	0.00	0.00	0.00	0.00	0.00	0.00	0.00	0.00	0.00	0.00
Karreriella bradyi	15.95	19.57	3.85	6.06	9.09	7.73	2.19	10.81	6.51	12.18	17.18	5.69	7.69	21.38	18.12	22.22
Lagena semistriata	0.00	0.00	0.00	0.00	0.00	0.00	0.00	0.00	0.00	0.51	0.38	0.00	0.00	0.00	0.00	0.00
Lagena sulcata	1.23	0.00	0.00	0.00	0.00	0.00	0.00	0.00	0.00	0.00	1.53	0.00	0.00	0.63	0.67	0.00
Melonis barleeanum	9.20	13.04	2.56	14.14	4.04	1.03	3.83	15.44	13.03	13.71	13.74	13.01	20.88	12.58	22.82	18.06
Melonis pompilioides	0.61	0.00	0.00	0.00	0.00	0.00	0.00	0.00	0.00	0.00	0.38	0.00	0.00	0.00	0.00	0.00
Nummoloculina irregularis	0.00	0.00	0.00	0.00	0.00	0.00	0.00	0.00	0.00	0.00	0.00	0.00	0.00	0.00	0.00	0.00
Pullenia bulloides	0.00	0.00	0.00	0.00	0.00	0.00	0.00	0.00	0.00	0.00	0.00	0.00	0.00	0.00	0.00	0.00
Pullenia subcarinata	0.61	1.45	5.13	0.00	0.00	0.00	0.00	1.54	1.53	0.51	0.76	0.00	0.00	1.89	0.67	0.00
Pyrgo depressa	1.84	0.72	0.00	0.00	0.00	0.00	0.00	0.00	0.38	1.02	0.76	1.63	0.00	1.26	0.00	0.69
Pyrgo murrhina	0.00	0.72	0.00	0.00	0.00	0.00	0.00	0.00	0.00	0.00	0.00	0.00	0.00	0.63	0.00	0.00
Pyrgo sarsi	0.00	0.00	0.00	0.00	0.00	0.00	0.00	0.00	0.00	0.00	0.00	0.00	0.00	0.00	0.00	0.00
Pyrgo serrata	0.00	0.00	0.00	0.00	0.00	0.00	0.00	0.00	0.00	0.00	0.00	0.00	0.00	0.00	0.00	0.00
Pyrgo williamsoni	0.00	0.72	0.00	1.01	1.01	0.00	0.00	0.00	0.00	0.00	0.00	0.00	0.00	0.00	0.00	0.00
Quinqueloculina arctica	0.00	0.00	0.00	0.00	0.00	0.00	0.00	0.00	0.00	0.00	0.00	0.00	0.00	0.00	0.00	0.00
Quinqueloculina seminulum	4.29	7.25	21.79	5.05	5.05	1.55	5.46	3.47	2.68	3.55	2.67	9.76	13.19	3.14	0.67	0.00
Quinqueloculina striata	0.00	0.00	0.00	0.00	0.00	0.00	0.00	0.00	0.00	0.00	0.00	0.00	0.00	0.00	0.00	0.00
Rupertina stabilis	7.36	10.87	17.95	13.13	13.13	33.51	42.62	14.29	19.16	15.23	11.83	4.07	2.20	0.63	2.01	2.08

Appendix B - Benthic foraminifera assemblage data

Core 9/97-03
Relative abundance - Benthic foraminifera 500-250um

Sample depth (cm)	3	6	9	13	19	23	27	31	35	39	43	47	51	55	59	63
Sigmoilopsis schlumbergeri	14.72	5.80	3.85	9.09	9.09	6.70	5.46	3.09	2.68	3.55	3.05	4.88	6.59	8.18	7.38	8.33
Siphotextularia rolshauseni	4.29	0.72	1.28	0.00	0.00	0.00	0.00	0.39	1.53	0.51	1.15	0.00	0.00	0.00	1.34	0.69
Trifarina angulosa	0.61	0.00	0.00	4.04	4.04	0.00	0.00	0.39	1.15	2.03	3.44	0.00	0.00	0.63	0.67	1.39
Trifarina sp.	0.00	0.00	0.00	0.00	0.00	0.00	0.00	0.00	0.00	0.00	0.00	0.00	0.00	0.00	0.00	0.00
Uvigerina celtica	0.00	0.72	0.00	0.00	0.00	0.00	0.00	0.00	0.00	0.00	1.15	0.00	0.00	0.00	3.36	0.00
Uvigerina peregrina	0.61	2.17	0.00	4.04	4.04	2.58	1.09	5.41	6.13	6.09	4.58	2.44	3.30	0.00	2.01	2.08

Appendix B - Benthic foraminifera assemblage data

Core 9/97-03
Relative abundance - Benthic foraminifera 500-250um

Sample depth (cm)	67	71	75	79	83	87	
Bullimina aculeata	7.53	1.70	1.05	1.22	0.00	0.00	
Bullimina inflata	0.00	0.00	0.00	0.00	0.00	0.00	
Bullimina marginata	6.45	10.64	10.47	12.20	16.25	9.91	
Cassidulina laevigata	1.08	0.00	0.00	0.00	0.00	0.00	
Cibicides kullenbergi	0.00	1.70	3.66	2.44	2.50	7.21	
Cibicides lobatulus	6.45	1.70	1.05	1.22	0.00	0.00	
Cibicides pachyderma	0.00	0.00	0.00	0.00	0.00	0.00	
Cibicides wuellerstorfi	8.60	25.53	25.65	4.88	2.50	18.92	
Cyclammina pusilla	0.00	0.00	0.00	0.00	0.00	0.00	
Dentalina communis	0.00	0.00	0.00	0.00	0.00	0.00	
Eggerella bradyi	0.00	0.00	0.00	0.00	0.00	0.00	
Epistominella exigua	4.30	0.85	1.05	2.44	5.00	3.60	
Fissurina marginata	0.00	0.85	0.52	1.22	2.50	0.90	
Fissurina porcupinensis	0.00	0.00	0.00	0.00	0.00	0.00	
Gyroidina soldanii	0.00	0.43	0.52	0.00	0.00	0.90	
Hoeglundia elegans	0.00	2.13	1.05	3.66	6.25	0.90	
Hormosina globulifera	0.00	0.00	0.00	0.00	0.00	0.00	
Karreriella bradyi	26.88	6.38	9.95	10.98	13.75	8.11	
Lagena semistriata	0.00	0.43	0.00	0.00	0.00	0.00	
Lagena sulcata	2.15	0.00	0.00	0.00	0.00	0.00	
Melonis barleeanum	11.83	13.62	16.75	17.07	10.00	9.01	
Melonis pompilioides	0.00	0.00	0.00	0.00	0.00	0.00	
Nummoloculina irregularis	0.00	0.00	0.00	0.00	0.00	0.00	
Pullenia bulloides	0.00	0.43	0.00	0.00	0.00	0.00	
Pullenia subcarinata	4.30	0.85	1.05	1.22	1.25	4.50	
Pyrgo depressa	2.15	0.00	0.00	0.00	0.00	0.00	
Pyrgo murrhina	0.00	1.28	0.00	1.22	2.50	1.80	
Pyrgo sarsi	0.00	0.00	0.00	0.00	0.00	0.00	
Pyrgo serrata	0.00	0.00	0.00	0.00	0.00	0.00	
Pyrgo williamsoni	0.00	0.00	0.52	0.00	0.00	0.00	
Quinqueloculina arctica	0.00	0.00	0.00	0.00	0.00	0.00	
Quinqueloculina seminulum	0.00	1.70	1.57	1.22	1.25	0.00	
Quinqueloculina striata	0.00	0.00	0.00	0.00	0.00	0.00	
Rupertina stabilis	1.08	12.34	3.66	4.88	2.50	9.01	

Appendix B - Benthic foraminifera assemblage data

Core 9/97-03

Relative abundance - Benthic foraminifera 500-250um

Sample depth (cm)	67	71	75	79	83	87
Sigmoilopsis schlumbergeri	12.90	11.91	12.57	8.54	11.25	21.62
Siphotextularia rolshauseni	3.23	0.00	0.00	0.00	0.00	0.00
Trifarina angulosa	0.00	0.00	0.00	0.00	0.00	0.00
Trifarina sp.	0.00	0.00	0.00	0.00	0.00	0.00
Uvigerina celtica	0.00	0.00	0.00	0.00	0.00	0.00
Uvigerina peregrina	1.08	5.53	8.90	25.61	22.50	3.60

Appendix B - Benthic foraminifera assemblage data

Core 9/97/04
Relative abundance - Benthic foraminifera 500-250um

Sample depth (cm)	1	2	5.5	9	13	21	25	33	37	39	43	45	48	52	56
Alabaminella weddellensis	0.78	1.10	0.00	0.00	0.00	0.00	0.00	0.00	0.00	0.00	0.00	0.00	0.00	0.00	0.00
Amphycorina scalaris	0.00	0.00	0.00	0.00	0.00	0.00	0.00	0.00	0.00	0.00	0.00	0.00	0.00	0.00	0.00
Astacolus hyalacrulus	0.00	0.00	0.00	0.00	0.00	0.00	0.00	0.00	0.00	0.00	0.00	0.00	0.00	0.00	0.00
Astacolus sp.	0.00	0.00	0.00	0.00	0.00	0.00	0.00	0.00	0.00	0.00	0.00	0.00	0.00	0.00	0.00
Bolivina albatrossi	0.00	0.00	0.00	0.00	0.00	0.00	0.00	0.00	0.00	0.00	0.00	0.00	0.00	0.00	0.00
Bolivina pseduopunctata	0.00	0.00	0.00	0.00	0.00	0.00	0.00	0.00	0.00	0.00	0.00	0.80	0.00	0.00	0.00
Bolivina sp.	0.00	0.00	0.00	0.00	0.00	0.00	0.00	0.00	0.00	0.00	0.00	0.00	0.00	0.00	0.00
Bolivina spinescens	0.00	0.00	0.00	0.00	2.67	0.00	0.00	0.00	0.00	0.00	0.00	0.00	0.00	0.00	0.00
Bolivina subspinescens	0.00	0.00	0.00	0.00	0.00	0.00	0.00	0.00	0.00	0.00	0.00	0.00	0.00	0.00	0.00
Brizalina cf. robusta	0.00	0.00	0.00	0.00	0.00	0.00	0.00	0.00	0.00	0.00	0.00	0.00	0.00	0.00	0.00
Brizalina variabilis	0.00	0.00	0.00	0.00	0.00	0.00	0.00	0.00	0.00	0.00	0.00	0.00	0.00	0.00	0.00
Bulimina aculeata	0.00	0.00	0.00	0.00	1.33	0.00	0.00	0.00	0.00	3.76	0.00	0.80	0.00	0.00	0.00
Bullimina cf. gibba	0.78	0.00	1.43	3.42	0.00	2.33	6.12	0.00	11.27	12.03	5.26	6.40	7.77	3.88	5.03
Bulimina inflata	0.00	0.00	0.00	0.00	0.00	0.00	0.00	0.00	0.00	0.00	0.00	0.00	0.00	0.00	0.00
Bullimina marginata	0.00	0.00	1.43	0.00	0.00	0.00	0.00	0.00	2.82	2.26	0.00	0.80	0.00	0.00	0.00
Cassidulina laevigata	0.00	0.00	0.00	0.00	30.67	0.00	0.00	0.00	0.00	0.00	1.32	0.80	0.00	0.00	0.00
Cassidulina obtusa	0.00	0.00	0.00	0.00	0.00	0.00	0.00	0.00	0.00	0.00	0.00	0.00	0.00	0.00	0.00
Chilostomella oolina	0.00	0.00	0.00	0.00	0.00	0.00	0.00	0.00	0.00	0.75	2.63	0.00	0.00	0.00	0.00
Cibicides kullenbergi	0.78	5.49	2.14	3.42	4.00	0.00	0.00	2.33	0.00	0.00	2.63	0.80	0.00	3.88	0.56
Cibicides lobatulus	2.34	6.59	7.86	1.71	0.00	1.16	0.00	0.00	0.00	0.00	0.00	1.60	0.00	3.88	3.35
Cibicides pachyderma	0.00	0.00	0.00	0.00	0.00	0.00	0.00	0.00	0.00	0.00	0.00	0.00	0.00	0.00	0.00
Cibicides sp.	0.00	0.00	0.00	0.00	1.33	0.00	0.00	0.00	0.00	0.00	0.00	0.00	0.00	0.00	0.00
Cibicides wuellerstorfi	9.38	15.38	11.43	23.93	5.33	4.65	0.00	4.65	21.13	21.05	2.63	17.60	12.62	10.78	16.20
Cyclammina pusilla	0.00	0.00	0.00	0.00	0.00	0.00	4.08	0.00	0.00	1.50	0.00	0.00	0.00	0.00	0.00
Dentalina communis	0.00	0.00	0.00	0.00	0.00	0.00	0.00	0.00	0.00	0.00	0.00	0.00	0.00	0.00	0.00
Dentalina sp.	0.00	0.00	0.00	0.00	0.00	0.00	0.00	0.00	0.00	0.00	0.00	0.80	0.00	0.00	0.00
Eggerella bradyi	0.78	1.10	2.86	0.00	1.33	0.00	10.20	9.30	22.54	8.27	7.89	4.80	4.85	7.76	6.70
Ehrenbergina serrata	0.00	0.00	0.00	0.00	0.00	0.00	0.00	0.00	0.00	0.00	0.00	0.00	0.00	0.00	0.00
Epistominella exigua	0.78	0.00	0.00	0.00	0.00	0.00	0.00	0.00	0.00	0.75	0.00	0.80	0.00	0.00	1.12
Eponides pusillus	0.00	0.00	0.00	0.00	0.00	0.00	0.00	0.00	0.00	0.00	0.00	0.00	0.00	1.29	0.00
Fissurina marginata	0.78	0.00	0.00	0.85	4.00	0.00	2.04	4.65	2.82	1.50	0.00	0.00	0.00	1.29	1.12
Fissurina orbignyana	0.00	0.00	0.00	0.00	1.33	0.00	0.00	0.00	0.00	0.00	0.00	0.80	0.00	0.00	0.56
Fissurina porcupinensis	0.00	0.00	0.71	0.00	0.00	1.16	0.00	0.00	5.63	0.75	1.32	0.80	0.97	0.00	0.00

Appendix B - Benthic foraminifera assemblage data

Core 9/97/04
Relative abundance - Benthic foraminifera 500-250um

Sample depth (cm)	1	2	5.5	9	13	21	25	33	37	39	43	45	48	52	56
Fissurina varioperforata	0.00	0.00	0.00	0.85	0.00	0.00	0.00	0.00	0.00	0.00	0.00	0.00	0.00	0.00	0.00
Fursenkoina complanata	0.00	0.00	0.00	0.00	0.00	0.00	0.00	0.00	2.82	0.75	0.00	0.00	0.00	0.00	0.00
Gavelinopsis lobatus	0.00	0.00	0.00	0.00	0.00	0.00	0.00	0.00	0.00	0.00	0.00	0.00	0.00	0.00	0.00
Globobulimina auriculata	0.00	0.00	0.00	0.00	0.00	0.00	0.00	0.00	0.00	0.00	0.00	0.00	0.00	0.00	0.00
Globobullimina affinis	0.00	0.00	0.00	0.00	1.33	0.00	0.00	0.00	0.00	0.00	0.00	0.00	0.97	0.00	0.00
Gyroidina soldanii	5.47	6.59	3.57	1.71	1.33	0.00	0.00	0.00	5.63	5.26	3.95	3.20	1.94	7.76	5.03
Hoeglundia elegans	0.00	0.00	0.00	14.53	0.00	0.00	0.00	0.00	0.00	0.75	1.32	1.60	2.91	7.76	7.26
Hormosina globulifera	0.00	0.00	0.00	0.00	0.00	0.00	0.00	0.00	0.00	0.00	15.79	0.00	0.00	0.00	0.00
Indeterminate	0.00	0.00	0.00	0.00	0.00	0.00	0.00	0.00	0.00	0.00	0.00	0.00	0.00	0.00	0.00
Karreriella bradyi	28.13	8.79	14.29	0.00	5.33	10.47	4.08	9.30	2.82	9.02	0.00	13.60	5.83	5.17	6.15
Lagena cf. acuticosta	0.00	0.00	0.00	0.00	0.00	0.00	0.00	0.00	0.00	0.00	0.00	0.00	0.00	0.00	0.00
Lagena cf. interrupta	0.00	0.00	0.00	0.85	0.00	0.00	0.00	0.00	0.00	0.00	0.00	0.00	0.00	0.00	0.00
Lagena semistriata	0.00	0.00	0.00	0.00	0.00	0.00	0.00	0.00	0.00	0.00	0.00	0.00	0.00	0.00	0.00
Lagena sulcata	0.00	0.00	0.00	0.00	0.00	0.00	0.00	0.00	0.00	0.75	0.00	0.80	0.97	0.00	0.00
Melonis barleeanum	4.69	8.79	2.14	0.00	1.33	8.14	6.12	2.33	0.00	6.02	5.26	2.40	2.91	5.17	1.68
Melonis pompilioides	0.78	0.00	0.00	0.00	0.00	0.00	2.04	0.00	0.00	0.00	0.00	0.00	0.00	0.00	0.00
Nodosaria sp.	0.00	0.00	0.00	0.00	0.00	0.00	0.00	0.00	0.00	0.00	0.00	0.00	0.00	0.00	0.00
Nonionella auricula	0.00	0.00	0.00	0.00	0.00	0.00	0.00	0.00	0.00	0.00	0.00	0.00	0.00	0.00	0.00
Nonionella turgida	0.00	0.00	0.00	0.00	0.00	1.16	0.00	0.00	0.00	0.00	0.00	0.00	0.00	0.00	0.00
Nummoloculina irregularis	0.00	0.00	0.00	0.00	0.00	3.49	0.00	2.33	0.00	0.00	0.00	0.00	0.00	0.00	0.00
Oolina apiopleura	0.00	0.00	0.00	0.00	0.00	0.00	0.00	0.00	0.00	0.00	0.00	0.00	0.00	0.00	0.00
Oolina heronalleni	0.00	0.00	0.00	0.00	0.00	0.00	0.00	0.00	0.00	0.00	0.00	0.00	0.00	0.00	0.00
Oolina hexagona	0.00	0.00	0.00	0.00	0.00	0.00	0.00	0.00	0.00	0.00	0.00	0.00	0.00	0.00	0.00
Oolina intercalata	0.00	0.00	0.00	0.00	0.00	0.00	0.00	0.00	0.00	0.00	0.00	0.00	0.00	0.00	0.00
Oolina melo	0.00	0.00	0.00	0.00	0.00	0.00	0.00	0.00	0.00	0.00	0.00	0.00	0.00	0.00	0.00
Oolina squamosa	0.00	0.00	0.00	0.00	0.00	0.00	0.00	0.00	0.00	0.00	0.00	1.60	0.00	0.00	0.56
Oridorsalis umbonatus	0.00	0.00	0.00	0.00	0.00	0.00	0.00	0.00	0.00	0.00	0.00	0.00	0.00	0.00	0.00
Pseudofissurina mccullochae	0.00	0.00	0.00	0.00	0.00	0.00	0.00	0.00	0.00	0.00	3.95	0.80	0.00	0.00	0.00
Pseudosolenina borealis	0.00	0.00	0.00	0.00	0.00	0.00	0.00	0.00	0.00	0.00	0.00	0.00	0.00	0.00	0.00
Pullenia bulloides	1.56	1.10	0.00	8.55	20.00	18.60	8.16	11.63	0.00	5.26	7.89	7.20	2.91	2.59	3.35
Pullenia subcarinata	0.78	0.00	0.00	0.00	2.67	0.00	0.00	0.00	0.00	0.75	2.63	3.20	3.88	2.59	0.00
Pyrgo depressa	0.00	0.00	0.00	0.00	0.00	0.00	0.00	0.00	0.00	0.00	0.00	0.00	0.00	0.00	0.00
Pyrgo lacernula	0.00	0.00	0.00	0.00	0.00	0.00	0.00	0.00	0.00	0.00	0.00	0.00	0.00	0.00	0.00

Appendix B - Benthic foraminifera assemblage data

Core 9/97/04
Relative abundance - Benthic foraminifera 500-250um

Sample depth (cm)	1	2	5.5	9	13	21	25	33	37	39	43	45	48	52	56
Pyrgo murrhina	0.78	2.20	3.57	0.00	0.00	1.16	8.16	11.63	2.82	0.75	1.32	0.80	3.88	3.88	8.94
Pyrgo oblonga	0.00	0.00	0.00	0.00	0.00	0.00	0.00	0.00	0.00	0.00	0.00	0.00	0.00	0.00	0.56
Pyrgo rotalia	0.00	0.00	0.00	0.00	0.00	1.16	0.00	0.00	0.00	0.00	0.00	0.00	0.00	0.00	0.00
Pyrgo sarsi	0.78	0.00	0.00	0.00	0.00	1.16	0.00	0.00	0.00	0.75	0.00	2.40	1.94	0.00	0.56
Pyrgo serrata	0.00	0.00	0.00	0.00	0.00	0.00	0.00	0.00	2.82	1.50	0.00	0.80	0.00	0.00	8.94
Pyrgo sp.	0.00	0.00	0.00	0.00	0.00	0.00	0.00	0.00	0.00	0.00	0.00	0.00	0.00	0.00	0.00
Pyrgo williamsoni	0.00	0.00	0.00	0.00	0.00	0.00	0.00	0.00	0.00	0.00	0.00	0.80	0.00	0.00	0.00
Quinqueloculina arctica	0.00	0.00	0.00	2.56	5.33	6.98	0.00	11.63	0.00	0.00	0.00	0.00	0.97	1.29	0.00
Quinqueloculina bicornis	0.00	0.00	0.00	0.00	0.00	0.00	0.00	0.00	0.00	0.00	0.00	0.00	0.00	0.00	0.00
Quinqueloculina cliarensis	0.00	0.00	0.00	0.00	0.00	0.00	0.00	0.00	0.00	0.00	0.00	0.00	0.00	0.00	0.00
Quinqueloculina elongata	0.00	0.00	0.00	0.00	0.00	0.00	0.00	0.00	0.00	0.00	0.00	0.00	0.00	0.00	0.00
Quinqueloculina lata	0.00	0.00	0.00	0.00	0.00	0.00	0.00	0.00	0.00	0.00	0.00	0.00	0.00	0.00	0.00
Quinqueloculina seminulum	0.00	0.00	0.00	2.56	2.67	3.49	8.16	4.65	0.00	0.00	0.00	1.60	0.00	0.00	0.00
Quinqueloculina sp.	0.00	0.00	0.00	0.00	0.00	0.00	0.00	0.00	0.00	0.00	0.00	0.00	0.00	0.00	0.00
Quinqueloculina stalkeri	0.00	0.00	0.00	0.00	0.00	0.00	0.00	0.00	0.00	0.00	0.00	0.00	0.00	0.00	0.00
Quinqueloculina striata	0.00	0.00	0.00	0.00	0.00	0.00	0.00	0.00	0.00	0.00	0.00	0.00	0.00	0.00	0.00
Rupertina stabilis	6.25	7.69	17.14	22.22	1.33	13.95	4.08	9.30	5.63	7.52	22.37	7.20	19.42	9.05	16.20
Sigmoilopsis schlumbergeri	25.78	30.77	29.29	3.42	0.00	10.47	30.61	11.63	5.63	5.26	2.63	4.00	9.71	9.05	1.12
Siphotextularia rolhauseni	4.69	0.00	1.43	2.56	1.33	9.30	0.00	4.65	2.82	1.50	7.89	8.00	9.71	9.05	3.91
Solenina radiata	0.00	0.00	0.00	1.71	0.00	0.00	2.04	0.00	0.00	0.00	1.32	0.00	0.00	0.00	0.56
Spiroloculina limbata	0.00	0.00	0.00	0.00	0.00	0.00	0.00	0.00	0.00	0.00	0.00	0.00	0.00	0.00	0.00
Spiroloculina rotunda	0.78	0.00	0.00	0.00	0.00	0.00	0.00	0.00	0.00	0.00	0.00	0.00	0.00	1.29	0.00
Stainforthia (Fursenkoina) fusiform	0.00	0.00	0.00	0.00	0.00	0.00	0.00	0.00	0.00	0.00	0.00	0.00	0.00	0.00	0.00
Stainforthia loeblichi	0.00	0.00	0.00	0.00	0.00	0.00	0.00	0.00	0.00	0.00	0.00	0.00	0.00	0.00	0.00
Stainforthia schreibersiana	0.00	0.00	0.00	0.00	0.00	0.00	0.00	0.00	0.00	0.00	0.00	0.00	0.00	0.00	0.00
Trifarina angulosa	0.00	0.00	0.00	0.00	4.00	0.00	0.00	0.00	0.00	0.00	0.00	0.00	2.91	2.59	0.56
Trifarina bradyi	0.00	0.00	0.00	0.00	0.00	0.00	0.00	0.00	0.00	0.00	0.00	0.00	0.00	0.00	0.00
Trifarina sp.	0.00	0.00	0.00	0.00	0.00	0.00	0.00	0.00	0.00	0.00	0.00	0.00	0.00	0.00	0.00
Triloculina tricarinata	0.00	0.00	0.00	0.00	0.00	1.16	0.00	0.00	0.00	0.00	0.00	0.00	0.00	0.00	0.00
Uvigerina celtica	0.78	2.20	0.00	0.00	0.00	0.00	0.00	0.00	2.82	0.75	0.00	0.80	0.00	0.00	0.00
Uvigerina cf. pigmea	0.00	0.00	0.00	0.00	0.00	0.00	0.00	0.00	0.00	0.00	0.00	0.00	0.00	0.00	0.00
Uvigerina peregrina	2.34	2.20	0.71	0.00	0.00	0.00	0.00	0.00	0.00	0.00	0.00	0.80	0.97	0.00	0.00
Virgulina advena	0.00	0.00	0.00	0.00	1.33	0.00	2.04	0.00	0.00	0.00	0.00	0.00	0.00	0.00	0.00

Appendix B - Benthic foraminifera assemblage data

Core 9/97/04
Relative abundance - Benthic foraminifera 500-250um

Sample depth (cm)	60	64	68	72	76	80	84	88
Alabaminella weddellensis	2.50	1.54	1.55	0.00	0.00	0.00	0.00	1.33
Amphycorina scalaris	0.00	0.00	0.00	0.00	0.00	0.00	0.00	0.00
Astacolus hyalacrulus	0.00	0.00	1.55	2.03	0.00	0.00	0.00	1.33
Astacolus sp.	0.00	0.00	0.00	0.00	0.00	0.00	0.00	0.00
Bolivina albatrossi	0.00	0.00	0.00	0.00	0.00	0.00	0.00	0.00
Bolivina pseduopunctata	0.00	0.00	0.00	0.00	0.00	0.00	0.00	0.00
Bolivina sp.	0.00	0.00	0.00	0.00	0.00	0.00	0.00	0.00
Bolivina spinescens	0.00	0.00	0.00	0.00	0.00	0.00	0.00	0.00
Bolivina subspinescens	0.00	1.54	0.00	0.00	0.00	0.00	0.00	1.33
Brizalina cf. robusta	0.00	0.00	0.00	0.00	0.00	0.00	0.00	0.00
Brizalina variabilis	0.00	0.00	0.00	0.00	0.00	0.00	0.00	0.00
Bulimina aculeata	0.63	0.00	0.00	0.00	0.00	5.88	2.22	2.67
Bullimina cf. gibba	2.50	6.15	9.30	2.03	12.07	7.06	4.44	5.33
Bulimina inflata	0.00	0.00	0.00	0.00	0.00	0.00	0.00	0.00
Bullimina marginata	0.00	1.54	1.55	2.03	0.00	1.18	0.00	0.00
Cassidulina laevigata	0.00	0.00	0.00	0.00	0.00	0.00	0.00	0.00
Cassidulina obtusa	0.00	0.00	0.00	0.00	0.00	0.00	0.00	0.00
Chilostomella oolina	0.63	0.00	0.00	0.00	0.00	0.00	0.00	0.00
Cibicides kullenbergi	0.63	0.00	0.00	0.00	0.00	0.00	0.00	0.00
Cibicides lobatulus	0.00	0.00	3.10	0.00	3.45	4.71	3.33	1.33
Cibicides pachyderma	0.63	0.00	0.00	0.00	0.00	0.00	0.00	0.00
Cibicides sp.	0.00	0.00	0.00	0.00	0.00	0.00	0.00	0.00
Cibicides wuellerstorfi	16.88	0.00	11.63	16.89	0.00	0.00	24.44	2.67
Cyclammina pusilla	0.00	1.54	0.00	0.00	0.00	2.35	1.11	0.00
Dentalina communis	0.00	0.00	0.00	0.00	0.00	0.00	0.00	0.00
Dentalina sp.	0.63	0.00	0.00	0.00	0.00	0.00	0.00	0.00
Eggerella bradyi	10.00	4.62	3.10	8.11	18.97	7.06	2.22	2.67
Ehrenbergina serrata	0.00	0.00	0.00	0.00	0.00	0.00	0.00	0.00
Epistominella exigua	0.63	0.00	0.00	0.00	0.00	2.35	2.22	4.00
Eponides pusillus	0.00	0.00	0.00	0.00	0.00	0.00	0.00	0.00
Fissurina marginata	3.13	1.54	1.55	0.00	6.90	2.35	2.22	1.33
Fissurina orbignyana	0.00	0.00	1.55	0.00	1.72	1.18	1.11	0.00
Fissurina porcupinensis	0.00	3.08	0.00	0.00	1.72	0.00	0.00	0.00

Appendix B - Benthic foraminifera assemblage data

Core 9/97/04
Relative abundance - Benthic foraminifera 500-250um

Sample depth (cm)	60	64	68	72	76	80	84	88
Fissurina varioperforata	0.00	0.00	0.00	0.00	0.00	0.00	0.00	0.00
Fursenkoina complanata	0.00	0.00	0.00	0.00	0.00	0.00	0.00	0.00
Gavelinopsis lobatus	0.00	0.00	0.00	0.00	0.00	0.00	0.00	0.00
Globobulimina auriculata	0.00	0.00	0.00	0.00	0.00	0.00	0.00	0.00
Globobullimina affinis	0.00	0.00	0.00	0.00	0.00	2.35	1.11	0.00
Gyroidina soldanii	5.00	10.77	6.20	8.11	10.34	7.06	5.56	10.67
Hoeglundia elegans	9.38	3.08	9.30	4.05	0.00	0.00	0.00	2.67
Hormosina globulifera	0.00	0.00	0.00	0.00	0.00	0.00	0.00	0.00
Indeterminate	0.00	0.00	0.00	0.00	0.00	0.00	0.00	0.00
Karreriella bradyi	7.50	13.85	1.55	12.16	5.17	7.06	4.44	2.67
Lagena cf. acuticosta	0.00	0.00	0.00	0.00	0.00	0.00	0.00	0.00
Lagena cf. interrupta	0.00	0.00	0.00	0.00	0.00	0.00	0.00	0.00
Lagena semistriata	0.00	0.00	0.00	0.00	0.00	0.00	0.00	0.00
Lagena sulcata	0.63	0.00	0.00	0.00	1.72	0.00	0.00	0.00
Melonis barleeanum	5.63	6.15	4.65	4.05	1.72	2.35	3.33	8.00
Melonis pompilioides	0.00	0.00	1.55	0.00	1.72	0.00	0.00	0.00
Nodosaria sp.	0.63	0.00	0.00	0.00	0.00	0.00	0.00	0.00
Nonionella auricula	0.00	0.00	0.00	0.00	0.00	0.00	0.00	0.00
Nonionella turgida	0.00	0.00	0.00	0.00	0.00	0.00	0.00	0.00
Nummoloculina irregularis	0.00	0.00	0.00	0.00	0.00	0.00	0.00	0.00
Oolina apiopleura	0.00	0.00	0.00	0.00	0.00	0.00	0.00	0.00
Oolina heronalleni	0.00	0.00	0.00	0.00	0.00	0.00	0.00	0.00
Oolina hexagona	0.00	0.00	0.00	0.00	1.72	1.18	0.00	0.00
Oolina intercalata	0.00	0.00	3.10	0.00	0.00	0.00	0.00	0.00
Oolina melo	0.00	0.00	0.00	0.00	0.00	0.00	0.00	0.00
Oolina squamosa	0.00	0.00	0.00	2.03	0.00	1.18	0.00	0.00
Oridorsalis umbonatus	0.00	0.00	0.00	0.00	0.00	0.00	0.00	0.00
Pseudofissurina mccullochae	0.00	0.00	0.00	0.00	0.00	0.00	0.00	0.00
Pseudosolenina borealis	0.00	0.00	0.00	0.00	0.00	0.00	0.00	0.00
Pullenia bulloides	7.50	1.54	0.00	2.03	1.72	2.35	1.11	2.67
Pullenia subcarinata	0.00	0.00	0.00	0.00	1.72	1.18	1.11	1.33
Pyrgo depressa	0.00	0.00	0.00	0.00	0.00	0.00	0.00	0.00
Pyrgo lacernula	0.00	0.00	0.00	0.00	0.00	0.00	0.00	0.00

Appendix B - Benthic foraminifera assemblage data

Core 9/97/04
Relative abundance - Benthic foraminifera 500-250um

Sample depth (cm)	60	64	68	72	76	80	84	88
Pyrgo murrhina	3.75	4.62	3.10	4.05	6.90	5.88	4.44	0.00
Pyrgo oblonga	0.00	0.00	1.55	2.03	0.00	0.00	0.00	0.00
Pyrgo rotalia	0.00	1.54	0.00	0.00	0.00	0.00	0.00	0.00
Pyrgo sarsi	0.00	4.62	1.55	2.03	0.00	0.00	0.00	0.00
Pyrgo serrata	0.00	0.00	0.00	0.00	0.00	0.00	0.00	0.00
Pyrgo sp.	0.00	0.00	0.00	0.00	0.00	0.00	0.00	0.00
Pyrgo williamsoni	0.00	0.00	0.00	0.00	0.00	0.00	0.00	0.00
Quinqueloculina arctica	3.75	0.00	3.10	0.00	0.00	0.00	0.00	2.67
Quinqueloculina bicornis	0.00	0.00	0.00	0.00	0.00	0.00	0.00	0.00
Quinqueloculina cliarensis	0.00	0.00	0.00	0.00	0.00	0.00	0.00	0.00
Quinqueloculina elongata	0.00	0.00	0.00	0.00	0.00	0.00	0.00	0.00
Quinqueloculina lata	0.00	0.00	0.00	0.00	0.00	0.00	0.00	0.00
Quinqueloculina seminulum	0.63	0.00	0.00	0.00	0.00	1.18	1.11	0.00
Quinqueloculina sp.	0.00	0.00	0.00	0.00	0.00	0.00	0.00	0.00
Quinqueloculina stalkeri	0.00	0.00	0.00	0.00	0.00	0.00	0.00	0.00
Quinqueloculina striata	0.00	0.00	0.00	0.00	0.00	0.00	0.00	0.00
Rupertina stabilis	5.63	9.23	13.95	10.14	6.90	4.71	5.56	6.67
Sigmoilopsis schlumbergeri	5.00	9.23	6.20	4.05	13.79	25.88	22.22	34.67
Siphotextularia rolhauseni	4.38	1.54	4.65	2.03	0.00	0.00	4.44	2.67
Solenina radiata	0.00	0.00	0.00	2.03	0.00	1.18	1.11	0.00
Spiroloculina limbata	0.00	0.00	0.00	0.00	0.00	0.00	0.00	0.00
Spiroloculina rotunda	1.25	3.08	1.55	2.03	0.00	0.00	1.11	0.00
Stainforthia (Fursenkoina) fusiform	0.00	0.00	0.00	0.00	0.00	0.00	0.00	0.00
Stainforthia loeblichi	0.00	0.00	0.00	0.00	0.00	0.00	0.00	0.00
Stainforthia schreibersiana	0.00	0.00	0.00	0.00	0.00	0.00	0.00	0.00
Trifarina angulosa	0.63	9.23	1.55	6.08	1.72	1.18	0.00	0.00
Trifarina bradyi	0.00	0.00	0.00	0.00	0.00	0.00	0.00	0.00
Trifarina sp.	0.00	0.00	0.00	0.00	0.00	0.00	0.00	0.00
Triloculina tricarinata	0.00	0.00	0.00	0.00	0.00	0.00	0.00	0.00
Uvigerina celtica	0.00	0.00	0.00	0.00	0.00	0.00	0.00	0.00
Uvigerina cf. pigmea	0.00	0.00	0.00	0.00	0.00	0.00	0.00	0.00
Uvigerina peregrina	0.00	0.00	0.00	0.00	0.00	0.00	0.00	0.00
Virgulina advena	0.00	0.00	0.00	0.00	0.00	0.00	0.00	0.00

Appendix B - Benthic foraminifera assemblage data

Core 9/97/14
Relative abundance - Benthic foramifera 500-250um

Sample depth (cm)	1	11	12.5	20	23	26	27.5	31	35	39	43	49	51	54	57
Alabaminella weddellensis	0.00	0.00	0.00	0.00	0.00	0.00	0.00	0.00	0.00	0.00	0.00	0.00	0.00	0.00	1.23
Amphycorina scalaris	0.00	0.00	0.00	0.00	0.00	0.00	0.00	0.00	0.00	0.00	0.00	0.00	0.00	0.00	0.00
Astacolus hyalacrulus	0.00	0.00	2.83	0.00	0.00	0.00	0.00	1.08	1.19	1.31	0.00	0.00	0.76	1.20	1.23
Astacolus sp.	0.00	0.00	0.00	0.00	0.00	0.00	0.00	0.00	0.00	0.00	0.00	0.00	0.00	0.00	0.00
Bolivina albatrossi	0.00	0.00	0.00	0.00	0.00	0.00	0.00	0.00	0.00	0.00	0.00	0.00	0.00	0.00	0.00
Bolivina pseduopunctata	0.00	0.00	0.00	0.00	0.00	0.00	0.00	0.00	0.00	0.00	0.00	0.00	0.00	0.00	0.00
Bolivina sp.	0.00	0.00	0.00	0.00	0.00	0.00	0.00	0.00	0.00	0.00	0.00	0.00	0.00	0.00	0.00
Bolivina spinescens	0.00	0.00	0.00	0.00	0.00	0.00	0.00	0.00	0.00	0.00	0.00	0.00	0.00	0.00	0.00
Bolivina subspinescens	0.00	0.00	0.00	0.00	0.00	0.00	0.00	0.00	0.00	0.00	0.00	0.00	0.00	0.00	0.00
Brizalina cf. robusta	0.00	0.00	0.00	0.00	0.00	0.00	0.00	0.00	0.00	0.00	0.00	0.00	0.00	0.00	0.00
Brizalina variabilis	0.00	0.00	0.00	0.00	0.00	0.00	0.00	0.00	0.00	0.00	0.00	0.00	0.00	0.00	0.00
Bulimina aculeata	0.00	0.00	0.00	0.00	2.82	5.56	0.00	1.81	1.19	0.65	6.11	4.00	5.34	3.61	9.88
Bullimina cf. gibba	1.23	0.00	0.00	0.98	1.41	0.93	0.00	1.44	1.19	0.98	0.00	1.33	0.76	0.00	0.00
Bulimina inflata	0.00	0.00	0.00	0.00	0.00	0.00	0.00	0.00	0.00	0.00	0.00	0.00	0.00	0.00	0.00
Bullimina marginata	0.00	0.00	0.00	0.00	0.00	0.00	0.00	0.00	0.00	0.00	3.05	0.00	0.00	0.00	0.00
Cassidulina laevigata	2.47	3.13	0.00	0.00	0.00	0.00	0.00	0.72	1.19	0.98	0.00	0.00	0.00	3.61	0.00
Cassidulina obtusa	0.00	0.00	0.00	0.00	0.00	0.00	0.00	0.00	0.00	0.00	0.00	0.00	0.00	0.00	0.00
Chilostomella oolina	0.00	0.00	0.00	0.00	1.41	0.93	0.76	0.00	0.00	0.00	0.00	0.00	0.00	0.00	0.00
Cibicides kullenbergi	0.00	0.00	0.00	1.96	0.00	0.00	0.00	3.61	2.38	3.92	9.16	4.00	6.87	1.20	0.00
Cibicides lobatulus	0.00	0.00	0.00	1.96	2.82	5.56	1.52	0.36	0.00	0.00	1.53	2.67	1.53	1.20	0.00
Cibicides pachyderma	1.23	0.00	0.00	14.71	5.63	2.78	0.00	0.00	0.00	0.00	1.53	0.00	0.76	1.20	0.00
Cibicides sp.	0.00	0.00	0.00	0.00	0.00	0.00	0.00	0.00	0.00	0.00	0.00	0.00	0.00	0.00	0.00
Cibicides wuellerstorfi	35.80	31.25	20.75	35.29	36.62	12.04	20.45	24.91	23.81	22.22	11.45	18.67	18.32	26.51	4.94
Cyclammina pusilla	0.00	0.00	0.00	0.00	0.00	0.00	3.79	0.00	0.00	0.00	0.00	0.00	0.76	0.00	0.00
Dentalina communis	0.00	0.00	0.00	0.00	0.00	0.00	0.00	0.00	0.00	0.00	0.00	0.00	0.00	0.00	0.00
Dentalina sp.	0.00	0.00	0.00	0.00	0.00	0.00	0.00	0.00	0.00	0.00	0.00	0.00	0.00	0.00	0.00
Eggerella bradyi	3.70	2.08	5.66	1.96	2.82	1.85	3.79	3.97	3.57	4.25	0.00	1.33	5.34	1.20	3.70
Ehrenbergina serrata	0.00	0.00	0.00	0.00	0.00	0.00	0.00	0.00	0.00	0.00	0.00	0.00	0.00	0.00	0.00
Epistominella exigua	0.00	6.25	8.49	0.98	4.23	9.26	11.36	9.39	9.52	9.48	0.00	1.33	0.00	1.20	0.00
Eponides pusillus	0.00	0.00	0.00	0.00	1.41	0.93	0.00	0.00	0.00	0.00	0.00	0.00	0.00	0.00	0.00
Fissurina marginata	1.23	0.00	0.00	0.00	1.41	2.78	0.00	0.00	0.00	0.00	0.00	1.33	0.00	0.00	2.47
Fissurina orbignyana	0.00	0.00	0.00	0.00	0.00	0.00	0.00	0.00	0.00	0.00	0.00	0.00	0.00	0.00	0.00
Fissurina porcupinensis	0.00	0.00	0.00	0.00	0.00	0.00	0.00	0.00	0.00	0.00	0.00	0.00	0.00	0.00	0.00

Appendix B - Benthic foraminifera assemblage data

Core 9/97/14
Relative abundance - Benthic foramifera 500-250um

Sample depth (cm)	1	11	12.5	20	23	26	27.5	31	35	39	43	49	51	54	57
Fissurina varioperforata	0.00	0.00	0.00	0.00	0.00	0.00	0.00	0.00	0.00	0.00	0.00	0.00	0.00	0.00	0.00
Fursenkoina complanata	0.00	0.00	0.00	0.00	0.00	0.00	0.00	0.00	0.00	0.00	0.00	0.00	0.00	0.00	1.23
Gavelinopsis lobatus	0.00	0.00	0.00	0.00	0.00	0.00	0.00	0.00	0.00	0.00	0.00	0.00	0.00	0.00	0.00
Globobulimina auriculata	0.00	0.00	0.00	0.00	0.00	0.00	0.00	0.00	0.00	0.00	0.00	0.00	0.00	0.00	0.00
Globobullimina affinis	0.00	0.00	0.00	0.00	0.00	0.00	0.00	0.00	0.00	0.33	1.53	0.00	0.00	0.00	1.23
Gyroidina soldanii	8.64	0.00	0.00	2.94	0.00	0.00	7.58	3.97	3.57	4.90	7.63	4.00	6.11	1.20	3.70
Hoeglundia elegans	8.64	1.04	0.00	0.00	1.41	0.93	0.76	0.00	0.00	0.00	9.16	6.67	1.53	1.20	0.00
Hormosina globulifera	0.00	0.00	0.00	0.00	0.00	0.00	0.00	0.00	0.00	0.00	0.00	0.00	0.00	0.00	0.00
Indeterminate	0.00	0.00	0.00	0.00	0.00	0.00	0.00	0.00	0.00	0.00	0.00	0.00	0.00	0.00	0.00
Karreriella bradyi	3.70	4.17	5.66	4.90	1.41	8.33	15.15	10.11	10.71	9.15	0.00	5.33	1.53	0.00	6.17
Lagena cf. acuticosta	0.00	0.00	0.00	0.00	0.00	0.00	0.00	0.00	0.00	0.00	0.00	0.00	0.00	0.00	0.00
Lagena cf. interrupta	0.00	0.00	0.00	0.00	0.00	0.00	0.00	0.00	1.19	1.31	0.00	0.00	0.00	0.00	0.00
Lagena semistriata	0.00	0.00	0.00	0.00	0.00	0.00	0.00	0.00	0.00	0.00	0.00	0.00	0.00	0.00	0.00
Lagena sulcata	0.00	1.04	2.83	0.98	0.00	0.00	0.00	0.36	0.00	0.00	0.00	0.00	0.00	0.00	1.23
Melonis barleeanum	1.23	2.08	2.83	0.00	1.41	3.70	3.79	4.69	3.57	3.59	9.16	2.67	4.58	3.61	1.23
Melonis pompilioides	0.00	14.58	16.98	3.92	2.82	1.85	3.79	0.72	3.57	4.58	4.58	0.00	0.76	2.41	0.00
Nodosaria sp.	0.00	0.00	0.00	0.00	0.00	0.00	0.00	0.00	0.00	0.00	0.00	0.00	0.00	1.20	0.00
Nonionella auricula	0.00	0.00	0.00	0.00	0.00	0.00	0.00	0.00	0.00	0.00	0.00	0.00	0.00	0.00	0.00
Nonionella turgida	0.00	0.00	0.00	0.00	0.00	0.00	0.00	0.00	0.00	0.00	0.00	0.00	0.00	0.00	0.00
Nummoloculina irregularis	0.00	0.00	0.00	0.00	0.00	0.00	0.00	0.00	0.00	0.00	0.00	0.00	0.00	0.00	0.00
Oolina apiopleura	0.00	0.00	0.00	0.00	0.00	0.00	0.00	0.00	0.00	0.00	0.00	0.00	0.00	0.00	0.00
Oolina heronalleni	0.00	0.00	0.00	0.00	0.00	0.00	0.00	0.00	0.00	0.00	0.00	0.00	0.00	0.00	0.00
Oolina hexagona	0.00	0.00	0.00	0.00	0.00	0.00	0.00	0.00	0.00	0.00	0.00	0.00	0.00	0.00	0.00
Oolina intercalata	0.00	0.00	0.00	0.00	0.00	0.00	0.00	0.00	0.00	0.00	0.00	0.00	0.00	0.00	0.00
Oolina melo	0.00	0.00	0.00	0.00	0.00	0.00	0.00	0.00	0.00	0.00	0.00	0.00	0.00	0.00	0.00
Oolina squamosa	0.00	0.00	0.00	0.00	0.00	0.00	0.00	0.00	0.00	0.00	0.00	0.00	0.76	0.00	0.00
Oridorsalis umbonatus	0.00	0.00	0.00	0.00	0.00	0.00	0.00	0.00	0.00	0.00	0.00	0.00	0.00	0.00	0.00
Pseudofissurina mccullochae	0.00	0.00	0.00	0.98	1.41	0.00	0.00	1.08	1.19	0.65	1.53	0.00	0.76	0.00	2.47
Pseudosolenina borealis	0.00	0.00	0.00	0.00	0.00	0.00	0.00	0.00	0.00	0.00	0.00	0.00	0.00	0.00	0.00
Pullenia bulloides	1.23	11.46	8.49	9.80	16.90	21.30	15.15	10.47	9.52	8.82	3.05	8.00	6.11	12.05	17.28
Pullenia subcarinata	1.23	2.08	2.83	0.98	1.41	2.78	0.00	1.81	1.19	0.00	1.53	1.33	1.53	2.41	0.00
Pyrgo depressa	0.00	0.00	0.00	0.00	0.00	0.00	0.00	0.00	0.00	0.00	0.00	0.00	0.00	0.00	0.00
Pyrgo lacemula	0.00	0.00	0.00	0.00	0.00	0.00	0.00	0.00	0.00	0.00	0.00	0.00	0.00	0.00	0.00

Appendix B - Benthic foraminifera assemblage data

Core 9/97/14
Relative abundance - Benthic foramifera 500-250um

Sample depth (cm)	1	11	12.5	20	23	26	27.5	31	35	39	43	49	51	54	57
Pyrgo murrhina	6.17	0.00	0.00	2.94	1.41	1.85	0.76	4.69	3.57	3.27	3.05	5.33	3.05	6.02	4.94
Pyrgo oblonga	0.00	0.00	0.00	0.00	0.00	0.00	0.00	0.00	0.00	0.00	0.00	0.00	0.00	1.20	0.00
Pyrgo rotalia	0.00	0.00	0.00	0.00	0.00	0.00	0.00	0.00	0.00	0.00	0.00	0.00	0.00	0.00	0.00
Pyrgo sarsi	0.00	0.00	0.00	0.00	0.00	0.00	0.00	0.00	0.00	0.00	0.00	0.00	0.00	0.00	0.00
Pyrgo serrata	0.00	0.00	0.00	0.00	0.00	0.00	0.00	0.00	0.00	0.00	0.00	0.00	0.00	0.00	0.00
Pyrgo sp.	0.00	0.00	0.00	0.00	0.00	0.00	0.00	0.00	0.00	0.00	0.00	0.00	0.00	0.00	0.00
Pyrgo williamsoni	0.00	0.00	0.00	0.00	0.00	0.00	0.00	0.00	0.00	0.00	0.00	1.33	0.00	0.00	0.00
Quinqueloculina arctica	0.00	13.54	14.15	0.00	0.00	0.00	0.00	0.00	0.00	0.00	0.00	1.33	0.00	0.00	0.00
Quinqueloculina bicornis	0.00	0.00	0.00	0.00	0.00	0.00	0.00	0.00	0.00	0.00	0.00	0.00	0.00	0.00	0.00
Quinqueloculina cliarensis	0.00	0.00	0.00	0.00	0.00	0.00	0.00	0.00	0.00	0.00	0.00	0.00	0.00	0.00	0.00
Quinqueloculina elongata	0.00	0.00	0.00	0.00	0.00	0.00	0.00	0.00	0.00	0.00	0.00	0.00	0.00	0.00	0.00
Quinqueloculina lata	0.00	0.00	0.00	0.00	0.00	0.00	0.00	0.00	0.00	0.00	0.00	0.00	0.00	0.00	0.00
Quinqueloculina seminulum	1.23	5.21	2.83	2.94	0.00	0.00	0.00	0.00	0.00	0.00	0.00	1.33	0.00	0.00	0.00
Quinqueloculina sp.	0.00	0.00	0.00	0.00	0.00	0.00	0.00	0.00	0.00	0.00	0.00	0.00	0.00	0.00	0.00
Quinqueloculina stalkeri	0.00	0.00	0.00	0.00	0.00	0.00	0.00	0.00	0.00	0.00	0.00	0.00	0.00	0.00	0.00
Quinqueloculina striata	0.00	0.00	0.00	0.00	0.00	0.00	0.00	0.00	0.00	0.00	0.00	0.00	0.00	0.00	0.00
Rupertina stabilis	4.94	0.00	0.00	1.96	0.00	0.00	3.79	0.00	0.00	0.65	1.53	2.67	1.53	2.41	8.64
Sigmoilopsis schlumbergeri	16.05	1.04	2.83	7.84	8.45	11.11	7.58	13.36	11.90	12.09	22.90	24.00	29.77	19.28	16.05
Siphotextularia rolhauseni	1.23	0.00	0.00	1.96	2.82	5.56	0.00	0.00	5.95	6.86	1.53	0.00	0.76	3.61	1.23
Solenina radiata	0.00	0.00	0.00	0.00	0.00	0.00	0.00	0.00	0.00	0.00	0.00	0.00	0.00	0.00	0.00
Spiroloculina limbata	0.00	0.00	0.00	0.00	0.00	0.00	0.00	0.00	0.00	0.00	0.00	0.00	0.00	0.00	0.00
Spiroloculina rotunda	0.00	0.00	0.00	0.00	0.00	0.00	0.00	0.00	0.00	0.00	0.00	0.00	0.00	0.00	0.00
Stainforthia (Fursenkoina) fusiform	0.00	0.00	0.00	0.00	0.00	0.00	0.00	0.00	0.00	0.00	0.00	0.00	0.00	0.00	0.00
Stainforthia loeblichi	0.00	0.00	0.00	0.00	0.00	0.00	0.00	0.00	0.00	0.00	0.00	0.00	0.00	0.00	0.00
Stainforthia schreibersiana	0.00	0.00	0.00	0.00	0.00	0.00	0.00	0.00	0.00	0.00	0.00	0.00	0.00	0.00	0.00
Trifarina angulosa	0.00	0.00	0.00	0.00	0.00	0.00	0.00	1.44	0.00	0.00	0.00	0.00	0.00	0.00	0.00
Trifarina bradyi	0.00	0.00	0.00	0.00	0.00	0.00	0.00	0.00	0.00	0.00	0.00	0.00	0.00	0.00	0.00
Trifarina sp.	0.00	0.00	0.00	0.00	0.00	0.00	0.00	0.00	0.00	0.00	0.00	0.00	0.00	0.00	0.00
Triloculina tricarinata	0.00	0.00	0.00	0.00	0.00	0.00	0.00	0.00	0.00	0.00	0.00	0.00	0.00	0.00	0.00
Uvigerina celtica	0.00	0.00	0.00	0.00	0.00	0.00	0.00	0.00	0.00	0.00	0.00	0.00	0.00	0.00	8.64
Uvigerina cf. pigmea	0.00	0.00	0.00	0.00	0.00	0.00	0.00	0.00	0.00	0.00	0.00	0.00	0.00	0.00	0.00
Uvigerina peregrina	0.00	0.00	0.00	0.00	0.00	0.00	0.00	0.00	0.00	0.00	0.00	0.00	0.76	2.41	0.00
Virgulina advena	0.00	1.04	2.83	0.00	0.00	0.00	0.00	0.00	0.00	0.00	0.00	0.00	0.00	0.00	1.23

Appendix B - Benthic foraminifera assemblage data

Core 9/97/14
Relative abundance - Benthic foramifera 500-250um

Sample depth (cm)	62	77	78	81	84	87	90	93
Alabaminella weddellensis	0.00	0.00	0.00	0.00	0.00	2.04	0.00	0.00
Amphycorina scalaris	0.00	0.00	0.00	0.00	1.29	0.00	0.00	0.00
Astacolus hyalacrulus	0.00	0.00	0.00	0.00	1.29	0.00	0.00	0.00
Astacolus sp.	0.00	0.00	0.00	0.00	0.00	0.00	0.00	0.00
Bolivina albatrossi	0.00	0.00	0.00	0.00	0.00	0.00	0.00	0.47
Bolivina pseduopunctata	0.00	0.00	0.00	0.00	0.00	0.00	0.00	0.00
Bolivina sp.	0.00	0.00	0.00	0.00	0.00	0.00	0.00	0.00
Bolivina spinescens	0.00	0.00	0.00	0.00	0.00	0.00	0.00	0.00
Bolivina subspinescens	0.00	0.00	0.00	0.00	0.00	2.04	0.00	0.00
Brizalina cf. robusta	0.00	0.00	0.00	0.00	0.00	0.00	0.00	0.00
Brizalina variabilis	0.00	0.00	0.00	0.00	0.00	0.00	0.00	0.00
Bulimina aculeata	15.25	0.00	0.00	0.00	0.00	6.12	6.38	3.27
Bullimina cf. gibba	0.00	1.92	0.00	0.00	1.29	0.00	0.00	0.00
Bulimina inflata	0.00	0.00	0.00	0.00	0.00	0.00	0.00	0.00
Bullimina marginata	0.00	0.00	0.00	0.00	0.00	4.08	1.06	0.93
Cassidulina laevigata	1.69	0.00	1.39	1.69	0.00	2.04	1.06	0.00
Cassidulina obtusa	0.00	0.00	0.00	0.00	0.00	0.00	0.00	0.00
Chilostomella oolina	0.00	0.00	0.00	0.00	0.00	0.00	0.00	0.00
Cibicides kullenbergi	1.69	0.00	4.86	5.08	2.58	4.08	1.06	2.80
Cibicides lobatulus	0.00	0.00	0.00	0.00	0.00	0.00	0.00	0.00
Cibicides pachyderma	0.00	0.00	2.78	6.78	0.00	2.04	0.00	1.40
Cibicides sp.	0.00	0.00	0.00	0.00	0.00	0.00	0.00	0.00
Cibicides wuellerstorfi	20.34	3.85	4.86	11.86	14.59	24.49	36.17	35.05
Cyclammina pusilla	0.00	0.00	0.00	0.00	0.00	0.00	0.00	0.00
Dentalina communis	0.00	0.00	0.00	0.00	0.00	0.00	0.00	0.00
Dentalina sp.	0.00	0.00	0.00	0.00	0.00	0.00	0.00	0.00
Eggerella bradyi	1.69	7.69	3.47	10.17	9.01	2.04	1.06	0.47
Ehrenbergina serrata	0.00	0.00	0.00	0.00	0.00	0.00	0.00	0.00
Epistominella exigua	0.00	5.77	6.94	5.08	6.44	4.08	0.00	9.35
Eponides pusillus	0.00	0.00	0.00	0.00	0.00	0.00	0.00	0.00
Fissurina marginata	0.00	0.00	0.00	0.00	0.00	4.08	0.00	0.00
Fissurina orbignyana	0.00	0.00	0.00	0.00	1.29	0.00	0.00	0.00
Fissurina porcupinensis	0.00	0.00	0.00	0.00	0.00	0.00	0.00	0.00

Appendix B - Benthic foraminifera assemblage data

Core 9/97/14
Relative abundance - Benthic foramifera 500-250um

Sample depth (cm)	62	77	78	81	84	87	90	93
Fissurina varioperforata	0.00	0.00	0.00	0.00	0.00	0.00	0.00	0.00
Fursenkoina complanata	0.00	0.00	0.00	0.00	0.00	0.00	0.00	0.00
Gavelinopsis lobatus	0.00	0.00	0.00	0.00	0.00	0.00	0.00	0.00
Globobulimina auriculata	0.00	0.00	0.00	0.00	0.00	0.00	0.00	0.00
Globobullimina affinis	0.00	0.00	0.00	0.00	0.00	2.04	0.00	0.00
Gyroidina soldanii	3.39	1.92	2.78	1.69	0.00	0.00	2.13	3.27
Hoeglundia elegans	0.00	0.00	8.33	6.78	15.45	2.04	2.13	4.67
Hormosina globulifera	0.00	0.00	0.00	0.00	0.00	0.00	0.00	0.00
Indeterminate	0.00	0.00	0.00	0.00	0.00	0.00	0.00	0.00
Karreriella bradyi	0.00	5.77	4.86	5.08	2.58	2.04	3.19	1.87
Lagena cf. acuticosta	0.00	0.00	0.00	0.00	0.00	0.00	0.00	0.00
Lagena cf. interrupta	0.00	0.00	0.00	0.00	0.00	0.00	0.00	0.00
Lagena semistriata	0.00	0.00	0.00	0.00	0.00	0.00	0.00	0.00
Lagena sulcata	0.00	1.92	0.00	0.00	0.00	0.00	0.00	0.00
Melonis barleeanum	5.08	17.31	2.78	0.00	0.00	0.00	1.06	3.27
Melonis pompilioides	1.69	3.85	2.08	1.69	2.58	4.08	3.19	1.40
Nodosaria sp.	0.00	0.00	0.00	0.00	0.00	0.00	0.00	0.00
Nonionella auricula	0.00	0.00	0.00	0.00	0.00	0.00	0.00	0.00
Nonionella turgida	0.00	0.00	0.00	0.00	0.00	0.00	0.00	0.00
Nummoloculina irregularis	0.00	0.00	0.00	0.00	0.00	0.00	0.00	0.00
Oolina apiopleura	0.00	0.00	0.00	0.00	0.00	0.00	0.00	0.00
Oolina heronalleni	0.00	0.00	0.00	0.00	0.00	0.00	0.00	0.00
Oolina hexagona	0.00	0.00	0.00	0.00	0.00	0.00	0.00	0.00
Oolina intercalata	0.00	0.00	0.00	0.00	0.00	0.00	0.00	0.00
Oolina melo	0.00	0.00	0.00	0.00	0.00	0.00	0.00	0.00
Oolina squamosa	0.00	0.00	0.00	0.00	0.00	0.00	0.00	0.00
Oridorsalis umbonatus	0.00	0.00	0.00	0.00	0.00	0.00	0.00	0.00
Pseudofissurina mccullochae	1.69	0.00	0.00	0.00	0.00	0.00	0.00	0.00
Pseudosolenina borealis	0.00	0.00	0.00	0.00	0.00	0.00	0.00	0.00
Pullenia bulloides	6.78	19.23	15.28	10.17	2.58	12.24	2.13	4.67
Pullenia subcarinata	3.39	0.00	0.00	0.00	1.29	2.04	7.45	1.87
Pyrgo depressa	0.00	0.00	0.00	0.00	0.00	0.00	0.00	0.00
Pyrgo lacernula	0.00	0.00	0.00	0.00	0.00	0.00	0.00	0.00

Appendix B - Benthic foraminifera assemblage data

Core 9/97/14
Relative abundance - Benthic foramifera 500-250um

Sample depth (cm)	62	77	78	81	84	87	90	93
Pyrgo murrhina	0.00	1.92	2.08	1.69	3.86	0.00	0.00	3.27
Pyrgo oblonga	0.00	0.00	0.00	0.00	0.00	0.00	0.00	0.93
Pyrgo rotalia	0.00	0.00	0.00	0.00	0.00	0.00	0.00	0.00
Pyrgo sarsi	0.00	0.00	0.00	0.00	0.00	0.00	1.06	2.34
Pyrgo serrata	0.00	0.00	0.00	0.00	0.00	0.00	0.00	0.00
Pyrgo sp.	0.00	0.00	0.00	0.00	0.00	0.00	0.00	0.00
Pyrgo williamsoni	0.00	1.92	0.69	0.00	0.00	0.00	0.00	2.34
Quinqueloculina arctica	1.69	0.00	0.00	0.00	0.00	2.04	0.00	0.00
Quinqueloculina bicornis	0.00	0.00	0.00	0.00	0.00	0.00	0.00	0.00
Quinqueloculina cliarensis	0.00	0.00	0.00	0.00	0.00	0.00	0.00	0.00
Quinqueloculina elongata	0.00	0.00	0.00	0.00	0.00	0.00	0.00	0.00
Quinqueloculina lata	0.00	0.00	0.00	0.00	0.00	0.00	0.00	0.00
Quinqueloculina seminulum	0.00	0.00	0.00	0.00	0.00	0.00	0.00	0.00
Quinqueloculina sp.	0.00	0.00	0.00	0.00	0.00	0.00	0.00	0.00
Quinqueloculina stalkeri	0.00	0.00	0.00	0.00	0.00	0.00	0.00	0.00
Quinqueloculina striata	0.00	0.00	0.00	0.00	0.00	0.00	0.00	0.00
Rupertina stabilis	5.08	0.00	0.00	0.00	0.00	0.00	1.06	3.27
Sigmoilopsis schlumbergeri	13.56	25.00	26.39	20.34	29.61	12.24	24.47	10.28
Siphotextularia rolhauseni	1.69	0.00	0.00	0.00	1.29	2.04	0.00	0.00
Solenina radiata	3.39	0.00	0.00	0.00	0.00	2.04	0.00	0.00
Spiroloculina limbata	0.00	0.00	0.00	0.00	0.43	0.00	0.00	0.00
Spiroloculina rotunda	0.00	0.00	0.00	0.00	0.00	0.00	0.00	0.00
Stainforthia (Fursenkoina) fusiform	0.00	0.00	0.00	0.00	0.00	0.00	0.00	0.00
Stainforthia loeblichi	0.00	0.00	0.00	0.00	0.00	0.00	0.00	0.00
Stainforthia schreibersiana	0.00	0.00	0.00	0.00	0.00	0.00	0.00	0.00
Trifarina angulosa	0.00	0.00	0.00	0.00	0.00	0.00	0.00	0.00
Trifarina bradyi	0.00	0.00	0.00	0.00	0.00	0.00	0.00	0.00
Trifarina sp.	0.00	0.00	0.00	0.00	0.00	0.00	0.00	0.00
Triloculina tricarinata	0.00	0.00	0.00	0.00	0.00	0.00	1.06	0.00
Uvigerina celtica	0.00	1.92	10.42	10.17	2.58	0.00	3.19	0.93
Uvigerina cf. pigmea	0.00	0.00	0.00	0.00	0.00	0.00	0.00	0.00
Uvigerina peregrina	8.47	0.00	0.00	1.69	0.00	0.00	1.06	1.40
Virgulina advena	0.00	0.00	0.00	0.00	0.00	0.00	0.00	0.00

Appendix B - Benthic foraminifera assemblage data

Core 9/97-08
Relative abundance - Benthic foraminifera 250-63um

Sample depth (cm)	3	7	11	15	19	23	27	31	35
Alabaminella weddellensis	0.00	0.00	3.68	4.23	8.72	3.51	0.00	1.74	0.00
Amphycorina scalaris	0.00	0.00	0.00	0.00	0.00	0.00	0.00	0.00	1.96
Astacolus hyalacrulus	0.00	0.00	0.00	0.00	0.00	0.00	0.00	0.00	1.96
Astacolus sp.	0.00	0.00	0.00	0.00	0.00	0.00	0.00	0.00	0.00
Bolivina albatrossi	0.00	0.00	0.00	0.00	0.00	2.63	0.00	0.00	1.96
Bolivina pseduopunctata	0.00	1.00	0.53	0.94	0.00	0.00	0.00	0.00	0.00
Bolivina sp.	0.00	0.00	0.00	0.00	0.00	0.00	0.00	0.00	0.00
Bolivina spinescens	0.00	6.00	3.16	1.88	0.00	0.00	0.00	0.00	0.00
Bolivina subspinescens	2.06	3.00	0.53	0.94	3.36	1.75	3.06	3.48	0.00
Brizalina cf. robusta	0.00	0.00	0.00	0.00	0.00	0.88	0.00	0.00	0.00
Brizalina variabilis	0.00	0.00	0.00	0.00	0.00	0.00	0.00	0.00	0.00
Bulimina aculeata	0.00	0.00	0.00	0.00	0.00	7.02	0.00	0.00	0.00
Bullimina cf. gibba	0.00	0.00	0.00	0.00	0.00	0.00	0.00	0.00	0.00
Bulimina inflata	0.00	0.00	0.00	0.00	0.00	0.00	0.00	0.00	5.88
Bullimina marginata	0.00	0.00	1.05	0.00	0.00	11.40	0.00	0.00	7.84
Cassidulina laevigata	59.79	17.00	40.00	35.21	44.97	21.05	4.08	60.00	1.96
Cassidulina obtusa	0.00	0.00	0.00	0.00	0.00	0.00	0.00	0.00	0.00
Chilostomella oolina	0.00	0.00	0.00	0.00	0.00	0.00	0.00	0.00	0.00
Cibicides kullenbergi	0.00	11.00	7.37	5.63	0.67	3.51	3.06	0.00	0.00
Cibicides lobatulus	0.00	0.00	0.00	0.00	0.00	0.88	2.04	0.00	0.00
Cibicides pachyderma	0.00	1.00	0.00	1.41	0.00	0.88	3.06	0.00	0.00
Cibicides sp.	0.00	0.00	0.00	0.00	0.00	0.00	0.00	0.00	0.00
Cibicides wuellerstorfi	0.00	0.00	0.53	0.47	0.67	1.75	6.12	0.00	3.92
Cyclammina pusilla	0.00	0.00	0.00	0.00	0.00	0.00	0.00	0.00	0.00
Dentalina communis	0.00	0.00	0.00	0.00	0.00	0.00	0.00	0.00	0.00
Dentalina sp.	0.00	0.00	0.00	0.00	0.00	0.00	0.00	0.00	0.00
Eggerella bradyi	0.00	0.00	0.00	0.00	0.00	0.00	0.00	0.00	0.00
Ehrenbergina serrata	0.00	0.00	0.00	0.00	0.00	0.00	0.00	0.00	0.00
Epistominella exigua	14.43	18.00	10.53	6.10	3.36	2.63	4.08	2.61	5.88
Eponides pusillus	0.00	0.00	0.00	0.00	0.00	0.00	0.00	0.00	0.00
Fissurina marginata	0.00	3.00	1.58	5.63	6.04	0.00	0.00	0.00	1.96
Fissurina orbignyana	0.00	0.00	0.00	0.00	0.00	0.00	0.00	0.00	0.00
Fissurina porcupinensis	0.00	0.00	0.00	0.00	0.00	0.00	0.00	0.00	0.00
Fissurina varioperforata	0.00	0.00	0.00	0.00	0.00	0.00	0.00	0.00	0.00
Fursenkoina complanata	0.00	0.00	0.00	0.00	0.00	0.00	0.00	0.00	0.00
Gavelinopsis lobatus	0.00	0.00	0.00	0.00	0.00	0.00	0.00	0.00	0.00
Globobulimina auriculata	0.00	0.00	0.00	0.00	0.00	0.00	0.00	0.00	0.00
Globobullimina affinis	0.00	0.00	0.00	0.00	0.00	0.00	0.00	0.00	0.00
Gyroidina soldanii	0.00	0.00	0.53	0.00	2.01	0.00	0.00	0.00	0.00
Hoeglundia elegans	0.00	0.00	0.00	0.00	0.00	0.00	0.00	0.00	0.00
Hormosina globulifera	0.00	0.00	0.00	0.00	0.00	0.00	0.00	0.00	0.00
Indeterminate	0.00	0.00	0.00	0.00	0.00	0.00	0.00	0.00	0.00
Karreriella bradyi	0.00	0.00	0.00	0.94	0.00	0.00	0.00	0.00	0.00
Lagena cf. acuticosta	0.00	0.00	0.00	0.00	0.00	0.00	0.00	0.00	0.00
Lagena cf. interrupta	0.00	0.00	0.00	0.00	0.00	0.00	0.00	0.00	0.00
Lagena semistriata	0.00	0.00	0.00	0.00	0.00	0.00	0.00	0.00	0.00

Appendix B - Benthic foraminifera assemblage data

Core 9/97-08
Relative abundance - Benthic foraminifera 250-63um

Sample depth (cm)	3	7	11	15	19	23	27	31	35
Lagena sulcata	0.00	0.00	0.00	0.00	0.00	0.00	0.00	0.00	0.00
Melonis barleeanum	16.49	7.00	8.42	9.39	12.08	12.28	24.49	23.48	17.65
Melonis pompilioides	0.00	0.00	0.00	0.00	0.00	0.00	0.00	0.00	0.00
Nodosaria sp.	0.00	0.00	0.00	0.00	0.00	0.00	0.00	0.00	0.00
Nonionella auricula	0.00	0.00	0.00	0.00	0.00	0.00	0.00	0.00	0.00
Nonionella turgida	0.00	0.00	0.00	0.00	0.00	0.00	0.00	0.00	0.00
Nummoloculina irregularis	0.00	0.00	0.00	0.00	0.00	0.00	0.00	0.00	0.00
Oolina apiopleura	0.00	0.00	0.00	0.00	0.00	0.00	0.00	0.00	0.00
Oolina heronalleni	0.00	0.00	0.00	0.00	0.00	0.00	0.00	0.00	0.00
Oolina hexagona	0.00	0.00	0.00	0.00	0.00	0.88	0.00	0.00	1.96
Oolina intercalata	0.00	0.00	0.00	0.00	0.00	0.00	0.00	0.00	0.00
Oolina melo	0.00	1.00	0.53	0.94	0.00	0.00	0.00	0.00	0.00
Oolina squamosa	0.00	0.00	0.00	0.00	0.00	0.00	0.00	0.00	0.00
Oridorsalis umbonatus	0.00	0.00	0.00	0.00	0.00	0.00	0.00	0.00	0.00
Pseudofissurina mccullochae	0.00	0.00	0.00	0.00	0.00	0.00	0.00	0.00	0.00
Pseudosolenina borealis	0.00	0.00	0.00	0.00	0.00	0.00	0.00	0.00	0.00
Pullenia bulloides	0.00	7.00	5.26	7.51	6.04	0.00	9.18	0.00	0.00
Pullenia subcarinata	0.00	0.00	0.00	0.47	0.00	0.88	0.00	0.87	1.96
Pyrgo depressa	0.00	0.00	0.00	0.00	0.00	0.00	0.00	0.00	0.00
Pyrgo lacernula	0.00	0.00	0.00	0.00	0.00	0.00	0.00	0.00	0.00
Pyrgo murrhina	0.00	0.00	0.00	0.00	0.00	0.00	0.00	0.00	0.00
Pyrgo oblonga	0.00	0.00	0.00	0.00	0.00	0.00	0.00	0.00	0.00
Pyrgo rotalia	0.00	0.00	0.00	0.00	0.00	0.00	0.00	0.00	0.00
Pyrgo sarsi	0.00	0.00	0.00	0.00	0.00	0.00	0.00	0.00	0.00
Pyrgo serrata	0.00	0.00	0.00	0.00	0.00	0.00	0.00	0.00	0.00
Pyrgo sp.	0.00	0.00	0.00	0.00	0.00	0.00	0.00	0.00	0.00
Pyrgo williamsoni	0.00	0.00	0.00	0.00	0.00	0.00	0.00	0.00	0.00
Quinqueloculina arctica	0.00	0.00	0.00	0.00	0.67	0.00	0.00	0.00	1.96
Quinqueloculina bicornis	0.00	0.00	0.00	0.00	0.00	0.00	0.00	0.00	0.00
Quinqueloculina cliarensis	0.00	1.00	0.53	0.00	0.00	0.00	0.00	0.00	0.00
Quinqueloculina elongata	0.00	1.00	0.53	0.00	0.00	0.00	0.00	0.00	0.00
Quinqueloculina lata	0.00	0.00	0.00	0.00	0.00	0.00	0.00	0.00	0.00
Quinqueloculina seminulum	0.00	0.00	0.53	0.94	1.34	5.26	1.02	0.87	3.92
Quinqueloculina sp.	0.00	0.00	0.00	0.00	0.00	0.00	0.00	0.00	0.00
Quinqueloculina stalkeri	0.00	1.00	0.00	0.00	0.00	0.00	0.00	0.00	0.00
Quinqueloculina striata	0.00	1.00	0.53	0.47	0.00	0.00	1.02	0.00	0.00
Rupertina stabilis	0.00	0.00	0.00	0.00	0.00	0.00	0.00	0.00	0.00
Sigmoilopsis schlumbergeri	0.00	3.00	1.58	2.35	0.00	3.51	0.00	1.74	9.80
Siphotextularia rolhauseni	0.00	0.00	0.00	0.00	0.00	0.00	0.00	0.00	0.00
Solenina radiata	0.00	0.00	0.00	0.00	0.00	0.00	0.00	0.00	0.00
Spiroloculina limbata	0.00	0.00	0.00	0.00	0.00	0.00	0.00	0.00	0.00
Spiroloculina rotunda	0.00	2.00	1.05	0.94	0.00	0.00	1.02	0.00	0.00
Stainforthia (Fursenkoina) fusiformis	0.00	0.00	0.00	0.00	0.00	0.00	0.00	0.00	0.00
Stainforthia loeblichi	0.00	1.00	0.53	0.00	0.00	0.00	0.00	0.00	0.00
Stainforthia schreibersiana	0.00	0.00	0.00	0.00	0.00	0.00	0.00	0.00	0.00
Trifarina angulosa	7.22	10.00	8.95	10.33	9.40	4.39	30.61	5.22	21.57

Appendix B - Benthic foraminifera assemblage data

Core 9/97-08
Relative abundance - Benthic foraminifera 250-63um

Sample depth (cm)	3	7	11	15	19	23	27	31	35
Trifarina bradyi	0.00	0.00	0.00	0.00	0.00	0.00	0.00	0.00	0.00
Trifarina sp.	0.00	0.00	0.00	0.00	0.00	0.00	0.00	0.00	0.00
Triloculina tricarinata	0.00	1.00	0.53	0.47	0.00	0.00	0.00	0.00	0.00
Uvigerina celtica	0.00	0.00	0.00	0.00	0.00	0.00	0.00	0.00	0.00
Uvigerina cf. pigmea	0.00	0.00	0.00	0.00	0.00	0.00	0.00	0.00	0.00
Uvigerina peregrina	0.00	4.00	1.58	2.82	0.67	14.91	7.14	0.00	7.84
Virgulina advena	0.00	0.00	0.00	0.00	0.00	0.00	0.00	0.00	0.00

Appendix B - Benthic foraminifera assemblage data

Core 9/97-08
Relative abundance - Benthic foraminifera 250-63um

Sample depth (cm)	39	43	47.5	51.5	55.5	59.5	63.5	76	80
Alabaminella weddellensis	3.77	1.00	0.00	0.00	0.00	5.31	0.00	0.00	0.00
Amphycorina scalaris	0.00	0.00	0.00	0.00	0.00	0.00	0.00	0.00	0.00
Astacolus hyalacrulus	0.00	0.00	0.00	0.00	0.00	0.00	0.00	0.00	0.00
Astacolus sp.	0.00	0.00	0.00	0.00	0.00	0.00	0.00	0.00	0.00
Bolivina albatrossi	0.00	3.00	5.50	0.00	0.00	1.77	2.22	12.20	18.00
Bolivina pseduopunctata	0.00	0.00	0.00	0.00	0.00	0.00	0.00	0.00	0.00
Bolivina sp.	0.00	0.00	0.00	0.00	0.00	0.00	0.00	2.44	1.00
Bolivina spinescens	0.00	0.00	0.00	0.00	0.00	0.00	0.00	1.22	3.00
Bolivina subspinescens	0.00	2.00	1.83	0.00	1.43	2.65	0.00	0.00	0.00
Brizalina cf. robusta	0.00	1.00	0.92	0.00	0.00	0.00	0.00	0.00	0.00
Brizalina variabilis	0.00	0.00	0.00	0.00	0.00	0.00	0.00	0.00	0.00
Bulimina aculeata	0.00	6.00	4.59	0.00	0.00	6.19	0.00	0.00	0.00
Bullimina cf. gibba	0.00	0.00	0.00	0.00	0.00	0.00	0.00	0.00	0.00
Bulimina inflata	0.00	1.00	0.00	0.00	0.00	0.88	1.11	0.00	0.00
Bullimina marginata	0.00	13.00	15.60	2.22	0.00	7.08	0.00	0.00	0.00
Cassidulina laevigata	28.30	6.00	4.59	2.22	52.86	25.66	3.33	15.85	13.00
Cassidulina obtusa	0.00	0.00	0.00	0.00	0.00	0.00	0.00	0.00	0.00
Chilostomella oolina	0.00	0.00	0.00	0.00	0.00	0.00	0.00	0.00	0.00
Cibicides kullenbergi	1.89	11.00	4.59	6.67	1.43	0.00	15.56	10.98	6.00
Cibicides lobatulus	0.00	1.00	0.92	0.00	0.00	2.65	0.00	0.00	1.00
Cibicides pachyderma	0.00	4.00	0.92	0.00	0.00	2.65	5.56	4.88	6.00
Cibicides sp.	0.00	0.00	0.00	0.00	0.00	0.00	0.00	0.00	0.00
Cibicides wuellerstorfi	0.00	2.00	0.92	4.44	0.00	0.00	7.78	0.00	5.00
Cyclammina pusilla	0.00	0.00	0.92	0.00	0.00	0.00	0.00	0.00	0.00
Dentalina communis	0.00	0.00	0.00	0.00	0.00	0.00	0.00	0.00	0.00
Dentalina sp.	0.00	0.00	0.00	0.00	0.00	0.00	0.00	0.00	0.00
Eggerella bradyi	0.00	0.00	0.92	0.00	0.00	0.00	0.00	1.22	2.00
Ehrenbergina serrata	0.00	0.00	0.00	0.00	0.00	0.00	0.00	0.00	0.00
Epistominella exigua	0.00	3.00	7.34	4.44	5.71	6.19	1.11	3.66	6.00
Eponides pusillus	0.00	0.00	0.00	0.00	0.00	0.00	1.11	0.00	0.00
Fissurina marginata	0.00	0.00	0.00	0.00	0.00	0.00	1.11	1.22	1.00
Fissurina orbignyana	0.00	0.00	0.00	0.00	0.00	0.00	0.00	0.00	0.00
Fissurina porcupinensis	0.00	0.00	0.00	0.00	0.00	0.00	0.00	0.00	0.00
Fissurina varioperforata	0.00	0.00	0.00	0.00	0.00	0.00	0.00	0.00	0.00
Fursenkoina complanata	0.00	0.00	0.00	0.00	0.00	0.00	0.00	0.00	0.00
Gavelinopsis lobatus	0.00	0.00	0.00	0.00	0.00	0.00	0.00	0.00	0.00
Globobulimina auriculata	0.00	0.00	0.00	0.00	0.00	0.00	0.00	0.00	0.00
Globobullimina affinis	0.00	0.00	0.00	0.00	0.00	0.00	0.00	0.00	0.00
Gyroidina soldanii	0.00	1.00	0.00	0.00	0.00	0.88	2.22	2.44	1.00
Hoeglundia elegans	0.00	0.00	0.00	0.00	0.00	0.00	2.22	0.00	1.00
Hormosina globulifera	0.00	0.00	0.00	0.00	0.00	0.00	0.00	0.00	0.00
Indeterminate	0.00	0.00	0.00	0.00	0.00	0.00	0.00	0.00	0.00
Karreriella bradyi	0.00	0.00	0.00	0.00	0.00	0.00	0.00	0.00	0.00
Lagena cf. acuticosta	0.00	0.00	0.00	0.00	0.00	0.00	0.00	0.00	0.00
Lagena cf. interrupta	0.00	0.00	0.00	0.00	0.00	0.00	0.00	0.00	0.00
Lagena semistriata	0.00	0.00	0.00	0.00	0.00	0.00	0.00	0.00	0.00

Appendix B - Benthic foraminifera assemblage data

Core 9/97-08
Relative abundance - Benthic foraminifera 250-63um

Sample depth (cm)	39	43	47.5	51.5	55.5	59.5	63.5	76	80
Lagena sulcata	0.00	0.00	0.00	0.00	0.00	0.00	0.00	0.00	0.00
Melonis barleeanum	1.89	14.00	16.51	13.33	10.00	7.96	14.44	23.17	13.00
Melonis pompilioides	0.00	0.00	0.00	0.00	0.00	0.00	0.00	0.00	0.00
Nodosaria sp.	0.00	0.00	0.00	2.22	0.00	0.00	0.00	0.00	0.00
Nonionella auricula	0.00	0.00	0.00	0.00	0.00	0.00	0.00	0.00	0.00
Nonionella turgida	0.00	0.00	0.00	0.00	0.00	0.00	0.00	0.00	0.00
Nummoloculina irregularis	0.00	0.00	0.00	0.00	0.00	0.00	0.00	0.00	0.00
Oolina apiopleura	0.00	0.00	0.00	0.00	0.00	0.00	0.00	0.00	0.00
Oolina heronalleni	0.00	0.00	0.00	0.00	0.00	0.00	0.00	0.00	0.00
Oolina hexagona	0.00	1.00	0.92	0.00	0.00	0.88	0.00	0.00	0.00
Oolina intercalata	0.00	0.00	0.00	0.00	0.00	0.00	1.11	3.66	1.00
Oolina melo	0.00	0.00	0.00	0.00	0.00	0.00	0.00	0.00	0.00
Oolina squamosa	0.00	0.00	0.00	0.00	0.00	0.00	0.00	0.00	0.00
Oridorsalis umbonatus	0.00	0.00	0.00	0.00	0.00	0.00	0.00	0.00	0.00
Pseudofissurina mccullochae	0.00	0.00	0.00	0.00	0.00	0.00	0.00	0.00	0.00
Pseudosolenina borealis	0.00	0.00	0.00	0.00	0.00	0.00	0.00	0.00	0.00
Pullenia bulloides	0.00	0.00	0.92	2.22	0.00	0.00	1.11	3.66	3.00
Pullenia subcarinata	0.00	1.00	1.83	0.00	0.00	1.77	0.00	0.00	0.00
Pyrgo depressa	0.00	0.00	0.00	0.00	0.00	0.00	0.00	0.00	0.00
Pyrgo lacernula	0.00	0.00	0.00	0.00	0.00	0.00	0.00	0.00	0.00
Pyrgo murrhina	7.55	0.00	0.00	0.00	1.43	0.00	0.00	0.00	0.00
Pyrgo oblonga	0.00	0.00	0.00	0.00	0.00	0.00	0.00	0.00	0.00
Pyrgo rotalia	0.00	0.00	0.00	0.00	0.00	0.00	0.00	0.00	0.00
Pyrgo sarsi	0.00	0.00	0.00	0.00	0.00	0.00	0.00	0.00	0.00
Pyrgo serrata	0.00	0.00	0.00	0.00	0.00	0.00	0.00	0.00	0.00
Pyrgo sp.	0.00	0.00	0.00	0.00	0.00	0.00	0.00	0.00	0.00
Pyrgo williamsoni	0.00	0.00	0.00	0.00	0.00	0.00	0.00	0.00	0.00
Quinqueloculina arctica	0.00	0.00	0.00	0.00	0.00	0.00	0.00	0.00	0.00
Quinqueloculina bicornis	0.00	0.00	0.00	0.00	0.00	0.00	0.00	0.00	0.00
Quinqueloculina cliarensis	0.00	0.00	0.00	0.00	0.00	0.00	0.00	0.00	0.00
Quinqueloculina elongata	0.00	0.00	0.00	0.00	0.00	0.00	0.00	0.00	0.00
Quinqueloculina lata	0.00	0.00	0.00	0.00	0.00	0.00	0.00	0.00	0.00
Quinqueloculina seminulum	1.89	6.00	5.50	0.00	2.86	3.54	3.33	1.22	0.00
Quinqueloculina sp.	0.00	0.00	0.00	0.00	0.00	0.00	0.00	0.00	0.00
Quinqueloculina stalkeri	0.00	0.00	0.00	0.00	0.00	0.00	0.00	0.00	0.00
Quinqueloculina striata	0.00	0.00	0.00	0.00	0.00	0.00	0.00	0.00	1.00
Rupertina stabilis	0.00	0.00	0.00	0.00	0.00	0.00	0.00	0.00	0.00
Sigmoilopsis schlumbergeri	0.00	4.00	3.67	8.89	1.43	1.77	2.22	2.44	2.00
Siphotextularia rolhauseni	0.00	0.00	0.00	0.00	0.00	0.00	0.00	0.00	0.00
Solenina radiata	0.00	0.00	0.00	0.00	0.00	0.00	0.00	0.00	0.00
Spiroloculina limbata	0.00	0.00	0.00	0.00	0.00	0.00	0.00	0.00	0.00
Spiroloculina rotunda	0.00	0.00	0.00	0.00	0.00	0.00	0.00	0.00	0.00
Stainforthia (Fursenkoina) fusiformis	0.00	0.00	0.00	0.00	0.00	0.00	0.00	0.00	0.00
Stainforthia loeblichi	0.00	0.00	0.00	0.00	0.00	0.00	0.00	0.00	0.00
Stainforthia schreibersiana	0.00	0.00	0.00	0.00	0.00	0.00	0.00	0.00	0.00
Trifarina angulosa	50.94	5.00	8.26	35.56	20.00	4.42	26.67	9.76	11.00

Appendix B - Benthic foraminifera assemblage data

Core 9/97-08
Relative abundance - Benthic foraminifera 250-63um

Sample depth (cm)	39	43	47.5	51.5	55.5	59.5	63.5	76	80
Trifarina bradyi	0.00	0.00	0.00	0.00	0.00	0.00	0.00	0.00	0.00
Trifarina sp.	0.00	0.00	0.00	0.00	0.00	0.00	0.00	0.00	0.00
Triloculina tricarinata	0.00	0.00	0.00	0.00	0.00	0.00	0.00	0.00	0.00
Uvigerina celtica	0.00	0.00	0.00	0.00	0.00	0.00	0.00	0.00	0.00
Uvigerina cf. pigmea	0.00	0.00	0.00	0.00	0.00	0.00	0.00	0.00	0.00
Uvigerina peregrina	3.77	14.00	12.84	17.78	2.86	17.70	7.78	0.00	5.00
Virgulina advena	0.00	0.00	0.00	0.00	0.00	0.00	0.00	0.00	0.00

Appendix B - Benthic foraminifera assemblage data

Core 9/97-10
Relative abundance - Benthic foraminifera 250-63um

Sample depth (cm)	3	7	11	16	20	27	31	35	39	43
Alabaminella weddellensis	0.00	0.00	0.00	0.00	0.00	0.00	0.00	0.00	0.00	0.00
Amphycorina scalaris	0.00	0.00	0.00	0.00	0.00	0.00	1.35	0.00	1.03	1.50
Astacolus hyalacrulus	0.00	1.54	0.32	1.01	0.00	0.00	0.00	0.00	0.00	0.00
Astacolus sp.	0.00	0.00	0.00	0.00	0.00	0.00	0.00	0.00	0.00	0.00
Bolivina albatrossi	0.23	0.51	0.32	0.00	0.00	0.00	0.68	0.00	1.55	1.50
Bolivina pseduopunctata	0.00	1.54	0.32	0.00	0.00	0.00	0.00	0.00	0.00	0.00
Bolivina sp.	0.00	0.00	0.00	0.00	0.00	0.00	0.00	0.00	0.00	0.00
Bolivina spinescens	0.00	0.51	0.32	0.00	0.00	0.00	0.00	0.00	1.55	0.00
Bolivina subspinescens	0.00	0.51	0.00	2.02	0.00	0.00	0.00	2.36	0.00	0.00
Brizalina cf. robusta	0.00	1.03	0.16	0.00	0.00	0.00	2.03	0.00	0.52	0.75
Brizalina variabilis	0.00	0.00	0.00	0.00	0.00	0.00	0.00	0.00	0.00	0.00
Bullimina aculeata	0.00	0.00	0.00	0.00	0.00	0.00	0.00	0.00	0.00	0.00
Bullimina cf. gibba	0.00	0.00	0.00	0.00	0.00	0.00	0.00	0.00	0.00	0.00
Bullimina inflata	0.23	0.00	0.63	0.00	0.00	0.00	1.35	3.77	1.55	0.75
Bullimina marginata	0.46	0.00	0.07	0.00	0.00	0.00	0.00	0.00	0.52	3.76
Cassidulina laevigata	0.00	9.74	3.17	42.42	70.89	65.83	16.89	41.98	15.98	26.32
Cassidulina obtusa	0.00	0.00	0.00	0.00	0.00	0.00	0.00	0.00	0.00	0.00
Chilostomella oolina	0.00	0.00	0.00	0.00	0.00	0.00	0.00	0.00	0.00	0.00
Cibicides kullenbergi	5.47	1.03	1.03	4.04	12.66	5.00	1.35	9.43	1.03	0.75
Cibicides lobatulus	0.23	1.03	0.63	4.04	0.00	0.83	0.00	0.00	1.55	1.50
Cibicides pachyderma	0.68	1.03	0.63	0.00	0.00	0.00	2.70	0.00	3.61	3.01
Cibicides sp.	0.00	0.00	0.00	0.00	0.00	0.00	0.00	0.00	0.00	0.00
Cibicides wuellerstorfi	14.81	1.03	7.62	3.03	2.53	5.83	2.70	5.66	2.58	0.00
Cyclammina pusilla	0.00	0.00	0.00	0.00	0.00	0.00	0.00	0.00	0.00	0.00
Dentalina communis	0.00	0.00	0.00	0.00	0.00	0.00	0.00	0.00	0.00	0.00
Dentalina sp.	0.00	0.00	0.00	0.00	0.00	0.00	0.00	0.00	0.00	0.00
Eggerella bradyi	0.23	0.51	0.12	0.00	0.00	0.00	0.00	0.94	1.03	0.00
Ehrenbergina serrata	0.00	0.00	0.00	0.00	0.00	0.00	0.00	0.00	0.00	0.00
Epistominella exigua	9.79	6.15	8.89	1.01	6.33	5.83	3.38	0.00	9.79	12.78
Eponides pusillus	0.00	0.00	0.00	0.00	0.00	0.00	0.00	0.00	0.00	0.00
Fissurina marginata	0.91	1.03	0.31	10.10	1.27	0.00	6.76	0.00	2.06	2.26
Fissurina orbignyana	0.00	0.51	0.32	0.00	0.00	0.00	0.00	0.00	0.00	0.00
Fissurina porcupinensis	0.00	0.00	0.00	0.00	0.00	0.00	1.35	0.00	0.52	0.00
Fissurina varioperforata	0.00	0.00	0.00	0.00	0.00	0.00	0.68	0.00	0.52	0.75
Fursenkoina complanata	0.00	0.00	0.00	0.00	0.00	0.00	0.00	0.00	0.00	0.00
Gavelinopsis lobatus	0.00	0.00	0.00	0.00	0.00	0.00	0.00	0.00	0.00	0.00
Globobulimina auriculata	0.00	0.00	0.00	0.00	0.00	0.00	0.00	0.00	0.00	0.00
Globobullimina affinis	0.00	0.00	0.00	0.00	0.00	0.00	0.00	0.00	0.00	0.00
Gyroidina soldanii	6.38	2.05	1.34	0.00	0.00	0.00	0.00	0.00	1.03	0.00
Hoeglundia elegans	0.00	0.00	0.00	0.00	0.00	0.00	2.03	0.00	1.03	0.00
Hormosina globulifera	0.00	0.00	0.00	0.00	0.00	0.00	0.00	0.00	0.00	0.00
Indeterminate	0.00	0.51	0.63	0.00	0.00	0.00	0.00	0.00	0.00	0.00
Karreriella bradyi	0.00	0.00	0.00	0.00	0.00	0.00	0.00	0.00	0.00	0.00
Lagena cf. acuticosta	0.00	0.00	0.00	0.00	0.00	0.00	0.00	0.00	0.00	0.00
Lagena cf. interrupta	0.00	0.00	0.00	0.00	0.00	0.00	0.00	0.00	0.00	0.00
Lagena semistriata	0.00	0.51	0.00	0.00	0.00	0.00	0.00	0.00	0.00	0.00

Appendix B - Benthic foraminifera assemblage data

Core 9/97-10
Relative abundance - Benthic foraminifera 250-63um

Sample depth (cm)	3	7	11	16	20	27	31	35	39	43
Lagena sulcata	0.00	0.51	0.63	1.01	0.00	0.00	0.68	0.00	0.52	0.00
Melonis barleeanum	20.05	39.49	26.35	10.10	2.53	6.67	26.35	16.51	18.56	19.55
Melonis pompilioides	0.00	0.00	0.00	0.00	0.00	0.00	0.00	0.00	0.00	0.00
Nodosaria sp.	0.00	0.00	0.00	0.00	0.00	0.00	0.00	0.00	0.00	0.00
Nonionella auricula	0.00	0.00	0.00	0.00	0.00	0.00	0.00	0.00	0.00	0.00
Nonionella turgida	0.00	0.00	0.00	0.00	0.00	0.00	2.70	0.00	0.52	0.75
Nummoloculina irregularis	0.00	0.00	0.00	3.03	0.00	0.83	0.00	0.00	0.00	0.00
Oolina apiopleura	0.00	0.00	0.00	0.00	0.00	0.00	0.00	0.00	0.00	0.00
Oolina heronalleni	0.00	0.51	0.32	1.01	0.00	0.00	0.00	0.00	0.00	0.00
Oolina hexagona	0.00	0.00	0.00	0.00	0.00	0.00	0.00	0.00	0.00	0.00
Oolina intercalata	0.00	0.00	0.00	0.00	0.00	0.00	0.00	0.00	0.00	0.00
Oolina melo	0.00	1.03	0.16	4.04	0.00	0.00	1.35	0.00	1.03	0.75
Oolina squamosa	0.00	0.00	0.00	1.01	0.00	0.83	0.00	0.00	0.00	0.00
Oridorsalis umbonatus	0.00	0.00	0.00	0.00	0.00	0.00	0.00	0.00	0.00	0.00
Pseudofissurina mccullochae	0.00	0.00	0.00	1.01	0.00	0.00	0.00	0.00	0.00	0.00
Pseudosolenina borealis	0.00	2.05	0.33	0.00	0.00	0.00	0.00	0.00	1.03	0.00
Pullenia bulloides	0.23	1.54	0.28	3.03	2.53	5.00	1.35	0.00	1.03	1.50
Pullenia subcarinata	0.00	1.03	0.16	0.00	1.27	0.83	1.35	7.08	0.00	0.00
Pyrgo depressa	0.00	0.00	0.00	0.00	0.00	0.00	0.00	0.00	0.00	0.00
Pyrgo lacemula	0.00	0.00	0.00	0.00	0.00	0.00	0.00	0.00	0.00	0.00
Pyrgo murrhina	6.15	0.00	4.44	0.00	0.00	0.00	0.00	0.00	0.00	0.00
Pyrgo oblonga	0.00	0.00	0.00	0.00	0.00	0.00	0.00	0.00	0.00	0.00
Pyrgo rotalia	0.00	0.00	0.00	0.00	0.00	0.00	0.00	0.00	0.00	0.00
Pyrgo sarsi	0.00	0.00	0.00	0.00	0.00	0.00	0.00	0.00	0.00	0.00
Pyrgo serrata	0.23	0.00	0.32	0.00	0.00	0.00	0.00	0.00	0.00	0.00
Pyrgo sp.	0.00	0.00	0.00	0.00	0.00	0.00	0.00	0.00	0.00	0.00
Pyrgo williamsoni	0.00	0.00	0.00	0.00	0.00	0.00	0.00	0.00	0.00	0.00
Quinqueloculina arctica	0.00	0.00	0.00	0.00	0.00	0.00	0.00	0.00	0.00	0.00
Quinqueloculina bicornis	0.00	0.00	0.00	0.00	0.00	0.00	0.00	0.00	0.00	0.00
Quinqueloculina cliarensis	0.00	0.00	0.00	0.00	0.00	0.00	0.00	0.00	0.00	0.00
Quinqueloculina elongata	0.00	0.00	0.00	0.00	0.00	0.00	0.00	0.00	0.00	0.00
Quinqueloculina lata	0.00	0.00	0.00	0.00	0.00	0.00	0.00	0.00	0.00	0.00
Quinqueloculina seminulum	3.19	0.00	0.51	7.07	0.00	1.67	1.35	2.83	1.03	0.75
Quinqueloculina sp.	0.00	0.00	0.00	0.00	0.00	0.00	0.00	0.00	0.00	0.00
Quinqueloculina stalkeri	0.00	0.00	0.00	0.00	0.00	0.00	0.00	0.00	0.00	0.00
Quinqueloculina striata	0.00	0.00	0.00	0.00	0.00	0.00	0.00	0.00	0.00	0.00
Rupertina stabilis	0.46	0.00	0.07	0.00	0.00	0.00	0.00	0.00	0.00	0.00
Sigmoilopsis schlumbergeri	12.76	8.21	3.33	0.00	0.00	0.00	1.35	0.47	1.03	0.00
Siphotextularia rolhauseni	0.00	0.00	0.00	0.00	0.00	0.00	0.00	0.00	0.00	0.00
Solenina radiata	0.00	0.00	0.00	0.00	0.00	0.00	0.00	0.00	0.00	0.00
Spiroloculina limbata	0.00	0.00	0.00	0.00	0.00	0.00	0.00	0.00	0.00	0.00
Spiroloculina rotunda	0.00	0.51	0.32	0.00	0.00	0.00	0.00	0.00	0.00	0.00
Stainforthia (Fursenkoina) fusiformis	0.00	0.00	0.00	0.00	0.00	0.00	0.68	0.00	0.52	2.26
Stainforthia loeblichi	0.00	0.51	0.32	0.00	0.00	0.83	0.00	0.00	0.00	0.00
Stainforthia schreibersiana	0.00	0.00	0.00	0.00	0.00	0.00	0.00	0.00	0.00	0.00
Trifarina angulosa	0.00	11.28	1.79	1.01	0.00	0.00	18.92	8.96	22.68	12.78

Appendix B - Benthic foraminifera assemblage data

Core 9/97-10
Relative abundance - Benthic foraminifera 250-63um

Sample depth (cm)	3	7	11	16	20	27	31	35	39	43
Trifarina bradyi	0.00	0.00	0.00	0.00	0.00	0.00	0.00	0.00	0.00	0.00
Trifarina sp.	0.00	0.00	0.00	0.00	0.00	0.00	0.00	0.00	0.00	0.00
Triloculina tricarinata	0.23	0.51	0.12	0.00	0.00	0.00	0.00	0.00	1.55	1.50
Uvigerina celtica	0.00	0.00	0.00	0.00	0.00	0.00	0.00	0.00	0.00	0.00
Uvigerina cf. pigmea	0.00	0.00	0.00	0.00	0.00	0.00	0.00	0.00	0.00	0.00
Uvigerina peregrina	17.31	2.05	3.07	0.00	0.00	0.00	0.68	0.00	3.09	4.51
Virgulina advena	0.00	0.00	0.00	0.00	0.00	0.00	0.00	0.00	0.00	0.00

Appendix B - Benthic foraminifera assemblage data

Core 9/97-10
Relative abundance - Benthic foraminifera 250-63um

Sample depth (cm)	47	51.5	55.5	59.5	63.5	67.5	79.5	83
Alabaminella weddellensis	0.00	0.00	0.00	0.00	0.00	0.00	0.00	0.00
Amphycorina scalaris	0.00	0.00	0.00	0.00	0.00	0.00	0.00	0.00
Astacolus hyalacrulus	0.00	0.00	0.00	1.60	1.02	1.11	0.00	0.00
Astacolus sp.	0.00	0.00	0.00	0.00	0.00	0.00	0.00	0.00
Bolivina albatrossi	0.00	0.78	0.00	0.53	2.04	2.22	1.52	2.86
Bolivina pseduopunctata	0.00	0.00	0.00	0.00	0.00	0.00	0.00	0.00
Bolivina sp.	0.00	0.00	0.00	0.00	0.00	0.00	0.00	0.00
Bolivina spinescens	0.00	1.56	0.00	0.53	2.04	0.00	0.00	0.00
Bolivina subspinescens	3.35	0.00	0.00	1.06	2.04	3.33	0.00	0.00
Brizalina cf. robusta	0.00	0.00	0.00	1.06	0.00	0.00	0.00	0.00
Brizalina variabilis	0.00	0.00	0.00	0.00	0.00	0.00	0.00	0.00
Bullimina aculeata	0.00	0.00	0.00	0.00	0.00	0.00	0.00	0.00
Bullimina cf. gibba	0.00	0.00	0.00	0.00	0.00	0.00	0.00	0.00
Bullimina inflata	1.91	4.69	7.46	0.00	9.18	8.89	0.00	0.00
Bullimina marginata	0.96	0.00	0.00	0.00	0.00	0.00	0.00	0.00
Cassidulina laevigata	44.50	7.81	11.94	12.23	9.18	13.33	49.24	62.14
Cassidulina obtusa	0.00	0.00	0.00	0.00	0.00	0.00	0.00	0.00
Chilostomella oolina	0.00	0.00	0.00	0.00	0.00	0.00	0.00	0.00
Cibicides kullenbergi	9.57	0.78	0.00	1.06	1.02	1.11	10.61	7.14
Cibicides lobatulus	0.48	0.00	0.50	1.06	0.00	0.00	0.00	0.00
Cibicides pachyderma	0.00	0.00	0.00	0.53	0.00	0.00	0.00	0.00
Cibicides sp.	0.00	0.00	0.00	0.00	0.00	0.00	0.00	0.00
Cibicides wuellerstorfi	2.87	0.78	6.97	0.53	3.06	4.44	15.15	5.71
Cyclammina pusilla	0.00	0.00	0.00	0.00	0.00	0.00	0.00	0.00
Dentalina communis	0.00	0.00	0.00	0.00	0.00	0.00	0.00	0.00
Dentalina sp.	0.00	0.00	0.00	0.00	0.00	0.00	0.00	0.00
Eggerella bradyi	0.48	0.78	0.00	0.53	1.02	1.11	0.00	0.00
Ehrenbergina serrata	0.00	0.00	0.00	0.00	0.00	0.00	0.00	0.00
Epistominella exigua	0.00	1.56	0.00	2.13	1.02	1.11	0.00	1.43
Eponides pusillus	0.00	0.00	0.00	0.00	0.00	0.00	0.00	0.00
Fissurina marginata	0.48	0.00	0.00	0.00	2.04	2.22	0.00	0.00
Fissurina orbignyana	0.00	2.34	0.00	1.06	1.02	0.00	0.00	0.00
Fissurina porcupinensis	0.00	0.00	0.00	0.00	0.00	0.00	0.00	0.00
Fissurina varioperforata	0.00	0.00	0.00	0.00	0.00	0.00	0.00	0.00
Fursenkoina complanata	0.00	0.00	0.00	0.00	0.00	0.00	0.00	0.00
Gavelinopsis lobatus	0.00	0.00	0.00	0.00	0.00	0.00	0.00	0.00
Globobulimina auriculata	0.00	0.00	0.00	0.00	0.00	0.00	0.00	0.00
Globobullimina affinis	0.00	0.00	0.00	0.00	0.00	0.00	0.00	0.00
Gyroidina soldanii	0.48	3.13	1.99	2.13	9.18	4.44	0.00	0.00
Hoeglundia elegans	0.00	0.00	0.00	0.00	0.00	0.00	0.00	0.00
Hormosina globulifera	0.00	0.00	0.00	0.00	0.00	0.00	0.00	0.00
Indeterminate	0.00	0.00	0.00	0.53	0.00	0.00	0.00	0.00
Karreriella bradyi	0.00	0.00	3.98	0.00	0.00	0.00	0.00	0.00
Lagena cf. acuticosta	0.00	0.00	0.00	0.00	0.00	0.00	0.00	0.00
Lagena cf. interrupta	0.00	0.00	0.00	0.00	0.00	0.00	0.00	0.00
Lagena semistriata	0.00	1.56	1.49	0.53	1.02	3.33	0.00	0.00

Appendix B - Benthic foraminifera assemblage data

Core 9/97-10
Relative abundance - Benthic foraminifera 250-63um

Sample depth (cm)	47	51.5	55.5	59.5	63.5	67.5	79.5	83
Lagena sulcata	0.00	0.00	0.00	0.53	0.00	0.00	0.00	0.00
Melonis barleeanum	17.70	35.94	27.86	42.02	25.51	32.22	6.06	2.86
Melonis pompilioides	0.00	0.00	0.00	0.00	0.00	0.00	0.00	0.00
Nodosaria sp.	0.00	0.00	0.00	0.00	0.00	0.00	0.00	0.00
Nonionella auricula	0.00	0.00	0.00	0.00	0.00	0.00	0.00	0.00
Nonionella turgida	0.00	0.78	0.00	0.00	1.02	1.11	0.00	0.00
Nummoloculina irregularis	0.00	0.00	0.00	0.00	0.00	0.00	0.00	0.00
Oolina apiopleura	0.00	0.00	0.00	0.00	0.00	0.00	0.00	0.00
Oolina heronalleni	0.00	0.00	0.00	0.53	0.00	0.00	0.00	0.00
Oolina hexagona	0.00	0.00	0.00	0.00	0.00	0.00	0.00	0.00
Oolina intercalata	0.00	0.00	0.00	0.00	1.02	1.11	0.00	0.00
Oolina melo	0.00	0.00	0.00	1.06	0.00	0.00	0.00	0.00
Oolina squamosa	0.00	0.00	0.00	0.00	0.00	0.00	0.00	0.00
Oridorsalis umbonatus	0.00	0.00	0.00	0.00	0.00	0.00	0.00	0.00
Pseudofissurina mccullochae	0.00	0.00	0.00	0.00	0.00	0.00	0.00	0.00
Pseudosolenina borealis	0.00	1.56	0.00	1.60	2.04	2.22	0.00	0.00
Pullenia bulloides	0.00	5.47	0.00	1.60	5.10	2.22	0.00	0.71
Pullenia subcarinata	4.78	5.47	0.00	1.06	2.04	1.11	1.52	0.71
Pyrgo depressa	0.00	0.00	0.00	0.00	0.00	0.00	0.00	0.00
Pyrgo lacernula	0.00	0.00	0.00	0.00	0.00	0.00	0.00	0.00
Pyrgo murrhina	0.00	0.00	0.00	0.00	0.00	0.00	0.00	0.00
Pyrgo oblonga	0.00	0.00	0.00	0.00	0.00	0.00	0.00	0.00
Pyrgo rotalia	0.00	0.00	0.00	0.00	0.00	0.00	0.00	0.00
Pyrgo sarsi	0.00	0.00	0.00	0.00	0.00	0.00	0.00	0.00
Pyrgo serrata	0.00	0.00	0.00	0.00	0.00	0.00	0.00	0.00
Pyrgo sp.	0.00	0.00	0.00	0.00	1.02	0.00	0.00	0.00
Pyrgo williamsoni	0.00	0.00	0.00	0.00	0.00	0.00	0.00	0.00
Quinqueloculina arctica	0.00	0.00	0.00	0.00	0.00	0.00	0.00	0.00
Quinqueloculina bicornis	0.00	0.00	0.00	0.00	0.00	0.00	0.00	0.00
Quinqueloculina cliarensis	0.00	0.00	0.00	0.00	0.00	0.00	0.00	0.00
Quinqueloculina elongata	0.00	0.00	0.00	0.00	0.00	0.00	0.00	0.00
Quinqueloculina lata	0.00	0.00	0.00	0.00	0.00	0.00	0.00	0.00
Quinqueloculina seminulum	1.44	0.00	1.49	0.00	0.00	0.00	0.76	1.43
Quinqueloculina sp.	0.00	0.00	0.00	0.00	0.00	0.00	0.00	0.00
Quinqueloculina stalkeri	0.00	0.00	0.00	0.00	0.00	0.00	0.00	0.00
Quinqueloculina striata	0.00	0.00	0.00	0.00	0.00	0.00	0.00	0.00
Rupertina stabilis	0.00	0.00	0.00	0.00	0.00	0.00	0.00	0.00
Sigmoilopsis schlumbergeri	0.00	1.56	12.94	7.98	4.08	1.11	9.09	11.43
Siphotextularia rolhauseni	0.00	0.00	0.00	0.00	0.00	0.00	0.00	0.00
Solenina radiata	0.00	0.78	0.00	0.00	1.02	1.11	0.00	0.00
Spiroloculina limbata	0.00	0.00	0.00	0.00	0.00	0.00	0.00	0.00
Spiroloculina rotunda	0.00	0.78	0.00	0.00	1.02	0.00	0.00	0.00
Stainforthia (Fursenkoina) fusiformis	0.00	0.00	0.00	0.00	0.00	0.00	0.00	0.00
Stainforthia loeblichi	0.00	0.00	0.00	0.53	0.00	0.00	0.00	0.00
Stainforthia schreibersiana	0.00	0.00	0.00	0.00	0.00	0.00	0.00	0.00
Trifarina angulosa	11.00	21.88	23.38	13.30	10.20	10.00	6.06	3.57

Appendix B - Benthic foraminifera assemblage data

Core 9/97-10
Relative abundance - Benthic foraminifera 250-63um

Sample depth (cm)	47	51.5	55.5	59.5	63.5	67.5	79.5	83
Trifarina bradyi	0.00	0.00	0.00	0.00	0.00	0.00	0.00	0.00
Trifarina sp.	0.00	0.00	0.00	0.00	0.00	0.00	0.00	0.00
Triloculina tricarinata	0.00	0.00	0.00	0.53	0.00	0.00	0.00	0.00
Uvigerina celtica	0.00	0.00	0.00	0.00	0.00	0.00	0.00	0.00
Uvigerina cf. pigmea	0.00	0.00	0.00	0.00	0.00	0.00	0.00	0.00
Uvigerina peregrina	0.00	0.00	0.00	2.13	1.02	1.11	0.00	0.00
Virgulina advena	0.00	0.00	0.00	0.00	0.00	0.00	0.00	0.00

Appendix B - Benthic foraminifera assemblage data

Core 9/97-04
Relative abundance - Benthic foraminifera 250-63um

Sample depth (cm)	1	2	5.5	9	13	17	21	25	25	29
Alabaminella weddellensis	0.00	0.00	0.00	0.00	17.54	0.00	0.00	0.00	0.00	3.00
Amphycorina scalaris	0.00	0.00	0.00	0.00	0.00	0.00	0.00	0.00	0.00	0.00
Astacolus hyalacrulus	0.00	0.00	0.00	0.00	0.00	0.00	0.00	0.00	0.00	0.00
Astacolus sp.	0.00	0.00	0.00	0.00	0.00	0.00	0.00	0.00	0.00	0.00
Bolivina albatrossi	0.00	0.00	0.00	0.00	0.00	0.00	0.00	0.00	0.00	0.00
Bolivina pseduopunctata	1.96	1.82	0.00	0.00	0.00	0.00	0.00	0.00	0.00	0.00
Bolivina sp.	0.00	0.00	0.00	0.00	0.00	0.00	0.00	0.00	0.00	0.00
Bolivina spinescens	0.98	0.00	0.00	0.00	0.00	0.00	0.00	0.00	0.00	0.00
Bolivina subspinescens	0.00	0.00	0.00	0.00	7.02	0.00	1.18	0.00	0.00	2.00
Brizalina cf. robusta	0.00	0.00	0.00	0.00	0.00	0.00	0.00	0.00	0.00	0.00
Brizalina variabilis	0.00	0.00	0.00	0.00	0.00	0.00	0.00	0.00	0.00	0.00
Bullimina aculeata	0.00	0.00	0.00	0.00	0.00	0.00	0.00	0.00	0.00	1.00
Bullimina cf. gibba	0.00	0.00	0.00	0.00	0.00	0.00	0.00	0.00	0.00	0.00
Bullimina inflata	1.96	4.55	3.00	3.28	0.00	0.00	0.00	1.50	1.13	6.00
Bullimina marginata	0.98	0.00	1.00	0.00	0.00	0.00	0.00	0.00	0.00	0.00
Cassidulina laevigata	28.43	38.18	20.00	9.02	7.02	39.62	32.94	5.26	3.96	15.00
Cassidulina obtusa	0.00	0.00	0.00	0.00	0.00	0.00	0.00	0.00	0.00	0.00
Chilostomella oolina	0.00	0.00	0.00	0.00	0.00	0.00	0.00	0.00	0.00	0.00
Cibicides kullenbergi	0.00	0.00	0.00	3.28	0.00	0.94	1.18	0.00	0.00	1.00
Cibicides lobatulus	0.00	0.00	0.00	1.64	0.00	0.00	0.00	0.00	0.00	0.00
Cibicides pachyderma	7.84	10.91	14.00	0.00	0.00	0.00	0.00	0.00	0.00	0.00
Cibicides sp.	0.00	0.00	0.00	0.00	0.00	0.00	0.00	0.00	0.00	0.00
Cibicides wuellerstorfi	0.98	0.91	3.00	3.28	0.00	0.00	0.00	0.00	0.00	0.00
Cyclammina pusilla	0.00	0.00	0.00	0.00	0.00	0.00	0.00	3.01	2.26	4.00
Dentalina communis	0.00	0.00	0.00	0.00	0.00	0.00	0.00	0.00	0.00	0.00
Dentalina sp.	0.00	0.00	0.00	0.00	0.00	0.00	0.00	0.00	0.00	0.00
Eggerella bradyi	19.61	15.45	32.00	0.00	0.00	0.94	2.35	14.29	10.74	2.00
Ehrenbergina serrata	0.00	0.00	0.00	0.00	0.00	0.00	0.00	0.00	0.00	0.00
Epistominella exigua	3.92	0.00	4.00	0.00	50.88	18.87	4.71	1.50	1.13	1.00
Eponides pusillus	0.00	0.00	0.00	0.00	0.00	0.00	0.00	0.00	0.00	0.00
Fissurina marginata	1.96	0.00	1.00	0.82	0.00	1.89	3.53	1.50	1.13	2.00
Fissurina orbignyana	0.00	0.00	0.00	0.00	0.00	0.00	1.18	0.00	0.00	0.00
Fissurina porcupinensis	0.98	0.91	1.00	0.00	0.00	0.00	0.00	0.00	0.00	0.00
Fissurina varioperforata	4.90	4.55	4.00	0.82	0.00	8.49	3.53	0.00	0.00	0.00
Fursenkoina complanata	2.94	1.82	3.00	0.00	0.00	0.94	1.18	0.00	0.00	0.00
Gavelinopsis lobatus	0.00	0.00	0.00	0.00	0.00	0.00	0.00	0.00	0.00	0.00
Globobulimina auriculata	0.00	0.00	0.00	0.00	0.00	0.00	0.00	0.00	0.00	0.00
Globobullimina affinis	0.00	0.00	0.00	0.00	0.00	0.00	0.00	0.00	0.00	0.00
Gyroidina soldanii	0.98	0.91	0.00	1.64	0.00	0.00	1.18	0.00	0.00	0.00
Hoeglundia elegans	0.00	0.00	0.00	23.77	0.00	0.00	0.00	0.00	0.00	0.00
Hormosina globulifera	0.00	0.00	0.00	0.00	0.00	0.00	0.00	0.00	0.00	0.00
Indeterminate	0.00	0.00	0.00	0.82	0.00	0.00	0.00	0.00	0.00	0.00
Karreriella bradyi	3.92	3.64	0.00	0.00	0.00	0.00	0.00	3.01	2.26	4.00
Lagena cf. acuticosta	0.00	0.00	0.00	0.00	0.00	0.00	0.00	0.00	0.00	0.00
Lagena cf. interrupta	0.00	0.00	0.00	0.82	0.00	0.00	0.00	0.00	0.00	0.00
Lagena semistriata	0.98	2.73	2.00	8.20	0.00	0.00	0.00	0.00	0.00	0.00

Appendix B - Benthic foraminifera assemblage data

Core 9/97-04
Relative abundance - Benthic foraminifera 250-63um

Sample depth (cm)	1	2	5.5	9	13	17	21	25	25	29
Lagena sulcata	0.00	0.00	0.00	0.00	0.00	0.00	0.00	0.00	0.00	0.00
Melonis barleeanum	5.88	3.64	6.00	0.00	0.00	7.55	10.59	4.51	3.39	2.00
Melonis pompilioides	0.00	0.00	0.00	0.00	0.00	0.00	0.00	3.01	2.26	0.00
Nodosaria sp.	0.00	0.00	0.00	0.00	0.00	0.00	0.00	0.00	0.00	0.00
Nonionella auricula	0.00	0.00	0.00	0.00	0.00	0.00	0.00	0.00	0.00	0.00
Nonionella turgida	0.98	0.91	1.00	0.00	0.00	0.94	1.18	0.00	0.00	1.00
Nummoloculina irregularis	0.00	0.00	0.00	0.00	0.00	0.00	0.00	0.00	0.00	0.00
Oolina apiopleura	0.00	0.00	0.00	0.00	0.00	0.94	1.18	0.00	0.00	0.00
Oolina heronalleni	0.00	0.00	0.00	0.00	0.00	0.00	0.00	0.00	0.00	0.00
Oolina hexagona	0.98	0.91	0.00	0.00	0.00	0.00	0.00	0.00	0.00	0.00
Oolina intercalata	0.00	0.00	0.00	0.00	0.00	0.94	1.18	0.00	0.00	0.00
Oolina melo	0.00	0.00	0.00	0.00	0.00	1.89	1.18	0.00	0.00	0.00
Oolina squamosa	0.00	0.00	0.00	0.00	0.00	0.00	0.00	0.00	0.00	0.00
Oridorsalis umbonatus	0.00	0.00	0.00	0.00	0.00	0.00	0.00	0.00	0.00	0.00
Pseudofissurina mccullochae	0.98	1.82	1.00	0.00	0.00	0.00	0.00	0.00	0.00	0.00
Pseudosolenina borealis	0.00	0.00	0.00	0.00	0.00	0.00	0.00	0.00	0.00	0.00
Pullenia bulloides	0.00	0.00	0.00	14.75	17.54	0.00	4.71	6.02	4.52	4.00
Pullenia subcarinata	0.00	0.00	0.00	0.00	0.00	0.00	0.00	0.00	0.00	3.00
Pyrgo depressa	0.00	0.00	0.00	0.00	0.00	0.00	0.00	0.00	0.00	0.00
Pyrgo lacernula	0.00	0.00	0.00	0.00	0.00	0.00	0.00	0.00	0.00	0.00
Pyrgo murrhina	0.00	0.00	0.00	0.00	0.00	0.00	0.00	9.02	6.78	8.00
Pyrgo oblonga	0.00	0.00	0.00	0.00	0.00	0.00	0.00	0.00	0.00	0.00
Pyrgo rotalia	0.00	0.00	0.00	0.00	0.00	0.00	0.00	0.00	0.00	0.00
Pyrgo sarsi	0.00	0.00	0.00	0.00	0.00	0.00	0.00	0.00	0.00	0.00
Pyrgo serrata	0.00	0.00	0.00	0.00	0.00	0.00	0.00	0.00	0.00	0.00
Pyrgo sp.	0.00	0.00	0.00	0.00	0.00	0.00	0.00	0.00	0.00	0.00
Pyrgo williamsoni	0.00	0.00	0.00	0.00	0.00	0.00	0.00	0.00	0.00	1.00
Quinqueloculina arctica	0.00	0.00	0.00	2.46	0.00	0.00	0.00	0.00	0.00	2.00
Quinqueloculina bicornis	0.00	0.00	0.00	0.00	0.00	0.00	0.00	0.00	0.00	0.00
Quinqueloculina cliarensis	0.00	0.00	0.00	0.00	0.00	0.00	0.00	0.00	0.00	0.00
Quinqueloculina elongata	0.00	0.00	0.00	0.00	0.00	3.77	4.71	1.50	1.13	0.00
Quinqueloculina lata	0.00	0.00	0.00	0.00	0.00	0.00	0.00	0.00	0.00	0.00
Quinqueloculina seminulum	0.00	0.00	0.00	2.46	0.00	4.72	9.41	6.02	4.52	4.00
Quinqueloculina sp.	0.00	0.00	0.00	0.00	0.00	0.00	0.00	0.00	0.00	0.00
Quinqueloculina stalkeri	0.00	0.91	0.00	0.00	0.00	0.00	0.00	0.00	0.00	1.00
Quinqueloculina striata	0.00	0.00	0.00	0.00	0.00	0.00	1.18	0.00	0.00	0.00
Rupertina stabilis	0.00	0.00	0.00	0.00	0.00	0.00	0.00	3.01	2.26	16.00
Sigmoilopsis schlumbergeri	3.92	1.82	0.00	22.13	0.00	0.00	0.00	34.59	26.00	12.00
Siphotextularia rolhauseni	0.00	0.00	0.00	0.00	0.00	0.00	0.00	0.00	0.00	4.00
Solenina radiata	0.98	0.91	1.00	0.82	0.00	0.00	0.00	0.75	0.57	0.00
Spiroloculina limbata	0.00	0.00	0.00	0.00	0.00	0.00	0.00	0.00	0.00	0.00
Spiroloculina rotunda	0.00	0.00	0.00	0.00	0.00	0.00	0.00	0.00	0.00	0.00
Stainforthia (Fursenkoina) fusiformis	0.00	0.00	0.00	0.00	0.00	1.89	2.35	0.00	0.00	0.00
Stainforthia loeblichi	0.00	0.00	0.00	0.00	0.00	0.00	0.00	0.00	0.00	0.00
Stainforthia schreibersiana	0.00	0.00	0.00	0.00	0.00	0.00	0.00	0.00	0.00	0.00
Trifarina angulosa	1.96	2.73	2.00	0.00	0.00	1.89	2.35	0.00	0.00	0.00

Appendix B - Benthic foraminifera assemblage data

Core 9/97-04
Relative abundance - Benthic foraminifera 250-63um

Sample depth (cm)	1	2	5.5	9	13	17	21	25	25	29
Trifarina bradyi	0.00	0.00	0.00	0.00	0.00	0.00	0.00	0.00	0.00	0.00
Trifarina sp.	0.00	0.00	0.00	0.00	0.00	0.00	0.00	0.00	0.00	0.00
Triloculina tricarinata	0.98	0.00	1.00	0.00	0.00	0.94	2.35	0.00	0.00	0.00
Uvigerina celtica	0.00	0.00	0.00	0.00	0.00	0.00	0.00	0.00	0.00	0.00
Uvigerina cf. pigmea	0.00	0.00	0.00	0.00	0.00	0.00	0.00	0.00	0.00	0.00
Uvigerina peregrina	0.00	0.00	0.00	0.00	0.00	1.89	2.35	0.00	0.00	0.00
Virgulina advena	0.00	0.00	0.00	0.00	0.00	0.94	2.35	1.50	1.13	1.00

Appendix B - Benthic foraminifera assemblage data

Core 9/97-04
Relative abundance - Benthic foraminifera 250-63um

Sample depth (cm)	33	35	37	41	43	45	48	52	56	60
Alabaminella weddellensis	0.00	0.00	0.00	0.00	0.00	0.00	1.69	0.00	0.00	0.00
Amphycorina scalaris	0.00	0.00	0.00	0.00	0.00	0.00	0.00	0.00	0.00	0.00
Astacolus hyalacrulus	0.00	0.00	0.00	0.00	0.00	0.00	1.69	0.00	0.00	0.00
Astacolus sp.	0.00	0.00	0.00	0.00	0.00	0.00	0.00	0.00	0.00	0.00
Bolivina albatrossi	0.00	0.00	0.00	2.02	0.00	0.00	0.00	0.00	0.00	0.00
Bolivina pseduopunctata	0.00	0.00	2.86	4.04	0.00	2.03	0.00	7.27	9.57	4.04
Bolivina sp.	0.00	0.00	0.00	0.00	0.00	0.00	0.00	0.00	0.00	0.00
Bolivina spinescens	0.00	2.17	1.90	0.00	0.00	0.00	0.00	0.00	0.00	2.02
Bolivina subspinescens	2.38	4.35	0.95	1.01	0.00	0.00	0.00	3.64	2.61	1.01
Brizalina cf. robusta	0.00	0.00	0.95	0.00	0.00	0.00	0.00	0.00	0.00	1.01
Brizalina variabilis	0.00	0.00	0.00	0.00	0.00	0.00	0.00	0.00	0.00	0.00
Bullimina aculeata	0.00	0.00	0.00	0.00	0.00	0.68	0.00	0.00	0.00	0.00
Bullimina cf. gibba	0.00	0.00	0.00	0.00	0.00	0.00	0.00	0.00	0.00	0.00
Bullimina inflata	0.00	3.26	4.76	4.04	4.94	5.41	10.17	4.55	0.00	5.05
Bullimina marginata	0.00	0.00	0.00	0.00	0.00	1.35	1.69	0.00	0.00	0.00
Cassidulina laevigata	38.10	38.04	32.38	27.27	0.00	4.05	0.00	26.36	28.70	36.36
Cassidulina obtusa	0.00	0.00	0.00	0.00	0.00	0.00	0.00	0.00	0.00	0.00
Chilostomella oolina	0.00	0.00	0.00	0.00	0.00	0.00	0.00	0.00	0.00	0.00
Cibicides kullenbergi	1.19	1.09	0.95	1.01	2.47	1.35	0.00	0.00	0.87	1.01
Cibicides lobatulus	0.00	1.09	0.00	0.00	0.00	0.68	3.39	0.00	0.00	1.01
Cibicides pachyderma	0.00	0.00	0.00	1.01	0.00	0.00	0.00	0.00	0.00	0.00
Cibicides sp.	0.00	0.00	0.00	0.00	0.00	0.00	0.00	0.00	0.00	0.00
Cibicides wuellerstorfi	0.00	0.00	0.00	1.01	0.00	0.00	3.39	0.00	0.00	0.00
Cyclammina pusilla	0.00	0.00	0.00	0.00	0.00	0.00	0.00	0.00	0.00	0.00
Dentalina communis	0.00	0.00	0.00	0.00	0.00	0.00	0.00	0.00	0.00	0.00
Dentalina sp.	0.00	0.00	0.00	0.00	0.00	1.35	0.00	0.00	0.00	0.00
Eggerella bradyi	0.00	6.52	5.71	5.05	7.41	4.05	3.39	5.45	5.22	6.06
Ehrenbergina serrata	0.00	0.00	0.00	0.00	0.00	0.00	0.00	0.00	0.00	0.00
Epistominella exigua	5.95	1.09	1.90	2.02	0.00	0.68	0.00	0.00	3.48	1.01
Eponides pusillus	0.00	0.00	0.00	0.00	0.00	0.00	0.00	0.00	0.00	0.00
Fissurina marginata	7.14	1.09	1.90	3.03	0.00	0.00	1.69	0.91	0.00	1.01
Fissurina orbignyana	2.38	0.00	0.00	0.00	0.00	1.35	1.69	0.00	0.00	0.00
Fissurina porcupinensis	0.00	0.00	0.00	0.00	1.23	0.68	0.00	0.00	0.00	0.00
Fissurina varioperforata	3.57	0.00	0.00	1.01	0.00	0.00	0.00	0.00	0.00	0.00
Fursenkoina complanata	5.95	0.00	0.00	0.00	0.00	0.00	0.00	0.00	0.00	0.00
Gavelinopsis lobatus	0.00	0.00	0.00	0.00	0.00	0.00	0.00	0.00	0.00	0.00
Globobulimina auriculata	0.00	0.00	0.00	0.00	0.00	0.00	0.00	0.00	0.00	0.00
Globobullimina affinis	0.00	0.00	0.00	0.00	0.00	0.00	0.00	0.00	0.00	0.00
Gyroidina soldanii	1.19	0.00	0.00	0.00	3.70	8.78	6.78	0.00	0.00	0.00
Hoeglundia elegans	0.00	4.35	0.95	0.00	1.23	1.35	10.17	2.73	5.22	1.01
Hormosina globulifera	0.00	0.00	0.00	0.00	22.22	0.00	0.00	0.00	0.00	0.00
Indeterminate	0.00	0.00	0.00	0.00	0.00	0.00	0.00	0.00	0.00	0.00
Karreriella bradyi	0.00	0.00	0.00	0.00	0.00	17.57	1.69	0.00	0.00	0.00
Lagena cf. acuticosta	0.00	0.00	0.00	0.00	0.00	0.00	0.00	0.00	0.00	0.00
Lagena cf. interrupta	0.00	0.00	0.00	0.00	0.00	0.00	0.00	0.00	0.00	0.00
Lagena semistriata	0.00	0.00	0.95	1.01	0.00	0.68	0.00	3.64	4.35	1.01

Appendix B - Benthic foraminifera assemblage data

Core 9/97-04
Relative abundance - Benthic foraminifera 250-63um

Sample depth (cm)	33	35	37	41	43	45	48	52	56	60
Lagena sulcata	0.00	0.00	0.00	0.00	0.00	0.00	0.00	0.00	0.00	0.00
Melonis barleeanum	5.95	8.70	3.81	10.10	4.94	2.03	5.08	1.82	1.74	6.06
Melonis pompilioides	0.00	0.00	0.00	0.00	0.00	0.00	1.69	0.00	0.00	0.00
Nodosaria sp.	0.00	0.00	0.00	0.00	0.00	0.00	0.00	0.00	0.00	0.00
Nonionella auricula	0.00	0.00	0.00	0.00	0.00	0.00	0.00	0.00	0.00	0.00
Nonionella turgida	1.19	1.09	1.90	0.00	0.00	0.00	0.00	0.91	0.87	1.01
Nummoloculina irregularis	0.00	0.00	0.00	0.00	0.00	0.00	0.00	0.00	0.00	0.00
Oolina apiopleura	3.57	0.00	0.00	1.01	0.00	0.00	0.00	0.00	0.00	0.00
Oolina heronalleni	0.00	0.00	0.00	0.00	0.00	0.00	0.00	0.00	0.00	0.00
Oolina hexagona	0.00	0.00	0.00	0.00	0.00	0.00	0.00	0.00	0.00	0.00
Oolina intercalata	2.38	0.00	0.00	0.00	0.00	0.00	3.39	0.00	0.00	0.00
Oolina melo	0.00	0.00	0.00	0.00	0.00	0.00	0.00	0.00	0.00	0.00
Oolina squamosa	0.00	0.00	0.00	1.01	0.00	2.70	0.00	0.00	0.00	0.00
Oridorsalis umbonatus	0.00	0.00	0.00	0.00	0.00	0.00	0.00	0.00	0.00	0.00
Pseudofissurina mccullochae	0.00	1.09	0.95	1.01	3.70	0.68	0.00	0.91	0.87	1.01
Pseudosolenina borealis	0.00	0.00	0.00	3.03	0.00	0.00	0.00	0.00	0.00	0.00
Pullenia bulloides	3.57	1.09	0.95	1.01	11.11	6.08	0.00	0.91	0.87	1.01
Pullenia subcarinata	0.00	0.00	0.00	0.00	2.47	2.70	0.00	0.00	0.00	0.00
Pyrgo depressa	0.00	0.00	0.00	0.00	0.00	0.00	0.00	0.00	0.00	0.00
Pyrgo lacernula	0.00	0.00	0.00	0.00	0.00	0.00	0.00	0.00	0.00	0.00
Pyrgo murrhina	0.00	0.00	0.00	0.00	2.47	0.68	3.39	0.00	0.00	0.00
Pyrgo oblonga	0.00	0.00	0.00	0.00	0.00	0.00	1.69	0.00	0.00	0.00
Pyrgo rotalia	0.00	0.00	0.00	0.00	0.00	0.00	0.00	0.00	0.00	0.00
Pyrgo sarsi	0.00	0.00	0.00	0.00	0.00	2.03	1.69	0.00	0.00	0.00
Pyrgo serrata	0.00	0.00	0.00	0.00	0.00	0.68	0.00	0.00	0.00	0.00
Pyrgo sp.	0.00	0.00	0.00	0.00	0.00	0.00	0.00	0.00	0.00	0.00
Pyrgo williamsoni	0.00	0.00	0.00	0.00	0.00	0.68	0.00	0.00	0.00	0.00
Quinqueloculina arctica	0.00	0.00	0.00	0.00	0.00	0.00	3.39	0.00	0.00	0.00
Quinqueloculina bicornis	0.00	0.00	0.00	0.00	0.00	0.00	0.00	0.00	0.00	0.00
Quinqueloculina cliarensis	0.00	0.00	0.00	0.00	0.00	0.00	0.00	0.00	0.00	0.00
Quinqueloculina elongata	2.38	2.17	1.90	1.01	0.00	0.00	0.00	1.82	0.00	2.02
Quinqueloculina lata	0.00	0.00	0.00	0.00	0.00	0.00	0.00	0.00	0.00	0.00
Quinqueloculina seminulum	3.57	0.00	0.00	1.01	0.00	1.35	0.00	0.00	0.00	0.00
Quinqueloculina sp.	0.00	0.00	0.00	0.00	0.00	0.00	0.00	0.00	0.00	0.00
Quinqueloculina stalkeri	0.00	0.00	0.00	1.01	0.00	0.00	1.69	0.00	0.00	0.00
Quinqueloculina striata	1.19	0.00	0.00	0.00	0.00	0.00	0.00	0.00	0.00	0.00
Rupertina stabilis	0.00	0.00	0.00	0.00	20.99	6.08	15.25	0.00	0.00	0.00
Sigmoilopsis schlumbergeri	0.00	0.00	0.00	0.00	2.47	6.76	6.78	0.00	0.00	0.00
Siphotextularia rolhauseni	0.00	0.00	0.00	0.00	7.41	14.19	5.08	0.00	0.00	0.00
Solenina radiata	0.00	0.00	0.00	0.00	1.23	0.00	0.00	0.00	0.00	0.00
Spiroloculina limbata	0.00	0.00	0.00	0.00	0.00	0.00	0.00	0.00	0.00	0.00
Spiroloculina rotunda	0.00	0.00	0.00	0.00	0.00	0.00	1.69	0.00	0.00	0.00
Stainforthia (Fursenkoina) fusiformis	2.38	1.09	0.00	4.04	0.00	0.00	0.00	0.91	0.87	1.01
Stainforthia loeblichi	0.00	0.00	0.00	0.00	0.00	0.00	0.00	0.00	0.00	0.00
Stainforthia schreibersiana	0.00	0.00	0.00	0.00	0.00	0.00	0.00	0.00	0.00	0.00
Trifarina angulosa	1.19	21.74	33.33	14.14	0.00	0.00	1.69	36.36	33.91	25.25

Appendix B - Benthic foraminifera assemblage data

Core 9/97-04
Relative abundance - Benthic foraminifera 250-63um

Sample depth (cm)	33	35	37	41	43	45	48	52	56	60
Trifarina bradyi	0.00	0.00	0.00	0.00	0.00	0.00	0.00	0.00	0.00	0.00
Trifarina sp.	0.00	0.00	0.00	0.00	0.00	0.00	0.00	0.00	0.00	0.00
Triloculina tricarinata	2.38	0.00	0.95	6.06	0.00	0.00	0.00	1.82	0.87	1.01
Uvigerina celtica	0.00	0.00	0.00	0.00	0.00	0.00	0.00	0.00	0.00	0.00
Uvigerina cf. pigmea	0.00	0.00	0.00	0.00	0.00	0.00	0.00	0.00	0.00	0.00
Uvigerina peregrina	0.00	0.00	0.00	1.01	0.00	0.68	0.00	0.00	0.00	0.00
Virgulina advena	2.38	0.00	0.00	1.01	0.00	0.00	0.00	0.00	0.00	0.00

Appendix B - Benthic foraminifera assemblage data

Core 9/97-04
Relative abundance - Benthic foraminifera 250-63um

Sample depth (cm)	64	68	72	76	80	84	88
Alabaminella weddellensis	1.22	0.00	0.00	0.00	0.00	0.00	0.00
Amphycorina scalaris	0.00	0.00	0.00	0.79	0.00	1.00	0.00
Astacolus hyalacrulus	0.00	0.00	0.00	0.00	0.89	0.00	0.00
Astacolus sp.	0.00	0.00	0.00	0.00	0.00	0.00	0.00
Bolivina albatrossi	0.00	0.00	0.00	1.59	0.00	2.00	0.00
Bolivina pseduopunctata	0.00	1.10	9.76	0.00	0.00	1.00	0.00
Bolivina sp.	0.00	0.00	0.00	0.00	0.00	0.00	0.00
Bolivina spinescens	0.00	0.00	0.00	0.79	0.00	1.00	0.00
Bolivina subspinescens	2.44	0.00	2.44	3.17	2.68	1.00	1.83
Brizalina cf. robusta	0.00	0.00	1.63	0.00	0.00	0.00	0.00
Brizalina variabilis	0.00	0.00	0.00	0.00	0.00	0.00	0.00
Bullimina aculeata	0.00	0.55	0.00	0.00	1.79	0.00	4.59
Bullimina cf. gibba	0.00	0.00	0.00	0.00	0.00	0.00	0.00
Bullimina inflata	4.88	4.42	0.00	1.59	3.57	2.00	5.50
Bullimina marginata	1.63	0.55	0.00	0.00	0.00	0.00	0.92
Cassidulina laevigata	0.00	0.55	25.20	17.46	5.36	7.00	1.83
Cassidulina obtusa	0.00	0.00	0.00	0.00	0.00	0.00	0.00
Chilostomella oolina	0.00	0.00	0.00	0.00	0.00	0.00	0.00
Cibicides kullenbergi	0.41	0.55	0.81	0.00	0.00	0.00	0.00
Cibicides lobatulus	0.00	2.76	0.81	0.79	0.89	0.00	3.67
Cibicides pachyderma	0.00	0.00	0.00	0.79	0.00	1.00	0.00
Cibicides sp.	0.00	0.00	0.00	0.00	0.00	0.00	0.00
Cibicides wuellerstorfi	0.00	0.00	0.00	0.00	1.79	0.00	0.00
Cyclammina pusilla	0.00	0.00	0.00	0.00	0.00	0.00	1.83
Dentalina communis	0.00	0.00	0.00	0.00	0.00	0.00	0.92
Dentalina sp.	0.00	0.55	0.00	0.00	0.00	0.00	0.00
Eggerella bradyi	3.66	3.31	4.88	4.76	0.00	3.00	5.50
Ehrenbergina serrata	0.00	0.00	0.00	0.00	0.00	0.00	0.00
Epistominella exigua	0.00	0.55	3.25	7.94	9.82	9.00	0.92
Eponides pusillus	0.00	0.00	0.00	0.00	0.00	0.00	0.00
Fissurina marginata	0.00	0.00	0.00	2.38	1.79	5.00	1.83
Fissurina orbignyana	0.00	0.55	0.00	0.00	0.00	0.00	0.92
Fissurina porcupinensis	2.44	0.55	0.00	0.00	0.00	0.00	0.00
Fissurina varioperforata	0.00	0.00	0.00	0.00	0.00	0.00	0.00
Fursenkoina complanata	0.00	0.00	0.00	0.00	0.00	0.00	0.00
Gavelinopsis lobatus	0.00	0.00	0.00	0.00	0.00	0.00	0.00
Globobulimina auriculata	0.00	0.00	0.00	0.00	0.00	0.00	0.00
Globobullimina affinis	0.00	0.00	0.00	0.00	0.00	0.00	1.83
Gyroidina soldanii	7.32	4.97	0.00	0.00	16.07	0.00	0.00
Hoeglundia elegans	1.63	1.10	4.88	0.00	1.79	0.00	0.00
Hormosina globulifera	0.00	0.00	0.00	0.00	0.00	0.00	0.00
Indeterminate	0.00	0.00	0.00	0.00	0.00	0.00	0.00
Karreriella bradyi	15.04	19.89	0.00	0.00	1.79	0.00	5.50
Lagena cf. acuticosta	0.00	0.00	0.00	0.00	0.00	0.00	0.00
Lagena cf. interrupta	0.00	0.00	0.00	0.00	0.00	0.00	0.00
Lagena semistriata	0.00	0.55	4.07	0.00	0.00	0.00	0.00

Appendix B - Benthic foraminifera assemblage data

Core 9/97-04
Relative abundance - Benthic foraminifera 250-63um

Sample depth (cm)	64	68	72	76	80	84	88
Lagena sulcata	0.00	0.55	0.00	0.00	0.00	0.00	0.00
Melonis barleeanum	7.32	1.66	1.63	2.38	3.57	3.00	1.83
Melonis pompilioides	0.00	0.00	0.00	0.00	0.00	0.00	0.00
Nodosaria sp.	0.00	0.00	0.00	0.00	0.00	0.00	0.00
Nonionella auricula	0.00	0.00	0.00	0.00	0.00	0.00	0.00
Nonionella turgida	0.00	0.00	0.81	0.79	0.00	1.00	0.00
Nummoloculina irregularis	0.00	0.00	0.00	0.00	0.00	0.00	0.00
Oolina apiopleura	0.00	0.00	0.00	0.79	0.00	1.00	0.00
Oolina heronalleni	0.00	0.00	0.00	0.00	0.00	0.00	0.00
Oolina hexagona	0.00	0.00	0.00	0.00	0.00	0.00	0.92
Oolina intercalata	0.00	0.00	0.00	0.00	0.00	0.00	0.00
Oolina melo	0.00	0.00	0.00	0.00	0.00	0.00	0.00
Oolina squamosa	0.00	1.10	0.00	0.00	0.00	0.00	0.92
Oridorsalis umbonatus	0.00	0.00	0.00	0.00	0.00	0.00	0.00
Pseudofissurina mccullochae	0.00	0.55	0.81	0.00	0.00	0.00	0.00
Pseudosolenina borealis	0.00	0.00	0.00	0.00	0.00	0.00	0.00
Pullenia bulloides	0.81	4.97	0.81	0.00	1.79	3.00	1.83
Pullenia subcarinata	0.00	9.94	0.00	0.79	1.79	1.00	0.92
Pyrgo depressa	0.00	0.00	0.00	0.00	0.00	0.00	0.00
Pyrgo lacernula	0.00	0.00	0.00	0.00	0.00	0.00	0.00
Pyrgo murrhina	4.47	0.55	0.00	0.00	0.00	0.00	1.83
Pyrgo oblonga	0.00	0.00	0.00	0.00	0.00	0.00	0.00
Pyrgo rotalia	1.22	0.00	0.00	0.00	0.00	0.00	0.00
Pyrgo sarsi	3.66	1.66	0.00	0.00	0.00	0.00	0.00
Pyrgo serrata	0.00	0.55	0.00	0.00	0.00	0.00	0.00
Pyrgo sp.	0.00	0.00	0.00	0.00	0.00	2.00	0.00
Pyrgo williamsoni	0.00	0.55	0.00	0.00	0.00	0.00	0.00
Quinqueloculina arctica	0.00	0.00	0.00	0.00	1.79	0.00	0.00
Quinqueloculina bicornis	0.81	0.00	0.00	0.00	0.00	0.00	0.00
Quinqueloculina cliarensis	0.00	0.00	0.00	0.00	0.00	0.00	0.00
Quinqueloculina elongata	0.00	0.00	0.00	1.59	0.00	2.00	0.00
Quinqueloculina lata	0.00	0.00	0.00	0.00	0.00	0.00	0.00
Quinqueloculina seminulum	0.00	1.10	0.00	0.79	0.00	1.00	0.92
Quinqueloculina sp.	0.00	0.00	0.00	0.00	0.00	0.00	0.00
Quinqueloculina stalkeri	0.00	0.00	0.00	0.00	0.89	0.00	0.00
Quinqueloculina striata	0.00	0.00	0.00	0.00	0.00	0.00	0.00
Rupertina stabilis	8.94	7.73	0.00	0.00	4.46	0.00	3.67
Sigmoilopsis schlumbergeri	7.72	2.76	0.00	0.79	23.21	1.00	29.36
Siphotextularia rolhauseni	1.22	5.52	0.00	0.00	1.79	0.00	0.00
Solenina radiata	0.00	0.00	0.00	0.00	0.00	0.00	0.92
Spiroloculina limbata	0.00	0.00	0.00	0.00	0.00	0.00	0.00
Spiroloculina rotunda	8.13	1.66	0.00	0.79	0.00	1.00	0.00
Stainforthia (Fursenkoina) fusiformis	0.00	0.00	0.81	0.00	0.00	0.00	0.00
Stainforthia loeblichi	0.00	0.00	0.00	0.00	0.00	0.00	0.00
Stainforthia schreibersiana	0.00	0.00	0.00	0.00	0.00	0.00	0.00
Trifarina angulosa	15.04	15.47	36.59	44.44	12.50	48.00	18.35

Appendix B - Benthic foraminifera assemblage data

Core 9/97-04
Relative abundance - Benthic foraminifera 250-63um

Sample depth (cm)	64	68	72	76	80	84	88	
Trifarina bradyi	0.00	0.00	0.00	0.00	0.00	0.00	0.00	
Trifarina sp.	0.00	0.00	0.00	0.00	0.00	0.00	0.00	
Triloculina tricarinata	0.00	0.00	0.81	1.59	0.00	1.00	0.00	
Uvigerina celtica	0.00	0.00	0.00	1.59	0.00	2.00	0.92	
Uvigerina cf. pigmea	0.00	0.00	0.00	1.59	0.00	0.00	0.00	
Uvigerina peregrina	0.00	0.55	0.00	0.00	0.00	0.00	0.00	
Virgulina advena	0.00	0.00	0.00	0.00	0.00	0.00	0.00	

Appendix B - Benthic foraminifera assemblage data

Core 9/97-14
Relative abundance - Benthic foraminifera 250-63um

Sample depth (cm)	1	23	51	54	57	62	81	90	93
Alabaminella weddellensis	4.00	0.00	2.04	5.10	0.00	11.22	3.06	4.08	0.00
Amphycorina scalaris	0.00	0.00	0.00	0.00	0.00	0.00	0.00	0.00	0.00
Astacolus hyalacrulus	1.00	1.02	0.00	0.00	0.00	0.00	0.00	1.02	0.00
Astacolus sp.	0.00	0.00	0.00	0.00	0.00	0.00	0.00	0.00	0.00
Bolivina albatrossi	0.00	0.00	3.06	0.00	0.00	1.02	1.02	0.00	0.00
Bolivina pseduopunctata	9.00	1.02	1.02	0.00	0.00	4.08	0.00	5.10	8.16
Bolivina sp.	0.00	0.00	0.00	0.00	0.00	0.00	0.00	0.00	0.00
Bolivina spinescens	0.00	0.00	1.02	0.00	0.00	1.02	3.06	0.00	0.00
Bolivina subspinescens	0.00	1.02	0.00	2.04	0.00	0.00	0.00	0.00	9.18
Brizalina cf. robusta	0.00	0.00	0.00	0.00	0.00	0.00	0.00	0.00	0.00
Brizalina variabilis	0.00	0.00	0.00	0.00	0.00	0.00	0.00	0.00	0.00
Bullimina aculeata	0.00	0.00	0.00	6.12	0.00	0.00	0.00	0.00	2.04
Bullimina cf. gibba	0.00	0.00	0.00	0.00	0.00	0.00	0.00	0.00	0.00
Bullimina inflata	0.00	0.00	0.00	0.00	0.00	0.00	0.00	0.00	0.00
Bullimina marginata	0.00	0.00	7.14	4.08	0.00	0.00	0.00	0.00	2.04
Cassidulina laevigata	14.00	15.31	13.27	39.80	43.88	32.65	1.02	10.20	23.47
Cassidulina obtusa	0.00	0.00	0.00	0.00	0.00	0.00	0.00	0.00	0.00
Chilostomella oolina	0.00	0.00	0.00	0.00	0.00	0.00	0.00	0.00	0.00
Cibicides kullenbergi	0.00	0.00	1.02	4.08	9.18	0.00	0.00	1.02	2.04
Cibicides lobatulus	0.00	0.00	2.04	0.00	0.00	0.00	0.00	0.00	0.00
Cibicides pachyderma	0.00	0.00	0.00	2.04	1.02	1.02	1.02	0.00	0.00
Cibicides sp.	0.00	0.00	0.00	0.00	0.00	0.00	0.00	0.00	0.00
Cibicides wuellerstorfi	0.00	0.00	0.00	0.00	0.00	0.00	0.00	0.00	0.00
Cyclammina pusilla	2.00	3.06	0.00	8.16	10.20	2.04	2.04	3.06	0.00
Dentalina communis	0.00	0.00	0.00	0.00	0.00	0.00	0.00	0.00	0.00
Dentalina sp.	0.00	0.00	0.00	0.00	0.00	0.00	0.00	0.00	0.00
Eggerella bradyi	4.00	0.00	0.00	2.04	2.04	1.02	0.00	4.08	0.00
Ehrenbergina serrata	0.00	0.00	0.00	0.00	0.00	0.00	0.00	0.00	0.00
Epistominella exigua	21.00	9.18	33.67	18.37	17.35	14.29	14.29	22.45	32.65
Eponides pusillus	1.00	1.02	1.02	0.00	0.00	2.04	1.02	1.02	0.00
Fissurina marginata	2.00	3.06	4.08	2.04	0.00	4.08	0.00	9.18	0.00
Fissurina orbignyana	0.00	0.00	0.00	0.00	0.00	0.00	0.00	0.00	0.00
Fissurina porcupinensis	0.00	0.00	0.00	0.00	0.00	0.00	0.00	0.00	0.00
Fissurina varioperforata	0.00	0.00	1.02	0.00	0.00	0.00	0.00	0.00	0.00
Fursenkoina complanata	1.00	2.04	0.00	0.00	0.00	1.02	6.12	1.02	5.10
Gavelinopsis lobatus	0.00	0.00	0.00	0.00	0.00	0.00	0.00	0.00	0.00
Globobulimina auriculata	0.00	0.00	0.00	0.00	0.00	0.00	0.00	2.04	2.04
Globobullimina affinis	0.00	0.00	0.00	2.04	0.00	0.00	0.00	0.00	0.00
Gyroidina soldanii	13.00	3.06	4.08	0.00	2.04	5.10	11.22	2.04	2.04
Hoeglundia elegans	1.00	0.00	3.06	2.04	4.08	0.00	0.00	0.00	0.00
Hormosina globulifera	0.00	0.00	0.00	0.00	0.00	0.00	0.00	0.00	0.00
Indeterminate	0.00	1.02	0.00	0.00	0.00	0.00	0.00	0.00	0.00
Karreriella bradyi	0.00	0.00	0.00	2.04	1.02	0.00	0.00	0.00	0.00
Lagena cf. acuticosta	0.00	0.00	0.00	0.00	0.00	0.00	0.00	0.00	2.04
Lagena cf. interrupta	0.00	1.02	0.00	0.00	0.00	0.00	0.00	0.00	0.00
Lagena semistriata	0.00	1.02	0.00	0.00	0.00	0.00	0.00	0.00	0.00

Appendix B - Benthic foraminifera assemblage data

Core 9/97-14
Relative abundance - Benthic foraminifera 250-63um

Sample depth (cm)	1	23	51	54	57	62	81	90	93
Lagena sulcata	0.00	0.00	0.00	0.00	0.00	0.00	0.00	0.00	0.00
Melonis barleeanum	7.00	9.18	0.00	0.00	0.00	5.10	12.24	2.04	2.04
Melonis pompilioides	0.00	1.02	0.00	4.08	4.08	0.00	4.08	0.00	0.00
Nodosaria sp.	0.00	0.00	0.00	0.00	0.00	0.00	0.00	0.00	0.00
Nonionella auricula	0.00	0.00	0.00	0.00	0.00	0.00	0.00	0.00	0.00
Nonionella turgida	1.00	2.04	0.00	0.00	0.00	0.00	0.00	1.02	0.00
Nummoloculina irregularis	1.00	0.00	0.00	0.00	0.00	0.00	0.00	1.02	0.00
Oolina apiopleura	0.00	1.02	0.00	0.00	0.00	0.00	0.00	0.00	0.00
Oolina heronalleni	0.00	0.00	0.00	0.00	0.00	0.00	0.00	0.00	0.00
Oolina hexagona	1.00	0.00	0.00	0.00	0.00	0.00	0.00	1.02	0.00
Oolina intercalata	0.00	0.00	0.00	0.00	0.00	0.00	0.00	0.00	0.00
Oolina melo	0.00	0.00	0.00	0.00	0.00	0.00	0.00	0.00	0.00
Oolina squamosa	0.00	0.00	0.00	0.00	0.00	0.00	0.00	0.00	0.00
Oridorsalis umbonatus	0.00	0.00	0.00	0.00	0.00	0.00	0.00	0.00	0.00
Pseudofissurina mccullochae	0.00	2.04	0.00	0.00	0.00	0.00	0.00	0.00	2.04
Pseudosolenina borealis	5.00	1.02	2.04	0.00	0.00	0.00	0.00	5.10	0.00
Pullenia bulloides	1.00	8.16	3.06	12.24	2.04	4.08	4.08	1.02	5.10
Pullenia subcarinata	0.00	0.00	0.00	2.04	0.00	1.02	0.00	0.00	0.00
Pyrgo depressa	0.00	0.00	0.00	0.00	0.00	0.00	0.00	0.00	0.00
Pyrgo lacernula	0.00	0.00	0.00	0.00	0.00	0.00	0.00	0.00	0.00
Pyrgo murrhina	0.00	0.00	0.00	0.00	4.08	0.00	0.00	0.00	0.00
Pyrgo oblonga	0.00	0.00	0.00	0.00	0.00	0.00	0.00	0.00	0.00
Pyrgo rotalia	0.00	0.00	0.00	0.00	0.00	0.00	0.00	0.00	0.00
Pyrgo sarsi	0.00	0.00	0.00	0.00	0.00	0.00	0.00	0.00	0.00
Pyrgo serrata	0.00	0.00	0.00	0.00	0.00	0.00	0.00	0.00	0.00
Pyrgo sp.	0.00	1.02	0.00	0.00	0.00	0.00	0.00	0.00	0.00
Pyrgo williamsoni	0.00	0.00	0.00	0.00	0.00	0.00	1.02	0.00	0.00
Quinqueloculina arctica	0.00	0.00	0.00	2.04	0.00	0.00	0.00	0.00	0.00
Quinqueloculina bicornis	0.00	0.00	0.00	0.00	0.00	0.00	0.00	0.00	0.00
Quinqueloculina cliarensis	0.00	0.00	0.00	0.00	0.00	0.00	0.00	0.00	0.00
Quinqueloculina elongata	0.00	0.00	0.00	0.00	0.00	0.00	1.02	0.00	0.00
Quinqueloculina lata	0.00	0.00	0.00	0.00	0.00	0.00	0.00	0.00	0.00
Quinqueloculina seminulum	1.00	8.16	3.06	0.00	0.00	0.00	0.00	4.08	0.00
Quinqueloculina sp.	0.00	0.00	0.00	0.00	0.00	0.00	0.00	0.00	0.00
Quinqueloculina stalkeri	0.00	0.00	0.00	0.00	0.00	0.00	0.00	0.00	0.00
Quinqueloculina striata	0.00	0.00	0.00	0.00	0.00	0.00	0.00	0.00	0.00
Rupertina stabilis	0.00	0.00	0.00	0.00	0.00	0.00	0.00	0.00	0.00
Sigmoilopsis schlumbergeri	2.00	8.16	10.20	12.24	29.59	7.14	2.04	2.04	2.04
Siphotextularia rolhauseni	0.00	0.00	0.00	2.04	0.00	0.00	0.00	0.00	0.00
Solenina radiata	2.00	0.00	0.00	2.04	0.00	0.00	0.00	2.04	0.00
Spiroloculina limbata	0.00	0.00	0.00	0.00	0.00	0.00	0.00	0.00	0.00
Spiroloculina rotunda	0.00	0.00	0.00	0.00	0.00	0.00	0.00	0.00	0.00
Stainforthia (Fursenkoina) fusiformis	0.00	2.04	0.00	0.00	0.00	5.10	9.18	0.00	8.16
Stainforthia loeblichi	0.00	0.00	0.00	0.00	0.00	1.02	0.00	0.00	0.00
Stainforthia schreibersiana	0.00	0.00	0.00	0.00	0.00	0.00	0.00	0.00	0.00
Trifarina angulosa	6.00	12.24	5.10	0.00	0.00	2.04	7.14	6.12	11.22

Appendix B - Benthic foraminifera assemblage data

Core 9/97-14
Relative abundance - Benthic foraminifera 250-63um

Sample depth (cm)	1	23	51	54	57	62	81	90	93	
Trifarina bradyi	0.00	0.00	0.00	0.00	0.00	0.00	0.00	0.00	0.00	
Trifarina sp.	0.00	0.00	0.00	0.00	0.00	0.00	0.00	0.00	0.00	
Triloculina tricarinata	0.00	0.00	0.00	0.00	0.00	0.00	13.27	4.08	0.00	
Uvigerina celtica	0.00	1.02	0.00	0.00	1.02	0.00	0.00	0.00	0.00	
Uvigerina cf. pigmea	0.00	0.00	0.00	0.00	0.00	0.00	0.00	0.00	0.00	
Uvigerina peregrina	0.00	0.00	0.00	0.00	4.08	0.00	0.00	0.00	0.00	
Virgulina advena	0.00	0.00	0.00	0.00	0.00	0.00	0.00	0.00	0.00	

Appendix B - Benthic foraminifera assemblage data

Core 9/97-27/II
Relative abundance - Benthic foraminifera 250-63um

Sample depth (cm)	3	7	11	15	19	73	147	151	155.5
Alabaminella weddellensis	23.53	17.53	35.29	20.00	42.11	0.00	3.00	3.37	2.17
Amphycorina scalaris	0.00	0.00	0.00	0.00	0.00	0.00	0.00	0.00	0.00
Astacolus hyalacrulus	0.00	0.00	0.00	0.00	0.00	0.00	0.00	0.00	0.00
Astacolus sp.	0.00	0.00	0.00	0.00	0.00	0.00	0.00	0.00	0.00
Bolivina albatrossi	0.00	0.00	0.00	0.00	0.00	0.00	1.00	1.12	1.09
Bolivina pseduopunctata	4.41	3.09	0.00	3.53	1.32	1.01	0.00	0.00	0.00
Bolivina sp.	0.00	0.00	0.00	0.00	0.00	0.00	0.00	0.00	0.00
Bolivina spinescens	2.94	2.06	0.00	2.35	0.00	1.01	3.00	0.00	0.00
Bolivina subspinescens	0.00	0.00	0.00	0.00	0.00	0.00	0.00	0.00	0.00
Brizalina cf. robusta	0.00	0.00	0.00	0.00	0.00	0.00	0.00	0.00	0.00
Brizalina variabilis	0.00	0.00	0.00	0.00	0.00	0.00	0.00	0.00	0.00
Bullimina aculeata	0.00	0.00	0.00	0.00	0.00	0.00	0.00	0.00	0.00
Bullimina cf. gibba	0.00	0.00	0.00	0.00	0.00	0.00	0.00	0.00	0.00
Bullimina inflata	0.00	0.00	0.00	0.00	0.00	0.00	0.00	0.00	0.00
Bullimina marginata	0.00	0.00	0.00	0.00	0.00	0.00	0.00	0.00	0.00
Cassidulina laevigata	0.00	0.00	0.00	0.00	0.00	3.03	1.00	2.25	1.09
Cassidulina obtusa	0.00	0.00	0.00	0.00	0.00	0.00	0.00	0.00	0.00
Chilostomella oolina	0.00	0.00	0.00	0.00	0.00	0.00	0.00	0.00	0.00
Cibicides kullenbergi	0.00	0.00	0.00	0.00	0.00	0.00	0.00	0.00	0.00
Cibicides lobatulus	0.00	0.00	0.00	0.00	0.00	0.00	0.00	0.00	0.00
Cibicides pachyderma	0.00	0.00	0.00	0.00	0.00	0.00	1.00	1.12	2.17
Cibicides sp.	0.00	0.00	0.00	0.00	0.00	0.00	0.00	0.00	0.00
Cibicides wuellerstorfi	0.00	0.00	2.94	0.00	5.26	1.01	1.00	1.12	0.00
Cyclammina pusilla	0.00	0.00	0.00	0.00	0.00	0.00	0.00	0.00	0.00
Dentalina communis	0.00	0.00	0.00	0.00	0.00	0.00	0.00	0.00	0.00
Dentalina sp.	0.00	0.00	0.00	0.00	0.00	0.00	0.00	0.00	0.00
Eggerella bradyi	0.00	0.00	0.00	0.00	0.00	0.00	0.00	0.00	0.00
Ehrenbergina serrata	0.00	0.00	0.00	0.00	0.00	0.00	0.00	0.00	0.00
Epistominella exigua	27.94	43.30	47.06	32.94	36.84	0.00	14.00	17.98	15.22
Eponides pusillus	1.47	1.03	0.00	1.18	0.00	0.00	1.00	1.12	1.09
Fissurina marginata	1.47	3.09	0.00	3.53	0.00	1.01	1.00	1.12	3.26
Fissurina orbignyana	0.00	0.00	0.00	0.00	0.00	0.00	0.00	0.00	0.00
Fissurina porcupinensis	0.00	0.00	0.00	0.00	0.00	0.00	0.00	0.00	0.00
Fissurina varioperforata	0.00	0.00	0.00	0.00	0.00	0.00	0.00	0.00	0.00
Fursenkoina complanata	1.47	1.03	0.00	1.18	0.00	30.30	6.00	3.37	19.57
Gavelinopsis lobatus	0.00	0.00	0.00	0.00	0.00	0.00	0.00	0.00	0.00
Globobulimina auriculata	0.00	0.00	0.00	0.00	0.00	0.00	0.00	0.00	0.00
Globobullimina affinis	0.00	0.00	0.00	0.00	0.00	0.00	0.00	0.00	0.00
Gyroidina soldanii	2.94	1.03	0.00	2.35	0.00	2.02	8.00	2.25	4.35
Hoeglundia elegans	2.94	4.12	0.00	9.41	1.32	1.01	0.00	0.00	0.00
Hormosina globulifera	0.00	0.00	0.00	0.00	0.00	0.00	0.00	0.00	0.00
Indeterminate	1.47	1.03	0.00	1.18	0.00	0.00	0.00	0.00	0.00
Karreriella bradyi	2.94	2.06	0.00	0.00	0.00	0.00	0.00	0.00	0.00
Lagena cf. acuticosta	0.00	0.00	0.00	0.00	0.00	0.00	0.00	0.00	0.00
Lagena cf. interrupta	0.00	0.00	0.00	0.00	0.00	1.01	0.00	0.00	0.00
Lagena semistriata	5.88	1.03	0.00	1.18	0.00	0.00	0.00	0.00	0.00

Appendix B - Benthic foraminifera assemblage data

Core 9/97-27/II
Relative abundance - Benthic foraminifera 250-63um

Sample depth (cm)	3	7	11	15	19	73	147	151	155.5
Lagena sulcata	0.00	0.00	0.00	0.00	0.00	0.00	0.00	0.00	0.00
Melonis barleeanum	1.47	5.15	13.24	3.53	11.84	1.01	12.00	20.22	6.52
Melonis pompilioides	1.47	1.03	0.00	0.00	0.00	2.02	4.00	4.49	2.17
Nodosaria sp.	0.00	0.00	0.00	0.00	0.00	0.00	0.00	0.00	0.00
Nonionella auricula	0.00	0.00	0.00	0.00	0.00	0.00	0.00	0.00	1.09
Nonionella turgida	0.00	0.00	0.00	0.00	0.00	0.00	0.00	0.00	0.00
Nummoloculina irregularis	0.00	0.00	0.00	0.00	0.00	0.00	0.00	0.00	0.00
Oolina apiopleura	0.00	0.00	0.00	0.00	0.00	0.00	0.00	0.00	0.00
Oolina heronalleni	0.00	0.00	0.00	0.00	0.00	0.00	0.00	0.00	0.00
Oolina hexagona	0.00	0.00	0.00	0.00	0.00	0.00	0.00	0.00	0.00
Oolina intercalata	0.00	0.00	0.00	0.00	0.00	0.00	0.00	0.00	0.00
Oolina melo	0.00	0.00	0.00	0.00	0.00	0.00	0.00	0.00	0.00
Oolina squamosa	0.00	0.00	0.00	0.00	0.00	0.00	0.00	0.00	0.00
Oridorsalis umbonatus	0.00	0.00	0.00	0.00	0.00	0.00	0.00	0.00	0.00
Pseudofissurina mccullochae	0.00	0.00	0.00	0.00	0.00	1.01	0.00	0.00	0.00
Pseudosolenina borealis	4.41	3.09	0.00	2.35	0.00	1.01	0.00	0.00	0.00
Pullenia bulloides	2.94	2.06	1.47	2.35	1.32	1.01	4.00	0.00	4.35
Pullenia subcarinata	0.00	0.00	0.00	0.00	0.00	0.00	0.00	0.00	0.00
Pyrgo depressa	0.00	0.00	0.00	0.00	0.00	0.00	0.00	0.00	0.00
Pyrgo lacernula	0.00	0.00	0.00	0.00	0.00	0.00	0.00	0.00	0.00
Pyrgo murrhina	0.00	0.00	0.00	0.00	0.00	0.00	0.00	0.00	0.00
Pyrgo oblonga	0.00	0.00	0.00	0.00	0.00	0.00	0.00	0.00	0.00
Pyrgo rotalia	0.00	0.00	0.00	0.00	0.00	0.00	0.00	0.00	0.00
Pyrgo sarsi	0.00	0.00	0.00	0.00	0.00	0.00	0.00	0.00	0.00
Pyrgo serrata	0.00	0.00	0.00	0.00	0.00	0.00	0.00	0.00	0.00
Pyrgo sp.	0.00	0.00	0.00	0.00	0.00	0.00	0.00	0.00	0.00
Pyrgo williamsoni	0.00	0.00	0.00	0.00	0.00	0.00	1.00	0.00	3.26
Quinqueloculina arctica	0.00	0.00	0.00	0.00	0.00	0.00	0.00	0.00	0.00
Quinqueloculina bicornis	0.00	0.00	0.00	0.00	0.00	0.00	0.00	0.00	0.00
Quinqueloculina cliarensis	0.00	0.00	0.00	0.00	0.00	0.00	0.00	0.00	0.00
Quinqueloculina elongata	0.00	0.00	0.00	0.00	0.00	0.00	1.00	1.12	1.09
Quinqueloculina lata	0.00	0.00	0.00	0.00	0.00	0.00	0.00	0.00	0.00
Quinqueloculina seminulum	0.00	1.03	0.00	1.18	0.00	2.02	7.00	7.87	7.61
Quinqueloculina sp.	0.00	0.00	0.00	0.00	0.00	0.00	0.00	0.00	0.00
Quinqueloculina stalkeri	0.00	0.00	0.00	0.00	0.00	0.00	0.00	0.00	0.00
Quinqueloculina striata	0.00	0.00	0.00	0.00	0.00	0.00	0.00	0.00	0.00
Rupertina stabilis	0.00	0.00	0.00	0.00	0.00	0.00	0.00	0.00	0.00
Sigmoilopsis schlumbergeri	2.94	2.06	0.00	2.35	0.00	0.00	2.00	0.00	2.17
Siphotextularia rolhauseni	0.00	0.00	0.00	0.00	0.00	0.00	0.00	0.00	0.00
Solenina radiata	0.00	0.00	0.00	0.00	0.00	0.00	0.00	0.00	0.00
Spiroloculina limbata	0.00	0.00	0.00	0.00	0.00	0.00	0.00	0.00	0.00
Spiroloculina rotunda	0.00	0.00	0.00	0.00	0.00	0.00	0.00	0.00	0.00
Stainforthia (Fursenkoina) fusiformis	0.00	1.03	0.00	0.00	0.00	40.40	9.00	13.48	10.87
Stainforthia loeblichi	0.00	0.00	0.00	0.00	0.00	1.01	0.00	0.00	0.00
Stainforthia schreibersiana	0.00	0.00	0.00	0.00	0.00	0.00	0.00	0.00	0.00
Trifarina angulosa	1.47	1.03	0.00	5.88	0.00	0.00	7.00	2.25	8.70

Appendix B - Benthic foraminifera assemblage data

Core 9/97-27/II
Relative abundance - Benthic foraminifera 250-63um

Sample depth (cm)	3	7	11	15	19	73	147	151	155.5
Trifarina bradyi	0.00	0.00	0.00	0.00	0.00	0.00	0.00	0.00	0.00
Trifarina sp.	0.00	0.00	0.00	0.00	0.00	0.00	0.00	0.00	0.00
Triloculina tricarinata	5.88	3.09	0.00	3.53	0.00	9.09	13.00	15.73	2.17
Uvigerina celtica	0.00	0.00	0.00	0.00	0.00	0.00	0.00	0.00	0.00
Uvigerina cf. pigmea	0.00	0.00	0.00	0.00	0.00	0.00	0.00	0.00	0.00
Uvigerina peregrina	0.00	0.00	0.00	0.00	0.00	0.00	0.00	0.00	0.00
Virgulina advena	0.00	0.00	0.00	0.00	0.00	0.00	0.00	0.00	0.00

Appendix B - Benthic foraminifera assemblage data

Core 9/97-27/II
Relative abundance - Benthic foraminifera 250-63um

Sample depth (cm)	183	196.5	200.5	204.5	208.5	212.5	216.5	241.5	245.5	249.5	253.5
Alabaminella weddellensis	1.98	22.64	15.58	12.12	15.00	17.14	15.58	4.55	3.03	9.76	5.48
Amphycorina scalaris	0.00	1.89	0.00	0.00	1.25	4.29	0.00	0.00	0.00	0.00	0.00
Astacolus hyalacrulus	0.99	1.89	1.30	1.01	1.25	1.43	0.00	0.00	0.00	0.00	0.00
Astacolus sp.	0.00	0.00	0.00	0.00	0.00	0.00	0.00	0.00	0.00	0.00	0.00
Bolivina albatrossi	0.00	0.00	0.00	0.00	0.00	0.00	0.00	0.00	0.00	0.00	0.00
Bolivina pseduopunctata	1.98	1.89	1.30	1.01	1.25	1.43	1.30	2.27	2.02	2.44	0.00
Bolivina sp.	0.00	0.00	0.00	0.00	0.00	0.00	0.00	0.00	0.00	0.00	0.00
Bolivina spinescens	0.99	1.89	1.30	1.01	1.25	1.43	1.30	0.00	0.00	0.00	0.00
Bolivina subspinescens	0.00	0.00	0.00	0.00	0.00	0.00	0.00	0.00	0.00	0.00	0.00
Brizalina cf. robusta	0.00	1.89	1.30	1.01	1.25	1.43	1.30	0.00	0.00	0.00	0.00
Brizalina variabilis	0.00	0.00	0.00	0.00	0.00	0.00	0.00	0.00	0.00	0.00	0.00
Bullimina aculeata	0.00	0.00	0.00	0.00	0.00	0.00	0.00	0.00	0.00	0.00	0.00
Bullimina cf. gibba	0.00	0.00	0.00	0.00	0.00	0.00	0.00	0.00	0.00	0.00	0.00
Bullimina inflata	0.00	0.00	0.00	0.00	0.00	0.00	0.00	0.00	0.00	0.00	0.00
Bullimina marginata	0.99	0.00	0.00	0.00	0.00	0.00	0.00	0.00	0.00	0.00	0.00
Cassidulina laevigata	3.96	1.89	1.30	2.02	6.25	2.86	2.60	2.27	9.09	4.88	8.22
Cassidulina obtusa	0.00	0.00	0.00	0.00	0.00	0.00	0.00	0.00	0.00	0.00	0.00
Chilostomella oolina	0.00	0.00	0.00	0.00	0.00	0.00	0.00	0.00	0.00	0.00	0.00
Cibicides kullenbergi	0.00	0.00	0.00	0.00	0.00	0.00	0.00	0.00	0.00	0.00	0.00
Cibicides lobatulus	0.00	0.00	0.00	0.00	0.00	0.00	0.00	0.00	0.00	0.00	0.00
Cibicides pachyderma	0.99	0.00	0.00	0.00	0.00	0.00	0.00	1.14	1.01	0.00	0.00
Cibicides sp.	0.00	0.00	0.00	0.00	0.00	0.00	0.00	0.00	0.00	0.00	0.00
Cibicides wuellerstorfi	2.97	0.00	0.00	2.02	2.50	7.14	2.60	2.27	2.02	2.44	2.74
Cyclammina pusilla	0.00	0.00	0.00	0.00	0.00	0.00	0.00	0.00	0.00	0.00	0.00
Dentalina communis	0.00	0.00	0.00	0.00	0.00	0.00	0.00	0.00	0.00	0.00	0.00
Dentalina sp.	0.00	0.00	0.00	0.00	0.00	0.00	0.00	0.00	0.00	0.00	0.00
Eggerella bradyi	1.98	0.00	0.00	0.00	0.00	0.00	0.00	1.14	1.01	1.22	1.37
Ehrenbergina serrata	0.00	0.00	0.00	0.00	0.00	0.00	0.00	0.00	0.00	0.00	0.00
Epistominella exigua	23.76	1.89	2.60	9.09	2.50	4.29	11.69	34.09	25.25	24.39	19.18
Eponides pusillus	0.99	1.89	1.30	1.01	1.25	1.43	1.30	0.00	0.00	0.00	0.00
Fissurina marginata	1.98	1.89	1.30	1.01	0.00	1.43	0.00	0.00	2.02	0.00	0.00
Fissurina orbignyana	0.00	0.00	0.00	0.00	0.00	0.00	0.00	0.00	0.00	0.00	0.00
Fissurina porcupinensis	0.00	0.00	0.00	0.00	0.00	0.00	0.00	0.00	0.00	0.00	0.00
Fissurina varioperforata	0.00	0.00	0.00	0.00	0.00	0.00	0.00	0.00	0.00	0.00	0.00
Fursenkoina complanata	7.92	0.00	0.00	0.00	0.00	0.00	0.00	3.41	3.03	3.66	4.11
Gavelinopsis lobatus	0.00	0.00	0.00	0.00	0.00	0.00	0.00	0.00	0.00	0.00	0.00
Globobulimina auriculata	0.00	0.00	0.00	0.00	0.00	0.00	1.30	0.00	0.00	0.00	0.00
Globobullimina affinis	0.00	0.00	0.00	0.00	0.00	0.00	0.00	0.00	0.00	0.00	0.00
Gyroidina soldanii	11.88	3.77	9.09	16.16	11.25	14.29	18.18	19.32	13.13	14.63	13.70
Hoeglundia elegans	0.00	0.00	0.00	0.00	0.00	0.00	0.00	1.14	1.01	1.22	0.00
Hormosina globulifera	0.00	0.00	0.00	0.00	0.00	0.00	0.00	0.00	0.00	0.00	0.00
Indeterminate	0.00	0.00	0.00	0.00	0.00	0.00	0.00	0.00	0.00	0.00	0.00
Karreriella bradyi	0.00	0.00	0.00	0.00	0.00	0.00	0.00	0.00	0.00	0.00	0.00
Lagena cf. acuticosta	0.00	0.00	0.00	0.00	0.00	0.00	0.00	0.00	0.00	0.00	0.00
Lagena cf. interrupta	0.99	0.00	0.00	0.00	0.00	0.00	0.00	1.14	1.01	0.00	1.37
Lagena semistriata	0.00	0.00	0.00	0.00	0.00	0.00	0.00	0.00	0.00	0.00	0.00

Appendix B - Benthic foraminifera assemblage data

Core 9/97-27/II
Relative abundance - Benthic foraminifera 250-63um

Sample depth (cm)	183	196.5	200.5	204.5	208.5	212.5	216.5	241.5	245.5	249.5	253.5
Lagena sulcata	0.00	0.00	0.00	0.00	0.00	0.00	0.00	0.00	0.00	0.00	0.00
Melonis barleeanum	4.95	18.87	27.27	21.21	23.75	7.14	12.99	5.68	9.09	13.41	13.70
Melonis pompilioides	1.98	1.89	0.00	1.01	0.00	1.43	1.30	0.00	2.02	0.00	2.74
Nodosaria sp.	0.00	0.00	0.00	0.00	0.00	0.00	0.00	0.00	0.00	0.00	0.00
Nonionella auricula	0.00	0.00	0.00	0.00	0.00	0.00	0.00	0.00	0.00	0.00	0.00
Nonionella turgida	0.00	0.00	0.00	0.00	0.00	0.00	0.00	0.00	0.00	0.00	0.00
Nummoloculina irregularis	0.00	0.00	0.00	0.00	0.00	0.00	0.00	0.00	0.00	0.00	0.00
Oolina apiopleura	0.00	0.00	0.00	0.00	0.00	0.00	0.00	0.00	0.00	0.00	0.00
Oolina heronalleni	0.00	0.00	0.00	0.00	0.00	0.00	0.00	0.00	0.00	0.00	0.00
Oolina hexagona	0.00	0.00	0.00	0.00	0.00	0.00	0.00	0.00	0.00	0.00	0.00
Oolina intercalata	0.00	0.00	0.00	0.00	0.00	0.00	0.00	0.00	0.00	0.00	0.00
Oolina melo	0.00	0.00	0.00	0.00	0.00	0.00	5.19	0.00	0.00	0.00	0.00
Oolina squamosa	0.00	0.00	0.00	0.00	0.00	0.00	0.00	0.00	0.00	0.00	0.00
Oridorsalis umbonatus	0.00	0.00	0.00	0.00	0.00	0.00	0.00	0.00	0.00	0.00	0.00
Pseudofissurina mccullochae	0.00	0.00	0.00	0.00	0.00	0.00	0.00	1.14	1.01	1.22	1.37
Pseudosolenina borealis	0.00	0.00	0.00	0.00	0.00	0.00	0.00	0.00	0.00	0.00	0.00
Pullenia bulloides	0.00	0.00	0.00	0.00	0.00	0.00	0.00	0.00	4.04	4.88	5.48
Pullenia subcarinata	0.00	0.00	0.00	0.00	0.00	0.00	0.00	0.00	0.00	0.00	0.00
Pyrgo depressa	0.00	0.00	0.00	0.00	0.00	0.00	0.00	0.00	0.00	0.00	0.00
Pyrgo lacernula	0.00	0.00	0.00	0.00	0.00	0.00	0.00	0.00	0.00	0.00	0.00
Pyrgo murrhina	0.00	0.00	0.00	0.00	0.00	0.00	0.00	0.00	0.00	0.00	0.00
Pyrgo oblonga	0.00	0.00	0.00	0.00	0.00	0.00	0.00	0.00	0.00	0.00	0.00
Pyrgo rotalia	0.00	0.00	0.00	0.00	0.00	0.00	0.00	0.00	0.00	0.00	0.00
Pyrgo sarsi	0.00	0.00	0.00	0.00	0.00	0.00	0.00	0.00	0.00	0.00	0.00
Pyrgo serrata	0.00	0.00	0.00	0.00	0.00	0.00	0.00	0.00	0.00	0.00	0.00
Pyrgo sp.	0.00	0.00	0.00	0.00	0.00	0.00	0.00	3.41	3.03	2.44	4.11
Pyrgo williamsoni	3.96	1.89	1.30	1.01	1.25	1.43	1.30	1.14	1.01	1.22	1.37
Quinqueloculina arctica	0.00	0.00	0.00	0.00	0.00	0.00	0.00	0.00	0.00	0.00	0.00
Quinqueloculina bicornis	0.00	0.00	0.00	0.00	0.00	0.00	0.00	0.00	0.00	0.00	0.00
Quinqueloculina cliarensis	0.00	0.00	0.00	0.00	0.00	0.00	0.00	0.00	0.00	0.00	0.00
Quinqueloculina elongata	0.00	1.89	1.30	1.01	1.25	1.43	1.30	0.00	0.00	0.00	0.00
Quinqueloculina lata	0.00	0.00	0.00	0.00	0.00	0.00	0.00	0.00	0.00	0.00	0.00
Quinqueloculina seminulum	0.00	11.32	2.60	2.02	0.00	2.86	5.19	2.27	2.02	2.44	2.74
Quinqueloculina sp.	0.00	0.00	0.00	0.00	0.00	0.00	0.00	0.00	0.00	0.00	0.00
Quinqueloculina stalkeri	0.00	0.00	0.00	0.00	0.00	0.00	0.00	0.00	0.00	0.00	0.00
Quinqueloculina striata	0.00	0.00	0.00	0.00	0.00	0.00	0.00	0.00	0.00	0.00	0.00
Rupertina stabilis	0.00	0.00	0.00	0.00	0.00	0.00	0.00	0.00	0.00	0.00	0.00
Sigmoilopsis schlumbergeri	1.98	0.00	3.90	3.03	0.00	4.29	0.00	1.14	5.05	4.88	1.37
Siphotextularia rolhauseni	0.00	0.00	0.00	0.00	0.00	0.00	0.00	0.00	0.00	0.00	0.00
Solenina radiata	0.00	0.00	0.00	0.00	0.00	0.00	0.00	0.00	0.00	0.00	0.00
Spiroloculina limbata	0.00	0.00	0.00	0.00	0.00	0.00	0.00	0.00	0.00	0.00	0.00
Spiroloculina rotunda	0.00	0.00	0.00	0.00	0.00	0.00	0.00	0.00	0.00	0.00	0.00
Stainforthia (Fursenkoina) fusiformis	17.82	0.00	0.00	0.00	0.00	0.00	0.00	0.00	0.00	0.00	0.00
Stainforthia loeblichi	0.99	0.00	0.00	0.00	0.00	0.00	0.00	0.00	0.00	0.00	0.00
Stainforthia schreibersiana	0.00	0.00	0.00	0.00	0.00	0.00	0.00	0.00	0.00	0.00	0.00
Trifarina angulosa	2.97	18.87	24.68	13.13	21.25	12.86	5.19	1.14	2.02	1.22	1.37

Appendix B - Benthic foraminifera assemblage data

Core 9/97-27/II
Relative abundance - Benthic foraminifera 250-63um

Sample depth (cm)	183	196.5	200.5	204.5	208.5	212.5	216.5	241.5	245.5	249.5	253.5
Trifarina bradyi	0.00	0.00	0.00	0.00	0.00	0.00	0.00	0.00	0.00	0.00	0.00
Trifarina sp.	0.00	0.00	0.00	0.00	0.00	0.00	0.00	0.00	0.00	0.00	0.00
Triloculina tricarinata	0.00	0.00	0.00	0.00	0.00	0.00	0.00	9.09	6.06	2.44	8.22
Uvigerina celtica	0.99	1.89	2.60	10.10	7.50	10.00	10.39	2.27	1.01	1.22	1.37
Uvigerina cf. pigmea	0.00	0.00	0.00	0.00	0.00	0.00	0.00	0.00	0.00	0.00	0.00
Uvigerina peregrina	0.00	0.00	0.00	0.00	0.00	0.00	0.00	0.00	0.00	0.00	0.00
Virgulina advena	0.00	0.00	0.00	0.00	0.00	0.00	0.00	0.00	0.00	0.00	0.00

Appendix C

Geochemical data

Bottom water temperature equation

$Mg/Ca = 0.85xe^{0.11*BWT}$ Martin *et al.* (2002)

Where BWT = bottom water temperature (°C)

Oxygen (seawater) equation (*Cibicides wuellerstorfi*)

$T\ (°C) = 16.9 - 4.0(d_c - d_{sw})$ Shackleton (1974)

Where T = temperature, d_c = oxygen isotope ratio of calcite and d_{sw} = oxygen isotope ratio of seawater

Cadmium/Calcium to Phosphorus

Phosphorus (µmol/kg) = $Cd_{sw} \times 2.1x10^{-4}$ Boyle (1988)

Where Cdsw = Cd concentration of seawater (nmol/kg)

D = Cd(foram) / Cd_{sw} (nmol/kg)
Boyle (1992)

Where Cd(foram) = Cd concentration in foraminifera (µmol/mol) and D = empirical relationship between seawater and foraminiferal cadmium concentrations

Appendix C

Geochemical data

Core	D
9/97-10	2.3
9/97-04	2.2
9/97-14	2.7

From Bertram *et al.* (1995)

Surface temperature from oxygen (*Globigerina bulloides*)

T (°C) = –4.89 ($d_c - d_{sw}$) + 13.20 Bemis *et al.* (1998)

Species-specific equation for calculating SST from *G.bulloides,* where d_c = oxygen isotope ratio of foraminiferal calcite and d_{sw} = oxygen isotope ratio of seawater. Values for d_{sw} derived from Elderfield and Ganssen (2000).

Appendix C

Core 9/97-10 Planktonic geochemical data

Sample depth (cm)	$d^{13}C$ ‰ VPDB	$d^{18}O$ ‰ VPDB	Sample depth (cm)	$d^{13}C$ ‰ VPDB	$d^{18}O$ ‰ VPDB
3	-0.11	1.98	**103**	-0.75	1.44
7	-0.45	1.91	**111**	-0.71	2.44
11	-0.68	1.29	**115**	-0.66	2.86
16	-1.20	3.61	**120**	-1.12	2.72
20	-0.59	2.52	**123**	-1.10	2.77
27	-0.27	2.99	**132**	-0.62	2.47
31	-0.11	2.62	**136**	-0.91	1.59
35	-0.16	2.83	**142**	-1.65	1.81
39	-0.38	2.84	**146**	-0.27	2.51
43	-0.60	2.00	**150**	-0.60	2.42
47	-0.76	2.02	**156**	-0.39	1.48
51	0.03	2.44	**160**	-1.04	2.75
55	-0.40	1.50	**168**	-0.52	2.36
59	-0.62	1.55	**172**	-0.80	2.61
63	-0.43	2.38	**176**	-0.38	2.70
67	-0.24	2.12	**180**	-0.23	3.09
71	-0.27	1.73	**184**	-0.89	1.67
75	-0.63	1.54	**188**	-0.48	2.44
79	-0.59	3.10	**192**	-0.48	2.50
83	-0.95	3.09	**196**	-0.36	2.37
87	-0.95	2.80	**200**	-0.38	1.78
91	-0.80	2.94	**204**	-0.74	1.09
95	-1.00	3.03	**213**	-1.18	3.34
99	-0.63	2.09	**236**	-1.06	2.56

Appendix C
Geochemical data

Core 9/97-10 - Benthic geochemistry

Sample depth (cm)	Sr/Ca (mmol/mol)	SD	Cd/Ca (µmol/mol)	SD	Cdsw (nmol/kg)	P (µmol/kg)	Ba/Ca (µmol/mol)	SD	Mg/Ca (mmol/mol)	SD	BWT (°C)	SE	$\delta^{13}C$ ‰ VPDB	SD	$\delta^{18}O$ ‰ VPDB	SD
3	1.42	0.00	0.09	0.00	0.21	1.01	2.21	0.01	1.72	0.00	6.41	1.40	1.07	0.08	1.98	0.09
11	1.42	0.00	0.06	0.00	0.14	0.68	1.72	0.00	1.79	0.01	6.78	1.40	1.50	0.08	1.29	0.09
15	1.45	0.01	0.07	0.00	0.15	0.71	1.71	0.01	1.85	0.00	7.09	1.40	1.66	0.08	3.61	0.09
16	1.41	0.00	0.04	0.00	0.10	0.49	1.75	0.00	1.63	0.01	5.91	1.40	1.60	0.08	4.19	0.09
20	1.47	0.00	0.08	0.00	0.18	0.84	2.03	0.01	1.83	0.01	6.97	1.40	1.50	0.08	2.52	0.09
21	1.38	0.00	0.05	0.00	0.11	0.51	1.73	0.00	1.50	0.01	5.18	1.40	1.70	0.08	4.01	0.09
27	1.44	0.01	0.08	0.00	0.17	0.83	1.75	0.00	1.78	0.01	6.73	1.40	1.70	0.08	3.99	0.09
35	1.47	0.00	0.08	0.00	0.18	0.84	3.65	0.00	1.74	0.01	6.51	1.40	1.57	0.08	3.69	0.09
39	1.43	0.00	0.14	0.00	0.31	1.49	1.64	0.01	1.69	0.00	6.23	1.40	1.91	0.08	3.93	0.09
43	1.43	0.01	0.07	0.00	0.15	0.71	1.68	0.01	1.61	0.00	5.78	1.40	1.55	0.08	3.43	0.09
51.5	1.42	0.00	0.14	0.00	0.31	1.50	2.04	0.00	1.62	0.01	5.84	1.40	2.47	0.08	4.24	0.09
67.5	1.47	0.00	0.14	0.00	0.32	1.54	3.00	0.02	2.04	0.00	7.97	1.40	0.88	0.08	3.44	0.09
91	1.42	0.00	0.12	0.00	0.28	1.35	2.09	0.01	1.68	0.01	6.21	1.40	2.07	0.08	4.37	0.09

Sample depth (cm)	Sr/Ca (mmol/mol)	SD	Cd/Ca (µmol/mol)	SD	Cdsw (nmol/kg)	P (µmol/kg)	Ba/Ca (µmol/mol)	SD	Mg/Ca (mmol/mol)	SD	BWT (°C)	SE	$\delta^{13}C$ ‰ VPDB	SD	$\delta^{18}O$ ‰ VPDB	SD
1	1.32	0.00	0.19	0.00	0.41	1.94	2.89	0.00	1.46	0.01	5.42	1.40	1.21	0.08	2.64	0.09
2	1.32	0.01	0.13	0.00	0.29	1.39	2.71	0.01	1.18	0.00	4.49	1.40	1.15	0.08	2.76	0.09
4	1.33	0.00	0.14	0.00	0.32	1.51	3.17	0.01	1.51	0.01	6.77	1.40	1.16	0.08	2.69	0.09
8	1.40	0.01	0.06	0.00	0.12	0.58	1.86	0.01	1.78	0.01	5.23	1.40	1.62	0.08	4.35	0.09
17	1.42	0.01	0.07	0.00	0.15	0.71	2.64	0.02	1.63	0.01	4.46	1.40	1.53	0.08	4.26	0.09
29	1.40	0.01	0.11	0.00	0.23	1.10	2.11	0.01	1.92	0.01	5.94	1.40	-	-	-	-
36	1.37	0.01	0.09	0.00	0.21	0.99	2.90	0.01	1.42	0.00	6.19	1.40	1.90	0.08	4.42	0.09
38	1.47	0.01	0.09	0.00	0.19	0.93	1.84	0.01	1.80	0.00	5.33	1.40	1.09	0.08	3.96	0.09
44	1.37	0.00	0.07	0.00	0.15	0.71	2.64	0.01	1.63	0.00	4.46	1.40	2.03	0.08	4.51	0.09
47	1.33	0.01	0.09	0.00	0.21	0.98	2.26	0.01	1.43	0.00	5.23	1.40	1.58	0.08	4.05	0.09
51	1.38	0.00	0.11	0.00	0.23	1.10	2.11	0.00	1.92	0.00	5.94	1.40	1.38	0.08	3.95	0.09
55	1.34	0.01	0.19	0.00	0.41	1.97	3.61	0.01	1.39	0.00	4.98	1.40	1.74	0.08	4.12	0.09
59	1.35	0.00	0.09	0.00	0.19	0.91	2.29	0.00	1.64	0.00	4.50	1.40	2.24	0.08	4.62	0.09
63	1.44	0.01	0.23	0.00	0.50	2.36	1.96	0.00	1.79	0.00	5.29	1.40	-	-	-	-
67	1.36	0.00	0.12	0.00	0.26	1.26	2.13	0.01	1.62	0.00	4.39	1.40	1.89	0.08	4.06	0.09
71	1.37	0.00	0.14	0.00	0.31	1.48	2.50	0.00	2.23	0.00	7.29	1.40	-	-	-	-
83	1.37	0.01	0.16	0.00	0.35	1.66	2.56	0.00	1.66	0.00	4.59	1.40	1.44	0.08	3.34	0.09

Appendix C Geochemical data 9/97-14

Sample depth (cm)	Sr/Ca (mmol/mol)	SD	Cd/Ca (µmol/mol)	SD	Cdsw (nmol/kg)	P (µmol/kg)	Ba/Ca (µmol/mol)	SD	Mg/Ca (mmol/mol)	SD	BWT (°C)	SE	$\delta^{13}C$ ‰ VPDB	SD	$\delta^{18}O$ ‰ VPDB	SD
1	1.32	0.00	0.19	0.00	0.41	1.94	2.89	0.00	1.46	0.01	5.42	1.40	1.21	0.08	2.64	0.09
2	1.32	0.01	0.13	0.00	0.29	1.39	2.71	0.01	1.18	0.00	4.49	1.40	1.15	0.08	2.76	0.09
4	1.33	0.00	0.14	0.00	0.32	1.51	3.17	0.01	1.51	0.01	6.77	1.40	1.16	0.08	2.69	0.09
8	1.40	0.01	0.06	0.00	0.12	0.58	1.86	0.01	1.78	0.01	5.23	1.40	1.62	0.08	4.35	0.09
17	1.42	0.01	0.07	0.00	0.15	0.71	2.64	0.02	1.63	0.01	4.46	1.40	1.53	0.08	4.26	0.09
29	1.40	0.01	0.11	0.00	0.23	1.10	2.11	0.01	1.92	0.01	5.94	1.40	-	-	-	-
36	1.37	0.01	0.09	0.00	0.21	0.99	2.90	0.01	1.42	0.00	6.19	1.40	1.90	0.08	4.42	0.09
38	1.47	0.01	0.09	0.00	0.19	0.93	1.84	0.01	1.80	0.00	5.33	1.40	1.09	0.08	3.96	0.09
44	1.37	0.00	0.07	0.00	0.15	0.71	2.64	0.01	1.63	0.00	4.46	1.40	2.03	0.08	4.51	0.09
47	1.33	0.01	0.09	0.00	0.21	0.98	2.26	0.01	1.43	0.00	5.23	1.40	1.58	0.08	4.05	0.09
51	1.38	0.00	0.11	0.00	0.23	1.10	2.11	0.00	1.92	0.00	5.94	1.40	1.38	0.08	3.95	0.09
55	1.34	0.01	0.19	0.00	0.41	1.97	3.61	0.01	1.39	0.00	4.98	1.40	1.74	0.08	4.12	0.09
59	1.35	0.00	0.09	0.00	0.19	0.91	2.29	0.00	1.64	0.00	4.50	1.40	2.24	0.08	4.62	0.09
63	1.44	0.01	0.23	0.00	0.50	2.36	1.96	0.00	1.79	0.00	5.29	1.40	-	-	-	-
67	1.36	0.00	0.12	0.00	0.26	1.26	2.13	0.01	1.62	0.00	4.39	1.40	1.89	0.08	4.06	0.09
71	1.37	0.00	0.14	0.00	0.31	1.48	2.50	0.00	2.23	0.00	7.29	1.40	-	-	-	-
83	1.37	0.01	0.16	0.00	0.35	1.66	2.56	0.00	1.66	0.00	4.59	1.40	1.44	0.08	3.34	0.09

Sample depth (cm)	Sr/Ca (mmol/mol)	SD	Cd/Ca (µmol/mol)	SD	Cdsw (nmol/kg)	P (µmol/kg)	Ba/Ca (µmol/mol)	SD	Mg/Ca (mmol/mol)	SD	BWT (°C)	SE	$\delta^{13}C$ ‰ VPDB	SD	$\delta^{18}O$ ‰ VPDB	SD
1	1.41	0.01	0.17	0.00	0.45	2.13	2.96	0.02	1.78	0.00	6.72	1.40	1.43	0.08	3.79	0.09
5	1.45	0.00	0.06	0.00	0.15	0.73	2.60	0.01	1.50	0.01	5.19	1.40	1.31	0.08	4.38	0.09
7.5	1.38	0.01	0.14	0.00	0.37	1.74	2.28	0.01	1.69	0.00	6.27	1.40	1.28	0.08	3.71	0.09
12	1.40	0.01	0.09	0.00	0.25	1.19	2.39	0.01	1.58	0.00	5.62	1.40	1.24	0.08	4.36	0.09
19	1.43	0.00	0.08	0.00	0.21	1.00	5.66	0.04	1.50	0.00	5.17	1.40	1.36	0.08	4.15	0.09
23	1.39	0.01	0.15	0.00	0.40	1.91	2.21	0.02	1.83	0.01	6.97	1.40	1.13	0.08	4.08	0.09
27	1.45	0.00	0.10	0.00	0.27	1.28	2.34	0.01	1.58	0.00	5.61	1.40	1.34	0.08	3.86	0.09
35	1.39	0.00	0.12	0.00	0.32	1.53	1.90	0.00	1.58	0.01	5.65	1.40	1.34	0.08	3.84	0.09
39	1.41	0.00	0.11	0.00	0.31	1.46	2.05	0.01	1.63	0.00	5.92	1.40	1.50	0.08	4.11	0.09
41	1.38	0.00	0.12	0.00	0.32	1.53	2.19	0.02	1.60	0.00	5.76	1.40	1.57	0.08	4.09	0.09
43	1.38	0.00	0.09	0.00	0.25	1.17	2.42	0.00	1.62	0.01	5.89	1.40	1.52	0.08	4.22	0.09
49	1.39	0.00	0.16	0.00	0.44	2.12	2.98	0.00	1.82	0.01	6.93	1.40	1.34	0.08	4.09	0.09
51	1.37	0.00	0.15	0.00	0.41	1.95	2.53	0.00	1.93	0.01	7.47	1.40	1.17	0.08	3.64	0.09
54	1.39	0.00	0.12	0.00	0.32	1.53	2.66	0.01	1.61	0.01	5.83	1.40	0.98	0.08	4.18	0.09
59	1.46	0.00	0.14	0.00	0.37	1.76	2.93	0.00	1.92	0.00	7.41	1.40	1.01	0.08	3.97	0.09
62	1.41	0.00	0.14	0.00	0.39	1.86	2.90	0.01	1.68	0.00	6.21	1.40	0.96	0.08	4.16	0.09
73	1.44	0.00	0.11	0.00	0.30	1.41	2.46	0.00	1.56	0.00	5.51	1.40	0.62	0.08	4.41	0.09
97	1.37	0.00	0.06	0.00	0.17	0.82	2.65	0.01	1.78	0.01	6.74	1.40	0.92	0.08	4.34	0.09

Appendix D

BFAR and Fragmentation Indices

Core 9/97-08 - BFAR and Fragmentation Indices

Sample depth (cm)	Dry bulk density	Specimens per gram dry sediment	BFAR	Fragmentation index	FLS (%)
3	1.31	226.18	0.01	32.00	5.56
7	1.21	56.24	0.02	29.00	5.06
11	0.95	211.71	0.00	21.00	3.72
15	1.03	134.78	0.01	18.00	3.20
19	1.20	63.93	0.02	12.00	2.16
23	1.55	264.44	0.01	13.00	2.33
27	1.55	166.54	0.01	13.00	2.33
31	1.43	168.23	0.01	7.00	1.27
35	1.07	238.54	0.00	10.00	1.81
39	1.48	450.73	0.00	14.00	2.51
43	1.50	492.73	0.00	8.00	1.45
47.5	1.61	25.40	0.06	2.00	0.37
51.5	1.40	175.59	0.01	3.00	0.55
55.5	1.33	112.74	0.01	4.00	0.73
59.5	1.23	198.86	0.01	4.00	0.73
63.5	1.48	169.15	0.01	12.00	2.16
68	1.79	119.55	0.01	18.00	3.20
72	1.58	137.74	0.01	11.00	1.98
76	1.24	27.53	0.05	3.00	0.55
80	1.36	84.36	0.02	4.00	0.73
84	1.34	170.83	0.01	7.00	1.27
88	1.25	245.56	0.01	16.00	2.86
92	1.53	460.88	0.00	9.00	1.63

Appendix D

BFAR and Fragmentation Indices

Core 9/97-08 - BFAR and Fragmentation Indices

Sample number	Dry bulk density	Specimens per gram dry sediment	BFAR	Fragmentation index	FLS (%)
96.5	1.13	410.18	0.00	10.00	1.81
100.5	1.30	41.47	0.03	4.00	0.73
105	1.13	72.75	0.02	8.00	1.45
109	0.81	361.13	0.00	5.00	0.91
113	0.87	629.72	0.00	3.00	0.55
117.5	1.00	259.38	0.00	5.00	0.91
121.5	1.01	149.04	0.01	26.00	4.56
125.5	1.09	107.67	0.01	6.00	1.09
129.5	1.18	220.43	0.01	34.00	5.88
133.5	1.34	539.71	0.00	14.00	2.51
137.5	1.60	546.39	0.00	17.00	3.03
141.5	1.67	123.10	0.01	6.00	1.09
145.5	1.33	639.98	0.00	4.00	0.73
149.5	1.48	699.39	0.00	3.00	0.55
154	1.20	657.43	0.00	11.00	1.98
162	1.51	117.46	0.01	8.00	1.45
166	1.18	434.48	0.00	8.00	1.45
170	1.34	416.21	0.00	4.00	0.73
174	1.30	96.93	0.01	3.00	0.55
178	1.01	23.00	0.04	2.00	0.37
182	1.15	141.79	0.01	4.00	0.73

Appendix D

BFAR and Fragmentation Indices

Core 9/97-10 - BFAR and Fragmentation Indices

Sample depth (cm)	Dry bulk density	Specimens per gram dry sediment	BFAR	Fragmentation index (%)	FLS (%)
3	1.49	93.93	35.42	16.00	2.86
7	1.42	36.65	13.82	11.00	1.98
11	1.53	106.68	40.23	13.00	2.33
16	1.27	172.17	432.08	5.00	0.91
20	1.70	70.67	342.48	0.00	0.00
27	1.50	43.54	210.98	12.00	2.16
31	1.41	112.24	543.90	4.00	0.73
35	1.57	89.83	435.30	5.00	0.91
39	1.28	89.36	85.15	8.00	1.45
43	1.45	112.83	164.70	7.00	1.27
47	1.66	144.29	210.61	10.00	1.81
51.5	1.12	253.14	982.04	17.00	3.03
55.5	0.82	212.98	826.24	18.00	3.20
59.5	1.06	155.11	111.50	14.00	2.51
63.5	1.22	267.99	192.65	18.00	3.20
67.5	1.12	107.26	759.94	17.00	3.03
71.5	1.66	118.31	838.23	17.00	3.03
75.5	1.59	54.85	388.61	8.00	1.45
79.5	1.35	121.23	590.35	6.00	1.09
83	1.64	93.23	107.17	8.00	1.45

Appendix D

BFAR and Fragmentation Indices

Core 9/97-03 - BFAR and Fragmentation Indices

Sample depth (cm)	Dry bulk density	Specimens per gram dry sediment	BFAR	Fragmentation index	FLS (%)
3	1.67	84.70	354.40	28.00	4.90
6	1.58	76.04	309.49	14.00	2.51
9	1.59	44.53	120.24	7.00	1.27
13	1.41	15.47	41.78	7.00	1.27
19	1.68	41.24	111.37	6.00	1.09
23	1.54	149.03	402.41	22.00	3.89
27	1.57	118.13	318.97	8.00	1.45
31	1.35	188.60	509.26	6.00	1.09
35	1.17	227.94	615.49	7.00	1.27
39	1.22	107.35	289.87	7.00	1.27
43	1.46	188.90	594.99	11.00	1.98
47	1.45	67.62	261.87	15.00	2.68
51	1.51	57.71	223.52	23.00	4.06
55	1.05	218.31	756.28	6.00	1.09
59	0.95	173.61	787.52	11.00	1.98
63	0.98	279.71	1012.71	17.00	3.03
67	1.06	401.50	1453.68	19.00	3.37
71	1.35	197.79	245.88	15.00	2.68
75	1.37	167.53	208.27	5.00	0.91
79	1.10	217.49	505.31	25.00	4.39
83	1.29	152.57	157.54	7.00	1.27
87	1.78	121.65	125.61	11.00	1.98
91	1.48	154.76	185.15	3.00	0.55
95	1.38	205.52	245.88	8.00	1.45

Appendix D

BFAR and Fragmentation Indices

Core 9/97-04 - BFAR and Fragmentation Indices

Sample depth (cm)	Dry bulk density	Specimens per gram dry sediment	BFAR	Fragmentation index	FLS (%)
1	2.51	127.77	53.88	10.00	1.81
2	3.36	78.48	141.91	4.00	0.73
4	2.73	89.76	130.86	5.00	0.91
9	2.71	85.39	32.32	4.00	0.73
13	2.46	95.31	35.62	3.00	0.55
17	2.48	143.33	318.46	2.00	0.37
21	2.43	99.95	222.08	3.00	0.55
25	2.55	52.84	117.41	4.00	0.73
29	2.51	95.87	160.88	8.00	1.45
33	3.20	141.50	167.65	7.00	1.27
37	3.57	183.12	302.58	5.00	0.91
39	3.53	211.45	6027.32	6.00	1.09
41	3.98	114.58	807.73	3.00	0.55
43	3.20	204.13	1221.56	5.00	0.91
45	3.42	229.55	30.43	4.00	0.73
48	3.05	155.84	153.99	11.00	1.98
52	3.03	138.76	137.11	9.00	1.63
56	2.51	173.42	171.36	7.00	1.27
60	2.86	93.24	82.81	10.00	1.81
68	2.07	110.63	92.14	12.00	2.16
72	2.10	97.08	95.27	9.00	1.63
76	2.04	90.52	83.60	15.00	2.68
80	2.07	49.47	77.95	13.00	2.33
84	2.22	63.61	42.60	12.00	2.16

Appendix D

BFAR and Fragmentation Indices

Core 9/97-14 - BFAR and Fragmentation Indices

Sample depth (cm)	Dry bulk density	Specimens per gram dry sediment	BFAR	Fragmentation index	FLS (%)
1	3.62	64.91	387.21	14.00	2.51
5	2.37	79.06	69.00	1.00	0.18
7.5	3.43	29.76	22.40	2.00	0.37
9	4.48	24.56	29.97	1.00	0.18
12.5	3.10	49.74	60.70	3.00	0.55
16	2.62	53.80	45.99	4.00	0.73
20	3.22	48.48	26.61	7.00	1.27
23	3.18	67.03	34.70	8.00	1.45
27.5	2.66	39.16	320.40	3.00	0.55
31	2.60	38.45	297.59	10.00	1.81
35	3.15	63.83	494.07	9.00	1.63
39	3.21	48.57	24.75	5.00	0.91
43	2.81	38.80	116.72	11.00	1.98
49	1.58	131.47	196.51	12.00	2.16
51	1.44	145.59	134.83	9.00	1.63
54	3.64	67.34	122.79	5.00	0.91
57	3.04	75.87	181.89	13.00	2.33
62	3.17	52.75	53.28	6.00	1.09
74	2.83	46.66	45.99	2.00	0.37
78	2.70	61.83	60.94	11.00	1.98
81	2.85	66.65	116.12	4.00	0.73
84	2.29	87.90	171.20	3.00	0.55
87	2.37	65.74	37.43	2.00	0.37
90	2.83	42.37	20.91	5.00	0.91
93	2.73	37.40	18.46	6.00	1.09
95	2.90	49.94	15.87	8.00	1.45

Appendix D BFAR and Fragmentation Indices

Core 9/97-27/II - BFAR and Fragmentation Indices

Sample depth (cm)	Dry bulk density	Specimens per gram dry sediment	BFAR	Fragmentation Index	FLS (%)
3	1.25	37.92	6.66	16.00	2.86
7	1.13	30.66	13.00	10.00	1.81
11	1.35	34.99	6.81	15.00	2.68
15	1.10	19.91	3.87	4.00	0.73
19	1.31	22.21	6.11	4.00	0.73
33	1.14	17.48	0.31	13.00	2.33
37	1.22	1.49	0.03	15.00	2.68
41	1.16	7.04	0.13	7.00	1.27
45	1.24	2.56	0.05	6.00	1.09
49	1.16	9.38	3.63	8.00	1.45
53	1.00	12.72	1.70	13.00	2.33
57	1.26	11.56	1.55	1.00	0.18
61	1.07	27.26	6.34	15.00	2.68
65	1.07	10.22	2.37	4.00	0.73
69	0.95	15.24	1.83	8.00	1.45
73	1.20	12.15	3.68	4.00	0.73
77	1.18	5.42	1.64	5.00	0.91
81	1.69	2.69	0.81	2.00	0.37
85	1.26	5.80	0.29	4.00	0.73
90	1.00	5.44	0.90	7.00	1.27
94	1.22	2.99	0.22	8.00	1.45
98	1.16	7.86	0.64	23.00	4.06
103	1.41	10.32	0.84	9.00	1.63
107	1.06	10.29	0.45	11.00	1.98
111	1.22	29.85	1.31	2.00	0.37
115	1.10	19.82	3.27	8.00	1.45
119	1.28	3.56	0.77	1.00	0.18
123	1.21	1.88	0.69	4.00	0.73
127	1.09	2.91	0.32	2.00	0.37
131.5	1.11	3.27	0.36	4.00	0.73
135	1.32	2.76	1.08	2.00	0.37
139.5	1.50	16.99	6.65	3.00	0.55
143	1.35	12.11	2.92	6.00	1.09
147	1.48	23.42	5.64	8.00	1.45
151	1.36	58.65	14.12	17.00	3.03
155.5	1.40	41.58	10.01	16.00	2.86
159.5	1.28	17.10	2.44	18.00	3.20
163.5	1.15	6.31	0.90	5.00	0.91
167.5	1.48	2.46	0.35	4.00	0.73

Appendix D

BFAR and Fragmentation Indices

Core 9/97-27/II - BFAR and Fragmentation Indices

Sample depth (cm)	Dry bulk density	Specimens per gram dry sediment	BFAR	Fragmentation Index	FLS (%)
171.5	1.78	3.07	0.12	1.00	0.18
176	1.41	12.95	0.69	6.00	1.09
180	1.31	26.28	4.69	11.00	1.98
184	1.49	35.33	6.31	12.00	2.16
188	1.39	28.80	19.85	12.00	2.16
192	1.20	54.35	4.86	14.00	2.51
196.5	1.42	18.62	1.66	15.00	2.68
200.5	1.38	57.87	5.17	16.00	2.86
204.5	1.10	165.13	14.76	13.00	2.33
208.5	1.33	57.62	5.15	6.00	1.09
212.5	1.45	16.28	1.46	1.00	0.18
216.5	1.30	27.98	2.50	9.00	1.63
220.5	1.07	11.89	1.06	7.00	1.27
224.5	0.97	9.40	0.21	7.00	1.27
229.5	1.21	9.02	0.20	12.00	2.16
233.5	1.30	12.62	0.69	4.00	0.73
237.5	1.23	2.96	0.31	5.00	0.91
241.5	1.43	43.13	3.28	9.00	1.63
245.5	1.28	22.66	1.73	10.00	1.81
249.5	1.16	21.94	1.67	3.00	0.55
253.5	1.19	24.40	1.86	15.00	2.68
258.5	1.24	46.90	3.57	8.00	1.45
262	1.24	29.22	2.23	17.00	3.03

Appendix D BFAR and Fragmentation Indices

Core 9/97-20 - BFAR and Fragmentation Indices

Sample depth (cm)	Dry bulk density	Specimens per gram dry sediment	BFAR	Fragmentation index	FLS (%)
1.5	2.34	42.82	8.86	11.00	1.98
3	1.23	100.66	20.82	9.00	1.63
5.5	2.50	21.60	4.47	10.00	1.81
9	1.29	75.96	22.33	7.00	1.27
11.5	2.61	39.15	11.51	6.00	1.09
15	1.15	114.49	33.66	3.00	0.55
19	1.22	42.68	12.55	4.00	0.73
20.5	2.52	38.05	11.19	13.00	2.33
23	1.22	94.79	50.05	4.00	0.73
25.5	2.80	54.97	29.03	6.00	1.09
27.5	3.02	51.05	26.95	3.00	0.55
30.5	2.81	44.20	14.30	2.00	0.37
33	2.06	18.41	11.51	4.00	0.73
34.5	2.63	57.03	35.65	4.00	0.73
37	1.23	66.58	41.62	3.00	0.55
40.5	2.57	10.91	6.82	2.00	0.37
43.5	2.41	7.46	4.66	2.00	0.37
45	0.79	20.23	6.77	3.00	0.55
48	2.99	76.13	25.47	4.00	0.73
50.5	2.69	12.62	4.03	3.00	0.55
52	1.13	40.75	10.01	3.00	0.55
55.5	2.78	12.96	3.18	4.00	0.73
57.5	2.53	1.58	0.76	2.00	0.37
59.5	2.58	9.31	4.48	3.00	0.55
63	1.03	23.20	11.16	2.00	0.37
66.5	2.82	14.19	6.83	3.00	0.55
68.5	2.46	0.81	0.39	2.00	0.37
70.5	2.58	5.42	2.61	5.00	0.91
72.5	2.30	0.87	0.13	2.00	0.37
74.5	2.35	0.85	0.13	4.00	0.73
76.5	2.36	11.02	1.71	2.00	0.37
78.5	2.27	3.52	2.29	3.00	0.55
80.5	2.53	15.82	4.44	3.00	0.55
82	1.72	8.12	2.28	3.00	0.55
87	1.25	9.58	1.60	4.00	0.73
90.5	2.96	14.21	2.38	9.00	1.63
92.5	2.91	17.88	5.10	4.00	0.73
94.5	3.16	7.60	0.58	8.00	1.45
96.5	3.37	8.89	0.68	6.00	1.09

Appendix D BFAR and Fragmentation Indices

Core 9/97-20 - BFAR and Fragmentation Indices

Sample depth (cm)	Dry bulk density	Specimens per gram dry sediment	BFAR	Fragmentation index	FLS (%)
97.5	3.21	5.60	0.43	2.00	0.37
101	1.74	2.30	0.11	2.00	0.37
103.5	2.51	4.78	0.23	2.00	0.37
106.5	2.61	1.53	0.07	3.00	0.55
108.5	2.39	0.84	0.04	2.00	0.37
110.5	2.26	2.65	0.13	2.00	0.37
112.5	2.60	1.54	0.07	4.00	0.73
114.5	2.33	4.29	0.21	2.00	0.37
116.5	2.75	5.09	0.58	1.00	0.18
121	1.11	0.00	0.00	2.00	0.37
123.5	2.08	4.81	0.55	2.00	0.37
125.5	2.10	1.91	0.22	3.00	0.55
129.5	2.87	1.39	0.46	4.00	0.73
131.5	2.68	8.21	2.71	5.00	0.91
133.5	2.62	7.63	2.52	6.00	1.09
135.5	2.64	12.90	4.26	4.00	0.73
137.5	2.52	18.28	5.31	3.00	0.55
139.5	2.71	16.25	4.72	4.00	0.73
141.5	2.62	3.05	0.40	3.00	0.55
143.5	2.08	3.84	0.51	2.00	0.37
145.5	3.01	7.30	0.57	2.00	0.37
158	1.25	4.79	0.37	2.00	0.37
162.5	3.33	10.81	1.15	9.00	1.63
164.5	3.53	27.19	2.89	6.00	1.09
166.5	3.55	34.36	4.88	7.00	1.27
168.5	3.57	60.45	8.59	5.00	0.91
170.5	3.53	37.97	5.40	7.00	1.27
172	1.34	149.71	21.28	9.00	1.63
175.5	3.06	172.57	24.53	5.00	0.91
177.5	2.93	83.32	11.85	13.00	2.33
180	2.82	136.39	19.39	9.00	1.63
183	2.85	5.62	0.80	6.00	1.09
185.5	3.60	1.11	0.16	1.00	0.18
188	1.66	1.20	0.31	1.00	0.18
191.5	3.89	5.66	1.45	4.00	0.73
193.5	3.60	14.46	3.72	6.00	1.09
195.5	3.55	15.19	3.90	3.00	0.55
197.7	3.59	44.06	11.32	5.00	0.91

Appendix D

BFAR and Fragmentation Indices

Core 9/97-20 - BFAR and Fragmentation Indices

Sample depth (cm)	Dry bulk density	Specimens per gram dry sediment	BFAR	Fragmentation index	FLS (%)
199.5	3.39	38.95	10.01	6.00	1.09
200	1.26	229.76	59.05	4.00	0.73
201	2.93	42.37	10.89	2.00	0.37
206.5	4.04	31.22	8.02	7.00	1.27

Appendix E
Age model data

Raw ^{14}C AMS radiocarbon dates and calculated reservoir ages					
Site	Core depth (cm)	C-14 Age (years BP)	1 sigma error	Correlated age (yr B.P.)	Reservoir age
Core 9/97/27/II	7	8840	35	8818.22	22
	33	12355	45	11585.26	770
	53	16305	50	15101.82	1203
	69	18875	55	17338.91	1536
	85	20150	60	20220.50	71
	135	26515	110	28063.54	1549
	180	33890	220	34975.03	1085
	196.5	41,600	500	40739.89	860
	208.5	42,400	600	41037.50	1362
Core 9/97/10	9	10320	35	11501.13	1181
	16	17,355	50	16403.37	952

Appendix E

Age model data

Core 9/97-10

Sample depth (cm)	Age (yr B.P.)
3	5640.00
7	9860.00
11	11500.00
16	16403.37
20	18101.13
27	35668.71
31	45707.32
35	55745.94
39	66336.63
43	85720.46
47	89560.16
51.5	96128.47
55.5	101966.97
59.5	109128.24
63.5	123992.34
67.5	126867.87
71.5	129743.40
75.5	132618.93
79.5	136511.06
83	161032.39
87	180511.06
91	185651.32
95	190249.51
99	194847.69
103	204732.87
107	209944.43
111	215262.31

Sample depth (cm)	Age (yr B.P.)
115	227913.82
120	243728.22
123	253216.85
132	275336.70
136	285107.22
142	297588.65
146	316834.69
150	334826.03
156	340266.05
160	346836.04
164	353359.86
168	359190.54
172	368230.80
176	377271.07
180	386311.33
184	395351.59
188	401463.86
192	403817.14
196	406152.21
200	408301.61
204	410451.02
207	412809.95
213	420709.53
217	427224.85
223	437010.59
230	446224.24
236	454035.50

Appendix E

Age model data

Core 9/97-10

Age (yr B.P.)	Sedimentation rate (cm /kyr)
12959.56	2.65
17878.26	0.40
65191.51	0.21
85724.05	1.05
89487.33	0.69
107007.57	0.26
123843.64	1.39
135379.66	0.14
160426.10	0.21
181220.64	0.87
194856.34	0.39
204478.17	0.77
215081.53	0.32
253814.92	0.41
285742.68	0.49
297369.15	0.21
316239.87	0.22
335094.05	1.20
339855.00	0.61
353118.39	0.73
358382.17	0.44
400433.45	1.70
405960.18	1.86
411548.05	0.76
420745.16	0.61
437508.72	0.77
453612.14	0.77

Appendix E

Age model data

Core 9/97-03

Sample depth (cm)	Age (yr B.P.)
3	1004.00
6	4074.01
9	16506.20
13	20500.00
19	24800.00
23	30500.00
27	41000.00
31	52500.00
35	64750.00
39	75800.00
43	86425.00
47	90300.00
51	96000.00
55	102000.00
59	109500.00
63	116750.00
67	124000.00
71	145000.00
75	160000.00
79	210000.00
83	243556.18
87	250763.65
91	255548.00
95	259250.81
99	262565.39
103	266045.92
107	270246.56
111	277358.43
115	296764.98

Sample depth (cm)	Age (yr B.P.)
119	327150.81
123	340789.40
127	371660.59
131	400730.24
135	411969.48
139	415800.47
143	416414.24
147	418001.84
151	423410.13
155	430444.49
159	437513.72
163	443826.05
167	449273.32
171	453919.02
175	457826.68
180	461782.84
183	463731.32
187	465918.40
191	467725.15
195	469248.94
199	470587.15
203	471837.14
207	473075.06
211	474312.98
215	475550.90
219	476788.82
222	477717.26
225	478645.70
229	479883.62

Appendix E

Age model data

Core 9/97-03

Age (yr B.P.)	Sedimentation rate (cm / kyr)
3509.57	0.24
16454.86	0.25
124728.39	0.37
136578.16	0.32
165511.32	0.26
180879.59	0.29
195865.52	0.22
215186.21	0.28
225693.56	0.80
242730.94	0.43
255339.75	0.97
270395.63	0.84
296871.53	0.14
326642.59	0.19
341098.73	0.21
400097.22	0.24
418012.64	1.15
423960.88	0.59
437524.68	0.59
457604.69	1.11
471720.65	3.23

Appendix E

Age model data

Core 9/97-04

Sample depth (cm)	Age (yr B.P.)	Age (yr B.P.)	Sedimentation rate (cm / kyr)
1	989.67	1040.38	2.37
2	1833.06	1864.27	0.55
4	5320.04	5207.29	0.69
8	11151.52	12238.45	2.64
12	13470.23	13469.94	2.68
16	14964.98	17970.27	0.45
20	16459.73	26626.00	0.60
24	17954.48	33048.76	0.84
28	26730.08	38168.14	0.61
32	33326.87	41741.07	0.04
36	38065.88	88694.53	0.14
38	41330.27	103397.73	0.17
40	89428.77	115756.16	7.54
42	103508.50	117200.14	1.01
44	115476.79	121297.68	1.13
47	116147.62	131880.39	1.16
51	116677.81	138791.55	1.16
55	117258.77		
59	121211.26		
67	128324.61		
71	131876.91		
75	135321.67		
79	138766.32		
83	142210.98		

Appendix E

Age model data

Core 9/97-14

Sample depth (cm)	Age (yr B.P.)	Age (yr B.P.)	Sedimentation rate (cm / kyr)
1	2533.26	2968.76	0.17
5	17282.35	15720.79	1.15
7.5	19170.09	17327.35	1.33
9	20299.01	21860.19	0.82
12	21804.25	25042.41	1.17
15	23599.92	27137.71	1.82
19	25314.20	29164.32	1.93
23	27024.02	30828.70	0.12
27	29254.86	54402.49	0.13
31	30807.70	65760.77	1.96
35	55005.29	67696.31	0.33
39	65817.05	79476.43	0.67
43	67600.74	85477.04	1.08
49	79164.65	89120.26	0.55
51	85300.12	99835.62	0.42
54	89071.83	104636.75	0.99
57	100006.46	110879.07	1.01
62	104706.03	115612.49	0.57
75	107736.22	126215.07	0.51
78	110766.41	131981.70	1.76
81	115762.70	135410.61	2.03
84	126216.35	138839.53	3.15
87	132004.31	141654.44	3.15
90	133712.19		
93	135418.81		

Appendix E

Age model data

Core 9/97-27/2

Sample depth (cm)	Age (yrs B.P.)	Sample depth (cm)	Age (yrs B.P.)
3	8041.33	139.5	28063.54
7	8818.22	143	28322.76
11	9595.10	147	28619.01
15	10371.98	151	28990.37
19	11144.02	155.5	30765.48
33	11585.26	159.5	32117.19
37	12290.64	163.5	32343.20
41	12449.99	167.5	32604.00
45	12680.39	171.5	33281.22
49	14305.13	176	34116.21
53	15101.82	180	34497.24
57	15820.74	184	34975.03
61	16168.25	188	37771.53
65	16516.10	192	38370.20
69	17338.91	196.5	39512.71
73	18051.64	200.5	40739.89
77	18607.37	204.5	40818.83
81	19212.23	208.5	40897.78
85	20220.50	212.5	41037.50
90	20960.60	216.5	41225.95
94	21552.68	220.5	41414.39
98	21774.94	224.5	42129.29
103	21966.07	229.5	42506.26
107	22440.12	233.5	42756.57
111	22764.17	237.5	43249.71
115	23141.06	241.5	43771.60
119	23525.80	245.5	44293.49
123	24199.10	249.5	44596.22
127	25635.07	253.5	44872.84
131.5	27040.30	258.5	45209.19
135	27727.92	262	45387.45

Appendix E Age model data

Core 9/97-27/2

Age (yrs B.P.)	Sedimentation rate (cm / kyr)
8245.65	5.70
8874.42	2.36
10580.06	5.14
11376.62	3.64
13021.61	56.28
13234.22	2.59
14814.69	7.46
15825.75	4.30
16788.33	10.76
17189.18	8.33
19121.06	3.30
20177.96	20.09
20599.17	6.08
21224.80	13.86
22168.92	12.30
22893.58	22.78
23256.11	6.06
23885.23	4.63
25556.07	2.73
27319.58	9.12
27720.30	8.46
28243.21	2.56
31110.39	4.15
32083.71	6.15
32841.35	7.02
33408.22	25.19
33731.03	14.06
33996.50	17.06
34230.77	18.63
34475.87	1.61
36869.83	5.60
38330.27	1.45
41443.45	11.19
42515.67	44.81
42769.80	18.31
43530.40	9.65
44304.65	13.13
45200.80	13.13

Appendix E Age model data Core 9/97-20

Sample depth (cm)	Age (yrs B.P.)	Sample depth (cm)	Age (yrs B.P.)
1.5	215.05	103.5	29596.34
3	525.33	106.5	29825.33
5.5	1042.46	108.5	29977.99
9	1766.45	110.5	30130.65
11.5	2283.58	112.5	30283.30
15	3007.56	114.5	30435.96
19	3834.97	116.5	30545.02
20.5	4145.25	121	30761.53
23	4670.76	123.5	30881.81
25.5	5405.80	125.5	30978.03
27.5	5993.83	129.5	31196.37
30.5	6923.41	131.5	31423.17
33	8229.59	133.5	31649.97
34.5	8714.90	135.5	31876.78
37	9523.74	137.5	32155.69
40.5	10656.12	139.5	32815.82
43.5	11626.73	141.5	33466.26
45	12480.95	143.5	34047.22
48	14356.59	145.5	34324.26
50.5	15230.54	158	35976.17
52	15732.42	162.5	36332.13
55.5	16838.41	164.5	36495.82
57.5	17329.87	166.5	36708.18
59.5	17821.32	168.5	36920.55
63	18681.37	170.5	37132.92
66.5	19541.42	172	37292.20
68.5	20032.87	175.5	37663.84
70.5	20524.33	177.5	37876.21
72.5	21477.21	180	38141.67
74.5	22439.54	183	38460.22
76.5	23356.03	185.5	38725.68
78.5	23666.65	188	39045.32
80.5	24033.02	191.5	39542.90
82	24993.30	193.5	39827.24
87	26395.54	195.5	40111.57
90.5	27377.06	197.7	40485.44
92.5	27713.96	199.5	40948.06
94.5	28284.84	200	41076.56
96.5	28855.72	201	41333.58
97.5	29138.37	206.5	42747.14
101	29405.52		

Appendix E

Age model data Core 9/97-20

Age (yrs B.P.)	Sedimentation Rate (cm / kyr)
1720.64	4.83
4642.50	3.40
6816.16	1.89
8207.64	3.09
11716.39	1.60
14437.24	2.99
15789.75	3.13
16788.68	4.07
20534.19	2.08
23334.18	6.44
23959.77	1.54
24981.89	3.57
27376.98	5.98
27707.95	3.50
29137.35	13.10
30470.69	20.79
31151.40	8.82
32076.31	3.03
33395.11	3.44
34070.58	7.57
35986.01	12.79
36468.23	9.42
38831.27	7.03
40348.70	3.89
41409.13	3.89

Appendix F Principle component scores

	1	2	3	4
3_8	8.8679	-7.1688	0.93664	5.7125
7_8	19.498	-6.0542	15.282	-9.3776
15_8	15.632	0.83445	27.033	-9.871
19_8	17.925	3.0503	29.018	-7.9521
23_8	47.612	-5.1322	13.782	-7.6947
27_8	69.4	-6.4143	12.801	-10.048
31_8	12.728	-5.4516	0.162	8.0699
35_8	71.697	-6.6488	11.872	-9.1208
39_8	9.5914	-9.8532	-5.7024	-1.9737
43_8	46.375	-8.579	8.217	-15.339
47.5_8	51.193	-8.4356	8.6581	-16.155
51.5_8	65.511	-4.8091	15.146	-10.915
55.5_8	66.373	-5.2398	13.909	-10.383
59.5_8	55.696	-4.2692	16.034	-9.9913
63.5_8	9.2748	-3.1255	7.6853	2.0903
68_8	13.325	-9.8	6.4555	-10.903
80_8	1.4467	-6.4108	10.808	-8.7176
3_10	11.832	-12.638	-0.02632	-13.689
7_10	1.7142	-11.75	0.24294	-6.926
11_10	-6.3527	-5.8304	14.865	-9.4708
16_10	-5.1644	2.3777	26.492	12.681
20_10	-8.9327	1.6089	27.978	11.779
27_10	-7.8855	1.9393	26.664	15.851
31_10	-2.8203	-1.5622	16.728	3.688
35_10	-4.5091	-1.0109	19.413	-2.3089
39_10	-9.4962	-0.06373	22.529	12.913
43_10	-8.9939	-3.3559	13.236	6.5664
47_10	-9.8605	-5.0143	11.469	-3.6881
51.5_10	-9.4159	-9.3959	2.3323	-13.752
55.5_10	-8.8993	-10.523	2.2078	-10.07
59.5_10	-10.719	-9.6346	4.5191	-16.915
63.5_10	-9.5189	-13.497	-3.0082	-14.325
67.5_10	-9.1316	-16.141	-8.2979	-17.329
71.5_10	-9.2087	-13.878	-3.9111	-15.479
79.5_10	-9.0444	-0.2565	19.061	6.923
83_10	-9.5626	-3.3688	12.422	1.4792

Appendix F Principle component scores

	1	2	3	4
1_4	-10.495	-15.305	-4.2634	-13.814
2_4	-10.349	-13.438	1.8074	-15.085
5.5_4	-11.112	-13.701	-0.61077	-9.0738
9_4	-9.3247	2.4223	20.261	6.8965
13_4	-2.9676	-1.0486	2.8011	-1.6789
21_4	-7.0965	-8.8486	-1.0881	1.334
25_4	-7.5141	-16.239	-11.641	-11.728
33_4	-6.6847	-7.6784	-1.5525	-1.9596
37_4	-7.9244	-0.39592	11.916	-3.4691
39_4	-8.9815	-2.6339	11.416	-3.1898
43_4	-3.5643	-4.1319	0.79249	17.002
45_4	-8.0689	-2.0956	9.9175	-3.5642
48_4	-7.7906	-4.8429	7.0192	4.5955
52_4	-6.54	-5.3571	4.2385	-0.54774
56_4	-7.2642	-0.43811	12.219	6.4299
60_4	-7.8416	-2.8693	9.0129	-3.432
64_4	-4.6264	-9.8508	-5.616	3.8199
68_4	-6.2533	-3.3682	7.2193	4.3562
72_4	-7.7381	-3.162	9.3729	0.8276
76_4	-5.1417	-9.6063	-6.7796	-0.73446
80_4	-6.4952	-13.745	-9.879	-10.394
84_4	-10.948	-5.8863	10.297	-15.709
88_4	-7.2048	-16.848	-11.769	-12.693

Appendix F Principle component scores

	1	2	3	4
1_14	-12.381	-0.24936	21.297	-16.293
11_14	-9.6779	9.8131	23.643	-13.909
12.5_14	-7.4621	7.9569	15.646	-11.11
20_14	-11.021	3.0812	22.499	-17.055
23_14	-11.537	3.7673	23.289	-18.429
26_14	-7.7184	-4.5176	3.098	-13.639
27.5_14	-9.5363	-2.2304	9.8563	-14.544
31_14	-10.509	-3.0777	11.765	-17.21
35_14	-9.9002	-1.9722	11.902	-16.584
39_14	-9.7806	-1.3076	10.821	-16.349
43_14	-6.64	-8.0606	3.1637	-14.257
49_14	-9.7805	-7.8174	6.0217	-19.514
51_14	-9.596	-10.009	4.4233	-20.855
54_14	-10.487	-2.9146	12.445	-19.876
57_14	-6.5755	-1.7049	-6.0083	-7.231
62_14	-0.51238	-3.7868	11.136	-11.899
77_14	-6.987	-15.412	-11.721	-12.918
78_14	-6.9719	-3.2486	-9.0863	-17.926
81_14	-7.5268	0.20439	-2.3078	-15.699
84_14	-9.6946	-9.7093	1.0264	-19.918
87_14	-8.7792	0.80364	14.691	-16.457
90_14	-12.749	-2.1466	18.448	-25.064
93_14	-10.925	3.2701	22.192	-18.028
3_27	-9.9922	1.9446	23.975	-18.547
7_27	-7.1954	7.3138	28.907	-13.124
15_27	-9.813	14.848	36.707	-16.055
19_27	-12.103	10.55	34.569	-17.588
147_27	4.0544	18.359	-6.9983	-8.5734
151_27	1.84	41.365	-0.56682	-11.225
155.5_27	5.2636	49.945	-21.441	-5.4386
159.5_27	9.4739	47.283	-19.252	-6.2319
192_27	5.858	30.218	1.7861	-8.325
200.5_27	2.785	33.158	0.79822	-10.864
204.5_27	9.0499	37.457	-8.9548	-8.5174
212.5_27	7.7429	33.98	-1.1474	-10.88
216.5_27	5.3886	28.726	-8.8306	-6.3083
241.5_27	-6.0049	27.194	15.698	-13.376
249.5_27	-14.085	11.014	33.27	-23.352
253.5_27	-10.216	13.095	27.878	-16.499

Appendix G - Lithofacies scheme courtesy of Toms (in prep.)

Carbonate Facies

CM Calcareous mud/sandy mud



(9/97-13)

CO Calcareous ooze

C0-1 Nannofossil ooze



(9/97-10)

C0-2 Clay-rich nannofossil ooze



(9/97-13)

C0-3 Foraminifera ooze

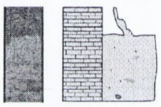

(9/97-10)

FS Foraminifera sand

FS-1 Foraminifera sand

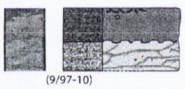

(9/97-10)

FS-2 Muddy foraminifera sand



(9/97-13)

CNO Consolidated calcareous nannofossil ooze



(10/97-16)

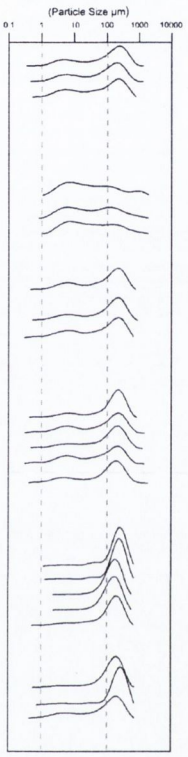

Siliciclastic Facies

BM Hemipelagic brown muds

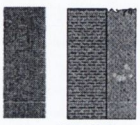

(9/97-27/II)

BM-1 Thin bioturbated muds



(9/97-03)

BM-2 Containing nannofossil banding

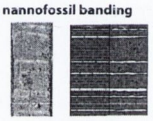

(10/97-19)

BM-3 Containing sponge spicules

GM Hemipelagic grey muds

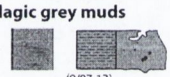

(9/97-13)

SM Brown sandy muds

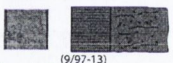

(9/97-13)

RM Red sandy muds



(9/97-13)

G Gravel

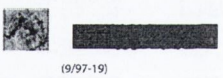

(9/97-19)

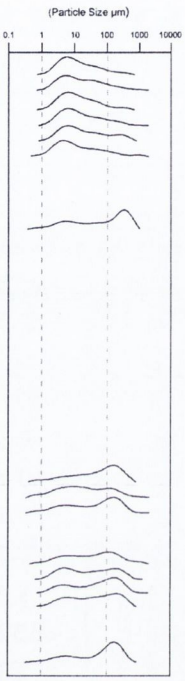

Remobilised Facies

R1 Muddy sands



(10/97-16)

R2 Chaotically organised bedding



(9/97-01)